Recalibrating the breakup history of SW Gondwana: The first U-Pb chronostratigraphy for the Uitenhage Group, South Africa

Robert Anthony Muir

A thesis submitted to the Faculty of Science, University of Cape Town, in fulfilment of the requirements for the degree of Doctor of Philosophy

December 2018

Supervisor: Assoc. Prof. Emese Bordy

Declaration

I declare that this thesis is my own, unaided work, except where specified in the text. It is being submitted for the Degree of Doctor of Philosophy in the University of Cape Town and has not been previously submitted to any other University or academic institution.

(Signature of candidate)

27th day of December 2018

I confirm that I have been granted permission by the University of Cape Town's Doctoral Degrees Board to include the following publication(s) in my thesis, and where co-authorships are involved, my co-authors have agreed that I may include the publication(s):

Publication 1:

Muir, R., Bordy, E.M., Reddering, J.S.V.; Viljoen, J.H.A. 2017. Lithostratigraphy of the Enon Formation (Uitenhage Group), South Africa. South African Journal of Geology 120.2: 273–280 • doi:10.2113/gssajg.120.2.273

Publication 2:

Muir, R., Bordy, E.M., Reddering, J.S.V.; Viljoen, J.H.A. 2017. Lithostratigraphy of the Kirkwood Formation (Uitenhage Group), including the Bethelsdorp, Colchester and Swartkops members, South Africa. South African Journal of Geology 120.2: 281–293 • doi:10.2113/gssajg.120.2.281

The papers form sections 2.2.1 and 2.2.2 of this thesis respectively and are found after the appendices.

Abstract

Syn-rift deposits often provide the only means to determine the processes for initiation and evolution of rift basins and passive margins. The structurally preserved erosional remnants of several rift basins that formed during the Mesozoic breakup of Gondwana are located within the southern Cape region of South Africa. These onshore basins contain the Suurberg and Uitenhage Groups, which are predominantly continental, taphrogenic, fossiliferous strata interbedded with volcaniclastics. Their significance in the Gondwanan breakup events is poorly understood due to a lack of precise and accurate radioisotopic ages. The development of SW Gondwana into the modern passive margins of southern Africa, South America and Antarctica, as well as the evolution of life recorded in the regional strata are difficult to evaluate without a high resolution chronostratigraphic framework. By integrating field observations with U-Pb geochronology of over 4000 detrital and primary volcanic zircons from pyroclastic, mixed-origin volcaniclastic and sedimentary rocks by Laser Ablation Inductively Coupled Plasma Mass Spectrometry (LA-ICPMS), this thesis presents the first radioisotopic ages for the Uitenhage Group and provides a new chronostratigraphic framework for the onshore Jurassic – Cretaceous in the southern Cape. To further improve precision and accuracy, a selection of crystals from four pyroclastic deposits in key stratigraphic positions were selected for single-zircon Chemical Abrasion – Thermal Ionisation Mass Spectrometry (CA-TIMS) analysis to minimize the effects of Pb-loss and constrain depositional age uncertainties to < 1%. These new age constraints show that the Suurberg Group was deposited rapidly during the emplacement of the Karoo and Ferrar Large Igneous Province in the Early Jurassic (Pliensbachian) and likely predates the main phase of rifting in the southern Cape, whereas the Uitenhage Group was deposited over a prolonged (> 40 Ma) period from the Early Jurassic into the Early Cretaceous and records two phases of rifting: an initial Jurassic episode that roughly coincides with the separation of East and West Gondwna and is contemporaneous with widespread volcanism in SW Gondwana; and a subsequent period of renewed rifting during the Early Cretaceous opening of the South Atlantic. Trace element geochemical and zircon morphological assessments indicate that the volcanic source that supplied ash into the growing rift basins in the southern Cape during Gondwana breakup was situated in modern-day Patagonia and the Antarctic Peninsula, which were proximal to the southern Cape in the Jurassic and Early Cretaceous. The valuable geological framework presented in this dissertation illustrates the complexity of long-lived, rift-basin sedimentation and highlights the importance of high-resolution chronostratigraphy when investigating the tectonic, palaeontological and palaeogeographical records from the final moments of a unified Gondwana.

Acknowledgements

I would never have completed this thesis if it were not for the wealth of support I am privileged to have around me. Firstly, I thank my supervisor, Emese Bordy, who was with me from beginning to end through times both joyous and stressful. Your guidance in scientific matters, mentorship and encouragement throughout my postgraduate studies at UCT are deeply appreciated. Thanks for always believing in me, listening to me, and for your wholehearted commitment to this endeavor.

Enduring the most taxing aspects of this research journey would have been impossible without the support of my dear family and friends – Thank you all for your encouragement, kindness and patience. Special thanks go to my father, Andy, and brother, Matt, my aunt, Irene, and friend, Mieng, who were unwavering in thier belief that I would complete this task.

This research benefitted from the numerous discussions I had with academics at UCT and elsewhere. I will not mention everyone by name because I pestered so many, but I do want to specifically thank Goonie Marsh for being a wealth of knowledge on the Suurberg Group and the Karoo Large Igneous Province; Alastair Sloan for insightful discussions concerning tectonics; Robyn Pickering, for helping improve aspects of the thesis; and Laura Bracciali, Clarisa Vorster, Dirk Frei and Roland Mundil for chats about the U-Pb radioisotopic system.

I also thank Jurie Viljoen, who helped me immensely in this project. Indeed, your work mapping the Uitenhage Group and its volcaniclastic component is the foundation upon which this research is based. You did a superb job and a great service to South African geoscience during your long career at the Council. Enjoy your well-deserved retirement!

A word of thanks goes to all the field assistants with whom I had the pleasure of working: Yambi, Mieng, Devon, Chris, John, Isabel, Bakang, Travis and Chelsea. I had tons of fun working with each of you in some beautiful places. For lab assistance, I thank Lorena, Genna, Brent, Shaakirah and Mareli.

I was lucky to encounter those in the field that would become invaluable guides. To this end I thank: Yoann Hoibian, a geologist working at Cape Bentonite in Heidelberg; Stephen Drew from Vantell brickworks in Plettenberg Bay; Francoir Whittle and Kieth Barbier, who guided me to exposures of the Suurberg Group; and Jono Berry from the Gondwana Nature Reserve near Mossel Bay. I also appreciate the remote guidance I received on several occasions from John Almond, who has great experience conducting fieldwork in the Western Cape.

Finally, I appreciate the generosity of the various funders that chose to support me over the last few years. This research was conducted through grants awarded by the National Research Foundation (NRF) and the DST-NRF Centre of Excellence in Palaeosciences (CoE-Pal) and I personally relied on bursaries from these same sources too, for which I am grateful. The support of the NRF, Palaeontological Scientific Trust (PAST), and the UCT in covering travel expenses to the USA and Australia are also appreciated.

To my mother, Pam

Contents

Chapter 1: Introduction

1.1 Motivation and aims

The breakup of Gondwana into the present-day continental configuration of the Southern Hemisphere and India began shortly after the extensive Pliensbachian – Toarcian outpouring of continental flood basalts of the Karoo and Ferrar large igneous provinces (LIP) (Storey, 1995; Encarnación et al., 1996; Svensen et al., 2012; Burgess et al., 2015). Initially, a seaward transfer of magmatism from continental sites occurred in the Early Jurassic (Seton et al., 2012; Gaina et al., 2013) as spreading centres developed between East (Antarctica, India, Australia) and West Gondwana (Africa and South America). However, it was not until the Early Cretaceous that West Gondwana itself separated with the emplacement of the Parana-Etendeka LIP (Renne et al., 1996; de Assis Janasi at al., 2011) and the onset of ocean spreading between South America and Africa (Koopman et al., 2014). Conversely, the present-day region of South Africa, specifically its southern Cape region, which incorporates the southernmost extremity of Africa and the continental shelf (Fig. 1.1), did not experience the same pattern of voluminous magmatic outpouring proceeded by ocean floor spreading (Torsvik and Cocks, 2013; Will and Frimmel, 2018). Instead, there was little to no igneous activity in the southern Cape, where several rift basins developed sometime between the breakup of E and W Gondwana and the eventual separation of Africa and South America (Dingle et al., 1983; McMillan et al., 1997). Compared to adjacent spreading centres to the northeast and northwest from the southern Cape, this lack of incipient magmatic activity and subsequent datable igneous rocks limits the assessment of the a timing of rift initiation; the movement and rotation of the Falkland Islands (Aide, 1952; Ben-Avraham et al., 1993; Marshall, 1994); and the role of crustal anisotropy in rifting (Fouché et al., 1992; Paton & Underhill, 2004; Paton, 2006; Will and Frimmel, 2018).

The rifting of Gondwana coincided with important evolutionary changes in fauna and flora. Of special interest are the evolutionary trends in: a) angiosperms (flowering plants) in a ‘fiery’ Cretaceous (Bond and Scott, 2010; Brown et al., 2012; Lamont and He, 2012; Muir et al., 2015; He et al., 2016), and b) sauropodomorph dinosaurs, which suffer a global decrease in diversity across the Jurassic – Cretaceous boundary globally (Mannion et al., 2011), but potentially with exceptions (McPhee et al., 2016). The syn-rift deposits of the southern Cape, the Uitenhage Group comprising the Enon, Kirkwood and Sundays River formations, offer an opportunity to further our understanding in these fields, however a lack of robust age constraints for this continental unit severely hinders the establishment of any time-sensitive geological trends. Characterizing and providing the first ever radiometric ages for these strata allow detailed considerations of the evolution of landscape and life in SW Gondwana during the Jurassic – Cretaceous.

The Uitenhage Group is confined to the erosional remnants of numerous rift basins onshore of the southern Cape and has subsurface distributions in basins offshore (Dingle et al., 1983; McMillan et al., 1997; Muir et al., 2017a, b). It comprises primarily continental conglomerates and red beds in its lower part (i.e., Enon and Kirkwood formations), as well as marine mud- and sandstones in its upper part (i.e., Sundays River Formation). The marine deposits of the Uitenhage Group have garnered much attention for their chronostratigraphic and palaeoenvironmental significance in aid of hydrocarbon exploration efforts in the southern Cape, while their continental counterparts have to date yielded few datable rocks and are therefore poorly constrained in age by comparison. Vertebrate and plant macrofossils from the Kirkwood Formation can only be used to ascribe a broadly Latest Jurassic (145 Ma) – Early Cretaceous (134 Ma) depositional age (McLachlan and McMillan, 1976; McLachlan and McMillan 1979; Gomez et al., 2002; McMillan, 2003; Shone, 2006), and although the youngest age is more accepted for the majority of the Kirkwood Formation, this has been inferred from biostratigraphic constrains of the overlying Sundays River Formation based on ammonites (Kitchin, 1908; Spath, 1930; McLachlan and McMillan, 1976, McLachlan and McMillan, 1979; Cooper, 1983) and foraminifera (McMillan, 2003) . These invertebrate biostratigraphic results provide only relative age control and may not be accurate due to uncertainty about the stratigraphic nature of the contact that separates the two formations. If a stratigraphic gap exists, then the validity of the age for the Kirkwood Formation is brought into question (Gomez et al., 2002; Shone, 2006). Additionally, the foraminiferally dated uppermost Tithonian (~145

Numerous boreholes drilled and seismic surveys conducted across the offshore depocentres in the southern Cape, collectively known as the Outeniqua Basin (McMillan et al., 1997), have provided sparse insights into the age continental deposits of the Uitenhage Group with micropalaeontological biostratigraphic models being entirely restricted to marine units. The oldest of such deposits is dated Tithonian, although workers acknowledge that in some cases a significant thickness of continental deposits that are barren of microfossils, or remain entirely undrilled, lie below (McMillan et al., 1997). Most authors agree that these basal deposits are Upper Jurassic with oldest estimates being either Kimmeridgian (Dingle, 1983; Shone, 2006; Green et al., 2016) or Oxfordian (McMillan et al., 1997; Broad et al., 2012). Unfortunately, these estimates of the maximum age of the Uitenhage Group are influenced by dubious and unpublished K-Ar age of 162 ± 7 Ma for basalts from the underlying Suurberg Group that was quoted in McLachlan and McMillan (1976). However, the age of the Suurberg Group has not been established reliably and further, may be separated from the overlying Uitenhage Group by a hiatus of unknown duration (Hill, 1972; Marsh et al., 1979; Dingle, 1983; McMillan, 2010). Without a robust age and depositional model, the role of the Suurberg Group in the Mesozoic breakup of SW Gondwana and use as a lower limit of Uitenhage Group deposition are cautioned.

Despite the poorly age-diagnostic continental fossils in the Uitenhage Group and the uncertainty of its relationship with the underlying Suurberg Group, there is great potential for accurately and directly dating this unit using the volcaniclastic deposits hosted in primarily the Kirkwood Formation (Muir et al., 2017b). Several bentonite deposits are described from the Heidelberg and Plettenberg Bay basins, which were, and in the former case still are, sites of bentonite mining. There are also brief mentions of ‘tuffaceous material’ from the Worcester, Oudtshoorn, Robertson and Mossel Bay basins (Dingle et al., 1983; Rigassi and Dixon, 1972) that were seldom mapped apart from efforts of Malan and Viljoen (1990) and Viljoen (1992). Volcaniclastic deposits are also reported from the Suurberg Group in the northern Algoa Basin both below and interbedded with the basalts of the Mimosa Formation (Hill, 1972), and thus offer an opportunity to verify the depositional age of these enigmatic rocks using the U-Pb system in zircons. A robust chronology of the Uitenhage Group will help establish the physical evolution of rifting in the Jurassic – Cretaceous; improve tectonostratigraphic models relied upon for

Ma) Bethelsdorp Member, a < 300 m thick, marine intercalation in the basal Kirkwood Formation that was deposited during a transgressive event in the southern Cape (Dingle, 1973; McMillan, 2010), cannot be extrapolated throughout the > 2000 m thickness of the Kirkwood Formation (McLachlan and McMillan, 1979; McMillan et al., 1997; Muir et al., 2017b). Moreover, Bethelsdorp Member, similar to the Sundays River Formation, is only present in the Algoa Basin and therefore provides no reliable chronostratigraphic constraint to the other continental deposits in the isolated rift basins elsewhere in the southern Cape (Fig. 2.1).

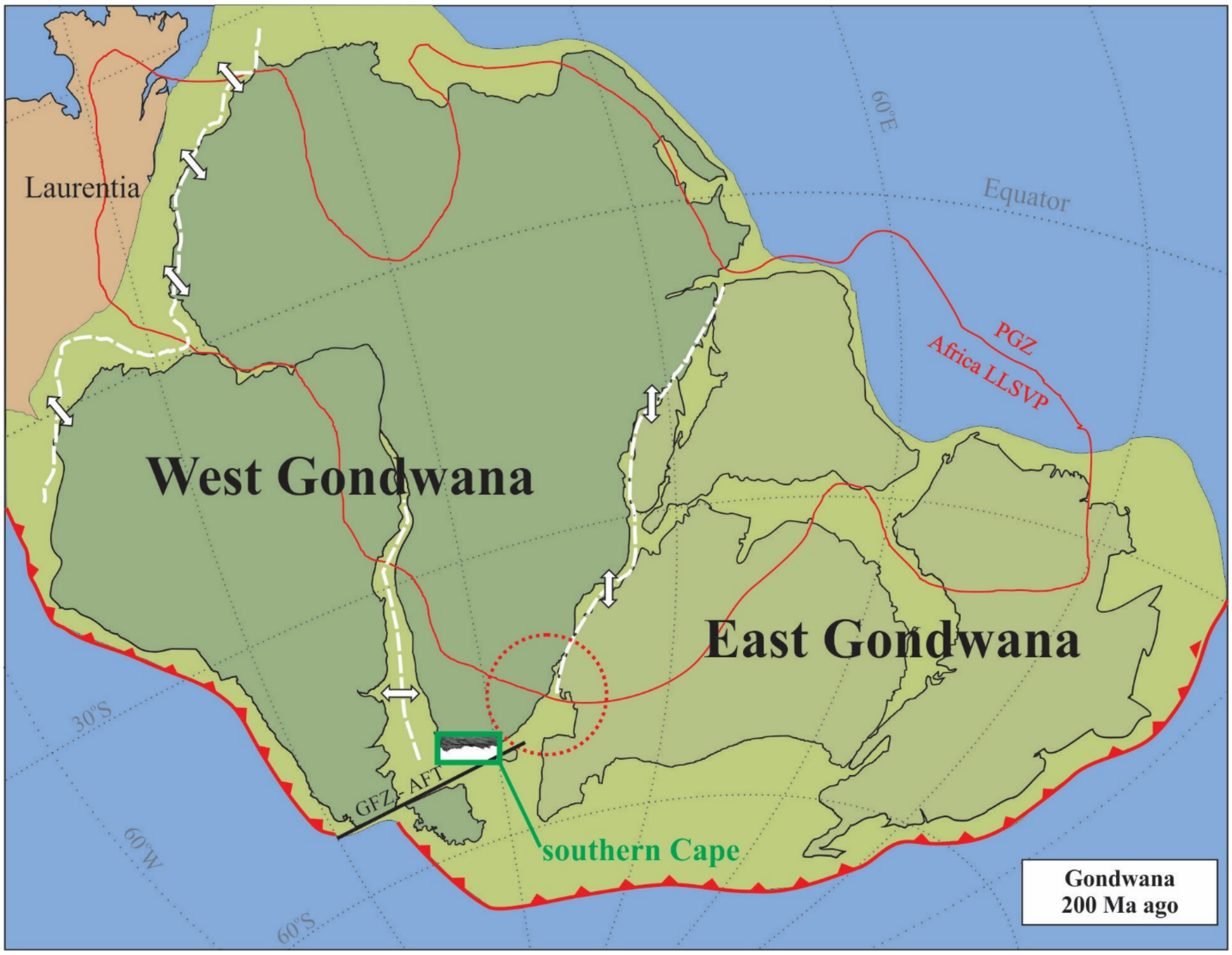

Fig. 1.1. Gondwana 200 MA ago as it was still largely united within Pangea. Red toothed lines are subduction zones, red solid line represent approximate position of Plume Generation Zone (PGZ) on the edge of the Large Low-Shear-Velocity Province (LLSVP) and red dotted circle delineates approximate position of plume responsible for the Karoo-Ferrar LIP. White dashed lines indicate regions of future rifting to form North Atlantic, Indian and South Atlantic Oceans ~195 Ma, ~175 Ma and ~135 Ma ago, respectively. Black line delineates the Gastre Fault Zone (GFZ) and Aghulas Falkland Transform (AFT). Green rectangle highlights the study area in modern day southern Cape of South Africa. Island arcs and minor terranes have been omitted (modified after Torsvick and Cocks, 2013 with additional information from White and McKenzie, 1989).

hydrocarbon exploration; and finally, place non-age-diagnostic fossils hosted in the syn-rift deposits of the southern Cape in the radiometrically-dated chronostratigraphic context needed to determine evolutionary trends in Mesozoic ecosystems of SW Gondwana. The overall aims of this study are as follows:

1. Locate poorly described and new volcaniclastic deposits in the Uitenhage and Suurberg Groups and assess whether they are primary (pyroclastic) or of mixed volcanogenic and detrital origin (reworked/resedimented).
2. Date volcaniclastic deposits of the Uitenhage and Suurberg groups using the U-Pb system in zircons by Laser Ablation Inductively Coupled Plasma Mass Spectrometry (LA-ICPMS) and Chemical Abrasion Thermal Ionisation Mass Spectrometry (CA-TIMS) to determine an age of deposition (if primary) or maximum deposition (if reworked). These methods will be used to test the hypothesis that the entire Uitenhage Group is Upper Jurassic – Lower Cretaceous with ages that algin with existing constraints from the Algoa Basin.
3. Date detrital zircons through the U-Pb system by LA-ICPMS from sedimentary samples of the fossiliferous deposits, and some non-fossiliferous but stratigraphically important sites, to improve their geochronological context and compile a combined U-Pb-based and bio-chronostratigraphic framework for the Uitenhage Group.
4. Determine the volcanic provenance of the volcaniclastic deposits in the Uitenhage and Suurberg groups.

1.2 Layout of the thesis

The multidisciplinary nature of this study, involving isotope geochemical techniques and geological fieldwork requires a unique layout in order to improve the flow of the thesis. *Chapter 2* includes the necessary geological background for this study. Firstly, the regional geological context to the Mesozoic of SW Gondwana is provided, with a special emphasis on the Uitenhage Group of the southern Cape in South Africa. Inevitably such an overview of the relevant stratigraphy will require both a review of literature published, but also incorporates the observations from the several fieldtrips to each rift basin. Special care will be taken to differentiate previously established geological characteristics and those established through undertaking this doctoral research project. The background of the Uitenhage Group lithostratigraphy in this chapter follows the layout recommended by the South African Committee for Stratigraphy (SACS) and includes two published, peer-reviewed journal articles that cover the lithostratigraphy of the Enon and Kirkwood formations, which are the most widespread deposits of the onshore Uitenhage Group and the principal units investigated in this thesis. Following this, in *Chapter 3*, the methods used in the subsequent chapters are described in detail. This includes a review of U-Pb geochronology in general as well as the specific U-Pb analytical techniques applied. However, the methods used in Chapter 6 are not included here, because it comprises a stand-alone assessment that does not apply geochronological techniques. *Chapter 4* concerns the age of the Suurberg Group, which underlies the Uitenhage Group and has traditionally provided a maximum age constraint for the overlying strata. *Chapter 5* follows this with a basin-by-basin evaluation of the age of the Uitenhage Group, a discussion on the chronostratigraphy of the Jurassic – Cretaceous southern Cape, and implications for the tectonic setting during the breakup of Gondwana. *Chapter 6* is a stand-alone investigation of the volcanic provenance of the volcaniclastic deposits in the Uitenhage and Suurberg Groups by applying both geochemical and zircon morphological assessments. Finally, *Chapter 7* summarises key findings of this study in the form of a concise geological history of the southern Cape within SW Gondwana during the Jurassic and Early Cretaceous. *Chapters 8* and *9* include a reference list and appendices, respectively.

Chapter 2: Geological background

2.1 Tectonic setting

East and West Gondwana, which comprise the Gondwanan superterrane that formed a part of Pangea, separated in the Early Jurassic due to their position above the African Large Low Shear-Wave Velocity Province (LLSVP) and associated Plume Generation Zone (PGZ) (Fig. 1.1; Burke et al., 2008; Gaina et al., 2013; Torsvik and Cocks, 2013). The extensive Lower Jurassic magmatic rocks of the Karoo, Ferrar, and Chon Aike large igneous provinces were emplaced across much of the supercontinent, heralding the subsequent breakup Gondwana (Pankhurst et al., 1998; Torsvik and Cocks, 2013; Burgess et al., 2015). However, it was only in the Early Cretaceous that separation began between Africa and South America (e.g., Renne et al., 1996; de Assis Janasi at al., 2011; Koopman et al., 2014; Will and Frimmel, 2018). Sometime during, or between, these two significant events during continental breakup, a series of normal faults developed in the southern Cape, which provided accommodation space for the Uitenhage Group to accumulate in numerous rift basins (Fig. 2.1), commonly referred to as the Outeniqua Basin (used here to refer to the offshore Bredasdorp, Pletmos, Gamtoos and Algoa Basin depocentres their southern extension, the Southern Outeniqua Basin) and its onshore basin inliers (McLachlan and McMillan, 1976; McMillan et al., 1997; Richardson et al., 2017). During the entire Jurassic and into the Early Cretaceous the southern Cape region was fixed at around 44° S based on three Global Apparent Polar Wonder Path models retrieved from www.paeleolatitude.org (using data from Besse and Courtillot, 2002; Kent and Irving, 2010; Torsvik et al., 2012).

Regional E-W orientation of gravity and positive magnetic anomalies, foliations, fold axes and trust planes (Dingle et al., 1983; Hälbich, 1983; De Beer, 1989; Booth and Shone, 1999; Pits et al., 1992; Hälbich, 1992); E-W stratigraphic continuity in the Cape Supergroup (Tankard et al., 1982; Veevers et al., 1994); and congruous crustal depth profiles (Parsiegla et al., 2009; Lindique et al., 2011) all evidence deep crustal anisotropy in the southern part of South Africa inherited from Palaeozoic compression and earlier. In turn, Mesozoic extensional normal faults of the southern Cape were influenced by this crustal anisotropy and propagated along pre-existing weaknesses in the Cape Fold Belt (Fig. 2.1; Fig. 2.2A), specifically, exploiting Permian – Triassic thrust planes (e.g., Lock et al., 1975; Dingle et al., 1983; Fouché et al., 1992; McMillan et al., 1997; Paton and Underhill, 2004; Paton, 2006). The resulting fault-bounded rift basins of the Outeniqua Basin and onshore inliers are therefore roughly parallel and follow the structural grain of the Cape Fold Belt, E-W in the central southern Cape and NW-SE to N-S in the Eastern Cape (Lock et al., 1975; Paton and Underhill, 2004; Paton, 2006) and are, with the exceptions of the Algoa and Bredasdorp basins, bounded by two exceptionally long series of normal faults (Paton, 2006), namely the Worcester and the Cango-Baviaanskloof-Gamtoos Fault Arrays (Fig. 2.1).

With improved constraints on the timing of regionally significant Gondwanan rifting events, such as the emplacement of Chon Aike, Karoo and Ferrar large igneous provinces (LIPs), the Early Jurassic onset of spreading between E and W Gondwana and Early Cretaceous opening of the South Atlantic, the formation of rift basins in the southern Cape can be placed into broader tectonic contexts. Importantly, only once the timing of movement along the Aghulas Falkland Transform was established, which coincides with the opening of the South Atlantic (Ben-Avraham et al., 1993; Marshall, 1994; Ben-Avraham et al., 1997) in the Early Cretaceous, did it become clear that rifting in the southern Cape began, at least in part, as an earlier event. McMillan et al. (1997) was the first to be more specific than simply ascribing their opening to *the breakup of Gondwana* and speculated that the rifting occurred during the opening of the Riiser Larson and Weddell Seas. Although others also noted that rifting initiated before the onset of the Aghulas Falkland Transform, they did not offer any specific event that accounted for the extension witnessed in the southern Cape in the Jurassic (Jungslager, 1996; Parsiegla et al., 2009; Broad et al., 2012).

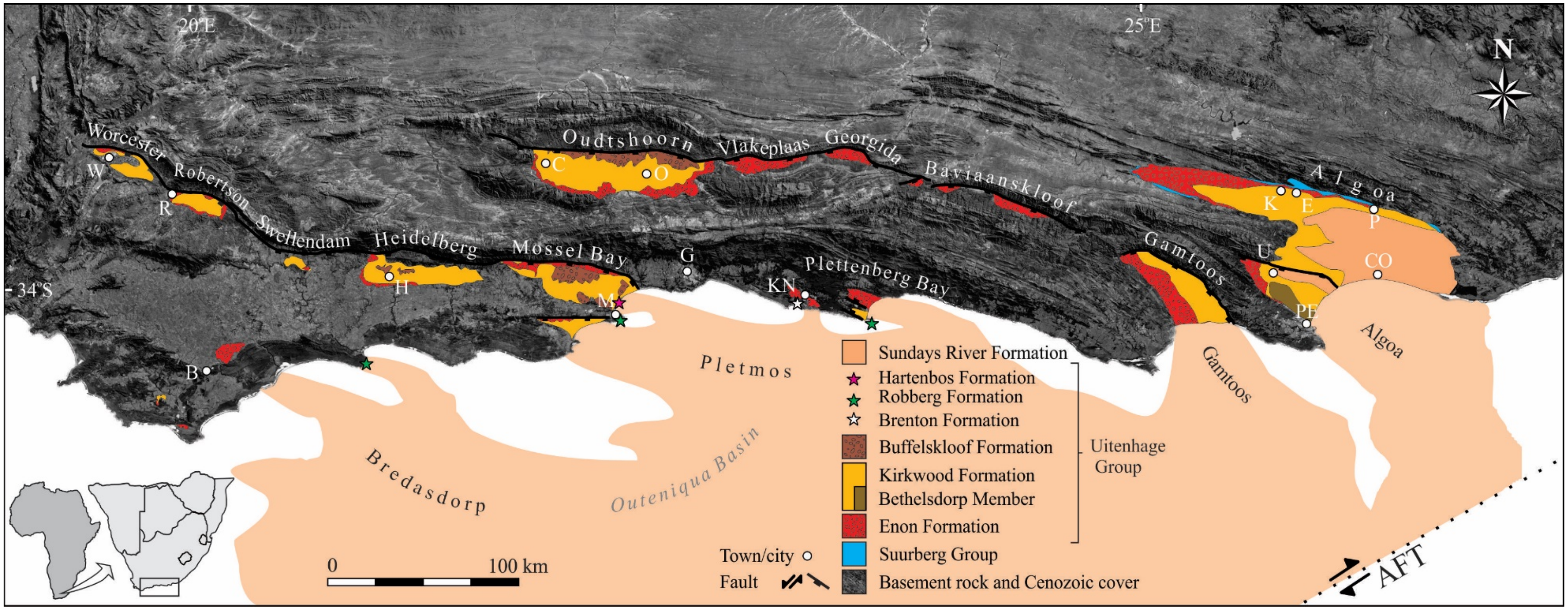

Fig. 2.1. Mesozoic rift basins in the southern Cape of South Africa and major onshore units of the Uitenhage Group. The offshore extension of the Uitenhage Group is only shown schematically in light orange. The Worcester-Pletmos basin line links the Worcester, Robertson, Swellendam, Heidelberg, Mossel Bay, Knysna and Plettenberg Bay basins, whereas the Gamtoos-Oudtshoorn basin line links the Oudtshoorn, Vlakteplaas, Georgida, Baviaanskloof and Gamtoos basins. The exceptionally long, parallel fault arrays (Cango-Baviaans-Gamtoos and Worcester faults) exploit pre-existing weaknesses in the Cape Fold Belt (Fouche et al., 1992; Paton, 2006). The Jurassic Suurberg Group is shown in the Algoa Basin, but the contentious Suurberg Fault, supposedly bounding the Algoa Basin to the north, is not included (Toerien, 1991). The Robberg, Hartenbos and Brenton formations, which are also constituents of the Uitenhage Group, are not shown due to their small aerial extent although the areas where they outcrop are indicated by stars. Abbreviations: AFT = Aghulas-Falkland Transform; E = Enon; B = Bredasdorp; BT = Bethelsdorp; C = Calitzdorp; CO = Colchester; G = George; H = Heidelberg; HN = Hankey; HR = Herbertsdale; I = Cape Infanta; K = Kirkwood; M = Mossel Bay; O = Oudtshoorn; P = Paterson; PE = Port Elizabeth; R = Robertson; U = Uitenhage; W=Worcester.

Low-temperature thermochronological studies conducted along transects in the Western and Eastern Cape provinces reveal periods of intensive denudation since at least the Early Cretaceous (Tinker, et al., 2008a, b; Guillocheau et al., 2012; Wildman et al., 2015; Green et al., 2016). From these data, periods of cooling-uplift have been identified, and point to Mesozoic movement along normal fault arrays during the breakup of Gondwana followed by several periods of regional uplift during the 'drift' stages of breakup in the Late Cretaceous and Cenozoic. Post-rifting uplift lead to the deep erosion of rift basins and in some cases entirely removed the sedimentary packages that were accommodated onshore (Wildman et al., 2015; Green et al., 2016).

Fig. 2.2 (following page). Generalized stratigraphic and structural context of the Mesozoic strata in the southern Cape of South Africa. (A) Schematic N-S cross-section through the southern Cape, perpendicular to Cape Fold Belt structures demonstrating the structural inversion of compressional features such as thrust planes during Mesozoic extension in the modern day on- and off-shore regions of the southern Cape. Reproduced from Paton, 2006. (B) Highly schematic graphic summary of the lithostratigraphy of the southern part of South Africa including the pre-cape groups and intrusive Cape Granite Suite; the overlying Cape and Karoo Supergroups including the volcanics and pervasive network of dykes and sills of the Karoo LIP (shown in red and purple); the Uitenhage and Suurberg groups, which outcrop in the southern Cape only, are the focus of this study. Folds, thrust, and normal faults are included schematically only. Modified from Linol and de Wit (2016). (C) Schematic representation of the main units of the Uitenhage Group and their stratigraphic positions in Mesozoic rift basins (not to scale). Not all these units or the volcaniclastic deposits (vvvv) are present in all basins. Suurberg Group is excluded and detailed in chapter 4 (Fig. 4.1).

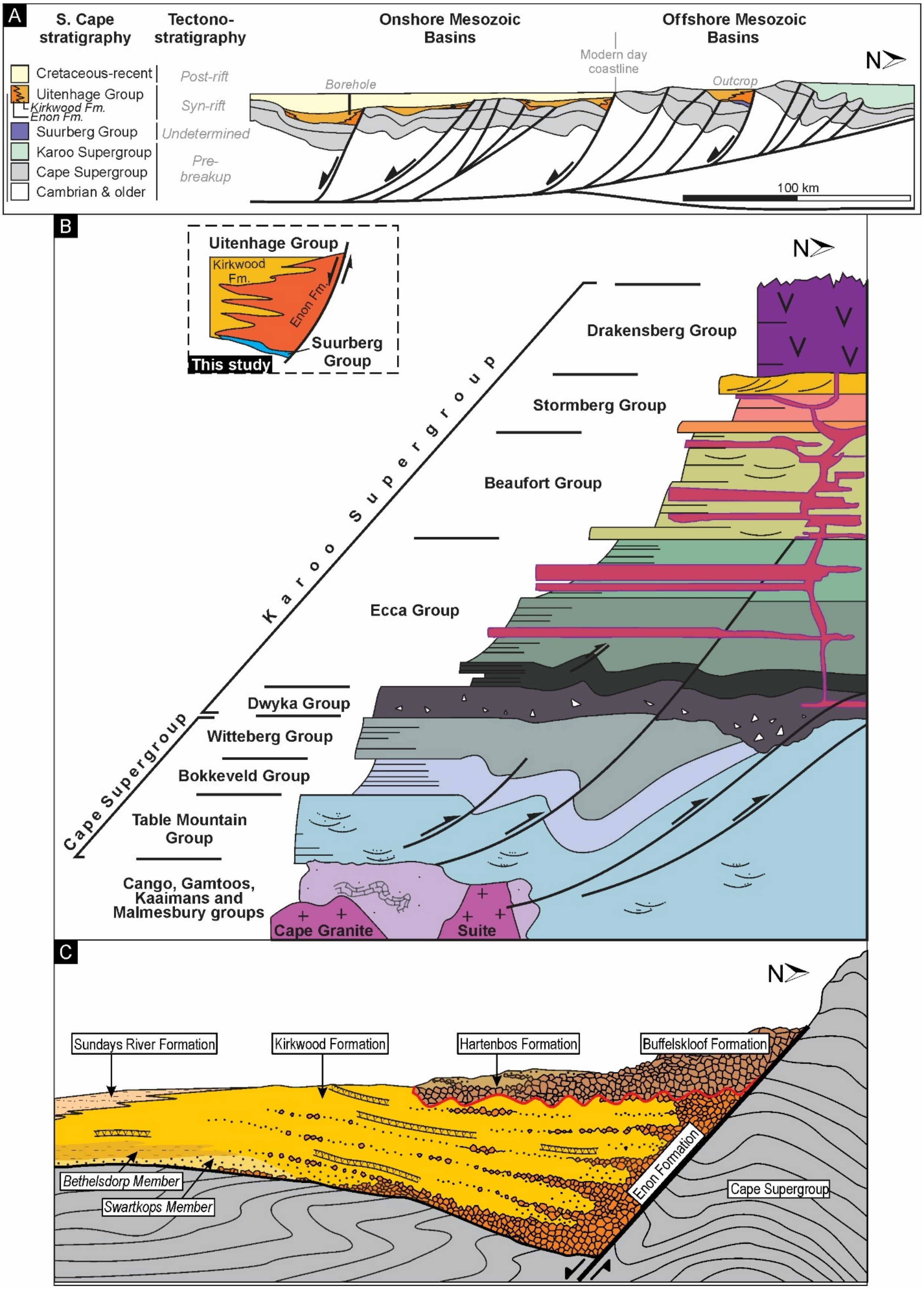

A
S. Cape stratigraphy
Tectono-stratigraphy
Onshore Mesozoic Basins
Offshore Mesozoic Basins
Cretaceous-recent
Post-rift
Uitenhage Group
Kirkwood Fm.
Enon Fm.
Syn-rift
Suurberg Group
Undetermined
Karoo Supergroup
Cape Supergroup
Pre-breakup
Cambrian & older
Borehole
Modern day coastline
Outcrop
N
100 km
B
Uitenhage Group
Kirkwood Fm.
Enon Fm.
Suurberg Group
This study
N
Drakensberg Group
Stormberg Group
Beaufort Group
Ecca Group
Karoo Supergroup
Dwyka Group
Witteberg Group
Bokkeveld Group
Table Mountain Group
Cape Supergroup
Cango, Gamtoos, Kaaimans and Malmesbury groups
Cape Granite
Suite
C
N
Sundays River Formation
Kirkwood Formation
Hartenbos Formation
Buffelskloof Formation
Bethelsdorp Member
Swartkops Member
Enon Formation
Cape Supergroup

2.2 Lithostratigraphy of the Uitenhage Group

The lithostratigraphy of the southern parts of South Africa are referenced widely in this section and is summaries schematically (Fig. 2.2B). The lithostratigraphy of the Enon and Kirkwood formations (Fig. 2.2.C) is of particular importance to this study and will be detailed in the following two sections (2.2.1 and 2.2.2). These two units garner priority in importance in this study for several reasons. Firstly, the Enon and Kirkwood formations have a widespread occurrence all rift basins and therefore demand much more thorough descriptions than other, locally restricted units (e.g., the Robberg, Brenton and Hartenbos formations). Additionally, all previous descriptions of these units are focused on borehole and outcrop observations from the Algoa Basin, which introduces a spatial bias in formal descriptions (Shone, 1976; Dingle et al., 1983; McMillan et al., 1997; Shone, 2006). The new lithostratigraphic descriptions of these two units attempt to rectify this by introducing descriptions from a wide range of rift basins. Secondly, the Kirkwood Formation contains abundant zircon-bearing volcaniclastic deposits that can be dated by U-Pb methods and provide the potential means to determine Uitenhage Group deposition. It also contains all the important continental palaeontological discoveries in the Uitenhage Group and therefore has elevated palaeoenvironmental significance over the fossil-poor Enon Formation. Finally, the basal position that the Enon and Kirkwood formations occupy in rift basin stratigraphy means that depositional ages acquired from these units will be the closest approximation of rift-initiation in the southern Cape, which is important for understanding the tectonic evolution SW Gondwana. It is with these factors in mind that in this section emphasis has been placed on describing the Enon and Kirkwood formations above other lithostratigraphic units in the Uitenhage Group. Further, considerable input has been paced on characterizing these two units as a part of this PhD research and their descriptions therefore contain a combination of previously established characteristics and those described for the first time. The format of these lithostratigraphic descriptions below follows the SACS (South African Committee of Stratigraphy) guidelines ascribed by Johnson (1987). This chapter begins with two published manuscripts that comprise the lithostratigraphy of the Enon and Kirkwood formations respectively, which are followed by similar lithostratigraphic reviews of more localized formations of the Uitenhage Group that are unpublished but adopt an identical layout.

2.2.1 Enon Formation (see published, peer-reviewed paper 1 after appendices)

2.2.2 Kirkwood Formation (see published, peer-reviewed paper 2 after appendices)

2.2.3 Sundays River Formation

Stratigraphic position and age

The Sundays River Formation occupies the uppermost part of the Uitenhage Group in the Algoa Basin, overlying and possibly also interfingering with parts of the Kirkwood Formation. The relationship between these units remains unclear and the possibility that an unconformity separates them cannot be disregarded (Winter, 1973; McLachlan and McMillan, 1976; Shone, 1978 for contrasting theories). Despite the stratigraphic relations of this unit being uncertain, its depositional age is well-constrained to Lowermost Valanginian – Hauterivian based on foraminiferal (McMillan, 2003), and ammonite assemblages (Kitchin, 1908; Spath, 1930; McMillan and McLachlan, 1976, 1979; Cooper, 1983).

Geological description

Basic unifying features: The Sundays River Formation is distinguished from the underlying and partial lateral equivalent, the Kirkwood Formation, by consisting of predominantly green-grey laminated mudstones compared to the red-mottled palaeosol-rich mudstones of the latter. The Sundays River Formation also contains abundant marine invertebrate fossils that are absent from the Kirkwood Formation. The unconformably overlying Cenozoic Algoa Group is generally sandstone and conglomerate-dominated as opposed to the primarily argillaceous Sundays River Formation and can easily be distinguished based on this grain size difference.

Thickness: The thickness of the Sundays River Formation is highly variable, due to the shape of the Algoa Basin and erosion. Boreholes intersect up to 1860 m of the unit near the depositional center of the Algoa Basin, constituting the maximum recorded thickness. Alternatively, a stratigraphic thickness of just 108 m is reported in a borehole near Paterson (Shone, 1976).

Lithology: *Sandstone (10 – 30%)*: Grey to olive grey very fine- to medium-grained sandstone beds interbedded with mudstones that dominate the unit (Fig. 2.3A). Typically these beds are thinly interlaminated with light grey siltstone lenses with abundant soft sediment deformation features. Rip-up mudclasts, shells (or fragments thereof), charcoal and scour marks occur at the base of some of the sandstone beds, which usually also exhibit ripple cross-laminations, flaser bedding, or cross-bedding (both planar and trough cross-beds). From a distance the sandstone units, which are positive features in outcrops due to preferential weathering of interbedded mudstones, appear laterally continuous for hundreds of meters although on closer inspection actually grade laterally into the mudstones or pinch out entirely only to reappear several cm laterally at a similar stratigraphic level (Shone, 1976).

Mudstones (70 – 90%): Grey, olive green, dark green and mottled purple/green mudstones dominate the unit and give an overall grey weathering appearance. Mudstones are typically thinly interlaminated with light grey very fine sand lenses with soft sediment deformation, localized slumping structures, ripple-cross lamination (Fig. 2.3B) and fine-grained or carbonaceous material (?charcoal). Massive mudstone units are much rarer, and are generally thinner than 1m before being truncated by a sandstone bed or lens.

Calcareous layers (0 – 5%): Shell fragments and whole calcareous invertebrate body fossils are found both scattered throughout and as discrete calcareous interbeds in the sand- and mudstones that dominate the Sundays River Formation.

Palaeontology: The Sundays River Formation hosts diverse shallow-marine and estuarine macrofossils including Early Cretaceous ammonites, belemnites, bivalves, gastropods, echinoids, crustaceans, polychaetes, corals and fragmentary reptile remains (Rogers and Swartz, 1901; Kitchin, 1908; Haughton, 1928; Spath, 1930; Cooper, 1970; McLachlan and McMillan, 1976; Dingle et al., 1983). Numerous studies of the microfossil assemblages in the Sundays River Formation were conducted during hydrocarbon explorations and record spores, pollen, dinoflagellates, ostracods and foraminifera (Dingle, 1969; McLachlan and McMillan, 1976 and 1979; McMillan, 2003).

Genesis: The Sundays River Formation was deposited during a marine transgression in SW Gondwana evidenced by the abundant shallow marine, estuarine and tidal-flat fossil invertebrate taxa. A bimodal palaeocurrent direction measured from sandstone cross-beds also supports a tidally influenced shallow marine depositional environment (Shone, 1976). Supplementary information comes from the study of microfossil assemblages of the Formation that describe a wide range of both shallow and deep water taxa, pointing to a broader depositional environment that extends to the continental shelf and even slope settings (McMillan, 2003).

Fig. 2.3. (Following page). Representative photographs of the locally distributed formations in the Uitenhage Group. (A) Laterally continuous green-grey mudstones overlain by pale green sandstones typical of the Sundays River Formation in the Algoa Basin. Cenozoic terrace gravel deposits of the Kudus Kloof Formation overlie unconformably, delineated by the red dashed line. Photo courtesy of the late K. Reddering. (B) Thinly alternating mudstone (green-grey) and very fine sandstone (pale grey) that exhibit ripple-cross lamination from a core sample of the Sundays River Formation. (C) Clayey sandstones of the Brenton Formation, near Knysna unconformably (dashed line) overlain by poorly consolidated sediment and soil. (D) Sandstone and mudstone units of the Hartenbos Formation in the Mossel Bay Basin (blue line separates the two facies). White dashed line delineates scree from *in-situ* outcrop. (E) Conglomerates with subordinate sandstone lenses of the Buffelskloof Formation in the Mossel Bay Basin. Green dashed lines delineate a clastic dyke (*CD*), which are a common secondary dewatering feature. (F) Tilted quartzites of the Table Mountain Group unconformably overlain by the Robberg Formation breccias and conglomerates (below blue dotted line) and sandstones and mudstones (above). Red dashed line highlights the angular unconformity. Blue dotted line is ~80 m above sea level.

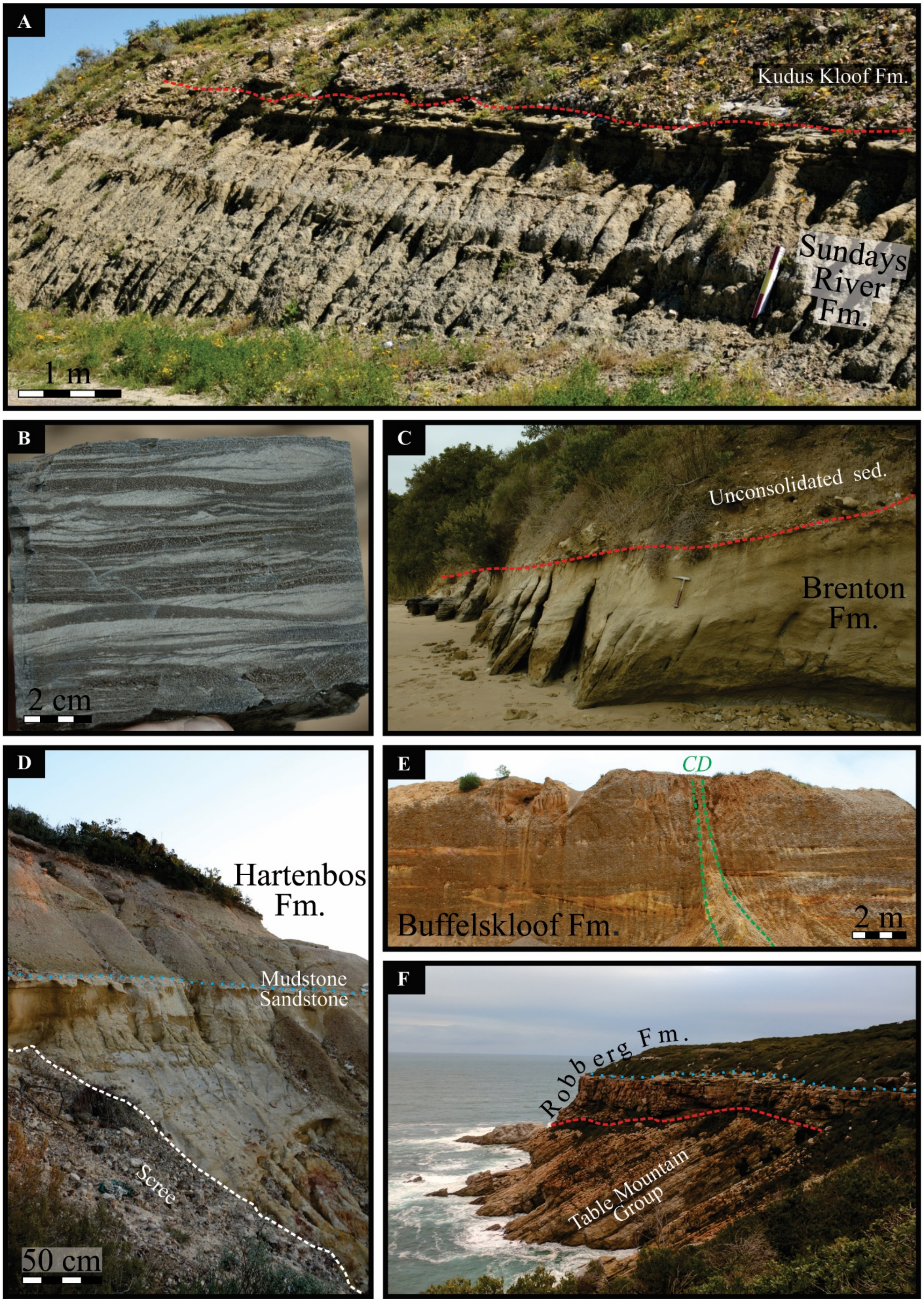
A
Kudus Kloof Fm.
Sundays River Fm.
1 m
B
2 cm
C
Unconsolidated sed.
Brenton Fm.
D
Hartenbos Fm.
Mudstone
Sandstone
Scree
50 cm
E
CD
Buffelskloof Fm.
2 m
F
Robberg Fm.
Table Mountain Group

Boundaries

Lower and lateral: Numerous boreholes drilled in the Algoa Basin pass through the green-grey Sundays River Formation before reaching the red beds of the Kirkwood Formation (e.g., CO1/67 but see McMillan et al., 1997 for others). This contact was described as unconformable by Winter (1973), although both the duration of the hiatus and the lateral extent had been brought into question (McLachlan and McMillan, 1976). Evidence has since been presented that the two units are conformable and interfinger, at least in part (Shone, 1978). The lower contact of the Sundays River Formation remains unresolved despite it being of considerable stratigraphic importance because most authors infer an Early Cretaceous age for the Kirkwood Formation in the Algoa Basin based on a lateral continuity between the units (Shone, 2006; McPhee et al., 2016; Muir et al., 2015). To this end, the lateral contact is not readily seen in the field, nor previously documented. Outcrops at Dunbrody in the Algoa Basin, and in some areas near Uitenhage offer the best expression of the gradational nature of the contact, with marine sandstone beds intersecting red mudstones that contain palaeosols. These outcrops likely represent an isolated snapshot of the transitional zone (where facies that are characteristic of both the Kirkwood and Sundays River formations are present) that exists between the two units, the full extent of which is not exposed anywhere.

Upper: The upper contact of the Sundays River Formation is always unconformable. In the southern parts of the Algoa Basin it is overlain by the Cenozoic Algoa Group (both the Alexandra and Salnova formations), while Cenozoic terrace-gravel deposits of the Kudus Kloof Formation overly it in the basin interior.

Subdivision

Four members of the Sundays River Formation are formally accepted by SACS (Joubert and Johnson, 1998) although they are seldom referred to in the literature, probably because their entirely subsurface descriptions. Venter (1972) identified four units in the Sundays River Formation, which he assigned Member status, from boreholes. From stratigraphically bottom to top these are the: Amsterdamhoek (337 m), Soetgenoeg (358 m), Addo (182 m) and Vetmaak (105 m) members. Each of the units is defined by the proportion and grain sizes of sandstone beds and shale beds with distinctive down-hole geophysical properties selected as physical boundaries (Winter, 1979). A separate subdivision that is unrecognized by SACS includes 'Upper', 'Middle' and 'Lower' members that are defined by their proportion of sandstone beds (Rigassi and Dixon, 1972). None of these members of particularly useful for the present study except for the following reasons: 1) there is consensus is that if there is lateral boundary shared with the Kirkwood Formation, it would exist in the bottommost portions of the Sundays River Formation (Rigassi and Dixon, 1972; McLachlan and McMillan, 1976; Dingle et al., 1983); 2) Two thin 'tuff beds' ranging from 1 – 10 cm thick are mentioned in a brief description of the Sundays River Formation (Rigassi and Dixon, 1972), although on review (during this study) of numerous cores and outcrop that span the interval no volcaniclastic beds can be confirmed.

Regional aspects

Geographic distribution: The Sundays River Formation outcrops exclusively in the onshore sector of the Algoa Basin in both the Sundays River and Uitenhage Troughs, but also exists in the subsurface in each of the offshore basins along the southern Cape (Bredasdorp, Pletmos, Gamtoos and Algoa basins). However, it is seldom referred to by its lithostratigraphic name by authors working on the Mesozoic successions offshore, who tend to prefer a sequence stratigraphic classification (Dingle et al., 1983; McMillan et al., 1997; Broad et al., 2012). Its onshore occurrences are best seen on the banks of the Sundays River, in road and railway cuttings, and at brick quarries near Coega, ~20 km north of Port Elizabeth.

Criteria for lateral extension: The green-grey mudstone and sandstone units that host marine fossils can be extended between isolated outcrops in the Algoa Basin only.

Correlation: In addition to correlations between onshore Sundays River Formation outcrops in the Algoa Basin with numerous boreholes that intersect the unit offshore, there is a probable correlation between it and several onshore Uitenhage Group formations. Firstly, the Robberg Formation that outcrops at Robberg (Plettenberg Bay) contains poorly preserved marine fossils in sandstones that have been correlated to the Sundays River Formation (Reddering, 2000; 2003), although several authors consider the fossil assemblage as Late Jurassic in age, and therefore preclude this correlation (Rigassi and Dixon, 1972; Cooper, 1974). Further, the speculative temporal correlation with the Sundays River Formation may not apply to other isolated Robbberg Formation outcrops (Mossel Bay and Cape Infanta) which are fossil-poor. Secondly, the Brenton Formation, which only outcrops in Knysna, has been correlated with the Sundays River Formation based on foraminiferal evidence (McLachlan et al., 1976), although likewise, there are alternate age interpretations based on the recovery of a single Late Jurassic ammonite specimen and ostracod assemblages (Dingle and Klinger, 1971). Finally, it is speculated that the continental Buffelskloof Formation also correlates with the Sundays River Formation (Viljoen, personal communication 2016, 27 June) although this argument, which is based entirely on lithostratigraphic grounds, only points out that the conglomeratic unit, like the Sunday River Formation, occupies an uppermost position of respective rift basin stratigraphy.

2.2.4 Brenton Formation

Stratigraphic position and age

The Brenton Formation is a fully marine unit in the Uitenhage Group that is a suspected chronostratigraphic correlative of the Sundays River Formation based on the Late Valanginian foraminiferal assemblages, especially *Reinholdella valendisnsis* and *Astacolus gibber* (McLachlan et al., 1976). Alternatively, the unit is Upper Jurassic, a view based on ostracod assemblages and a single ammonite specimen (*Hybonoticeras aff. hildebrandti*). that was recovered from these rocks (Dingle and Klinger, 1972). Nevertheless, the Brenton Formation is often regarded as Lower Cretaceous, with authors arguing that the Jurassic ostracods and the single fragmentary ammonite fossil described in Dingle and Klinger (1972) are either miss-identified or reworked (McLachlan et al., 1976). Since neither alternative can be regarded as unequivocal, its age remains inconclusive. Similarly, there is uncertainty regarding the stratigraphic relation of the marine beds that outcrop on the southern banks of the Knysna Estuary and the continental Enon Formation that outcrops ~3.5 km away on its northern margin (Fig. 2.1).

Geological description

Basic unifying features: Greenish grey and beige sand- and mudstones with predominantly marine fossils and rare pebble conglomerate interbeds.

Thickness: 6 – 20 m of the Brenton Formation is exposed along the southern margin of the Knysna Estuary at low tide (Dingle and Klinger, 1972; Rigassi and Dixon, 1972).

Lithology: *Mudstone (40 – 100%):* Green-grey massive claystones, siltstones and sandy siltstones with marine fossils confined to calcareous concretions, disseminated throughout or forming defined layers of shell-fragments. The mudstones are generally exposed on flat-lying surfaces but are also found as grey-weathering vertical cliffs up to 5 m thick. The true extent of the mudstone is unknown due to poor vertical and lateral exposure, and lack of boreholes intersecting the unit in subsurface. One borehole was drilled at Brenton in 2012 by the Council for Geoscience with the aim of determining the exact thickness and stratigraphy of the Brenton Formation but unfortunately the core and its unpublished description have since been lost.

Sandstone (0 – 50%): Grey-green and beige sandstone beds (Fig. 2.3C) that are massive or exhibit cross-bedding, soft sediment deformation structures and rare well-rounded quartzite pebbles and charcoal fragments. The sandstone beds often form at least 3 m high vertical cliffs along the estuary banks, in contrast to the above-mentioned mudstone-dominated units that are preferentially eroded and form flat-lying surfaces. Sandstone units are generally clay-rich and have discrete layers of shell-fragments and subordinate conglomerates.

Conglomerates (0 – 5%): Grey oligomictic clast-supported conglomerates with a sandy matrix are present in the northwestern extremity of the Brenton Formation outcrops. The conglomerates are confined to a channel-shaped body that cuts into sandstone strata.

Palaeontology: The Brenton Formation has drawn much attention because of its marine fossils that have important chronostratigraphic implications. A diversity of bivalves, a single ammonite specimen, echinoid spines, reptile teeth and a diversity of microfossils (foraminifera, ostracoda and coccoliths) are reported from the unit (Kitchin, 1908; Schwarz, 1915; Dingle and Klinger, 1972; Rigassi and Dixon, 1972; Beer, 1972; McLachlan et al., 1976). The majority of these specimens were found in either the lowermost greenish-grey mudstone unit, or as fallen blocks eroded from poorly exposed overlying conglomeratic layers (McLachlan et al., 1976).

Genesis: As attested by its marine faunal assemblage, the Brenton Formation was deposited during a marine transgressive event either in the Late Jurassic or Early Cretaceous. Without high resolution sedimentological studies, the depositional setting of the Brenton Formation remains poorly understood. However, its shallow marine faunal assemblage suggests that the deposition occurred during a marine transgressive event either in the Late Jurassic or Early Cretaceous. Common vertical and lateral grain-size variations indicate fluctuating energy levels in a nearshore setting.

Boundaries

Lower and lateral: The limited lateral and vertical extent of the Brenton Formation outcrops makes understanding its position in Uitenhage Group stratigraphy of the Knysna Basin difficult. Specifically, the Knysna Estuary covers the contact between the mudstone-dominated marine strata in Brenton, and its continental, conglomeratic counterparts in the northern parts of the Knysna Basin, ~3.5 km to the north (Fig. 2.1). Most authors prefer a gradational lateral contact between the two facies based on the rare conglomerate beds in the Brenton Formation (at the western extent of the exposures) that resemble those of the Enon Formation (Rogers 1909; Dingle and Klinger, 1972; Rigassi and Dixon, 1972; McLachlan et al., 1976). The unfortunate loss of the only stratigraphic borehole drilled at Brenton has hampered investigations of the Uitenhage Group stratigraphy in the Knysna Basin and because the outcrop extent is severely limited, all boundaries for the unit can only be inferred.

Upper: Unconsolidated sediments of the post-Cretaceous overlie the Brenton Formation near Featherbed, and these indicate that an unconformity exists at the top of the Brenton Formation, at least where visible.

Subdivision

There are no official subdivisions of the Brenton Formation, although McLachlan et al. (1976) described 7 discrete lithostratigraphic units based mainly on grainsize and colour variation along the southern banks of the Knysna Estuary, although due to landscape changes and the loss of outcrop some of the exposures visited in that study no longer exist.

Regional aspects

Geographic distribution: The Brenton Formation is a highly localized unit, only outcropping in the southern banks of the Knysna Estuary at Brenton, Western Cape. Its subsurface extent is unknown, due to the lack of boreholes near Knysna (and missing reference material and core from the 2012 drilling efforts) and may be distributed offshore and beneath the modern estuarine sediments at Knysna.

Criteria for lateral extension: The green-grey mudstone, sandstone and minor conglomerate with marine fossils.

Correlation: Correlation of the Brenton Formation with other Uitenhage Group deposits remains contentious. The stratigraphy in the Knysna Basin itself is unclear because the unit has limited outcrops and poor constraints on its subsurface extent. Further, the age of the Brenton Formation is yet unresolved, making correlations based on marine fossils with either the Colchester Member of the Kirkwood Formation (Dingle and Kinger, 1972) or the Sundays River Formation possible (McLachlan et al., 1976). A correlation with the latter is supported by a similarity of foraminiferal assemblages between the Brenton Formation and the upper portions of the PB A/1 offshore well, which is assigned to the Sundays River Formation (McLachlan et al., 1976).

2.2.5 Buffelskloof Formation

Stratigraphic position and age

The Buffelskloof Formation is a locally restricted conglomerate-dominated unit in the Jurassic – Cretaceous Uitenhage Group, and is separated from the underlying the Enon and Kirkwood formations with an angular unconformity (Theron et al., 1991; Malan and Viljoen, 1990; Malan et al., 1994). Consequently, the unit occupies an upper portion of the Uitenhage Group and is probably Lower Cretaceous. It laterally interfingers with the Hartenbos Formation in the Mossel Bay Basin (Malan and Viljoen, 1990) and is sporadically overlain by post-Cretaceous silcretes of the Grahamstown Formation, various clastic rocks of the Eocene to Holocene Algoa Group and the Miocene to Holocene Bredasdorp Group in the Mossel Bay Basin (Malan and Viljoen, 1990).

Geological description

Basic unifying features: A conglomerate-dominated massive or crudely bedded unit that unconformably overlies the Enon and Kirwkwood formations.

Thickness: The thickness of the Buffelskloof Formation is highly variable, probably due to post-Cretaceous erosion that partially (or entirely) removed the unit. In the northern Oudtshoorn Basin, in the Buffelskloof farming district, it reaches a maximum thickness of ~450 m, but becomes thinner towards south and southwest in the Mossel Bay and Heidelberg basins, where its maximum thickness is ~150 and ~100 m, respectively (Du Plessis, 1947; Malan and Viljoen, 1990; Fig. 2.1).

Lithology: *Conglomerate (80 – 100%):* Mostly sandstone and quartzitic clasts derived from the Table Mountain Group (Fig. 2.3D) with the addition of phyllites and quartzites from the Cango Group in the Oudtshoorn Basin (Dinis, 2018). Rare intra-basinal sandstone, mudstone and volcaniclastic clasts are present in the Mossel Bay Basin, and, on lithological grounds, appear to be derived from the underlying Kirkwood Formation. Clast sizes range from granules to very large boulders, and sorting is highly variable ranging from very poor, especially in parts of the northern Oudtshoorn Basin where matrix supported breccias are exposed, to well-sorted clast-supported conglomerates in other parts of the Oudtshoorn Basin, the Mossel Bay and Heidelberg basins (Fig. 2.1).

Sandstone (0 – 10%): Very fine- to very coarse-grained grey, white, red and beige sandstone lenses and beds are commonly interbedded with conglomerates. The larger lenses and beds often contain cross-bedding, pebble stringers and fine upwards.

Mudstones (0 – 10%): Sandy grey, white, red small (< 1 m) mudstone lenses are found in conglomerates, or at upper portions of fining-upward sand lenses and beds.

Palaeontology: Rare silicified logs, wood fragments and charcoal were reported from the conglomerate and sandstone beds.

Genesis

This conglomerate-dominated unit was likely deposited on high energy alluvial fans and braided rivers in proximal regions of the subsiding rift basins. This is indicated by the coarse clast sizes, and a general decrease in clast size along palaeocurrents, which point away from basin marginal faults (Malan and Viljoen, 1990; Holzforster, 2007). The angular unconformity with underlying Enon and Kirkwood formations suggests that the Buffelskloof Formation was deposited subsequent or during movement along the Worcester and Cango faults (Fig. 2.1).

Boundaries

Lower: Unconformable and with an angular relation to the underlying Enon and Kirkwood formations, however this contact is far more easily noticeable where it overlies the latter, a strongly contrasting lithological unit. Where it overlies the Enon Formation in the Mossel Bay and Heidelberg basins and perhaps in the subsurface of the Oudtshoorn Basin, the unconformable relationship at the boundary of the two conglomeratic units is usually only apparent as contrasting clast compositions.

Upper: Conformably overlain by the Hartenbos Formation in the Mossel Bay Basin, with which it also shares a partial lateral contact, and unconformably overlain by unconsolidated gravels, soil in many places in the Oudtshoorn and Heidelberg basins. In the latter, the Buffelskloof Formation is sometimes overlain unconformably by silcretes of the Grahamstown Formation (Viljoen, 1992; Viljoen, personal communication 2016, 27 June).

Lateral: Shares a lateral, gradational, interfingering boundary with the Hartenbos Formation in the Mossel Bay Basin. Although this contact is gradational and poorly exposed in the vicinity of Hartenbos (Fig. 2.1), it exists where the conglomerates give way to sandstone and mudstone dominated lithologies (Viljoen, 1992).

Subdivision

There are no established subdivisions of the Buffelskloof Formation although matrix-supported breccia and clast-supported conglomerate facies are present in the Oudtshoorn Basin.

Regional aspects

Geographic distribution: Outcrops in the Oudtshoorn, Mossel Bay and Heidelberg basins (Fig. 2.1) and may have a subsurface distribution in offshore basins. Although the Buffelskloof Formation is at present only mapped in three of the onshore basins, it is possible that it was deposited in other onshore rift basins in the southern Cape too, but it is either unrecognized (e.g., lumped with the lithologically similar Enon Formation) or entirely removed through by erosion. Offshore boreholes do not intersect the Buffelskloof Formation per se, although there remains uncertainty whether or not conglomerates that overlie mudstones and sandstones of the Kirkwood Formation, and are possibly equivalent to the Buffelskloof Formation, although without exposures or quality seismic profiles that display an angular unconformity below the interval of interest and adequate lateral resolution, these conglomerates could equally be coarser-grained facies of the Hartenbos or Kirkwood formations or a tongue of the laterally interfingering Enon Formation.

Criteria for lateral extension: Conglomerate-dominated unit with minor sandstone and mudstone interbeds overlying the Enon and Kirkwood Formation unconformably.

Correlation: Tentative correlation with the Sundays River Formation of the Algoa Basin has been proposed (Viljoen, personal communication 2016, 27 June), although this argument is based solely on both units occupying an upper portion of the Uitenhage Group in their respective basins. Similarly, the reliance of an angular relationship with the underlying, lithologically similar Enon Formation leaves a possibility for correlation between it and uppermost Enon Formation in some basins where no angular unconformity is identified within the thick conglomeratic units of the Uitenhage Group (e.g., the Knysna and Gamtoos basins).

2.2.6 Hartenbos Formation

Stratigraphic position and age

The Hartenbos Formation conformably overlies and interfingers with the Buffelskloof Formation in the Mossel Bay Basin (Theron et al., 1991; Malan and Viljoen, 1990; Viljoen, personal communication 2016, 27 June). Although the lower contact of the Hartenbos Formation is not exposed in outcrops, the Buffelskloof Formation, which is its partial lateral correlative, overlies the Kirkwood Formation with an angular unconformity. The Hartenbos Formation is therefore considered younger than the Kirkwood Formation and is probably Lower Cretaceous, although there is no direct chronostratigraphic evidence to constrain a depositional age for this unit. The Pliocene De Hoopvlei Formation (of the Miocene to Holocene Bredasdorp Group) para-unconformably overlie the Hartenbos Formation in some areas (Malan and Viljoen, 1990).

Geological description

Basic unifying features: Often poorly consolidated fine- to medium-grained sandstones and clay-rich sandstones interbedded with sandy mudstones, subordinate conglomerates and sporadic carbonaceous layers (Viljoen, personal communication 2016, 27 June).

Thickness: Due to limited outcrop, the thickness of the Hartenbos Formation cannot accurately be estimated although at least 100 m was recorded in stratigraphic borehole HA1/88 (Malan and Viljoen, 1990; Viljoen, personal communication 2016, 27 June).

Lithology: *Sandstone (70 – 90%):* Moderately consolidated, upward fining, fine- to coarse-grained yellowish grey to greyish orange sandstones (Fig. 2.3E) that are either massive or contain horizontal laminations and rip-up mudclasts.

Mudstones (~20%): Poorly consolidated and friable clayey and sandy siltstones that are medium to light grey with pale red mottles or yellowish brown to medium brown with greenish grey mottles. Mudstones are mostly massive, or contain poorly developed horizontal laminations. Weathers to both a light grey or reddish brown colour and dark grey-brown where carbonaceous layers are present.

Conglomerate (<2%): Very coarse pebble- to granule-sized quartzite clasts that occur as pebble stringers in sandstone units, often at the base of upward fining successions that are xxx m thick.

Palaeontology: Rare silicified wood fragments and charcoalified plant material in association with laminated carbonaceous mudstones.

Genesis: Likely represents a fluvial or estuarine deposition although poor lateral and vertical extent of the rare outcrops and an absence of diagnostic fossils make a reliable depositional environment reconstruction for the Hartenbos Formation difficult.

Boundaries:

Lower and lateral: Conformable and gradational with the Buffelskloof Formation, with which it also shares a lateral boundary in places. This contact is defined by the abundance of conglomerates, where the Hartenbos Formation is sandstone and mudstone-dominated, while the Buffelskloof Formation comprises predominantly conglomerates. Presumably, the Hartenbos Formation unconformably overlies the Kirkwood and/or Enon formations in places where the Buffelskloof Formation is not developed.

Upper: The Hartenbos Formation is unconformably overlain by the Dehoop and Klein Brak formations of the Miocene to Holocene Bredasdorp Group although outcrops of this contact are not commonly seen in the field. However, borehole HA1/88 shows an abrupt change in lithology at around 20 m depth, which can be interpreted as an unconformity (Viljoen, personal communication 2016, 27 June).

Subdivision

No subdivision can be applied to the Hartenbos Formation except for a change from coarsening-upward to fining-upward vertical grain size trends at around 44 m depth in the HA1/88 borehole (Viljoen, personal communication 2016, 27 June).

Regional aspects

Geographic distribution: Restricted exclusively to the Mossel Bay Basin in the vicinity of Hartenbos (Fig. 2.1) but may also have an offshore distribution.

Criteria for lateral extension: Fine- to medium-grained sandstones, clay-rich sandstones and sandy mudstones with subordinate conglomerates that occupy a stratigraphically higher position than the lithologically similar Kirkwood Formation in the Mossel Bay Basin.

Correlation:

No definite correlations can be made due to the poor geochronological constraints for the Hartenbos Formation, which is only recognized in the Mossel Bay Basin. However, the parts of the Sundays River Formation that overly the Kirkwood Formation in the Algoa Basin may be a correlative because both units occur in the upper part of the Uitenhage Group stratigraphy in their respective basins.

2.2.7 Robberg Formation

Stratigraphic position and age

The Robberg Formation is a constituent of the Jurassic – Cretaceous Uitenhage Group with outcrops in three isolated coastal locations in the Bredasdorp and Pletmos basins at Cape Infanta, Mossel Bay and

Robberg. In each case, it unconformably overlies the Peninsula Formation of the Palaeozoic Table Mountain Group and is overlain by recent unconsolidated sand and colluvium that caps Cenozoic wave-cut terraces. Traditionally, the Robberg Formation was considered Upper Jurassic (Rigassi and Dixon, 1972; Tankard et al., 1982; Dingle, 1983) based on the presence of recrystallized coccoliths, although more recent biostratigraphic evidence based on poorly preserved ammonites, a Spatangoid echinoid, and microfossil assemblages suggests that it is Lower Cretaceous, albeit tentatively (Reddering, 2000; 2003; McMillan, personal communications 2017, 19 June). The generally poor preservation of fossils from this unit renders all these biostratigraphically determined ages tentative. Additionally, the three spatially isolated Robberg Formation outcrops have not been conclusively demonstrated as coeval, further complicating the chronostratigraphy of the Robberg Formation.

Geological description

Basic unifying features: Sandstone with subordinate conglomerate and breccia layers and minor mudstone interbeds. These form southward-thickening wedges in three isolated localities, each containing a basalmost breccio-conglomerate layer (Reddering, 2003).

Thickness: Maximum recorded thicknesses are: 94 m at Robberg, 69 m at Mossel Bay and 60 m at Cape Infanta and thins towards the north (Reddering, 2003).

Lithology: *Sandstone (7 – 100%):* Thick litho- packages (up to 42 m) are composed of 0.5 – 2 m thick beds and lenses of very fine- to medium-grained sandstone that in places contains planar and trough cross-bedding, flaser bedding, ripple marks and soft sediment deformation (Reddering, 2003).

Conglomerate & breccia (0 – 93%): 2 – 8 m thick beds of yellow – red, very poorly sorted conglomerates and breccias are common. Clasts range from very angular to subrounded granules to boulders of quartzite, and rare rip-up mudclast pebbles. At Cape Infanta and Robberg,these beds form 30 m thick litho-packages comprising 1.5 m tabular beds and lenses, well-sorted, imbricated conglomerates with well-rounded clasts are exposed at Cape Infanta and Robberg.

Mudstone (0 – 40%): < 1 cm – 5 m thick units of thinly bedded, lenticular and laminated mudstones (mostly siltstones) that are light grey, pale yellow or pale orange in colour. Laminations are parallel, lenticular and wavy.

Palaeontology: The Robberg Formation contains poorly preserved macrofossils as casts in sandstone, microfossils, and trace fossils, none of which are strongly age-diagnostic, although tentatively suggest Early Cretaceous deposition.

Macrofossils: Poorly preserved invertebrate casts of molluscs (mostly trigonod bivalves), two ammonite casts, and one spatangoid echinoid have been described (Reddering, 2000; 2003). Casts of logs and wood fragments are common, as are coalified plant remains. Plant taxa include cycadophytes, coniferophytes, pteridophytes and sphenophytes, which are all continental, age undiagnostic and mostly lack features necessary for detailed taxanomic classification. However, some fossils from Cape Infanta that are better preserved have been identified as *Zamites* sp. (cycad) and *Cladophlebis browinia* (fern) by Malan and Viljoen (1990).

Microfossils: Marine dinoflagellates and acritarchs have been recovered, along with spores and pollen that correspond with the floral assemblages represented by plant macrofossils (Reddering, 2000). The dinoflagellates recovered are somewhat age-diagnostic and suggest a Berrisian – Valanginian (Early Cretaceous) age. Rigassi and Dixon (1972) describe recrystallized coccoliths, although their occurrence is not well documented and is rather speculative (McLachlan and McMillan, 1976). A single sample of grey mudstone at Robberg yielded a diverse assemblage of foraminifera (McMillan, personal communications 2017, 19 June).

Trace fossils: Sandstones commonly bare trace fossils at Robberg, which are scarcely preserved elsewhere. They consist primarily of feeding and dwelling traces, while crawling and escape traces are rare (Reddering, 2000).

Genesis: The Robberg Formation was deposited in a coastal setting with significant palaeoenvironmental variability. The breccia/conglomerates at the base of the unit (St Sebastian Point Member) were deposited by mass-flow processes in rough topography, whereas rounded conglomerate units were deposited as beach and gravel barriers. Some sandstone-dominated portions show evidence of tidal influence (bimodal palaeocurrents, marine invertebrate and trace fossils, and flaser bedding), and thus were interpreted as estuarine deposits (Reddering, 2003).

Boundaries:

Lower: Always unconformable, mostly expressed as an angular unconformity but in places as a paraconformity (e.g., at Robberg) atop the Peninsula Formation of the Palaeozoic Table Mountain Group (Fig. 2.3F).

Upper: Always unconformable, as the unit is truncated by wave-cut terraces and overlain by recent unconsolidated sand.

Subdivision

Comprising of subangular clasts, the basal conglomerate and breccia unit with subordinate sandstone and mudstones is assigned to the St Sebastian Point Member. This 0.5 – 60-m-thick member rests on the Table Mountain Group with an angular unconformity, and is overlain, supposedly unconformably by other units of the Robberg Formation (Reddering, 2003).

Regional aspects

Geographic distribution: The Robberg Formation outcrops in coastal cliffs at Cape Infanta, Mossel Bay and Robberg (Plettenberg Bay) in the Bredasdorp and Pletmos basins (Fig. 2.1).

Criteria for lateral extension: Predominantly sandstone with subordinate conglomerate and breccia layers, especially at the base of the Formation, and minor mudstone interbeds that unconformably overlie the Table Mountain Group. The Robberg Formation is distinguished from other lithologically similar units in the Uitenhage Group by the presence of tidally- influenced facies characteristics.

Correlation:

Invertebrate palaeontological evidence affords some tentative correlation of sandstone units in the Robberg Formation at Robberg with the Sundays River Formation (Reddering, 2000; 2003).

2.2.8 Infanta Formation

Stratigraphic position and age

Unlike all other formations in the Uitenhage Group, the Infanta Formation has an entirely subsurface distribution in the Outeniqua Basin (Dingle et al., 1983) and is infrequently referenced in the literature, presumably falling away to the more favoured tectonostratigraphic 'syn-rift' nomenclature adopted by McMillan et al. (1997) and subsequent workers. The poorly described grey mudstone-dominated unit is regarded as the offshore equivalent of the Kirkwood Formation in the Bredasdorp and Pletmos basins underlying the Sundays River Formation (Du Toit, 1976; Dingle et al., 1983; Johnson, 1998).

Geological description

Basic unifying features: Light to dark grey mudstones with rare calcareous and sandstone horizons in the offshore Bredasdorp and Pletmos basins only (Du Toit, 1976).

Thickness: Highly varied from 1132 m in the Gb-Gemsbok 1 borehole (Pletmos Basin) to 82 m in the northern Bredasdorp Basin (Dingle et al., 1983).

Lithology: *Mudstones (>95%):* Homogenous light, medium and occasionally dark grey siltstones, claystones and shales.

Sandstones (<5%): Rare, minor sandstones occur in the northern Bredasdorp Basin and above the Superior Ridge, SW Pletmos Basin, where they are calcareous.

Palaeontology: Generally described as poorly fossiliferous (Du Toit, 1976; Winter, 1979; Dingle et al., 1983), and although foraminifera have been recovered in syn-rift deposits from numerous boreholes in the

Bredasdorp Basin from shallow marine intervals that presumably correspond to the Infanta Formation, those workers do not recognize those unnamed units as the Infanta Formation (Broad et al., 2012).

Genesis: The Infanta Formation was deposited in a shallow marine setting, possibly in a low-energy estuarine, lagoonal environment (Du Toit, 1975; Broad et al., 2012).

Boundaries:

Lower and lateral: possibly conformable with the Enon Formation in some boreholes (e.g., Winter, 1979; Dingle et al., 1983). Presumably, it shares a lateral gradational, interfingering contact with the Kirkwood Formation.

Upper: possibly unconformable with the Sundays River Formation (Dingle et al., 1983).

Subdivision

No subdivisions are described.

Regional aspects

Geographic distribution: Restricted to the offshore Bredasdorp and Pletmos basins only (Fig. 2.1).

Criteria for lateral extension: Grey mudstones with rare calcareous and sandstone horizons in the offshore Bredasdorp and Pletmos basins overlying the Enon Formation and underlying the Sundays River formations.

Correlation:

The Infanta Formation is described as the probable marine correlative of the continental Kirkwood Formation (Du Toit, 1975; Dingle et al., 1983) although this is at odds with lithostratigraphic description of the Kirkwood Formation, which clearly contains the Bethelsdorp Member (in the Algoa Basin – see Muir et al., 2017b). It is likely that the Infanta Formation is more reasonably considered the lithostratigraphic equivalent of the Bethelsdorp Member and may warrant a review in future SACS descriptions of this unit.

2.3 Summary of historic chronostratigraphic information

The stratigraphic units in the Uitenhage Group suffer from poor chronostratigraphic constraints that depend solely on rare age-diagnostic marine fossils. The only undisputed age constraints come from dated foraminifera and ammonite assemblages recovered from the Sundays River Formation and Bethelsdorp Member of the Kirkwood Formation in the Algoa Basin, while other marine units (i.e., Robberg and Brenton formations) have contentious and poorly-defined ages. Ages for the rest of the Group, which is largely continental and therefore does not have datable marine fossils, are only inferred from these ages. The continental Enon and Kirkwood formations are especially poorly constrained in age yet have the most widespread occurrence across rift basins in which they occupy basalmost stratigraphic positions.

Table 2.1. Summary of the sparse chronostratigraphic constraints of the Uitenhage Group. formations are ordered from oldest (bottom) to youngest (top) where chronostratigraphic constraints allow.

Formation	Geological age	Source of age determination	References
Hartenbos	Lower Cretaceous	None. Inferred from lateral correlation with Buffelskloof Formation[a]	[a] Malan and Viljoen, 1990
Buffelskloof	Lower Cretaceous	None. Inferred from the basal angular unconformity with the Kirkwood Formation[a]	[a] Malan and Viljoen, 1990
Robberg	Lower Cretaceous	Poorly preserved cast fossils of two ammonites and an echinoid from sandstone units at Robberg, Plettenberg Bay[b]	[b] Reddering, 2000
Sundays River	Lower Cretaceous: Valanginian – Hauterivian	Valanginian foraminifera[c] and ammonite assemblages[d] in the lower parts of the Formation.	[c] McMillan, 2003; [d] Kitchin, 1908; Spath, 1930; McMillan and McLachlan, 1976; 1979; Cooper, 1983.
Brenton	Upper Jurassic OR Lower Cretaceous: Valanginian – Hauterivian	Controversial. Upper Jurassic ostrocods and an ammonite fragment[e] from Brenton, Knysna, and Valanginian ostrocods and foraminifera[f] from borehole PB-A/1, with which the outcrops at Brenton are correlated.	[e] Dingle and Klinger, 1972; [f] McLachlan et al., 1976
Infanta	Upper Jurassic – Lower Cretaceous	None. Correlation with Kirkwood Formation is based on lithostratigraphy only[g].	[g] Du Toit, 1976
Kirkwood	Upper Jurassic – Lower Cretaceous: Tithonian – Valanginian	Tithonian foraminifera from the basal Bethelsdorp Member, Algoa Basin[h]. Valanginian age inferred by correlation with lower Sundays River Formation, Algoa Basin[i]	[h] McMillan, 2010; [i] McLachlan and McMillan, 1976; Shone, 1978
Enon	Upper Jurassic – Lower Cretaceous	None. Age is inferred by correlation with Kirkwood Formation[j], and appearing below the Kirkwood Formation in numerous boreholes in the Algoa Basin[k] and above the contentiously dated Suurberg Group[l]	[j] Dingle et al., 1983; [k] McMillan, 2010; [l] McLachlan and McMillan, 1976; Kirstein, 1997; Marsh, 2016.

Chapter 3: Methods

3.1 U-Pb system in zircons

Zircon, $ZrSiO_4$, is a silicate mineral of extreme importance to the earth sciences and has enabled giant leaps in understanding of geological time, and the occurrence and nature of important events in Earth's history. These include amongst others, mass extinction events (e.g., Bowring, 1998; Mundil et al., 2004), the onset and evolution of plate tectonics (e.g., Hawkesworth and Kemp, 2006; Spencer et al., 2014), and the formation of the earliest crustal material (e.g., Maas, et al., 1992; Dhuime et al., 2012; Dhuime et al., 2015). What makes zircon so special in these cases are its abundance as an accessory mineral in various rock types, its chemical and physical resilience, and trace element diversity (e.g., Bowring et al., 2006; Harley and Kelly, 2007). Geochronologists rely on the tendency of zircon crystals to incorporate the element uranium ($U^{4+/6+}$) as a substitute for zirconium (Zr^{4+}) in the crystal lattice during crystallization, but exclude lead (Pb^{2+}), which enables it as an excellent geochronometer that has been utilized to date rocks since the mid-twentieth century (Tilton et al., 1955).

What makes U-Pb a particularly good chronometer compared to other radiogenic isotope systems is that it involves two independent decay schemes, ^{235}U to ^{207}Pb and ^{238}U to ^{206}Pb. These two decay schemes have different half-lives but involve the same chemical elements, allowing for a means to assess whether the zircons exhibit 'closed system behavior' through time – in a closed system all the Pb in a crystal comes from the radiogenic decay of U (through the two decay schemes), and no Pb was able to exit the system (Parrish and Noble, 2003; Bowring et al., 2006). In such an ideal system, the age of crystallization (t) can be calculated using either of the following two equations for the $^{238}U/^{206}Pb$ and $^{235}U/^{207}Pb$ systems:

$$t_{206} = \frac{1}{\lambda_{238}} ln\left(\frac{^{206}Pb}{^{238}U} + 1\right) \qquad (1)$$

$$t_{207} = \frac{1}{\lambda_{235}} ln\left(\frac{^{207}Pb}{^{235}U} + 1\right) \qquad (2)$$

where λ_{238} and λ_{235} represent decay constants 1.55125 e^{-10} and 9.8485 e^{-10} per year for the ^{238}U and ^{235}U systems, respectively (Jaffey et al., 1971). Typically, these notations are simply referred to as either the (1) $^{206}Pb/^{238}U$ age or (2) $^{207}Pb/^{235}U$ age and because the $^{235}U/^{238}U$ ratio is a natural constant = 137.818 (Hiess et al., 2012), a third $^{207}Pb/^{206}Pb$ age can be determined.

In reality, zircon crystals seldom behave as perfect closed systems and are prone to Pb-loss, especially at sites in the crystal lattice that have suffered radiation damage (e.g., Parrish and Nobel, 2003; Mundil et al., 2004; Bowring et al., 2006). In order to assess closed system behavior, Wetherill (1956) combined the two decay schemes to create the equation:

$$\frac{207Pb}{206Pb} = \frac{235U}{238U} \frac{(e^{\lambda 235t}-1)}{(e^{\lambda 238t}-1)} \qquad (3)$$

This can be plotted as the 'concordia curve', a line on the graphical plot of $^{206}Pb/^{238}U$ vs. $^{207}Pb/^{235}U$ (the concordia diagram) where the $^{206}Pb/^{238}U$ age is equal to the $^{207}Pb/^{235}U$ age (Wetherill, 1956). When $^{206}Pb/^{238}U$ and $^{207}Pb/^{235}U$ ratios from a zircon analysis is plotted on the concordia diagram, it should lie on the concordia curve, or in other words is *concordant*. If however the point lies off the curve, as when the calculated ages from each ratio are not equal, then the zircon age is *discordant*. Concordance can also be quantified (as a %) with the following equation:

Concordance = 100 [$^{206}Pb/^{238}U$ age / $^{207}Pb/^{206}Pb$ age] (4)

Or

Concordance = 100 [$^{206}Pb/^{238}U$ age / $^{207}Pb/^{235}U$ age] (5)

An alternate form of data presentation is the Tera-Wasserburg concordia diagram, where $^{207}Pb/^{206}Pb$ is plotted vs. $^{238}U/^{206}Pb$. In this plot, the gradient of the line, along which ages calculated from each system are equal, is less steep for young ages than in the conventional concordia diagram and therefore provides a better visualization of young zircon ages (Gehrels, 2011).

A common alternate way in which detrital U-Pb zircon data are displayed, especially when datasets are large and varied in age is the probability density diagram (e.g., Ludwig, 2000; Gehrels, 2011), which are often accompanied by a frequency histogram of zircon ages. In the probability density diagram: (1) concordant zircon ages are each assigned a normal (Gaussian) distribution based on age and analytical uncertainty; (2) the probability distribution of each analysis is summed into a singl curve. A normalized probability density diagram is simply a probability density diagram that is normalized to the number of dates used so that the area under each graph is equivalent, which can sometimes aid comparisons (Gehrels, 2011). Cumulative age probability diagrams can also aid detrital zircon comparisons, and these are constructed by plotting the cumulative probability vs. age for a set of U-Pb dates (Gehrels, 2011).

3.1.1 Analytical techniques

There are two approaches to U-Pb zircon geochronology, both of which are utilized in this study: Microbeam techniques and thermal ionization mass spectrometry (TIMS). The ‘conventional’ method of U-Pb dating zircons is by TIMS and involves isolating single crystals and dissolving them prior to analysis, whereas microbeam techniques, specifically, Laser Ablation Inductively Coupled Plasma Mass Spectrometry (LA-ICPMS) for the purposes of this study rather than Secondary Ionisation Mass Spectrometry (SIMS), are relatively new methods that allow rapid *in-situ* analysis and have revolutionized geochronology in the last several decades (Bowring et al., 2006; Schoene, 2014).

The development of improved and cheaper ICPMS and laser ablation instrumentation and the characterization of several zircon standards (Jackson et al., 2004) have propelled this method of U-Pb geochronology to become the most widely used among earth scientists. In short, this method utilizes a focused laser to vaporize a small volume of a crystal in a thin section or mounted in epoxy resin and then flushes the aerosol from the ablation stage into the ICPMS where isotopic masses are analysed. Typically, a relatively small spot size (typically 10 – 60 µm in diameter and up to 20 µm deep) is used and allows high spatial resolution when analyzing a crystal (Fig. 3.1). In this way, specific sites of interest in the polished zircon (e.g., xenocrystic cores, secondary growth rims and inclusions) can be targeted or avoided based on the user's interest (Corfu et al., 2003). In addition, analyses can be performed very rapidly, usually hundreds in a day in a highly automated protocol without much concern for contamination. However, the high special resolution and short analytical times come at a cost of analytical precision. Even the most sophisticated microbeam methods achieve analytical uncertainties an order of magnitude greater than modern TIMS methods (e.g., Ireland and Williams, 2003; Kosler and Sylvester, 2003; Karlstrom et al., 2018). Where 1 – 8% (2-σ) uncertainties are expected for LA-ICPMS U-Pb zircon dates (e.g., Bowring et al., 2006; Dickinson and Gehrels, 2009; Gehrels, 2011; Karlstrom et al., 2018), uncertainties of ~0.1 % (2-σ) are regularly achieved by TIMS (e.g., Mundil et al., 2004). The relatively low-precision of microbeam techniques present additional problems – zircons dates with large uncertainties cannot easily be resolved from one another and subtle Pb loss or inheritance cannot be identified using tests of concordance. It thus is possible to attain relatively inaccurate zircon U-Pb dates, as well as imprecise ones and severely limits the practicality of microbeam techniques in high-precision geochronology (Ireland and Williams, 2003; Bowring et al., 2006). However, due to the rapid analytical times (and higher cost efficiency), they remain the principal method for analyzing large sets of detrital zircons to reveal a maximum depositional age (Dickinson and Gehrels, 2009), or a low-precision depositional age of a pyroclastic deposit (e.g., Han, 2006; Roberts et al., 2012; McKay et al., 2015).

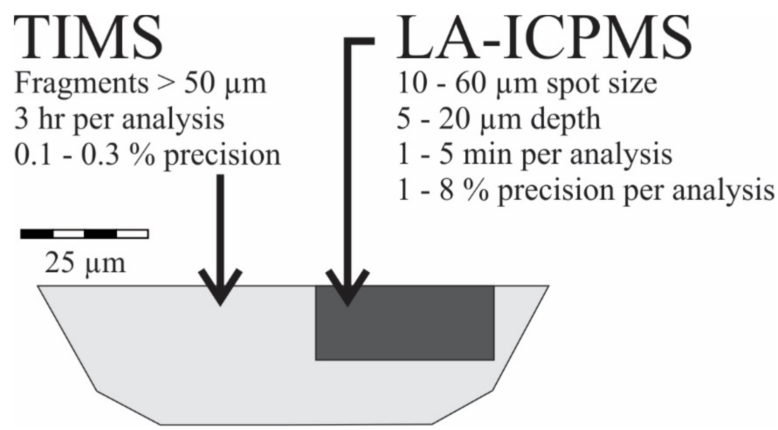

Fig. 3.1. Relative volumes of zircon, time and precision achieved by TIMS and LA-ICPMS analysis (modified from Bowring et al., 2006). Uncertainties quoted are at the 2σ level.

U-Pb dating zircons by TIMS has also seen massive improvements over the last half century (e.g., Parrish and Noble, 2003; Mattinson, 2005; Schoene et al., 2015). This method involves dissolving individual crystals (Fig. 3.1) in ultra-clean environments prior to performing a comparatively time-consuming analysis with minimal automation. By dissolving the crystals, any significant spatial resolution is precluded, but what is gained is a much higher precision analysis. This allows for more thorough scrutiny of concordance and overall more accurate and precise ages. Further, improvements to the method have come from subjecting crystals to a number of pre-dissolution treatments such as chemical abrasion (CA-TIMS). This method involves thermal annealing and partial dissolution of the crystals in HF followed by sequential cleaning (Mattinson, 2005). The parts of crystal that has had radiation damage and Pb loss are dissolved at a higher rate than other low U zones and the remaining crystal is more likely to be concordant. The success of chemical abrasion over other pretreatment methods such as air abrasion, which removes the outermost layer of a crystal, is that the HF affectively 'mines out' high U damaged zones that are often irregular and in central portions of a crystal's volume (e.g., Mundil et al., 2004; Bowring et al., 2006).

3.2 Methods employed in this study

3.2.1 Field observations

Extensive field work was undertaken in order to locate/discover and describe the poorly documented volcaniclastic deposits in the Uitenhage Group. Once found in the field, local evidence was collected in the form of stratigraphic and sedimentological macroscopic observations to document the vertical and horizontal distributions of sedimentary characteristics not only of the sampled layer but also of the host strata. In this chapter, field observations were limited to those that directly relate to characterizing the deposit as detrital or primary volcaniclastic following the recommendations of Bohor and Triplehorn (1993), Koniger and Stollhofen (2001), White and Houghton (2006) and Nemeth and Martin (2007) and recent volcaniclastic classifications (White and Houghton, 2006; Brown et al., 2012). Specifically, sedimentological characteristics that were used to help identify volcaniclastic material in the field were the presence of: 1) laterally continuous uniform bed character; 2) clay-dominated lithologies with rare (<5%) phenocrysts that are sand–silt sized; 3) No visible detrital quartz grains or lithic fragments; 4) ‘Popcorn texture’ surficial weathering that indicate an abundance of smectite clays such as montmorillonite; 5) Accretionary pellets; 6) Amorphous silica within unit or in adjacent beds that may indicate devitrification of original glass components during alteration to clay; 7) lack of sedimentological structures that may indicate lateral transport of material before deposition. This was done by systematically documenting the vertical and lateral sedimentological facies changes, including grain size, sediment colour and composition, bedding geometries and boundary surfaces at each site. Further, thin sections were made of competent specimens in order to determine if there was sedimentary rounding of constituent minerals or glass shards were present.

3.2.2 U-Pb zircon geochronology

3.2.2.1 LA-ICPMS

Approximately 2 kg of fresh, unweathered rock was collected from each sampled unit, regardless of its suspected origin (i.e., pyroclastic, volcaniclastic, or detrital). Slightly different mineral separation protocols were adhered to depending on the physical properties of the sampled lithology. Clay-rich bentonites disintegrated when left in water, and therefore all bentonitic samples were submerged in water in clean containers and periodically stirred to aid the breaking-down process and generation of a slurry. In some cases where stirring was insufficient, an ultrasonicator was used to ensure that the clay fraction of sample disintegrated and entered suspension. Following these steps, the slurries were removed of their clay fraction by successively stirring and pouring-off of the suspended fraction until only silt and sand sized particles remained. Samples that were composed of sandstone were more competent, and required being crushed instead of simply disintegration by mixing with water. This was done by first drying the samples overnight in an oven set at 60 ºC and then crushing the samples in a Sturtevant Model 4 rock crusher at the University of Cape Town, before being milled in a disc-mill at Central Analytical Facility (CAF) of Stellenbosch University. All subsequent sample preparation procedures for LA-ICPMS were conducted at CAF. The crushed, milled sample was subsequently sieved using 355 µm aperture mesh, to concentrate liberated crystals. The sieved material was then mixed with water and successively washed following the same procedure as the uncrushed bentonitic samples until the clay fraction was effectively removed and silt- and sand-sized grains remained. This fraction was then processed to concentrate heavy minerals by gravitational separation using an automatic panner and a handheld pipette. The heavy mineral separate was oven-dried in a petri-dish overnight before being subject to magnetic separation. Magnetic separation was achieved by running a small handheld magnet that was wrapped in clean paper over the sample several times until all ferromagnetic minerals were removed from the sample. The non-magnetic heavy mineral separate was further processed using standard heavy mineral separation techniques utilizing tetrabromoethane (TBE) (density = 2,97 g/cm^3) to concentrate heavy minerals on filter paper by removing light minerals. The heavy mineral separate was then washed thoroughly using water and acetone to remove excess TBE and help dry the sample. Once dried, the crystals were tipped onto a petri-dish for handpicking under the binocular light microscope. In order to minimize human-induced bias in the selection of zircons, and attain a representative selection of grains, crystals were picked from a defined field-of-view that was only moved once all zircons within were placed onto a strip of double-sided tape. Once ~80 crystals were picked, a focused effort was made to find and select the most pristine zircon crystals that were euhedral and contain no obvious blemishes until a total of ~100 crystals were picked. This was done to maximize the chance that the mounted sub-population contained a young volcanic proportion that could be suitably dated by LA-ICPMS (Gehrels, 2011). The picked zircons were then mounted onto a 25 mm epoxy resin puck that was polished so that their mid-sections were exposed. The polished mounts were then coated with a fine layer of carbon before being inserted into the Carl Zeiss: MERLIN–Field Emission Scanning Electron Microscope (SEM). Images of the zircons were attained using the cathodoluminescence (CL) detector that allowed the visualization of xenocrystic cores, microtextures, cracks and inclusions within the crystals and were used in the selection of appropriate analytical spots during LA-ICPMS analysis. Avoiding these features both enhances the chance of producing a successful analysis by excluding damaged parts of the crystal, areas with mixed ages, or inherited portions that clearly do not reflect the youngest crystallization event experienced.

LA-ICPMS analysis of zircons at the CAF happened over a period of four years from 2015 to 2018 in four discrete analytical campaigns. The first three campaigns were analysed at the CAF under the supervision of Dr. Dirk Frei and the final campaign was overseen by Dr. Laura Bracialli. During this time the analytical equipment, namely a 193 nm wavelength ASI Resolution laser ablation system coupled to a Thermo Scientific Element 2 single collector magnetic sector field inductively coupled plasma mass spectrometer (SC-SF-ICP-MS), remained unchanged. The procedures followed were almost identical too excluding a few subtle changes between the first three and the final campaigns, although all procedures closely follow the established procedural framework for U-Pb geochronological LA-ICPMS analysis described by Jackson et al. (2004). The metadata for LA-ICPMS analyses are given in Tables 2 and 3 and comprise the laser ablation, mass-spectrometry and data reduction methods. The principal differences between the first three campaigns and the last are the laser parameters, secondary reference zircons used for quality control, data reduction procedures and calculation of concordance. Importantly, all data in the first three campaigns are corrected for common Pb using the composition projected from the age following Stacey and Kramers (1975), whereas no common Pb correction was applied for data from campaign 4. This was due to Mercury contamination in the gas-line, precluding common Pb correction. All LA-ICPMS isotopic data for reference materials are plotted in Appendix A, Fig. A1. The resulting isotopic data for the samples from the Suurberg Group are tabulated in Appendix B, Tables B1 – B5. The data for samples from the Uitenhage Group are tabulated in Appendix D, Tables D1 – D24, and Appendix E, Table E1. For more information about and access to these data please direct an email to robert.muir@uct.ac.za.

Table 3.1. Metadata for LA-ICPMS U-Pb geochronological method employed for campaigns 1, 2 and 3, from 2015 – 2017 at the CAF, Stellenbosch University, South Africa

Laser ablation system	
Make, Model & type	ASI Resolution M-50-LR Excimer laser
Ablation cell & volume	Laurin Technic M-50 dual-volume cell
Laser wavelength	193 nm
Pulse width	15 ns
Fluence	2.0 J/cm^{-2}
Repetition rate	7 Hz
Spot size	26 µm
Sampling mode / pattern	Static spot ablation
Carrier gas	100% He in the cell, Ar make-up gas combined using a T-connector close to sample cell
Pre-ablation background collection	3 cleaning shots followed by 20 seconds background collection
Ablation duration	20 seconds
Wash-out delay	15 s
Cell carrier gas flow	0.35 l/min He
ICP-MS Instrument	
Make, Model & type	Thermo Scientific Element2 single collector HR-SF-ICP-MS
Sample introduction	Ablation aerosol via conventional tubing
RF power	1350 W
Make-up gas flow	1.0 l/min Ar
Detection system	Single collector secondary electron multiplier
Masses measured	202, 204, 206, 207, 208, 232, 235, 238
Integration time per peak (segment duration)	7, 14, 15, 18, 8, 8, 1, 13 ms, respectively
Total integration time per output datapoint	0.1 s
Sensitivity	30000 cps/ppm Pb
Dead time	6 ns
Data Processing	
Gas blank	20 s on peak prior to each measurement
Calibration strategy	GJ-1 used as primary reference material, Plešovice & M127 used as secondary reference ma (Quality Control). 91500 used in campaign 3 only.
Reference Material info	M127 (Nasdala et al. 2008; Mattinson 2010), 91500 (Wiedenbeck et al. 1995), GJ-1 (Jackson et al. 2004), Plešovice (Slama et al. 2008)
Data processing package used / Correction for LIEF	In-house spreadsheet data processing using intercept method for LIEF correction
Mass discrimination	Standard-sample bracketing with $^{207}Pb/^{206}Pb$ and $^{206}Pb/^{238}U$ normalized to reference material GJ-1
Common-Pb correction	204-method, Stacey & Kramers (1975) composition at the projected age of the mineral, 5% uncertainty assigned
Uncertainty level & propagation	Ages are quoted at 2 sigma absolute, propagation is by quadratic addition. Reproducibility and age uncertainty of reference material and common-Pb composition uncertainty are propagated.
Quality control / Validation	See Appendix A for quality control.
Determination of concordance	Concordance = 100 [$^{206}Pb/^{238}U$ age / $^{207}Pb/^{206}Pb$ age]

Table 3.2. Metadata for LA-ICPMS U-Pb geochronological method employed for campaign 4 in 2018 at the CAF, Stellenbosch University, South Africa.

Laser ablation system	
Make, Model & type	ASI Resolution M-50-LR Excimer laser
Ablation cell & volume	Laurin Technic M-50 dual-volume cell
Laser wavelength	193 nm
Pulse width	15 ns
Fluence	2.0 J/cm^{-2}
Repetition rate	7 Hz
Spot size	26 µm
Sampling mode / pattern	Static spot ablation
Carrier gas	100% He in the cell, Ar make-up gas combined using a T-connector close to sample cell
Pre-ablation background collection	13 s
Ablation duration	29 s
Wash-out delay	20 s
Cell carrier gas flow	0.35 l/min He
ICP-MS Instrument	
Make, Model & type	Thermo Scientific Element2 single collector HR-SF-ICP-MS
Sample introduction	Ablation aerosol via conventional tubing
RF power	1325 W
Make-up gas flow	0.9 l/min Ar
Detection system	Single collector secondary electron multiplier
Masses measured	202, 204, 206, 207, 208, 232, 235, 238
Integration time per peak (segment duration)	7, 14, 15, 18, 8, 8, 1, 13 ms, respectively
Total integration time per output datapoint	0.1 s
Sensitivity	0.3% U
Dead time	6 ns
Data Processing	
Gas blank	13 s on peak prior to each measurement
Calibration strategy	GJ-1 used as primary reference material
Reference Material info	GJ-1 (Jackson et al. 2004); Plešovice (Slama et al. 2008); Mud Tank (Black and Gulson 1978; Horstwood et al. 2016)
Data processing package used / Correction for LIEF	Iolite data reduction software package (Paton et al., 2011) in combination with the Visual Age add-on (Petrus and Kamber, 2012); LIEF modelled within each analytical session on the basis of combined analyses of the main reference material. LIEF correction assumes reference material and samples behave identically
Mass discrimination	Reference material-sample bracketing with $^{207}Pb/^{206}Pb$ and $^{206}Pb/^{238}U$ normalized to zircon GJ-1
Common-Pb correction	No common Pb correction applied to the data
Uncertainty level & propagation	Decay constant uncertainties, ratio uncertainty of primary reference material and long-term excess variance of secondary reference material are propagated by quadratic addition. Age uncertainties are quoted at the 2s absolute level.
Quality control / Validation	Plešovice: Wtd avg $^{206}Pb/^{238}U$ age = 337.0 ± 0.7 (95%, MSWD = 0.9; n = 109); Mud Tank Wtd avg $^{206}Pb/^{238}U$ age = 729.3 ± 2.1 (95%, MSWD = 0.8; n = 65);
Determination of concordance	Concordance = 100 [$^{206}Pb/^{238}U$ age / $^{207}Pb/^{235}U$ age]

3.2.2.2 CA-TIMS

Four pyroclasic samples analysed by LA-ICPMS that are in key stratigraphic positions were selected for secondary analysis by CA-TIMS. This was done by selecting the youngest and least complex zircons based on $^{206}Pb/^{238}U$ dates derived from the LA-ICPMS analysis and CL images. These were individually chiseled out of the epoxy mounts for pretreatment before final analysis following the procedure outlined in Mundil et al. (2004) and developed by Mattinson (2005). The selected zircons were placed within quartz crucibles in a high-temperature oven to be chemically annealed for 850ºC for 36 hours. Following this, the crystals were removed from the crucibles and placed into a concentrated solution of HF within individual Teflon capsules. These were place into pressurized containers that were heated to 220ºC for 16 hours, during which time the crystals were partially digested, or chemically abraded. The regions of each crystal that have suffered the most severe radiation damage, which are also typically regions of open system behavior and Pb-loss (Mundil et al., 2004; Mattinson, 2005) were preferentially dissolved. This minimized the effects of Pb-loss and the calculation of spuriously young dates during TIMS analysis. After this process was completed, each zircon was cleaned thoroughly by repeated exposure to aqua regia. Finally, the zircons were dissolved in their respective capsules, within a pressurized vessel for 6 days at 220 ºC along with a drop of phosphoric acid and the EARTHTIME spike standard. The resulting solution was placed onto rhenium filaments and analysed with a Micromass Sector54 thermal-ionization mass spectrometer. All CA-TIMS procedures were carried out at the Berkeley Geochronology Centre during October, November and December 2016 under the supervision of Dr. Roland Mundil, who reduced the data using in-house Excel protocols. The graphical determination of concordance of dates was followed for all samples acquired by CA-TIMS following laboratory preferences. The CA-TIMS isotopic data tabulated Table G1 in Appendix G, and all concordant data are plotted in Fig. H1 in Applendix H. For more information about and access to these data please direct an email to robert.muir@uct.ac.za.

3.2.2.3 Zircon geochronology statistical considerations

In this study, we use zircon as a chronometer in detrital sedimentary rocks, which include both terrigenous clastic and volcaniclastic rocks. In order to distinguish the types of volcaniclastic deposits sampled for zircons in this study, the terminology used is that of White and Houghton (2006), who reserve the term 'pyroclastic' for *primary* volcaniclastic deposits that do not involve any interim storage (e.g., layer of volcanic ash that fell from an eruption cloud), while non-primary volcaniclastic deposits (e.g., a reworked/resedimented volcanic ash layer) are named using sedimentary terminology with a prefix modifier that indicates a partial volcanic origin (e.g., tuffaceous sandstone). Deviation from this scheme is taken when describing a highly altered rock such as *bentonite*, which is a commonly used term for smectite-rich altered volcanic ash and continues to be employed in numerous geochronological studies (e.g., Bowring and Schmitz, 2003; Mundil et al., 2004; Wang et al., 2016; Rocholl et al., 2018). Nevertheless, because the way in which U-Pb zircon data are handled depends on the interpretation of a deposit being primary or reworked, each sampled deposit in this study will be clearly classified on a case-by-case basis based on sedimentary observations and zircon age distributions following methods outlined in Bohor and Triplehorn (1993) and Nemeth and Martin (2007) and listed in section 3.2.1. Further, CL and secondary election images were also colsulted along with the U-Pb data to make the final assessment of whether a specific sampled unit is primary or reworked. For terrigenous clastic and resedimented (detrital) volcaniclastic deposits, a maximum depositional age is calculated based on the age of the youngest age component in the zircon age distribution, while zircons in pyroclastic deposits can be used to determine the age of crystallization/eruption, which is assumed to be the true depositional age of the deposit. This geological classification therefore greatly affects the interpretation of the age of the sampled unit but there are also statistical considerations that warrant mention.

There are multiple approaches to defining a maximum depositional age from a given detrital zircon age population that is derived from a terrigenous clastic and resedimented volcaniclastic rocks. Dickinson and

Gehrels (2009) outline several of the commonly used metrics and compare their reliability and accuracy. The youngest concordant date in the sample, or *youngest single grain* (YSG), should reflect the maximum depositional age because inherently a rock cannot be older than its constituents assuming no metamorphic overprinting. However, the lack of reproducibility of the age of just a single zircon grain is a concern especially since subtle Pb-loss can occur resulting in spuriously young crystals that are still concordant (Bowring et al., 2006). However, in settings near where syn-depositional igneous activity occurs this metric can be a close reflection of the actual depositional age of the deposit (Dickinson and Gehrels, 2009). An alternate method used to define the youngest age component in a sample and therefore its maximum depositional age is the graphical approach – selecting the age that corresponds to the *youngest graphical peak* (supported by two or more dates) on a probability density diagram (YPP). This is a more robust measure of the maximum depositional age of the rock because it incorporates more than one date and is therefore at least somewhat reproducible, unlike the YSG metric (Dickinson and Gehrels, 2009). The downside of this metric is that no uncertainty can be quantified for the graphically-defined quantity. Nevertheless, YPP is a commonly used approach to defining a maximum depositional age of the detrital rock (e.g., Dickinson and Gehrels, 2009; Lawton and Bradford, 2011; Tucker et al., 2013). It should be noted that there are, however, quantifiable uncertainties associated with the individual dates that constitute the graphical peak (that are typically 2 – 8 % for LA-ICPMS) and therefore the uncertainty of this metric – although not itself quantifiable – should not be considered less than about half of this value (Ireland and Williams, 2003; Bowring et al., 2006)**.** Other methods attempt to retain a measure of uncertainty and employ a metric that uses more than one date (thereby improving reproducibility) by calculating weighted averages of a section of overlapping dates. For instance, a weighted mean of the youngest cluster of ages that overlap at 1σ or 2σ error, and comprise 2, 3 or more dates is sometimes used to define the maximum depositional age (e.g., Dickinson and Gehrels, 2009; Tucker et al., 2013). Although these metrics do retain a quantified uncertainty, they assume that the dates used to calculate the mean are co-genetic, and this assumption is especially tenuous when considering a detrital rock sample that clearly has multiple sources for constituent zircons (Bowring et al., 2006). Another approach is to run Monte Carlo statistical simulations to determine what the most likely youngest detrital age component is in the sample, which can be automatically performed using the *Youngest Detrital Zircon* (YDZ) operation within the Isoplot software package (Ludwig, 2000). Due to the array of different metrics used in determining the maximum depositional age of a detrital sample, each with their own merits, some authors prefer to quote multiple different metrics (e.g., Dickinson and Gehrels, 2009). Each of these metrics attamept to quantify the youngest age component in a detrital zircon population, which represents the maximum depositional age of the unit sampled. Importantly however, in most cases this does not approximate the actual depositional age of the sample at all, because the youngest zircons may long-predate their final incorporation into the final sedimentary host rock sampled. For a more robust constraining of depositional age, it is more useful to assess the U-Pb zircon geochronology of pyroclastic rocks.

There are also statistical considerations concerning zircon data from the numerous pyroclastic samples used in this study. In pyroclastic deposits, the dates attained for analyzing constituent zircons more closely reflect the age of the crystallization event and the true depositional age of the sampled horizon than in a detrital sample. Ideally, the constituent zircons in such a deposit are of equivalent age, form a single population, and are normally distributed around a mean value (the age of the rock). However, it is common that dates are skewed from this normal distribution, possibly due to subtle post-depositional Pb-loss (e.g., Mundil et al., 2004) or inheritance (e.g., Landing et al., 1998) and a create complex distributions of dates that are not simply caused by the analytical precision of the instrumentation used. This makes interpretations of an age of the rock difficult (Bowring et al., 2006). A statistical parameter that helps give an indication of whether the scatter of dates can be entirely attributed to the analytical imprecision, the mean square of the weighted deviates, or MSWD, is usually quoted with weighted average calculations. Simply put, when the MSWD is $>> 1$, then the scatter observed cannot be entirely attributed to analytical uncertainty and there could be real geological processes affecting the spread of dates. When the MSWD is ~1, the spread of dates used to calculate the weighted mean can be explained by the analytical uncertainties alone (Bowring et al., 2006). Finally, a MSWD value that is $<< 1$ indicates that the analytical uncertainties are overestimated. When the data do not form a coherent cluster (MSWD = 1), assigning an age for the pyroclastic rock become challenging. Selecting dates from a highly scattered population (MSWD >>1) often requires the trimming of data to arrive at a reasonable age (for instance the recognition an omission of dates effected by inheritance or Pb-loss). Generally, these decisions can only confidently be made with high-precision data produced by CA-TIMS, because the selection of a geological meaningful age from a population of scattered, imprecisely determined dates can become subjective (Bowring et al., 2006). In this study, weighted mean ages for zircon populations in pyroclastic rocks are therefore limited to data that are produced by the CA-TIMS method. These dates are generally higher-precision than those aquired by LA-ICPMS and have more varied uncertainties. However, most pyroclastic deposits analysed in this study have been dated using LA-ICPMS (yielding lower-precision U-Pb dates) and instead, a more automated approach of selecting a robust geological age is applied for these samples. In these cases, the TuffZirc algorithm in Isoplot (Ludwig, 2000) is employed to calculate an age in a scattered population without requiring extreme subjectivity. It works by selecting an age that incorporates the most coherent cluster of dates and therefore ignores inherited dates and is robust against spuriously young outliers that have likely been affected by Pb-loss. It should be noted that the TuffZirc algorithm is used for dates aquired from LA-ICPMS that have individual uncertainties that are typically ~3%, and any uncertainty quoted with the TuffZirc-calculated age should not be viewed as a high-precision age (c.f. those aquired from CA-TIMS) and is realistically no less that half that of the individual uncertainties of dates that constitute the coherent cluster (Ireland and Williams, 2003; Bowring et al., 2006). Further, where the individual U-Pb dates in a pyroclastic deposit are approximately continuous and no coherent cluster dominates the distribution, the TuffZirc age calculated has not been accepted as an adequate interpretation of depositional age.

Finally, the aims of this study relate to constraining the depositional age of the units sampled, and this also affects how the data are presented. Two standard graphical representations of U-Pb data are given – probability density diagrams and concordia plots. These are used widely throughout this thesis, but data older than 1.5 Ga are not included in these plots because: 1) these old crystals contribute nothing to determining the depositional age of the sampled unit; 2) it is not within the scope of the thesis to fully characterize the detrital zircon provenance of the Uitenhage or Suurberg Groups; 3) the number of > 1.5 Ga zircons never exceeds more than 5 grains in any given sample and therefore constitutes a very small proportion of each sample. Nevertheless, these data are included in all data sheets and are therefore fully accessible to the inquisitive reader (Appendices C, D and E).

In summary, there are lithological and statistical nuances that require attention throughout this thesis. These are navigated in the following way: firstly, an assessment of the origin of each sample is made (i.e., either detrital, be that terrigenous clastic or resedimented volcaniclastic, or pyroclastic). In the case of detrital samples, only maximum depositional ages are considered unless there are compelling, case-specific reasons to interpret that data differently. The YSG, YDZ and YPP metrics are given, although the most robust of the three is preferred (i.e., YPP), as it is the least likely to reflect a spuriously young maximum depositional age. Pyroclastic samples are treated differently. The TuffZirc algorithm is preferred for extracting a meaningful depositional age for the unit when lower-precision LA-ICPMS data are available, whereas a weighted mean is preferred for higher-precision CA-TIMS data. In all cases the final age interpretations are made using the dates derived from the $^{206}Pb/^{238}U$ isotopic system unless otherwise stated.

Chapter 4: Geochronology of the Suurberg Group

4.1 Introduction

Continental rifting is often accompanied, or closely proceeded by extensional volcanism, either as voluminous flood basaltic outpourings, as in the Karoo and Ferrar large igneous provinces (LIPs) and Central Atlantic Magmatic Province (CAMP), or less voluminous volcanism along weaknesses in the thinned crust incipient with rift-basin formation (Gust et al., 1985; Ebinger et al., 1993; Abebe et al., 2003; Will and Frimmel, 2018). However, volcanism can also be entirely absent during extensional basin formation (e.g., Wernicke and Burchfiel, 1982; Dewey, 1988). It is unclear which of these scenarios existed during the Jurassic – Cretaceous rifting of the southern Cape. The enigmatic volcaniclastic and volcanic-dominated Suurberg Group, which outcrops at the margin of the northern Algoa Basin in the Eastern Cape Province of South Africa (Fig. 4.1), has been attributed to volcanism prior to rifting (Hill, 1972), incipient with it (Roux and Davids, 2016) or instead largely unrelated to rifting (Marsh, 2016). An unequivocal view of its deposition and significance for Gondwanan rifting has been elusive largely due to extremely poor outcrops that hinder confident field observations, but also because existing radiometric ages for its constituent basalts are not reproducible, have large uncertainties and are of questionable accuracy. Literature report ages that include 'absolute age dating' of 80 to 100 Ma and 'early Upper Cretaceous' (sic), although no data nor the analytical dating technique used to derive these ages are mentioned. K-Ar analysis of a basaltic sample yielded an age of 162 ± 7 Ma (McLachlan and McMillan, 1976), and a single sample of plagioclase mineral separates is dated to 194 ± 11.9 Ma by Ar-Ar methods (Kirstein, 1997). However, none of these contrasting ages or the requisite datasets have been published nor sufficiently validated, and all of which are derived from just a single basaltic interval that may not represent the entire Suurberg Group. Improving the depositional age constraints of this stratigraphic unit would lend insights into the geodynamic evolution during the Jurassic – Cretaceous of SW Gondwana.

The Suurberg Group has also played an important role in pinning the physical evolution of rifting in the southern Cape to a chronological timeframe because it has (and continues to be) a datum used to infer the maximum age of the overlying, taphrogenic Uitenhage Group (Hill, 1972; McLachlan and McMillan, 1976; Wildman et al., 2015; Green et al., 2016; Richardson et al., 2017). Therefore knowing the age of the Suurberg Group would enable the robust determination of the maximum age for the Uitenhage Group that overlies it and by inference help constrain the timing of rift initiation in the southern Cape, which plays into one of the aims of this thesis.

The Suurberg Group consists of three discrete stratigraphic units that have a cumulative thickness generally less than ~200 m (Hill, 1972; Joubert and Johnson, 1998) that include the basalmost breccia and conglomerates of the Slagboom Formation, an overlying volcaniclastic-dominated Coerney Formation, comprising various discrete tuffaceous intervals, and the uppermost Mimosa Formation, which consists of basalts and rare tuffaceous interbeds (Hill, 1972; Fig. 4.1). The Group overlies the Palaeozoic Cape Supergroup and lowermost Karoo Supergroup with an angular unconformity and is separated from the overlying Uitenhage Group by a stratigraphic contact that is poorly understood and rarely exposed. Some authors regard the contact conformable (Dingle et al., 1983; McMillan et al., 1997) whereas others consider the two groups to be separated by an unconformity that is either very 'weak' (sic), with a short hiatus (Rigassi and Dixon, 1972), or possibly lengthier (McLachlan and McMillan, 1976; McMillan, 2010).

It remains unclear how any of these lithological units were deposited. The breccia-dominated Slagboom Formation has been attributed to explosive incipient volcanism (Hill, 1972), although the presence of rounded clasts in some areas, making the unit a conglomerate rather than a breccia, and no outcrops in the Suurberg Group that unequivocally exhibits cross-cutting dikes or volcanic pipes, leave the possibility that the unit has a sedimentary origin. Further, the clast composition of a volcanic breccia that erupts upward through country rock stratigraphy is expected to be heterolithic, or at least contain some juvenile components, but observations show that clasts are composed exclusively of quartzites from the Cape Supergroup, which outcrops widely in the basement that surrounds the Algoa Basin (Hill, 1972; Toerien, 1991). None of these observations bring absolute clarity on the petrogenesis of these deposits, yet it seems that the Slagboom Formation need not have a volcanic origin and may equally be attributed to talus-slope and alluvial fan deposition where such coarse-grained facies commonly result from colluvial and alluvial depositional processes. The deposition of ash is also expected if there was violent volcanism nearby, and Hill (1972) suggests such an origin for the tuffaceous strata in the Coerney and Mimosa formations. However, a distal, yet unknown, origin for the ash may also be possible (Marsh, 2016), especially since there is no strong evidence for volcanic 'vents' that are filled by tuffaceous rocks first proposed by Hill (1972). Finally, the origin of the basalts in the Mimosa Formation is also rather enigmatic. Geochemically, they are identical to the Karoo continental flood basalts of the Lesotho Formation in the Drakensberg Group

(Marsh et al., 1979; Marsh, 2016), but their position within the Cape Fold Belt – disconnected from the main body of the Karoo LIP volcanics and subvolcanics in the interior of South Africa – is unique (Marsh, 2016). The crust underlying the Cape Fold Belt is thickened and deformed (Paton, 2006; Lindique et al., 2011) and likely acted as a barrier preventing upward moving melts to reach the surface (Marsh, 2016). It therefore seems unlikely that the basalts in the Suurberg Group are derived from local dolerite intrusions as is the case further north. Instead of speculating on feeder dykes anomalously penetrating the Cape Fold Belt in the Algoa Basin, an alternate explanation is that the flood basalts that extruded during the Karoo LIP extended as far south as the Cape Fold Belt, flowing far from their original feeder dykes (fissures) and overstepping any potential topographic barriers presented by the Cape Mountains in the Early Jurassic (Pliensbachian-Toarcian), but are only preserved in rare instances such as in the northern Algoa Basin (Marsh, 2016). One of the main assumptions held by this depositional model for the basalts is that they are the same age as the ~183 Ma Drakensberg Group (Svensen et al., 2012; Burgess et al., 2015), which is to date unconfirmed.

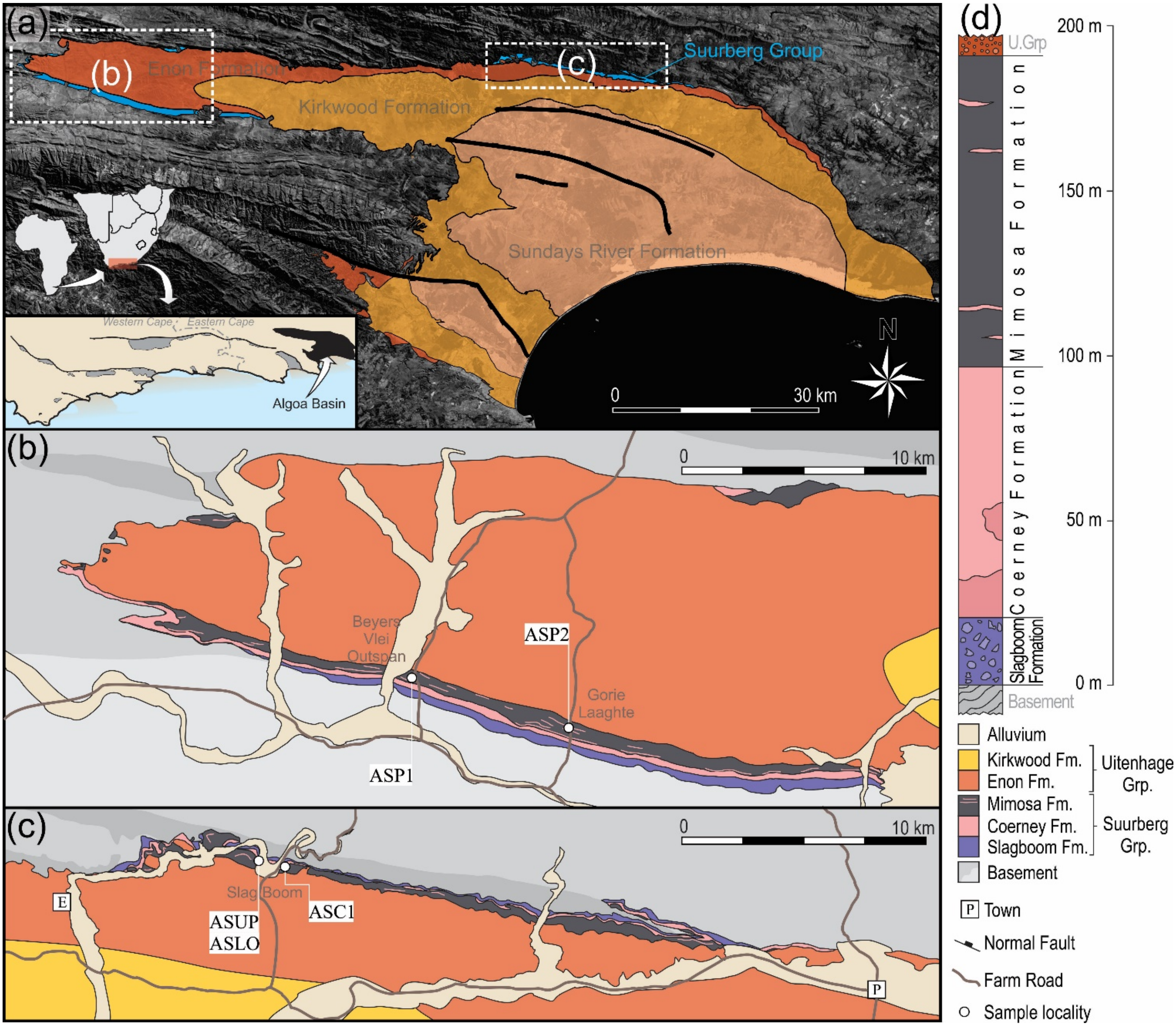

Fig. 4.1. Distribution of the Suurberg Group in the northern Algoa Basin. (A) Simplified geology of the Algoa Basin, the eastern most rift basin in the southern Cape (inset). Unshaded regions are basement and blue shaded regions are where the Suurberg Group outcrops. White dashed rectangles are the regions enlarged in figures B and C. (B) Geology of the Algoa Basin panhandle, where the Suurberg Group occupies the southern margin of the Basin. (C) Geology of the central northern Algoa Basin, where the Suurberg Group outcrops along the northern edge of the Basin. (D) Simplified stratigraphic log of the Suurberg Group at Slagboom after Hill (1972). Base map A is modified from the 1: 250 000 geological map sheets 3324 (Toerien, 1991) and 3326 (Roby and Johnson, 1995) of the Council for Geoscience overlain on ESRI satellite imagery; Maps B and C modified after Hill (1972).

There is a clear need for robust geochronological constraints for the Suurberg Group in order to assess possible connections with other Mesozoic LIPs that occurred shortly before the fragmentation of Gondwana; resolve how it was deposited; and to provide a maximum age constraint to the overlying Uitenhage Group. This study aims to achieve this by dating zircons separated from five volcaniclastic deposits (Table 4.1) in different locations and at separate stratigraphic intervals throughout the Suurberg Group using U-Pb isotopic system by LA-ICPMS. Additionally, field observations will accompany this geochronological study because it is important to assess whether the units are primary volcaniclastics (i.e., pyroclastics) originating directly from explosive or effusive eruption, or are secondary volcaniclastics originating from post-volcanic re-sedimentation process.

Table 4.1. All five samples from the Suurberg Group collected from the different formations and locations and analysed between 2016 – 2017 in two annual analytical campaigns.

Sample code	Location	Formation	Analytical campaign
ASP1	Beyers Vlei Outspan	Mimosa	2
ASP2	Gorie Laaghte	Mimosa	3
ASC3*	Slagboom	Unknown	3
ASUP*	Slagboom	Coerney	3
ASLO	Slagboom	Coerney	3

4.2 Results

4.2.1 Field observations

Beyers Vlei Outspan (sample ASP1)

The Suurberg Group exposures at Beyers Vlei Outspan, in the panhandle of the Algoa Basin (Fig. 4.1) are limited to cuttings along an unnamed farm road, adjacent a small ephemeral stream, and at several 'koppies' or ridges that punctuate the otherwise relatively flat topography. There is a general dip of 10 – 25 º N in the Suurberg Group in the region and a subsequent northward younging direction with the basalmost Slagboom Formation resting on Cape Supergroup basement (Fig. 4.2A). The Coerney Formation does not outcrop at Beyers Vlei Outspan as it is entirely covered by alluvium and loose scree, presumably because its less competent tuffaceous-dominated rock types are preferentially eroded. The overlying Mimosa Formation is also not well exposed, apart from several of the volcaniclastic interbeds in the mostly basaltic unit. These form positive features that protrude through scree and highly weathered basalt and are all comprise of massive pink tuffaceous sandstones, one of which was sampled (Fig. 4.2B).

Gorie Laaghte (sample ASP2)

The Suurberg Group sparsely outcrops at Gorie Laaghte, situated 12 km ESE of Beyers Vlei Outspan, also along the southern margin of the panhandle (Fig. 4.1). However, a few roadside cuttings can be found along a farm road that expose the Slagboom Formation and the lower part of the Coerney Formation, although the latter unit is extremely weathered. Stratigraphically overlying these, and further to the north, the Mimosa Formation is similarly poorly exposed. However, there are abundant loose, *ex situ* cobbles and boulders of pink tuffaceous sandstones adjacent the road that were clearly excavated during its construction and maintenance (Fig. 4.2C). The absence of a river or steep slope that could have aided the transportation of these boulders by more recent alluvial or colluvial processes suggest indeed that the boulders are likely derived from the immediate underlying volcaniclastic interbeds in the Mimosa Formation (Fig. 4.1).They exhibit surficial white staining, which was removed with the hammer during sampling, and are otherwise unweathered (Fig. 4.2D). 2 kg of this material was collected from three lithologically identical boulders.

Slagboom (samples ASLO, ASLUP and C3)

The Suurberg Group is exposed at Slagboom farm in the northern Algoa Basin (Fig. 4.1). Unfortunately, due to the recent construction of a game fence the historical roadside outcrops visited by Hill (1972) are completely destroyed and the only evidence that remains of the strata there are *ex situ* fragments of basalt and various tuffaceous rocks. One 45 cm boulder of unweathered light brown, massive tuffaceous sandstone was collected (sample C3), although it is unclear whether it was derived from the Coerney Formation or a volcaniclastic interval in the overlying Mimosa Formation. Fortunately, newly discovered superior exposures of the Suurberg Group exist nearby. A small farm track ~700 m east of the main Slagboom road intersects the Coerney Formation and exposes various unweathered volcaniclastic lithologies that are rarely exposed elsewhere (Fig. 4.2E). Three lithologies, each forming discrete layers, are exhibited in the outcrop, which overlie quarzitic breccias of the Slagboom Formation. These include: i) a basal, massive, beige and orange tuffaceous sandstone with poorly structured accretionary pellets and rare quarzitic pebbles (Fig. 4.2E, F); ii) an overlying breccia bed of variable thickness with angular clasts that are comprised of the same lithology that occupies the lower tuffaceous interval, as well as quarzitic clasts; iii) an uppermost pale green-white tuffaceous interval with extremely rare accretionary pellets and no quartzite clasts. The lower and upper tuffaceous intervals were collected (samples ASLO and ASUP, respectively) because they appear predominantly volcanic origin with minimal detrital input. Further, these two units are typical lithologies intersected by boreholes drilled through the Coerney Formation (Hill, 1972; Marsh, 2016).

Fig. 4.2. (Following page). Geological context of the Suurberg Group samples in the northern Algoa Basin. (A) N-S cross section along service road at Beyers Vlei Outspan, where the Suurberg Group is exposed (inset). Yellow star indicates the position of the ASP1 sample in map-view. Blue dashed line indicates a perennial river. (B) Field appearance of the raised koppies and ridges are composed of tuffaceous rocks that are more resistant to erosion than surrounding basalts. White arrow indicates sampled unit. (C) Roadside occurrence of *ex situ* tuffaceous boulders and cobbles Gorie Laaghte. (D) Close-up photograph of one of the sampled cobbles in Fig. 2C, exhibiting the unweathered pink tuffaceous lithology and white weathered surface. (E) Fresh outcrop of three lithological units in the Coerney Formation exposed along a farm road at Slagboom. The deposit consists of a light grey massive tuffaceous sandstone (i), breccia (ii)and massive silty sandstone with accretionary pellets (iii). White arrows point to the two sampled units. (F) Close-up of the lowermost interval in Fig. 2E exhibiting constituent accretionary pellets and quartzite clasts. White arrows point to accretionary pellets and the colourless arrow indicates a quartzite clast


A
Alluvium
Conglomerate
Sandstone
Uitenhage Grp.
Basalt
Volcaniclastics
Breccia
Suurberg Grp.
Basement
200 m
N
200 m
N
B
25 cm
C
D
2 cm
E
i
ii
iii
1 m
F
2 cm

4.2.2 U-Pb Geochronology

Beyers Vlei Outspan (sample ASP1)

Zircon crystals from this sample vary in size (~50 - ~100 μm) and shape, with common angular fragments or rounded grains and are rarely euhedral. Most are colourless although some were orange-pink presumably due to oxide staining that gives the entire rock a pinkish hue. Internally, their CL images show a great diversity of morphologies, with oscillatory zonation being common, although not always present (e.g., crystal 99 in Fig.4.3). Most Jurassic crystals show bright luminescence. The highest number of concordant dates (73 out of 105) of all five samples from the Suurberg Group is found in this sample. These range from Mesozoic (~36 %), Palaeozoic (36 %) and Precambrian (~28 %) and occupy a single youngest Jurassic peak at ~181 Ma (YPP) and several older subordinate peaks (Fig. 4.5; Table B1 in Appendix B; Fig. C1 in Appendix C). The youngest date in this dataset is 175 ± 4 Ma (YSG), while the youngest modelled date (YDZ) is at 172 +3.2/ -4.7 Ma (95% conf.). The presence of a few zircons that appear younger than the peak age of the youngest population is likely a reflection of subtle Pb-loss and not interpreted as actual younger components. We therefore consider ~181 Ma the most robust measure of the maximum deposition of this unit.

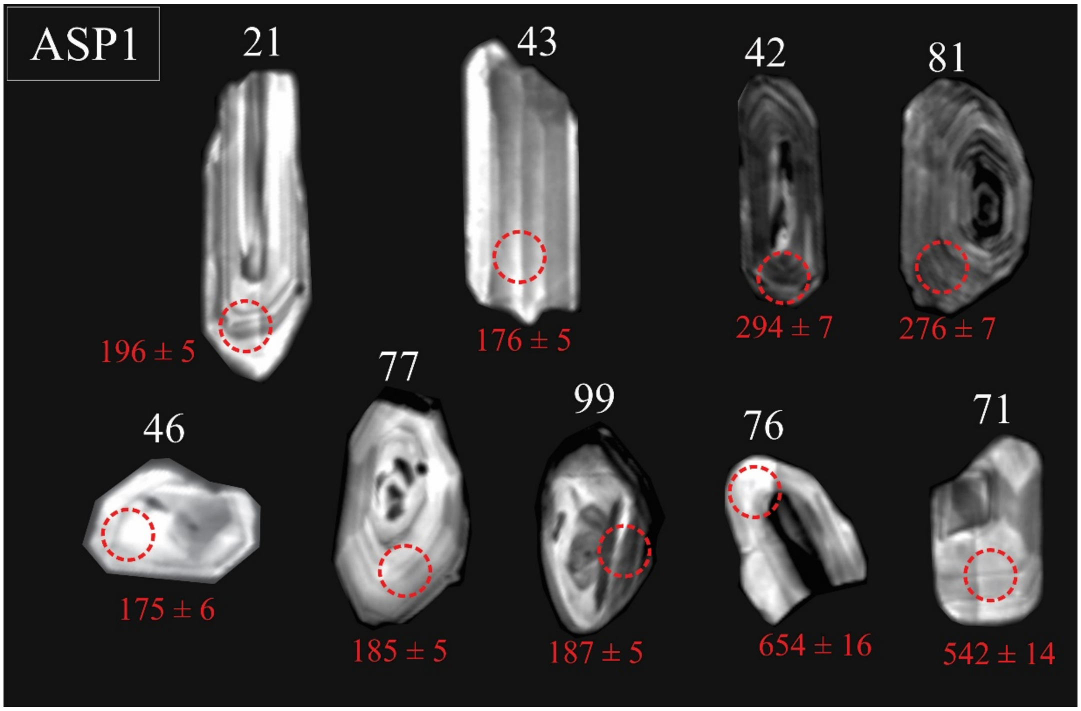

Fig. 4.3. Composite diagram of CL images of zircons that yield concordant dates from sample ASP1, Suurberg Group. Individual zircon indicated by white number; analytical spot (26 µm diameter) with respective $^{206}Pb/^{238}U$ date are in red.

Gorie Laaghte (sample ASP2)

Zircon crystals from this sample vary in size (~60 - ~120 µm) and shape, with common angular fragments or rounded grains and are rarely euhedral. Crystals were either colourless, beige or light orange. Internally, the crystals also show diversity, with common oscillatory zonation (e.g. crystals 1.2 and 1.10 in Fig. 4.4), although not always present (e.g., crystal 1.12 and 2.2 in Fig. 4.4) and in some cases CL images were too obscured to adequately determine the internal morphological character (e.g., crystal 2.41 and 2.50 in Fig. 4.4). Of the 88 zircons analysed, 64 yield concordant dates that span the Mesozoic (~34 %), Palaeozoic (~42 %) and Precambrian (~24 %) and comprise multiple age peaks. The youngest and largest population peaks at 181 Ma (YPP), with additional smaller Mesozoic peaks, and numerous Palaeozoic and Precambrian peaks (Fig. 4.5; Table B2 in Appendix B; Fig. C2 in Appendix C). The youngest population is attributable to the volcanic source inherent to the tuffaceous rock, while older peaks likely reflect detrital input during post- or syn-depositional resedimentation. Other analytical metrics are: YSG = 174 ± 3 Ma;

YDZ = 173.5 +2.5 / -3.5 Ma at (95% conf.). We consider the ~181 Ma graphical peak (YPP) as a robust measure of the youngest age component and maximum depositional age of unit.

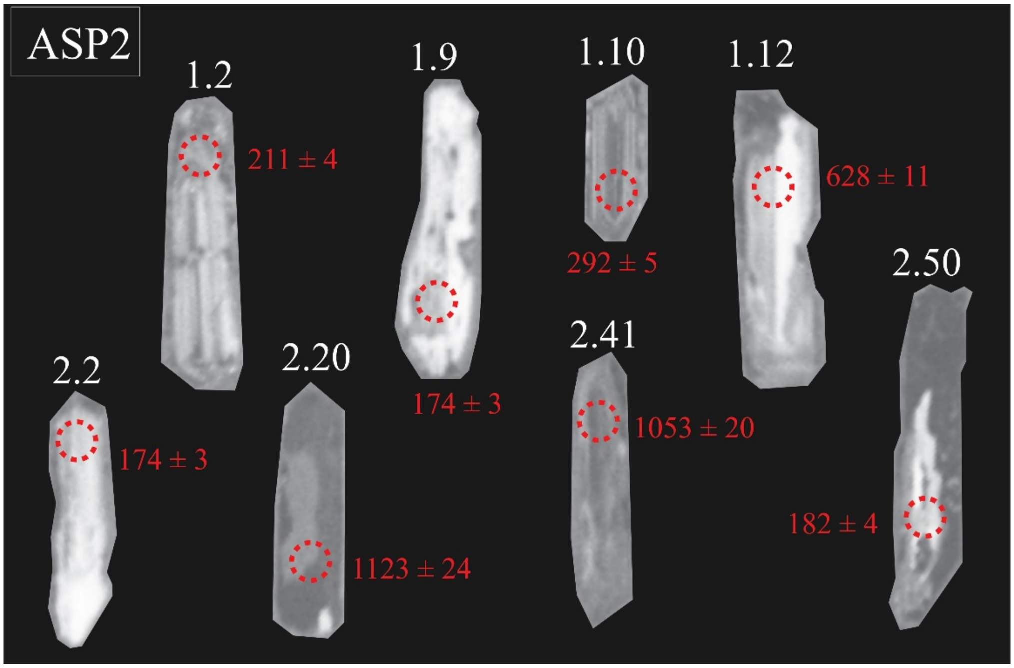

Fig. 4.4. Composite diagram of CL images of zircons that yield concordant dates from sample ASP2, Suurberg Group. Individual zircon indicated by white number following the system in Table B2 in Appendix B, analytical spot (26 µm diameter) with respective $^{206}Pb/^{238}U$ date are in red.

Fig. 4.5. (following page) Concordant $^{206}Pb/^{238}U$ dates for the five volcaniclastic deposits displayed as cumulative age probability diagrams (above) and as normalized probability density diagrams (below), where such that the coloured areas are equivalent for each sample. The age depicted for each sample is that which corresponds to the youngest graphically defined peak in this distribution (YPP). n = number of concordant dates.

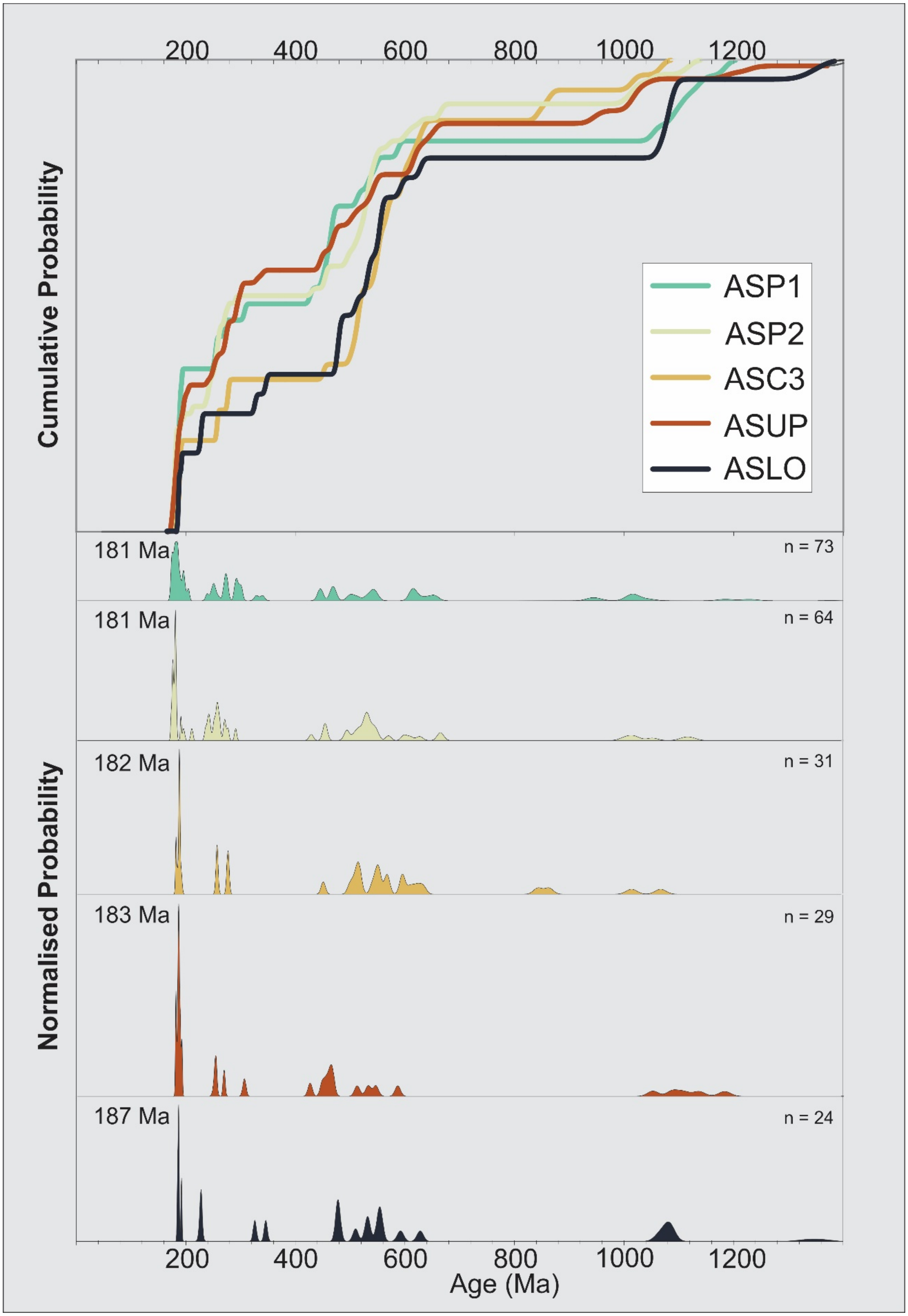

200
400
600
800
1000
1200
Cumulative Probability
ASP1
ASP2
ASC3
ASUP
ASLO
181 Ma
n = 73
181 Ma
n = 64
182 Ma
n = 31
183 Ma
n = 29
187 Ma
n = 24
Normalised Probability
200
400
600
800
1000
1200
Age (Ma)

Slagboom, central northern Algoa Basin

ASC3

Zircon crystals from this sample vary in size from 80 to 200 µm and have predominantly prismatic and some stalky habits. They are commonly angular fragments or show significant rounding and are rarely euhedral. Most crystals are colourless although some are orange-pink presumably due to oxide staining that gives the entire rock a pinkish hue. Internally, their CL images show a great diversity of morphologies, with oscillatory zonation being common (e.g., crystal 1, Fig. 4.6), although not always present (e.g., crystals 36 and 37, Fig. 4.6). In most cases, Jurassic aged zircons show typically brighter luminescence than older crystals (Fig. 4.6).

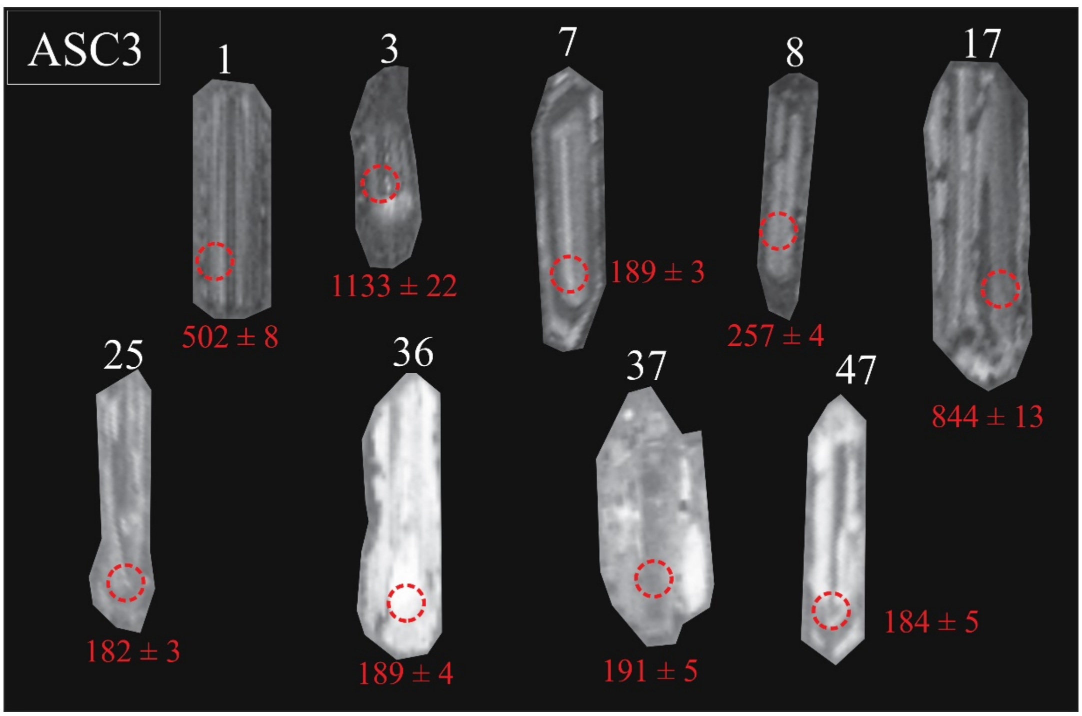

Fig. 4.6. Composite diagram of CL images of zircons that yield concordant dates from sample ASC3, Suurberg Group. Individual zircon indicated by white number; analytical spot (26 µm diameter) with respective $^{206}Pb/^{238}U$ date are in red.

Of the 54 zircons analysed, 36 yield concordant dates that span the Mesozoic (~17 %), Palaeozoic (~39 %) and Precambrian (~44 %) and comprise multiple age peaks. The youngest and largest population peaks at 181 Ma (YPP), with additional smaller Mesozoic peaks, and numerous Palaeozoic and Precambrian peaks

(Fig. 4.5; Table B3 in Appendix B; Fig. C3 in Appendix C). The youngest population of zircons with a peak at ~182 Ma is attributable to the volcanic source inherent to the tuffaceous rock, and older populations are likely derived from detrital input during post or syn-depositional resedimentation. Other analytical metrics are: YSG = 182 ± 3 Ma; YDZ = 181.9 +3.1 / -3.3 Ma (95% conf.). We consider the ~182 Ma graphical peak (YPP) as a robust measure of the youngest age component and maximum depositional age of unit. This estimation is corroborated by other metrics, which suggests that Pb-loss is negligible in this sample.

ASUP

Zircons from this sample have considerable morphological variation, both externally and internally. Small, rounded, euhedral and fragmentary ~50 µm crystals are common, and sizes range to ~120 µm. Most of the euhedral crystals occupy either stubby or stalky habits, and are rarely prismatic. All crystals were colourless or pale beige and have fine or medium oscillatory zoning (e.g., crystals 13 and 23 in Fig. 4.7) and rarely with inclusions (e.g., crystal 74 in Fig. 4.7).

Fig. 4.7. (Following page). Composite diagram of CL images of zircons that yield concordant dates from sample ASUP, Suurberg Group. Individual zircon indicated by white number; analytical spot (26 µm diameter) with respective $^{206}Pb/^{238}U$ date are in red.

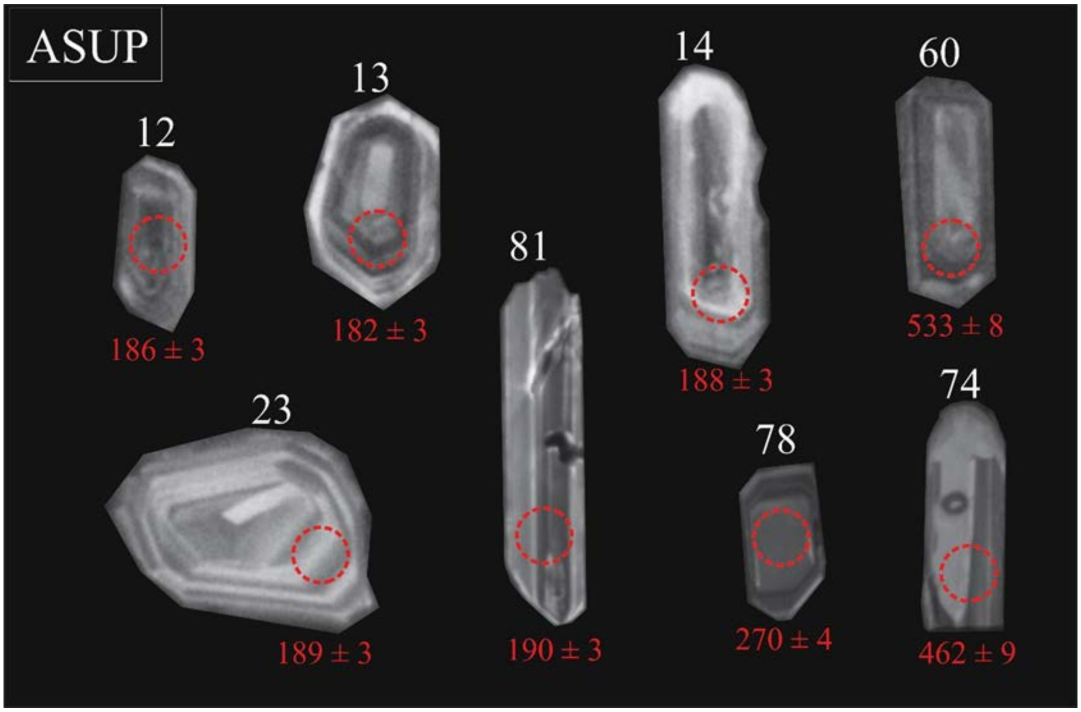

Of the 64 analysed crystals, 29 yield concordant dates, which are Mesozoic (~34 %), Palaeozoic (41 %) and Precambrian (25 %), occupying multiple age populations (Fig. 4.5; Table B4 in Appendix B; Fig. C4 in Appendix C). Of these, the largest and youngest age population is Jurassic and peaks at ~183 Ma (YPP), while older populations are subordinate. The youngest zircon in the sample is 182 ± 2 Ma (YSG) and the youngest modelled detrital zircon (YDZ) is 181.5 +2.5 / -2.9 Ma (95% conf.). All of these metrics overlap and definitively point to maximum deposition at ~183 Ma (YPP).

ASLO

Crystals are very similar in shape, colour and size to those found in the overlying sample ASUP (Fig. 4.2E). They range from 50 to 110 µm, and show either stubby or stalky elongation with rare short prisms. Some crystals are rounded (e.g., crystal 107 in Fig. 4.8), others fragmentary (e.g., crystal 99 in Fig. 4.8), and some euhedral. Internally, they show fine to medium oscillatory zoning, or the zoning is poorly developed. Some crystals have complex growth histories with inherited xenocrystic cores, inclusions and later overgrowths (e.g., crystal 107 in Fig. 4.8), while many do not show any of these features (e.g., crystal 46 in Fig. 4.8).

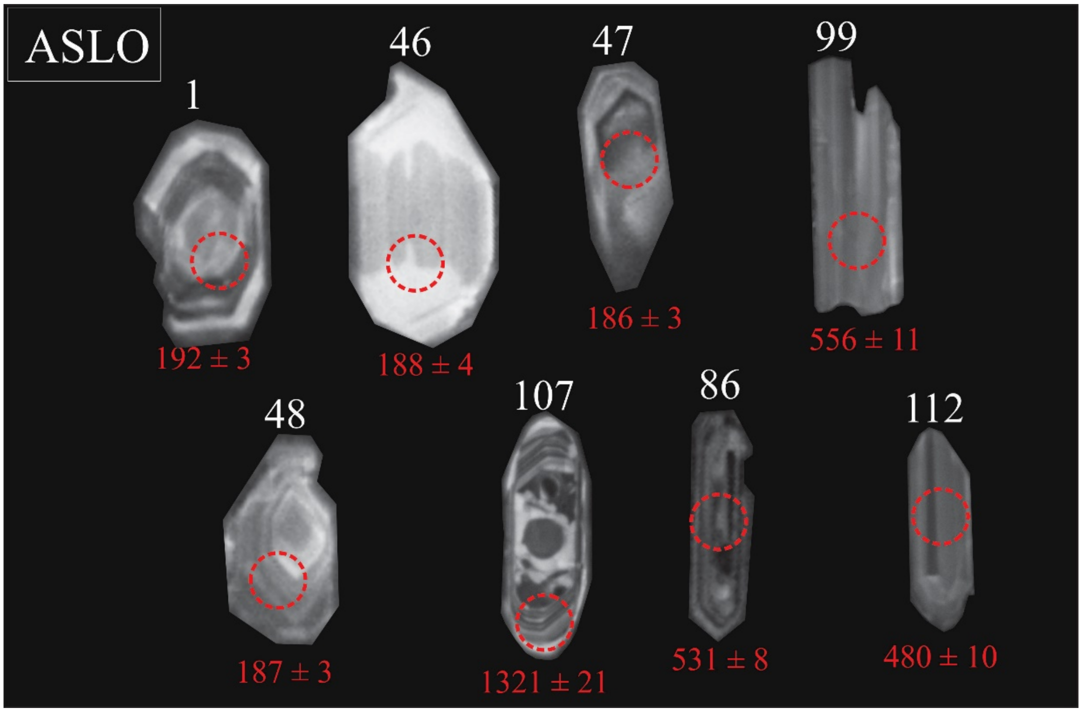

Fig. 4.8. Composite diagram of CL images of zircons that yield concordant dates from sample ASLO, Suurberg Group. Individual zircon indicated by white number; analytical spot (26 µm diameter) with respective $^{206}Pb/^{238}U$ date are in red.

Most of the 85 crystals analysed in this sample are discordant, leaving just 24 concordant dates, ranging from Mesozoic (25 %), Palaeozoic (~33 %) and Precambrian (~42 %). The youngest graphical population (YPP) is Jurassic and peaks around ~187 Ma (Fig. 4.5; Table B5 in Appendix B; Fig. C5 in Appendix C), although it is noted that a large number of discordant 178 – 191 Ma zircons are present in the sample but failed to pass the concordance threshold (Table B5 in Appendix B). The youngest date is 186 ± 3 Ma (YSG), and modelling yields a youngest detrital age (YDZ) of 185.2 +2.4 / -3 Ma (95% conf.). Both these metrics are compatible with a ~187 Ma (YPP) period of maximum deposition for the tuffaceous unit.

4.3 Discussion

Since samples were taken from tuffaceous interbeds within the dated basalts (ASP1 and ASP2), and from below them – in the Coerney Formation (ASC3, ASUP and ASLO) – it can be reasonably assumed that the youngest populations of these clearly mixed-origin volcaniclastic deposits are roughly equivalent to their actual depositional age. We are therefore able to definitively date the Suurberg Group as a Lower Jurassic and possibly Pliensbachian-Toarcian unit, based on the youngest populations of zircons from five volcaniclastic intervals in the Coerney and Mimosa formations that range from ~187 to ~181 Ma (Fig. 4.9). This is compatible with the highly uncertain 194 ± 11.9 Ma Ar-Ar age for basalts from the Mimosa Formation (Kirstein, 1997) and strongly suggests that the previously held notions of a younger age for the Suurberg Group based on K-Ar whole rock techniques reported by McLachlan and McMillan (1976) are spurious (Fig. 4.9).

Given the relatively imprecise U-Pb techniques employed here and the lack of primary pyroclastic deposits recovered from the Suurberg Group volcaniclastic intervals and the use of a graphically-defined youngest age component, there still remains a fairly large yet quantitatively undefined uncertainty associated with its Lower Jurassic age interpretation. Nevertheless, these new ages are compatible with the emplacement of the volumetric Karoo (183.0 ± 0.5 – 182.3 ± 0.6 Ma) and Ferrar (182.779 ± 0.033Ma – 182.430 ± 0.036 Ma) large igneous provinces (Svensen et al., 2012; Burgess et al., 2015). The new ages for the Suurberg Group are also compatible with an imprecisely dated dolerite swarm (188-178 Ma) exposed on the Falkland Islands (Richards et al., 1996; Richards et al., 2013), which was also relatively close to the northern Algoa Basin during the Early Jurassic (Jokat et at., 2003; Macdonald et al., 2003).

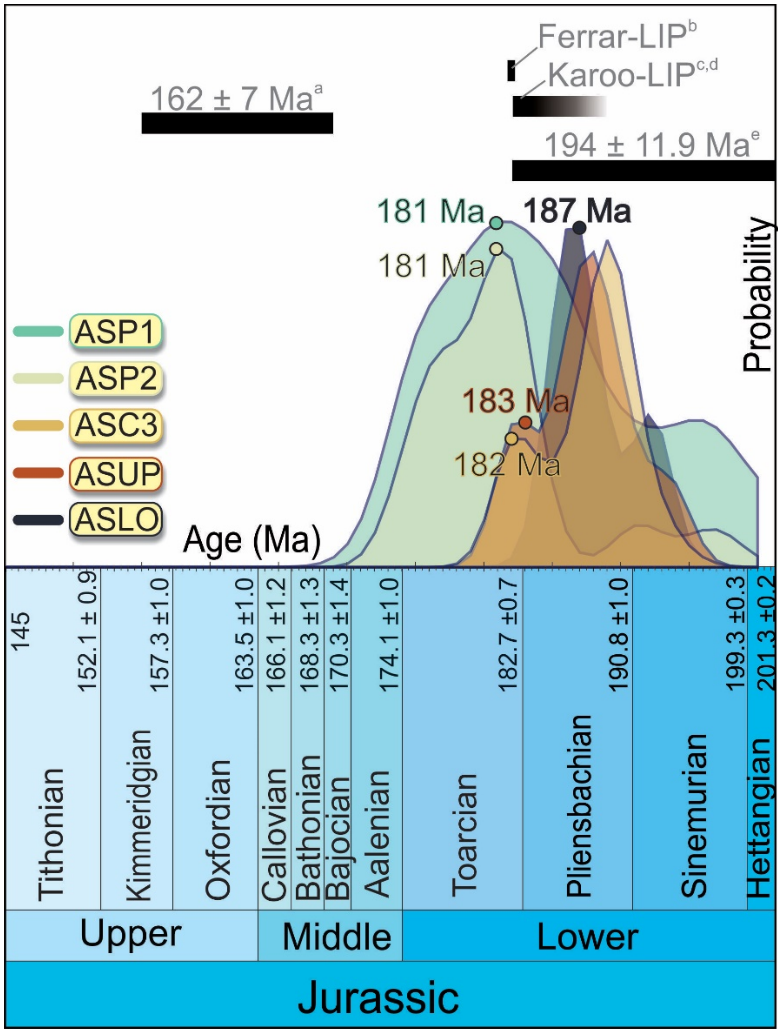

Fig. 4.9. Youngest age populations for each of the five samples plotted as a probability density diagrams along the timescale of Cohen et al., (2013) for the Jurassic, with corresponding graphically defined peaks (YPP). Crystallization ages for the Karoo and Ferrar large igneous provinces, and two historic ages of the Suurberg Group are plotted as horizontal black rectangles representing the associated 2σ error. a = McLachlan and McMillan, (1976); b = Burgess et al. (2015); c = Svensen et al. (2012); d = Moulin et al. (2017); e = Kirstein (1997).

Although dating the Suurberg Group by U-Pb methods has been a success, and this enables a definitive Lower Jurassic ~187 to ~181 Ma age determination, its exact age and correlation is still somewhat ambiguous based on the U-Pb data alone. However, it seems that the most parsimonious interpretation is that of Marsh (2016), who poroposes that the basalts in the Mimosa Formation are the distal expression of

Karoo continental flood basalts rather than the result of incipient volcanism in the Cape Fold Belt based on geochemical evidence. These new U-Pb data are consistent with the correlation between the Suurberg and Drakensberg groups and the most likey age for the Suurberg Group is therefore Pliensbachian – Toarcian, a time when there was extensive volcanism in SW Gondwana (e.g., Svenson et al., 2012; Burgess et al., 2015).

While there appears to be an association of the Suurberg Group with the contemporaneous Karoo and Ferrar large igneous provinces, its genesis and significance in the Mesozoic breakup of SW Gondwana remains somewhat enigmatic. In order to assess these aspects of the Group, its field relationships need to be described in detail, something that remains extremely challenging considering the exceptionally poor outcrop quality in the basin. An important question that remains unanswered is whether the Suurberg Group is a pre-rift or syn-rift succession within the Algoa Basin. The new U-Pb ages reported here are consistent with geochemical correlations with basalts of the Drakensberg Group of Marsh (2016) who proposed that the basalts in the Mimosa Formation are the distal expression of Karoo continental flood basalts rather than the result of incipient volcanism in the Cape Fold Belt. Nevertheless, this does not lend insights into whether the basalts were deposited into an actively subsiding Algoa Basin, or on a land surface that was downfaulted by subsequent rifting – either situation is possible. In order to answer this question, which relates to the overall significance of the Lower Jurassic unit in Gondwanan breakup, it needs to be determined whether: 1) the volcaniclastic units in the Coerney Formation underlying the basalts and those within them are derived from the same mafic volcanic source during the Karoo or Ferrar LIP events, or are entirely unrelated contemporaneous units; and 2) there is a hiatus between the Suurberg Group and the overlying clearly rift-related Uitenhage Group. Neither of these questions can be answered unequivocally in this chapter, although some thoughts are shared below.

The volcaniclastic interbeds found in the principally basaltic Mimosa Formation are considered especially important in determining the mechanism for the Suurberg Group deposition but the lack of quality outcrop makes describing field relationships difficult. Hill (1972) initially considered some of these units as ‘tuff dykes' that postdate and cross-cut basaltic intervals. Marsh (2016) suggests instead that flood basalts sourced from the north invaded poorly consolidated and recently deposited volcanicalstics to simply give the appearance of dykes, which removes the necessity for an incipient volcanic genesis for the Group. The new U-Pb data from five volcaniclastic deposits throughout the Mimosa and Coerney formations show that they are all roughly contemporaneous Pliensbachian – Toarcian. However, in order to assess whether any of the volcaniclastic interbeds in the Mimosa Formation are in fact dykes that postdate the deposition of basalt one needs to attain higher precision geochronological constraints on each of the lithologies, excavate a region in order to assess relative stratigraphic context and field relations, and date primary ash beds that have not been resedimented. Each of these tasks requires considerable effort and is beyond the scope of this study. One of the concerns raised by Marsh (2016) is that the source of the volcaniclastic material. The presence of ash beds in the upper Karoo Supergroup that have a Patagonian silicic volcanic source (e.g., Bordy and Abrahams, 2016), and outcrop commonly in the main Karoo Basin, invokes the possibility that the same volcanic source is responsible for the tuffaceous lithologies of the Suurberg Group (Marsh, 2016). Another distal origin for the ash is from the Karoo LIP, where volcaniclastic rocks are formed by explosive mafic volcanism under certain phreatic conditions (e.g., Lock et al., 1974; Holzförster, 2007; McClintock et al., 2008). Perhaps the volcaniclastic material was transported south from sites in the main Karoo Basin at ~183 Ma both before and during the flood basalt deposition. One of the problems with the Karoo LIP being a source for the tuffaceous rocks is that they contain an abundance of young, syn-depositional zircons, which is not the case in the zircon-poor flood basalts in the Drakensberg Group (Svensen et al., 2012). Nevertheless, the youngest zircons do look superficially similar to those recovered from rare intervals in the mafic subvolcanics of the Karoo LIP (see fig. 2 in Svensen et al., 2012), although morphological characterization of zircons of the Karoo LIP has not been carried out and would be necessary for a robust comparison to be made. Instead, future researchers interested in ascertaining whether the volcaniclastics of the Suurberg Group are derived from the Karoo LIP, or elsewhere might consider geochemical fingerprinting of the youngest zircons analysed in this study using trace element (Belousova et al., 2002) and Hf isotopes (Anderson et al., 2009).

In order to determine whether there is a hiatus between the Suurberg and Uitenhage Groups, improved chronology of the latter strata needs to be established. If the age of the lowermost Uitenhage Group were known, then the difference in age may be used to assess their stratigraphic relationship. If they are unconformable, differing in age to a large extent, then it is likely that rifting and subsidence in the Algoa Basin, and by inference extension in the southern Cape, occurred after the Karoo and Ferrar LIPs and not during it. Alternatively, if they are conformable, then it is probable that extension began during the emplacement of the Suurberg Group in the late Early Jurassic. Unfortunately, the lack of quality outcrops, especially of the contact between the two Groups, hinders any direct geological assessment of the contact. Further, it is not possible to determine whether the Suurberg Group was deposited during normal faulting or prior to it, whereas the deposition of the Uitenhage Group clearly coincides with active faulting – evidenced by the presence of syn-depositional faults (e.g., Shone, 1976, 2006; Tankard et al., 1982). The geochronology of the clearly rift-related Uitenhage Group follows in Chapter 5, which provides the basis for determining the breakup-history of SW Gondwana in the southern Cape. The new U-Pb data presented here has conclusively demonstrated a late Early Jurassic (Pliensbachian – Toarcian) age for the Suurberg Group and hopefully puts to rest the quoting of spuriously young and poorly recorded historic ages for the unit. Further, because the Suurberg Group underlies and is therefore older than the Uitenhage Group, its confirmed late Early Jurassic age pushes back the maximum age constraint for the Uitenhage Group from the frequently quoted Upper Jurassic (e.g., Green et al., 2016; Richardson et al., 2017; Baby et al., 2018) and raises the new possibility that the Uitenhage Group is older than previously envisioned.

Chapter 5: Chronostratigraphic framework for the Uitenhage Group

5.1 Introduction

Syn-rift deposits provide the only means to determine the processes for initiation and early history of fragmenting continental plates that led to the formation aulacogens, rift basins, and potentially even passive continental margins. Dating these early rift-related successions in various extensional settings has enabled considerable progress in understanding important tectonic, plate kinematic and geodynamic processes (e.g., Roberts et al., 2012). Unlike in other well-studied Mesozoic rift-related settings where syn-rift strata contain contemporaneous fault bound volcanic units, such as in the Newark basins of eastern North America (e.g., Sutter, 1988; Olsen, 1997), volcanism did not occur in the southern Cape during extension, and therefore there is a scarcity of datable volcanic interbeds that might have conveniently provided a means to determine the chronological evolution of rifting in this region. Although the Suurberg Group has been demonstrated to be Lower Jurassic, and contemporaneous with the Karoo and Ferrar LIPs (Encarnación et al., 1996; Burgess et al., 2015; see Chapter 4), its relation to the overlying syn-rift Uitenhage Group remains unclear (Hill., 1972; McMillan et al., 1997) and therefore can only provide a maximum age constraint to the Mesozoic rifting in the southern Cape. These U-Pb age constraints, presented in Chapter 4, already challenge previous assertions that the Uitenhage Group is no older the Upper Jurassic, and open the possibility that rifting in the southern Cape began earlier that previously understood. Here, we date zircons from the syn-rift Uitenhage Group in a number of onshore basins in the southern Cape using the U-Pb decay system with LA-ICPMS and CA-TIMS analytical methods in order to directly assess the age of the accommodated syn-rift strata and elucidate the evolution of rifting recorded in these strata.

Necessarily, this chapter presents a large database of U-Pb ages from zircons from pyroclastic, volcaniclastic and terrigenous clastic rock samples in order to constrain the timing of deposition of the Uitenhage Group in eight isolated basins and between isolated outcrops within each. These data are integrated with all other available chronostratigraphic information where possible in order to synthesize the chronostratigraphy of each basin (section 5.3) and then later build a chronostratigraphic framework for the entire southern Cape (section 5.4). As a cautionary note, pyroclastic deposits, due to their primary volcanic origin, are considered here as the most reliable means to determine a true depositional age, while volcaniclastic and terrigenous clastic rock samples are secondary as they can only provide maximum depositional ages of strata. This is an important distinction that will be reflected in the results section of this chapter where data is presented strictly on a basin-by-basin basis regardless of the medley of data types (detrital U-Pb and primary volcanic U-Pb). The decision to lay out the data in this fashion has been made following two practical considerations: 1) future workers considering palaeoenvironmental, palaeontological or lithological changes through time and depth benefit from considering individual basins rather than the entire Uitenhage Group across discontinuous basins; 2) the data are integrated closely on stratigraphic grounds, so that where one sample defines an age of maximum deposition, a sample from an overlying deposit with a true depositional age (in this or future studies) may provide constraints on the enveloped interval by stratigraphic bracketing.

The intensive Late Cretaceous and Cenozoic erosion of the southern Cape (e.g., Tinker et al., 2008a; Wildman et al., 2015; Green et al., 2016) has resulted in the severely discontinuous exposures of the Uitenhage Group that are themselves contained in the isolated erosional remnants of rift basins (Muir et al., 2017a, b). Therefore, it is deemed necessary to sample from a wide area, in as many parts of as many basins as possible in order to minimize potential geographical biases. In accordance, the dataset presented below consist of 33 samples spanning eight basins in the southern Cape (Table 5.1). Three of the tabled samples (i.e., AK5, ASH1 and RAE) were investigated by Isabel van Breda, under my close supervision from data collection to processing, as part of her BSc honours project at the University of the Western Cape in 2017 (van Breda, 2017). Sample processing procedures and equipment used in analyzing these three samples are identical to those described in section 3.2.2.1 of Chapter 3, and can therefore be meaningfully integrated with the rest of the samples presented in this section for a more complete and robust chronostratigraphic framework across the southern Cape.

Table 5.1. All samples from the Uitenhage Group collected from eight basins in the southern Cape and analysed from 2015 – 2018 in four annual analytical campaigns. * = van Breda (2017).

Sample code	Basin	Analytical campaign
ROBE	Robertson	3
AK5*	Robertson	3
ASH1*	Robertson	3
RAE*	Robertson	3
HBUP	Heidelberg	1
HBMB	Heidelberg	1
HBMill	Heidelberg	3
HBUE1	Heidelberg	3
KLIP	Mossel Bay	2
MATJ	Mossel Bay	3
SITT2	Mossel Bay	1
SITT3	Mossel Bay	1
VOEL	Mossel Bay	1
MBHF	Mossel Bay	4
OES1	Oudtshoorn	4
CALI	Oudtshoorn	2
DERU	Oudtshoorn	1
DERC1	Oudtshoorn	3
OKT1	Oudtshoorn	4
KNYE	Knysna	4
BREN2	Knysna	3
PLETT	Plettenberg Bay	1
RBGS1	Plettenberg Bay	4
GKT1	Gamtoos	4
GES3	Gamtoos	4
AECOC	Algoa	3
AKIRK	Algoa	3
AKSTR	Algoa	3
KDUNS	Algoa	3
KBCS2	Algoa	4
KBEZS1	Algoa	4
KWAS3	Algoa	4
SRFS1	Algoa	3

5.2 Basin-by-basin chronostratigraphy

5.2.1 Robertson Basin

The Robertson Basin is located in the vicinity of Robertson and Ashton in the Western Cape Province (Fig. 5.1). It is situated along the Worcester-Pletmos basin line and bounded to the north by the Worcester Fault. The Mesozoic rift strata that occupy the basin, the Enon and Kirkwood formations, rest unconformably atop the Cape Supergroup (Fig. 5.1), which occupies the southern downthrown side of the Worcester Fault immediately surrounding the basin. The presence of the uppermost Cape Supergroup (Witteberg Group) along the southern margin of the Basin and heterolithic diamictite clasts within the conglomerates in the Uitenhage Group indicates that the Dwyka Group probably exists in the subsurface basement beneath the basin depocentre. A ~3 km zone of Precambrian Malmesbury Group outcrops north of the Worcester Fault and beyond this, further north, lie erosion-resistant sandstone and quartzite of the Cape Supergroup that form the Langeberg Mountains. The Robertson Pluton, an easterly outlier of the Cape Granite Suite, lies immediately west of Robertson in the footwall of the Worcester Fault.

Outcrops of the Uitenhage Group are very sparse in the Robertson Basin and limited to several river-cut cliffs in and around Ashton along the banks of the Kogmanskloof River, road-cuttings along the R60, and furrows, road-cuttings and construction sites in the north of Robertson. No formal mapping of sedimentary facies variation was undertaken in the Robertson Basin although our limited observations indicate that finer-grained deposits occupy the central region of the basin, while conglomeratic deposits are closer to the edges. Despite a lack of exposures hindering our understanding of the basin-fill stratigraphy, it is estimated that 1.2 km of Uitenhage Group occupy the basin (Rigassi and Dixon, 1972; Dingle et al., 1983). Although no specific evidence is quoted by these authors, the 215.9 m deep W202 borehole did not reach basement before terminating and thus provides a compatible minimum thickness (see Fig. 8 of Muir et al., 2017b in section 2.2.2 of this thesis).

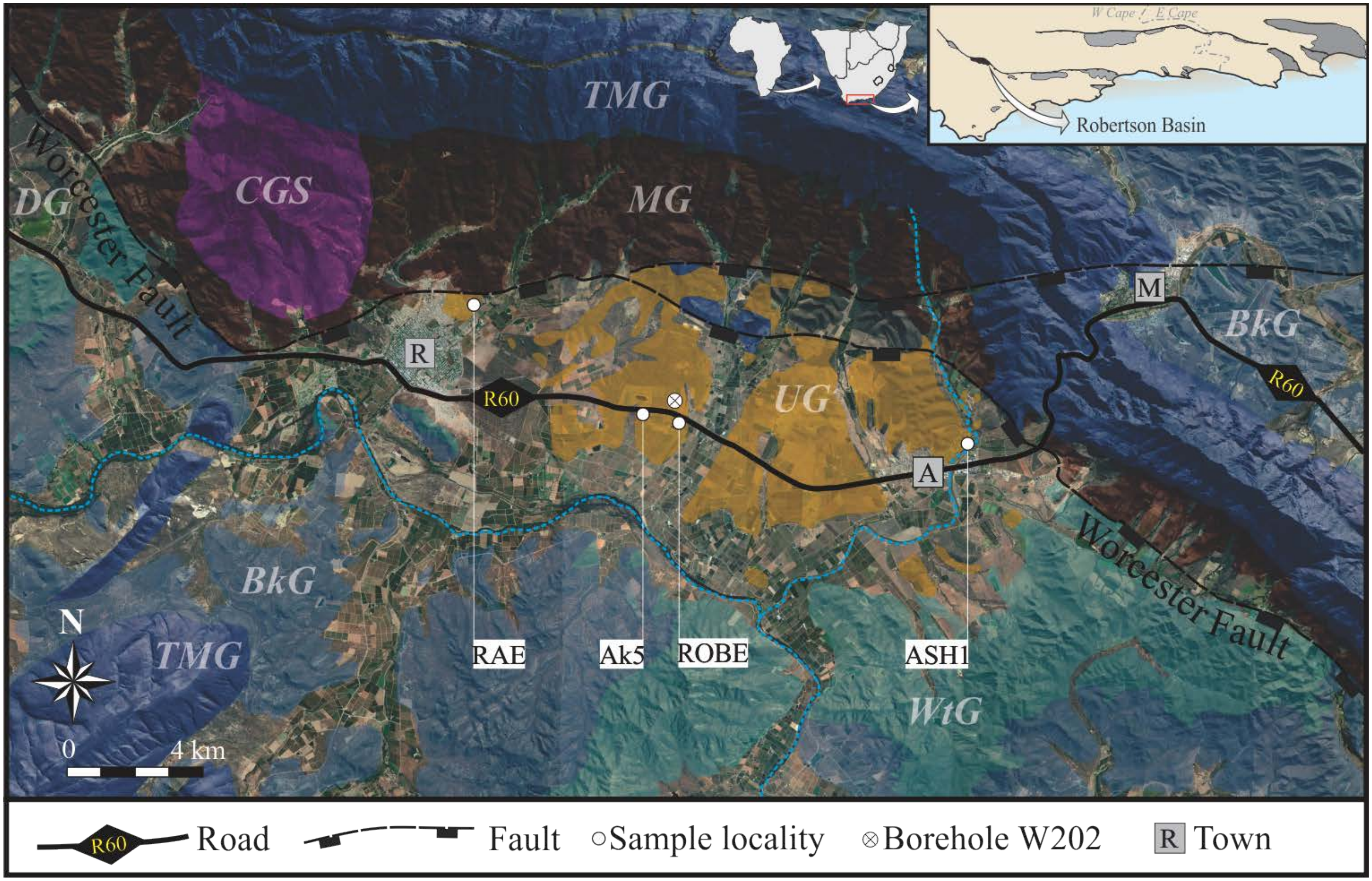

Fig. 5.1. Simplified geological map of the Robertson Basin. Letters and colours are lithostratigraphic units and unshaded areas are recent alluvium. Abbreviations: Towns: A = Ashton; M = Montagu; R = Robertson. Stratigraphic units arranged from oldest to youngest: MG = Malmesbury Group; CGS= Cape Granite Suite; TMG = Table Mountain Group; BkG = Bokkeveld Group; WtG = Witteberg Group; DG = Dwyka Group; UG = undifferentiated Uitenhage Group. Base maps modified from the 1: 250 000 geological maps sheets 3319 (Gresse ,1997) and 3320 (Theron ,1991) of the Council for Geoscience overlain on ESRI satellite imagery.

5.2.1.1 Outcrop description

Central Robertson Basin (samples ROBE and Ak5)

The roadside outcrop (33°49'10.39"S; 19°58'12.35"E; Fig. 5.1) is dominated by 50 cm to 3 m thick laminated red-grey mudstones and poorly developed varicoloured palaeosols and interbedded with subordinate 10 cm to 1 m thick medium-grained red-grey sandstone and massive ~ 2 m thick red oligomitic orthoconglomerate that all dip at ~ 20° to the NW (Fig. 5.2A). A massive, 10 – 50 cm thick, pink montmorillonite-rich bentonite (from which sample ROBE was taken) is interbedded with the laminated mudstones and was sampled. The bentonite is laterally extensive for 10 m before being lost due to outcrop limitations although it presumably extends well beyond the outcrop in the subsurface and is intersected by the nearby borehole W202 at ~17 m depth (Fig. 5.1 ; see Fig. 8 of Muir et al., 2017b in section 2.2.2 of this thesis for detailed log).

A second road-cutting approximately 1 km to the west of this locality along the R60 (33°49'5.09"S; 19°57'28.24"E; Fig. 5.1) comprises predominately 2 – 5 m thick horizontally laminated to massive silty-mudstone beds with subordinate 10 – 30 cm thick grey-brown silty-sandstone and red pebble conglomerate interbeds (Fig. 5.2B). All units dip ~ 45° NE and are largely covered by scree. One of the more prominent silty-sandstone beds was sampled (sample Ak5).

River cutting in Ashton (sample ASH1)

Crudely-bedded conglomerates outcrop in river-cut cliffs in Ashton (33°49'45.08"S; 20° 3'48.12"E; Fig. 5.1) with an overall red colour (Fig. 5.2C, D). Although unmapped previously, these outcrops are assigned here as the Enon Formation given their > 90% conglomeratic content. These predominately clast-supported conglomerates are polymictic with clasts consisting of diamictite, shale, quartzite, gneiss, granitoid, quartz and various other rock types reflecting a source from the Dwyka Group, which outcrops ~10 km to the east and probably exists in the in the basement beneath the Uitenhage Group. Additionally, some of the sandstone, quartzite and shale clasts are probably also derived from the Cape Supergroup. Clasts range from granule to cobble size and are in a coarse-grained sandstone matrix. In some places the conglomerate is matrix-supported, or entirely void of clasts, forming subordinate sandstone lenses, one of which was sampled.

Fig. 5.2. (Following page). Geological context of the Uitenhage Group samples in the Robertson Basin. (A) Laterally continuous sandstones and mudstone beds, with subordinate conglomerate deposits and a bentonite bed exposed at a roadside outcrop in the central Robertson Basin. (B) Sandstones and mudstones exposed in the central Robertson Basin. (C) River-cut cliff face exposing conglomerates of the Enon Formation in Ashton. White dashed line highlights the area enlarged in D. (D) Sandstone lens that was sampled in the conglomerate-dominated deposit. Inset: Typical disc-shaped clast composed of diamictite. (E) Conglomerate deposit exposed NE of Robertson in a weathered road-cutting. Pink arrows point to the precise location from where samples were extracted.

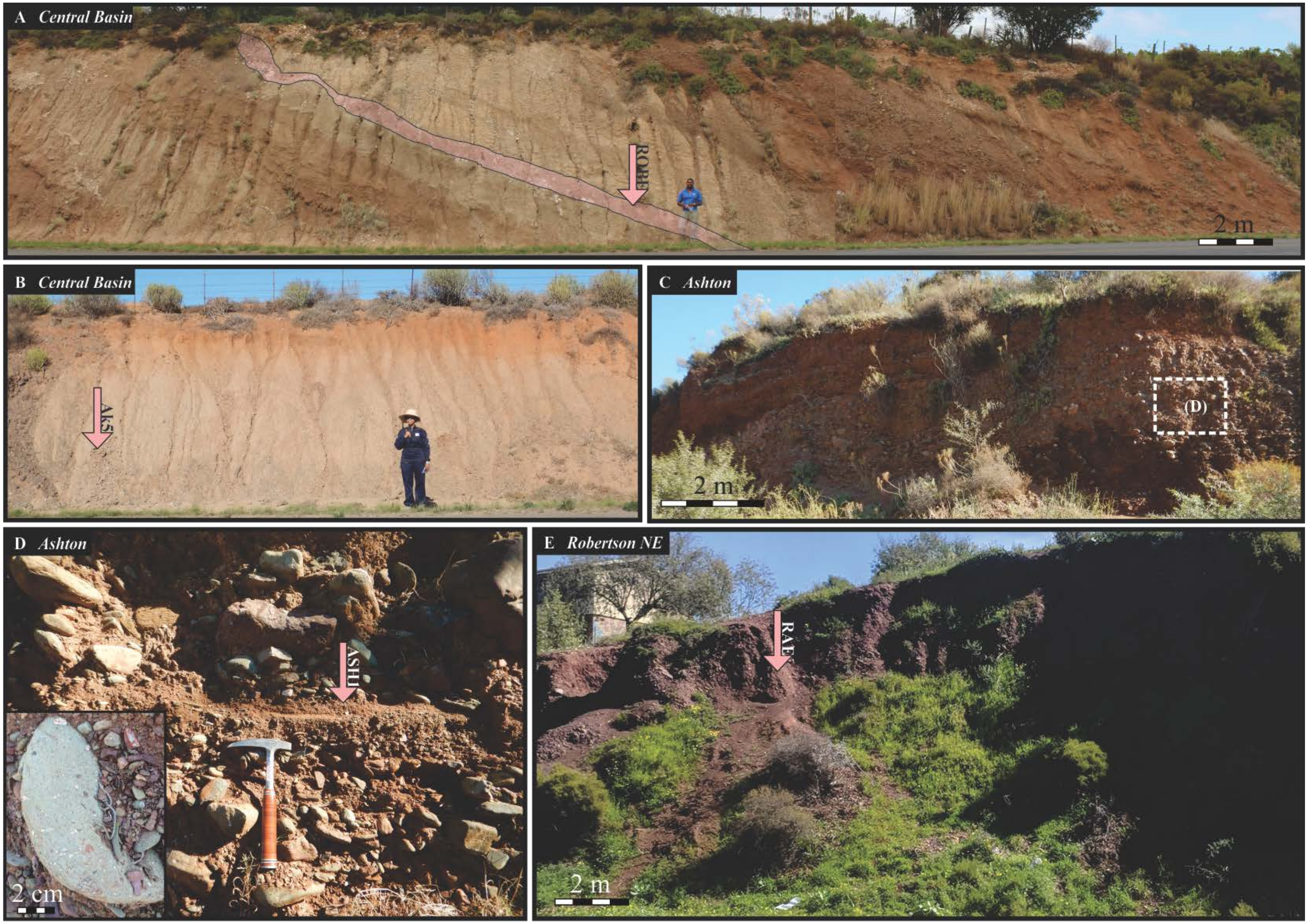
A Central Basin
ROBB
2 m
B Central Basin
AK5
C Ashton
(D)
2 m
D Ashton
ASHJ
2 cm
E Robertson NE
RAE
2 m

Road-cutting NE of Robertson (sample RAE)

Massive to crudely bedded oligomictic clast-supported conglomerates outcrop in an isolated roadside outcrop (Fig. 5.2E) north of Robertson that are assigned the Enon Formation (33°47'36.88"S; 19°54'1.50"E; Fig. 5.1). The sub- to well-rounded cobble clasts are composed of sandstone and quartzites and are probably sourced from Palaeozoic Table Mountain Group. The coarse-grained sandstone matrix of the conglomerate was sampled for its detrital zircon content.

5.2.1.2 U-Pb geochronology

ROBE

The crystals from the ROBE bentonite sample are strongly euhedral and range from needle to short-prismatic in shape, are colourless and have rare inclusions. Overall their lengths range from 50 – 200 µm although the short end of this range is predominately comprised of fragmentary grains. Internal crystal morphology revealed from CL images (Fig. 5.3) show fine to medium oscillatory zoning in all grains with very few exceptions where xenocrystic cores are present (e.g., crystal 8 in Fig. 5.3).

Of the 102 crystals analysed only 42 were concordant and yielded 90% Mesozoic, 7% Palaeozoic, and 3% Precambrian dates (Fig. 5.4; Table D1 in Appendix D; Fig. F1 in Appendix F). The lack of any significant detrital zircons, along with the purity of the massive montmorillonite that makes up the deposit suggests a primary volcanic origin. A single population of around ~ 152 Ma on the probability density diagram (Fig. 5.4) is formed by 38 Mesozoic dates. No concordia age can be calculated when plotted on the concordia diagram because of the relatively large spread of dates that do not all intersect at 2σ error (Fig. 5.5). The TuffZirc algorithm identifies the most coherent population of 35 dates at 151.6 +0.9/-1.0 Ma with 95% confidence (Fig. 5.5), which is considered a reasonable estimate for the age of the bentonite based on the LA-ICPMS data alone. CA-TIMS analyses of 9 crystals yield 6 concordant dates (Fig. 5.6; Table G1 in Appendix G), 5 are within error of each other (at 2σ) and have a weighted mean age of 150.3 ± 0.2 Ma with minimal scatter (MSWD = 0.61). This is interpreted as a depositional age of the pyroclastic deposit despite a single younger date of 141.8 ± 1.3 Ma. This crystal is excluded from the weighted mean calculation because it yielded a non-reproducible result and is interpreted as an outlier that suffered Pb loss due the imperfect chemical abrasion. More aggressive pretreatment and additional analyses would be needed to assess if there is actually a young ~142 Ma component to this deposit that is subordinate to the one at ~150 Ma but there remains a possibility that the unit was deposited approximately at this time. Notably, the weighted ean from the CA-TIMS U-Pb data is slightly younger than the age calculated using TuffZirc, which suggests that the TuffZirc algorithm is affected by subtle inheritance and is slightly too old.

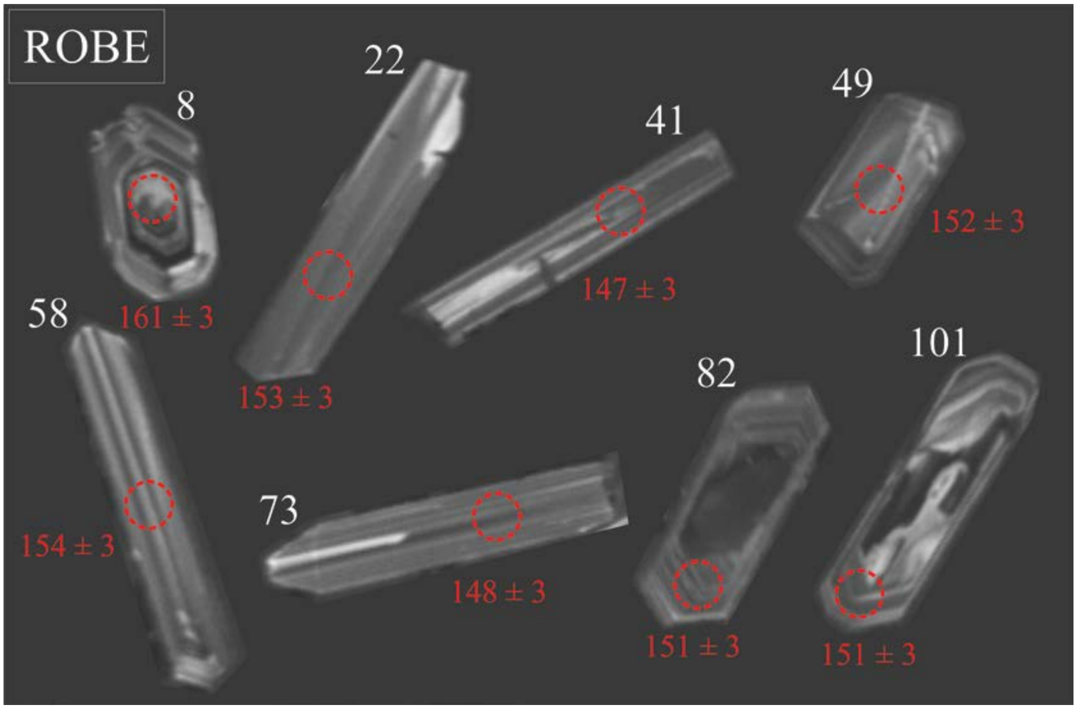

Fig. 5.3. (Following page). Composite diagram of CL images of zircons that yield concordant dates. Individual zircon indicated by white number and analytical spot (26 µm diameter) with respective $^{206}Pb/^{238}U$ date are red.

Fig. 5.4. (Following page). U-Pb dates of zircons from all samples in the Robertson Basin shown as age probability density diagrams (blue area) combined with frequency histograms (grey bars) with 20 Ma intervals. Only concordant data are shown: n = x/y means that x out of a total of y zircons yielded concordant dates. Youngest graphically-defined peak (YPP) is indicated. Note that data for samples AK5, ASH1 and RAE are extracted from van Breda (2016).

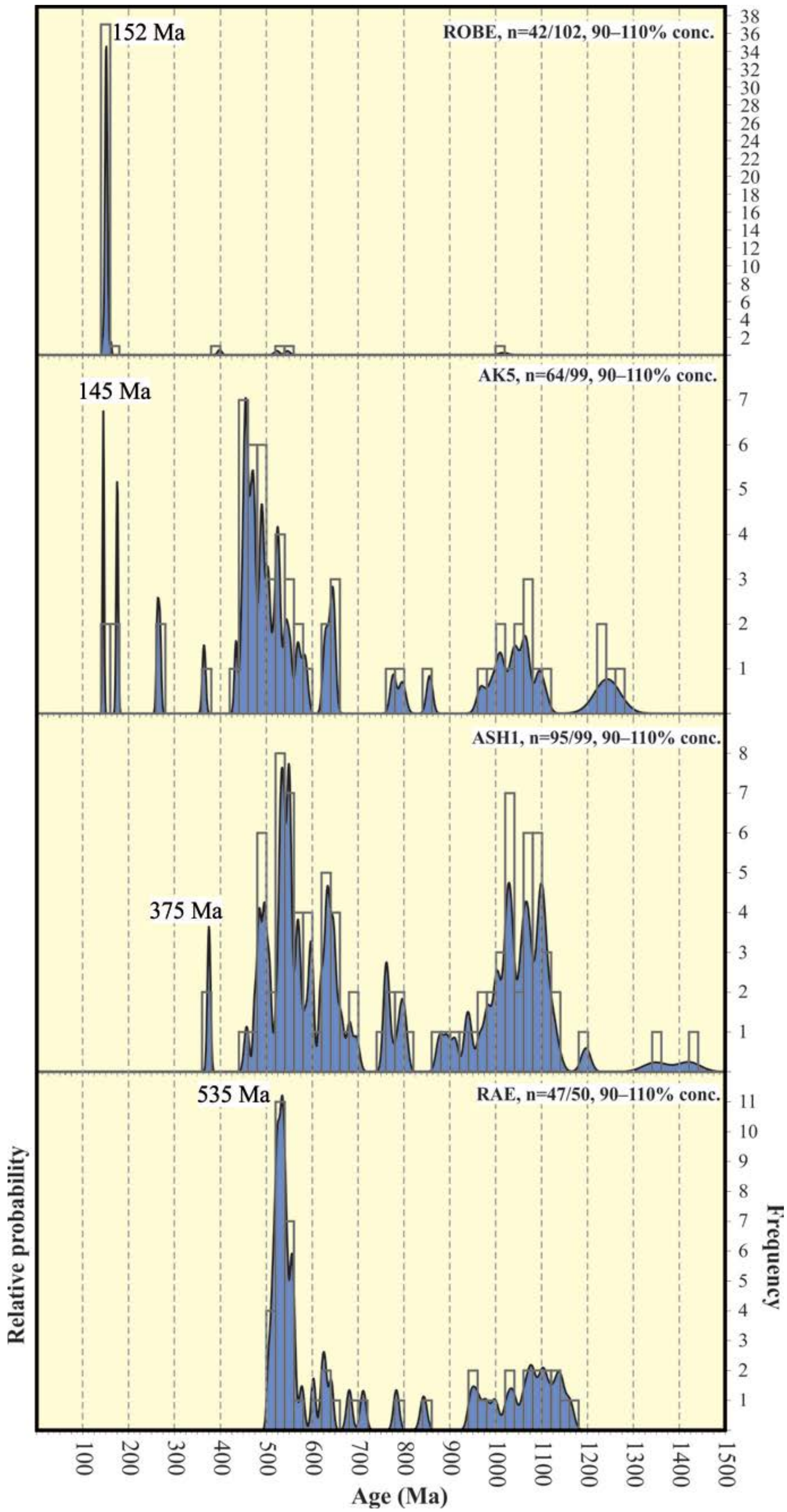
152 Ma
ROBE, n=42/102, 90–110% conc.
145 Ma
AK5, n=64/99, 90–110% conc.
ASH1, n=95/99, 90–110% conc.
375 Ma
535 Ma
RAE, n=47/50, 90–110% conc.
Relative probability
Frequency
Age (Ma)
100
200
300
400
500
600
700
800
900
1000
1100
1200
1300
1400
1500

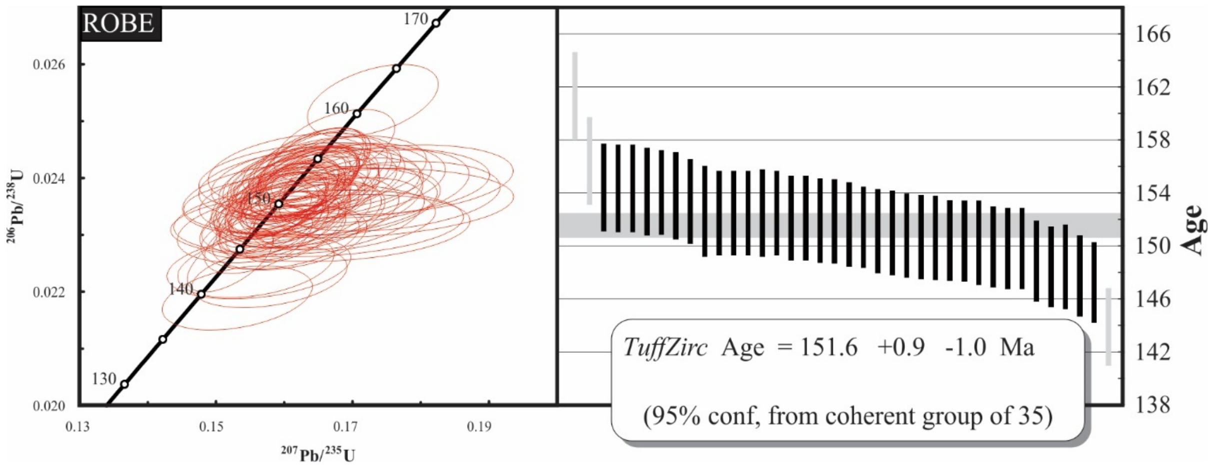

Fig. 5.5. Concordia diagram (left) and concordant $^{206}Pb/^{238}U$ dates arranged by age. Horizontal grey line is the age calculated by TuffZirc with vertical grey lines representing dates rejected from the age calculation. All individual errors are 2σ.

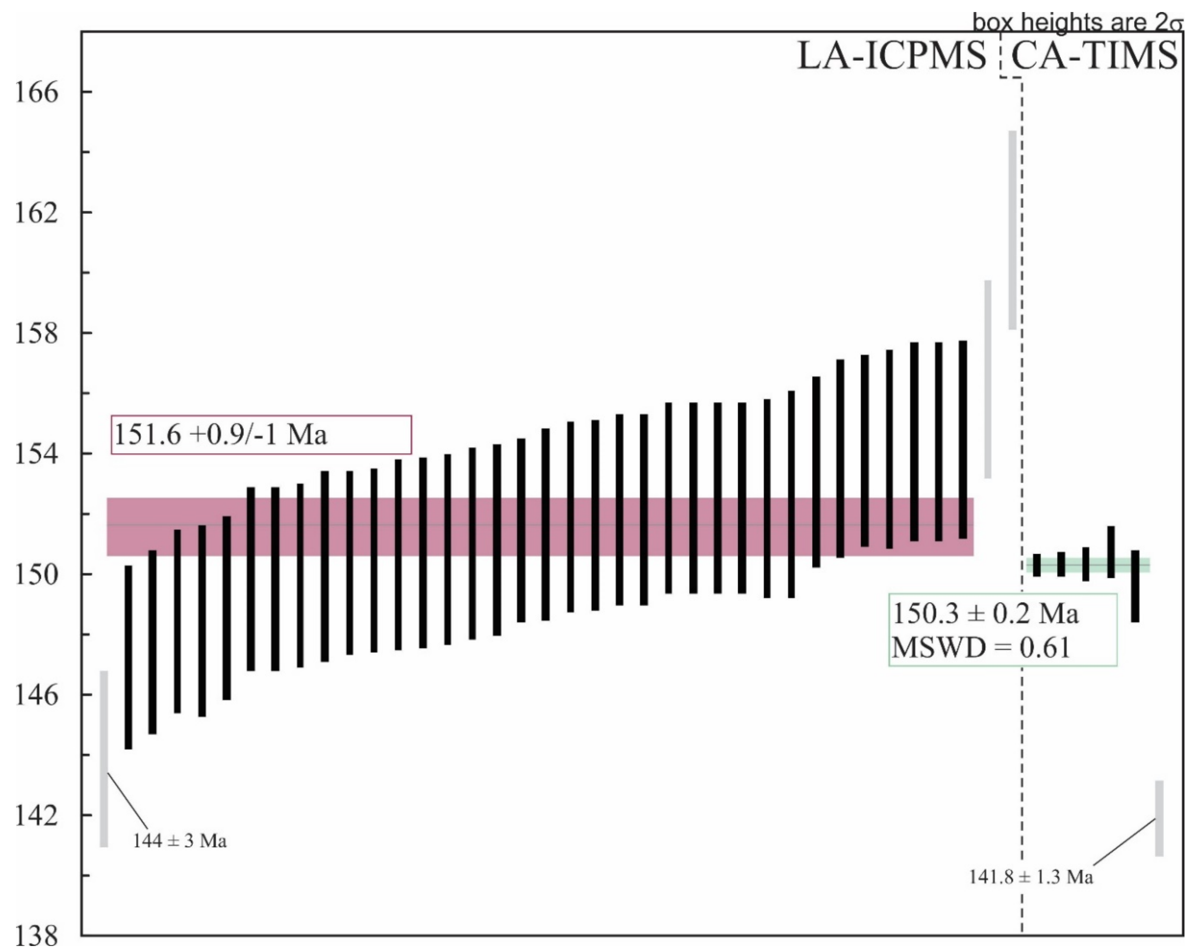

Fig. 5.6. U-Pb dates from LA-ICPMS (left) and CA-TIMS (right) analytical procedures ordered by age. Grey uncertainty ranges are dates that are excluded from age calculations. Both the TuffZirc age (red) and the weighted mean (green) calculated using 5 dates acquired by CA-TIMS are indistinguishable.

Ak5

Of the 99 analyses, 64 yield concordant dates of which 6% are Mesozoic, 48% Palaeozoic and 46% Precambrian (Fig. 5.4; Table D3 in Appendix D; van Breda, 2017). The wide range of dates with multiple peak ages on the probability density diagram is typical of a detrital zircon sample, and therefore dates are assessed to constrain maximum deposition of the sandstone sample. Analytical metrics are as follows: YSG = 145 ± 2 Ma; YDZ = 144.4 +3.0/-4.4 Ma (95% conf.); YPP = 145 Ma. An additional metric is included here because a concordia age can be calculated from the youngest 7 grains that intersect the concordia plot (Fig. F1A in Appendix F). These grains both define an equivalent population and are graphically concordant (Ludwig, 2003), and therefore provide a reliable concordia age of 147.0 ± 1.1 Ma. Following convention, the preferred maximum depositional age is 145 Ma (YPP), which is within error of YSG and YDZ ages, and is only slightly younger than the concordia age. Realistically however, the latter is roughly compatible with the graphically-derived YPP age given that no associated uncertainty is quoted with this metric.

ASH1

Of the 99 analyses, 95 yield concordant dates of that are 80 % Palaeozoic and 20% Precambrian (Fig. 5.4; Table D3 in Appendix D; Fig. F1B in Appendix F; van Breda, 2017). The wide range of dates with multiple peak ages on the probability density diagram is typical of a detrital zircon sample, and therefore dates are assessed to constrain maximum deposition. Analytical metrics are as follows: YSG = 374 ± 6; YDZ = 373.7 +5.1/-7.0 Ma (95% conf.); YPP = 375 Ma. The absence of Mesozoic grains precludes these data from helping refine the chronostratigraphy of the Robertson Basin and all metrics are older than the ~Jurassic – Cretaceous age range for the Uitenhage Group.

RAE

Of the 47 analyses, 50 yield concordant dates of that are 32 % Palaeozoic and 68% Precambrian (Fig. 5.4; Table D4 in Appendix D; Fig. F1C in Appendix F; van Breda, 2017). The wide range of dates with multiple peak ages on the probability density diagram is typical of a detrital zircon sample, and therefore dates are assessed to constrain maximum deposition. Analytical metrics are as follows: YSG = 505 ± 8 Ma; YDZ = 504.6 + 7.4/-8.3 Ma (95% conf.); YPP = 535 Ma. Since there are no Mesozoic grains in the sample, it cannot aid in refining the depositional age of the unit.

5.2.1.3 Basin synthesis

The U-Pb data from the Robertson Basin are somewhat helpful in determining the age of the Uitenhage Group fill in the Robertson Basin. The Tithonian primary ash deposit (sample ROBE) in the Kirkwood Formation and nearby sandstones that were not deposited before the latest Jurassic (~145 Ma) suggest that much of the exposed strata are Upper Jurassic to Lower Cretaceous. This correlates with the accepted, yet unconfirmed age for the Kirkwood Formation in the Algoa Basin. However, there is potentially > 1 km of Uitenhage Group buried in the depocentre of the basin, 215.9 m of which is intersected by borehole W202 (Fig. 8 of Muir et al., 2017b in section 2.2.2 of this thesis) suggesting that there are older, Middle and perhaps even Lower Jurassic deposits in the subsurface. The location of the borehole W202 and the outcropping Tithonian bentonite less than 300 m away (Fig. 5.1) also informs the chronostratigraphy of the basin. The dated bentonite (ROBE) probably correlates with the middle to upper parts of the borehole log (Fig. 5.7) based on bedding that dips 20º NW. Following this, it is probable that there are considerably older deposits that underlie the Tithonian interval in the Robertson Basin.

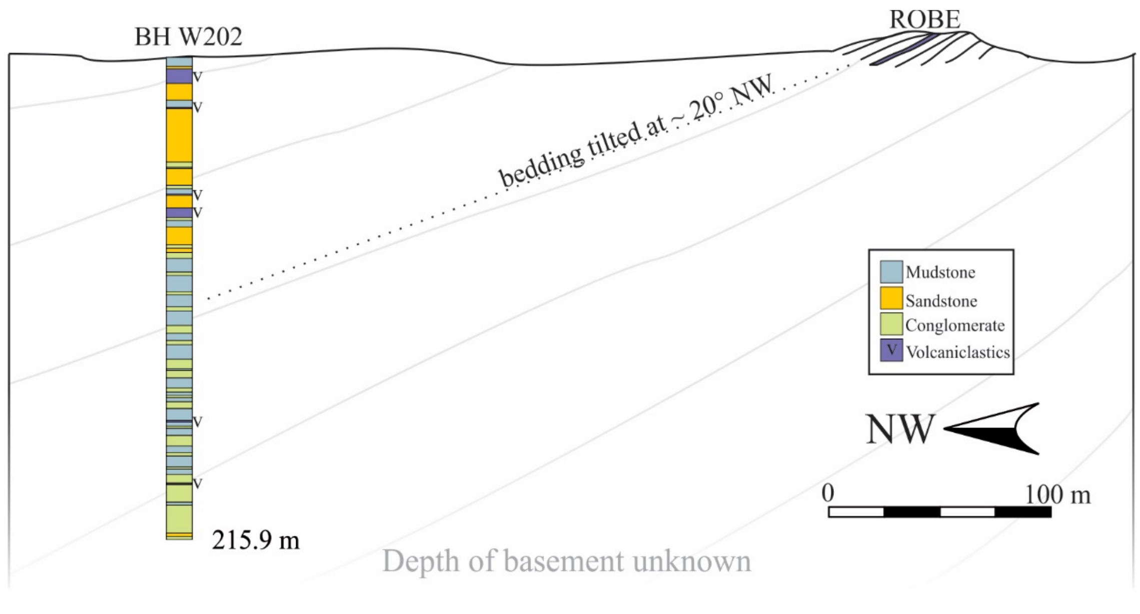

Fig. 5.7 Sketch diagram of the central Robertson Basin showing how the Tithonian bentonite (sample ROBE) correlates with the interval intersected by borehole W202 based on a consistent tilt of bedding ~20º NW.

The two samples from conglomeratic units close to the basin margin do not help resolve the intra-basin stratigraphy, because neither contain young, Jurassic – Cretaceous zircon populations. Perhaps the only noteworthy differences between the zircon distribution in these two samples is the proportion of Cambrian zircons that correspond to the Cape Supergroup, which is greater in the Enon Formation in the east of the basin compared to the west, and the presence of a younger, Devonian population present in the west but absent in the east. These subtle differences are probably caused by the local sourcing of detritus during their deposition, with the conglomerates in the west having an exclusively Table Mountain Group and Cape Granite Suite source and those in the east containing younger source rocks. Field observations corroborate these findings, as the conglomerates at Ashton contain clasts of diamictite, most probably derived from the Dwyka Group, that are absent in the conglomerates at Robertson (Fig. 2C, D, E).

5.2.2 Heidelberg Basin

The Heidelberg Basin is situated south of the Langeberg Range in the vicinity of Heidelberg and Riversdale in the Western Cape Province (Fig. 5.8). The Uitenhage Group exposures are confined to an ovoid-shaped area in map view spanning 70 km in the E-W direction, following the orientation of the Worchester Fault, and 10 to 15 km N-S. In this region, Uitenhage Group contains the Enon, Kirkwood and Buffelskloof formations, although the stratigraphic relationship between isolated outcrops of these formations is highly uncertain. The presence of horizontally bedded, conglomerate-dominated Buffeslkloof Formation overlying the Enon and Kirkwood formations, which generally dip shallowly to the north (Viljoen, 1992), remains the only reliable stratigraphic constraint and this angular, and likely unconformable stratigraphic relationship provides no quantitative assessment of the chronology of the units. Fortunately, the lacustrine facies of the Kirkwood Formation contain abundant bentonite layers that are previously undated and active bentonite mining provides excellent quality outcrops, which otherwise would be restricted to road- and river-cuttings.

5.2.2.1 Outcrop description

Upper Horizon bentonite (sample HBUP)

A grey-white massive bentonite layer is exposed in an active quarry ~ 8.5 km NE of Heidelberg on the northern side of the R322 (34° 3'33.83"S; 20°52'42.72"E; Fig. 5.8) within the lacustrine facies association of the Kirkwood Formation. It is overlain by horizontally laminated grey mudstones, subordinate sandstones and rare conglomerates, which form shallow troughs that truncate underlying strata. The laterally extensive bentonite, named the 'Upper Horizon' by mining geologists at Cape Bentonite, has a constant thickness of 1.5 m over the 30 m lateral extent of the quarry and dips 15º to the N (Fig. 5.9A). The high purity and constant dimensions of the montmorillonite-rich bentonite bed suggest a primary ash-fall origin. Conglomerates of the Buffelskloof Formation down-cut into the Kirkwood Formation, and the two formations are separated by an angular unconformity in the vicinity of the sample locality.

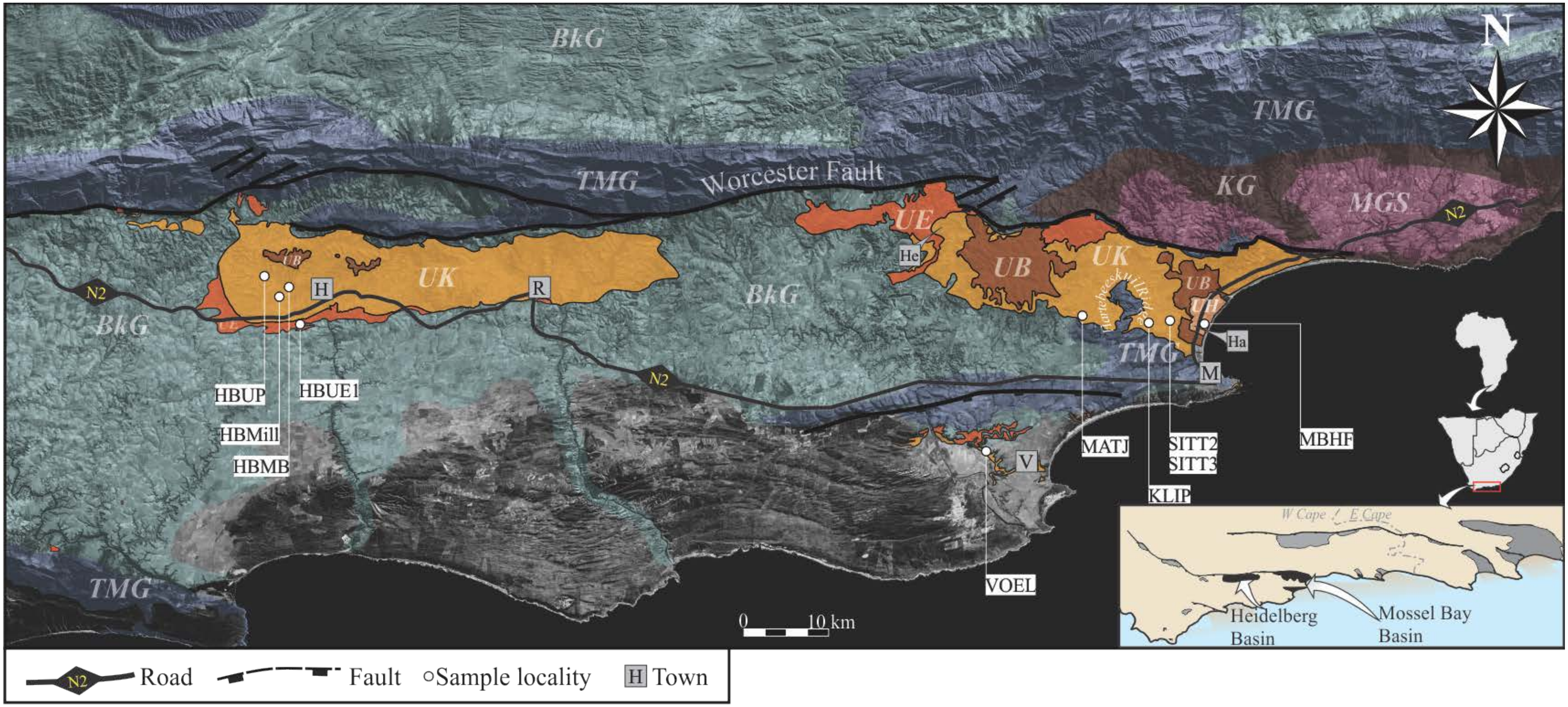

Fig. 5.8. Simplified geology of the Heidelberg (left) and Mossel Bay (right) basins. Letters and colours are stratigraphic units and unshaded areas are recent alluvium and Cenozoic deposits. Abbreviations: Towns: H = Heidelberg; Ha = Hartenbos; He = Herbertsdale; M = Mossel Bay; R = Riversdale; V = Vlees Bay. Stratigraphic units arranged from oldest to youngest: KG = Kaaimans Group; MGS = Maalgaten Granite Suite; TMG = Table Mountain Group; BkG = Bokkeveld Group; UE = Enon Formation; UK = Kirkwood Formation; UB = Buffelskloof Formation; UH = Hartenbos Formation. Base maps modified from the 1: 250 000 geological maps sheets 3420 (Malan, 1993), 3320 (Theron ,1991) and 3322 (Toerien and Roby, 1979) of the Council for Geoscience overlain on ESRI satellite imagery.

Main Bentonite Horizon (sample HBMB)

Quarries around the Cape Bentonite processing factory ~ 3 km NE of Heidelberg along the R322 expose a massive green-grey bentonite named the 'Main Horizon' (34° 4'11.37"S; 20°55'33.56"E; Fig. 5.8). It ranges between 1 and 1.5 m in thickness and is capped by either siltstones, conglomerates or a white or green zeolitic layer, all interpreted to form part of the lacustrine facies association of the Kirkwood Formation. The particular quarry from which this sample was taken has since been backfilled. (Fig. 5.9B).

Millenium Bentonite Horizon (Sample HBMill)

A quarry ~4.5 km west of Heidelberg (34° 5'22.60"S; 20°54'24.31"E; Fig. 5.8) exposes a 1.7 m thick light grey to white bentonite layer (aka the 'Millenium Horizon'; Fig. 5.9C). Although the bottommost ~1 m of the bentonite is a generally massive claystones, its upper part is horizontally laminated and comprises alternating white claystones and grey siltstone interlaminae. Locally, rare ripple-cross laminations replace the horizontal laminations. There are also lateral variations in grain-size in the bentonite, with subordinate silt, sand and granules occurring commonly in its eastern section but mostly absent further to the west. This grain size variation indicates syn-sedimentary reworking and significant detrital input. A sample was extracted from the massive claystone away from laminae.

Moordenaarskop road-cutting (Sample HBUE1)

The few isolated road-cuttings in the southern and southwestern margins of the Heidelberg Basin expose the Enon Formation. In one of these, at Moordenaarskop ~3 km SW of Heidelberg along the R322 south of the N2 highway (34° 7'1.85"S; 20°55'56.88"E; Fig. 5.8), crudely bedded red conglomerate beds have an overall dip of ~30º N, are composed principally of shale clasts from the Bokkeveld Group (Cape Supergroup) and contain rare lensoid sandstones (Fig. 5.9D). One of these rare red sandstone interbeds was sampled.

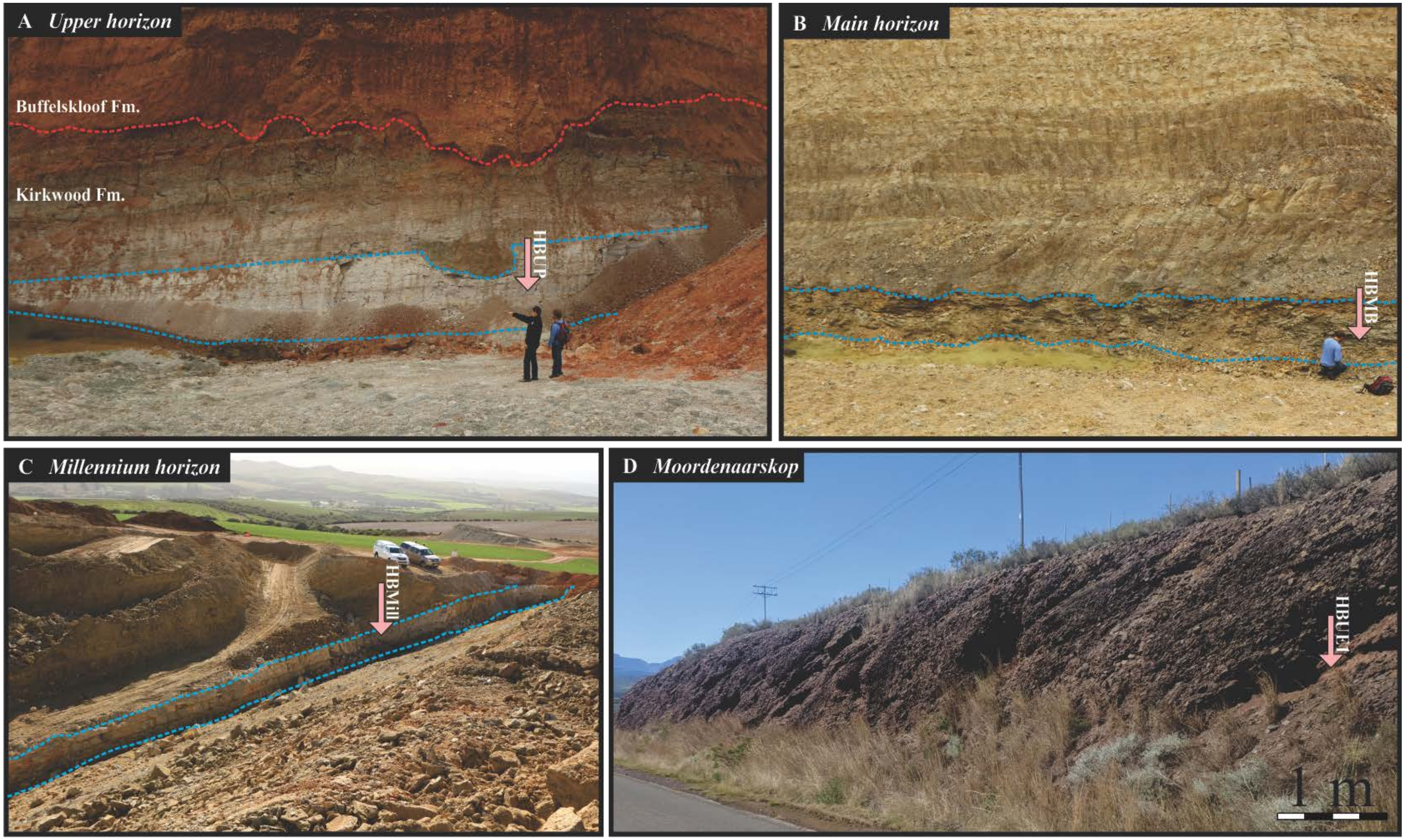

Fig. 5.9. Geological context of the Uitenhage Group samples in the Heidelberg Basin. (A) The Kirkwood Formation and overlying Buffelskloof Formation, separated by an angular unconformity (red dashed line), exposed in a bentontie quarry. Blue dashed lines highlight the ‘Upper horizon’ bentonite from which HBUP sample was taken. (B) Quarry that exposes the ‘Main horizon’ bentonite (outlined in blue dashed lines) within the Kirkwood Formation. It is overlain by conglomerates, sandstones and laminated mudstones. (C) Quarry exposure of the ‘Millennium horizon’ bentonite (outlined in blue dashed lines) within the Kirkwood Formation. (D) Conglomerate-dominated deposits at Moordenaarskop exposed in a road-side outcrop. Pink arrows indicate the position from which respective samples were extracted.

5.2.2.2 U-Pb geochronology

HBUP

Zircon crystals from the HMUP sample are strongly euhedral and range from 100 to 500 µm needles, prismatic and stalky-shaped crystals with very few fragmentary stubby grains. Internally, they exhibit consistent fine and medium oscillatory zoning with very rare inclusions and cores when imaged using the CL detector (Fig. 5.10). Of the 98 analyses, 56 are concordant and overwhelmingly (~95%) yield Mesozoic dates, with only 3 Proterozoic dates (Fig. 5.11). The Mesozoic dates form a single cluster around 162 Ma. The synchronicity of zircon crystal dates, lack of significant detritus, and similarity of crystal morphology and internal zonation are in agreement with the sedimentological classification of the deposit as pyroclastic. Analytical metrics are as follows: YSG = 159 ± 2 Ma; YDZ = 157.4 +1.4/-2.5 Ma (95% conf.); YPP = 162 Ma. The TuffZirc algorithm identifies the most coherent cluster around 162.3 +0.7/-0.9 Ma (at the 95% confidence interval) using 49 crystals and accounts for minor inheritance (Fig. 5.12). This earliest Oxfordian age is considered the best estimate of the depositional age of the pyroclastic deposit.

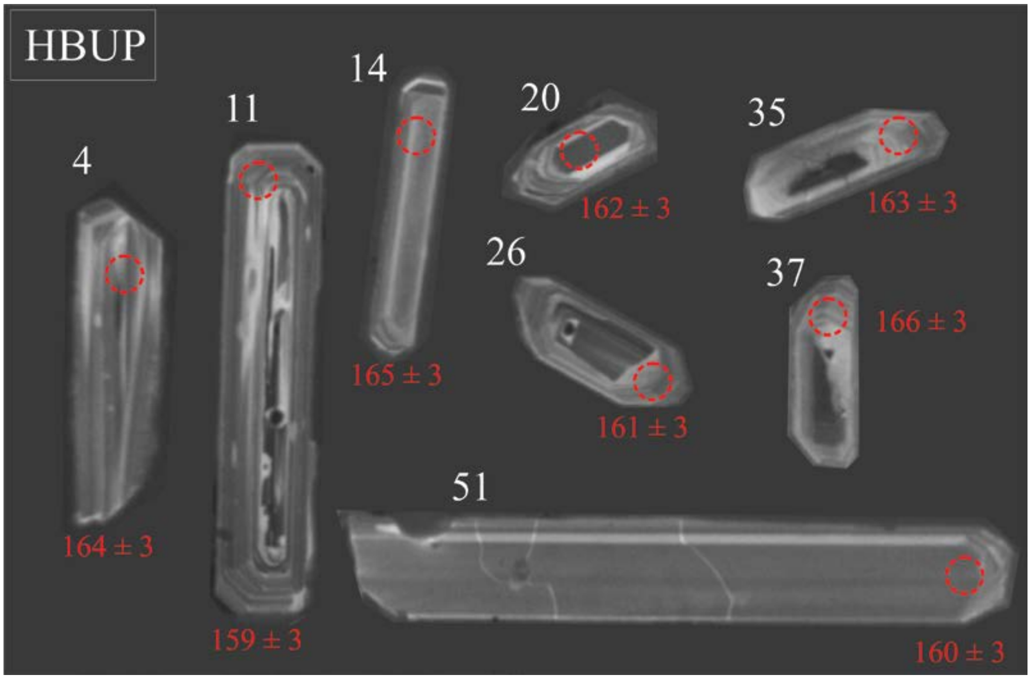

Fig. 5.10. Composite diagram of CL images of zircons that yield concordant dates in sample HBUP from the Heidelberg Basin. Individual zircon indicated by white number and analytical spot (26 µm diameter) with respective $^{206}Pb/^{238}U$ date are red.

Fig. 5.11. (Following page). U-Pb dates of zircons from all samples in the Heidelberg Basin shown as age probability density diagrams (blue area) combined with frequency histograms (grey bars) with 20 Ma intervals. Only concordant data are shown: n = x/y means that x out of a total of y zircons yielded concordant dates. Youngest graphically-defined peak (YPP) are indicated.

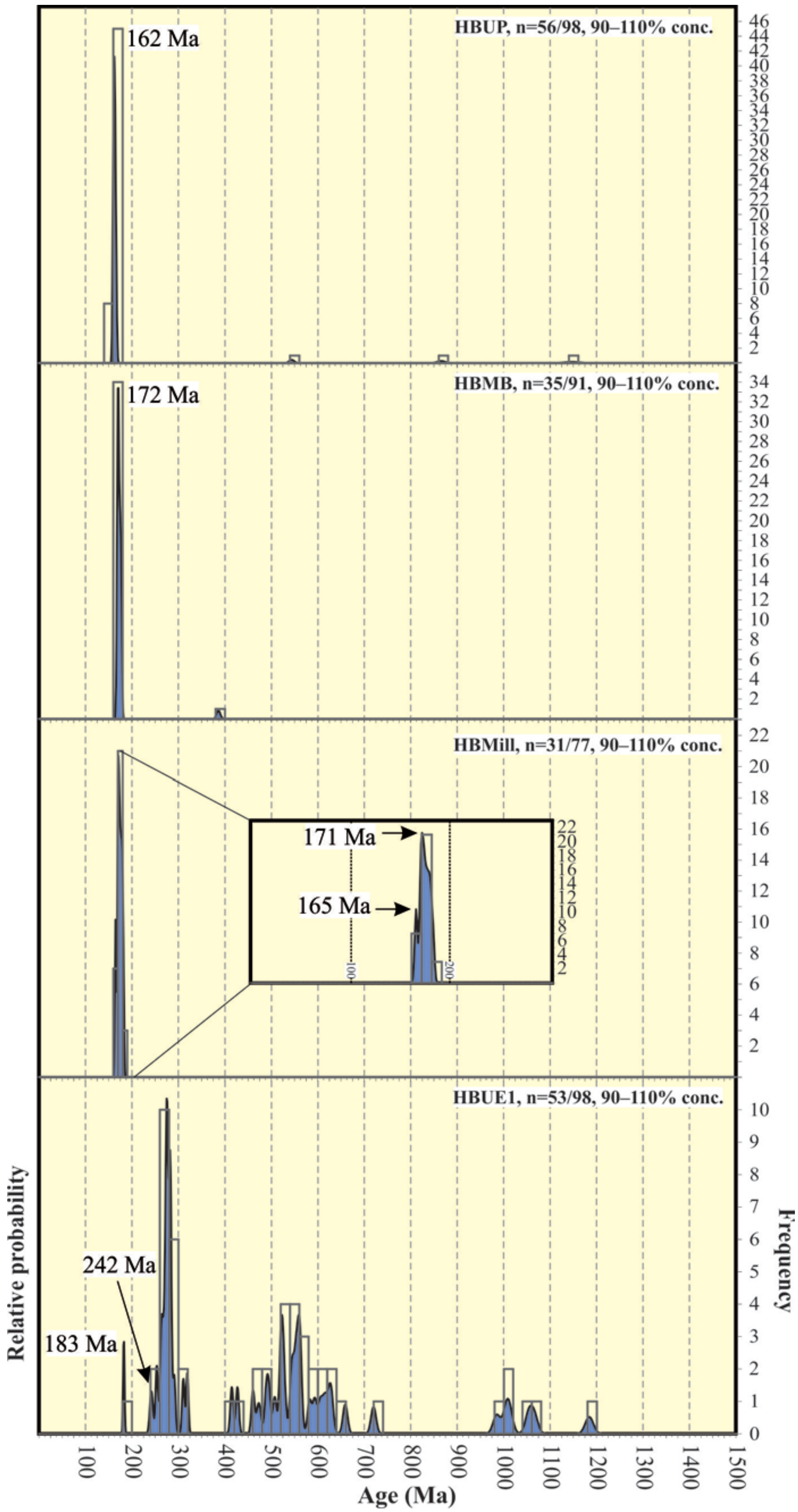
HBUP, n=56/98, 90–110% conc.
162 Ma
HBMB, n=35/91, 90–110% conc.
172 Ma
HBMill, n=31/77, 90–110% conc.
171 Ma
165 Ma
HBUE1, n=53/98, 90–110% conc.
242 Ma
183 Ma
Relative probability
Frequency
Age (Ma)

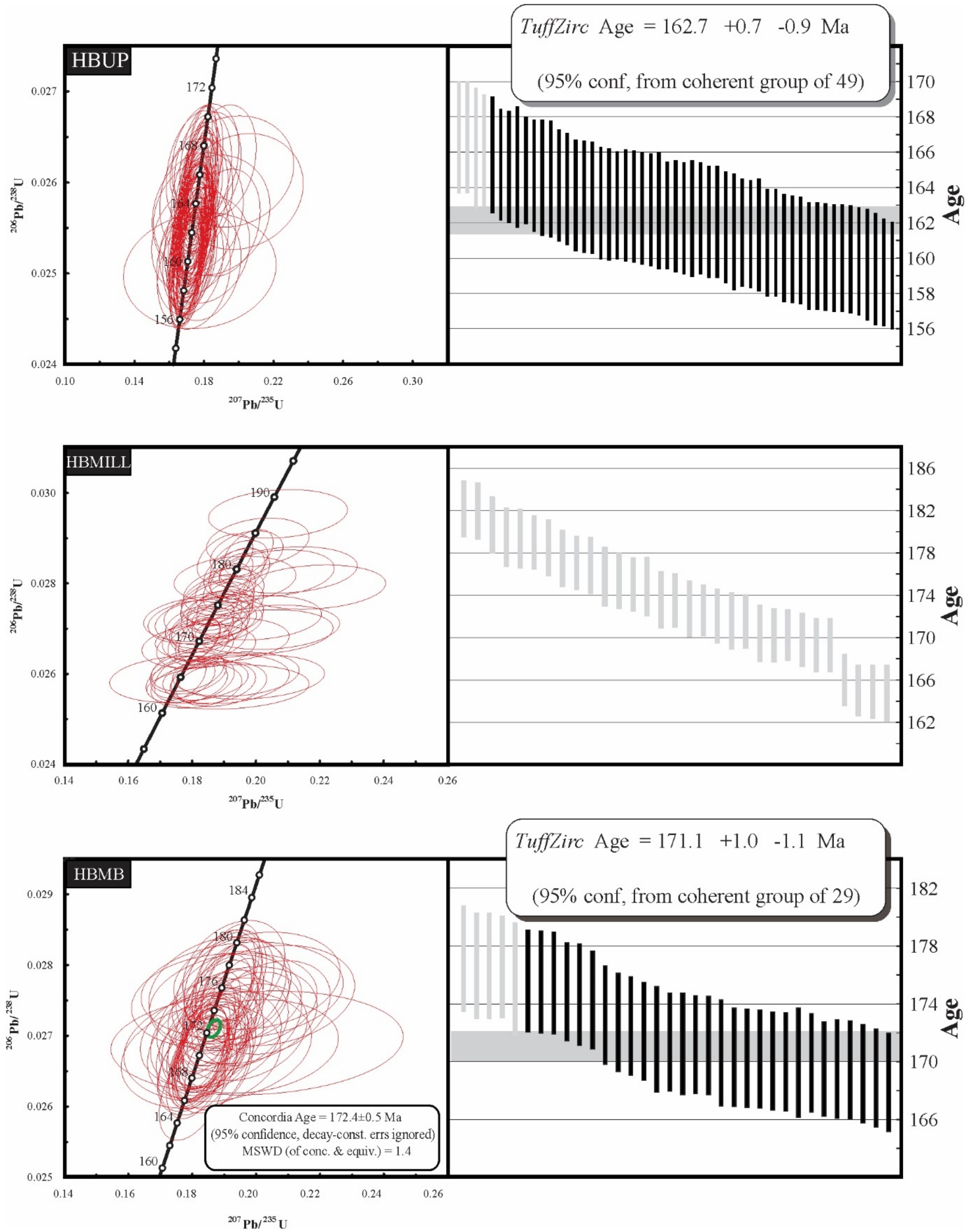

Fig. 5.12. Concordia diagrams (left) and concordant ^{206}Pb/^{238}U dates arranged by age (right) for the three pyroclastic deposits in the Heidelberg Basin. Horizontal grey line is the age calculated by TuffZirc with vertical grey lines representing dates rejected from the age calculation. All individual errors are 2σ.

HBMB

Zircon crystals in HBMB are similarly euhedral and range from 60 to 350 µm with prismatic and stalky habits, but unlike HBUP, the crystals are rarely needle-like. The smallest crystals generally comprise broken grain fragments. Overall the crystals were uniformly colourless except for infrequent inclusions and showed either medium to fine oscillatory zoning (e.g., crystal 9 and 39 in Fig. 5.13) or no visible zoning (e.g., crystal 1 in Fig. 5.13) when imaged though the CL detector.

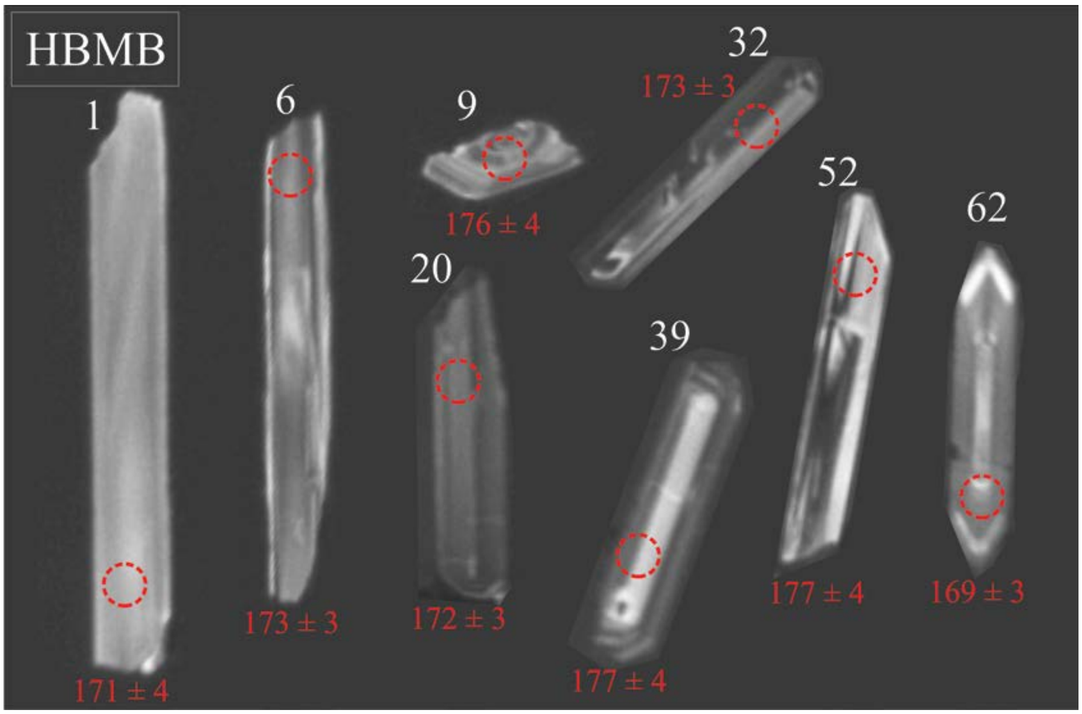

Fig. 5.13. Composite diagram of CL images of zircons that yield concordant dates in sample HBMB from the Heidelberg Basin. Individual zircon indicated by white number and analytical spot (26 µm diameter) with respective $^{206}Pb/^{238}U$ date are red.

Of the 91 crystals analysed, 35 are concordant, 34 of which occupy a single Mesozoic population around 172 Ma, and just 1 Palaeozoic crystal. Such a limited detrital component supports the pyroclastic interpretation for the bentonite (Fig. 5.11). Analytical metrics are: YSG = 169 ± 2 Ma; YDZ = 166.9 +1.6/-2.9 Ma (95% conf.); YPP 172 Ma. A concordia age can (Ludwig, 2000) be calculated as 172.4 ± 0.5 Ma using graphically concordant data-points that have overlapping uncertainties, and the TuffZirc algorithm yields a 171.1 +1.0/-1.1 Ma age from the most coherent cluster of 29 crystals (Fig. 5.12). This is indistinguishable from the concordia age, and both are fairly robust estimates for the depositional age of the ash. Further analysis of 15 zircons using the CA-TIMS method yield 15 concordant dates (Fig. 5.14; Table G1 in Appendix G). The higher precision associated with these dates compared to those acquired by LA-ICPMS suggests that there are multiple closely spaced crystallization events recorded in the zircon population. All 14 dates yield a weighted mean of 170.5 ± 0.6 Ma, which is regarded as the best estimate of the depositional age of the unit despite the excess scatter (MSWD = 3.8). The youngest crystal is 169.6 ± 0.8 Ma, which is the minimum depositional age of the unit, and there is probably also an inherited component at ~171 Ma, although interpretations of specific crystallization episodes would be subjective due to the indiscrete clustering of dates around the mean (Fig. 5.14). The 170.5 ± 0.6 Ma mean is probably a reasonable refelction of the age of this deposit because it is within error of the TuffZirc-defined age, although there may be slightly younger and older age components that are indecernable at the precision attained.

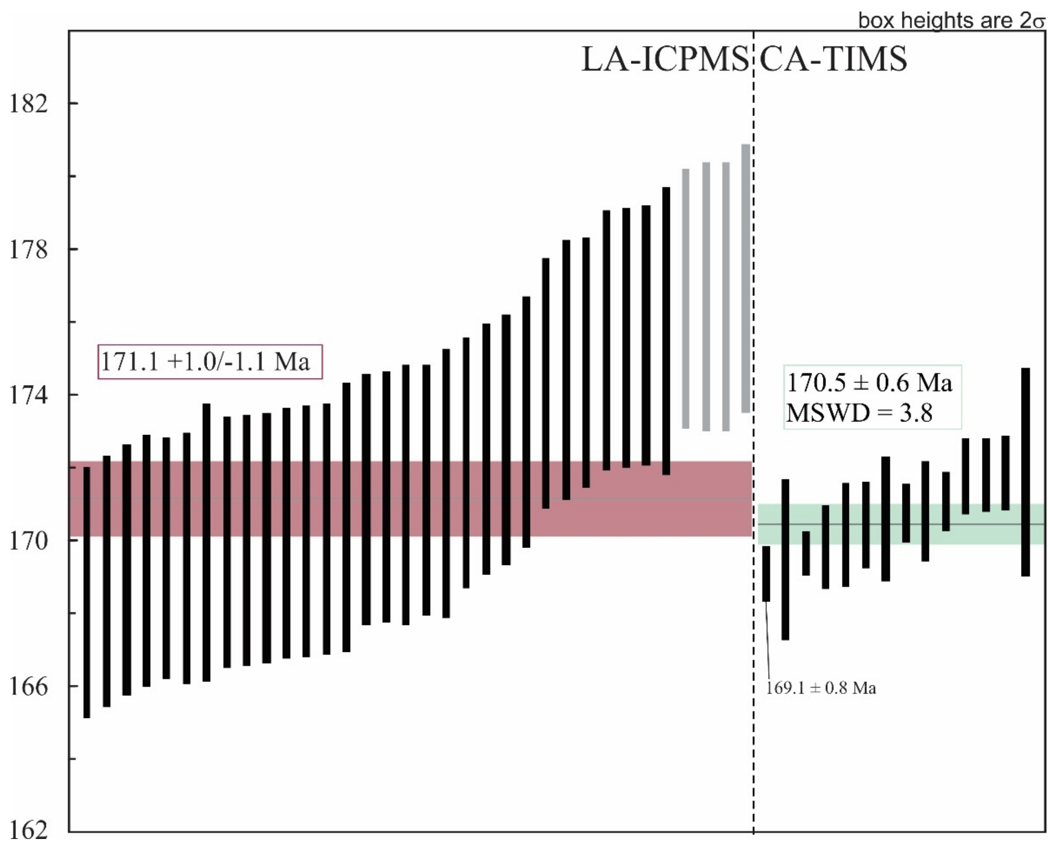

Fig. 5.14. U-Pb dates from LA-ICPMS (left) and CA-TIMS (right) analytical procedures ordered by age. Grey uncertainty ranges are dates that are excluded from age calculations. Both the TuffZirc age (red) and the weighted mean (green) of 14 dates acquired by CA-TIMS are indistinguishable.

HBMIL

The zircons extracted from the sample range in size from ~60 – 170 µm and are primarily prismatic to needle-like, with few stalky and stubby habits. All crystals exhibit fine oscillatory zonation under the CL detector. Some of the needle-shaped crystals were too narrow to analyse effectively and regularly yielded discordant ages presumably because ablation pits failed to fall entirely within the exposed crystal. Some of the youngest dates are derived from small stubby crystals that have pure oscillatory zoning and show no evidence of undergoing multiple episodes of crystallization (e.g., crystals 72 and 78 in Fig. 5.15). Conversely, some of the older dates are from the centres of zircons that have thin rims of sharply contrasting intensity under the CL detector (e.g., 4 and 10 in Fig. 5.15). This microtextural observation suggests a complex zircon crystallization history prior to eruption that is resolvable at 2σ error.

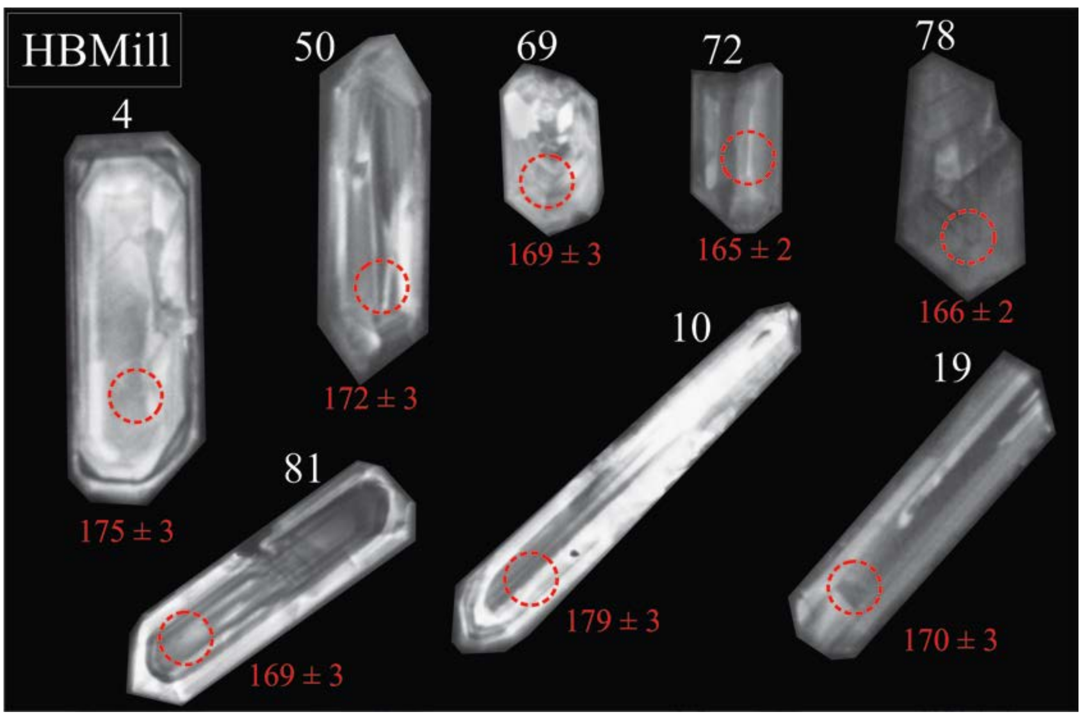

Fig. 5.15. Composite diagram of CL images of zircons that yield concordant dates in sample MBMill from the Heidelberg Basin. Individual zircon indicated by white number and analytical spot (26 µm diameter) with respective $^{206}Pb/^{238}U$ date are red.

Nevertheless, of the 77 crystals analysed, 31 yield concordant dates that are exclusively Mesozoic but occupied two discrete populations with peaks at 165 Ma and 171 Ma on the probability density diagram

(Fig. 5.11). Analytical metrics are as follows: YSG = 165 ± 3 Ma; YDZ = 163.8 +1.8/-2.4 Ma (95% conf.); YPP = 165 Ma. Although there are multiple age components present within the Mesozoic zircon dates, the lack of significant detrital zircons in the sample confirm limited or no reworking and a pyroclastic origin for the bentonite. Although the actual sampling site yielded no sedimentological evidence for reworking, there are clear signs of detrital mixing elsewhere within the bed. It is possible that the spread in dates can be accounted for by extremely subtle resedimentation during which older zircons are included into younger ash deposits during deposition. Alternatively, zircons of varying ages may have been incorporated into the same eruptive event by magmatic processes (i.e., prolonged or multiple zircon crystallization episodes within the magmatic system prior to an eruption; Reid et al., 1997; Reid and Coath, 2000; Bowring et al., 2006) or explosive processes (i.e., zircon inheritance derived from the pulverization or assimilation of slightly older igneous rocks located near the volcanically active site; Landing et al., 1998; Bowring et al., 2006). Although subtle inheritance can occur, equally cryptic Pb loss likely also played a role in broadening the distribution of zircon dates in this sample. The TuffZirc algorithm identifies the most coherent cluster of 14 dates at 171.6 +1.2/-1.4 Ma, although this age is unsatisfactory (nore reported in Fig. 5.12) because there is both an older ~175 Ma coherent grouping of dates and a younger ~165 Ma component which are almost as likely. Without resampling the deposit in a different area to minimize the chance of including old zircons derived from detrital input or using a CA-TIMS analytical procedure to improve precision and reduce the effect of lead-loss and therefore spuriously young dates, reporting a reliable depositional age for this unit without extreme subjectivity is not possible. Therefore, this bentonite should instead be considered simply as broadly Middle Jurassic, to reflect the large uncertainty associated with determining its deposition and no numeric age can be deduced from the data reliably (Fig. 5.12).

HBUE1

Zircons vary in length from 60 to 170 μm and have stubby to needle-like habits, with most crystals being prismatic and euhedral. They are frequently stained pale red, presumably due to the same secondary iron oxide weathering product that gives the whole outcrop a red hue. Typically, the crystals have fine oscillatory zoning without obvious core inheritance (e.g., crystal 97 in Fig. 5.16) or with subtle, poorly defined secondary growth rims (e.g., crystal 106 in Fig. 5.16) and some contain small opaque inclusions (e.g., crystal 106 in Fig. 5.16).

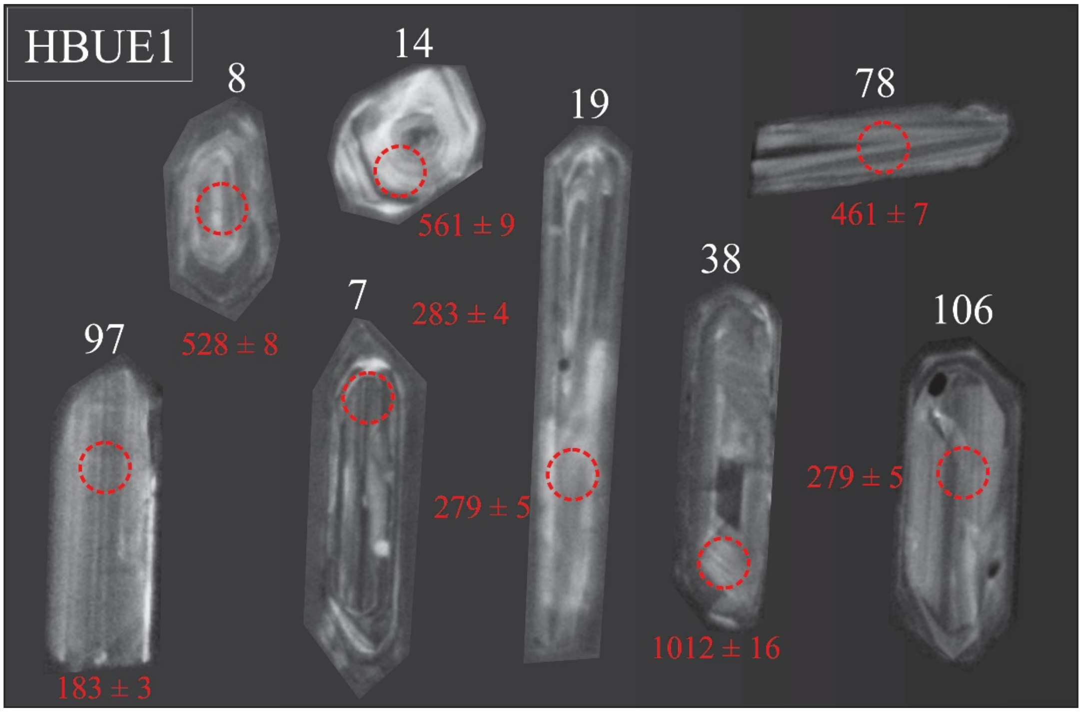

Fig. 5.16. Composite diagram of CL images of zircons that yield concordant dates in sample HBUE1 from the Heidelberg Basin. Individual zircon indicated by white number and analytical spot (26 µm diameter) with respective $^{206}Pb/^{238}U$ date are red.

A total of 98 zircons were analysed yielding 53 concordant dates. Zircons vary in age from Mesozoic (~4 %), Palaeozoic (~53 %) and Precambrian (43 %) defining multiple age peaks on a probability distribution diagram (Fig. 5.11). Analytical metrics are as follows: YSG = 183 ± 3 Ma; YDZ = 182.8 +3.1/-3.7 Ma (95% conf.); YPP = 265 Ma. Only 1 single zircon that passed the concordance test produced a Jurassic date. However, two additional dates that are below the concordance threshold lie along the concordia diagram when plotted in U^{238}/Pb^{206} vs. U^{235}/Pb^{207} space and yield a concordia age of 179.5 ± 5.0 Ma (Fig. F1 D). Following convention, the metric used to describe the maximum depositional age of the deposit is the YPP age of 265 Ma although a less repeatable, but perhaps geological meaningful constraint on maximum deposition is 179.5 ± 5.0 Ma because a young cluster of three dates exists when plotted along concordia that supports this age component.

5.2.2.3 **Basin synthesis**

Bentonite deposits that are well-exposed in the Heidelberg Basin are considered pyroclastic and allow for robust assessments of the depositional ages of the Uitenhage Group. The results show that much of the Kirkwood Formation in this basin was deposited in the Middle Jurassic indicated by 170.5 ± 0.6 Ma and 162.3 +0.7/-0.9 Ma depositional ages of the HBMB and HBUP bentonite layers, respectively. This strongly contrasts previous age estimates for the bentonitic mudstones, which were considered Portlandian (Viljoen, 1992) or younger (Rigassi and Dixon, 1972) and also contradicts all previous estimates for a maximum age of the Uitenhage Group (McLachlan and McMillan, 1976; Dingle et al., 1983; McMillan et al., 1997; Shone, 2006). Not only are 170.5 ± 0.6 Ma deposits more than 10 Ma older than any of these estimates, but further, the HBMB bentonite is not at the base of the Heidelberg Basin stratigraphy and therefore does not represent the absolute oldest syn-rift accumulations. In fact, we estimate that ~500 m of mudstones, sandstones and conglomerates underlie the unit based on a consistent northwards dip direction (Viljoen, 1992) and 5 km apparent thickness before the edge of southern end of the basin is reached (Fig. 5.9). This approximation is also supported by descriptions of a borehole log drilled in the basin near Riversdale, in which > 600 m of Uitenhage Group underlie the grey bentonitic facies of the Kirkwood Formation (Rigassi and Dixon, 1972). These underlying strata are older than 170.5 ± 0.6 Ma by an unknown period of time. If this thickness accumulated quickly, then the oldest strata in the basin are considerably older than the oldest dated bentonite; else, if the average sedimentation rate was slow, 170.5 ± 0.6 Ma is a good approximation of when accommodation began. In reality we do not know how much time this basal most 500 – 600 m sedimentary package represents but it is not unreasonable to assume a latest early Jurassic age for the lowermost beds of the Uitenhage Group in Heidelberg Basin. Further, since there are Lower Jurassic zircons in the HBUE1 sample at Moordenaarskop, which is on the southern margin of the half-graben and therefore probably occupies a basalmost position in the stratigraphy, it is likely that extension began between 179.5 ± 5.0 Ma and 170.5 ± 0.6 Ma, possibly as early as the Pliensbachian – Toarcian.

The Enon and Kirkwood formations exposed within the Heidelberg Basin therefore constitute some of the oldest parts of the Uitenhage Group in the southern Cape, and represent deposition that occurred soon after rifting began. Sometime in the Early Jurassic at ~183 Ma (an age compatible with the 179.5 ± 5.0 Ma maximum age of deposition of the basalmost dated strata at Moordenaarskop) normal faults developed through inversion of compressional weaknesses (cf. the Late Jurassic; Fouché et al., 1992; Viljoen, 1992; McMillan et al., 1997; Paton, 2006; Green et al., 2016) near present-day Heidelberg and Riversdale (Fig. 5.17). Continental conglomerates, sandstones and mudstones began to accumulate in the newly created, growing accommodation space. As extension continued into the Middle and Upper Jurassic, faults grew, became linked and continued to accumulate displacement. Deposition of terrigenous clastic sediments continued throughout this time but was interrupted by volcanic ash fall events that resulted in l pyroclastic layers that settled in intermountain lakes. There is no evidence for deposits that are younger than Oxfordian beneath the angular unconformity that separates the lower Enon and Kirkwood formations from the overlying Buffelskloof Formation. Nevertheless, it is reasonable to assume that deposition did continue into the Early Cretaceous, only that all Oxfordian to Lower Cretaceous deposits were removed subsequent to or during a reinvigoration of rifting and displacement along normal faults (Fig. 5.17). By the time this happened, probably sometime in the Early Cretaceous, the Worcester Fault had become the principal fault that accommodated extensional stress and therefore accumulated the most displacement (Paton, 2006). However, subordinate fault planes also remained active, especially at transfer zones between non-contiguous segments of the Worcester Fault (Viljoen, 2000). This tectonic reinvigoration steepened topographic gradients at the scarp and at nearby transfer zones, and generated new accommodation space south of the Worcester Fault in which the sediments that constitute the Buffelskloof Formation were deposited. Finally, as the landscape continued to evolve through the Upper Cretaceous and Cenozoic, much of the Buffelskloof Formation was removed, leaving behind just a few isolated koppies around Heidelberg and exposed the older, tilted Enon and Kirkwood Formation strata beneath (Fig. 5.17).

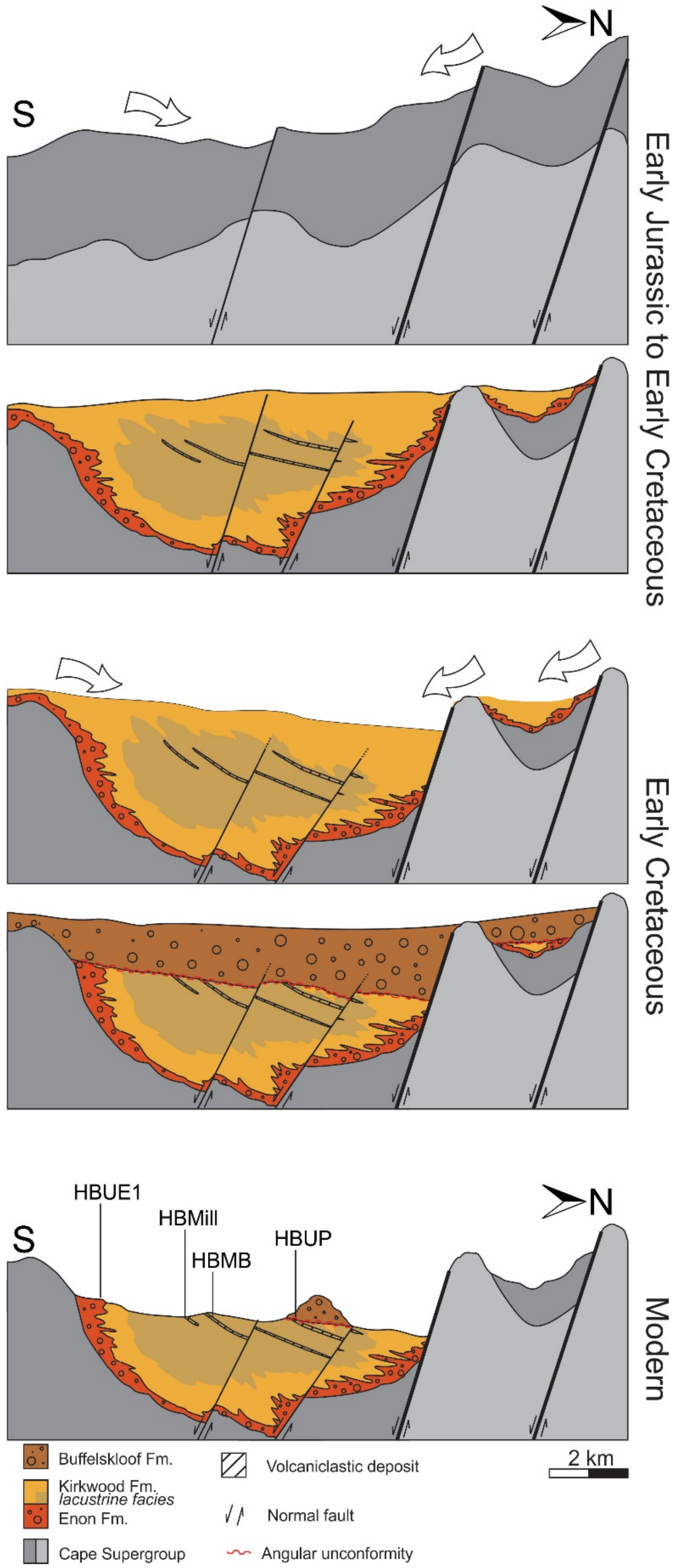

Fig. 5.17. Evolution of the Heidelberg Basin from the late Early Jurassic to present with inferred stratigraphic relationships and an overall northward dip direction of strata described by Viljoen (1992) and confirmed by U-Pb data. See text for details.

5.2.3 Mossel Bay Basin and Vlees Bay

The Mossel Bay Basin contains Uitenhage Group that outcrop around Mossel Bay and Herbertsdale. A few isolated outcrops at Vlees Bay, some ~25 km west of Mossel Bay are also considered part of the Basin (Fig. 5.8). The Uitenhage Group comprises the Enon, Kirkwood, Buffelskloof and Hartenbos formations in these areas and the latter two, the Buffelskloof and Hartenbos formations, are separated by an angular unconformity from the tilted strata of the underlying Enon and Kirkwood formations (Malan and Viljoen, 1990). Outcrops of the Enon and Kirkwood formations are mostly restricted to river valley and road-cuttings throughout the basin, whereas the Buffelskloof Formation is quarried for building material and is therefore well-exposed near Hartenbos, but also in natural cliff faces along the Nouga and Heuningklip rivers SE of Herbertsdale. Rare outcrops of its finer-grained lateral equivalent, the Hartenbos Formation, exist near Hartenbos and Kleinbrak in erosional gullies. The Mossel Bay Basin is bounded in the north by the Worcester Fault, which changes strike from ~ E-W at Herbertsdale, to ENE-WSW further east, controlled by the position of the George Pluton, where the Maalgaten Granite Suite outcrops (Fig. 5.8).

5.2.3.1 Outcrop description

Klipkop road-cutting (sample KLIP)

An upward fining package of conglomerate, sandstone and mudstone beds are exposed at Klipkop, 4.5 km west of Hartenbos, in a road-cutting (34° 7'38.00"S; 22° 2'58.66"E; Fig. 5.8). The upward-fining beds dip shallowly northwards and comprise a quart breccia-conglomerate overlain by clast-rich sandstone, which in turn is overlain by a clast rich sandy-mudstone bed. Each unit is roughly 1 m thick, and the uppermost tuffaceous sandy-mudstone exhibits popcorn texture weathering in places despite containing a fraction of sand-size grains (Fig. 5.18A, B, C). A sample was extracted from this bed based on it likely containing at least a partial volcanogenic fraction. Overall the unit falls within the Kirkwood Formation, attested by the mudstone-dominated lithologies in the few scattered outcrops within 100 m of the sample site on the gentle slopes north of Klipkop.

Matjiesdrift hill (sample MATJ)

A bentonite layer is poorly exposed at Matjiesdrift farmstead ~20 km NW of Mossel Bay and 2.3 km NE of the R327 in a hillside gully and in recent excavations (34° 5'56.98"S; 21°56'39.33"E; Fig. 5.8). Surficial popcorn texture and absence of significant sand-sized grains in the pure claystone are field evidence for a pyroclastic origin. The mottled pink and grey bentonite (Fig. 5.18 D) is interbedded with light grey massive mudstones and subordinate sandstone and conglomerate beds. Unfortunately, the lack of good exposure of this unit inhibits thorough description of its bedding geometry other than that it has at least 20 cm thick in places (blocks of such thickness were encountered eroding from recent excavation tailings) and that the bedding planes defined by erosion-resistant sandstone interbeds dip consistently at 25º N in the area

Fig. 5.18. Geological context of the Uitenhage Group samples in the Mossel Bay Basin. (A) Roadside outcrop exposing volcaniclastics at Klipkop. Conglomerate/breccia deposits pictured in B are to the left of the photograph, region enlarged in C is delineated by white dashed lines. (B) Sporadic conlgomerate/breccias that occur at Klipkop. (C) Clay-rich sandy bentonite with rare quarzite granules (inset). (D) Mottled grey and pink bentonite in a disturbed hillside exposure at Matjiesdrift. (E) Volcaniclastic deposit exposed on Sittingbourne Farm in a small quarry. (F) Well-rounded quartz pebble (white arrow), which are common in the volcaniclstic deposit at Sittingbourne. (G) *Ex-situ* fragments of red-black siliceous veins that weather to white in the in the outcrop. (H) Volcaniclastics exposed at Voëlvlei with white accretionary pellet-rich tuff outlined in blue dashed lines. (I) Clast-rich tuffaceous sandstone that overlies accretionary pellet-rich tuff. White arrow points to subrounded quartzite pebbles. (J) White, accretionary pellet-rich tuff with white arrows pointing to vertically compressed ovoid accretionary pellets that are preferentially weathered. (K) Sandstone and mudstone units of the Hartenbos Formation (blue line separates the two facies). White dashed line delineates scree from *in-situ* outcrop. Pink arrows indicate the exact position from which respective samples were extracted.

A Klipkop
C
B Klipkop
C Klipkop
KLIP
10 cm
D Matjiesdrif
MATJ
5 cm
E Sittingbourne
SITT2
F Sittingbourne
5 cm
G Sittingbourne
2 cm

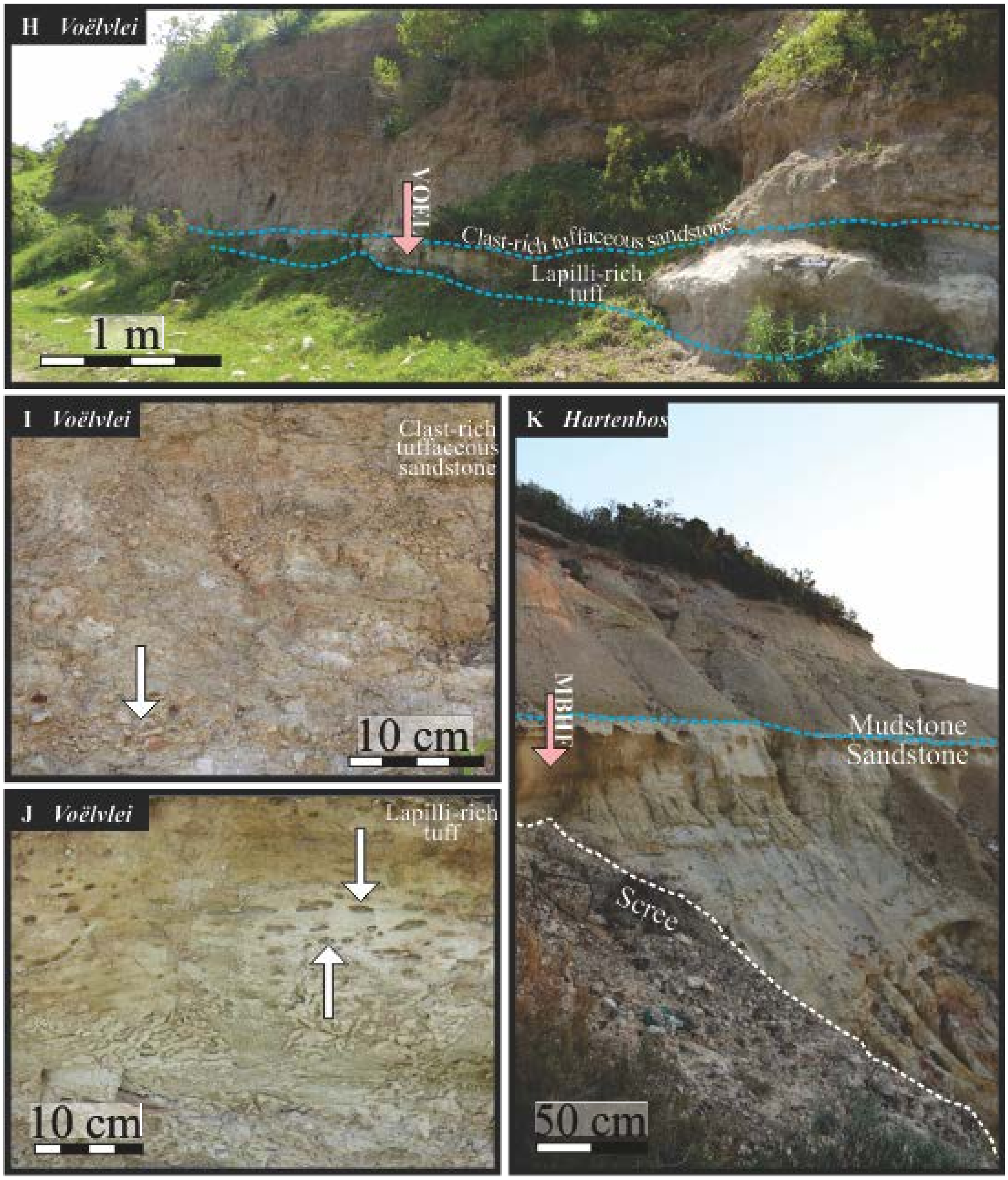

Sittingbourne small quarry (samples SITT2 and SITT3)

Accretionary pellet-rich tuffaceous sandstones commonly outcrop on the Sittingbourne Farm ~2 km west of Hartenbos along the R328 (Fig. 5.18), and in borehole SI 2/89 that was drilled there. Undifferentiated 'tuffaceous deposits' occupy most of the 80 m borehole (Viljoen, pers. com.), which no doubt correlate to the scattered outcrops around the aggregate-processing plant there. A 30 m long, 4 m high outcrop of poorly differentiated brown accretionary pellet-rich tuffaceous sandstone, with rare quartzite clasts, exists in a small farm quarry (34° 7'1.74"S; 22° 4'31.54"E). The light brown volcaniclastic deposit is composed of two crude beds of equal (~2 m) thickness (Fig. 5.18E). The basal unit is massive and rich in poorly-structured accretionary pellets, while the upper bed contains fewer pellets, although rare well-rounded quartzite clasts were found throughout both (Fig. 5.18F). Both white calcareous and red-black siliceous veining (Fig. 5.18F, G) are present in some areas that likely formed from during transport of mineral-rich fluids during devitrification of the ash deposit. Microscopic assessment revealed abundant glass-shards (Fig. 5.19) indicating that the unit has not undergone full alteration into clay minerals. A sample was extracted from the basal accretionary pellet-rich unit from an area that contained no visible quartzite clasts.

A second outcrop on the Sittingbourne Farm 500 m north of the previous site (34° 6'43.27"S; 22° 4'27.71"E; Fig. 5.8) exposes a similar tuffaceous sandstone deposit at approximately the same stratigraphic interval as SITT2, although here the proportion of accretionary pellets was reduced in comparison and the unit had an overall orange-brown colour.

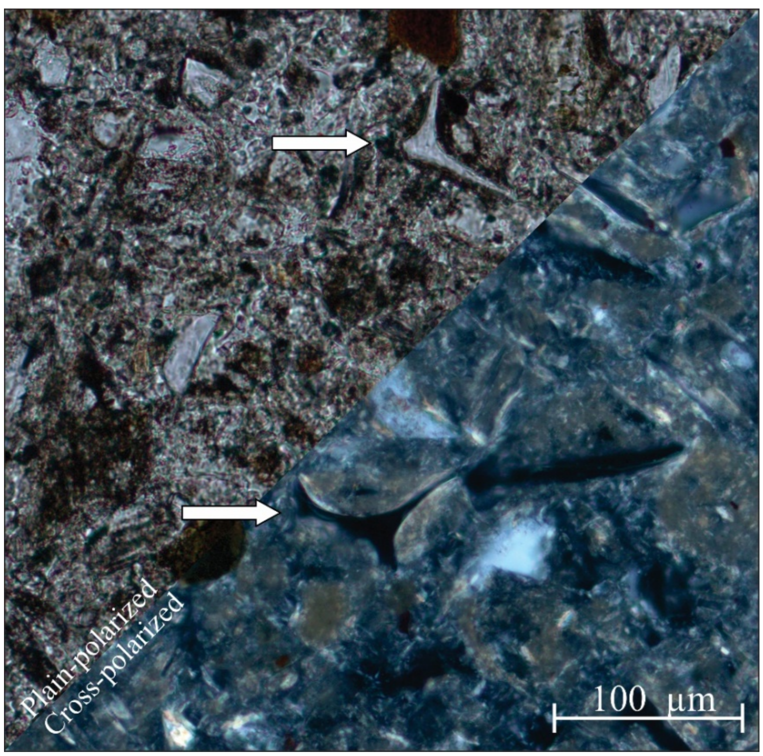

Fig. 5.19. Photomicrograph of a thin section produced from the volcaniclastic rock exposed in the small quarry at Sittingbourne Farm in the Mossel Bay Basin. White arrows point to tricuspate class shards.

Voëlvlei (sample VOEL)

Scattered outcrops of the Uitenhage Group exist near Vlees Bay and on the eastern banks of the Vogel valley, comprising the Enon and Kirkwood formations. Mudstone-dominated lithologies of fluvial origin outcrop around Voëlvlei and a distinctive volcaniclastic deposit outcrops in a river cutting there (34°16'1.13"S; 21°50'23.95"E; Fig. 5.8). The outcrop is 3 m high and comprises a 2.7 m brown-grey tuffaceous sandstone bed with rare quartzite pebbles overlying a 30 cm thick white and light-grey accretionary pellet-rich ash layer, which contains clay-sized particles that are powdery and friable (Fig. 5.18H, I J) and poorly structured accretionary pellets. The upper bed is likely re-sedimented ash mixed with siliciclastic detritus, whereas the basal bed is probably of pyroclastic origin, evidenced by the preservation of accretionary pellets, the consistently clay-sized grain constituents and the lack of any quartzite pebbles or grit (Fig. 5.18J).

Hartenbos parastratotype (sample MBHF)

The Hartenbos Formation is exposed in an old excavation east of the N2 highway at its parastratotype near Hartenbos (34° 7'8.63"S; 22° 6'30.57"E; Fig. 5.8). These sandstone and mudstone units (Fig. 5.18K) are the distal, finer-grained equivalent of the Buffelskloof Formation, which together overlie the Enon and Kirkwood formations in the Mossel Bay Basin (Muir et al., 2017b in section 2.2.2 of this thesis). Medium- to coarse-grained beige sandstone was sampled from this outcrop in order to constrain its age using detrital zircon U-Pb geochronology.

5.2.3.2 U-Pb geochronology

KLIP

Zircon crystals extracted from the sandy-mudstone bed range considerably in size from 50 to 225 µm and shape. Many of the crystals are rounded or are angular fragments, with only a small fraction that are unbroken euhedral. Both the euhedral and abraded/broken grains have stubby to prismatic habits. Internal structures revealed by CL imagery are diverse, with predominately fine and medium oscillatory zoning, but there also unzoned crystals (e.g., crystal 75 in Fig. 5.20). Core-and-rim textures are common in the sample suggesting multiple crystallization episodes (e.g., crystal 99 in Fig. 5.20).

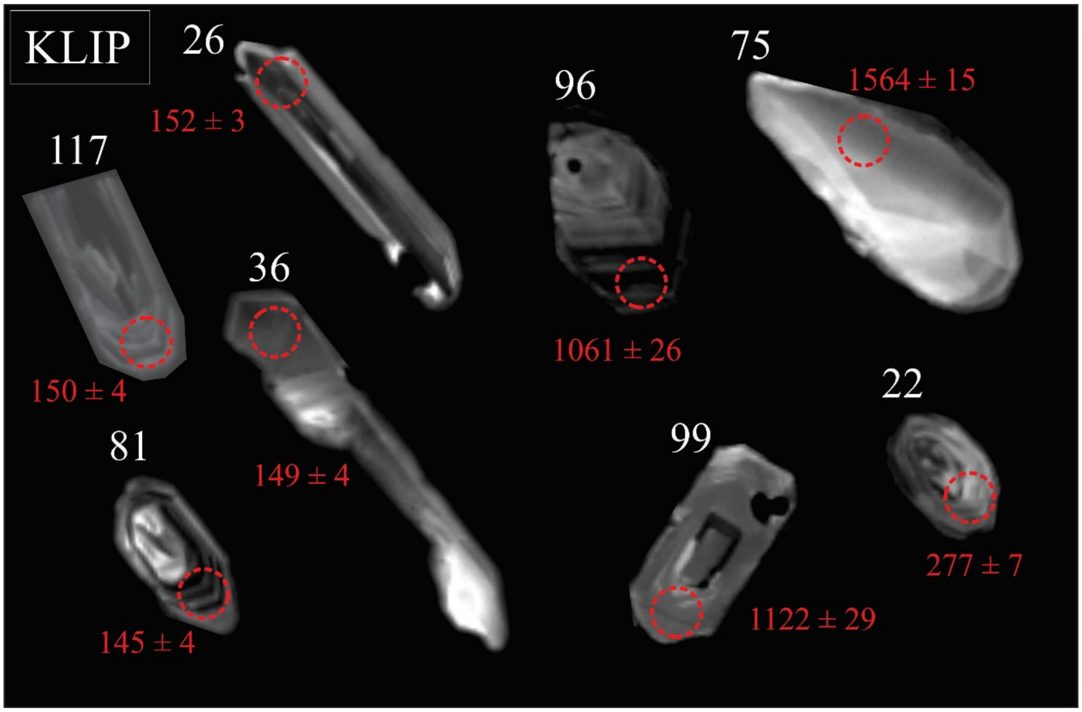

Fig. 5.20. Composite diagram of CL images of zircons that yield concordant dates in sample KLIP from the Mossel Bay Basin. Individual zircon indicated by white number and analytical spot (26 µm diameter) with respective $^{206}Pb/^{238}U$ date are red.

A total of 87 concordant analyses were obtained from the 129 crystals analysed. Crystals range in age from Mesozoic (33 %), Palaeozoic (30 %) to Precambrian (37 %) (Fig. 5.21; Table D9 in Appendix D; Fig. F2A in Appendix F). Mesozoic dates occupied several peaks on the probability density diagram (Fig. 5.21) including a largest, youngest peak around 150 Ma, which is considered a robust estimate of the maximum depositional age of this reworked volcaniclastic sample. Analytical metrics are as follows: YSG = 145 ± 4 Ma; YDZ = 144.5 +2.2/-3.8 Ma (95% conf.); YPP = 150 Ma.

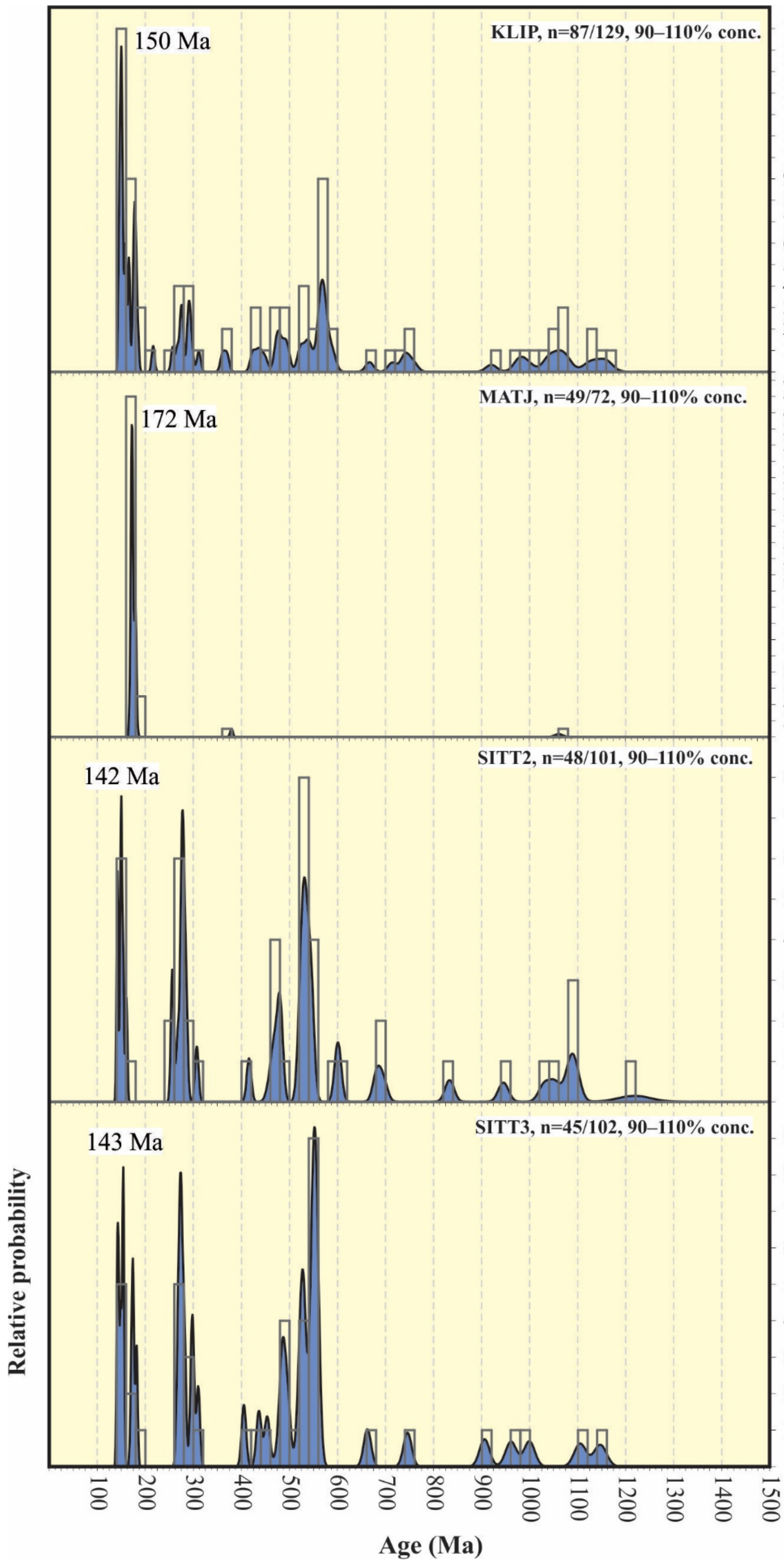
150 Ma
KLIP, n=87/129, 90–110% conc.
172 Ma
MATJ, n=49/72, 90–110% conc.
142 Ma
SITT2, n=48/101, 90–110% conc.
143 Ma
SITT3, n=45/102, 90–110% conc.
Relative probability
Age (Ma)

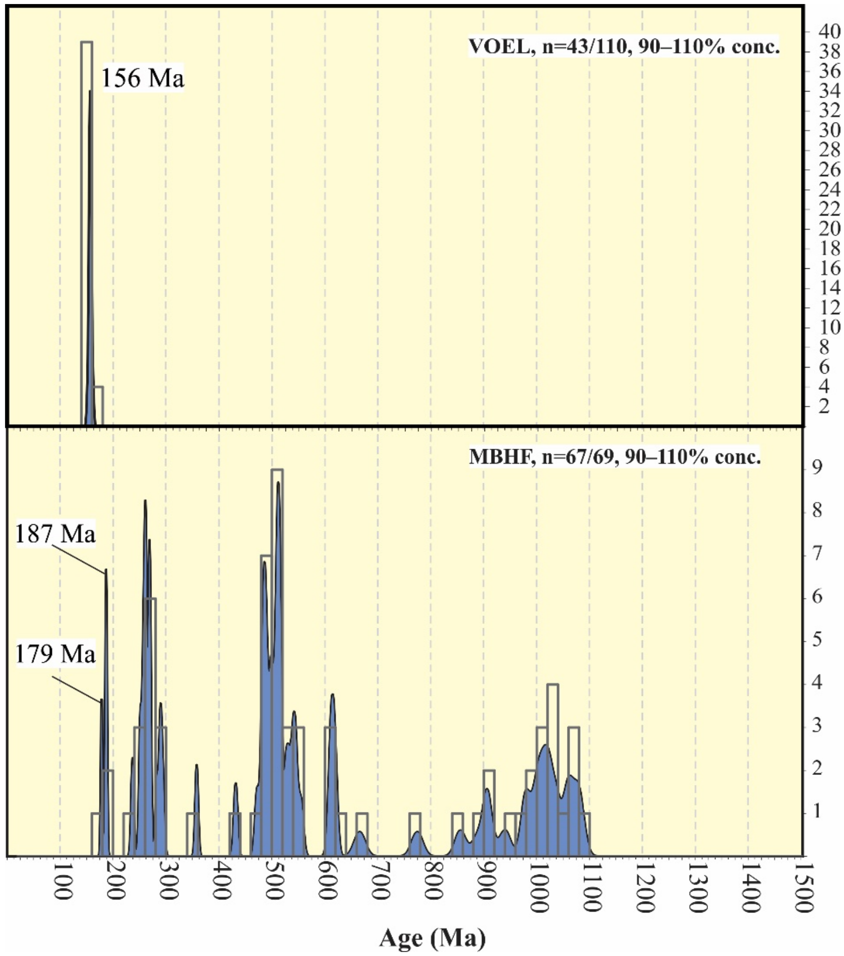

Fig. 5.21. U-Pb dates of zircons from all samples in the Mossel Bay Basin shown as age probability density diagrams (blue area) combined with frequency histograms (grey bars) with 20 Ma intervals. Only concordant data are shown: n = x/y means that x out of a total of y zircons yielded concordant dates. Youngest graphically-defined peak (YPP) are indicated.

MATJ

Zircons are strongly euhedral and range from 80 to 250 µm with predominantly stalky and prismatic habits, and also rare needle-shaped grains. All crystals are colourless and some contained inclusions. CL images reveal fine and medium oscillatory zoning patters usually without core-and-rim textures (e.g., crystals 3, 8 and 12 in Fig. 5.22), but some crystals have possible xenocrystic cores (e.g., crystal 35 in Fig. 5.22).

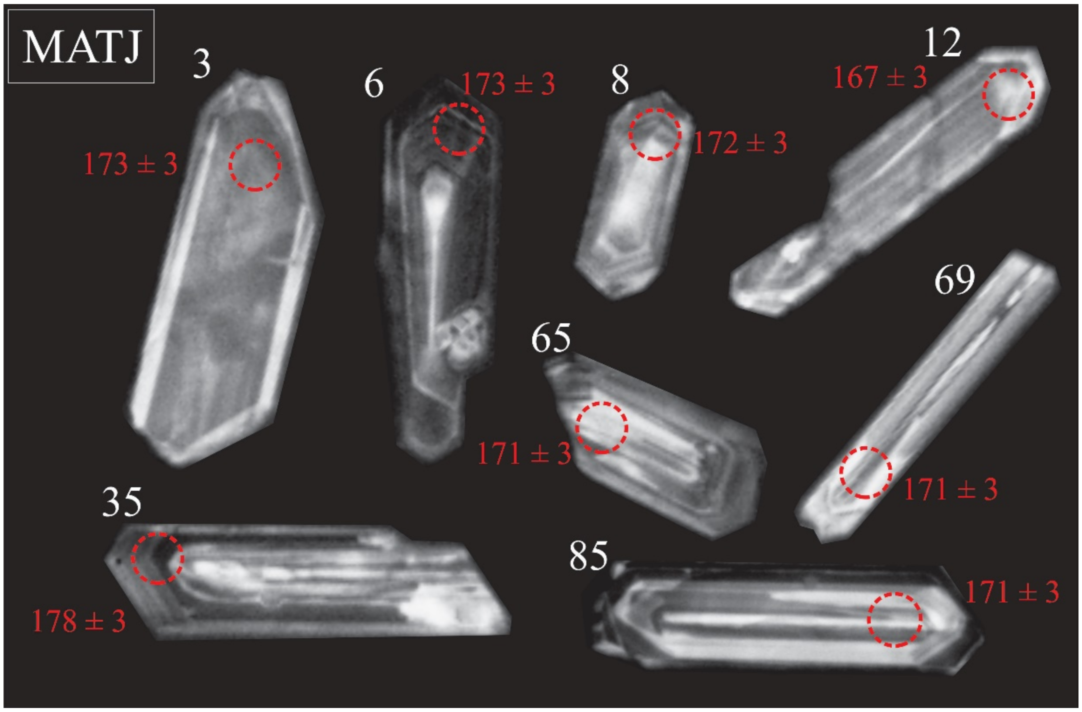

Fig. 5.22. Composite diagram of CL images of zircons that yield concordant dates in sample MATJ from the Mossel Bay Basin. Individual zircon indicated by white number and analytical spot (26 µm diameter) with respective $^{206}Pb/^{238}U$ date are red.

In this sample, 49 of the 72 analyses are concordant and mostly yield Mesozoic dates (~96 %), with just 1 Palaeozoic and 1 Precambrian dates (Fig. 5.21; Table D10 in Appendix D; Fig. F2B in Appendix F). The Mesozoic zircons farm a single population on the probability density diagram (Fig. 5.21) that contains a large peak at 172 Ma and subordinate peak at 179 Ma. The lack of significant detrital input, narrow distribution of zircon dates and the similarity of internal and external crystal morphologies further support the interpretation that this unit is of pyroclastic origin. Analytical metrics are as follows: YSG = 167 ± 3 Ma; YDZ = 166.9 +1.9/-3.1 Ma (95% conf.); YPP = 172 Ma. The most coherent grouping of 32 zircons identified by TuffZirc occurs at 172.62 +0.56/-0.94 Ma, which is a best estimate for the depositional age of the deposit (Fig. 5.23). It is likely that the youngest two dates that are excluded by the algorithm are spuriously young due to subtle Pb-loss, while there is clearly also an inherited ~180 Ma component in these data.

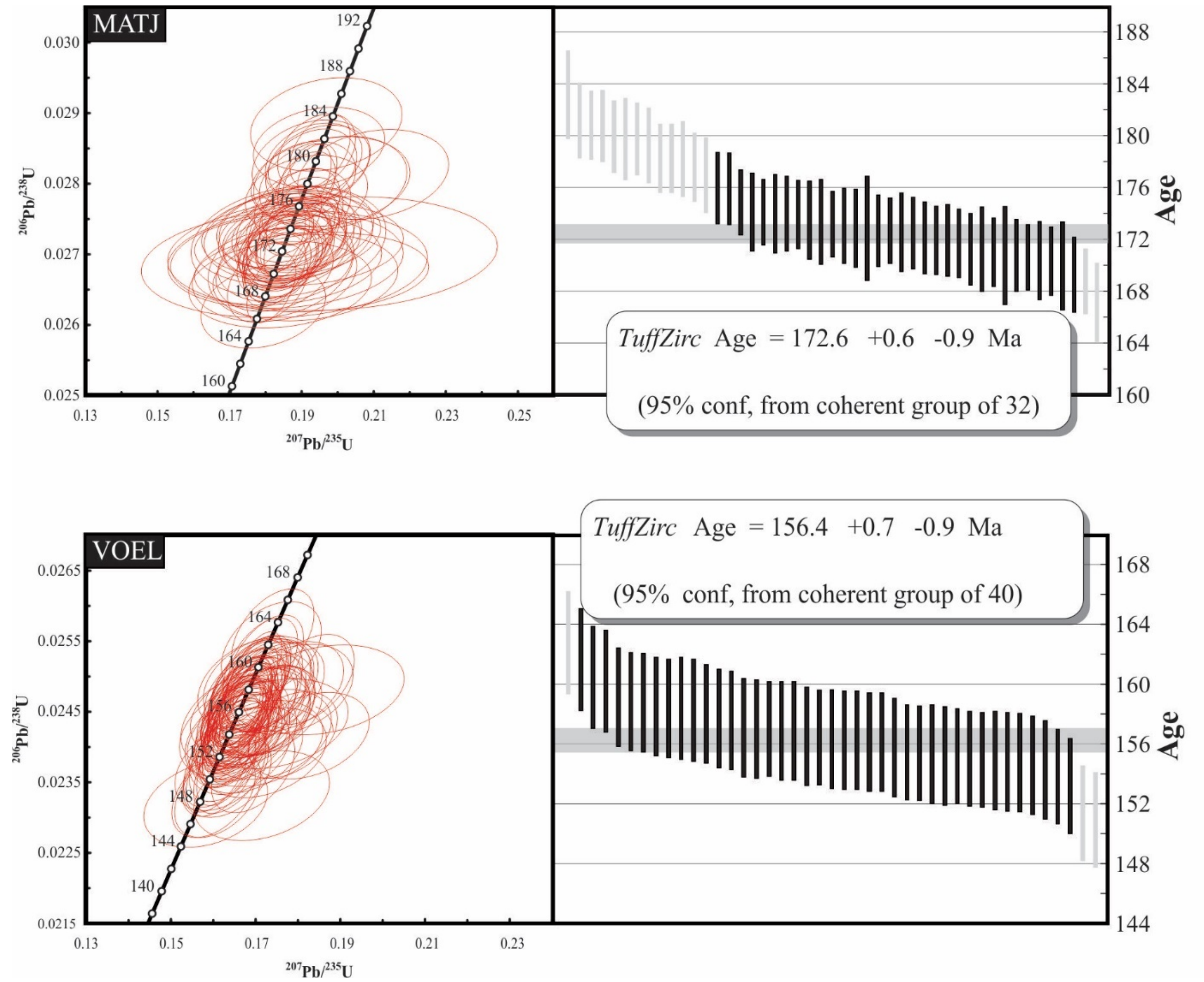

Fig. 5.23. Concordia diagrams (left) and concordant Mesozoic $^{206}Pb/^{238}U$ zircon dates arranged by age (right) for two pyroclastic deposits in the Mossel Bay Basin. Horizontal grey line is the age calculated by TuffZirc with vertical grey lines representing dates rejected from the age calculation. All individual errors are 2σ.

SITT2

Zircons from this sample vary in size and shape, ranging from 60 to 230 µm. They occur as small angular fragmentary and rounded grains and as larger crystals with varied degrees of elongation from stubby to prismatic. Internal textures included fine, medium and rarely broad oscillatory zoning (Fig. 5.24), some crystals had no clear zoning (e.g., crystal 8 in Fig. 5.24) and some contained xenocrystic cores (e.g., crystal 105 in Fig. 5.24). Some crystals contain inclusions and some are severely cracked.

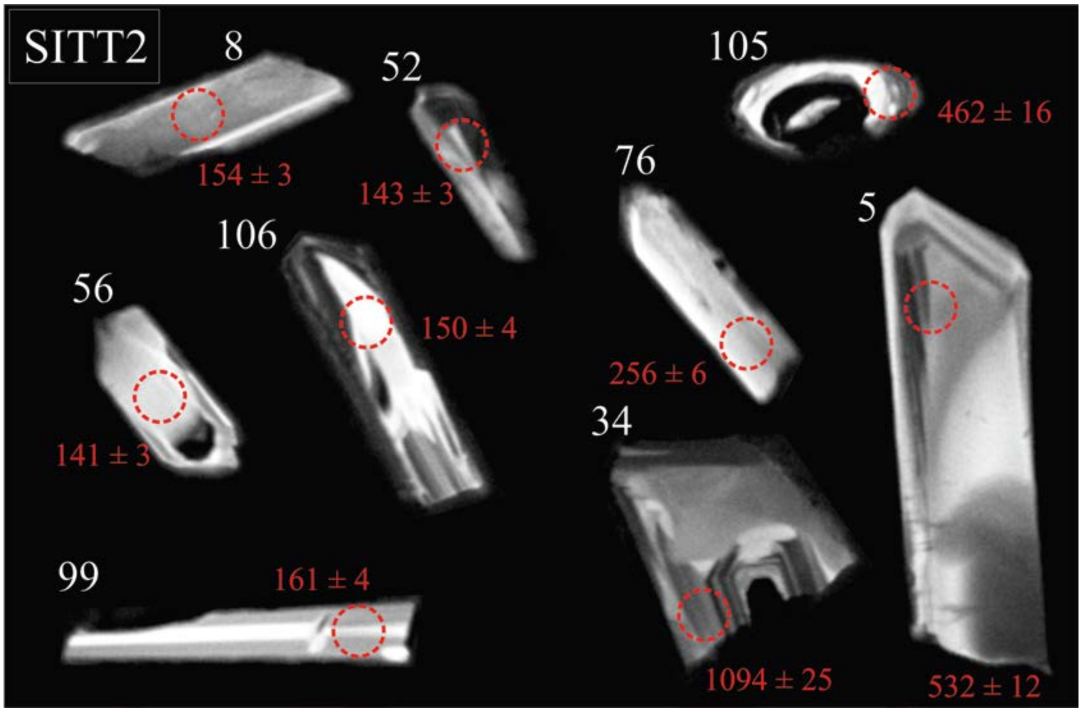

Fig. 5.24. Composite diagram of CL images of zircons that yield concordant dates in sample SITT2 from the Mossel Bay Basin. Individual zircon indicated by white number and analytical spot (26 µm diameter) with respective $^{206}Pb/^{238}U$ date are red.

Zircons are clearly derived from a variety of sources and concordant analyses span the Mesozoic (14 %), Palaeozoic (49 %) and Precambrian (37 %), with multiple age peaks (Fig. 5.21; Table D11 in Appendix D; Fig. F2C in Appendix F). Mesozoic dates form a youngest peak on the probability density diagram at 142 Ma, with an older and larger peak at 150 Ma (Fig. 5.21). The youngest (142 Ma) peak is supported by two grains, it is probably a robust reflection of the youngest age component and maximum depositional age of this mixed-origin volcaniclastic unit. Other analytical metrics are: YSG = 141 ± 3 Ma; YDZ = 141 +2.7-3.5 Ma (95% conf.).

SITT3

As in SITT2, zircons are morphologically diverse ranging from 70 µm stubby grains to crystals with a needle habit (and fragments thereof) that are up to 190 µm. Inclusions (e.g., crystals 31, 44 and 48 in Fig. 5.25) and xenocrystic cores (e.g., crystal 48 in Fig. 5.25) are common when imaged using the CL detector (Fig. 5.22) and fine to medium oscillatory zoning prevailed. The youngest concordant analysis (crystal 48 in Fig. 5.22) clearly reveals at least two periods of crystallization with contrasting zonation textures, however most crystal rims are too narrow for analysis using an analytical spot size of 26 µm.

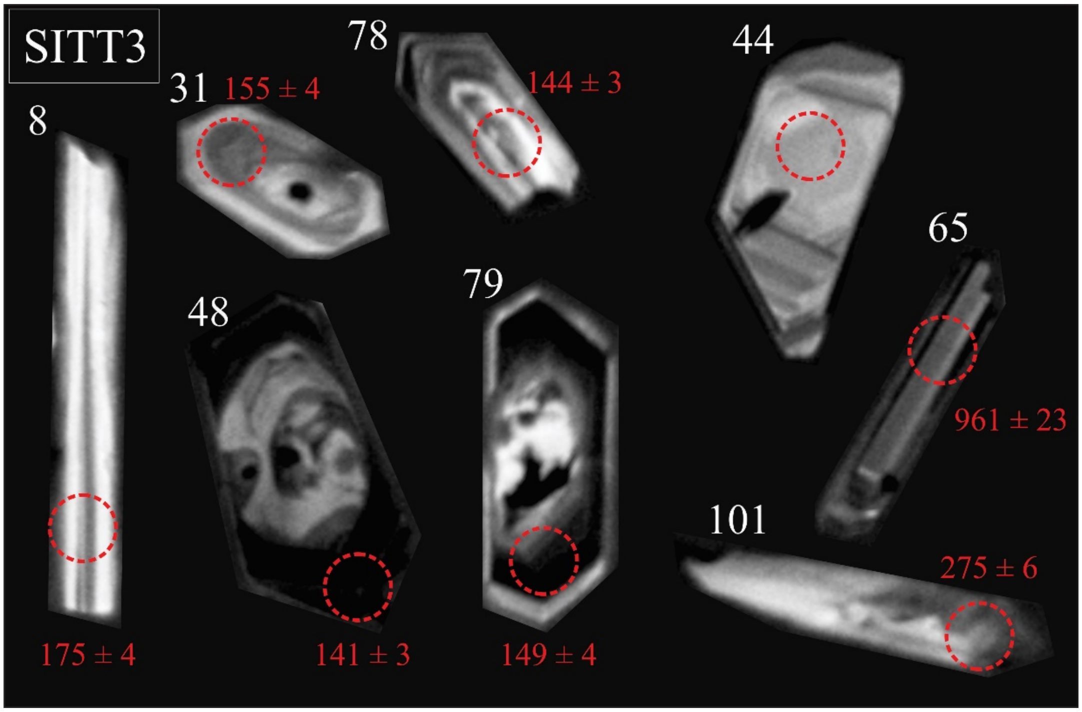

Fig. 5.25. Composite diagram of CL images of zircons that yield concordant dates in sample SITT3 from the Mossel Bay Basin. Individual zircon indicated by white number and analytical spot (26 µm diameter) with respective $^{206}Pb/^{238}U$ date are red.

Based on 46 concordant analyses (out of a total of 106), zircons are Mesozoic (17 %), Palaeozoic (45 %) and Precambrian (38 %) in age, and distributed into multiple age peaks on the probability density diagram (Fig. 5.21 Table D12 in Appendix D; Fig. F2D in Appendix F). The youngest peak with more than 1 date is 143 Ma (YPP), although older Mesozoic peaks also occur at 149 Ma, 154 Ma and 174 Ma. Other analytical metrics are: YSG = 141 ± 3 Ma; YDZ = 141.5 +3.1/-3.7 Ma (95% conf.). Although young crystals are rare in both SITT2 and SITT3, they show approximately equivalent youngest components and based on their close proximity and lithological similarity ought to be considered a single volcaniclastic package that was deposited shortly after the ~145 Ma Jurassic – Cretaceous transition.

VOEL

Zircon crystals range in size from 60 to 200 µm, with stalky and prismatic habits and the longest grains typically exhibiting a needle habit. Morphologies are compatible with the interpretation that the deposit is pyroclastic in that they are mostly euhedral with either fine or medium oscillatory zoning (e.g., crystals 46, 60 and 62), or no zoning at all (e.g., crystal 6 in Fig. 5.26). Under plain light they are all colourless except for a few opaque inclusions present in some of the grains.

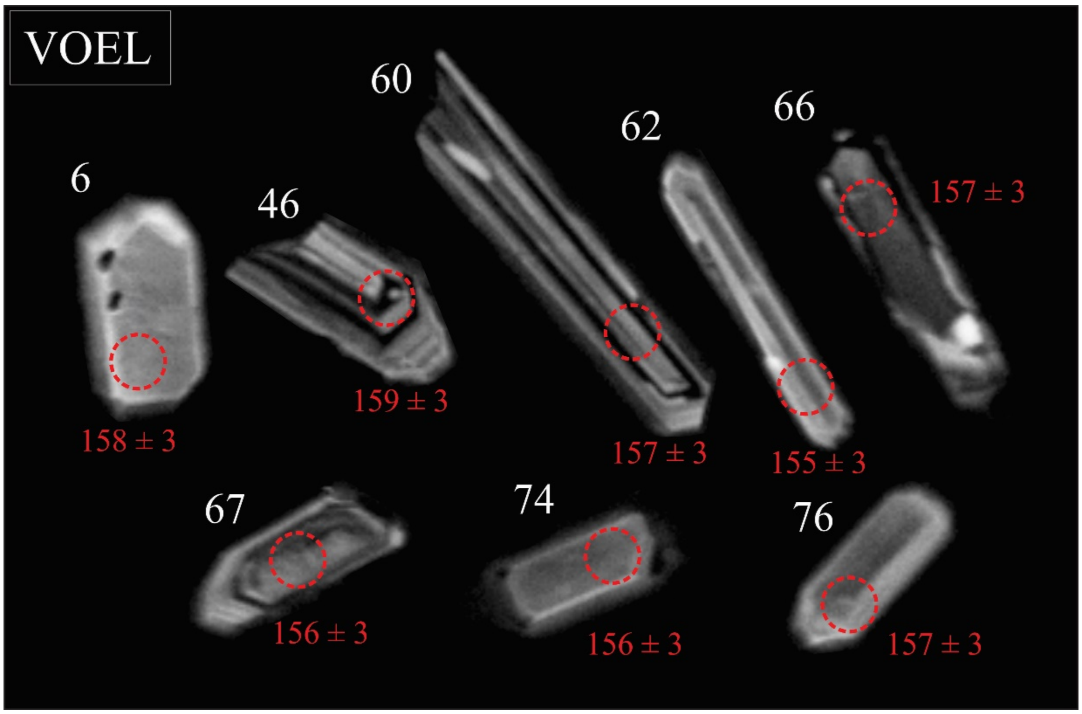

Fig. 5.26. Composite diagram of CL images of zircons that yield concordant dates in sample VOEL from the Mossel Bay Basin. Individual zircon indicated by white number and analytical spot (26 µm diameter) with respective $^{206}Pb/^{238}U$ date are red.

The 43 concordant dates (from a total of 110) show that all zircons are roughly of the same age ~156 Ma (Fig. 5.21; Fig. 5.23; Table D13 in Appendix D), which is the youngest (and only) graphical age component in the sample (YPP), with a youngest crystal (YSG) = 151 ± 3 Ma and YDZ = 150.2 +2.2/-3.1 Ma (95% conf.). The approximate equivalence of all zircons supports a single ash-fall event origin for the deposit, which dates to 156.4 +0.7/-0.9 Ma (Kimmeridgian), calculated using the most coherent clustering of dates identified by TuffZirc assuming minor inheritance and Pb-loss (Fig. 5.23).

MBHF

Zircons from this sample are some of the largest in the entire dataset. Most are over 100 µm long, and some reach 300 µm (e.g., crystal 56 in Fig. 5.27). Crystals that are < 100 µm long are typically fragments of larger grains (e.g., crystal 79 in Fig. 5.27). They range from colourless to beige and have prismatic and stalky habits that are usually euhedral and rarely rounded (e.g., crystals 49 and 73 in Fig. 5.27). Internally, they show fine oscillatory zoning that is simple, or with inherited cores and inclusions (e.g., crystals 55, 82 and 49 in Fig. 5.27).

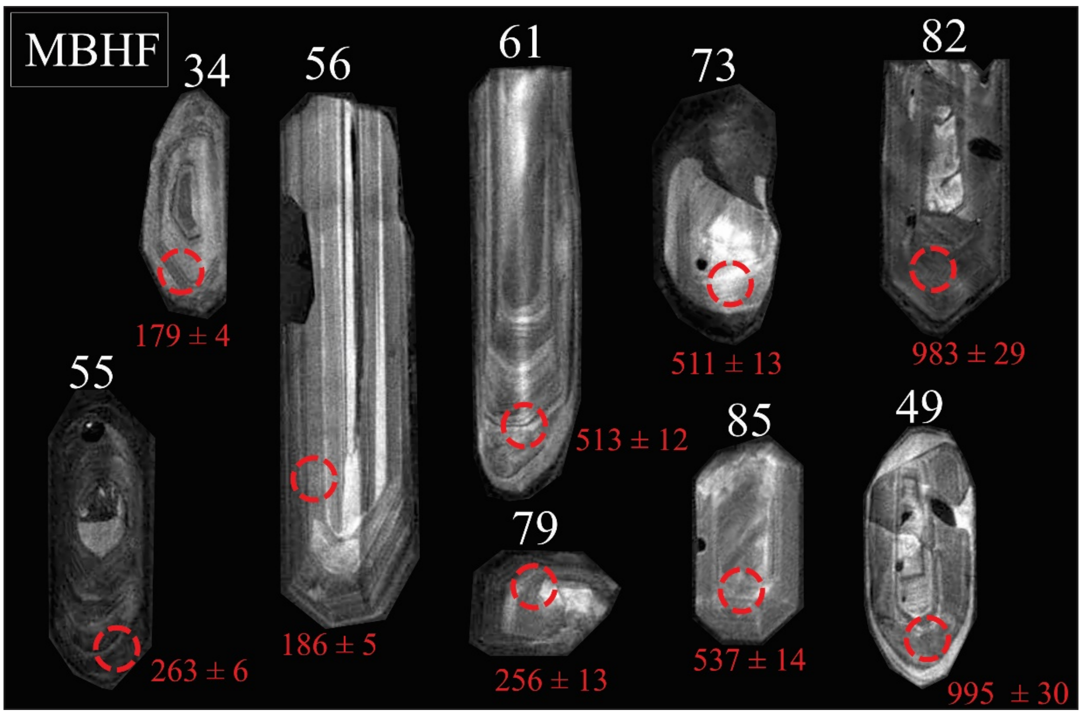

Fig. 5.27. Composite diagram of CL images of zircons that yield concordant date in sample MBHF from the Mossel Bay Basin. Individual zircon indicated by white number and analytical spot (26 µm diameter) with respective $^{206}Pb/^{238}U$ date are red.

A total of 67 concordant dates are Mesozoic (~7 %), Palaeozoic (~50 %) and Precambrian (~43 %) and occupy multiple complex populations most notably at ~260 Ma and ~500 Ma with subordinate Precambrian populations (Fig. 5.21; Table E1 in Appendix E; Fig. F3B in Appendix B). The youngest graphically-defined age component is at ~187 Ma (YPP), which is a robust measure of the maximum deposition of this unit. Other metrics are: YSG = 179 ± 4 Ma; YDZ = 178.3 +4.6 / -4.4 Ma (95% conf.). Stratigraphic field relationships dictate that the Hartenbos Formation is younger than the underlying Enon and Kirkwood formations (Malan and Viljoen, 1990), but the lack of young, Cretaceous zircons hampers further chronostratigraphic relationships between these strata. Furthermore, major Late Permian and Cambrian populations simply indicate Karoo and Cape Supergroups are likely sources, either directly or through recycling of the underlying Enon and Kirkwood formations. The presence of large, euhedral Cambrian zircons in the Hartenbos Formation may reflect a direct Maalgaten Granite Suite source because crystals are unlikely to have maintained such morphologies if they were significantly transported during Palaeozoic recycling episodes. The Maalgaten Granite Suite is a known source for the Uitenhage Group in parts of the Mossel Bay Basin nearby, where boulder-sized granitic clasts in conglomerate beds are described (Bordy and America, 2016).

5.2.3.3 Basin synthesis

The Mossel Bay Basin provides one of the best case studies for the onshore Uitenhage Group deposition because there are ample means to assess the depositional age of the accommodated strata. Firstly, there is an angular unconformity that separates the basal Enon and Kirkwood formations from the overlying Buffelskloof and Hartenbos formations. This implies that these strata record at least two phases of rift-related tectonism, and establishes relative age constraints – the Enon and Kirkwood predate the Buffelskloof and Hartenbos formations (Malan and Viljoen, 1990). Secondly, there are abundant volcaniclastic deposits in the Kirkwood Formation in the Mossel Bay Basin that provide a means to constrain the age of deposition.

The oldest dated deposits in the Mossel Bay Basin are Aalenian (sample MATJ), rough time-equivalents of those exposed in Heidelberg to the west and > 10 Ma older than all previous age estimates for the Kirkwood Formation (McLachlan and McMillan, 1976; Dingle et al., 1983; McMillan et al., 1997; Shone, 2006). These lowermost Middle Jurassic deposits presumably occupy a relatively basal position in the stratigraphic succession of the Uitenhage Group in the Mossel Bay Basin and were deposited shortly after the onset of rifting (Fig. 5.28). Subsidence and deposition continued throughout the Jurassic, with the majority of extension being taken up by displacement along the Worcester Fault, which follows the southern margin of the George Granite Pluton (Fig. 5.8), but also by subordinate intra-basinal faults (Fig. 5.28) and at fault transfer zones NE of Herbersdale (Fig. 5.8; Viljoen, 2000). Deposition continued into the Early Cretaceous, evidenced by Lower Cretaceous volcaniclastic interbeds in the Kirkwood Formation. Following this, also during the Early Cretaceous, displacement along boundary faults accelerated during a second phase of extension that generated additional accommodation space into which the Buffelskloof and Hartenbos formations were deposited (Fig. 5.28).

Importantly however, the dated volcaniclastics are not equally distributed across the areal extent of the Mossel Bay Basin, which complicates models of basin stratigraphy. The 172.6 +0.6/-0.9 Ma bentonite at Matjiesdrift is isolated from other dated strata in the east by a large ridge of Table Mountain Group basement on the Hartebeeskuil Farm (from here referred to as Hartebeeskuil Ridge). Conversely, the Kirkwood Formation exposures east of Hartebeeskuil Ridge at Kipkop (KLIP) and Sittingbourne (SITT2&3) are no older than Upper Jurassic – Lower Cretaceous, as indicated by their respective maximum depositional ages. Such an age discrepancy of the volcaniclastic interbeds might be explained by the differential erosion of the western and eastern portions of the Mossel Bay Basin (Fig. 26). If subsidence initiated during the Early Jurassic, as evidenced by the presence of lowermost Middle Jurassic strata, then greater denudation of the Uitenhage Group west of Hartebeeskuil Ridge would explain why the deposits that outcrop there are older than those to the east. However, the thick package of overlying Buffelskloof Formation in the west, and that the MATJ bentonite is exposed on a land surface that is not particularly incised compared to the those further east suggests that recent erosion does not account for the age discrepancy in the exposed volcaniclastic interbeds. Instead, the western Mossel Bay Basin may have experienced greater exhumation during the Early Cretaceous during a second phase of subsidence, when the Buffelskloof and Hartenbos formations were deposited. During this time, the underlying Enon and Kirkwood formations may have been more deeply truncated in the west than in the east. If displacement along boundary faults was greater in the east than west during the Early Cretaceous deposition of the Buffelskloof and Hartenbos formations (i.e., the depocentre was in the east), then more of the underlying strata would have been preserved there subsequent to incision by high-energy processes that acted during their deposition. Such a scenario in the Mossel Bay Basin does not seem unlikely considering that basin depocentres in the offshore Gamtoos Basin also migrated during the late Valanginian (Paton and Underhill, 2004).

Fig. 5.28. Evolution of the Mossel Bay Basin east of Hartebeeskuil Ridge from the Early Jurassic onset of rifting to present (see text for details). Map based on the 1: 50 000 Council for Geoscience map sheet 3422AA (Viljoen and Malan, 1993).

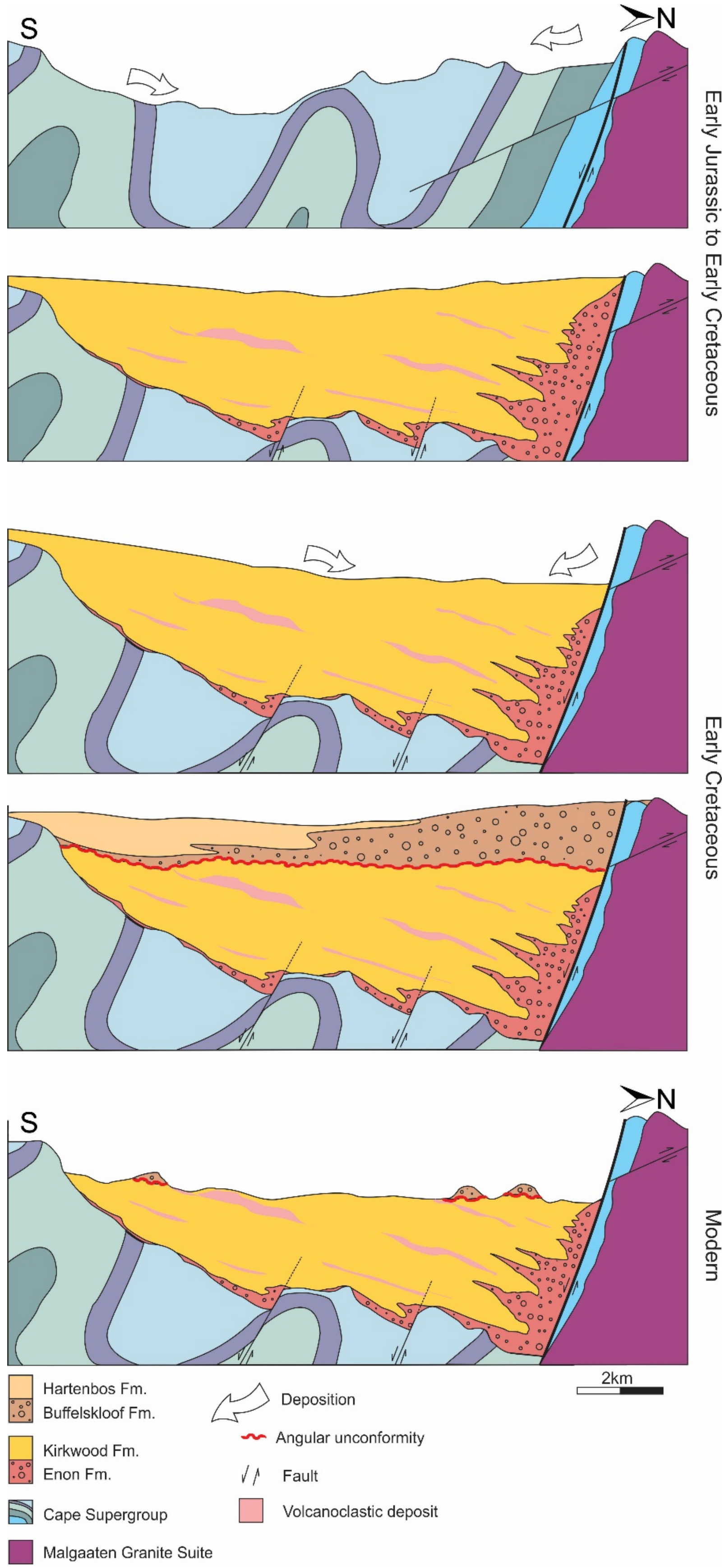

S
N
Early Jurassic to Early Cretaceous
Early Cretaceous
S
N
Modern
2km
Hartenbos Fm.
Buffelskloof Fm.
Kirkwood Fm.
Enon Fm.
Cape Supergroup
Malgaaten Granite Suite
Deposition
Angular unconformity
Fault
Volcanoclastic deposit

5.2.4 Oudtshoorn Basin

The Oudtshoorn Basin is situated in the interior of the Western Cape south in the 'Little Karoo' district, between the Outeniqua and Swartberg Mountain ranges (Fig. 5.29). This, half-graben, is bounded to the north by the Cango Fault, which is part of a larger Cango-Baviaans-Gamtoos fault array along which exist several Mesozoic rift basins – the Vlakteplaas, Goergida, Baviaanskloof and Gamtoos basins (Fig. 2.1). The Oudtshoorn Basin is 80 km long and ~ 20 km wide in the E-W and N-S directions, respectively. Just like the other Mesozoic rift basins along the southern Cape, it is an erosional and/or structural relict with its long axis running parallel to structural trends in the Palaeozoic basement. The basement rocks to the Oudtshoorn Basin are principally the Cape Supergroup, and in a few isolated localities directly north of the Basin, along Cango Fault. Apart from the rare occurrence of Cape Supergroup basement directly north of the Basin, this region is dominated by the Cango Group, which occupies the interior strata of a large anticline that formed in the Cape Orogenic episode, and acted as a separate structural block during the Mesozoic and Cenozoic (Green et al., 2016). The Basin is filled with an unknown thickness of Uitenhage Group deposits, although an estimated 3.1 km composite thickness is exposed in isolated outcrops of predominately conglomerates/breccias, sandstones and mudstones (Du Toit, 1974; Dingle et al., 1983). Some previous efforts have been made to map out sedimentary facies across the basin (Du Preez, 1944; Holzförster, 2007; Dinis, 2018), although it remains unclear how the isolated outcrops relate to each other stratigraphically limiting the usefulness of such mapping efforts in understanding basin dynamics through time. Despite this, the Uitenhage Group in the Oudtshoorn Basin can be divided into three discrete stratigraphic units fairly confidently: the Enon, Kirkwood and Buffelskloof formations. Although the Enon Formation comprises primarily conglomerates along the southern margin as well as the eastern and western flanks of the basin, a second conglomerate-breccia unit is mapped as the Buffelskloof Formation along the northern boundary of the Basin. This division is based purely on grainsize and facies differences (Lock et al., 1975) and an apparent angular relationship between the upper Buffelskloof Formation and the lower Enon and Kirkwood formations. Although a clear field example of the angular unconformity remains elusive, bedding is varied but often significantly tilted in the Enon and Kirkwood formations, while retaining subhorizontal to horizontal attitudes in the Buffelskloof Formation (Dingle et al., 1983; Malan and Viljoen, 1990). The sandstone and mudstone-dominated Kirkwood Formation generally occupies the central portion of the basin (Du Preez, 1944; Lock et al., 1975; Holzförster, 2007; Dinis, 2018) where the landscape is topographically flatter and outcrop is relatively sparse in comparison with the flanks of the basin. Apart from the topographically rough terrain along the basin margins, where natural exposures of the conglomerates in the Enon and Buffelskloof formations are very common (Lock et al., 1975; Dinis, 2018), outcrops can be found in quarries, road-, railway- and river-cuttings.

5.2.4.1 Outcrop description

Buffelskloof Formation cliffs (sample OES1)

A 30 m high cliff is accessible at a railway cutting in the north eastern part of the Oudtshoorn Basin adjacent the N12 roadway (33°32'17.74"S; 22°27'13.26"E; Fig. 5.29). The outcrop typifies those of the topographically rugged terrain in the northern basin where the immature, poorly sorted, polymictic breccia of the Buffelskloof Formation is mapped. The subrounded to angular clasts range from small pebble to boulder. The mostly clast-supported conglomerate contains several 30 cm thick, 1 m long sandstone lenses, in a bed that has an anomalously low clast to matrix ratio (Fig. 5.30A, B). Overall the breccia and sandstone units are a deep red colour and dip shallowly northwards.

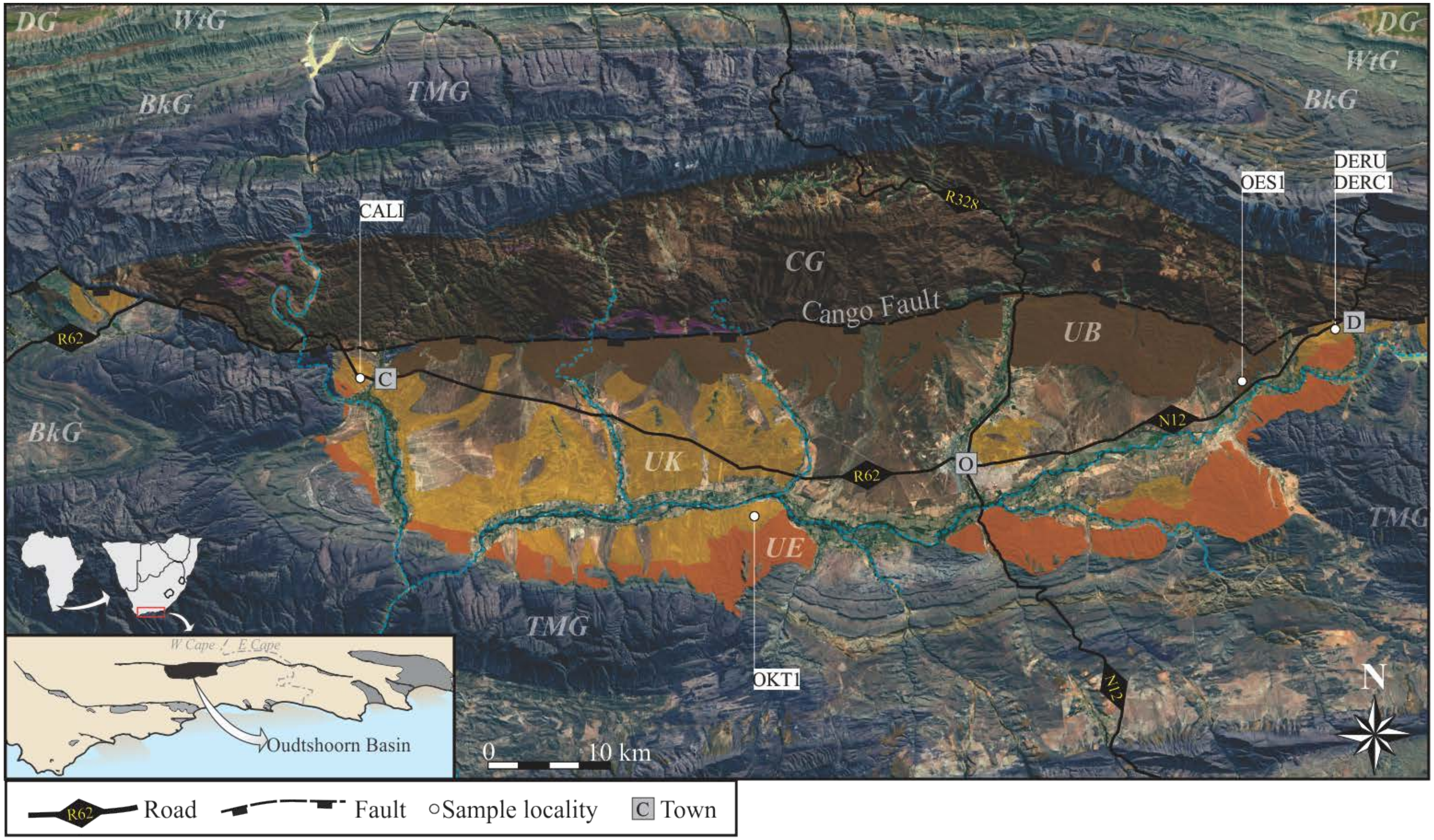

Fig. 5.29. Simplified geological map of the Oudtshoorn Basin. Sample localities are indicated by white circles. Letters and colours are lithostratigraphic units and inshaded areas are recent alluvium. Abbreviations: Towns: C = Calitzdorp; D = De Rust; O = Oudtshoorn. Stratigraphic units arranged from oldest to youngest: CG = Cango Group; TMG = Table Mountain Group; BkG = Bokkeveld Group; WtG = Witteberg Group; DG = Dwyka Group; UE = Enon Formation; UK = Kirkwood Formation; UB = Buffelskloof Formation; UH = Hartenbos Formation. Base maps modified from the 1: 250 000 geological maps sheets 3320 (Theron, 1991) and 3322 (Toerien, 1979) of the Council for Geoscience overlain on ESRI satellite imagery.

Calitzdorp cutting (sample CALI)

A laterally and vertically extensive, northward dipping (at 20º) succession of mudstones, sandstones and conglomerates outcrop in a road-cutting along the R62 on the western side of Calitzdorp (33°31'41.35"S; 21°40'34.16"E; Fig. 5.29). The mudstone packages are 3 – 10 m-thick, massive or horizontally laminated and red in colour. Sandstones and congloemrates are typically less than 20 cm thick, tabular and red, grey or beige. A pink and olive green 20 cm thick bentonite bed is found within the mudstones (Fig. 5.29C, D) and is laterally continuous for 7 m before being obscured by fallen scree at the edge of the outcrop. This bentonite appears without a significant silt-sized component, exhibited popcorn texture weathering (due to the high proportion of smectite clays present in its composition) and is therefore considered of likely ash fall origin.

Fig. 5.30. (Following page). Geological context of the Uitenhage Group samples in the Oudtshoorn Basin. (A) Clast-supported conglomerate-dominated outcrop of the Buffelskloof Formation with a bed that contains fewer clasts outlined in blue dashed line. White dashed lines delineate the area depicted in B. (B) Sandstone lenses outlined in green dashed lines within the low clast to matrix ratio conglomerate bed, outlined in blue dashed lines. (C) Road-cutting in Calitzdorp that exposes mudstones, sandstones and rare conglomerates where not obscured by scree White arrow points to area where bentonite is exposed and depicted in D. (D) Pink bentonite interbed within beige mudstones at Calitzdorp. (E) Naturally eroding ravines in the southern part of the Oudtshoorn Basin. A prominent 1.8 m thick red and white sandstone unit within predominantly mudstones is outlined with blue dashed lines. A bentonite bed is exposed (green dashed lines) or covered by a veneer of scree (green dotted line). Pink arrows indicate the precise location from which samples were taken.

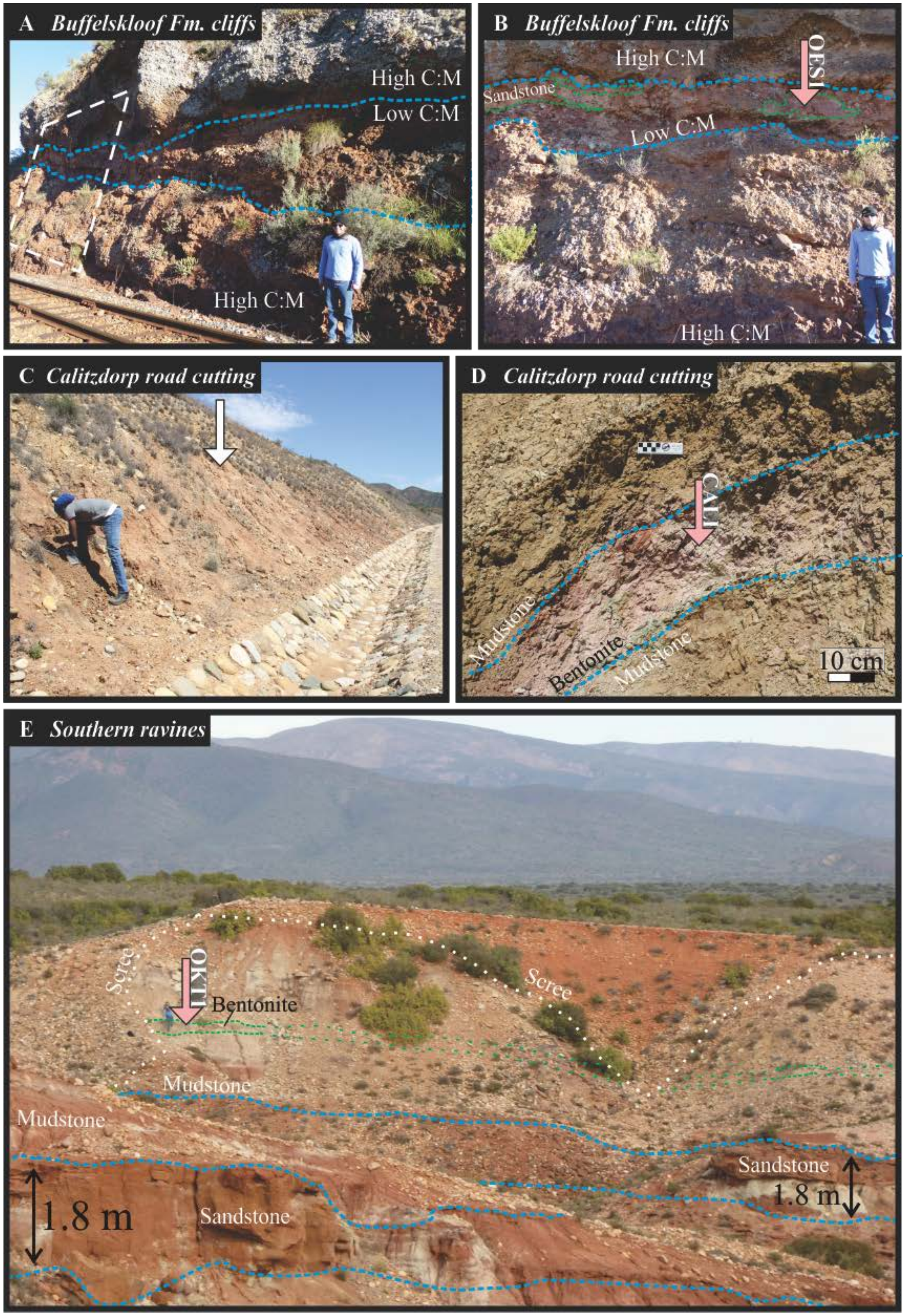
A Buffelskloof Fm. cliffs
High C:M
Low C:M
High C:M
B Buffelskloof Fm. cliffs
High C:M
OES1
Sandstone
Low C:M
High C:M
C Calitzdorp road cutting
D Calitzdorp road cutting
CAL1
Mudstone
Bentonite
Mudstone
10 cm
E Southern ravines
Scree
OKT1
Bentonite
Scree
Mudstone
Mudstone
Sandstone
1.8 m
1.8 m
Sandstone

Southern ravines (sample OKT1)

A natural ravine exposes laterally extensive mudstones and sandstones of the Kirkwood Formation in the south-central portions of the Oudtshoorn Basin (33°38'17.89"S; 21°59'0.18"E; Fig. 5.29). The subhorizontal attitude of bedding and steep sided gullies enables the lateral tracing out of deposits for 50 m or more. Most of the mudstones show palaeosol development with a mottled red-grey colouration and high silt content. A dark green, primarily massive 20 cm thick bentonite interbed can be traced for 50 m sandwiched between a yellow-beige sandstone bed and green-red siltstone, below and above, respectively (Fig. 5.29E). The bentonite is comprised of high purity clay particles with a very minor silt-sized grain component (less than 5%) and was sampled and is of probable pyroclastic origin.

De Rust quarry (samples DERU and DERC1)

A unique succession of rocks (i.e., sandstone, chert, silicified accretionary pellet-rich tuff and silicified breccia) with complex stratigraphic relations are exposed in a roadside quarry along the N12 road, 1 km south west of central De Rust (33°29'37.67"S; 22°31'32.15"E; Fig. 5.29; Fig. 5.31) was first described by Lock et al. (1975). The southern wall of the quarry exposes a number of volcaniclastic and terrigenous clastic rocks (Fig. 5.31B – D). A well-consolidated conglomerate bed defines the lower limit of the exposure on the southern wall of the quarry where not entirely covered with loose scree (Fig. 5.31E). Overlying this is a 1.7 m thick very well consolidated, silicified, accretionary pellet-rich tuffaceous sandstone (Fig. 5.31D) that contains both abraded quartz grains and tricuspate glass shards, as well as structureless accretionary pellets (Lock et al., 1975). A sample of this layer was taken for U-Pb zircon geochronological analysis. This in turn is overlain by a 1.4 m thick, friable, accretionary pellet-rich pink-grey mudstone unit (Fig. 5.31B, C). Black joints and modern roots are pervasive in this highly weathered unit, and the proportion of constituent accretionary pellets appear to decrease upward (normal grading) – although this could be a function of weathering, which increases in severity upsection. To minimize the chance of contamination, a second sample of the least weathered portion (near the base) of this friable unit was also taken. Finally, the uppermost unit on the southern wall of the quarry is a yellow-grey, highly fractured medium-grained sandstone that is separated from the underlying units by an undulating, erosive contact (Fig. 5.31B). On the eastern side of the quarry, green-grey sandstone beds dip in opposite directions, at 15º N and 25º S, over a short 3 m lateral distance, which gives the appearance of localized faulting and structural tilting (Fig. 5.31F). Such brittle deformation is not unexpected given the close proximity to the Cango Fault < 500 m north of the quarry (Fig. 5.29).

Fig. 5.31. (Following page). A) Roadside quarry south of De Rust exposing volcaniclastic deposits. Letters E and S refer to the eastern and southern walls of the quarry. Dashed white line indicates the location of log (Fig. 45C); B) Pink, friable accretionary pellet-rich mudstones overlain by fractured beige medium-grained sandstone. Red dashed line highlights the undulating, erosive contact that separates these units; C) Log of the various lithologies exposed on the southern wall of the quarry and location of DERU and DERC1 samples. Scale is in cm; D) Pink, accretionary pellet-rich tuffaceous sandstone; E) Silicified conglomerate with quartzite clasts; F) Dramatic change in dip angle and direction of beds (white dashed lines) and inferred fault plane (solid white line) on the eastern wall of the quarry.

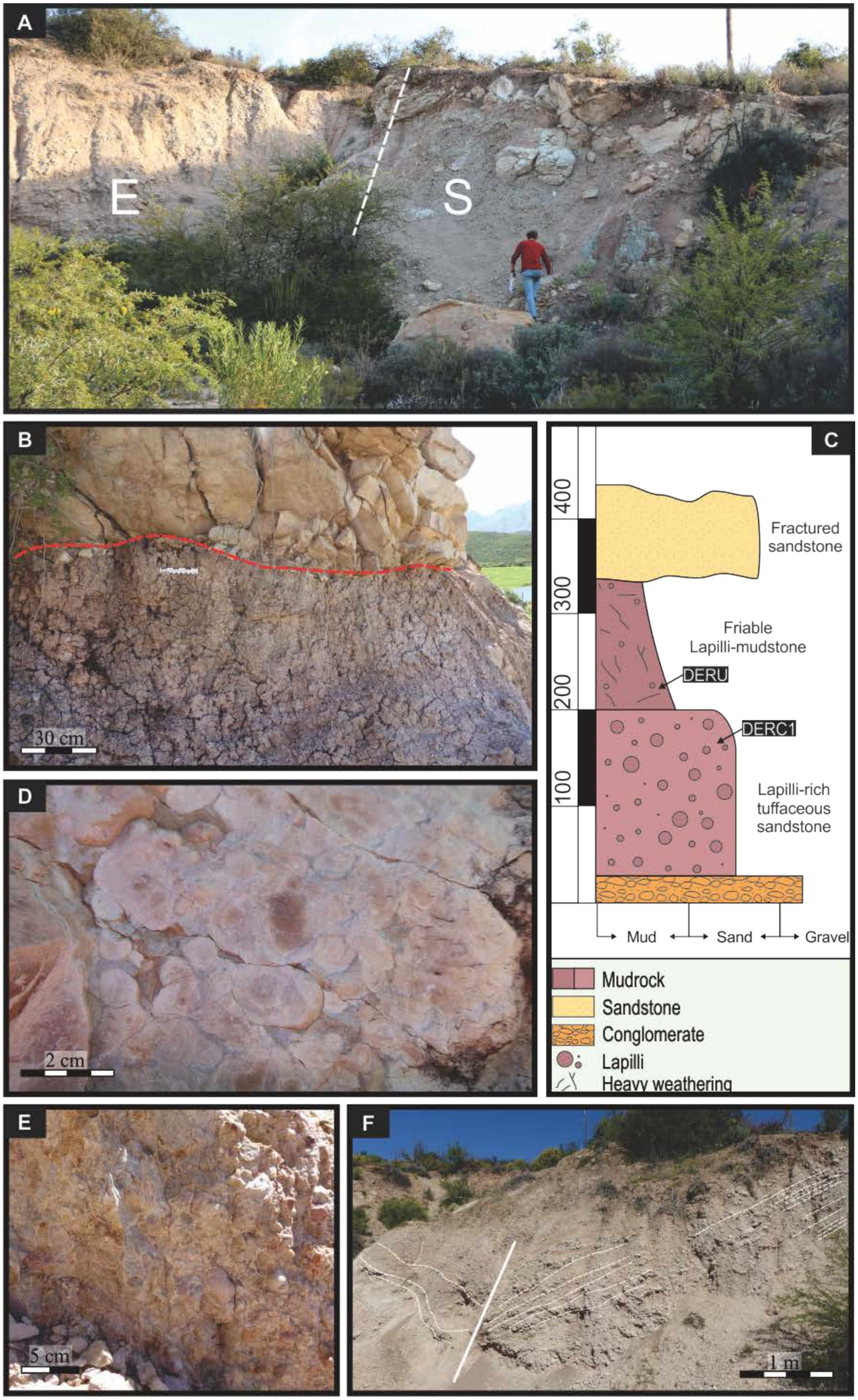
A
E
S
B
30 cm
C
400
300
200
100
Fractured sandstone
Friable Lapilli-mudstone
DERU
DERC1
Lapilli-rich tuffaceous sandstone
Mud
Sand
Gravel
Mudrock
Sandstone
Conglomerate
Lapilli
Heavy weathering
D
2 cm
E
5 cm
F
1 m

5.2.4.2 U-Pb geochronology

OES1

Zircons vary in colour and are pale brown, beige and colourless and size from 50 to 200 µm. Crystal shapes are stubby, stalky and rarely prismatic and are in many cases well-rounded or completely rounded. Angular fragments and euhedral crystals are also present. CL images reveal a wide range of internal morphologies, with oscillatory zoning common in the mantle of most crystals (e.g., crystals10, 6 16 and 71), often with very thin rims indicating secondary growth. Such rims are commonest in Precambrian crystals, which also commonly contain inclusions (e.g., crystals 6, 16, 52 in Fig. 5.32).

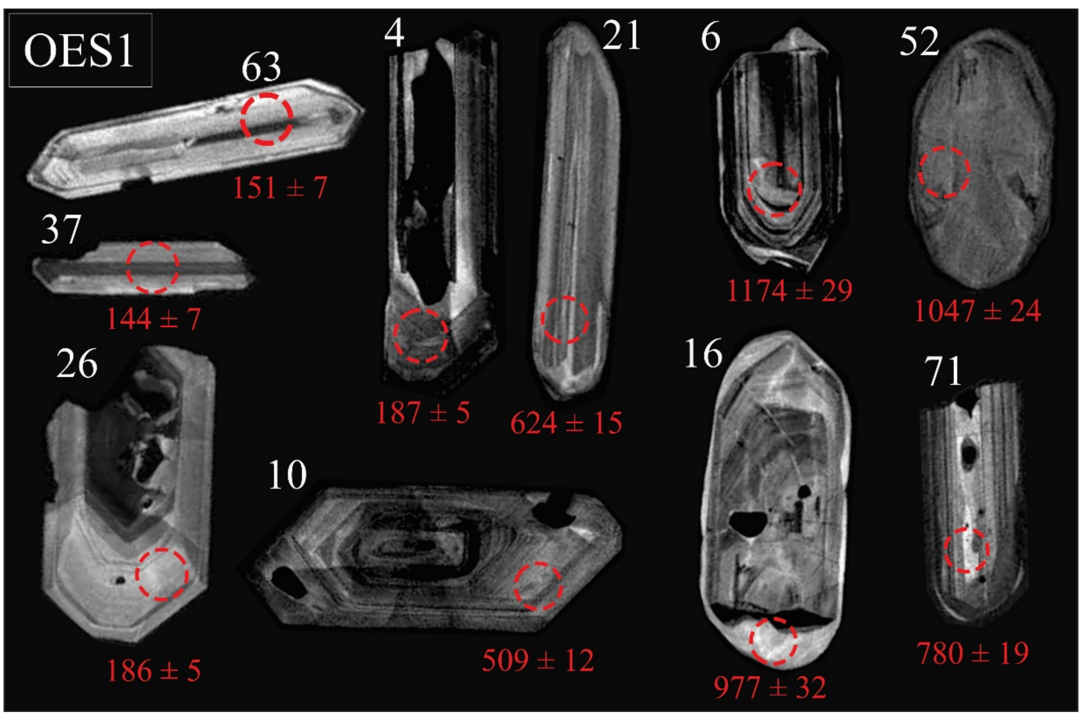

Fig. 5.32. Composite diagram of CL images of zircons that yield concordant dates in sample OES1 from the Oudtshoorn Basin. Individual zircon indicated by white number and analytical spot (26 µm diameter) with respective $^{206}Pb/^{238}U$ date are red.

Of 56 dates, 53 are concordant that from multiple Mesozoic (~19 %), Palaeozoic (~15 %) and Precambrian (~66 %) age populations (Fig. 5.33; Table E1 in Appendix E; Fig. F3A in Appendix F). Two Jurassic and Cretaceous zircons form the youngest overlapping age component at ~145 Ma (YPP), each displaying similar prismatic habits and oscillatory zoning, and there is a larger Jurassic population at ~186 Ma consisting of 7 zircons (Fig. 5.33). In addition to populations around 520 – 535 Ma, numerous Precambrian clusters occur. Notably, there no Permian or Triassic zircons in this sample, which probably reflects sediment sources from mainly the Table Mountain and Cango Groups. Other analytical metrics are: YSG = 144 ± 7 Ma; YDZ = 144.3 +5.5/-5.7 Ma (95% conf.).

Fig. 5.33. (Following page). U-Pb dates of zircons from all samples in the Oudtshoorn Basin shown as age probability density diagrams (blue area) combined with frequency histograms (grey bars) with 20 Ma intervals. Only concordant data are shown: n = x/y means that x out of a total of y zircons yielded concordant dates. Youngest graphically-defined peak (YPP) are indicated.

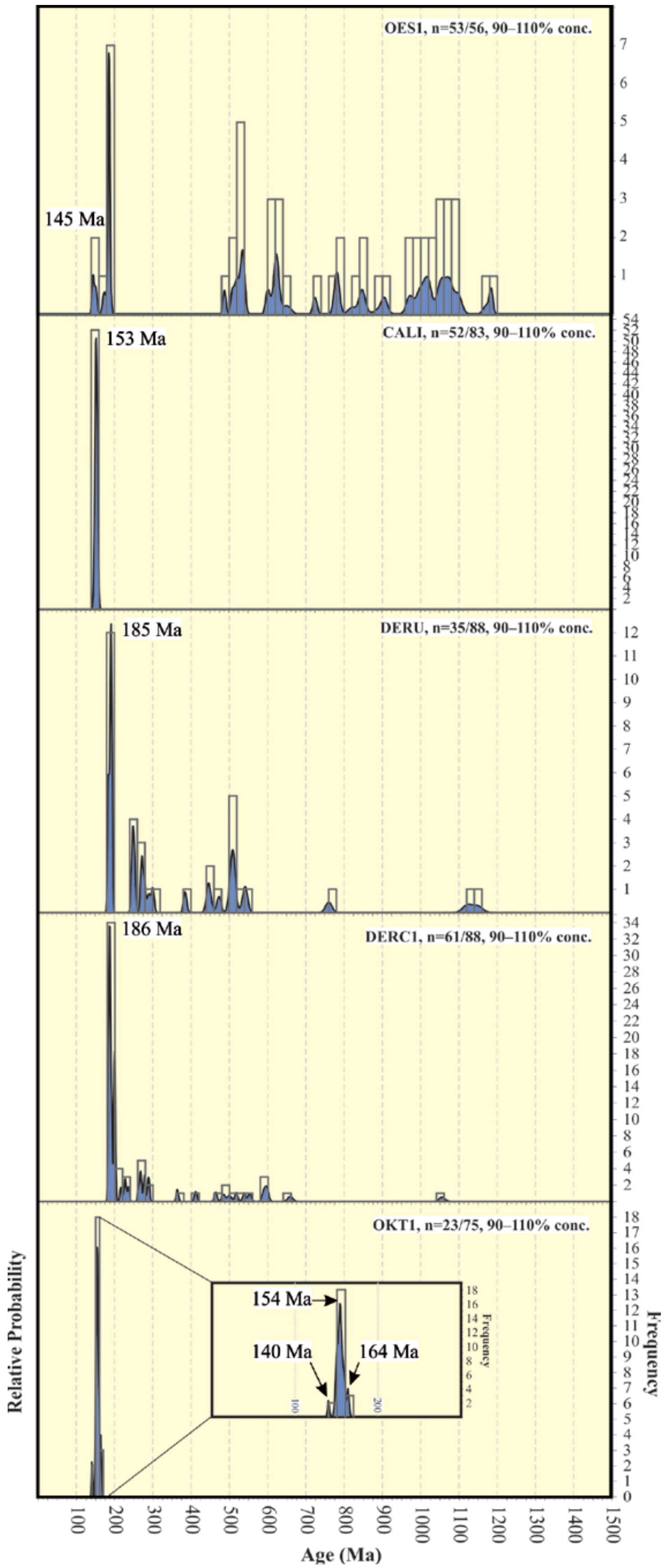
OES1, n=53/56, 90–110% conc.
145 Ma
CALI, n=52/83, 90–110% conc.
153 Ma
DERU, n=35/88, 90–110% conc.
185 Ma
DERC1, n=61/88, 90–110% conc.
186 Ma
OKT1, n=23/75, 90–110% conc.
154 Ma
140 Ma
164 Ma
Relative Probability
Frequency
Age (Ma)

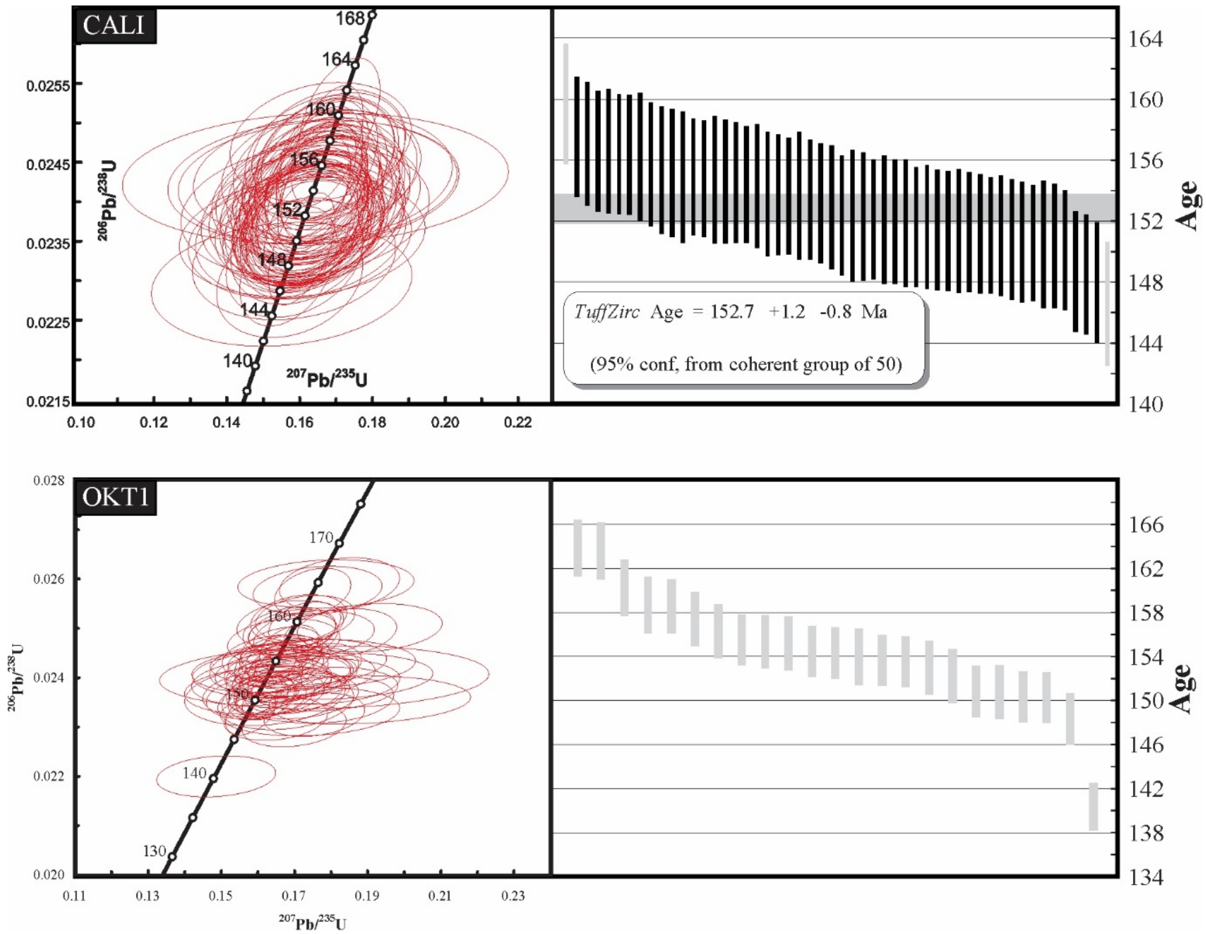

Fig. 5.34. U-Pb zircon dates from two pyroclastic deposits in the Oudtshoorn Basin plotted on concordia (left) and as individual ^{206}Pb/^{235}U dates arranged by age (right). Horizontal grey rectangles are the TuffZirc age, with quoted errors. Grey vertical rectangles are excluded from calculation. All individual dates have 2σ error.

CALI

Zircon crystals are strongly euhedral and stalky, with rare stubby and prismatic habits that range from 90 to 200 µm. They are the shortest yet volumetrically the largest by comparison with all other pyroclastic samples. No elongate 'needle-like' crystals are present in this sample, nor any significant quantity of fragmentary grains. All crystals are colourless and exhibit fine oscillatory zoning under the CL detector (Fig. 5.35).

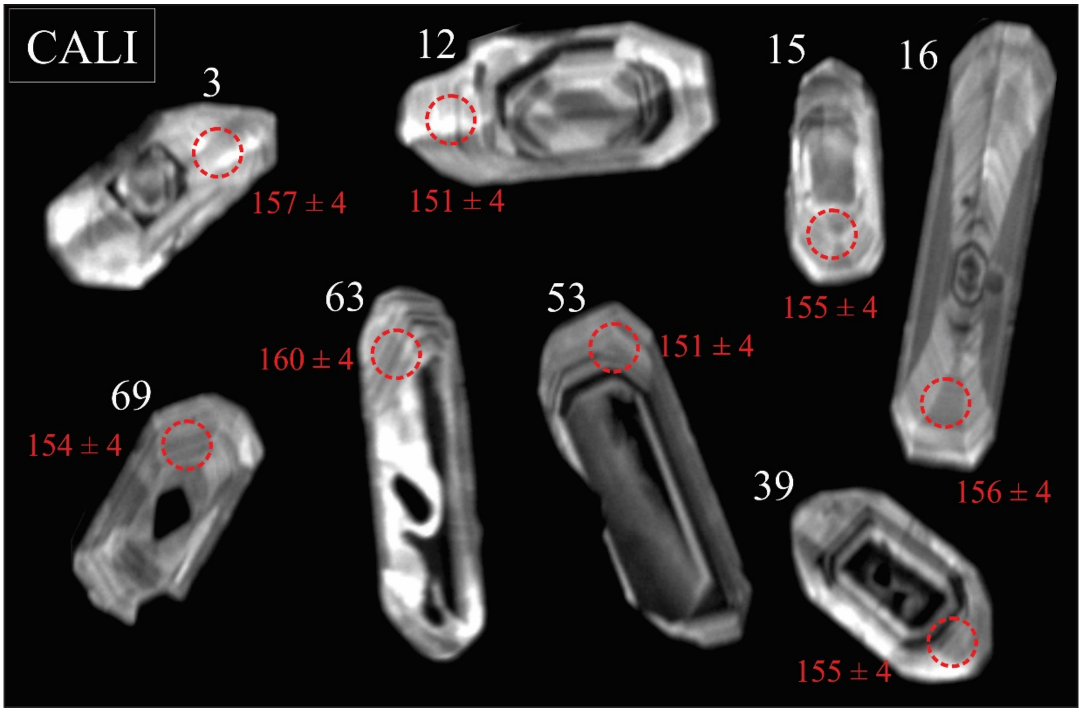

Fig. 5.35. Composite diagram of CL images of zircons that yield concordant dates in sample CALI from the Oudtshoorn Basin. Individual zircon indicated by white number and analytical spot (26 µm diameter) with respective $^{206}Pb/^{238}U$ date are red.

Of the 83 crystals analysed, 52 yielded concordant dates, all of which are Mesozoic and formed a single population ranging from 147 ± 4 Ma to 160 ± 4 Ma with a peak around 152 Ma on a probability density diagram (Fig. 5.33; Table D14 in Appendix D). Analytical metrics are as follows: YSG = 147 ± 4 Ma; YDZ = 145.8 +2.2/-4 Ma (95% conf.); YPP = 152 Ma. The similarity of zircon morphology (internal and external) and coherence of individual dates confirm a pyroclastic origin for the bentonite. Of the 52 zircons analysed in the sample, 50 yield concordant dates that form a coherent cluster around 152.7 + 1.2/ -0.8 Ma, as identified by the TuffZirc algorithm (Fig. 5.34). Further analysis of CA-TIMS analysis of 18 crystals yields 12 concordant dates that are indistinguishable from one another at 2σ error and have a weighted mean age of 153.8 ± 0.2 Ma (MSWD = 0.77), which is itself is indistinguishable from the TuffZirc age and provides the most reliable depositional age for the deposit (Fig. 5.36; Table G1 in Appendix G).

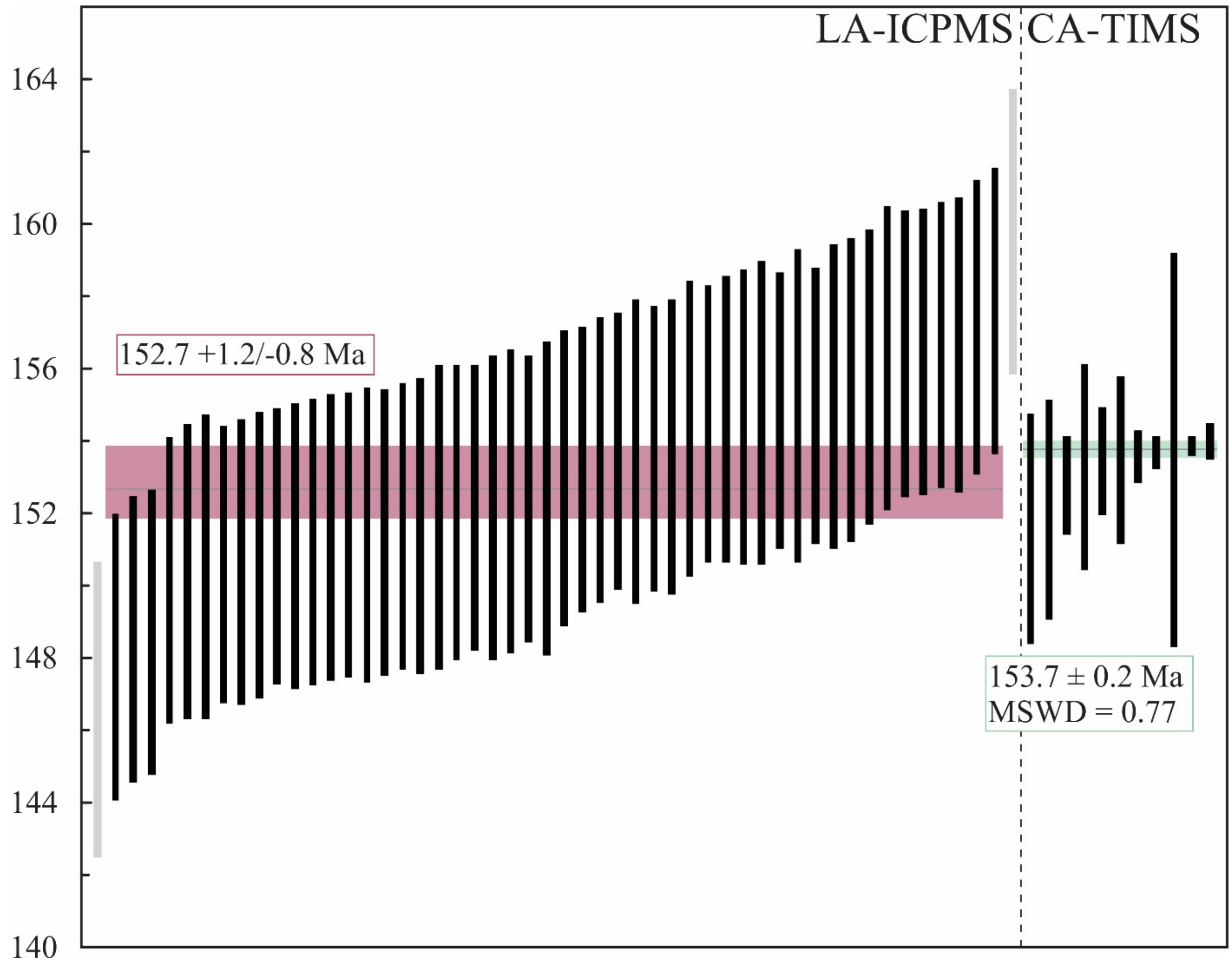

Fig. 5.36. U-Pb dates from LA-ICPMS (left) and CA-TIMS (right) analytical procedures ordered by age. Grey uncertainty ranges are dates that are excluded from age calculations. Both the TuffZirc age (red) and the weighted mean (green) calculated from 11 dates acquired by CA-TIMS are indistinguishable.

OKT1

Zircon crystals range from 40 to 180 µm and are consistently euhedral, prismatic and elongated, with very few fragmentary grains. All crystals are colourless and exhibit fine oscillatory zoning (Fig. 5.37), and rarely contain inclusions or xenocrystic cores (e.g., crystals 11 and 60 in Fig. 5.37).

Of the 75 analysed crystals, only 23 yield concordant Mesozoic dates. The dates define a complex population on a probability density diagram with a large peak at 154 Ma and two smaller peaks at 140 and 164 Ma (Fig. 5.33; Table D15 in Appendix D). Analytical metrics are as follows: YSG = 140 ± 2 Ma; YDZ = 140.2 + 2.6/-2.3 Ma (95% conf.); YPP = 152 Ma; YPP = 154 Ma. Internal and external grain morphologies, sedimentological observations and individual dates confirm a pyroclastic origin. However, the concordant analyses exhibit complex age components with a single date of 140 ± 2 Ma that does not overlap with the larger subpopulation of 22 dates at 2σ. The TuffZirc algorithm identifies the most coherent grouping of dates around 154.5 + 1.1 / -0.9 Ma with several discrete older and younger dates that also seem likely, making assigning an age for this deposit difficult (Fig. 5.34). A similarly wide spread of dates intersect concordia when plotted in $^{207}Pb/^{235}U$ vs $^{206}Pb/^{238}U$ space. Although the single young ~140 Ma date is considered unreliable, may have suffered from Pb-loss and is therefore not interpreted here as representing the youngest age component; the remaining dates, which show considerable overlap, probably reflect an inherited component and spuriously young dates that suffer from Pb loss. An exact depositional age is difficult to ascertain conclusively for this (~Upper Jurassic) sample because there is probably minor Pb loss and inheritance that cannot be resolved confidently at this precision (Fig. 5.34). To definitively date this deposit additional sampling and CA-TIMS analysis of the youngest crystals would be necessary.

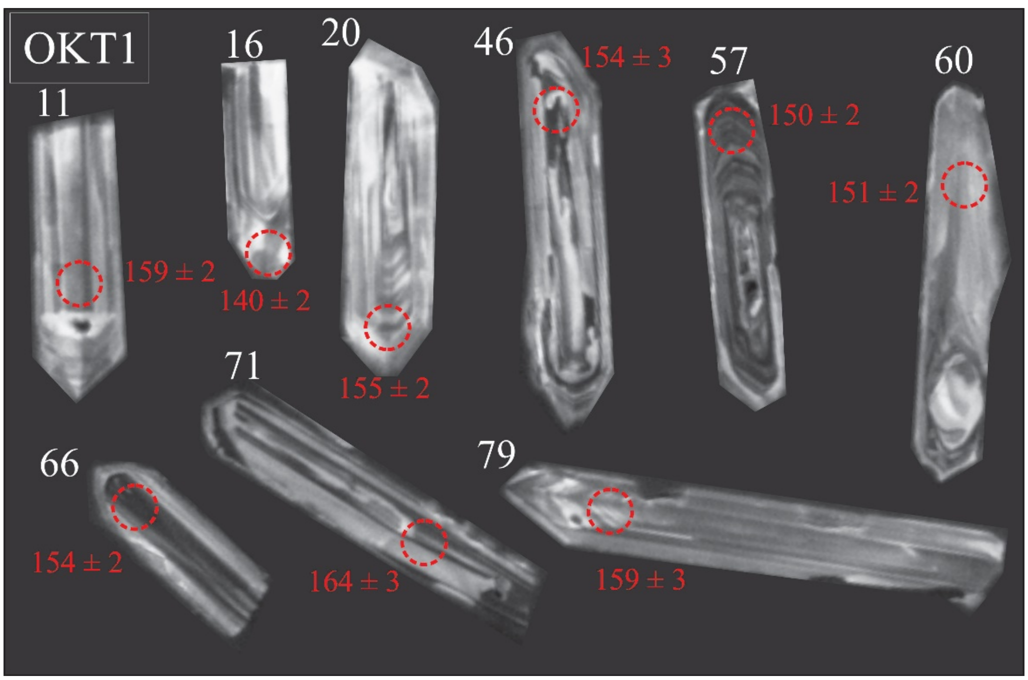

Fig. 5.37. Composite diagram of CL images of zircons that yield concordant dates in sample OKT1 from the Oudtshoorn Basin. Individual zircon indicated by white number and analytical spot (26 μm diameter) with respective $^{206}Pb/^{238}U$ date are red.

DERU & DERC1

Crystal morphologies and sizes in this sample DERU are highly varied ranging from euhedral, to rounded and fragmentary grains that are angular and range from 30 µm to 250 µm. Colourless, yellow and yellow-orange crystals are common and CL imagery reveals a diversity of fine to broad oscillatory zoning (Fig. 5.38), xenocrystic cores (e.g., crystal 12 in Fig. 5.38) and inclusions (crystals 70 and 31 in Fig. 5.38).

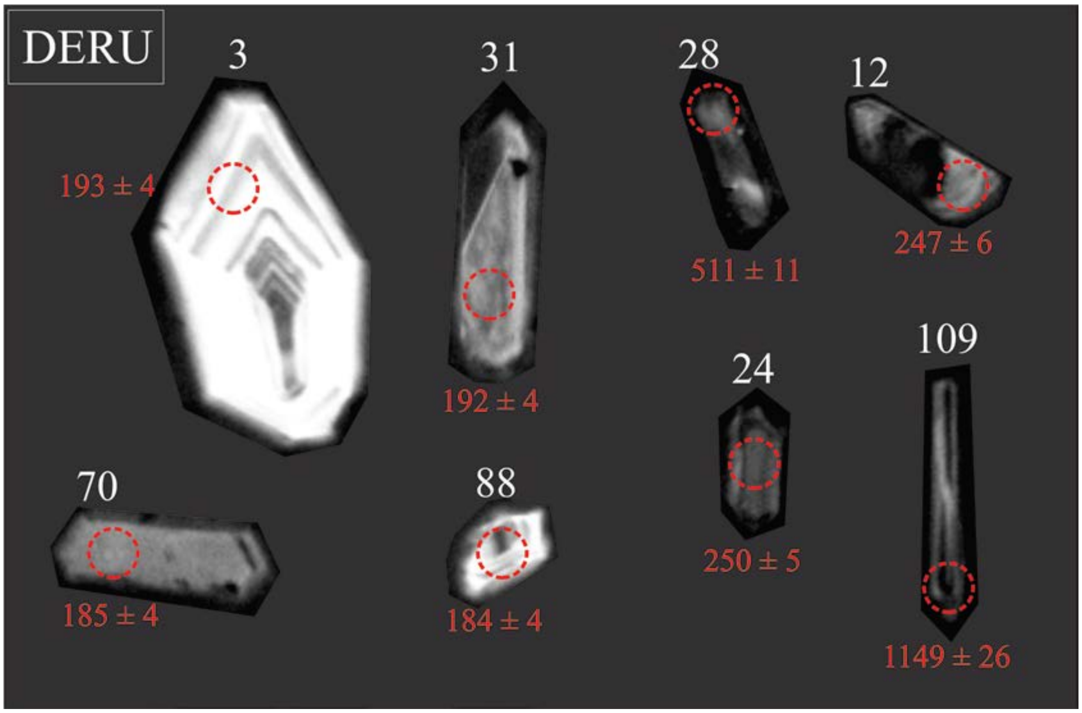

Fig. 5.38. Composite diagram of CL images of zircons that yield concordant dates in sample DERU from the Oudtshoorn Basin. Individual zircon indicated by white number and analytical spot (26 µm diameter) with respective $^{206}Pb/^{238}U$ date are red.

Of the 88 crystals analysed, 35 yield concordant dates that are Mesozoic (43 %), Palaeozoic (46 %) and Precambrian (11 %). Mesozoic dates define a single peak on a probability density diagram at 185 Ma, while there are several Palaeozoic and Precambrian peaks (Fig. 5.33; Table D16 in Appendix D; Fig. F3B in Appendix D). Analytical metrics are as follows: YSG = 184 ± 4 Ma; YDZ = 182.8 +3.1/ -3.8 Ma (95% conf.); YPP = 185 Ma. Variation in grain internal and external morphology and the wide spread of dates is compatible with a resedimented mixed-origin volcaniclastic deposit. However, the presence of glass shards and intact accretionary pellets suggest that reworking was likely not extensive because if there had been significant transport of ash prior to deposition, these delicate structures would probably have been destroyed. Nevertheless, no true depositional age can be extracted from the sample with confidence, and a maximum depositional age of 185 Ma is preferred.

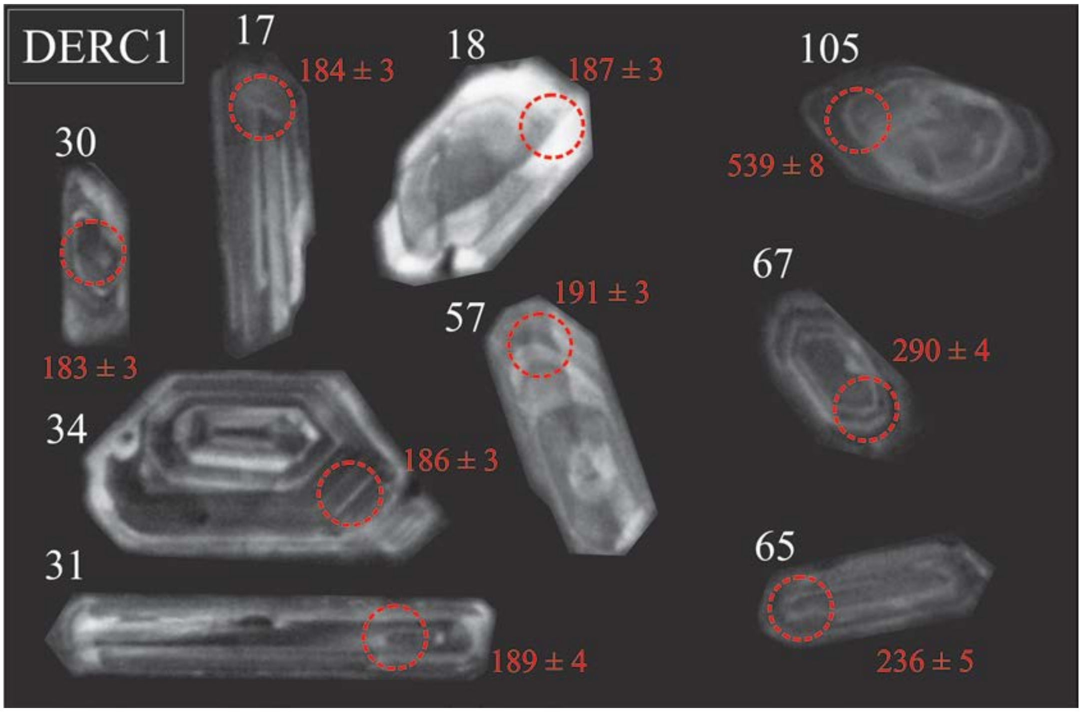

Fig. 5.39. Composite diagram of CL images of zircons that yield concordant dates in sample DERC1 from the Oudtshoorn Basin. Individual zircon indicated by white number and analytical spot (26 µm diameter) with respective $^{206}Pb/^{238}U$ date are red.

Crystal morphology, size and colour in sample DECR1 show similar variation to sample DERU. External crystal morphologies were either euhedral, angular fragments or rounded, while internal morphologies showed fine and medium oscillatory zoning, xenocrystic cores and inclusions (Fig. 5.39). Of the 88 analyses, 61 yield concordant dates and most zircons in this sample are Mesozoic (67 %) forming two large peaks on the probability density diagram at 183 Ma and 199 Ma, and smaller Triassic peaks (Fig. 5.33; Table D17 in Appendix D; Fig. F3C in Appendix D). The remaining zircons (23 % Palaeozoic and 10 % Precambrian) constitute multiple small peaks. Analytical metrics are: YSG = 183 ± 3 Ma; YDZ = 181.4 +1.8 / -2.6 Ma (95% conf.); YPP = 186 Ma. Like DERU, DERC1 is a mixed-origin volcaniclastic layer and not primary ash-fall deposit although in this case the proportion of young, volcanic zircons is greater, which may be a reflection of reduced detritus input in comparison to DERU. Alternatively, the lower proportion of Palaeozoic and Precambrian zircons may be an artifact of the sampling procedure the sampled horizon was highly friable and may have been contaminated by sediment that worked its way into the weathered rock through the pervasive cracks. DERC1 on the other hand was extracted from well-consolidated, unweathered rock, which precludes sample contamination. Despite this, only a maximum depositional age of 186 Ma can be confidently established and should be considered more-or-less equivalent to the directly overlying DERU sample.

5.2.4.3 Basin synthesis

The five samples presented above provide the first age constraint of the Uitenhage Group in the Oudtshoorn Basin, the lack of which hindered previous sedimentological (Du Preez, 1944; Holzförster, 2007; Richardson et al., 2017; Dinis, 2018), palaeontological (McLachlan and McMillan, 1976) and tectonic studies (Lock et al., 1975; Green et al., 2016).

The two bentonite layers, which are considered here as pyroclastic deposits, in the Kirkwood Formation near Calitzdorp (CALI) and in the south-central part of the Oudtshoorn Basin (OKT1) are both Late Jurassic. CALI has been dated with confidence, whereas OKT1 has a complicated spread of dates that are not easy to interpret beyond 'Late Jurassic'. Importantly, however, at least CALI and possibly also OKT1 are older than the oldest accepted (Portlandian) age for the Kirkwood Formation (McMillan et al., 1997). This is important for sedimentological assessments that rely on lithological correlations in order to assess models of basement infilling, and for dating no-age diagnostic fossils (De Klerk, 2000; Holzförster, 2007; Dinis, 2018). However, relative stratigraphic position of these bentonite layers within the basin fill succession remains unclear. Importantly, neither deposits seem to be near the base of the basin stratigraphy because there are considerble thicknesses of strata below each horizon evidenced by the numerous groundwater exploration boreholes that were drilled in each vicinity that failed to reach basement after 150 m (National Groundwater Archives, Department of Water and Sanitation). Therefore, these deposits are unlikely to have formed at the onset of rifting in the Oudtshoorn Basin and are underlain by an unknown >

150 m thickness of Uitenhage Group deposits. Further, conglomerates, sandstones and mudstones that outcrop on the eastern side of the basin that are not obviously contiguous (e.g., at Oudtshoorn) may also differ in age (i.e., can be pre- or syn- or post-Kimmeridgian).

The age of the oldest syn-rift units accommodated in the Oudtshoorn Basin may provide a minimum constraint of the onset of basin-forming tectonics. However, the depth at which these crucial deposits exist is presently unknown because neither deep drilling, nor seismic surveys have been conducted in any part of the Basin. Nevertheless, the complex history of the Cango Fault, which includes multiple periods of movement during the Mesozoic (Green et al., 2016), may yet give us access to these elusive deposits. It is likely that the volcaniclastic deposits at De Rust (from which samples DERU and DERC1 are derived) are rare portions of basal Uitenhage Group units that have been brought upward relative to surrounding younger strata by complex multi-phase faulting along the Cango Fault for three reasons.

Firstly, the volcaniclastic deposits at De Rust are Lower Jurassic basal portions of the Uitenhage Group based on lithological, geochronological, and zircon morphological characteristics. The presence of delicate glass shards and accretionary pellet structures preserved in these volcaniclastic deposits point to minimal reworking and transport as such structures would likely have been destroyed if significantly transported. Instead, the accretionary pellet-rich tuffaceous deposit is probably the result of a syn-depositional mixing of siliciclastic detritus with freshly deposited accretionary pellet-rich ash. If this is the case, then the Pliensbachian maximum depositional age of these strata roughly approximates its depositional age. This also implies that these deposits are age-correlatives of the Pliensbachian –Toarcian Suurberg Group, which outcrops in the Algoa Basin (see Chapter 4). The presence of constituent accretionary pellets, the overall silicification of the deposit, and proximity to these outcrops to the northern basin margin draw close similarity with the Pliensbachian tuffaceous deposits there. U-Pb zircon geochronology certainly supports such a correlation, with the De Rust samples (DERU and DERC1) showing identical detrital age components (albeit at different proportions) as tuffaceous units in the Suurberg Group (Fig. 5.40), although with noticeably different proportions of Jurassic aged zircons (a likely reflection of the degree of 'mixing' with siliciclastic component during deposition). Youngest age components, which presumably comprise syn-depostional late Early Jurassic zircons, are also indiscernible (Fig. 5.40).

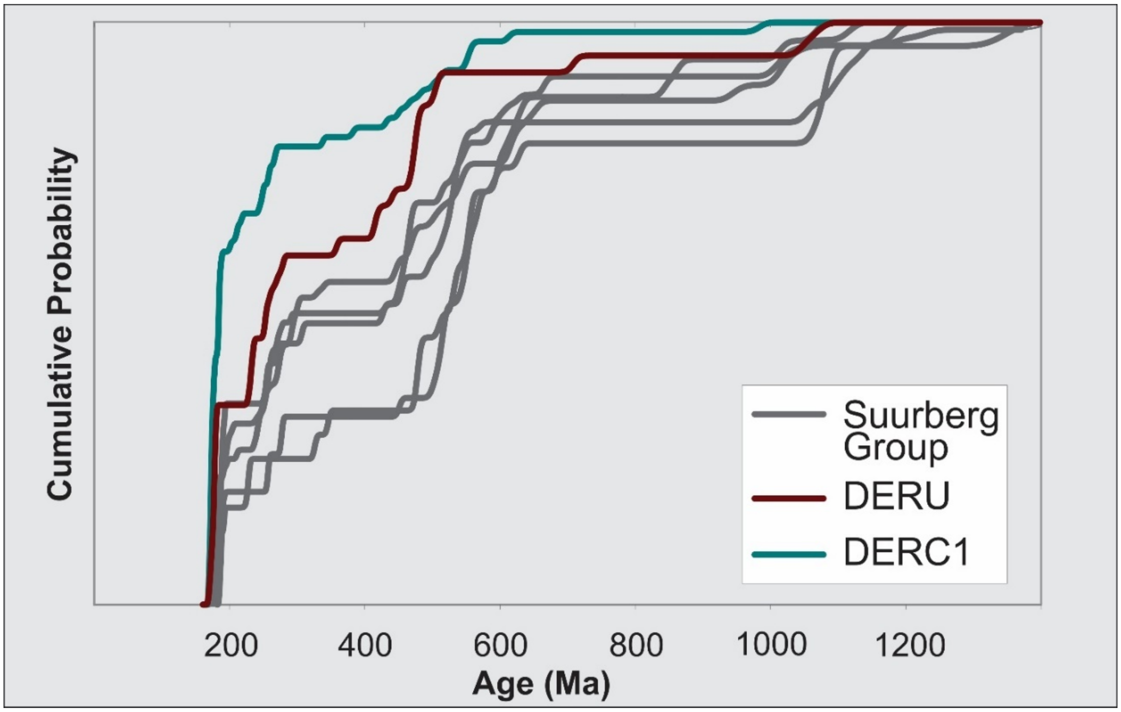

Fig. 5.40. Comparison of detrital zircon signatures of the Suurberg Group (Chapter 4) with the two samples of the volcaniclastic deposits exposed near De Rust, Oudtshoorn Basin. Data are displayed as cumulative probability density diagrams.

Notwithstanding the lithological, geochronological and zircon morphological similarities of these tuffaceous beds, a cogenesis in the two basins need not necessarily be invoked in order to assign the De Rust deposits as Lower Jurassic. Moreover, these deposits have clearly been deformed, probably during displacement along the Cango Fault. This basin-bounding feature lies less than 500 m north of the quarry exposures, which can explain this deformation. Small-scale faults may have occurred either through the local widening of the Cango Fault into a deformation zone, or the off-shooting of subordinate antithetic faults from the Cango Fault during slip. Smaller fault blocks adjacent the Cango Fault could have developed at some point after initial rifting that incorporated a portion of the early basin fill. These blocks may have been caught within the region of deformation during a subsequent episode of normal faulting that caused highly localized strain, in the form of small faults and tilting, and brought them upwards relative to surrounding younger units (Fig. 5.41).

Finally, the Cango Fault has a complex episodic history of reactivation and displacement, which would have provided several opportunities for such a scenario to develop. Faulting appears to have been sustained during the deposition of the Uitenhage Group in the Oudtshoorn Basin because there is a progressive upward shallowing of dip angles and syn sedimentary faults in the Buffelskloof Formation (Holzförster, 2007). Furthermore, low temperature thermochronological data from a N-S transect across the Cango Group Inlier indicate that it moved as a discrete tectonic block in the Early Cretaceous (Green et al., 2016) implying that significant displacement occurred at this time, subsequent to Jurassic basin initiation and deposition. Such an episodic displacement history during the Mesozoic would have provided ample opportunity for basal units that were deposited adjacent the Cango Fault to be successively deformed during later episodes of normal faulting. This not to mention the Cango Fault remained active into the Quarternary, evidenced by recent pediment surfaces along the fault scarp (Malan and Viljoen, 2016 p. 63).

Based on these Upper and Lower Jurassic volcaniclastic deposits, subsidence of the Oudtshoorn Basin clearly began sometime during the Early Jurassic (Fig. 5.41). The lack of stratigraphic context of the De Rust volcaniclastics remains a problem for reconstructions of basin history – where are they positioned in the basin stratigraphy? The presence of lowermost Middle Jurassic deposits within the Uitenhage Group at Mossel Bay to the south and Heidelberg to the southwest indicates that an extensional stress regime had commenced by the Middle Jurassic, probably beginning earlier, and that rifting in at least parts of the southern Cape initiated as early as the Early Jurassic. By inference, this suggests that subsidence in the Oudtshoorn Basin begun in the Early Jurassic, shortly after or during the deposition of the De Rust volcaniclastic unit (Fig. 5.41). As with time fault(s) grew through linkage to form the Cango Fault (Paton, 2006), the rest of the Enon and Kirkwood formations were deposited – during the Early, Middle and Upper Jurassic and possibly into the Early Cretaceous (Fig. 5.41). The clast composition of conglomerates in these units are exclusively sandstone and quartzites of the Table Mountain Group (Dinis, 2018), although Permo-Triassic zircons do contribute to the detrital component of the De Rust volcaniclastics (Fig. 5.33), so a partial Karoo Supergroup source is also expected at least for the oldest deposits in the Oudtshoorn Basin.

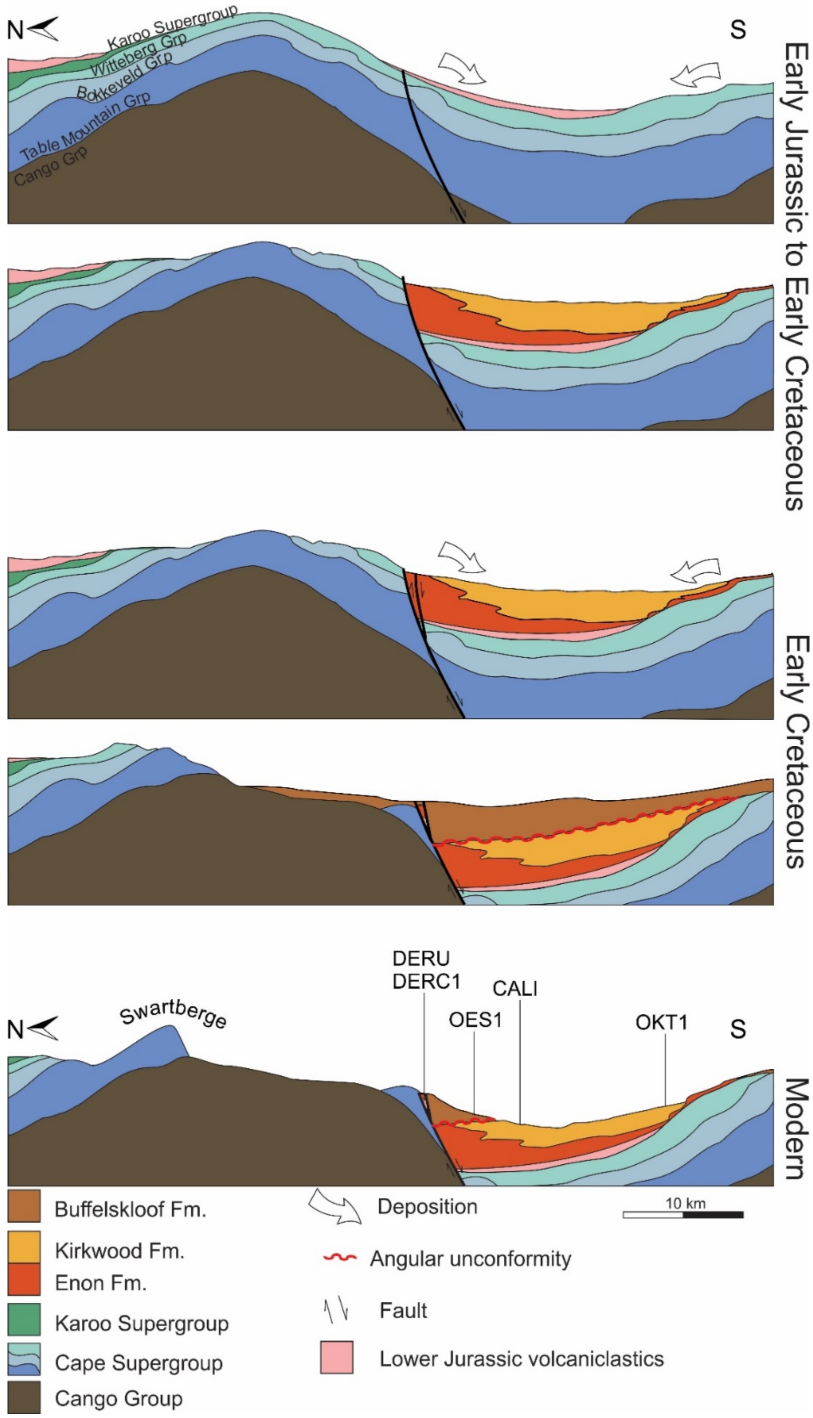

Fig. 5.41. Evolution of the Oudtshoorn Basin from the Early Jurassic to modern day. Note the reactivation of the Cango Fault in the Early Cretaceous, which created the accommodation space for the Buffelskloof Formation and possibly brought deeply buried Lower Jurassic volcaniclastics closer to the surface. The progressive unroofing of the large anticline north of the basin is idealized as the true southern extent of the Karoo Supergroup during at Early Jurassic times is unknown.

After the deposition of the Enon and Kirkwood formations, in the post- Kimmeridgian, the Cango Fault was reinvigorated, and the basin entered a second phase of subsidence (Fig. 5.41). It was probably during this time that the uppermost breccia/conglomerates, the Buffelskloof Formation, were deposited as evidenced by a ~145 Ma maximum depositional age of sample OES1. The youngest zircons in this sample may have been derived from cannibalized older deposits or syn-depositional volcanic ash input. Either way, this youngest component reveals that the Buffelskloof Formation is discernably younger than the exposed, dated Kimmeridgian strata of the underlying Enon and Kirkwood formations. Although certainly the Buffelskloof Formation is equal to or younger than ~145 Ma (by virtue of containing ~145 Ma zircons), is it probably Lower Cretaceous, as opposed to say, Upper Cretaceous or Cenozoic because: 1) Apatite fission track analysis indicates that Cango Group Inlier, which occupies the northern footwall of the Cango Fault, was uplifted sometime between 145 Ma and 130 Ma (Green et al., 2016); and 2) similar aged deposits exist elsewhere in the rift basins of the southern Cape (e.g., the Sundays River Formation of the Algoa Basin). The considerable uplift and denudation of the region immediately north of the Cango Fault also brought the Cango Group to surface at this time. This is evidenced by the presence of phyllite and conglomerate clasts derived from the Cango Group in Buffelskloof Formation, which are entirely absent in the Enon and Kirkwood formations (Dinis, 2018). Further, the absence of Permian – Triassic zircons in the Buffelskloof Formation suggests that this unroofing process entirely removed the Karoo Supergroup from the scarp by the end of the Jurassic (Fig. 5.41). Further denudation occurred at the end of the Early Cretaceous and Cenozoic (Green et al., 2016) that removed much of the Buffelskloof Formation (and probably also its distal finer-grained equivalent) resulting in its restricted present-day distribution of the stratigraphic units of the Uitenhage Group in the Oudtshoorn Basin.

5.2.5 Knysna Basin

The Knysna Basin is situated around the town of Knysna in the Western Cape (Fig. 30). The Enon Formation is abundant around Knysna and outcrops in cliffs on the banks of the Knysna River and Estuary (Fig. 5.42; Fig. 5.43). The detailed sedimentology of these Enon Formation strata is to date unstudied, and the rocks have only been considered in relation to the Brenton Formation, which is exposed in a series of small, isolated outcrops on the southern banks of the Knysna Estuary from Featherbed to Lake Brenton (Fig. 5.43). The green-grey mudstone-dominated Brenton Formation hosts marine invertebrate fossils that carry chronostratigraphic significance in that the faunal assemblages have been dated through global correlations with dated horizons although their exact age interpretation remains unconfirmed (see Dingle and Klinger, 1972 and McLachlan et al., 1976 for opposing opinions; and summarized in Chapter 2 of this thesis). Importantly, the relationship between these marine mudstones and the continental conglomerates to the north of the Knysna Estuary has remained elusive to date (Fig. 5.43).

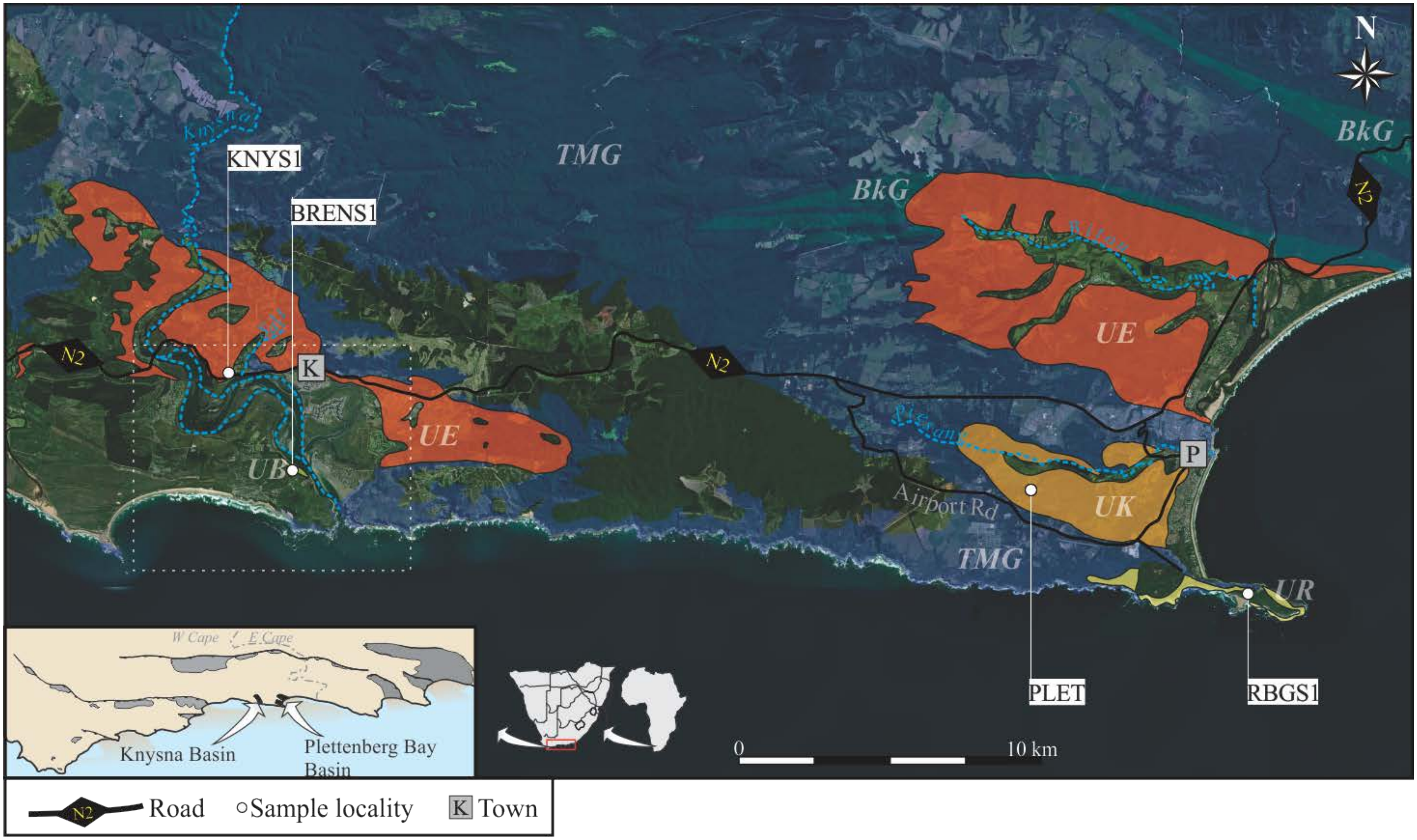

Fig. 5.42. Simplified Geology of the Knysna and Plettenberg Bay areas. Letters and colours are stratigraphic units and unshaded areas are recent alluvium and Cenozoic deposits. Abbreviations: Towns: K = Knysna; P = Plettenberg Bay. Stratigraphic units arranged from oldest to youngest: TMG = Table Mountain Group; BkG = Bokkeveld Group; UB = Brenton Formation; UE = Enon Formation; UK = Kirkwood Formation; UR = Robberg Formation. Base maps modified from the 1: 250 000 geological map sheet 3322 (Toerien and Roby, 1979) of the Council for Geoscience overlain on ESRI satellite imagery.

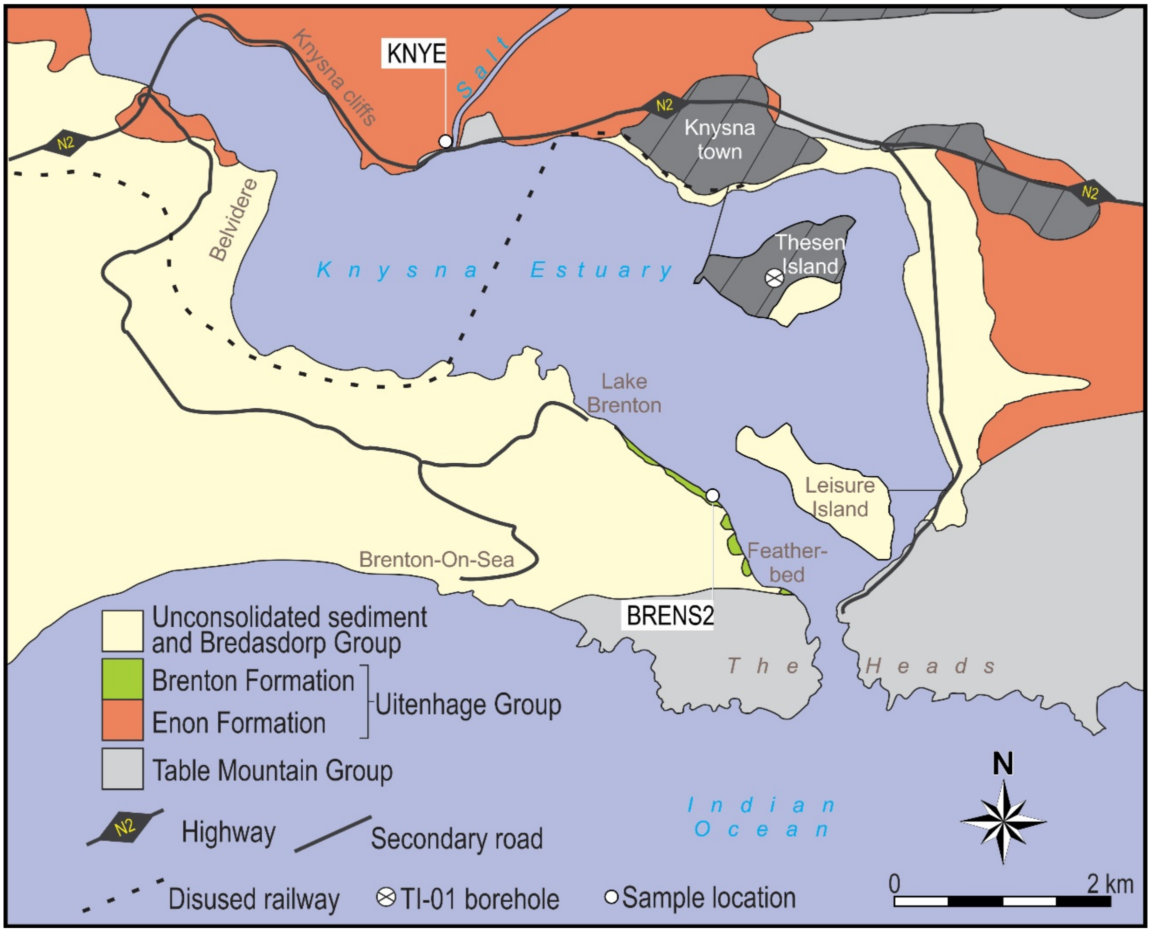

Fig. 5.43. Simplified geology of the southern part of the Knysna Basin based on McLachlan et al. (1976). Built-up regions are shaded dark grey.

5.2.5.1 Outcrop description

Salt River mouth (sample KNYE)

Most of the Uitenhage Group deposits around Knysna are conglomerate-dominated and mapped as the Enon Formation (Fig. 5.42; Fig. 5.43.). These are typified by the laterally extensive outcrops on the northern side of the Knysna Estuary along the N2 highway. Strata in one such outcrop (34° 2'12.96"S; 23° 1'28.27"E; Fig. 5.43) dip ~10º SW and comprise yellow-white sandstones and pebble conglomerates with sandstone and quartzite clasts identical to the rocks in the Table Mountain Group (Fig. 5.44B). A brown-orange medium-grained sandstone bed 20 cm thick that was sampled in the lower part of the outcrop, which predominantly exhibits conglomerates.

Estuary banks at Brenton (sample BREN2)

The best exposure of the Brenton Formation, which straddles the southern banks of the Knysna Estuary from Featherbed to Late Brenton, is at a ~ 5 high cliff face 800 m northwest of featherbed (Fig. 5.43.). The outcrop consists of a basal green-grey massive sandy mudstone unit that is only exposed at low tide. These are overlain by clay-rich grey-beige sandstones up to 3 m thick that are in paces horizontally laminated, massive or exhibit soft sediment deformation structures. This sandstone package was sampled for detrital zircon geochronological analysis. All bedding planes along the southern banks of the Knysna Estuary dip shallowly (8 – 18º) towards the NE (McLachlan et al., 1976).

Fig. 5.44. (Following page). Geological context of the Uitenhage Group samples in the Knysna and Plettenberg Bay basins. (A) Muddy sandstones of the Brenton Formation exposed between Fetherbed and Lake Brenton on the southern banks of the Knysna Esturay. (B) Sandstones and conglomerates of the Enon Formation exposed on the northern side of the Knysna Estuary at the mouth of the Salt River. (C) Vantell brickworks quarry with white dashed lines delineating the area shown in D where a bentonite layer is exposed. (D) Green bentonite lense that separates dark grey mudstones below the blue dashed line from the overlying matrix-supported polymictic conglomerates, above the red dashed line, which represents an erosive contact. (E) Sandstones at the uppermost interval of the Robberg Formation at the Robberg Peninsula. White arrow points to the signpost at 'The Gap'. Pink arrows indicate the exact position from which respective samples were extracted.

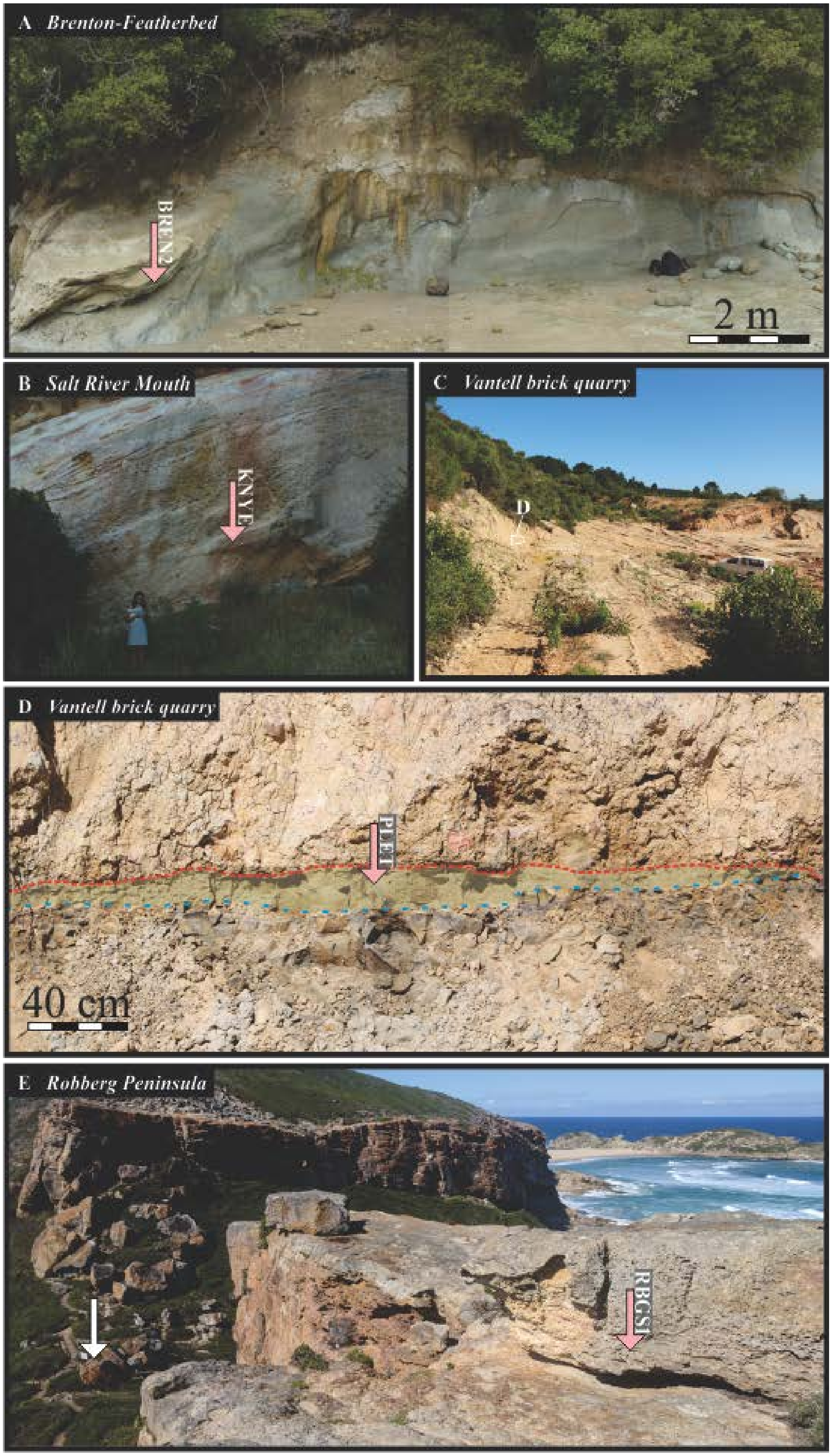

A Brenton-Featherbed
BREN2
2 m
B Salt River Mouth
KNYE
C Vantell brick quarry
D
D Vantell brick quarry
PLET
40 cm
E Robberg Peninsula
RBGS1

5.2.5.2 U-Pb geochronology

KNYE

Zircons vary in colour from pale brown to beige and size from 50 to 200 µm. Crystal are typically stubby, stalky and rarely prismatic and are in many cases well-rounded or completely rounded. Angular fragments and euhedral crystals are also present. The CL images reveal a wide range of internal morphologies, with oscillatory zoning common in the mantle of most crystals (e.g., crystals 5, 37 and 68 in Fig. 5.45). Many crystals contain inclusions (e.g., crystals 9 and 37 in Fig. 5.45) or have experienced zircon regrowth (e.g., crystal 25 in Fig. 5.45).

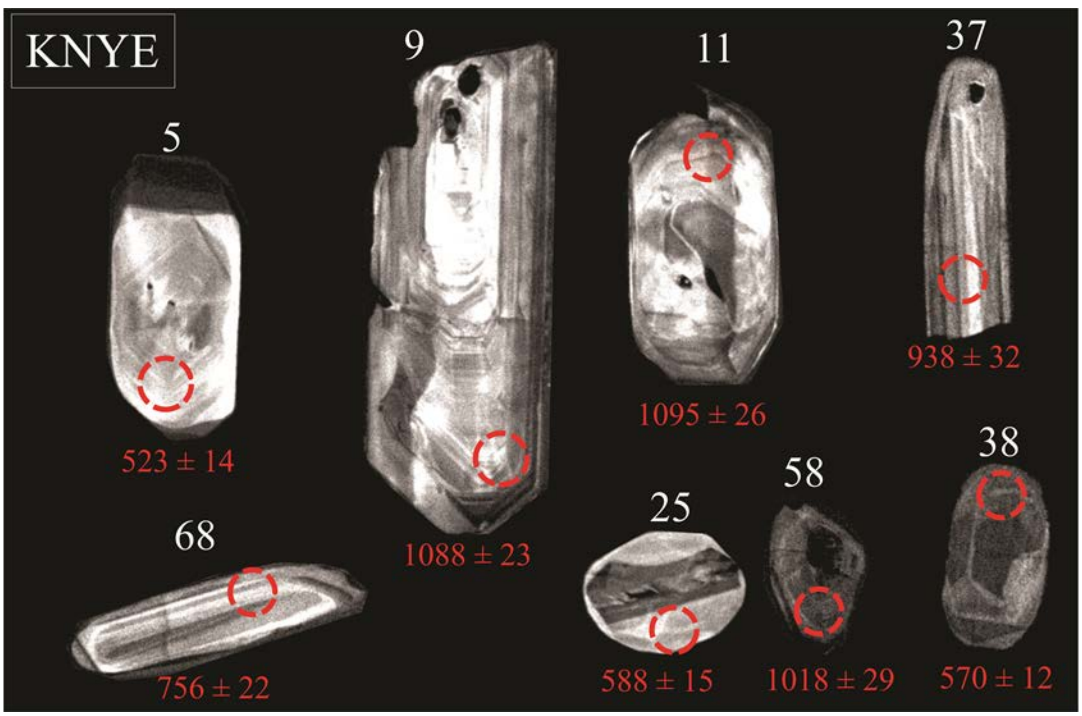

Fig. 5.45. Composite diagram of CL images of zircons that yield concordant dates in sample KNYE from the Knysna Basin. Individual zircon indicated by white number and analytical spot (26 µm diameter) with respective $^{206}Pb/^{238}U$ date are red.

Of 35 dates, 28 are concordant and from multiple Palaeozoic (~7 %) and Precambrian (~66 %) age populations (Fig. 5.46; Table E1 in Appendix E; Fig. F4A in Appendix F). There are no Mesozoic zircons in this sample, and just two Palaeozoic crystals comprising the youngest population. The absence of syn-depositional Jurassic or Cretaceous crystals makes constraining a depositional age for this unit impossible.

The presence of age populations at 500 – 600 Ma and 950 – 1200 Ma are expected for deposits that clearly are derived from the Cape Supergroup and contain exclusively quartzite to sandstone clasts of the Table Mountain Group, although the provenance has not been fully characterized given the small sample size of just 35 concordant dates. Analytical metrics are: YPP = 523 Ma; YSG = 523 ± 10 Ma; YDZ = 523.3 +5.2 / -6.6 Ma (95% conf.).

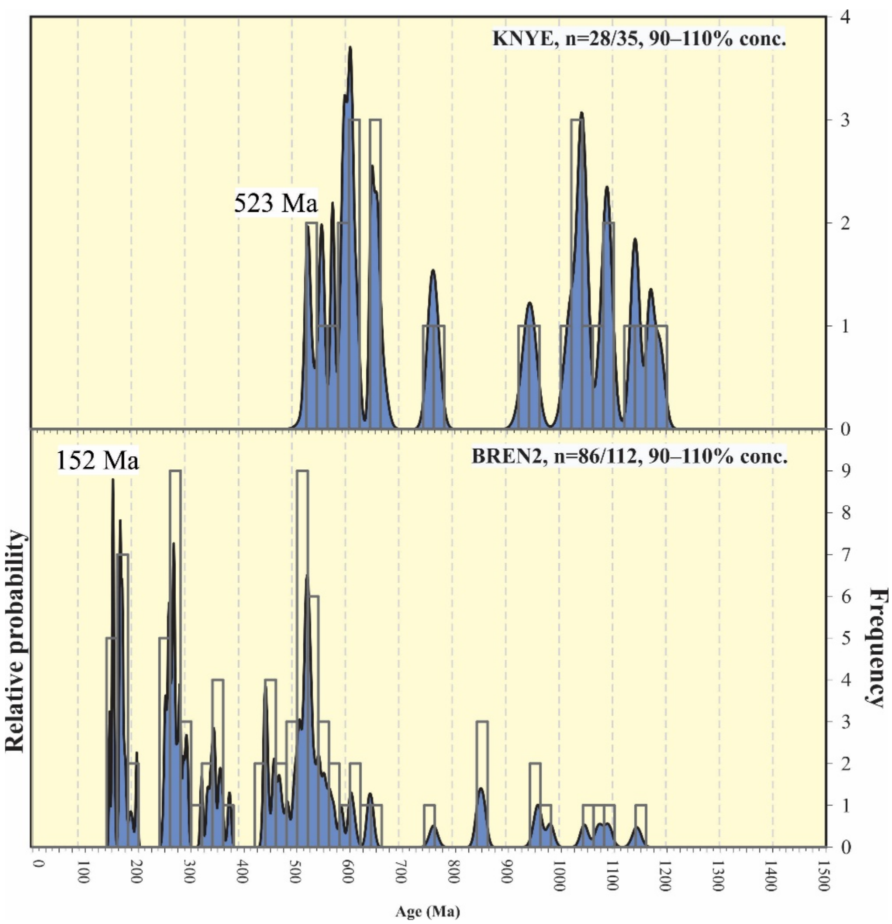

Fig. 5.46. U-Pb dates of zircons from the two samples in the Knysna Basin shown as age probability density diagrams (blue area) combined with frequency histograms (grey bars) with 20 Ma intervals. Only concordant data are shown: n = x/y means that x out of a total of y zircons yielded concordant dates. Youngest graphically-defined peak (YPP) are indicated.

BREN2

Crystal morphologies range in shape from euhedral and prismatic, with a number of long needle-shaped crystals, and a few that are rounded and fragmentary. Crystal sizes vary from 60 to 200 µm, and range from colourless to beige. Internally, fine and medium oscillatory zoning is almost unanimous, with (e.g., crystals 36 and 72 in Fig. 5.47) and without xenocrystic cores or inclusions (e.g., crystals 69 and 44 in Fig. 5.47).

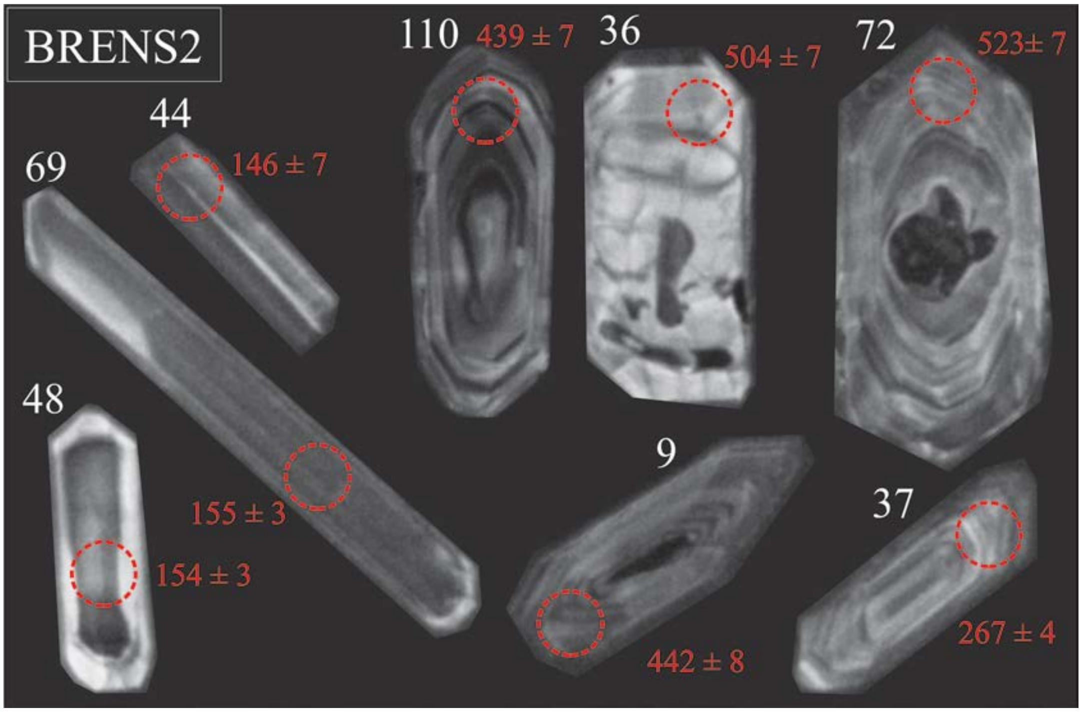

Fig. 5.47. Composite diagram of CL images of zircons that yield concordant dates in sample BRENS2 from the Knysna Basin. Individual zircon indicated by white number and analytical spot (26 µm diameter) with respective $^{206}Pb/^{238}U$ date are red.

Of the 117 crystals analysed, 91 yield concordant Mesozoic (18 %), Palaeozoic (54 %), and Precambrian (28 %) dates, forming multiple populations (Fig. 5.46; Table D18 in Appendix D; Fig. F4B in Appendix F). The majority of the Mesozoic dates are Jurassic. Analytical metrics are as follows: YSG = 146 ± 2 Ma; YDZ = 145.8 +2.7 / -2.7 Ma (95% conf.); YPP = 152 Ma. The single 146 ± 2 Ma date does not constitute a zircon population, and despite displaying concordance may have been affected by subtle Pb-loss and be spuriously young. Instead the 152 Ma graphically-defined peak age is regarded as a best estimate of the youngest reliable age component and therefore maximum depositional age of the unit. Therefore, it does not lend useful insights into the disputed age because it is compatible with both Early Cretaceous (McLachlan et al., 1976) and a Latest Jurassic (Dingle and Klinger, 1971) biostratigraphic age determinations.

5.2.5.3 Basin synthesis

The exposed Uitenhage Group around Knysna is Upper Jurassic to Lower Cretaceous, but underlain by an unknown thickness of older strata. The Brenton Formation, which outcrops in the south banks of the Knysna Estuary, remains the most significant chronostratigraphic constraint for deposition yet these new U-Pb data do not help resolve its contentious age. If the Early Cretaceous age is accepted, then it is likely that a significant thickness of Uitenhage Group exists beneath the Knysna Estuary.

A newly drilled borehole at Thesen Island ('TI-01'), more-or-less in the centre of the Knysna Estuary (Fig. 5.43), gives the first confirmation of Uitenhage Group at depth, and provides some insights into the sedimentary fill and its stratigraphy in the Knysna Basin. During late 2017, efforts were made to reach an aquifer hosted in Table Mountain Group but the drilling stopped ~178 m from the surface, before reaching the aquifer. The borehole intersected ~34 m of surficial unconsolidated grey-brown mud, sand and gravel that are assigned to the Cenozoic (Fig. 5.48). These Cenozoic strata are underlain by 144 m of consolidated varicoloured, mostly red, siltstones and rare beige sandstones. This lower unit is interpreted as the Kirkwood Formation and supports the interpretations of Dingle et al. (1983) who placed fine-grained continental red beds as lateral equivalents of the Enon and Brenton formations in subsurface, below the south and north banks of the Knysna Estuary. At 98 –105 m depth (Fig. 5.48), the drilling intersected several green-grey shelly mudstone units, one of which hosts rare foraminifera at 98 –105 m depth (Fig. 5.48), which imply a marine origin for these beds. If this interpretation is correct, then it supports a lateral interfingering of the Kirkwood Formation with the Brenton Formation in the subsurface. Although some authors have proposed that such a gradational relationship exists between the Enon, Kikwood and Brenton formations in Knysna (e.g., Dingle et al., 1983), borehole TI-01 provides the first evidence of the previously inferred stratigraphic relationships and the presence of fine-grained lateral equivalents of the conglomerate-dominated strata that ourcrop around Knysna (Fig. 5.43). However, there still remains much uncertainty regarding the general subsurface structure and stratigraphic architecture of the Knysna Basin, although a complex and compartmentalized horst-and-graben structure is likely (Fig. 5.49). The total thickness of Uitenhage Group in the depocentre of the Knysna Basin remains unknown, as is the presence or absence of marine intervals that are older than the Brenton Formation (Fig. 5.49).

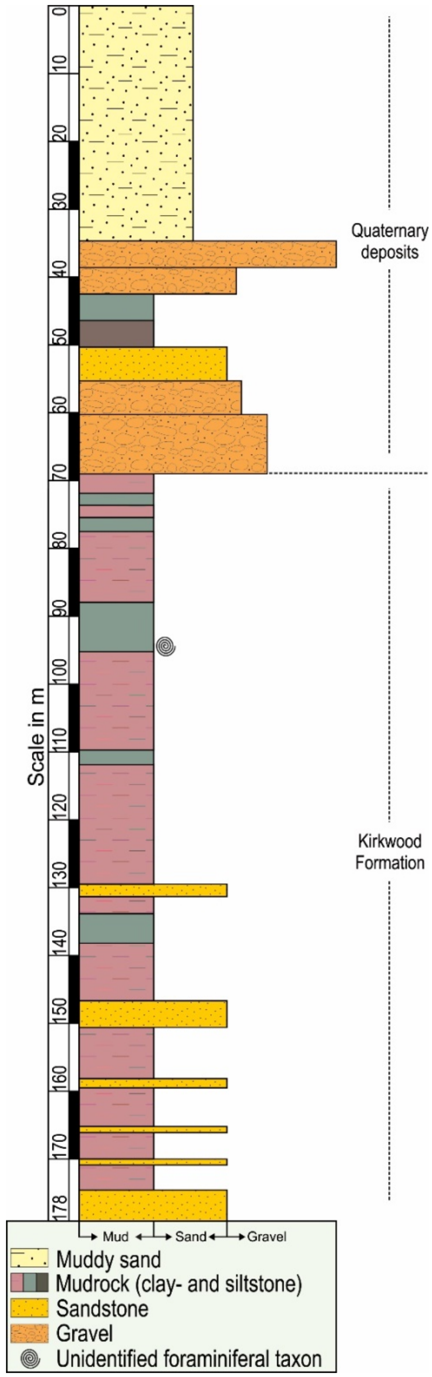

Fig. 5.48. Borehole log TI-01 from a groundwater borehole drilled in the Knysna Basin on Thesen Island with interpreted stratigraphic units on the right. Total depth is 178 m. For the location of the borehole in the Knysna Estuary, see Fig. 5.43.

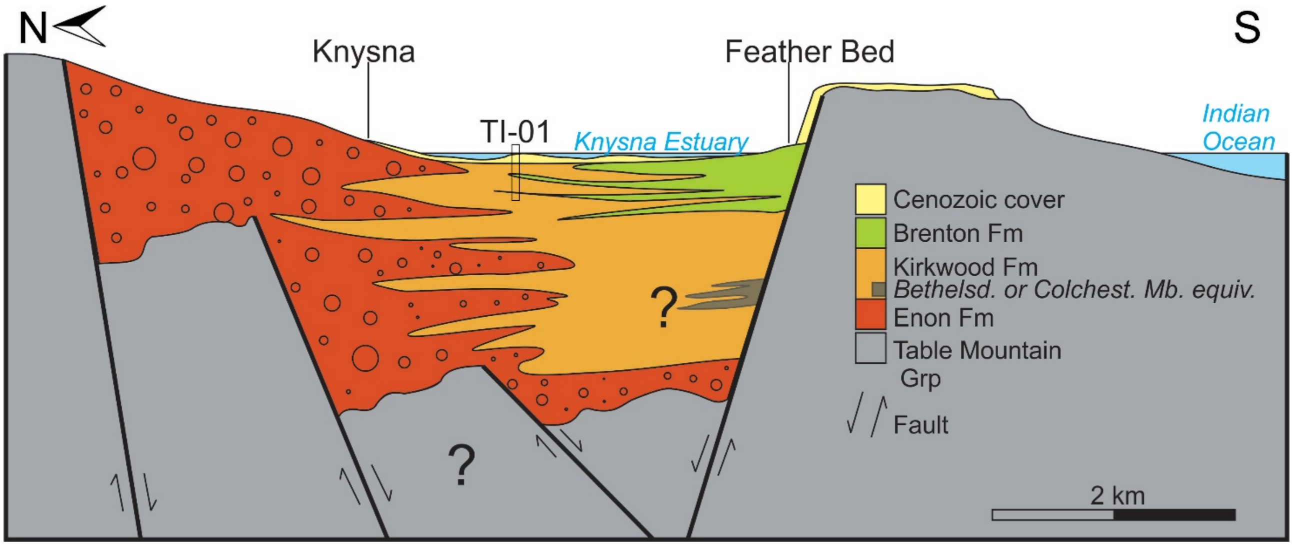

Fig. 5.49. Simplified geological cross-section of the Knysna Basin from N to S. Note the vertical scale is exaggerated to twice that of the horizontal. The total thickness of Uitenhage Group are unknown, as are the structures at depth. If the Brenton Formation is Lower Cretaceous, then Tithonian Bethelsdorp/Colchester Member equivalents are expected in the Kirkwood Formation at depth. Modified after Dingle et al. (1983).

5.2.6 Plettenberg Bay Basin

Uitenhage Group outcrops in several locations in the Plettenberg Bay Basin (Fig. 5.42), which can be subdivided into the Piesang Valley and Bitou sectors, each one probably bounded by an individual unmapped fault, and the numerous associated outcrops on the Robberg Peninsula, which is not fault-bound (Reddering, 2000). Although no thorough mapping of sedimentary rocks has been undertaken in this area other than at the well-studied outcrops on the Robberg Peninsula, which is the type locality for the Robberg Formation (Reddering, 2000), red conglomerates (Enon Formation) and finer-grained grey and red sand- and mudstones (Kirkwood Formation) exist in both the Bitou and Piesang Valley sectors (Rigassi and Dixon, 1972; Dingle et al., 1983; McMillan, 2010). The Uitenhage Group is estimated to be 2100 m and 1500 m thick in these two sectors, respectively (McLachlan and McMillan, 1976).

Most of the outcrops in the Bitou sector are exposed along the banks of the Bitou River and its unnamed tributaries and as road-cuttings along the N2 highway. Outcrops in the Piesang Valley are restricted to active brickworks, rehabilitated quarries and erosional gullies north of the Airport Road. Although exposures are very sparse in these two areas and previously undescribed in any detail, the outcrops at the Robberg Peninsula, are excellently exposed as steep-sided cliffs along the wave-cut terrace and have been studied extensively (Rigassi and Dixon, 1972; Reddering, 2000; 2003). To date, no adequate correlation between the Robberg Formation outcrops in the peninsula and those of the Enon and Kirkwood formations further inland in the Plettenberg Bay area has been made, nor has its Early Cretaceous age, based on trace fossil and microfossil assemblages (Reddering, 2000; McMillan personal communication 2016, 19 June) been verified. Here, we only consider the Uitenhage Group in the Piesang Valley and Robberg Peninsula.

5.2.6.1 Outcrop description

Vantell brickworks quarry (sample PLET)

A brickworks quarry in the Piesang Valley exposes red, purple, green, brown and grey claystones of the Kirkwood Formation (34° 4'21.73"S; 23°18'42.23"E; Fig. 5.42; Fig. 5.44 C). These varicoloured claystones are intersected by channel-shaped sandstone packages, and are overlain by a matrix-supported breccia that contains intra- and extra-basinal clasts of quartzite, sandstone and mudstone (Fig. 5.44D). Two bentonitic claystone lenses (2 and 4 m in length and up to 40 cm thick) occupy the same horizon at the top of the claystone-dominated package, directly beneath the overlying breccia. These lenses can be differentiated from surrounding claystones by their distinctive weathering that crumbles and is very uneven (popcorn texture), unlike the comparatively smooth and cracked weathering of surrounding claystones (Fig. 5.44D). The bentonitic claystone lenses were sampled, because they are interpreted as pyroclastic deposits that have been altered to montmorillonite.

Robberg Peninsula (sample RBGS1)

Excellent exposure of conglomerates, breccias, sandstones and mudstones of the Robberg Formation are displayed on the Robberg Peninsula (34° 6'3.42"S; 23°22'54.18"E; Fig. 5.42). In the upper portion of the Formation, medium to very fine-grained sandstones occur and are typified in an outcrop on the northern side of ‘The Gap’, which displays silty-sandstones with ripple cross laminations and soft-sediment deformation (Fig. 5.44E).

5.2.6.2 U-Pb geochronology

PLET

Zircons range from small, stubby ~60 µm long crystals to prismatic ones up to 150 µm long. Almost all are euhedral and unrounded although some elongated crystals are broken fragments. These zircons are all colourless under plain light and exhibit fine oscillatory zoning when imaged using the CL detector (Fig. 5.50).

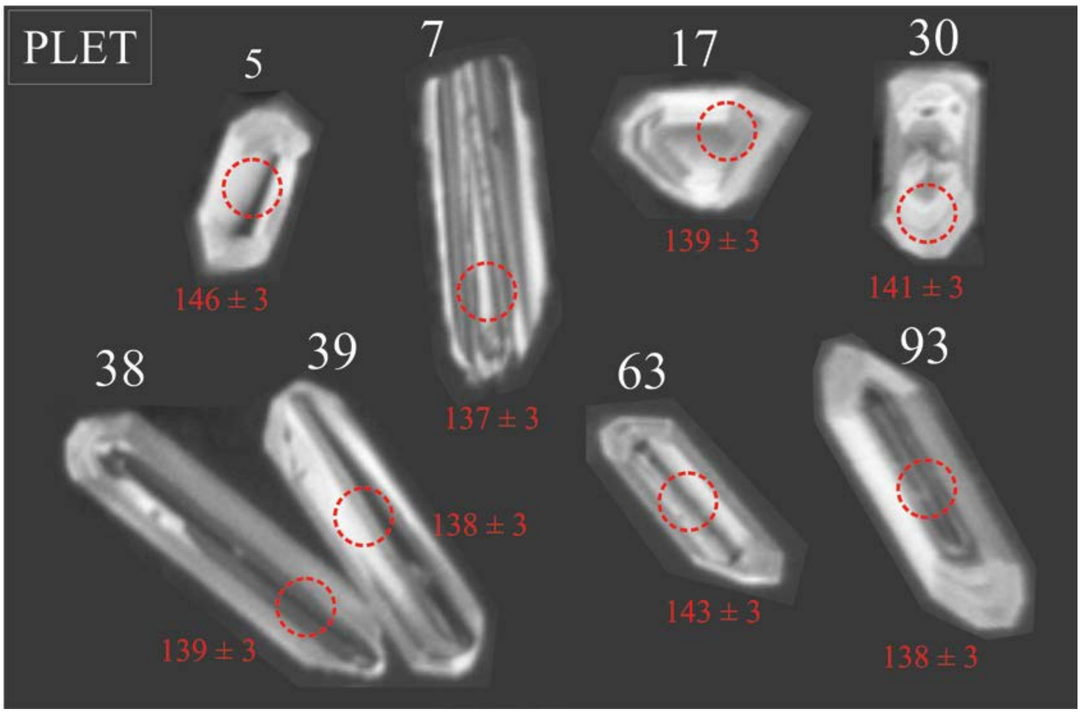

Fig. 5.50. Composite diagram of CL images of zircons that yield concordant dates in sample PLET from the Piesang Valley sector of the Plettenberg Basin Basin. Individual zircon indicated by white number and analytical spot (26 µm diameter) with respective $^{206}Pb/^{238}U$ date are red.

Of the 81 analyses, 25 yield concordant Mesozoic dates that form a population with peaks at ~138 Ma (YPP) and ~147 Ma (Fig. 5.51; Table D19 in Appendix D). Only a single older, Precambrian crystal exists in this sample, so the detrital zircon contribution in this deposit is negligible. Other analytical metrics are: YSG = 135 ± 3 Ma; YDZ = 134.2 +1.5 -2.8 Ma (95% conf.). Such a close clustering of zircon ages and ubiquitous oscillatory zonation are in agreement with field-based sedimentological interpretations of a pyroclastic origin for these bentonites. However, when plotted on the concordia diagram, 2σ ellipses are not equivalent (Fig. 5.52). $^{206}Pb/^{238}U$ dates yield a TuffZirc age of 137.9 +1.4/-0.9 Ma from a coherent cluster of 20, assuming minor inheritance (Fig. 5.52).

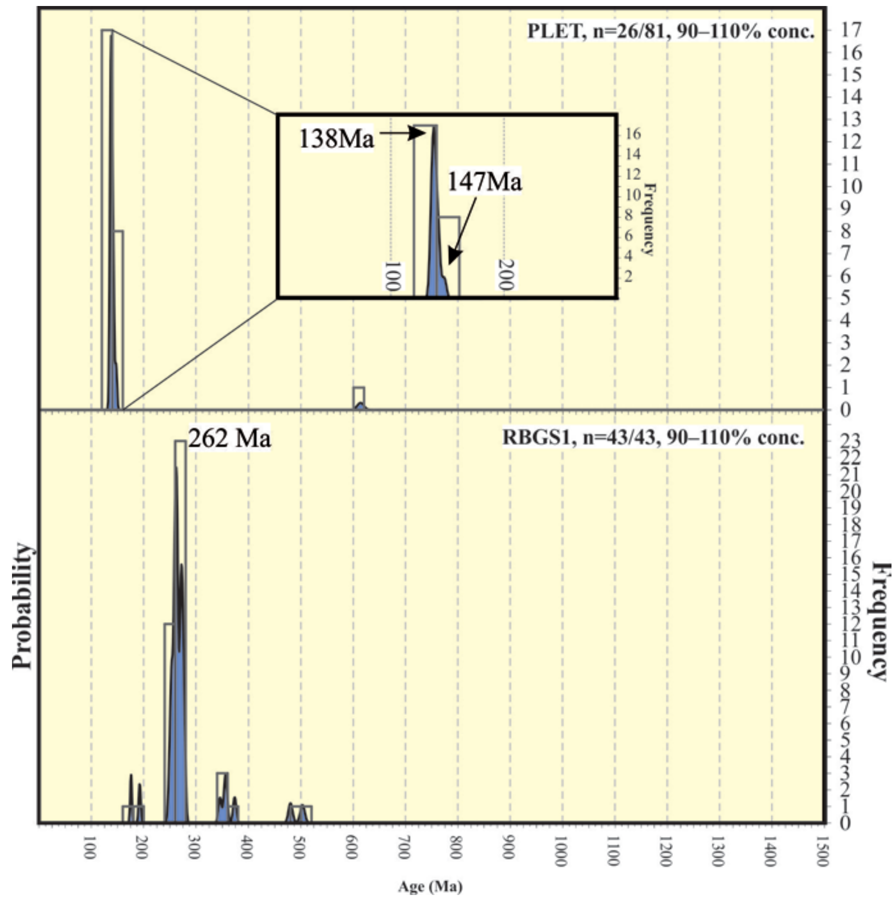

Fig. 5.51. U-Pb dates of zircons from the two samples in the Plettenberg Bay Basin shown as age probability density diagrams (blue area) combined with frequency histograms (grey bars) with 20 Ma intervals. Only concordant data are shown: n = x/y means that x out of a total of y zircons yielded concordant dates. Youngest graphically-defined peak (YPP) are indicated

CA-TIMS analysis of a selection of the youngest crystals yielded 11 concordant and reliable dates (Fig. 5.53; Table G1 in Appendix G). A weighted mean (139.9 ± 0.6 Ma) that includes all of these dates is undesirable because of the associated excess degree of scatter (MSWD = 2.6). This is largely due to the single youngest date that is discernibly younger than most other dates (at 2σ error). This 138.5 ± 0.3 Ma date only overlaps with other dates that have relatively large errors and is therefore interpreted as a spuriously young outlier that suffers lead loss. Ideally, more aggressive chemical abrasion parameters are used in order to test if this single date is repeatable. If so, then a ~138.5 Ma depositional age would be preferable to an older weighted mean of 140.2 ± 0.4 Ma (MSWD = 1.01), which is interpreted as the depositional age of the bentonite. This weighted mean is discernably older than the TuffZirc-defined age, suggesting that there is sublte Pb-loss that is not accounted for in the LA-ICPMS data.

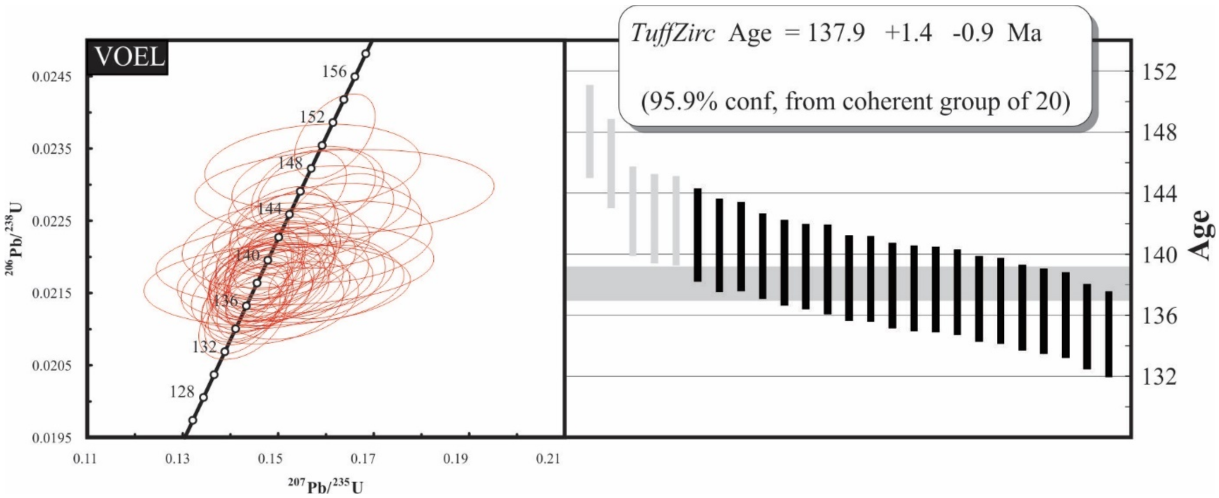

Fig. 5.52. Concordia diagram (left) and concordant $^{206}Pb/^{238}U$ dates arranged by age (right) for the pyroclastic deposit in the Plettenberg Bay Basin. Horizontal grey line is the age calculated by TuffZirc with vertical grey lines representing dates rejected from the age calculation. All individual errors are 2σ.

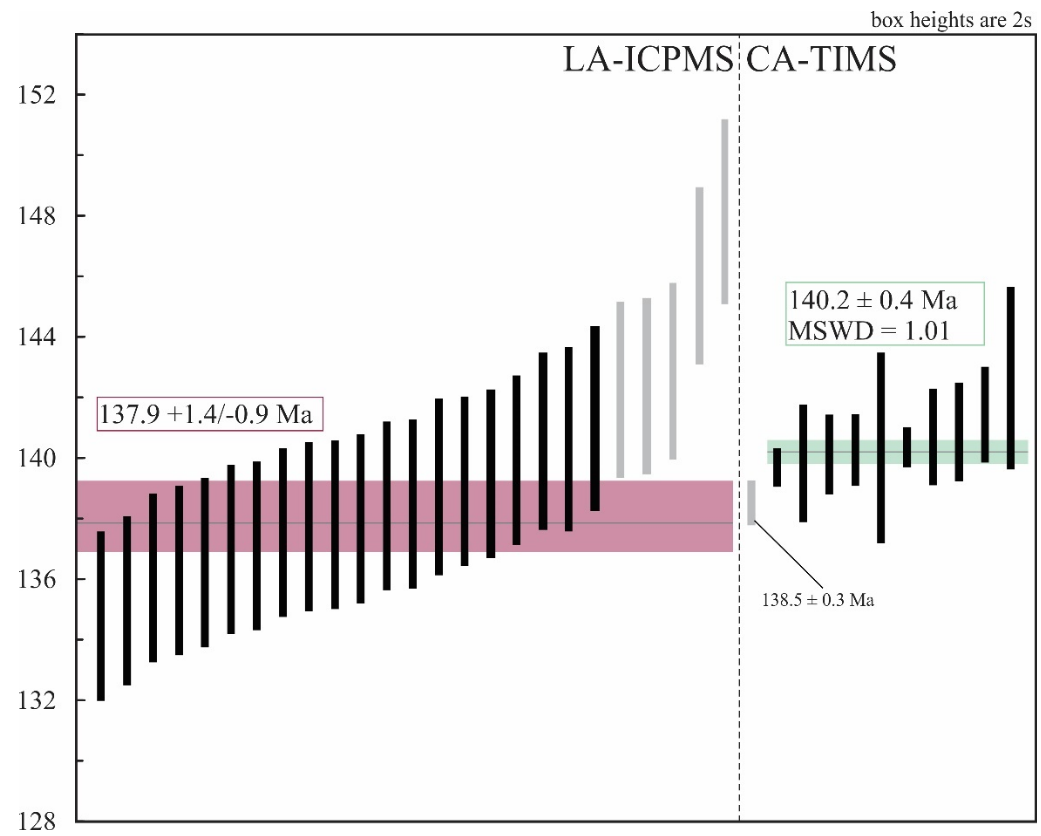

Fig. 5.53. U-Pb dates from LA-ICPMS (left) and CA-TIMS (right) analytical procedures ordered by age in sample PLET, Plettenberg Bay Basin. Grey uncertainty ranges are dates that are excluded from age calculations. The TuffZirc age (red) is younger than the weighted mean (green) calculated from 10 dates acquired by CA-TIMS.

RBGS1

Zircon crystals range from 75 to 130 µm in length and are primarily of euhedral stalky or stubby habit. Rarely, crystals displayed significant rounding and are mostly colourless or pale beige in colour. Internally, they all exhibit fine oscillatory zoning, commonly with inherited cores (e.g., crystals 17, 54 and 6 in Fig. 5.54).

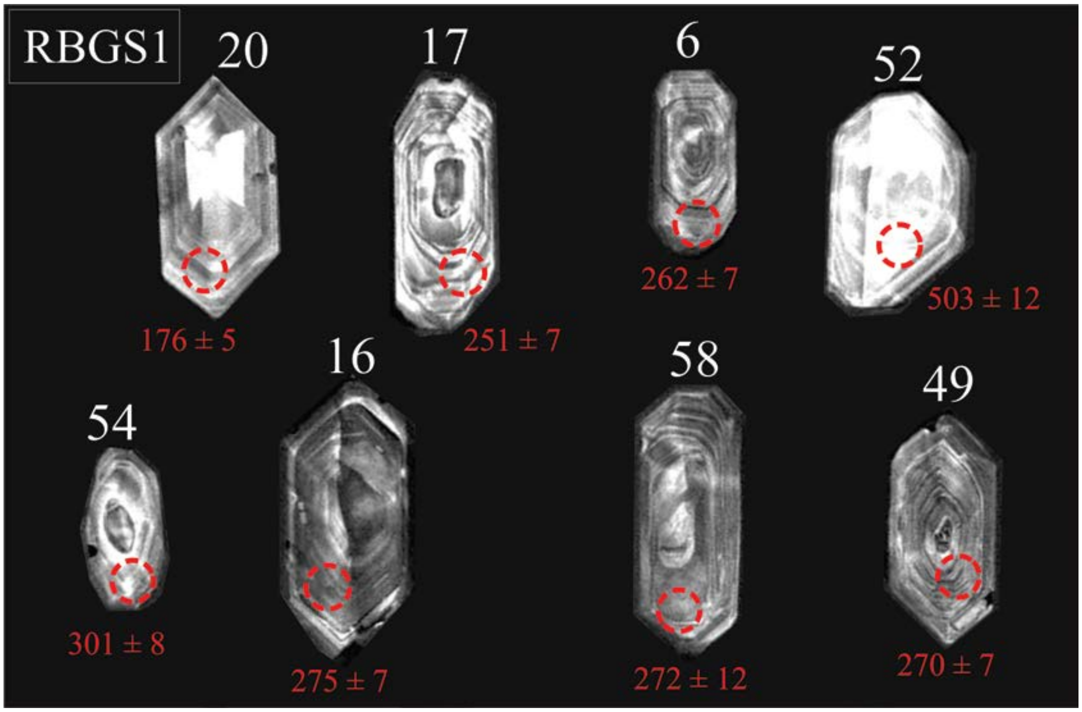

Fig. 5.54. Composite diagram of CL images of zircons that yield concordant dates in sample RBGS1 from the Robberg Peninsula of the Plettenberg Bay Basin. Individual zircon indicated by white number and analytical spot (26 µm diameter) with respective $^{206}Pb/^{238}U$ date are red.

Of the 54 crystals, 43 yielded concordant dates that form multiple Mesozoic (~10 %) and Palaeozoic (~90 %) populations on a probability density diagram (Fig. 5.51; Table E1 in Appendix E; Fig F4C in Appendix F). Only two non-overlapping (at 2σ error) Jurassic dates are present in the sample and therefore do not constitute a population. Most zircons in this sample form a complex Palaeozoic peaks at 262 Ma (YPP) and 272 Ma while there are just six Middle – Late Palaeozoic zircons. The youngest modelled detrital zircon age (YDZ) is 175.6 +3.8/-3.3 Ma (95% conf.). A rigorous measure of maximum deposition of this deposit is the graphically defined ~262 Ma, although the presence of rare Jurassic zircons suggests that deposition occurred much later than the Triassic. The biostratigraphically defined Early Cretaceous age for the

Robberg Formation at its type locality (Reddering, 2000) therefore is not further refined by detrital zircon geochronology, and is still the best estimate for its depositional age. Interestingly, the large proportions of Permian and Triassic zircons in the Robberg Formation, which both outcrops more than 100 km from presently outcropping Karoo Supergroup source and contains quartzite and sandstone clasts that are clearly derived from the Cape Supergroup and none from Karoo Supergroup lithologies. This suggests that either the Karoo Supergroup was exposed much further south than its present-day distribution or that the total transport distances and energy levels were large and transported sediment in a north to south direction.

5.2.6.3 Basin synthesis

With the exception of the Robberg Formation, the poorly exposed Uitenhage Group in the vicinity of Plettenberg Bay is scarcely considered in tectonostratigraphic models of the Mesozoic southern Cape (e.g., Dingle et al., 1983; McMillan et al., 1997; McMillan, 2010). This is largely because correlations with the Lower Cretaceous Robberg Formation have until now been impossible (Rigassi and Dixon, 1972).

The outcrops of Kirkwood Formation in the Piesang Valley are neither physically connected to those at Robberg, nor do they show the same transitional marine sedimentary facies that are described there (Reddering, 2000). However, a latest Berriasian to Valanginian pyroclastic deposit from the Piesang Valley sector (bentonite sample: PLET) allows for the first confident correlations to be made between the Kirkwood Formation in the Piesang Valley and elsewhere in the southern Cape and Robberg Formation at Robberg despite their contrasting lithological characteristics. This raises two interesting questions: 1) Why is the Robberg Formation well-cemented, while the coeval Kirkwood Formation just ~5 km from there coastal occurrence is poorly consolidated? 2) When did rift-related subsidence begin in the region of modern-day Plettenberg Bay?

To date, no suitable explanation has been provided for the unusually resistant nature of the Robberg Formation, a characteristic that is deemed highly significant by some authors (Rigassi and Dixon, 1972;

Reddering, 2000). In fact, its well-cemented nature, and lack of obvious fault planes at or near the outcrops has lead authors to believe that the deposition of the Robberg Formation predates the rifting in the southern Cape (Rigassi and Dixon, 1972). Here, we have shown that despite these differences in cementation (and thus resistance to weathering), the Robberg Formation can be considered coeval with the nearby Kirkwood Formation. This conclusively demonstrates that the two formations are facies equivalents with the Kirkwood Formation being the landward, continental equivalent of the Robberg Formation, which formed in the estuaries at the palaeocoastline in the Early Cretaceous. However, lateral sedimentary facies variations fail to account for the siliceous character of Robberg Formation. Reddering (2000) suggested that the silicification is a result of ~1 km burial and pointed out that the Robberg Formation is located on a horst structure, in contrast to the graben-fill units of the Kirkwood Formation in the Piesang Valley. However, how strata on a horst would have reached a greater burial depth than coeval graben-confined strata is unclear, especially since no later-stage fault seems to separate the Robberg Peninsula from the Piesang Valley. Perhaps a complex Cenozoic uplift and denudation history accounts for their present-day surface occurrence despite differential burial depths, or else silicious cementing is influenced by diagenetic factors other than burial depth such groundwater movement (Morad et al., 2002).

To date there is no definitive measure of the thickness of Uitenhage Group in the Piesang Valley sector, although 1500 m is estimated (McLachlan and McMillan, 1976). If the Berriasian – Valanginian bentonite horizon is near the up of this estimated section, then it is reasonable that Upper, Middle and possibly even Lower Jurassic deposits lie beneath. However, if this is an overestimation and the underlying strata have a much smaller cumulative thickness, then the earliest-deposited Uitenhage Group in the Piesang Valley sector likely is much younger. In order to properly asses the onset of rifting and Mesozoic accumulation at Plettenberg Bay, a better control of the stratigraphic position of the dated deposits need to be determined.

5.2.7 Gamtoos Basin

The Gamtoos Basin is an arcuate-shaped basin in the Eastern Cape Province that has both onshore and offshore distribution (Fig. 2.1). Its onshore sector is about 50 km in length and arcuate shape is strictly controlled by the Gamtoos Fault, which bounds the basin in the north and northeast (Fig. 5.55). Basement rocks comprise mostly of the Palaeozoic Table Mountain Group (Cape Supergroup) although an inlier of the Precambrian Gamtoos Group is exposed in the footwall of the Gamtoos Fault in the vicinity of Patensie (Fig. 5.55). The Gamtoos Fault has an extreme throw of ~12 km offshore (McMillan et al., 1997), but the total thickness of the Uitenhage Group onshore remains unknown (Dingle et al., 1983) and due to the lack of lithostratigraphic markers, the stratigraphic relationships between isolated outcrops are poorly established (van de Linde, 2017). The conglomerate-dominated Enon Formation and the sandstone-dominated Kirkwood Formation outcrop in the western and eastern part of the basin, respectively. These two outcrop regions are roughly separated by the Gamtoos River (Fig. 5.55).

Fig. 5.55. (Following page). Simplified Geology of the Algoa and Gamtoos basins. Letters and colours are lithostratigraphic units and unshaded areas are alluvium and Cenozoic cover sequences. Black stars with numbers are fossiliferous sites referred to in the text: 1 = Umlilo farm; 2 = Kirkwood Cliffs; 3 = Blue Cliffs; 4 = Bezuidenhouts River crossing; 5 = Dunbrody; 6 = Kwa Nobuhle township. Abbreviations: Towns: C = Colchester; E = Enon; H = Hankey; K = Kirkwood; P = Patensie; PE = Port Elizabeth; U = Uitenhage. Stratigraphic units arranged from oldest to youngest: GG = Gamtoos Group; TMG = Table Mountain Group; BkG = Bokkeveld Group; WtG = Witteberg Group; KSG = Karoo Supergroup; SG = Suurberg Group; UE = Enon Formation; UK = Kirkwood Formation; US = Sundays River Formation. Base maps modified from the 1: 250 000 geological maps sheets 3324 (Toerien, 1991) and 3326 (Roby and Johnson, 1995) of the Council for Geoscience overlain on ESRI satellite imagery.

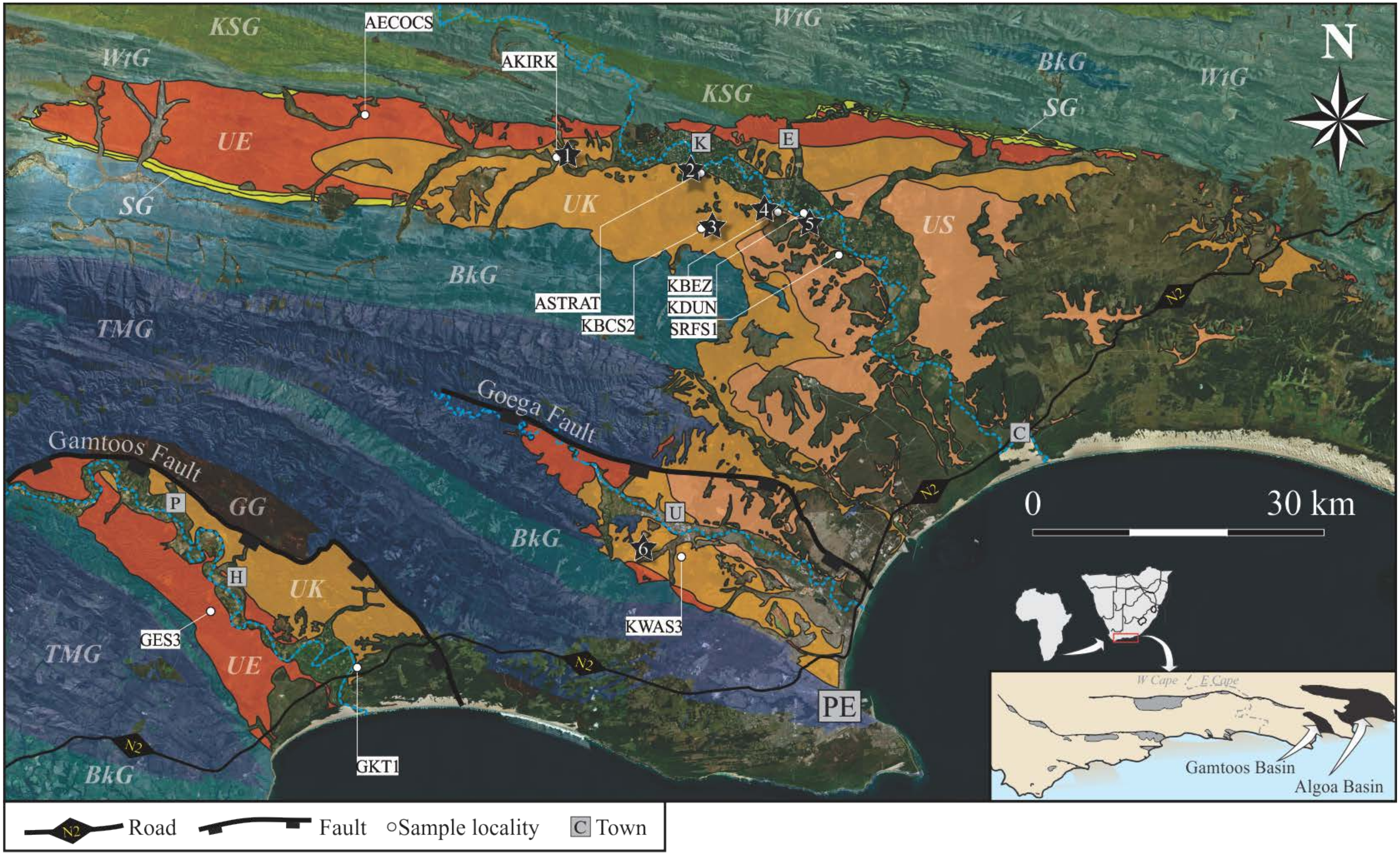

KSG
WtG
BkG
SG
UE
UK
US
TMG
GG
AECOCS
AKIRK
ASTRAT
KBCS2
KBEZ
KDUN
SRFS1
KWAS3
GES3
GKT1
K
E
C
U
P
H
PE
N2
Goega Fault
Gamtoos Fault
N
0
30 km
W Cape
E Cape
Gamtoos Basin
Algoa Basin
Road
Fault
Sample locality
Town

5.2.7.1 Outcrop description

Enon Formation stratotype quarry (sample GES3)

The Gamtoos Basin contains the newly proposed stratotype for the Enon Formation (see Fig. 5 in Muir et al., 2017a within section 2.2.1 of this thesis for details) in a roadside quarry (33°52'12.30"S; 24°51'15.31"E; Fig. 5.55) that presents high quality and easily accessible exposures of the unit, which otherwise show subtle lithofacies variations in the region (van de Linde, 2017). Overall, the Enon Formation is this quarry comprises massive to crudely bedded conglomerates with quartzite and sandstones clasts from the Table Mountain Group and white sandstone lenses, one of which was sampled for detrital zircons.

Gamtoos River cutting south (sample GKT1)

Good exposures of the Kirkwood Formation are situated in the southeastern part of the onshore basin, particularly along the banks of the Gamtoos River. A river-cut cliffs ~ 200 m north of the N2 highway (33°55'21.34"S; 25° 1'41.23"E; Fig. 5.55) displays a thick succession of mainly sandstones, with a thin, laterally extensive grey claystone layer of possible, yet unconfirmed volcaniclastic affinity (Fig. 5.56). In order to maximize the chances of sampling volcanic zircons, the 5 – 10 cm thick claystone was excavated along with some of the overlying sandstone.

Fig. 5.56. (Following page). Geological context of the Uitenhage Group samples in the Gamtoos Basin. (A) White sandstone lenses in a conglomerate-dominated outcrop that forms part of the proposed new stratotype for the Enon Formation (see Fig. 5 in Muir et al., 2017a, section 2.2.1 of this thesis). (B) White sandy claystone beds (outlined by blue dashed lines) in a sandstone-dominated outcrop of the Kirkwood Formation at the southern Gamtoos River Banks. (C) The clay-rich sandstone bed sampled, which is ~2 m to the right of B. Pink arrows indicate the exact position from which respective samples were extracted.

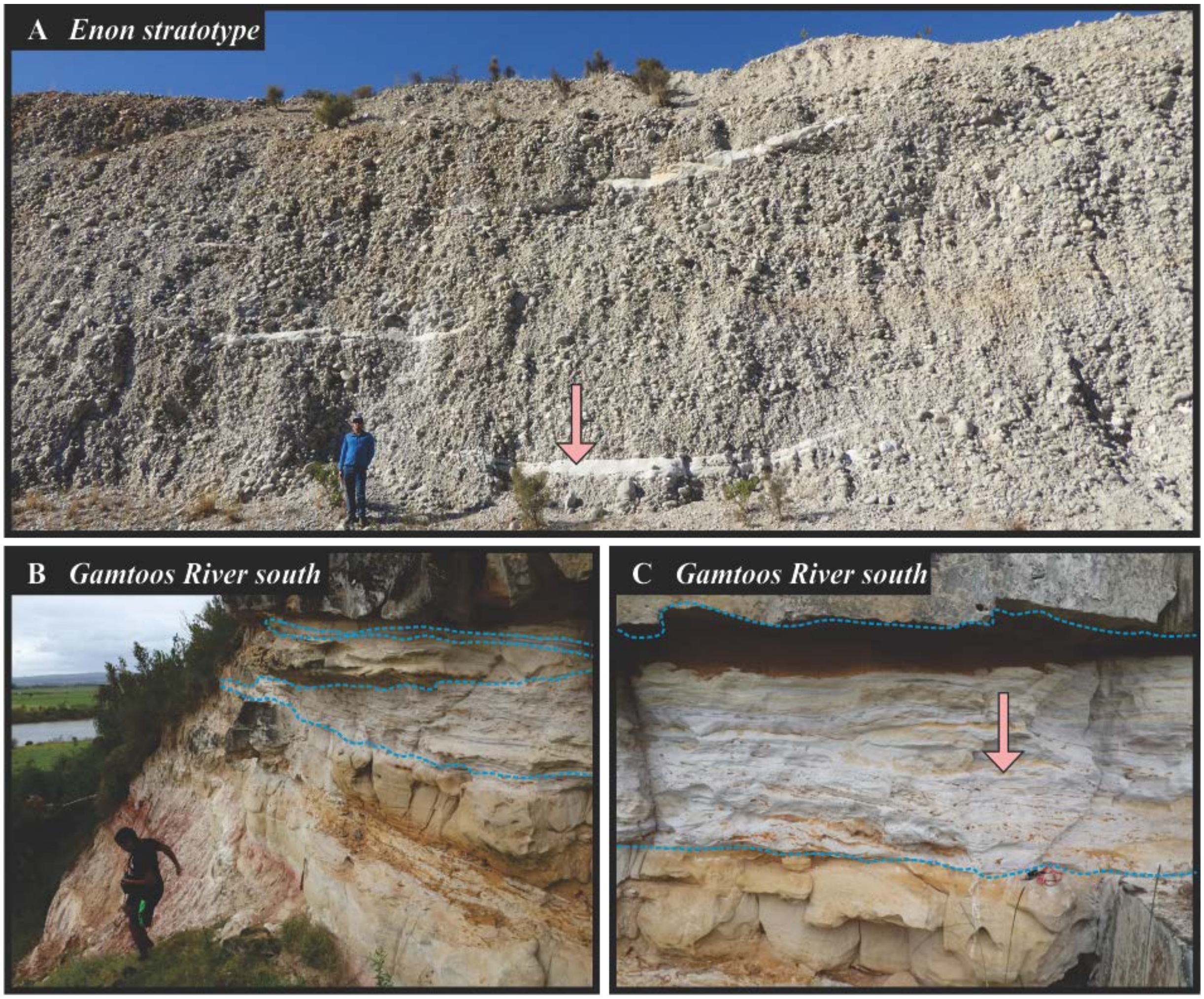

5.2.7.2 U-Pb geochronology

GES3

Crystals are between 60 and 210 µm, are well-rounded to euhedral, or are angular fragments. Commonly they take on prismatic and stalky habits, with rare, often broken needles (e.g., crystal 31 in Fig. 5.57). They are either beige, colourless, or deep orange in colour. Internally, the crystals show fine oscillatory zoning, sometimes with secondary recrystallization (e.g., 64 in Fig. 5.57). Many zircons contain xenocrystic cores (e.g., 58 and 72 in Fig. 5.57) and inclusions (e.g., 64 and 42 in Fig. 5.57), while others do not (e.g., 31 in Fig. 5.57).

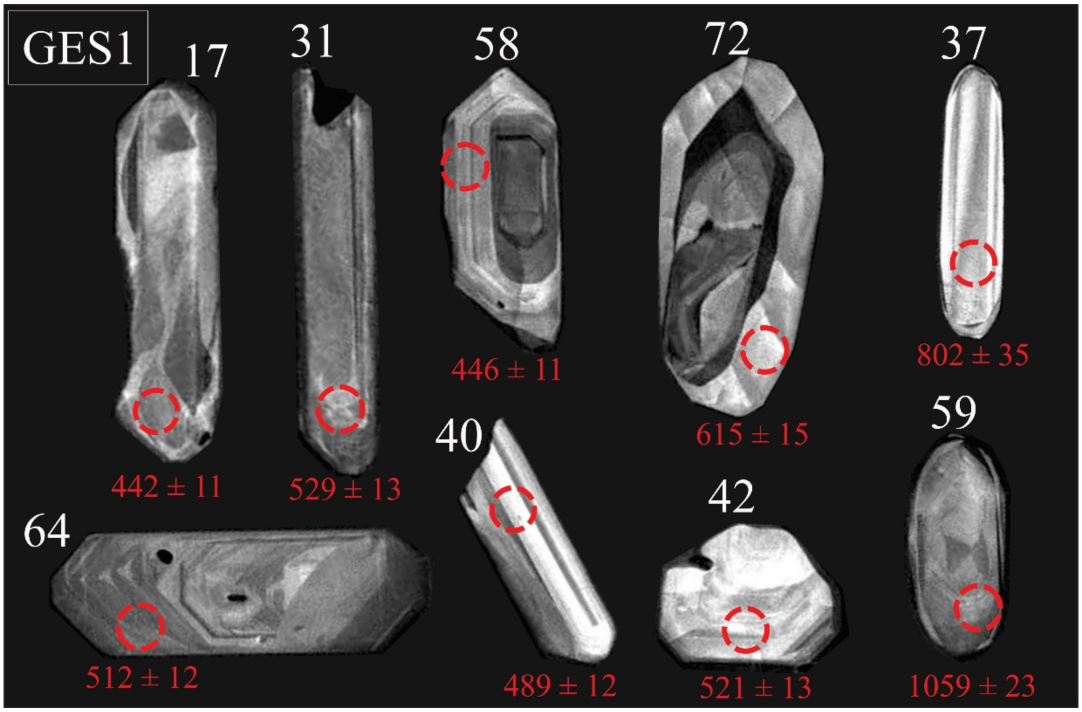

Fig. 5.57. Composite diagram of CL images of zircons that yield concordant dates in sample GES1 from the Gamtoos Basin. Individual zircon indicated by white number and analytical spot (26 µm diameter) with respective $^{206}Pb/^{238}U$ date are red.

Of the 64 zircons, 58 yield concordant dates, which are early Palaeozoic (~28 %) and Precambrian (~72%) and occupy complex age populations with notable Ordovician, Cambrian, and Neoproterozoic peaks (Fig. 5.58; Table E1 in Appendix E; Fig. F5A in Appendix F). The youngest age component is at ~445 Ma (YPP), which reflects a Late Ordovician maximum depositional age. However, this probably reflects a Cape Supergroup source and an absence, Mesozoic zircons. Other metrics are: YSG = 442 ± 11 Ma; YDZ = 441.3 +6.6/-8.2 Ma (95% conf.).

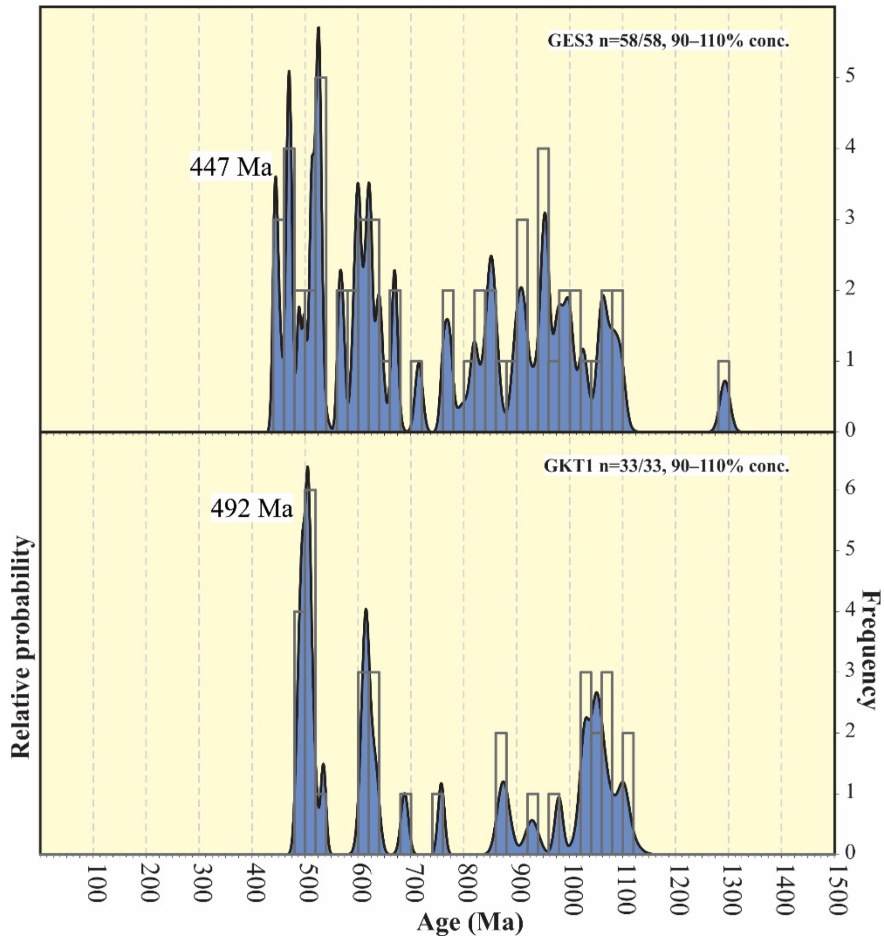

Fig. 5.58. U-Pb dates of zircons from all samples in the Gamtoos Basin shown as age probability density diagrams (blue area) combined with frequency histograms (grey bars) with 20 Ma intervals. Only concordant data are shown: n = x/y means that x out of a total of y zircons yielded concordant dates. Youngest graphically-defined peak (YPP) are indicated.

GKT1

Zircons are similar to those in sample GKT1 in many respects, although in general are smaller, and range in size from 50 to 130 µm. They likewise are colourless, beige, or deep orange under plain light. Typically, crystals are either stalky or prismatic and range from well-rounded (e.g., crystal 56 in Fig. 5.59) to euhedral (e.g., 5 in Fig. 5.59) with some angular fragments (e.g., 5 and 6 in Fig. 5.59). Internal textures under the CL detector are varied, with some crystals exhibiting clear signs of recrystallization (e.g., 14, 56 in Fig. 5.59) commonly with xenocrystic cores (e.g., 12 in Fig. 5.59). Fine oscillatory zoning is present in some grains (e.g., 5, 6 in Fig. 5.59) and absent in others (e.g., 60 in Fig. 5.59), as are inclusions.

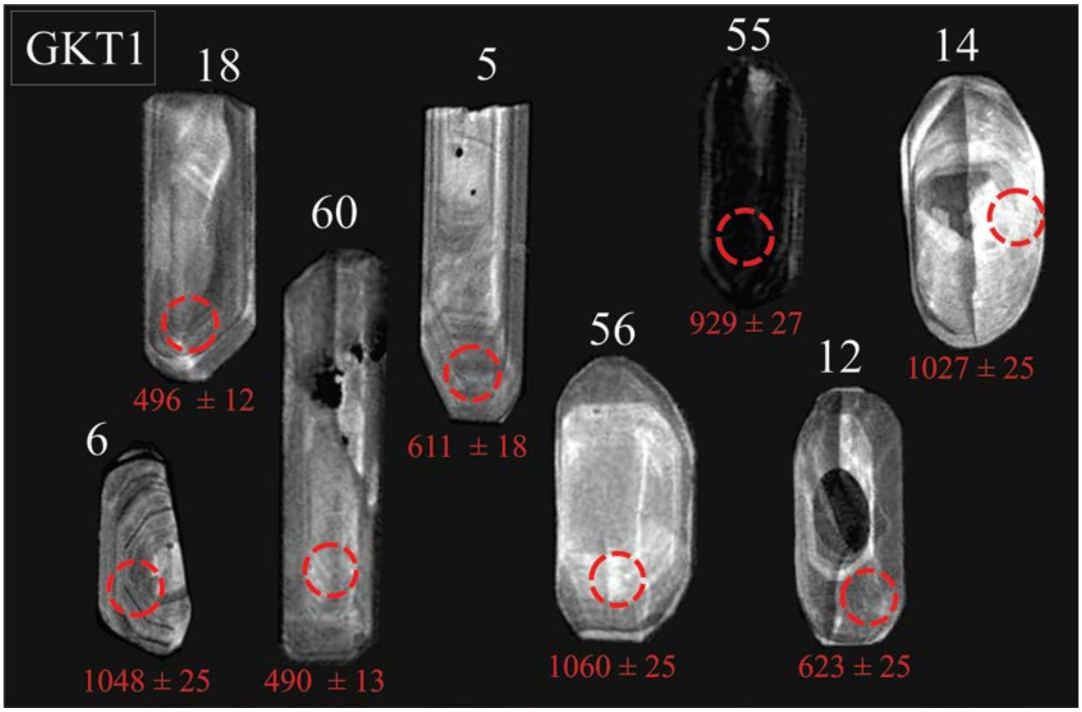

Fig. 5.59. Composite diagram of CL images of zircons that yield concordant dates in sample GKT1 from the Gamtoos Basin. Individual zircon indicated by white number and analytical spot (26 µm diameter) with respective $^{206}Pb/^{238}U$ date are red.

All 33 analytical dates are concordant in this sample, and comprise multiple populations, notably at ~505 Ma, which is the youngest and largest age component (YPP), as well as Neoproterozoic populations (Fig. 5.58; Table E1 in Appendix E; Fig. F5B in Appendix F). The detrital zircon age distribution is very similar to that of GES3 albeit a fewer number of analysed zircons make for a less representative age distribution. The absence of Mesozoic zircons and Cambrian maximum depositional age (YPP) is not consistent with the claystone interval being of volcanic origin and provides no means to refine deposition age. The youngest zircon (YSG) is 486 ± 15 Ma and the youngest modelled age (YDZ) is 489.2 +7/-12 Ma (95% conf.).

5.2.7.3 Basin synthesis

The onshore Gamtoos Basin contains thick accumulations of sandstones and conglomerates of the lower Uitenhage Group. Unfortunately, there are no Mesozoic zircons present in either of the two samples and therefore they offer no refinement of the depositional age of the exposed strata, nor of the stratigraphic relationships between units within the Gamtoos Basin. Furthermore, the detrital zircon distributions do not add a new meaningful detail to the provenance history of these sediments either, because the Early Palaeozoic – Precambrian zircon populations simply confirm that both the Enon and Kirkwood formations in the basin were derived from sources that are locally outcropping in and around the basin (i.e., the Table Mountain and Gamtoos Groups).

In light of this, offshore borehole microfossil assessments of the Uitenhage Group remain the most reliable means to date the strata in the Gamtoos Basin. McMillan et al. (1997) assigned the oldest dated strata of the Enon Formation to the Kimmeridgian, and the youngest to the Valanginian, and this probably also reflects the age interval of the exposed units onshore. This is compatible with the Late Jurassic – Early Cretaceous plant macrofossil assemblages that occur in rare lignites in the Kirkwood Formation onshore (McLachlan and McMillan, 1976). However, because there remains a thick package of undrilled and undated continental strata below the deepest boreholes drilled in the offshore Gamtoos Basin, there could also be vast thicknesses underlying those exposed onshore, especially adjacent the Gamtoos Fault. Therefore, it is likely that initial basin subsidence occurred in the Middle Jurassic or earlier.

5.2.8 Algoa Basin

The Algoa Basin is situated in the Eastern Cape Province largest of the onshore Mesozoic basins. It takes on an arcuate shape and is composed of a number of half-grabens that are filled with the Uitenhage Group and to a lesser degree the Suurberg Group (see Chapter 4) within Cape and Karoo Supergroups as basement. It contains abundant outcrops of the Enon, Kirkwood and Sundays River formations, which have been studied, among others, for their palaeontological (e.g., McLachlan and McMillan, 1976; Rich et al., 1983; de Klerk et al., 2000; Choiniere et al., 2012; Muir et al., 2015; McPhee et al., 2016), hydrocarbon (McMillan et al., 1997; Broad et al., 2012), and carbon sequestration potential (Viljoen et al., 2010). These multifaceted inquiries require a at least some chronostratigraphic information and therefore the age of the strata in the Algoa Basin have been previously investigated with considerably more effort than strata in any other rift basin of the southern Cape. In aid of this, the marine units contained in the basin, the Tithonian Bethelsdorp Member of the Kirkwood Formation and the Valanginian – Hauterivian Sundays River Formation has provided the only sound biostratigraphic time constraints to the Uitenhage Group. These constraints, in combination with historic ages for the Mimosa Formation of the underlying Suurberg Group (McLachlan and McMillan, 1976) account for all the chronostratigraphic information in the Algoa Basin. However, with new U-Pb ages for the Suurberg Group that push back constraints for maximum deposition of the Uitenhage Group by ~20 Ma (see Chapter 4) and a large range of ages reported from ashes in the Uitenhage Group in other basins, existing estimated depositional ages from the Algoa Basin require careful scrutiny, especially its continental deposits that have never been dated directly. Specifically, the Tithonian – Valanginian age reported for the Kirkwood Formation, including an entirely Early Cretaceous age for its uppermost fossil-bearing strata (e.g., McLachlan and McMillan, 1976; Shone, 2006), requires critical evaluation because this age determination is based on a correlation between the upper Kirkwood Formation and the Valanginian lower Sundays River Formation that is unconfirmed (contrast McLachlan and McMillan, 1976; Winter, 1979 and Shone, 1978). Further, if these units (i.e., upper Kirwoord and lower Sundays River formations) are age correlatives, how much time does the full 2000 m thickness of the underlying Kirkwood Formation represent?

5.2.8.1 Fossiliferous deposits of Kirkwood Formation in the Algoa Basin

The diversity of non-age diagnostic continental fauna (e.g., sauropod, ornithopod and theropod dinosaurs, frogs, turtles, sphenodontids, crocodiles) in the Algoa Basin come from the mudstones and sandstones of the Kirkwood Formation, mostly as poorly articulated and fragmentary remains in channel lag deposits and palaeosols (McLachlan and McMillan, 1976; Rich et al., 1983; de Klerk et al., 2000; Almond 2009; Forster et al., 2009; McPhee et al., 2016) although rare articulated specimens have also been found (de Klerk et al., 2000). Plant fossil remains (e.g., bryophytes, ferns, bennettitaleans, cycads, conifers, fossil logs, amber and charcoal) are common although usually comprise abraded fragments or logs weathering out of sandstones (McLachlan and McMillan, 1976; Anderson and Anderson, 1985; Banford, 1986). An exception is near the Buizedenhouts River crossing (Bamford, 1986; Muir et al., 2015) where well-preserved specimens are common in the grey mudstones. Including this important plant fossil locality, there are essentially six fossil sites in the Formation that have been subjected to systematic palaeontological studies (McLachlan and McMillan, 1976; Rich et al., 1983; Bamford, 1986; McPhee et al., 2016) and account for the diversity of fossil assemblages in the Kirkwood Formation. These include five sites in the northern part of the Basin near Kirkwood, within the Sundays River Trough, and one in the vicinity of Kwa-Nobuhle in the Uitenhage Trough (see black stars in Fig. 5.55).

One of the most fossil-rich sites in the Kirkwood Formation is on Umlilo farm, ~15 km west of Kirkwood (Fig. 5.55). Here, laterally extensive outcrops of mudstones and sandstones outcrop in erosional gullies and ravines. The first ornithomimosaurian dinosaur taxon known from Africa and the most articulated of such specimens from the whole Gondwanan supercontinent, *Nqwebasaurus thwasi*, was excavated from red sandy mudstones exposed in a natural cliff in the late 1990’s (de Klerk et al., 2000; Choiniere et al., 2012). In addition to yielding this important specimen, several other fragmentary sauropod remains have also been excavated here that have contributed to our understanding of their diversity in the Early Cretaceous (McPhee et al., 2016). None of these fossils are age diagnostic, and have been assigned as Early Cretaceous (Berriasian –Valanginian) based on an assumed partial lateral continuity of its upper strata with the Valanginian Sundays River Formation (Shone et al., 1978; McMillan, 2003). However, the Sundays River Formation does not outcrop in the immediate vicinity of Umlilo (the nearest exposures are more than 23 km away) making a lateral correlation potentially erroneous, especially considering that there is no compelling evidence that the deposits at Umlilo are indeed in the upper part of the thick Kirkwood Formation. Additionally, the stratigraphic relationship between these two stratigraphic units in the Algoa Basin remains unclear. They appear to be at least partial lateral correlatives (Shone, 1978), although the lack of exposure that clearly demonstrates this leaves the possibility that a stratigraphic gap exists between them (Winter, 1973), and if so, then the correlative inference is brought into question.

The stratotype locality for the Kirkwood Formation on the banks of the Sundays River (Fig. 5.55; Fig. 5 of Muir et al., 2017b in section 2.2.2 of this thesis) is one of the most palaeontological productive sites in the Mesozoic of the southern Cape and has contributed immensely to the reconstruction of the continental ecosystem of this region. The site has yielded a diverse faunal assemblage with fragmentary remains of crocodilia, theropoda, sauropoda, ornithischia and osteichthyes fish (McLachlan and McMillan, 1976; Rich et al., 1983, Forster, 2009; McPhee et al., 2016). These vertebrate fossils are assigned broadly a Late Jurassic – Lower Cretaceous age by comparison with similar vertebrate assemblages in North America (Rich et al., 1983). These fossiliferous deposits are difficult to conclusively date because like those at Umlilo, the stratigraphic position of this spatially isolated fossil locality relative to the better dated Valanginian lowermost Sundays River Formation is not obvious.

Outcrops of the Kirkwood Formation on the banks of the Sundays River at Dunbrody (Fig. 5.55) have been pivotal in understanding the stratigraphy of the Uitenhage Group in the Algoa Basin, because of the marine bivalve fossils that are found there. Sandstones and mudstones there contain abundant shell fragments and whole oyster shells, which signify a (at least partial) marine influence during deposition. Two stratigraphic interpretations can be invoked to satisfy there being marine conditions during deposition of the otherwise continental Kirkwood Formation at the Dunbrody site (Fig. 5.60). On the one hand, the thin marine Bethelsdorp Member of the Kirkwood Formation may extend laterally from its known coastal locality, 40 km south of Dunbrody with an entirely subsurface distribution to the Dunbrody area (Fig. 5.60). Alternatively, the presence of marine conditions could be attributed to thin ‘tongues’ of the marine Sundays River Formation that extend further north than the majority of the unit (Shone, 1978). After all, the Sundays River Formation does outcrop widely immediately south of Dunbrody (Fig. 5.55), so if the suspected gradational contact and lateral continuity occurs between the two units, then such thin marine interbeds are likely. The latter interpretation is generally accepted (McMillan et al., 1997) because nearby boreholes (AD1/68 and CK 1/68) intersect neither the Bethelsdorp nor the Colchester members of the Kirkwood Formation and therefore suggest a limited distribution for these units at least 10 km south of, rather than at, Dunbrody (McMillan, 2010; fig. 15 p. 42). However, there are no outcrops that display how the Kirkwood and Sundays River formations relate to each other. If the beds at Dunbrody represent an interfingering and lateral correlation between the units, then they should have a Valanginian age.

Good exposures of beige sandstones and grey mudstones are exposed in river cuttings along the Bezuindenhouts River around the Blue Cliffs railway station that have yielded freshwater bivalves and rare, fragmentary dinosaur remains (McLachlan and McMillan, 1976; Rich et al., 1983). Although this site has not significantly contributed to the fossil assemblages of the unit, its sedimentary characteristics and freshwater fossils indicate that lacustrine depositional settings did exist in the principally fluvial part of the Kirkwood Formation in the Algoa Basin (Muir et al., 2017b in section 2.2.2 of this thesis). However, how these lacustrine settings relate to the lacustrine Colchester Member and other stratigraphic units in the basin remains unclear.

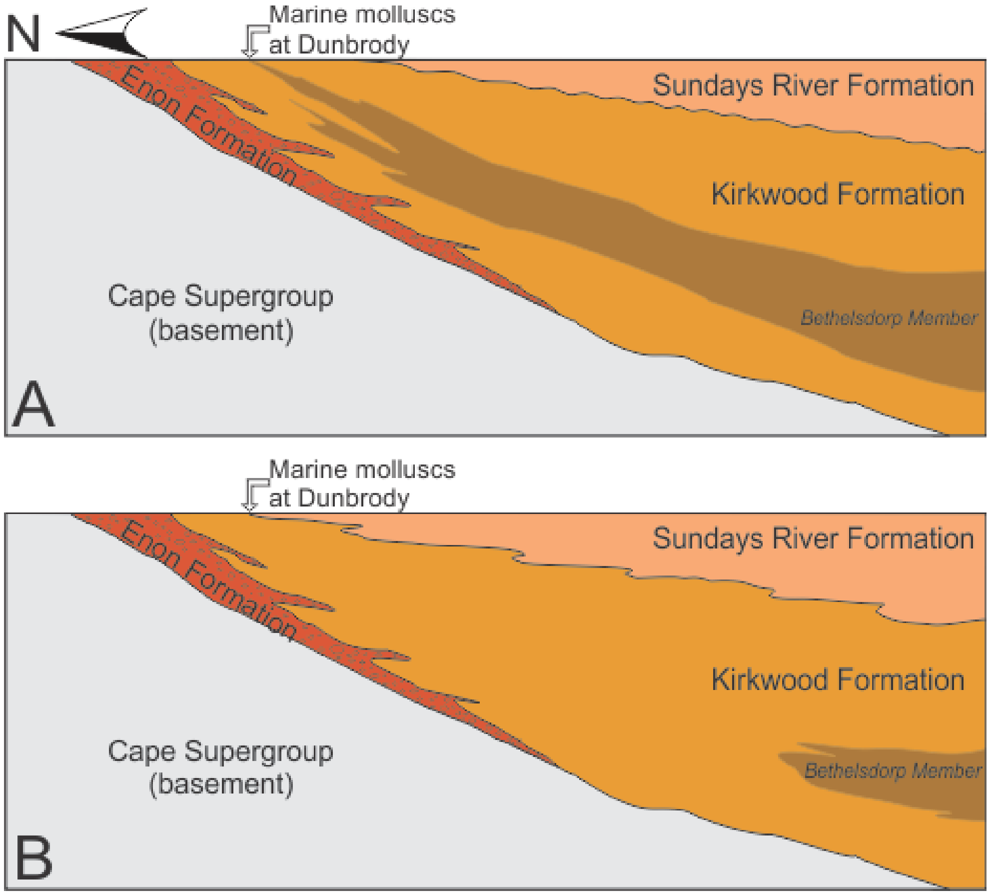

Fig. 5.60. Schematic diagram exhibiting two alternate stratigraphic relationships in the Algoa Basin that honor a partial marine depositional setting in the Kirkwood Formation at Dunbrody (modified after McLachlan and McMillan, 1976).

Grey mudstones, beige sandstones and subordinate charcoal-rich breccia-conglomerates outcrop in a river cutting some ~50 km north of Port Elizabeth at the Bezuindenhouts River Bridge (Fig. 5.55). The mudstones here have yielded exceptionally well-preserved fossil plant remains (Bamford, 1986), and coarser deposits contain fossil logs with a charred appearance and abundant charcoal, indicating that wildfires were active during deposition (Muir et al., 2015). Due to the close proximity of the Sundays River Formation, which outcrops less than 200 m to the SE, these fossiliferous deposits have been regarded as Lower Cretaceous (Muir et al., 2015). The age of this deposit is particularly important for furthering work on the effect of wildfires on vegetation structure and plant evolution because rising atmospheric oxygen levels are considered an Early Cretaceous phenomenon of global significance (e.g., Brown et al., 2012). If the deposit is Upper Jurassic, then the presence of intensive wildfires in the Algoa Basin may be driven by factors such as climate, vegetation structure or ignition source than it does with global atmospheric compositions.

Laterally extensive exposures of varicoloured palaeosol-rich mudstones are scattered at Kwa-Nobuhle township, 5 km south of Uitenhage, that have yielded important fragmentary sauropod vertebral remains (Broom, 1904; McPhee et al., 2016). These deposits have also been tentatively considered to be Lower Cretaceous (McPhee et al., 2016) although this remains unconfirmed. These outcrops of the Kirkwood Formation are unique because unlike those at the aforementioned sites in the northern Algoa Basin, the red bed here are underlain by the Tithonian marine Bethelsdorp Member, and are overlain (and possibly partially interfinger with) the Sundays River Formation (Fig. 5.55). As such, the red beds here are the only part of the Formation that can reasonably confidently be dated as probably post-Tithonian, and likely earliest Early Cretaceous by biostratigraphic methods.

5.2.8.2 Outcrop description

Roodekrans (sample AECOC)

Crudely-bedded conglomerates of the Enon Formation outcrop in a ~250 m long, and ~80 high river-cut cliff in the northern Algoa Basin Panhandle south of the R75at Roodekrans (33º22'31.86"S; 25º 2'14.90"E; Fig. 5.55). The crude beds dip 25ºS and comprise well-rounded to sub-rounded quartzite conglomerates, subordinate sandstone lenses and rare sandstone beds that are laterally extensive for ~50 m (Fig. 5.61A, B). The lower of two prominent sandstone beds was sampled.

Umlilo farm (sample AKIRK)

A sample from a thin sandstone layer (Fig. 5.61C) that intersects red mudstones on Umlilo farm at the exact locality where Nqwebasaurus (de Klerk, et al., 2000) was discovered (33°24'45.11"S; 25°15'44.42"E; Fig. 5.55) was extracted in order to assess the maximum depositional age of the fossil-bearing site directly and potentially provide constraints on its age.

Kirkwood Cliffs (sample AKSTRAT)

Interbedded beige sandstones and varicoloured silty mudstones outcrop on a north-facing cliff-face ('Kirkwood cliffs') on the southern banks of the Sundays River and is the formal type locality of the Kirkwood Formation (see Figs 4 and 5 in Muir et al., 2017b in section 2.2.2 of this thesis). A sample of a prominent beige sandstone bed exposed in the cliff face was taken for detrital zircon geochronology (33°25'40.93"S; 25°26'6.71"E; Fig. 5.55; Fig. 5.61D).

Dunbrody (sample KDUNS)

Alternating ~5 cm beds of light brown mudstone and medium-grained beige sandstone are exposed at Dunbrody (33°28'28.29"S; 25°33'48.06"E; Fig. 5.55) that may reflect the gradational contact between the Kirkwood and Sundays River formations (McMillan et al., 1997) and a transition between continental and shallow marine deposition (McLachlan and McMillan, 1976). One of the sandstone interbeds (Fig. 5.61E) was sampled in order to constrain the deposition age.

Fig. 5.61. Geological context of the Uitenhage Group samples in the Algoa Basin. (A) Cliffs at Roodekrans consisting of the conglomerate-dominated Enon Formation. Bedding (white lines) is tilted towards the south. White dashed lines delineate the area depictedin B. (B) A sandstone bed, outlined by blue dashed lines, within the conglomerate-dominated deposit at Roodekrans. (C) Sandstones and mudstones of the Kirkwood Formation on Umlilo farm at the *Nqwebasuarus* fossil locality. Blue dashed line separates the different facies. (D) Variagated mudstones and a sandstone bed (outlined with blue dashed lines) of the Kirkwood Formation at the 'Kirkwood Cliffs' stratotype locality. The conglomerate-dominated Kudus Kloof Formation overlies and is separated from underlying strata by an unconformity (red dashed line). Photo courtesey of Dr. Billy De Klerk. (E) Beige sandstones interbedded with grey mudstones that contain marine gastropod fossils within the Kirkwood Formation at Dunbrody. Blue dashed lines hilight some of the interbedded sandstones. (F) Cliffs composed of the sandstones, mudstones and conglomerates of the Kirkwood Formation near Blue Cliffs. White dashed line highlights the region depectedi in G and the white dotted line separates the underlying Kirkwood Formation from uncosolidated modern sediments and soil. (G) Prominent sandstone bed overlying mudstones. (H) Charcoal-rich fossiliferous interbed within beige sandstones at an outcrop of the Kirkwood Formation at the Bezuidenhouts River Bridge. (I) Charcoal-rich fossiliferous bed in H within a larger context at Bezuidenhouts River Bridge outcrop (adopted from Muir et al., 2015). (J) Red and grey mudstones and sandstones of the Kirkwood Foramtion on the outscirts of the Kwa-Nobuhle township near Uitenhage. Blue dashed line separate the different facies. (K) Sandstone lenses and bed (outlined in dashed blue lines) interbedded with mudstones in an outcropexposing the Sundays River Formation near Sunland. The Kudus Kloof Formation . Pink arrows indicate the exact position from which respective samples were extracted.

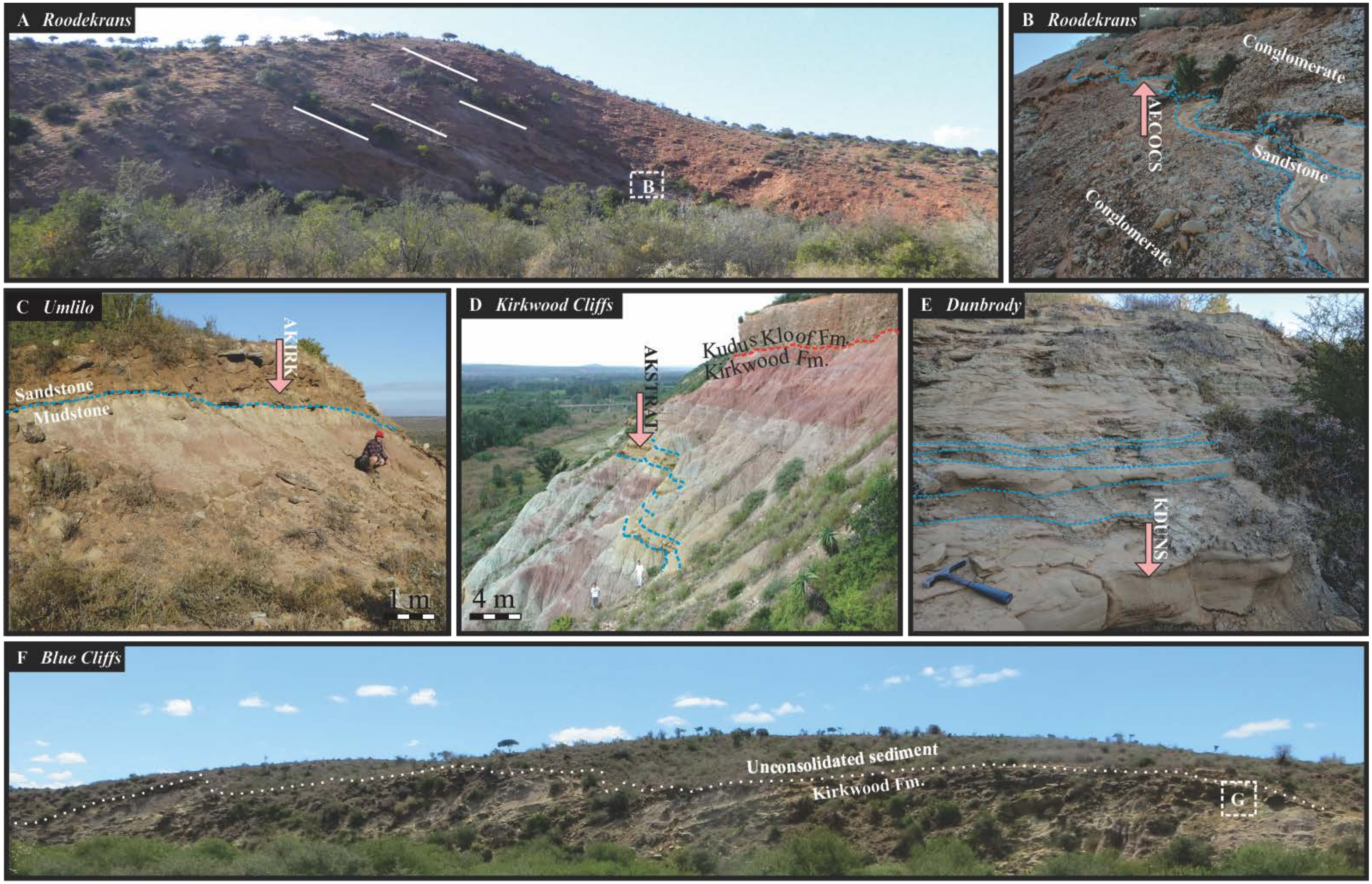
A Roodekrans
B
B Roodekrans
Conglomerate
AECOCS
Sandstone
Conglomerate
C Umlilo
AKIRK
Sandstone
Mudstone
1 m
D Kirkwood Cliffs
AKSTRAI
Kudus Kloof Fm.
Kirkwood Fm.
4 m
E Dunbrody
KDUNS
F Blue Cliffs
Unconsolidated sediment
Kirkwood Fm.
G

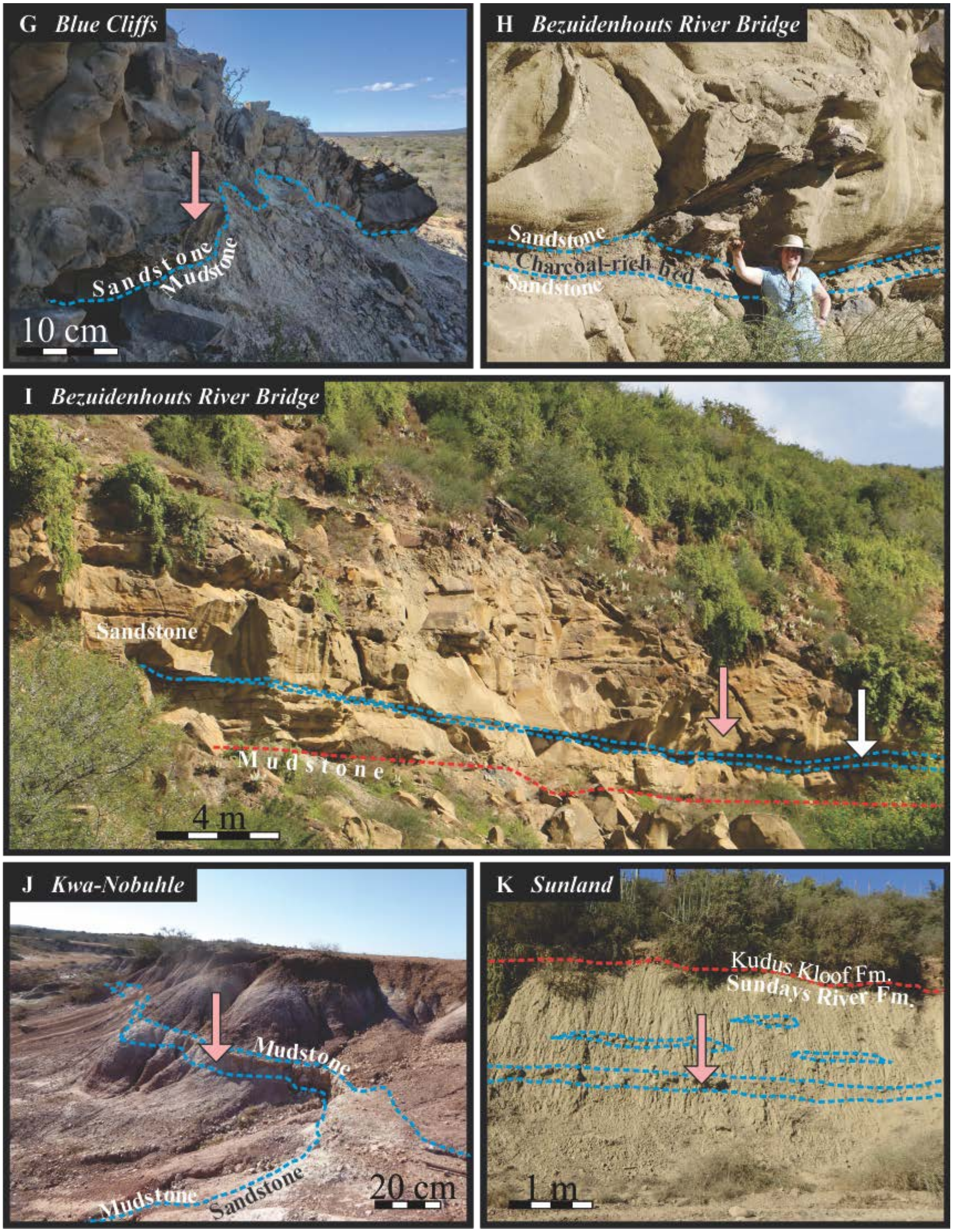
G Blue Cliffs
Sandstone
Mudstone
10 cm
H Bezuidenhouts River Bridge
Sandstone
Charcoal-rich bed
Sandstone
I Bezuidenhouts River Bridge
Sandstone
Mudstone
4 m
J Kwa-Nobuhle
Mudstone
Mudstone
Sandstone
20 cm
K Sunland
Kudus Kloof Fm.
Sundays River Fm.
1 m

Blue Cliffs (sample KBCS2)

Beige sandstone beds with fossiliferous pebble lag deposits at their bases comprise much of the cliff faces along the Bezuidenhouts River near the Blue Cliffs railway station (33°29'33.44"S; 25°26'17.17"E; Fig. 5.55). These beds (of which one was sampled; Fig. 5.61) truncate either red or grey mudstones.

Bezuidenhouts River Bridge (sample KBEZS1)

A laterally extensive medium-grained beige sandstone bed overlies grey fossiliferous mudstones and underlies a charcoal-rich bed at a river cutting adjacent the Bezuidenhouts River Bridge, ~50 km north of Port Elizabeth (33°28'14.28"S; 25°32'7.16"E; Fig. 5.55). Beige sandstones directly overlying the charcoal-rich bed were sampled (Fig. 5.61H, I).

Kwa-Nobuhle (KWAS3)

Laterally extensive varicoloured, principally red, mudstones are exposed in and around the Kwa-Nobuhle township, south of Uitenhage. A site on the eastern side of Kwa-Nobuhle, directly south of Nelson Mandela Bay Logistics Park exhibits the laterally extensive mudstones that typify the outcrops there (33°48'49.13"S; 25°25'27.76"E; Fig. 5.55) and one of the red/grey medium-grained sandstone interbed was sampled (Fig. 5.61J)

Sundays River Formation cutting (sample SRFS1)

Laterally extensive green-grey mudstones and sandstones of the Sundays River Formation outcrop widely in the Algoa Basin south of Dunbrody (Fig. 5.55). A roadside outcrop along the MR00470 near Sunland (33°30'56.88"S; 25°36'25.33"E; Fig. 5.55) exposes what is probably the lower part of the Sundays River Formation based on the close proximity of the underlying and/or laterally interfingering Kirkwood Formation. Rigassi and Dixon (1972) report two thin 'tuff bands' within the Sundays River Formation in exposed on the banks of the Sundays River, although no such deposits were confirmed in our field investigation. Several 10 – 50 cm thick green-grey sandstone interbeds are exposed in a sandy-mudstone-dominated deposit, one of which was sampled (Fig. 5.61K).

5.2.8.3 U-Pb Geochronology

Unfortunately, no volcaniclastic deposits were discovered in the Algoa Basin despite intensive fieldwork and reviewing of several cores housed at the South African National Core Library of the Council for Geoscience in Gauteng. Instead, eight sandstones samples from the Kirkwood, Enon and Sundays River formations of the Algoa basin were dated in order to constrain maximum depositional age of these units. Of the eight samples, one was extracted from the fossil-poor Enon Formation, one from the biostratigraphically well-constrained Valanginian – Hauterivian Sundays River Formation (McMillan, 2003) and seven samples were taken from the Kirkwood Formation at each of the above-mentioned fossil localities. The objective of sampling efforts in the Algoa Basin is to use detrital zircon geochronology to contextualize these important fossil localities of the Kirkwood Formation in terms of their maximum age of deposition. This will not only be the first attempt to place the vertebrate fauna and flora of the Kirkwood Formation in the Algoa Basin into a chronostratigraphic framework (with potential ramifications for evolutionary trends), but also help improve intrabasinal correlations between isolated outcrops and between other basins in the southern Cape that contain pyroclastic deposits and therefore better-constrained depositional ages.

AECOCS

Zircons were vary in shape and colour, including small, often colourless grain fragments and larger colourless, orange and beige crystals that were euhedral to subrounded. Sizes range from 40µm to 170 µm. Prismatic crystals regularly have broken terminations, while stubbier grains frequently preserve their original crystal habit, presumably due to their comparative resilience during transport. Internally, the crystals exhibit fine and medium oscillatory zoning (e.g., crystals 73, 77 and 81 in Fig. 5.62) and rare, black inclusions (e.g., crystal 70 in Fig. 5.62). Inherited cores were present too, although the width of the rims was seldom large enough to analyze separately (e.g., crystal 81 in Fig. 5.62).

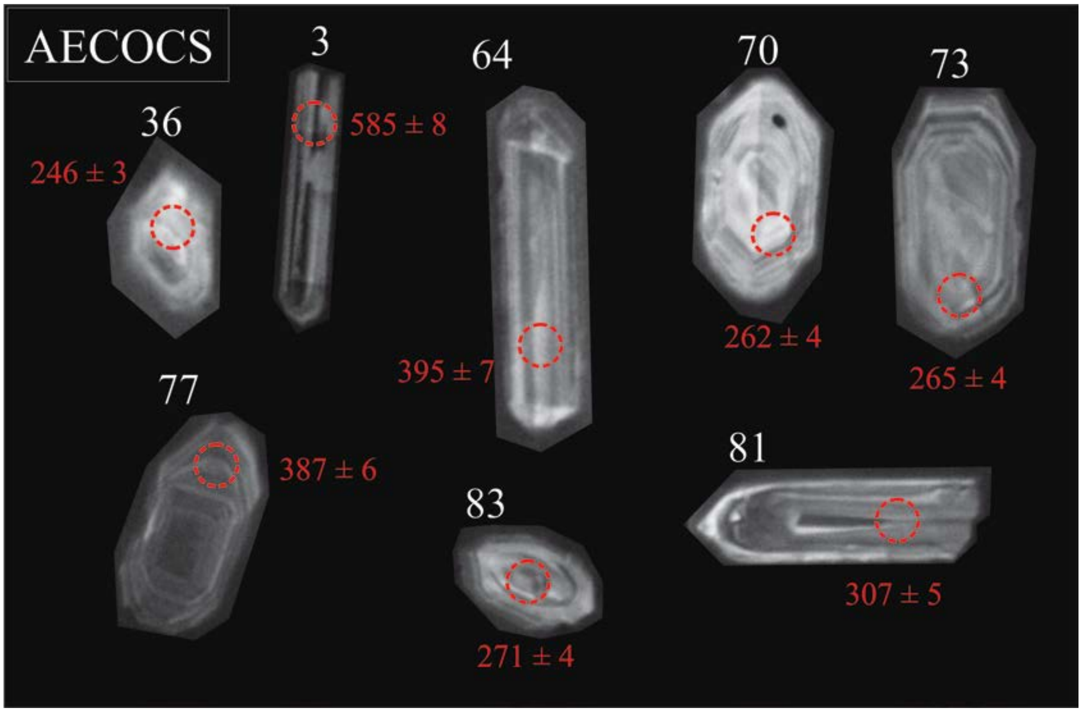

Fig. 5.62. Composite diagram of CL images of zircons that yield concordant dates in sample AECOCS from the Algoa Basin. Individual zircon indicated by white number and analytical spot (26 µm diameter) with respective $^{206}Pb/^{238}U$ date are red.

Of the 91 analyses performed on zircon in this sample, 71 have acceptable concordance and are considered further. Zircons were mostly Palaeozoic (78 %) although smaller contributions of Mesozoic (6 %) and Precambrian (16 %) grains occupy the distribution (Fig. 5.63; Table D20 in Appendix D; Fig. F6A), each with multiple age peaks. The largest peak is around 264 Ma although a smaller, younger peak at 248 Ma also exists, which is also the youngest age component in the sample (YPP). The zircons in this sample clearly are reflective of detrital input only, with no syn-depositional zircons present. The main source for the Palaeozoic zircons is probably the nearby Karoo Supergroup, which outcrops widely on the northern side of the Suurberg Mountains. Other analytical metrics are: YSG = 246 ± 4; YDZ = 245.2 +3.2/-4.6 Ma (95% conf.). The lack of younger Jurassic and/or Cretaceous zircons limits the usefulness of this dataset in meaningfully constraining the depositional age.

Fig. 5.63. (Following page). U-Pb dates of zircons from all samples in the Algoa Basin shown as age probability density diagrams (blue area) combined with frequency histograms (grey bars) with 20 Ma intervals. Only concordant data are shown: n = x/y means that x out of a total of y zircons yielded concordant dates. Youngest graphically-defined peak (YPP) are indicated.

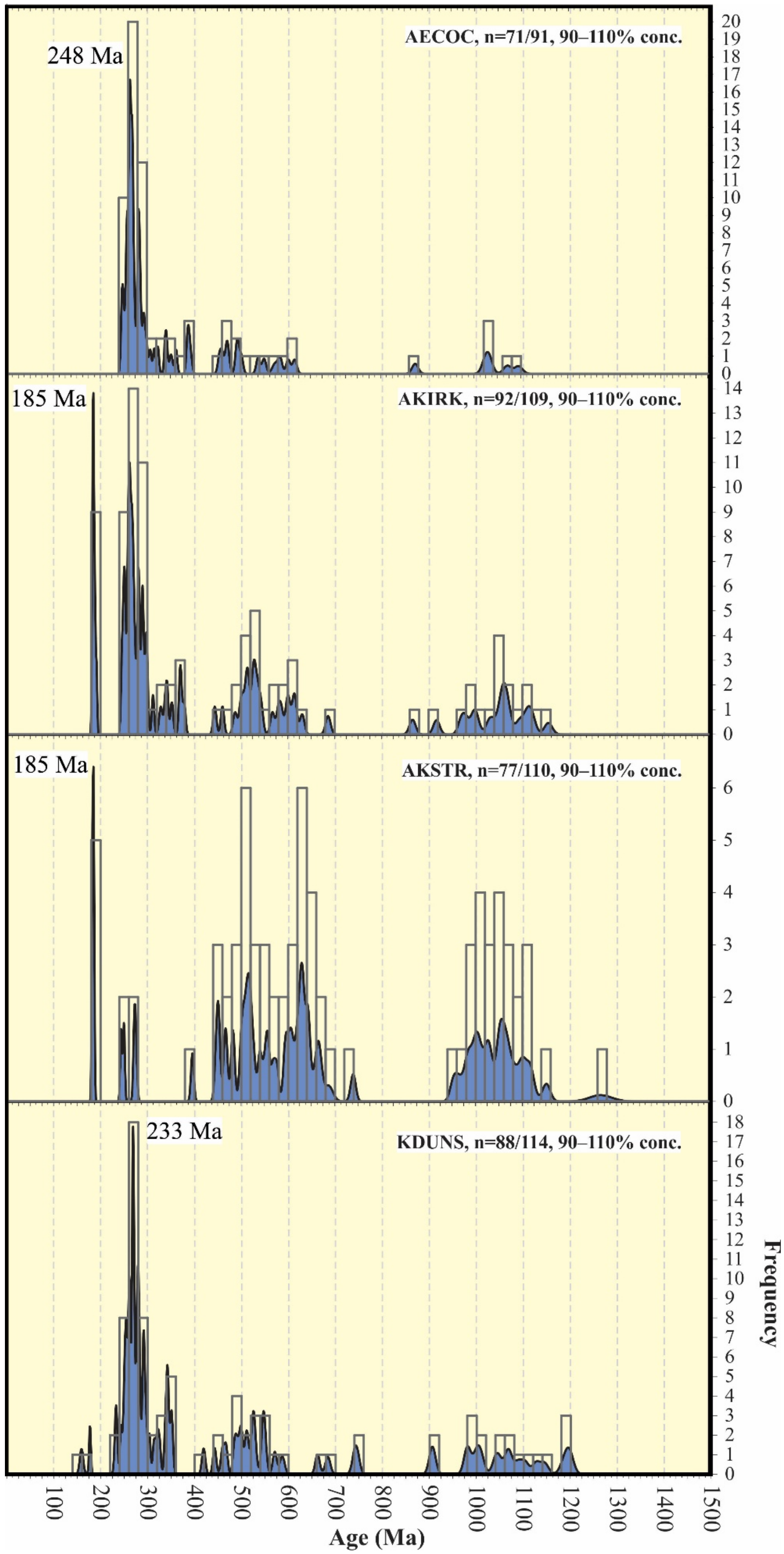
248 Ma
AECOC, n=71/91, 90–110% conc.
185 Ma
AKIRK, n=92/109, 90–110% conc.
185 Ma
AKSTR, n=77/110, 90–110% conc.
233 Ma
KDUNS, n=88/114, 90–110% conc.
Frequency
Age (Ma)

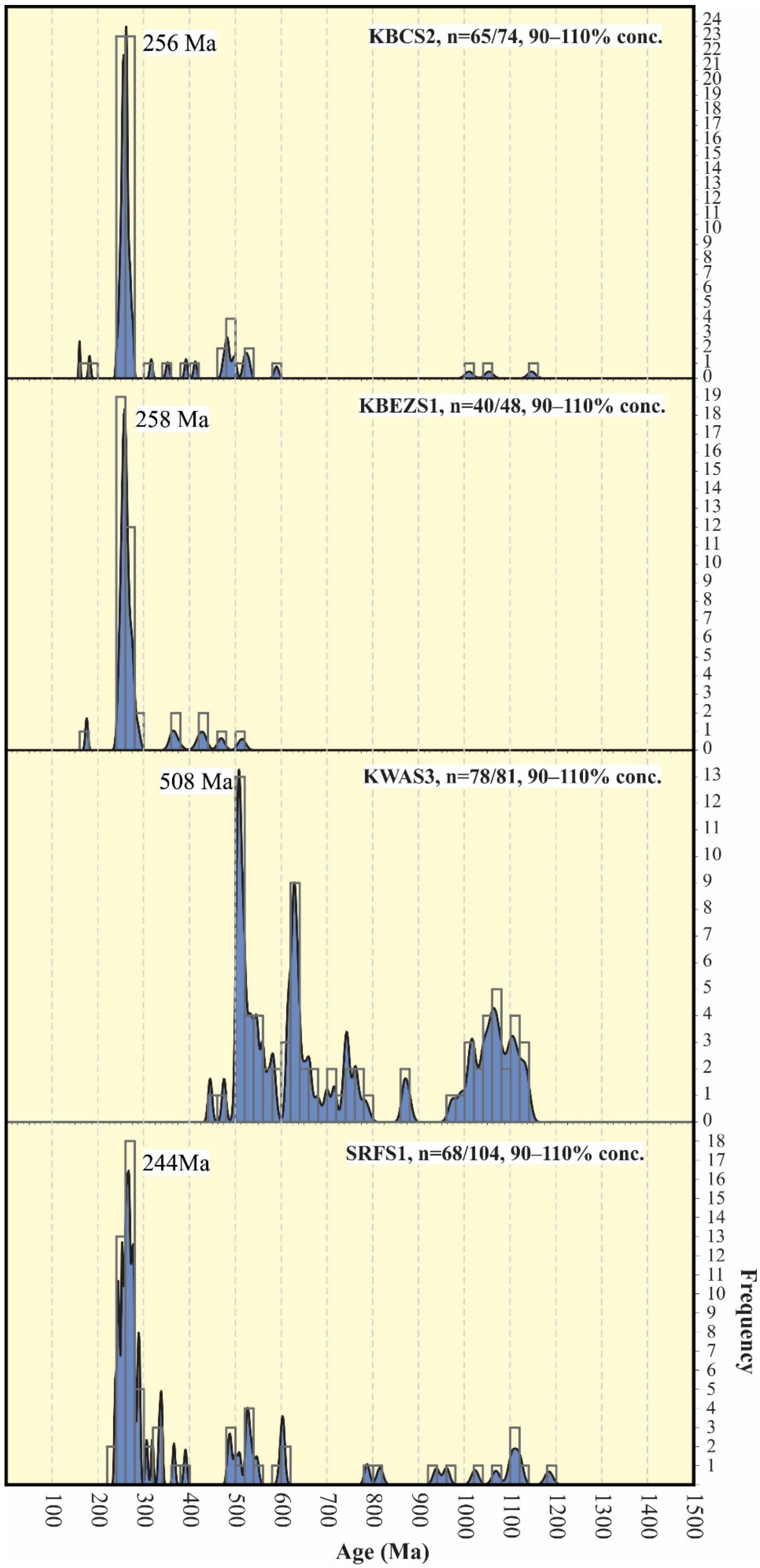
256 Ma
KBCS2, n=65/74, 90–110% conc.
258 Ma
KBEZS1, n=40/48, 90–110% conc.
508 Ma
KWAS3, n=78/81, 90–110% conc.
244Ma
SRFS1, n=68/104, 90–110% conc.
Frequency
Age (Ma)

AKIRK

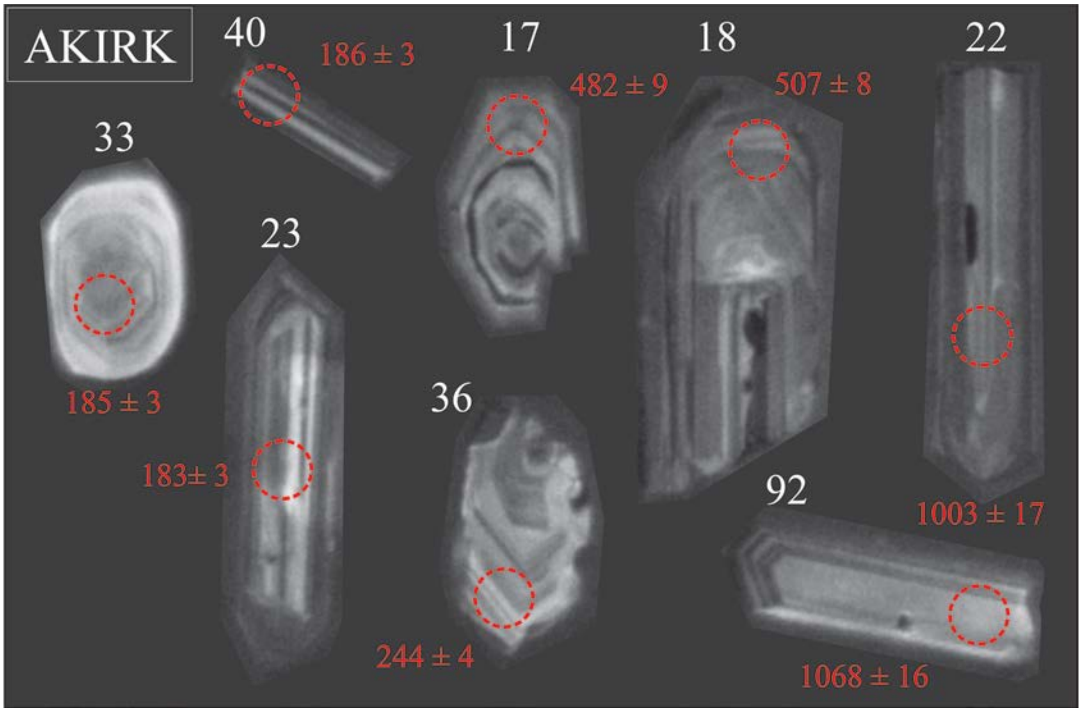

Fig. 5.64. Composite diagram of CL images of zircons that yield concordant dates in sample AKIRK from the Algoa Basin. Individual zircon indicated by white number and analytical spot (26 µm diameter) with respective 206Pb/238U date are red.

Zircons extracted are 50 to 120 µm in length and are usually fragmentary or rounded with only rare whole euhedral crystals. Colours vary from beige to deep orange although colourless grains are also present in the sample. Internally, the crystals exhibit fine oscillatory zoning, inclusions and rare inherited cores, especially in the stumpy crystals (e.g., crystals 17 and 36 in Fig. 5.64). Of the 109 crystals analysed, 92 yield concordant Mesozoic (15 %), Palaeozoic (54 %) and Precambrian (31 %) dates with multiple peaks on the probability density diagram (Fig. 5.63; Table D21 in Appendix D; Fig. F6B). A youngest population comprising 9 crystals clusters around 185 Ma, which is the graphically-defined youngest age component in the sample (YPP). The youngest crystal in the sample (YSG) is 183 ± 4 Ma and the youngest modelled zircon age is 182.5 +1.9/-3.1 Ma (YDZ). All these metrics are compatible with a Suurberg (or Drakensberg Group source), the former of which outcrops in the northern Algoa Basin and probably contributed towards the Lower Jurassic zircon component.

KSTRAT

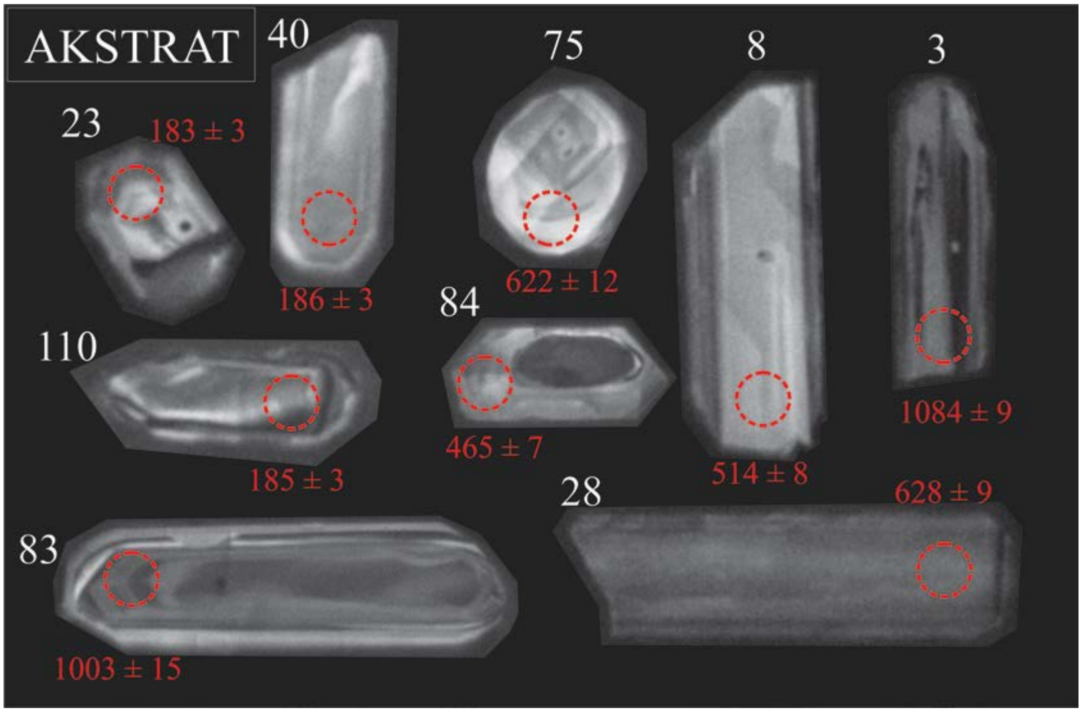

Fig. 5.65. Composite diagram of CL images of zircons that yield concordant dates in sample AKSTRAT from the Algoa Basin. Individual zircon indicated by white number and analytical spot (26 µm diameter) with respective $^{206}Pb/^{238}U$ date are red.

Zircons are morphologically diverse and include crystals with small, rounded habits as well as elongate crystals with varied degrees of rounding and many grain fragments. Typically, crystals are beige or colourless when viewed under the light microscope and range from 50 to 180 µm. CL images of the zircons exhibit fine and broad oscillatory zoning with (e.g., crystal 84 in Fig. 5.65) and without xenocrystic cores (e.g., crystals 75 and 28 in Fig. 5.65) and rare inclusions (e.g., crystal 23 in Fig. 5.65). Of 110 analyses, 77 yielded concordant Mesozoic (9 %), Palaeozoic (26 %) and Precambrian (65 %) dates (Fig. 5.63; Table D22 in Appendix D; Fig. F6C in Appendix F). The wide range of ages likely reflects the known Cape and Karoo Supergroup sources exposed in the Suurberg Mountains to the north. The youngest population of zircons ranging from 183 ± 3 Ma (YSG) to 186 ± 3 Ma with a graphical peak at 185 Ma (YPP) is likely derived from the Suurberg Group, which also outcrops in the Suurberg Mountains, in the panhandle, and presumably underlies the Uitenhage Group in at least parts of the northern Algoa Basin (Fig. 5.55). This youngest age component reflects maximum deposition but unfortunately does not allow any constraints beyond the known Tithonian – Valanginian biostratigraphic constraints.

KDUNS

Zircons are 60 to 210 µm long and range from stubby to needle-like, with most having a moderate stalky to prismatic elongation. Many of the grains are rounded or fragmentary, although some have euhedral habits. The crystals were either beige or colourless under plain light and have diverse internal structures (Fig. 5.66). Most grains exhibit fine and medium oscillatory zoning, often with inherited xenocrystic cores (e.g., crystals 50, 89 and 6 in Fig. 5.66). Inclusions are rare (e.g., crystals 44 and 89 in Fig. 5.66).

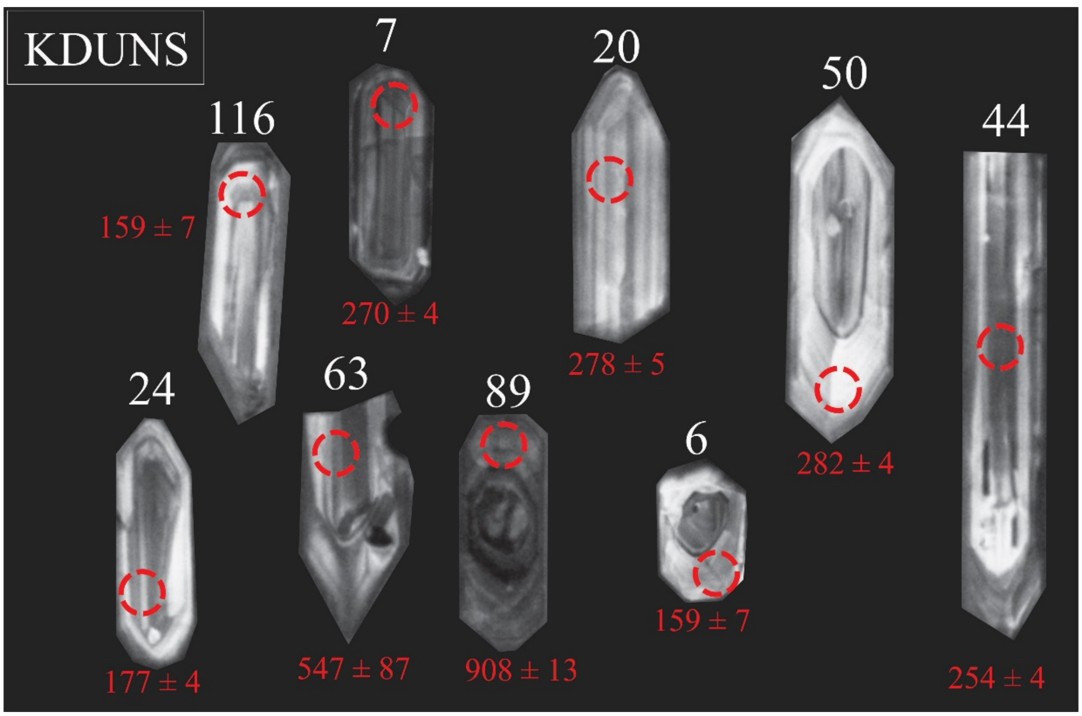

Fig. 5.66. Composite diagram of CL images of zircons that yield concordant dates in sample KDUNS from the Algoa Basin. Individual zircon indicated by white number and analytical spot (26 µm diameter) with respective $^{206}Pb/^{238}U$ date are red.

The 88 concordant zircon dates (out of 114) include multiple Mesozoic (9 %), Palaeozoic (60 %) and Precambrian (31 %) populations (Fig. 5.63; Table D23 in Appendix D; Fig. F6D in Appendix F). The majority of zircons form a complex set of peaks between 230 and 300 Ma. There are only 2 crystals that yield concordant Jurassic dates at 159 ± 7 Ma (YSG) and another at 177 ± 4 Ma while the youngest modelled detrital zircon age (YDZ) is 159.6 +7.9/-8.5 Ma (95% conf.). Neither of these grains constitute a youngest graphical population, which is 233 Ma in this sample (YPP) because they are singular dates that do not overlap (at 2σ error). Nevertheless, the presences of these two concordant dates, in addition to two zircons that yield only slightly discordant dates, suggest that a Middle Jurassic maximum depositional age is likely. Nevertheless, these data, with a Triassic (233 Ma) or Middle Jurassic youngest age component do not refine the depositional age of the strata at Dunbrody beyond the already established, albeit tentative Late Jurassic – Early Cretaceous age.

KBCS2

Zircon crystals extracted from the pebble-rich sandstones range in size from 90 to 140 µm and are either stalky or prismatic. Generally, they are colourless or pale beige. CL images reveal that fine oscillatory zoning dominates (e.g., crystals 60, 54 and 47 in Fig. 5.67), with rare xenocrystic cores and inclusions (crystals 55 and 66 in Fig. 5.67). Of 74 analyses, 65 yield concordant dates that are Mesozoic (~14 %), Palaeozoic (~78 %) and Precambrian (~8 %). Most zircons are Permian – Triassic and define the dominant population (Fig. 5.63; Table D24 in Appendix D; Fig. F6E in Appendix F). In most cases they are stalky and have fine oscillatory zoning. Two Jurassic dates of 160 ± 4 Ma (YSG) and 182 ± 6 Ma, as well as the modelled age (YDZ) of 160.2 +3.2 -3.7 Ma (95% conf.) are not unexpected since the ~256 Ma maximum depositional age defined graphically on the probability density diagram (YPP) certainly predates the true depositional age of the unit. A single date of 132 ± 4 Ma that is slightly discordant (2% lower than the 90% threshold) suggests that deposition was even earlier than the youngest concordant zircons reflect. In all likelihood this unit is Lower Cretaceous in age although the current detrital zircon signature from this unit does not definitively constrain the age of deposition.

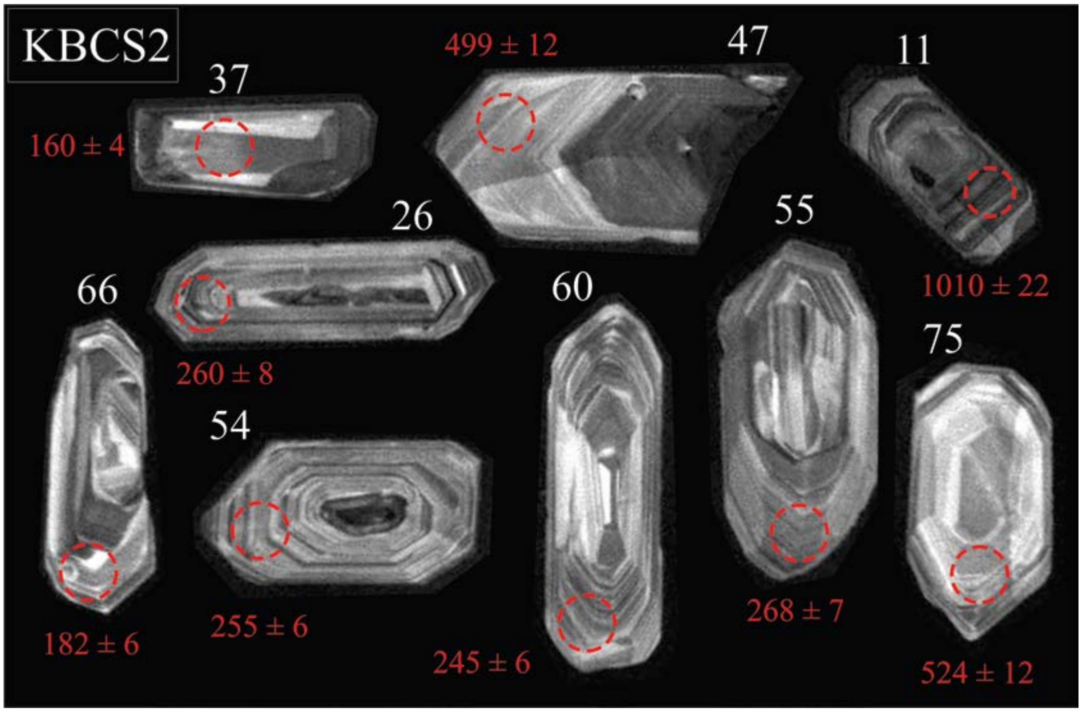

Fig. 5.67. Composite diagram of CL images of zircons that yield concordant dates in sample KBCS2 from the Algoa Basin. Individual zircon indicated by white number and analytical spot (26 µm diameter) with respective $^{206}Pb/^{238}U$ date are red.

KBEZ

Zircon crystals are generally euhedral and unbroken with stalky to prismatic elongation, ranging from 70 to 150 µm in length and are all colourless to very pale transparent beige. CL images of the crystals reveal a dominant fine oscillatory zonation on most of the crystals (Fig. 5.68), with fairly common inherited xenocrystic cores (e.g., crystals 2 and 31 in Fig. 5.68) inclusions (e.g., crystal 17 in Fig. 5.68). Of the 48 zircons analysed, 40 yield concordant dates that are mostly Palaeozoic (~85 %), with only a few Mesozoic (15 %) dates (Fig. 5.58; Table E1 in Appendix E; Fig. F6F in Appendix F). Most dates cluster around 258 Ma to form a largest youngest age population (YPP) with minor populations only supported by one or two dates. A single Jurassic zircon at 176 ± 6 Ma (YSG) and 176.3 +5.7 -7.3 Ma (95% conf.) youngest modelled detrital date (YDZ) do not provide a robust measure of maximum deposition, although the deposit is most likely younger still and contains no syn-depositional zircons.

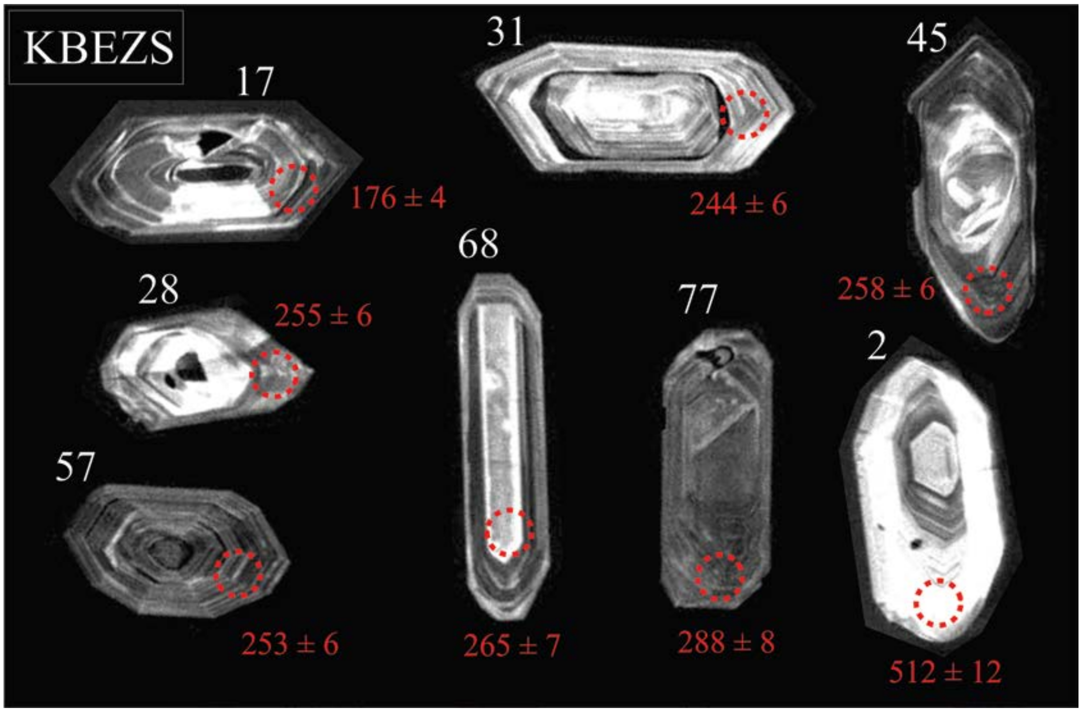

Fig. 5.68. Composite diagram of CL images of zircons that yield concordant dates in sample KBEZS from the Algoa Basin. Individual zircon indicated by white number and analytical spot (26 µm diameter) with respective $^{206}Pb/^{238}U$ date are red.

KWAS3

Zircons ranged from colourless transparent to pale beige in colour and ranged in length from 80 µm stubby to 200 µm stalky crystals. There are approximately equal parts whole crystals and crystal fragments, with few grains exhibiting any appreciable degree of roundness. CL images reveal that most of the crystals show medium to coarse oscillatory zoning, with fine oscillatory zoning a less common feature that is restricted to Precambrian aged components (Fig. 5.69). Many crystals had clearly inherited cores (e.g., crystal 36 and 34 in Fig. 5.69) and small inclusions (e.g., crystal 30 in Fig. 5.69). U-Pb dates are mostly concordant (78 out of 81) and either Palaeozoic (~26 %) or Precambrian (~74 %), with no Mesozoic aged crystals (Fig. 5.58; Table E1 in Appendix E; Fig. F6G in Appendix F). These dates occupy multiple age components with major population peaks on the probability density diagram at 508 Ma, 629 Ma and 1064 Ma. The absence of the common Permo-Triassic populations probably reflects the minimal contribution of the Karoo Supergroup as a detrital source for this deposit, which is not unexpected considering its distal location from any present-day outcrops of the Karoo Supergroup. Further, the lack of Early Jurassic ~183 Ma dates also likely reflects the absence of detritus derived from the Suurberg Group. Most likely the sediments in the Uitenhage Trough were entirely derived from the locally outcropping Cape Supergroup, although it should be cautioned this study has not fully characterized the zircon population for detailed provenance assessments. Two dates, at 445 ± 12 Ma (YSG) and 475 ± 12 Ma are discrete from the largest ~508 Ma population (YPP), although neither of these dates constitute a robust population. The youngest modelled detrital date (YDZ) is 444.2 +14/-13 Ma (95% conf.). The absence of young Jurassic – Cretaceous zircons makes it impossible to constrain the depositional age of these strata beyond what is already established from biostratigraphic and field relations.

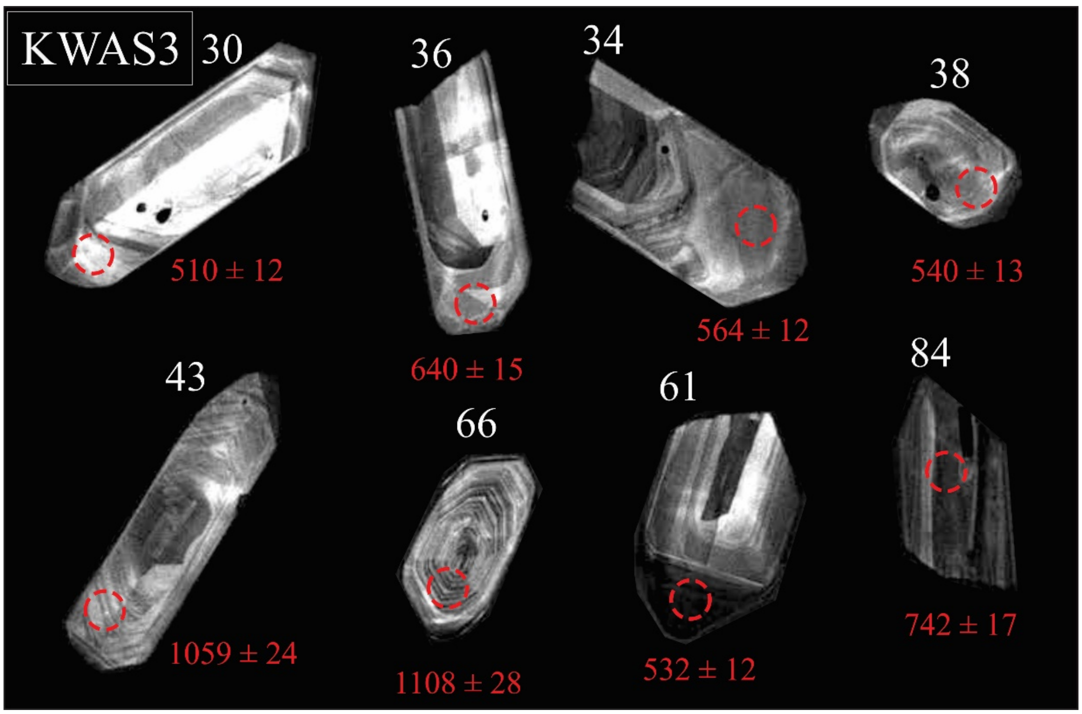

Fig. 5.69. Composite diagram of CL images of zircons that yield concordant dates in sample KWAS3 from the Algoa Basin. Individual zircon indicated by white number and analytical spot (26 µm diameter) with respective $^{206}Pb/^{238}U$ date are red.

SRFS1

Crystals from this unit of the Sundays River Formation are primarily colourless or pale transparent beige. They range from 100 – 140 µm and are euhedral to rounded. They are ubiquitously stubby and exhibit fine oscillatory zoning under the CL detector (Fig. 5.70), sometimes with complexities that appear to be from secondary crystallization (e.g., crystal 30 in Fig. 5.70).

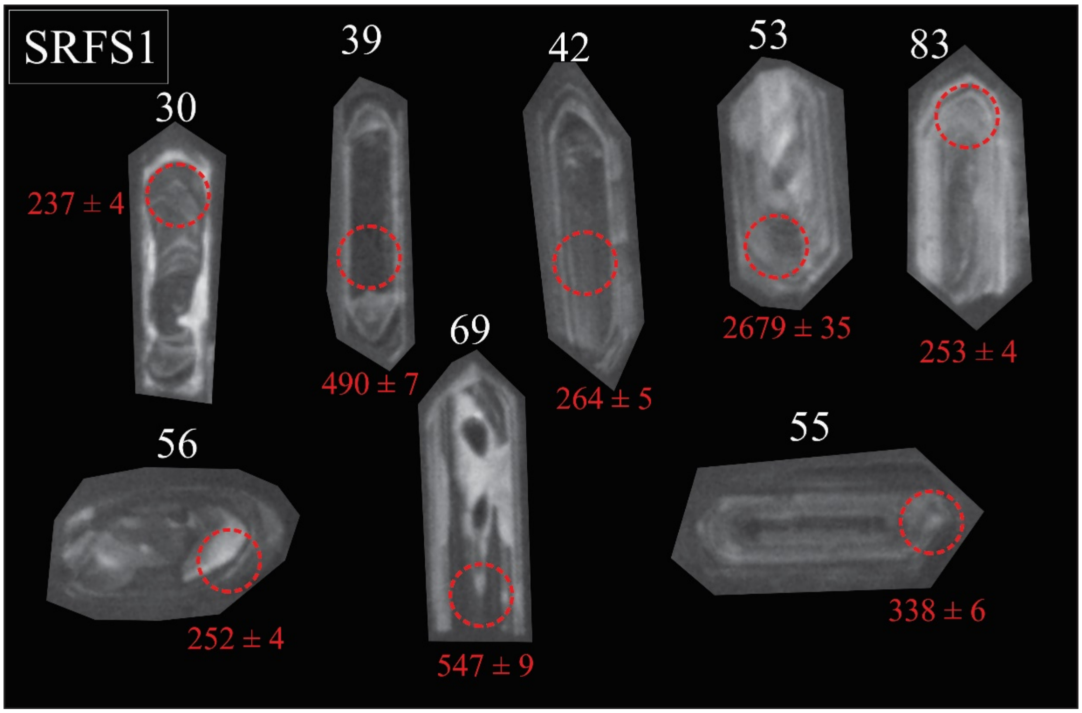

Fig. 5.70. Composite diagram of CL images of zircons that yield concordant dates in sample SRFS1 from the Algoa Basin. Individual zircon indicated by white number and analytical spot (26 µm diameter) with respective $^{206}Pb/^{238}U$ date are red.

Of the 104 analyses, 68 yield concordant dates with a dominant early Mesozoic – Late Palaeozoic population (18 % Mesozoic, 61 % Palaeozoic) with a minor Precambrian (~21 %) contribution (Fig. 5.58; Table D24 in Appendix D; Fig. F6H in Appendix F). None of the zircons were syn-depositional and therefore the age distribution entirely reflects a detrital source, which is likely the Karoo, and to a lesser extent Cape Supergroups. Analytical metrics are: YSG = 231 ± 4 Ma; YDZ = 229.8 +2.7/ -3.3 Ma (95% conf.); YPP = 244 Ma. To establish a maximum depositional age of ~244 Ma does not help constrain the age of this unit beyond the previously established Valanginian – Hauterivian age derived from foraminiferal assemblages (McMillan, 2003). Although the provenance of the unit is not fully characterized, there appears to be no change in detrital zircon provenance across the Sundays River Formation and the Kirkwood Formation at Dunbrody (Fig. 5.63), which supports a lateral continuity between the units.

5.2.8.4 Basin synthesis

The Algoa Basin is the largest of all onshore rift basins, is the best studied, and contains the most extensive exposures of Uitenhage Group. However, unlike most of the basins further to the west, it seems to contain neither primary nor reworked volcaniclastic deposits, and further, sedimentary strata rarely contain any volcanically-derived Jurassic – Cretaceous syn-depositional zircons. This makes drawing any depositional age interpretations from U-Pb zircon geochronology in the Algoa Basin rather impractical. However, based on a new Early Jurassic age for the underlying Suurberg Group, and well-dated Uitenhage Group in other rift basins, some insights into the geological evolution of the basin, and the age of its fossiliferous deposits can be made.

Shone (1976), using 2D seismic data from SOEKOR's earlier exploration efforts and measurements of bedding attitude, was the first to visualize the structure of the Algoa Basin, as a composite accumulation of graben and half-graben structures (Fig. 5.71). This sets it apart from other, more structurally simple, half-graben onshore basins. Nevertheless, the oldest exposed strata in the numerous half-graben sectors of the Algoa Basin are expected to be on the opposite side of large normal faults. This appears to be the case in the northern Algoa Basin east of Enon, where the underlying Suurberg Group is exposed. The lack of any direct depositional ages from the immediately overlying strata of the Uitenhage Group there, or anywhere else in the basin for that matter, makes assessing whether there is a hiatus separating these two groups and therefore the onset of rifting difficult. Two possibilities may be considered with both alternatives requiring a degree of inference: 1) the oldest Uitenhage Group were deposited in actively subsiding depocentres shortly after or during the onset of the Karoo and Ferrar LIPs; 2) there is a large unconformity separating the two Groups implying that initial extension occurred long after the Suurberg Group was deposited.

In order to evaluate the merits of each scenario, we must describe what we know about the age of the Uitenhage Group in the Algoa Basin. The youngest, most robust detrital zircon age across all the samples from the Uitenhage Group of the Algoa Basin is ~185 Ma, from sandstones in the Kirkwood Formation at the Umlilo Farm and Kirkwood Cliffs (Fig. 5.55).This does not help constrain the age of deposition any better than the well-dated underlying Suurberg Group, which is the probable source of the Jurassic zircons in overlying strata. The only other constraints in the northern Algoa Basin come from the Valanginian – Hauterivian Sundays River Formation based on foraminiferal assemblages (McMillan, 2003). Althoguh this age may reasonably be extrapolated across the apparent interfingering lateral contact into the Kirkwood Formation at nearby sites such as Dunbrody and Bezuidenhouts Bridge, extrapolating this relationship for distal sites is doubtful considering the vast > 2000 m thickness of the Kirkwood Formation (Shone, 2006; Muir et al., 2017b in section 2.2.2 of this thesis). This is especially the case considering that much of this total thickness underlies (and is therefore older than) the Sundays River Formation. Useful constraints come from the Bethelsdorp Member that outcrops in the Uitenhage Trough and is intersected in boreholes. This 480 m thick Tithonian (McMillan, 2010) marine interval helps constrain an oldest age for the Kirkwood Formation. Further, there is only <100 m of Uitenhage Group beneath this unit, composed of the Swartkops Member and Enon Formation, which in borehole SW 1/08 (see Fig. 7 in Muir et al., 2017b in section 2.2.2 of this thesis) rest directly on Table Mountain Group basement rocks. Based on the near basal position of the Bethelsdorp Member in the SW 1/08 borehole, and the spuriously young age for the Suurberg Group (McLachlan and McMillan, 1976), McMillan et al. (1997) assigned the oldest age of the Uitenhage Group as Kimmeridgian.

If we accept a Kimmeridgian age for the earliest infill of the Algoa Basin, then > 25 Ma separates the Suurberg Group from the overlying Uitenhage Group. In this scenario, basaltic lava would have flowed south from the center, or centers, of the Karoo LIP in the north and filled low-lying areas and intermountain valleys within the Early Jurassic Cape Fold Belt (Marsh, 2016), in the present-day region of the Suurberg Mountains (Fig. 5.71). Following this, erosion or non-deposition ensued for > 25 Ma during which there was no appreciable accumulation of sediments atop the crystalline basalts of the Mimosa Formation, Suurberg Group. During the Kimmeridgian, extension around the incipient Algoa Basin commenced and a series of normal faults developed and formed the accommodation space in which continental deposits began accumulating and was interrupted by intermittent marine incursions from the south (deposition of the Tithonian Bethelsdorp Member). As rifting continued in the Berriasian, predominantly continental deposition occurred in much of the Algoa Basin before widespread marine conditions began to develop, reflected by the deposition of the Valanginian – Hauterivian Sundays River Formation.

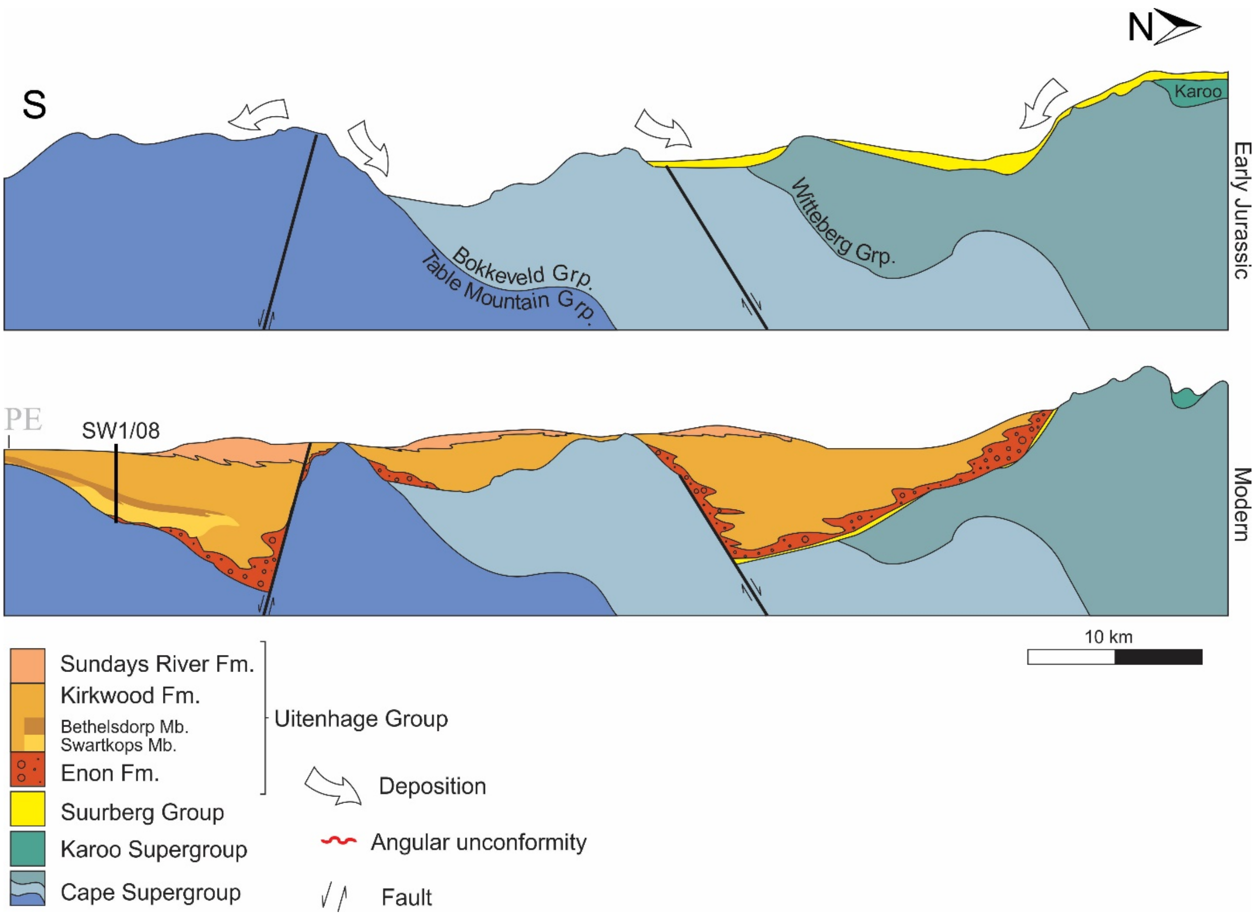

Fig. 5.71. Schematic cross section through the Sundays River and Uitenhage Troughs of the onshore Algoa Basin showing its Early Jurassic – Early Cretaceous evolution. See text for details.

However, there are three concerns with the assertion of a Kimmeridgian maximum age constraint for the Uitenhage Group in the Algoa Basin. Firstly, there is a distinct possibility that the SW 1/08 borehole used to ascertain the relative position of the Tithonian Bethelsdorp Member in relation to basement does not intersect the Uitenhage Group at its thickest. Instead there may be great thicknesses of undrilled Uitenhage Group elsewhere in the Uitenhage Trough as is certainly the case for many of the offshore boreholes (Dingle et al., 1983; McMillan et al., 1997), and possibly also in the CO 1/67 and CO 3/71 boreholes (Muir et al., 2017b in section 2.2.2 of this thesis), which do not intersect basement. Secondly, the Bethelsdorp Member does not exist in the subsurface in the northern Algoa Basin, and therefore cannot be used to assign an age to the strata there. It is possible that there are older elements of the Uitenhage Group in that part of the basin that do not exist further south. Finally, and importantly, there are unequivocally dated lowermost Middle Jurassic Uitenhage Group deposits in the Heidelberg and Mossel Bay basins that suggest that the onset of rifting was in the Early Jurassic and the extensional tectonic regime had already been established by the Middle Jurassic a in the region. Provided such extensional stress was wide-spread, it would be parsimonious to assume that rifting also began in the Early Jurassic in the Algoa Basin. This implies that it is reasonably realistic to expect undated Lower – Middle Jurassic deposits of the Uitenhage Group in subsurface of the deepest parts of the Algoa Basin.

If there are yet undetected Lower Jurassic deposits in the subsurface of the Algoa Basin, then we can assume a relatively short-lived hiatus, if any, between the Suurberg Group and overlying Uitenhage Group. Instead of erosion/non-deposition after the igneous actives associated with the Karoo LIP, active normal faulting closely followed, or was contemporaneous with widespread Lower Jurassic Karoo volcanism. Basaltic lava flows would have overstepped the Cape Fold Belt, which was already subdued in topography, and occupied low-lying areas in the incipient northern Algoa Basin (Marsh, 2016). As normal faults developed, conglomerates, sandstones and mudstones of the Uitenhage Group began to accumulate atop the basalts of the Mimosa Formation. Since we know that rifting was well underway by the Middle Jurassic in the west (evidenced by Middle Jurassic bentonites in the Uitenhage Group at Mossel Bay and Heidelberg) an Early Jurassic initial formation of the Algoa Basin is preferred. This honours a roughly synchronous initiation of rifting throughout the southern Cape by the inversion of structural weaknesses within the Cape Fold Belt (e.g., Fouché et al., 1991; Paton, 2006). For further discussion that considers the tectonic setting for the

Jurassic rift initiation throughout the southern Cape, see section 5.4. In order to fully ascertain whether rifting began at roughly the same time throughout the southern Cape in the Early Jurassic, more geochronological assessments of the lowermost Uitenhage Group in the Algoa Basin are needed, particularly from boreholes that reach basement near depocentres. Such future studies should also place emphasis on locating primary volcaniclastic deposits in the Algoa Basin strata to constrain depositional ages empirically because there remains a dire need for radiometric constraints of the vast continental deposits that are not in close stratigraphic and spatial proximity to the biostratigraphically-dated, marine Tithonian Bethelsdorp Member and the Valanginian – Hauterivian Sundays River Formation.

Age of fossiliferous deposits of the Algoa Basin

The lack of volcaniclastic deposits in the Algoa Basin, and scarcity of Jurassic – Cretaceous zircons in the detrital record mean that the fossiliferous strata of the Algoa Basin remain poorly constrained in age. However, the new Early Jurassic age for the underlying Suurberg Group and confirmation of Middle and even Lower Jurassic deposits in the depocentres of the rift basins in the southern Cape do tell us that the Uitenhage Group, including its fossiliferous Kirkwood Formation is older than previously accepted. Further, the continental deposits of the Uitenhage Group that are lithologically fairly homogenous, lack regional marker beds and are accessible in spatially isolated outcrops make establishing the age of a given fossiliferous deposit difficult. Perhaps the only way to adequately date any specific outcrop is to find volcaniclastic deposits to date nearby, and that can accurately be traced to the outcrop of interest. In the Algoa Basin, this appears to be impractical until volcaniclastic deposits are located. If datable ash beds are found, then fossiliferous outcrops of interest should be placed into the stratigraphic context specific to that part of the Algoa Basin that can be stratigraphically tied to the dated horizon. The Kirkwood Formation deposits at Dunbrody and the Bezuidenhouts River Bridge are geographically close to the region where Sundays River Formation outcrops and are therefore easier to envision as laterally interfingering with the Sundays River Formation if they are lateral correlatives (Fig. 50), whereas those more distal from the nearest outcrops of the Sundays River Formation, such as the fossiliferous deposits at Umlilo have comparatively poor age constraints and could be anything from Lower Jurassic to Early Cretaceous. Conversely, the fossil-bearing outcrops of the Kirkwood Formation near the Kwa Nobuhle township in the Uitenhage Trough are bracketed by the Tithonian Bethelsdorp Member and the Valanginian lower Sundays River Formation and therefore confidently placed in this time period (i.e., probably being Tithonian–Valanginian, and thus likely containing the Jurassic –Cretaceous boundary).

5.2.9 Other basins

A number of onshore basins that host Uitenhage Group are not considered in this study due to the lack of quality exposure in many, and the exceptionally large U-Pb zircon dataset that has been assembled from just these eight most prominent basins. There are certainly additional volcaniclastic deposits near Worcester and Swellendam, where bentonitic clays outcrop scarcely, and in the shallow subsurface of the Jubilee Hill Basin intersected by borehole DJH-I (Viljoen, personal communication, 2016). The various depocentres in the Baviaanskloof area have not been thoroughly examined although that region is dominated by conglomerates and are unlikely to contain datable pyroclastic deposits nor age-diagnostic fossils. Nevertheless, any meaningful comparisons between those conglomerates and the Buffelskloof Formation in the northern Oudtshoorn Basin, either chrono- or lithostratigraphic, might be useful in modelling the history of displacement along the Cango-Baviaans-Gamtoos Fault array and testing predictions made by Paton (2006).

5.3 Discussion: Chronostratigraphy of the Uitenhage Group

The extensive database of U-Pb zircon data marks the first radiometric constraints for the Uitenhage Group and the only direct constraints for the previously undated continental component that constitutes each basin. Pyroclastic deposits in the Robertson, Heidelberg, Mossel Bay, Oudtshoorn and Plettenberg Bay basins range in depositional age from 172.62 +0.56/-0.94 Ma (Aalenian) to 140.2 ± 0.36 Ma (Berriasian) from the fine-grained Kirkwood Formation. The presence of an estimated ~500 m of undated Uitenhage Group lying beneath the Aalenian bentonites in Mossel Bay and Heidelberg, points to an even earlier onset of deposition, conceivably in the latest Pliensbachian – Toarcian. The Uitenhage Group has therefore been demonstrated to be in part much older than previously thought and represents up to ~35 Ma of Mesozoic geological record in the southern Cape region. The hypothesis that the Uitenhage Group is entirely Late Jurassic – Early Cretaceous is therefore rejected based on these findings. This raises interesting questions about the tectonic setting that presided throughout the Jurassic of SW Gondwana and the palaeogeographic configuration during its breakup. Here, these topics and how they are informed by the new chronostratigraphic constraints for the southern Cape rift-related strata are addressed.

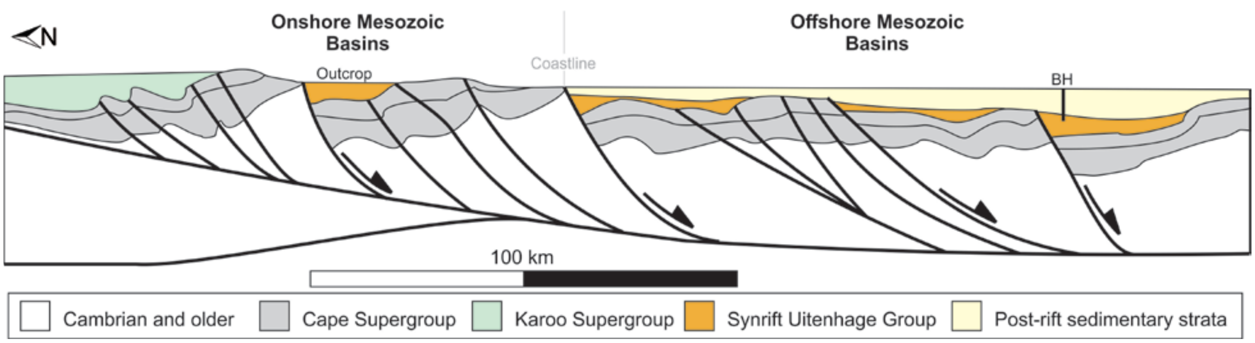

Fig. 5.72. Simplified structure and geology of the continental margin in the southern Cape modified after Paton (2006). Note that the connectivity of faults at depth is highly uncertain.

In order to draw suitable chronostratigraphic comparisons between the offshore syn-rift strata, imaged by seismic methods and intersected in boreholes, and those exposed onshore (Fig. 5.72), one needs to establish a common language to describe portions of the relevant stratigraphy. Up until this point, the use of conventional SACS-approved stratigraphic terminology has been strictly adhered to, which are easily applied to outcropping strata. However, the offshore Uitenhage Group, those continental and shallow marine strata confined to the Bredasdorp, Pletmos, Gamtoos and Algoa basins (collectively the Outeniqua Basin) are commonly described using tectonostratigraphic terminology (e.g., Dingle et al., 1983; Jungslager, 1996; McMillan et al., 1997; Broad et al., 2012), which will be discussed from this point forwards. Typically, these include: *syn-rift 1* for units that span from the basement seismic reflector and unconformity ‘D’ to a prominent, laterally continuous seismic reflector and unconformity named ‘1At1’ (McMillan, et al., 1997), and *syn-rift 2* (Jungslager, 1996) for units that lie above 1At1 and are fault-bounded (i.e., are strictly controlled by availability of accommodation space related to movement along normal faults). These terms are useful when considering time-equivalent packages that exist across multiple basins and for describing how basin development responds to tectonic changes. In order to assess how the onshore stratigraphy relates to those offshore, a chronostratigraphic framework for the Uitenhage Group is constructed, which incorporates biostratigraphic data (McMillan et al., 1997; McMillan, 2003; McMillan, 2010) with new U-Pb ages. This enables the first interbasinal correlations of continental strata in the Uitenhage Group and robust comparisons with existing offshore chronostratigraphic frameworks. Two main chronostratigraphic frameworks exist for the offshore Mesozoic strata of the southern Cape, which are representative of the Bredasdorp Basin in the west (Jungslager, 1996; Broad et al., 2012) and the Algoa and Gamtoos basins in the east (McMillan et al., 1997; Broad et al., 2012). Both are commonly used as a basis for ongoing hydrocarbon exploration efforts (e.g., Roux and Davids, 2016; van Bloemenstein, 2016; Makhubele and Bordy, 2018), landscape evolution (e.g., Tinker et al., 2008b; Wildman et al., 2015; Green et al., 2016; Richardson et al., 2017) and palaeoenvironmental studies (e.g., Muir et al., 2015; Van de Linde, 2017; Dinis, 2018); yet they have a strong bias favouring the marine strata that provide biostratigraphic age constraints. However, most of the boreholes that penetrate the offshore syn-rift sequences do not reach basement (Fig. 5.72) and datable marine units from associated cores become increasingly rare with depth (e.g., Jungslager, 1996; McMillan, et al., 1997) because the first marine conditions in SW Gondwana occurred during the Tithonian (Dingle, 1973). Therefore the earliest syn-rift deposits, which are both thick and invariably continental, have been largely overlooked. One of the main contributions of this thesis is correcting this bias by adding chronostratigraphic information from the exposed units onshore that are partial equivalents of the scarcely accessible basal strata of the offshore basins (Fig. 5.72).

5.3.1 Western basins

Syn-rift 1

The western basins that are included in this study, namely the Robertson, Heidelberg, Mossel Bay and Oudtshoorn basins, are well-constrained in comparison to those that are further east because of the abundance of pyroclastic deposits in the Uitenhage Group seems to decrease eastward in the southern Cape. Each of these four basins contains Jurassic – Lower Cretaceous deposits that are assigned the Enon and Kirkwood formations.

Syn-rift 1 deposits outcrop widely in each of the four western basins and the range of depositional ages from continental pyroclastic beds are mostly Jurassic. Near Robertson, the exposed units are Tithonian – Berriasian although there certainly are older, undated deposits below as evidenced by borehole W202 (Fig. 5.7; Fig. 8 in Muir et al., 2017b in section 2.2.2. of this thesis for detailed log). There is no evidence for the unconformity-bound syn-rift 2 deposits exposed here although such a package would go undetected in the absence of specific outcrops exhibiting the diagnostic angular relationship. The Heidelberg Basin contains deposits that span the Middle Jurassic, with elements that are probably Lower and Upper Jurassic as well and there is a very protracted hiatus separating syn-rift 1 and syn-rift 2 deposits in this basin, probably reflecting a renewed gradients and energy levels during the onset of transform motion along the AFT (Jungslager, 1996) and erosion of most Upper Jurassic – Lower Cretaceous deposits. This is also the case for the western Mossel Bay Basin, where exposed syn-rift 1 deposits are Lower to Middle Jurassic, as opposed to the Upper Jurassic – Lower Cretaceous components in the eastern part of the basin. The Oudtshoorn Basin contains Lower – Upper Jurassic and potentially Lower Cretaceous syn-rift 1 deposits, although the lower age constraint depends heavily on the interpretation of the highly deformed Lower Jurassic volcaniclastic deposits near De Rust.

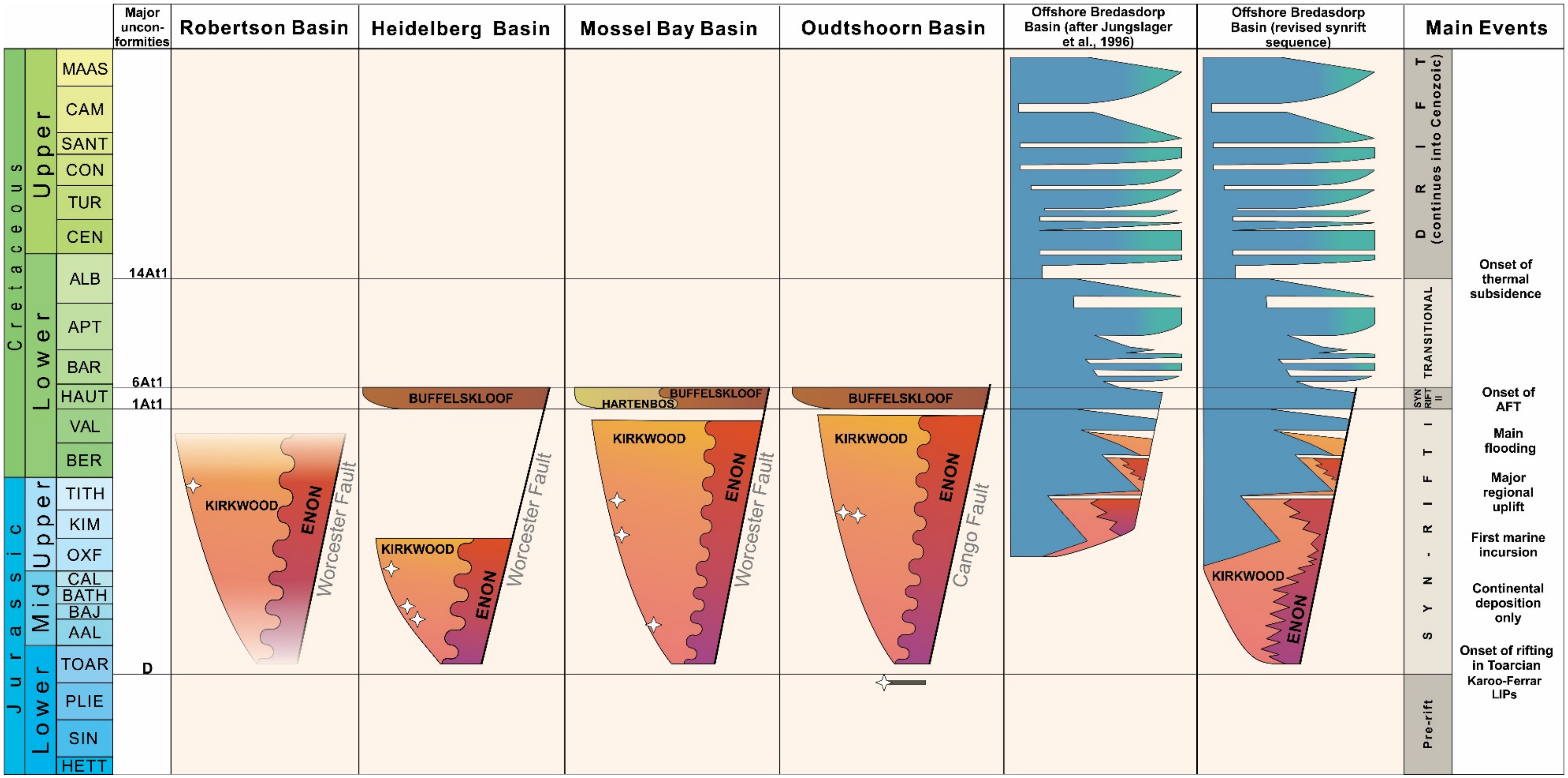

Fig. 5.73. Chronostratigraphy of the onshore Robertson, Heidelberg, Mossel Bay and Oudtshoorn basins compared to existing framework of Jungslager et al. (1994) from the Bredasdorp Basin (second from right) and an updated chronostratigraphy for the Bredasdorp Basin (far right). The main events that presided across the southern Cape during the Jurassic – Cretaceous are listed on the right. All charts are adjusted to the geologic time scale of Cohen et al. (2013) and post syn-rift 2 deposits are included for completeness. White shaded regions indicate areas with poor age and thickness constraints and white stars represent the depositional age information from pyroclastic deposits in this study.

The chronostratigraphic chart of the Bredasdorp Basin, which was initially constructed by Jungslager et al. (1996), includes two intervals that they describes as 'fluvial' – units intersected near the bottom of the abundant boreholes drilled in the basin that contain red mudstones, sandstones and conglomerates – which are assigned to the Upper Jurassic and Lower Cretaceous (Fig. 5.73). Most boreholes do not penetrate below the lower of these fluvial intervals, and none reach basement in the basin depocentre. These intervals are equated to the Enon and Kirkwood formations, and based on the prevalence of Middle and even Lower Jurassic syn-rift 1 deposits in the onshore basins, we propose that similarly aged continental deposits exist at depth in the Bredasdorp Basin, or in other words the lower fluvial unit of Jungslager et al. (1996) began to be deposited as early as the latest Pliensbachian – Toarcian, during the earliest rifting in the southern Cape (Fig. 5.73). Continental conditions were interrupted in the Tithonian, during which the southern Cape experienced the first marine transgressive events (Dingle, 1973). After a transition into marine conditions in the Bredasdorp Basin during the Late Jurassic, which occurred haphazardly due to complex relative sea level fluctuations and a rough pre-existing topography (Jungslager et al.,1996), renewed rifting occurred. This renewal conincides well with the onset of movement along the AFT, was widespread, and caused rapid accumulations on land and at sea (syn-rift 2). Following a period of transitional tectonics that saw a waning of normal fault movement, thermal subsidence caused the offshore syn-rift units to be draped in marine deposits (McMillan et al., 1997; McMillan, 2003). Any evidence of deposition onshore during this time has since been lost during extensive erosion that has clearly left different stratigraphic intervals of individual onshore basin stratigraphy exposed.

Syn-rift 2

All western basins of the southern Cape, except the Robertson Basin, contain the Buffelskloof Formation, which is younger than these basal Enon and Kirkwood formations, and represents a renewed pulse of rifting (Fig. 5.73). In Oudtshoorn, these stratigraphically higher strata are no older than ~145 Ma (Tithonian) and are probably Lower Cretaceous, based on the presence of a ~145 Ma youngest zircon age population. This is the only absolute age constraint for the Buffelskloof Formation, however based on the angular relationship between these and the underlying units in each basin, along with the generally coarse-grained nature of the deposits, they likely reflect a period of widespread renewed rifting in the Early Cretaceous. Further, In the Bredasdorp Basin a similar period of renewed rifting is identified from seismic and borehole data and those units that lie above the 1At1 unconformity there contain Hauterivian foraminiferal assemblages (Junglslager et al., 1996). In the onshore basins, this unconformity appears to correspond with the angular unconformity that separates the Buffelskloof and Hartenbos formations from the underlying Enon and Kirkwood formations. Therefore, in tectonostratigraphic terms, we tentatively assign the Buffelskloof and Hartenbos formations to syn-rift 2, and those below, the Enon and Kirkwood formations, to syn-rift 1 (Fig. 5.73). Although admittedly the former units are not well constrained in age, the fact that renewed rifting was a widespread and contemporaneous phenomenon across all offshore basins (Broad et al., 2012) supports the assertion that the syn-rift 2 strata (i.e., the Buffelskloof and Hartenbos formations) are Hauterivian and synchronous.

5.3.2 Eastern basins

The Algoa, Gamtoos, Plettenberg Bay and Knysna basins, referred to here as the eastern basins, contain continental deposits that have less well-constrained depositional ages than those in the west because they contain fewer dated volcaniclastic deposits. However, unlike in the western basins, in the Algoa, Plettenberg Bay and Knysna basins marine units that outcrop have been dated biostratigraphically. Therefore, despite the absence of abundant U-Pb constraints, biostratigraphy, a single well-constrained depositional age from Plettenberg Bay, and a revised age of the Suurberg Group allows for considerable reassessment of the chronostratigraphy of these basins.

Syn-rift 1

The Knysna, Plettenberg Bay, Gamtoos and Algoa basins each contain thick, primarily continental accumulations of syn-rift 1 deposits (Fig. 5.74). In the Algoa Basin, the maximum age constraint for the Uitenhage Group comes from the underlying Suurberg Group, which has confidently been dated to the Lower Jurassic (Pliensbachian – Toarcian) in this study (see Chapter 4). It should also be noted that boreholes drilled in the Algoa Basin seldom reach basement in basin depocentres and therefore rarely, if ever, intersect the basal most strata (McMillan et al., 1997). For instance, the SW1/08 borehole reaches basement in a shallow part of the Uitenhage Trough, where the Tithonian Bethelsdorp Member of the Kirkwood Formation is underlain by a relatively thin unit of sandstone (Swartkops Member) and conglomerate (Enon Formation) that probably are not much older than Kimmeridgian (McMillan, 2010). However, elsewhere in the basin, for instance in the offshore parts of the Uitenhage and Port Elizabeth Troughs, the thickness of strata beneath the Tithonian interval is much greater (McMillan et al., 1997) and presumably older. Similarly, it can be expected that in parts of the Sundays River Trough there are thick pre-Tithonian accumulations that are Middle Jurassic or even Lower Jurassic and were deposited soon after the Suurberg Group. Such is also the case for the Gamtoos Basin where the throw along sections of the Gamtoos Fault is ~12 km and there are ~7 km of undrilled syn-rift strata (McMillan et al., 1997). Deposition of the syn-rift 1 strata probably began in the Early Jurassic, coeval with the initial magmatic events of the Karoo-Ferrar LIP, and continued into the Early Cretaceous.

Much uncertainty surrounds the onshore deposits in Plettenberg Bay and Knysna. The Lower Cretaceous deposits exposed in Plettenberg Bay may be underlain by thick accumulations of Jurassic strata in the Piesang Valley, although there is no definitive geochronological or borehole data to test this. Similarly, the marine Brenton Formation at Knysna, which is probably Lower Cretaceous (McLachlan et al., 1976) but might be older (Dingle and Klinger, 1973), points to a Latest Jurassic (Tithonian) to Early Cretaceous age. Perhaps the Knysna Basin is much deeper than the minimum 178 m from the (TI-01) borehole on Thesen Island (Fig. 5.48) and Middle or even Lower Jurassic deposits lie deeply buried. Nevertheless, even if accurate assessments of the depth of the Knysna Basin were attained, the buried package of sediment would itself need to be dated in order to determine when it formed. If the oldest strata are young (e.g., Oxfordian) and the Knysna Basin formed long after the initial rifting in the latest Pliensbachian – Toarcian then there are certainly deep, undrilled sections at the depocentres of the contiguous offshore Pletmos Basin (McMillan et al., 1997) that probably Lower and Middle Jurassic.

Syn-rift 2

Syn-rfit 2 deposits are markedly different in the east compared to in the west. Whereas the 1At1 unconformity that defines the base of the late syn-rift units is a clear feature of the Bredasdorp Basin, and is expressed onshore as an angular unconformity in Heidelberg, Mossel Bay and Oudtshoorn, it is often absent, or is cryptic further eastwards. In the Port Elizabeth Trough of the Algoa Basin Hauterivian deposits are entirely absent due to erosive canyoning in the Aptian – Albian (Fig. 5.75). In the Sundays River and Uitenhage Troughs, the chronostratigraphic interval that corresponds with the 1At1 unconformity is present in the lower parts of the Sundays River Formation (McMillan et al., 1997; Broad et al., 2012), although a significant unconformity is absent there (McMillan et al., 1997). Equally, there is no evidence for an angular unconformity at this interval where it is exposed onshore, neither in the Sundays River Formation nor in the parts of the Kirkwood Formation that might be lateral correlatives, such as in exposures at Dunbrody. Conversely, syn-rift 2 deposits are present in the offshore Gamtoos and parts of the Pletmos Basin (McMillan et al., 1997).

The onshore exposures in Knysna and Plettenberg Bay are difficult to place chronostratigraphically, and it remains uncertain whether the conglomerates, sandstones and mudstones there are entirely syn-rift 1 packages, or whether there are younger elements. Notably, it remains unknown whether the Brenton Formation in Knysna, which may be correlated with the Sundays River Formation (McLachlan et al., 1976) would correlate with the lower, pre 1At1 parts of the latter, or the upper parts that correspond to the syn-rift 2 package (Fig. 5.75).

This uncertainty is fairly common in the onshore basins in the east and is not restricted to the Knysna area alone. Wherever there are neither chronostratigraphic markers, nor relative-age indicators (such as the angular unconformities seen in the west), it becomes impossible to discriminate between syn-rift 1 and 2. For instance, there are *probably* upper Valanginian – Hauterivian sandstones, mudstones and conglomerates in the onshore Algoa and Gamtoos basins, but without any strong evidence for an unconformity or datable horizons, such intervals are undetected. Therefore the purely lithostratigraphic terms favoured when describing strata onshore should not be equated directly to tectonostratigraphic terms; a point that future workers should heed carefully until the Early Cretaceous chronology of continental deposits in eastern basins is improved.

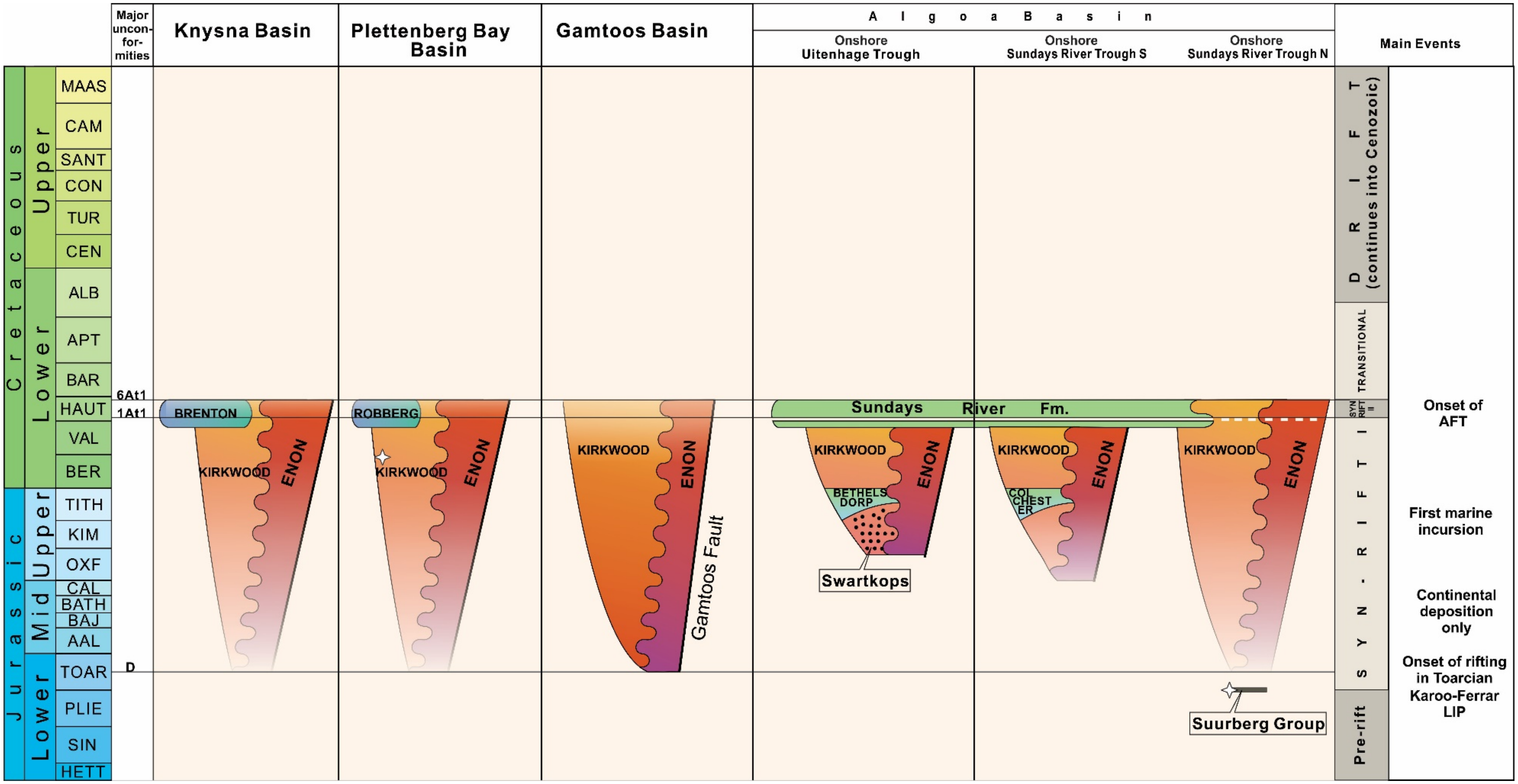

Fig. 5.74. Chronostratigraphy of the onshore Knysna, Plettenberg Bay, Gamtoos and Algoa basins. The main events that presided across the southern Cape during the Jurassic – Cretaceous are listed on the right. All charts are adjusted to the geologic time scale of Cohen et al. (2013). White shaded regions indicate areas with poor age and thickness constraints and white star represent the depositional age information from pyroclastic deposits in this study.

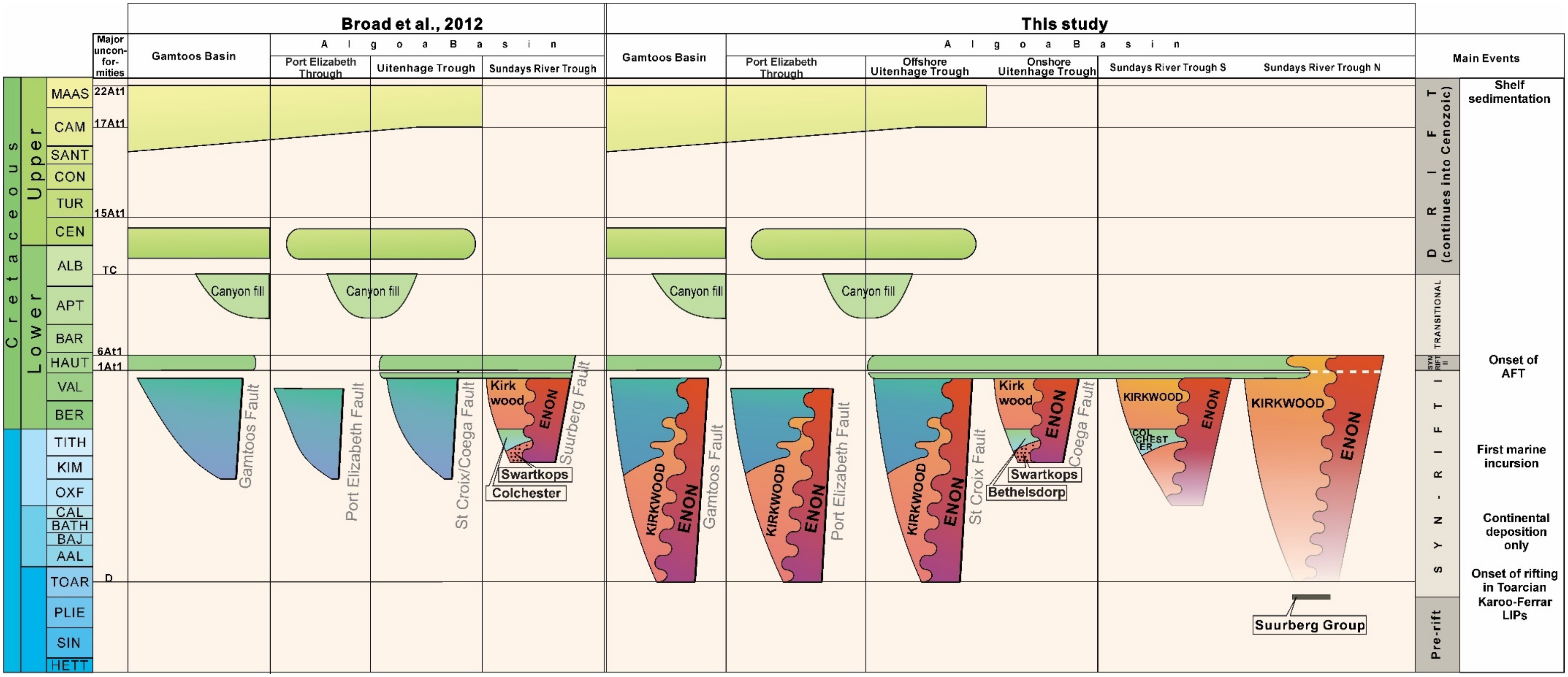

Fig. 5.75. Revised chronostratigraphy for the onshore and offshore sectors of the Algoa and Gamtoos basins. New chronostratigraphy proposed in this study (right) compared to the previously established framework Broad et al. (2012). The main events that presided across the southern Cape during the Jurassic – Cretaceous are listed on the right. All charts are adjusted to the geologic time scale of Cohen et al. (2013) and post syn-rift 2 deposits are included for completeness. White shaded regions indicate areas with poor age and thickness constraints. White dashed line indicates the unconfirmed extension of the 1At1 unconformity, or the time interval with which it is associated, into the Enon and Kirkwood formations. Sedimentary packages in the Gamtoos, and parts of the Algoa Basin are depicted in blue-green after (Broad et al. 2012) because information is derived purely from offshore seismic studies and boreholes where both continental and marine packages have been identified but not depicted separately.

5.3.3 The South African stratigraphic record

The revised age of the Uitenhage Group in the southern Cape contributes towards a revision of the established record of South African stratigraphy. Not only does the Uitenhage Group span a protracted > 40 Ma period of geological time, but also convention has the Uitenhage Group separated from the Karoo Supergroup by a large hiatus representing more than 30 Ma. This is determined from the difference between the ~183 Ma age of the youngest Karoo LIP strata of the uppermost Drakensburg Group and the Latest Jurassic – Early Cretaceous age for the Uitenhage Group (Svenson et al., 2012; McMillan et al., 1997; Shone, 2006). This long stratigraphic gap has been attributed to a period of erosion and/or prolonged non-deposition after the outpourings of flood basalts of the Karoo LIP. Instead, the data in this study show that there is no large hiatus between the emplacement of the Karoo LIP and the earliest deposition of the Uitenhage Group in the southern Cape if any at all. Tectonically, this implies a rapid and more-or-less unbroken transition from the Karoo retroarc forland basin and Cape Orogeny compressional tectonics to an extensional stress regime and rift basin formation in the southern Cape. Such a transition has been identified in the spreading centres that opened up during the separation of East and West Gondwana, namely the West Somali Basin and the Mozambique basins (Gaina et al., 2013, Torsvik and Cocks, 2013) but extension as early as this has never been unambiguously tracked to the southern Cape until now. The mechanisms for this Jurassic extension in the southern Cape are investigated in the next section (5.4), while here we consider only the early and protracted period of deposition, a revised stratigraphic record, and how this is hoped to influence future investigations into various aspects of the SW Gondwanan rock record.

5.3.3.1 Suurberg Group

The oldest units dated are those of the Suurberg Group in the northern Algoa Basin, and a still poorly understood volcaniclastic deposit near De Rust in the Oudtshoorn Basin. These units are of comparable age to the vast volcanics of the Drakensberg Group, although a source for the tuffaceous intervals, which are not common in the Drakensberg Group except for those derived from localized phreatic volcanism that occurred when mafic lavas interacted with groundwaters (McClintock et al., 2008). There is obvious scope for two investigations in aid of answering this question: 1) a high-precision geochronologically based investigation of the youngest zircons in the tuffaceous intervals, or Ar-Ar of feldspar crystals that may co-exist as well as a re-assessment of the poorly dated basalts in the Mimosa Formation of the Suurberg Group. This may resolve uncertainties that relate to the petrogenesis of the entire package and further, allow robust comparisons with the precisely dated Karoo and Ferrar LIPs. Additionally, trace element and Hf isotopes of these young zircons could help trace them back to a source, be that distal and simply interbedded with basalts as a mere coincidence or reveal a co-genesis; 2) stratigraphic investigations of the contact between the Suurberg and Uitenhage Group in the Algoa Basin, and the stratigraphic relationships of the De Rust volcaniclastic deposits. The lack of quality outcrop is still a major setback here, but expanded drill core database might help assess the nature of the contact and its subsurface distribution. A final assessment of whether or not there is an appreciable amount of time missing between the two units will help constrain how extension in the southern Cape progressed.

5.3.3.2 J-K transition

The addition of a number of precisely-dated pyroclastic deposits in the Uitenhage Group open up possibility of pinning down important chronostratigraphic boundaries. The Jurassic – Cretaceous transition contains an important record of global oceanographic and climatic changes (e.g., Gröcke et al., 2003; Weissert and Erba, 2004; Föllmi, 2012) as well as disruptions in continental and marine ecosystems that coincide with elevated extension rates (e. g., Hallam, 1986; Alroy, 2010; Upchurch et al., 2011; Butler et al., 2013; Tennant et al., 2017). Interestingly, while these global changes were underway, the Morokweng bolide impact occurred in the interior of South Africa (Hart et al., 1997; Koeberl et al., 1997), although it remains unclear how extensive the effects of this impact were on Late Jurassic – Early Cretaceous environments. Since the southern Cape is ~ 800 km south of the impact crater, the contemporaneous deposits of the

Uitenhage Group would be a good place to assess potential effects. At present there is very little known about the J-K transition from the South African rock record and it is hoped that this new chronostratigraphy may help pinpoint the interval in the Uitenhage Group and propel investigations into this important time in earth history. Previous chronostratigraphic assessments of the Uitenhage Group indicate that the Kirkwood Formation contains the interval because it spans the Latest Jurassic to Early Cretaceous (McLachlan and McMillan, 1976; Shone, 2006; McMillan, 2010; Muir et al., 2017b), but no further refinement of its position can be made based on the rare biostratigraphic markers. From the data presented in this chapter, the J-K boundary can be placed in many of the onshore basins, and is likely exposed in the central parts of the Roberson Basin, near the ROBE bentonite (150.3 ± 0.2 Ma) and sample Ak5 (which is younger than ~145 Ma based on detrital zircon geochronology), and in the W202 core, which is currently housed in the National Core Library also intersects this stratigraphic interval. A systematic sampling of the numerous volcaniclastic deposits along the length of the W202 core for high-precision geochronological analyses would help pin down the J-K boundary there provided the fluvial deposits contain a relatively unbroken sedimentary record. The Oudtshoorn, Mossel Bay, Plettenberg Bay and Knysna basins probably also contain the J-K boundary, although the absence of core and lateral discontinuity of outcrops makes locating the stratum that is most likely to contain the J-K boundary difficult. Nevertheless, the subhorizontal beds in the southern ravines of the Oudtshoorn Basin that host apoorly dated ~Upper Jurassic bentontie (OKT1), are a reasonable place to search for the J-K interval because there is a significant thickness of strata that clearly overly (and are therefore younger than) the dated horizon. In the Mossel Bay Basin the critical interval is somewhere near the Sittingbourne Farm based on the volcaniclastic deposits that are younger than the J-K interval (SITT2&3). One can also expect the interval to be exposed or in the subsurface in the Knysna and Plettenberg Bay basins, in the Upper Jurassic – Lower Cretaceous strata there. Additional high precision U-Pb zircon analyses in specific areas, or Ar-Ar geochronology on feldspars in selected volcaniclastics may help refine the J-K boundary further.

5.3.3.3 Sediment accumulation patterns

The new U-Pb chronostratigraphy of the Uitenhage Group presented here may help refine models of onshore denudation and offshore accumulation during the evolution of southern Africa since continental breakup. Low-temperature thermochronology to constrain two periods of major onshore denudation in the Cretaceous (Tinker et al. 2008a, b; Wildman et al., 2015; Green et al., 2016), the timing of which coincide well with periods of rapid accumulation in the offshore Outeniqua basins (Tinker et al., 2008b; Guillocheau et al., 2012). The calculated sum of denuded material onshore is an order of magnitude greater than the sediment volume preserved sinks offshore (Tinker et al., 2008b), although the 'missing' sediment may be traced to once contiguous basins that have been separated during breakup, specifically in the North Falkland Basin (Richardson et al., 2017). The data here highlights that deposition in the southern Cape – in the present-day onshore areas and in a wider region that encompasses the Outeniqua, and North Falklands basins – began in the late Early Jurassic. Initially, this would have been in small, isolated basins that are now the depocentres of larger basins with thick sedimentary accumulations. All the calculations of present-day sedimentary thicknesses only include the Lower Cretaceous and younger sedimentary packages, because they are: 1) well-dated using the established marine microfossil biostratigraphic framework; 2) are commonly intersected by boreholes offshore and are laterally extensive providing robust thickness estimates (Tinker et al., 2008). This is not the case for the Jurassic strata below, which are fault-bounded and therefore of variable and poorly defined thicknesses (leading to unreliable thickness estimations), suffer from poor age control, and are rarely intersected by boreholes. For accurate calculations of the total accumulated sediment, necessary to compare with estimates of the total denuded material in the interior of South Africa, not only should contiguous basins be considered (as in Richardson et al., 2017), but the Jurassic depositional record should be investigated in conjunction with the comparatively well-understood Cretaceous succession. For instance, one of the findings that the present study has brought to bear is that much of the sedimentary strata in the onshore basins are older than previously envisioned, which means that we have a record of landscape evolution and denudation of the interior of southern Africa that extends from the Early Jurassic into the Early Cretaceous. Additionally, the correlation of the base of the Buffelskloof and Hartenbos formations within onshore basins with the 1At1 unconformity described from core and seismic profiles offshore indicates that there are packages of Lower Cretaceous deposits preserved onshore that have been overlooked in previous calculations of the sediment budget that might be significant. It is hoped that the chronostratigraphy presented here will allow refinement of existing models and the sedimentary source-to-sink calculations upon which they are based.

The unconformities represented in the Uitenhage Group at the base of the Buffelskloof and Hartenbos formations in several basins remain quite ambiguous and interesting. A new question that has emerged from the chronology presented in this chapter is that there appears to be variation in the amount of time represented by this unconformity in different areas (named the 1At1 unconformity in offshore sequences). This could be simply because they renewed rifting steepened gradients and more energetic currents eroded the underlying Kirkwood and Enon formations during the deposition of the Buffelskloof and Hartenbos formations somewhat haphazardly. It may later be realized that this unconformity represents the systematic shifting of extension tectonism in the southern Cape, although currently there is no evidence for such inferences. For instance there appears to be a southerly sift in depocentres at this time in the Mossel Bay basin while a contemporaneous northerly shift is recorded in the Gamtoos Basin (Paton and Underhill, 2004). It would be intereting to interegate the lenth of the hiatus of the 1At1 unconformity across the southern Cape using evidence from the on- and off-shore data and compare with South American exhumation periods that are identified in several basins there that appear to correspond to periods of intermittent compression (Navarrette et al., 2016).

Finally, there is also great scope to further investigate the detrital zircon signature of the numerous detrital samples presented in this study. A robust characterization of the provenance of the Uitenhage Group is not the objective of this thesis although where possible some inferences are made. It appears that the majority of the detrital zircons dated are derived from recycling of the Cape and Karoo Supergroups with very few Jurassic – Cretaceous zircons included. This interpretation of sediment provenance has been mentioned by previous authors over the last several decades before detrital zircon studies became popular tools used to decifer provenance because the clasts in the conglomerates of the Uitenhage Group are primarily from the Cape and to a lesser extent the Karoo supergroups (e.g., Rigassi and Dixon, 1972; Dingle et al., 1983, Viljoen, 1992; Muir et al., 2017a, b) with a strong correlation to basement rocks that immediately surround the respective basin. Nevertheless, there is considerable scope to study the detrital record of these basins further, especially in combination with palaeocurrent observations and an improved chronology based on the true depositional age of the Uitenhage Group (see section 5.3.3.4).

5.3.3.4 Palaeoenvironmental considerations

Various attempts at reconstructing the palaeoenvironments recorded in the Uitenhage Group have been conducted, although none have done so with the chronostratigraphic framework necessary to elucidate evolutionary trends. Commonly, palaeontological studies that account for the fossil assemblages found in the Uitenhage Group, especially its Kirkwood Formation, have very limited chronostratigraphic constraints by nature of the fossil assemblages in the continental deposits being non-age-diagnostic (e.g., Gomez et al., 2002; McPhee et al., 2016). This study greatly assists workers assessing the fossiliferous Kirkwood Formation in western basins, which for the first time have a robust chronology. For instance, a recent discovery of dinosaur bones in the Heidelberg Basin (Almond, personal communication 2018, 12 September) can be placed to the Mid Jurassic by inference from a nearby dated bentonite deposit. The findings presented here also warn against the drawing of evolutionary trends through time without knowing the age of the strata from which palaeontological sampling occurred. For example, McPhee et al. (2016) describe sauropod dinosaur diversity in the Kirkwood Formation (of the Algoa Basin) that is elevated compared to other Lower Cretaceous localities worldwide, and hence tentatively propose a less dramatic decline in sauropod diversity at the J-K transition that evidenced elsewhere. However, they do not have a strong basis for confirming that the palaeontological samples all come from Lower Cretaceous stratigraphic intervals within the Kirkwood Formation, and follow the often-quoted Early Cretaceous age that is based on lithostratigraphic correlations. They do however acknowledge that this inference is unconfirmed and recognise that “Dating the Kirkwood Formation has proven problematic, especially given the absence of chronometric age determinations” (McPhee et al., 2016, p. 230). Although this study lacks absolute age constraints for Uitenhage Group in the Algoa Basin, and therefore cannot refute or confirm inferred Early Cretaceous age for the Kirkwood Formation there, the wealth of constraints from the unit in other basins and the Lower Jurassic maximum age constraint provided by the underlying Suurberg Group both highlight its long-lived nature. This raises additional concerns as to whether all the fossiliferous units investigated in that study (McPee et al., 2016) and others (e.g., Rich et al., 1983; Forster et al., 2009) are indeed coeval and Lower Cretaceous.

Palaeoecological changes triggered by wildfires in an increasingly oxygenated Early Cretaceous atmosphere (Bergman et al., 2004; Belcher and McElwain, 2008; Berner, 2009; Belcher et al., 2010; Glasspool and Scott, 2010) have been investigated at a single locality in the Kirkwood Formation (Muir et al., 2015), although any attempts to build on this work by establishing patterns of wildfire occurrence through time, and if indeed wildfire abundance increases with observed increases in atmospheric oxygen concentrations, will need to adhere to these new chronostratigraphic constraints. The presence of charcoal material in the Middle Jurassic strata of Kirkwood Formation in the Heidelberg Basin raises the possibility that wildfire frequency was no more frequent in the Jurassic southern Cape when compared to the Cretaceous, despite elevated atmospheric oxygen concentrations. Althoguh wildfires were generally more frequent at intense in the Cretaceous worldwide (Brown et al., 2012), this pattern remains unconfirmed in the South African rock record and remains an interesting aspect of the Mesozoic strata that warrants further study.

There is scope to expand on the notable presence of cyclicity preserved in parts of the Kirkwood Formation. Borehole W202 in the Robertson Basin (Fig. 8 in section 2.2.2.), and the outcrops in the Heidelberg and Mossel Bay basins exhibit cyclicity in grain size that ought to be studied further. Such patterns have been well-studied in other continental deposits around the globe (e.g., Olsen 1996; Kent et al., 2017), primarily in the Northern Hemisphere, to determine astronomically-placed climate fluctuations (e.g., Milankovitch cycles). With the new chronostratigraphic constraints provided in this thesis, coupled with additional high-precision ages from a relatively unbroken section and detailed sedimentological investigations, one could contribute towards improving the understanding of how mid-latitude continental environments and ecosystems in greenhouse worlds respond to astronomically-placed changes in climate. Information from the southern Cape of South Africa would be an especially welcome new perspective on this pressing issue, which requires a global perspective to uncover.

Finally, the characteristics of the sedimentary deposits that constitute the Enon and Kirkwood formations have been studied in an attempt to reconstruct drainage pattern evolution during and after rifting (Dingle et al., 1983; Malan and Viljoen, 1990; Richardson et al., 2017), but failed to take into account the chronostratigraphic relationships between isolated outcrops used to make these assessments. Each of these studies draw the same conclusion, that sediments in the Late Jurassic southern Cape are transported axially, along the Worcester-Pletmos and Cango-Baviaans-Gamtoos basin lines to the newly developed Jurassic coastline (Fig. 5.76). Each study includes some measure of palaeocurrent, which corroborates this transport direction, although never are the full palaeocurrent datasets made available, nor are the exact location and number of outcrops visited mentioned. Such assessments of palaeocurrent direction are not adequate by modern sedimentological standards, and additionally, fail to consider that deposits exposed in an isolated outcrop from which data are collected may not correlate at all with the next. Although these studies may resolve highly generalized transport directions, not only are averages from different localities been made, but also unknowingly the averages are calculated using data from highly varied snaps of geological time. The best way to reliably determine the sediment transport directions in the Uitenhage Group is to systematically measure palaeocurrent indicators from several different sedimentary facies and compare coeval deposits. At present this may only be viable for a few basins that have the greatest number of age constraints, and a full characterization of the palaeocurrent directions for the entire Uitenhage Group necessitates additional age determinations, coupled with stratigraphic control provided by borehole and seismic/geophysical data. Neither do such databases already exist, nor are there many deep boreholes from the onshore basins in the southern Cape, making the task one of considerable difficulty. Nevertheless, cognizance of the exceptionally long-lived nature of the Enon and Kirkwood formations and varied age of these units from one isolated outcrop to the next is necessary before sediment transport directions of the entire Mesozoic southern Cape can be confidently established.

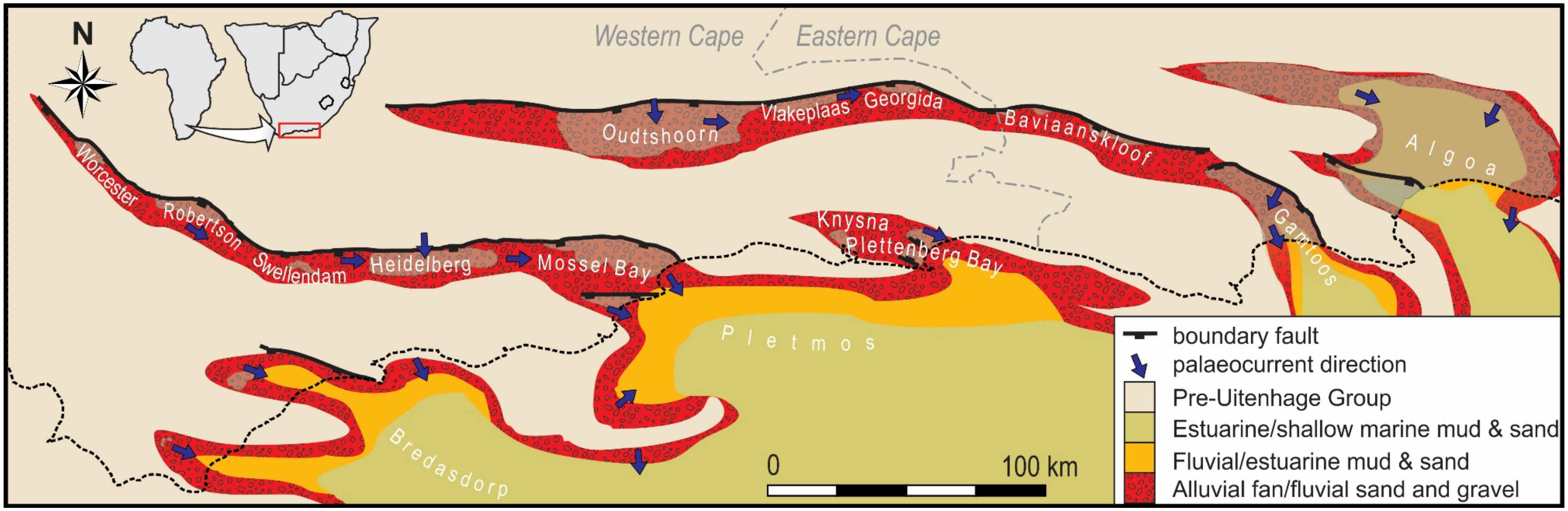

Fig. 5.76. Palaeogeography and sediment dispersion patterns of the southern Cape basins during the Tithonian (Late Jurassic). Black dashed line indicatesapproximate position of the present-day cpastline. Grey shaded areas are where the Uitenhage Group presently outcrops as erosional reminants. Map is based on Dingle et al. (1983) which was reproduced in Malan and Viljoen (2010) and share basic concepts with Richardson et al. (2017).

5.4 Discussion: Jurassic tectonic setting in SW Gondwana

The new chronostratigraphy presented highlight that deposition of the Uitenhage Group began earlier than previously envisioned and that accumulation in growing rift basins spanned a protracted >40 Ma. However, the tectonic setting of the Jurassic SW Gondwana, and specifically the driving mechanism behind the extensional stress necessary to create the rift basins during this time is yet unknown. Seismic and geophysical studies across once-contiguous margins enable ever-imporoving descriptions of the extensional history of SW Gondwana (e.g., Jungslager, 1996; McMillan et al., 1997; Macdonald; 2003; Parsiegla et al., 2009; Lindeque et al., 2011; Broad et al., 2012; Baby et al., 2018), however, a repeated shortcoming of these studies is the lack of robust chronostratigraphic constraints for continental units that are deeply buried in grabens and half grabens and therefore record the onset of rifting. The lack of robust age constraints from the initial rift-related deposits have slowed our understanding of the breakup history and this hindrance is largely because marine deposition in SW Gondwana only began when the first incursion occurred in the Late Jurassic, and therefore until now all dated horizons in the Uitenhage Group postdate this time period (Dingle, 1973; Dingle et al.,1983; McMillan et al., 1997). Until now we therefore have had little understanding of when extensional tectonics began during breakup. Initially, there was Permo-Triassic extension in South America before Gondwana breakup initiated, due to the steepening of the subducting slab (Ramos et al., 2011; Rocher et al., 2015; Riel et al., 2018). Following this rift-related extension began as early as the Latest Triassic in some parts of SW Gondwana, such as in the Neuquén Basin of Chile and Argentina (e.g., Uliana and Biddle, 1987; Uliana et al., 1989; Zerfaas et al., 2003) and the Colorado Basin offshore Argentina (Lovecchio et al., 2018). Conversely, new U-Pb data presented in this study indicate that extension begun the Early Jurassic (~latest Pliensbachian – Toarcian) in the southern Cape, before the opening of the South Atlantic (e.g., Koopman et al., 2014; Will and Frimmel, 2018) and associated strike-slip movement along the AFT (e.g., Ben-Avraham et al., 1997). There remains uncertainty surrounding what drove this Jurassic extension, with prominent workers preferring far-field stresses (McMillan et al., 1997; Broad et al., 2012). The onset of rifting and deposition of syn-rfit 1 packages may indeed have been caused by yet-unknown far-field stress regime change in accordance with these authors, or perhaps are attributable to other mechanisms. For instance, Thomson (1999) alludes to a geodynamically-driven cause for extension in the Gamtoos Basin and the gravitational collapse (Dewey, 1988) of the Cape Fold Belt may offer another often-overlooked driving force for extension. These two mechanisms might better explain the Jurassic rifting experienced in the southern Cape and are explored with respect to the broad tectonic setting of SW Gondwana during the Jurassic and in light of the new U-Pb ages presented in this thesis that indicate a late Early Jurassic (~latest Pliensbachian – Toarcian) onset of prolonged rifting.

Far-field stresses related to plate tectonic motion during continental breakup are tentatively proposed as the driving force behind the extensional rifting experienced in the southern Cape, although a consensus on the details of these stresses has not been reached (McMillan et al., 1997; Broad et al., 2012; Tankard et al., 2012). Tankard et al. (2012) proposes that there was strike-slip movement along inherited structures in the Cape Fold Belt in response to dextral movement along the Agulhas Falkland Transform (AFT), a view shared by others (Ben-Avraham et al., 1993; Roux and Davids, 2016). However, the arcuate shape of these basins need not necessarily have been derived by transtensional shear stresses, and instead can be attributed to a preexisting change in orientation of the Cape Fold Belt structures offshore the Eastern Cape (Johnston, 2000, Paton and Underhill, 2004; Paton, 2006). Further, the new U-Pb ages presented in this thesis also provide direct evidence that much of the Uitenhage Group, and therefore the rift basins that accommodate it, long predate strike-slip movement along the AFT, which only initiated in the Early Cretaceous (Ben-Avraham et al., 1997). Tankard et al. (2012) nevertheless mentions that 'strike-slip basins formed along the Cango and Worcester faults (see their fig. 23.20, p 920), yet cite no direct evidence in support of that sense of movement. Indeed the Oudtshoorn Basin has long been understood to be a half-graben, or composite of several half-grabens, that relate to normal faulting along the Cango Fault (Lock et al., 1975; Holzförster, 2007; Dinis, 2018). This view is preferred over a dextral pull-apart model for the basin because there is a good match between the location of the Oudtshoorn Basin directly south of a large anticline that exposes pre-Cape Supergroup stratigraphy of the Cango Group – a pattern that exists for several other rift basins in the southern Cape too (e.g., the Gamtoos and Mossel Bay basins) – suggesting a dip-slip rather than strike-slip sense displacement. The most likely scenario is that the Oudtshoorn Basin exists in its present location *because* the inherited compressional structures along the southern limb of the anticline were more prone to being reactivated there (Hälbich et al., 1983; Fouché et al., 1992; Paton, 2006). If there were instead strike-slip movement, and the Oudtshoorn Basin were a dextral pull-apart feature, then the position of the basin would be offset to the east relative to the exposed Cango Group in the centre of the anticline. We therefore are of the view that the sense of movement along the reactivated faults in the southern Cape was strictly dip-slip during the Jurassic, at least until the Early Cretaceous onset of strike-slip movement along the AFT.

McMillan et al. (1997), recognizing that the rift basins of the southern Cape began to develop prior to transform movement along the AFT, suggested instead that ~N-S orientated relative plate tectonic motion associated with East and West Gondwana separation and the opening of the Riiser-Larsen Sea might have provided the far-field stress that lead to rifting in the southern Cape. Although this seems more likely than dextral strike-slip movement, the new ages presented here that point to a Pliensbachian – Toarcian onset of rifting (far older than the Kimmeridgian age for rift initiation quoted by those authors) suggest that the timing and orientation of faulting in the southern Cape are not compatible with this interpretation. Flood basalt volcanism of the Karoo and Ferrar LIPs began at ~189 Ma (Moulin et al., 2017) and peaked at ~183 Ma (Encarnación et al., 1996; Duncan et al., 1997; Sevenson et al., 2012; Burgess et al., 2015), and there was a seaward transfer of spreading loci during the Early – Middle Jurassic commencing either at 170 Ma (Gaina et al., 2013) or 165 Ma (Seton et al., 2012) in the Riiser-Larson Sea, Western Somali and Mozambique basins. New radiometric age determinations for the Uitenhage Group presented here indicate that these spreading centres postdate the onset of rifting in the southern Cape, and that extensional stresses existed prior to the separation of East and West Gondwana. Further, the N-S relative plate motion and orientation of far-field stresses associated with this spreading is not consistent with the diverse orientation of normal faults in the southern Cape, which are tightly controlled by preexisting weaknesses in the crust that were developed during the Cape Orogeny (e.g., Fouche et al., 1991; Paton and Underhill, 2004; Paton et al., 2006). These large normal fault arrays strictly follow the inherited structural grain of the Cape Fold Belt, which is predominantly E-W orientated in the central southern Cape but approach a N-S orientation at the western syntaxis (de Beer, 1992) and the antitaxis (Johnston, 2000) in the east (Fig. 2.1), yet the fault displacement along N-S orientated fault planes are no less severe than those orientated E-W despite plate kinematics during East and West Gondwana dictating a N-S extension. The presence of N-S striking extensional faults that in places reached more than 12 km of throw (Dingle et al., 1983; McMillan et al., 1997) is at odds with a regional N-S extension transferred from spreading centers further north and extensional basins in the western margin of the Cape Fold Belt, since destroyed by uplift and erosion (Wildman et al., 2015), formed at equally incongruous E-W orientations. Perhaps the structural anisotropy in the Cape Fold Belt (Paton and Underhill, 2004) meant that extension was always confined to pre-existing weaknesses in the crust, even if they were not at obviously suitable orientations perpendicular to regional extension, however this mismatch may have an alternate explanation entirely. Instead of far-field stresses manifesting in normal faults with varied orientations in the southern Cape, is plausible that that a different source of stress central to the orogeny itself could have driven rifting. This might have happened either through the gravitational collapse of the Cape Orogeny, or by the introduction of hot, impinging asthenosphere during the Jurassic SW Gondwana. The merits of these non-mutually exclusive mechanisms are considered below.

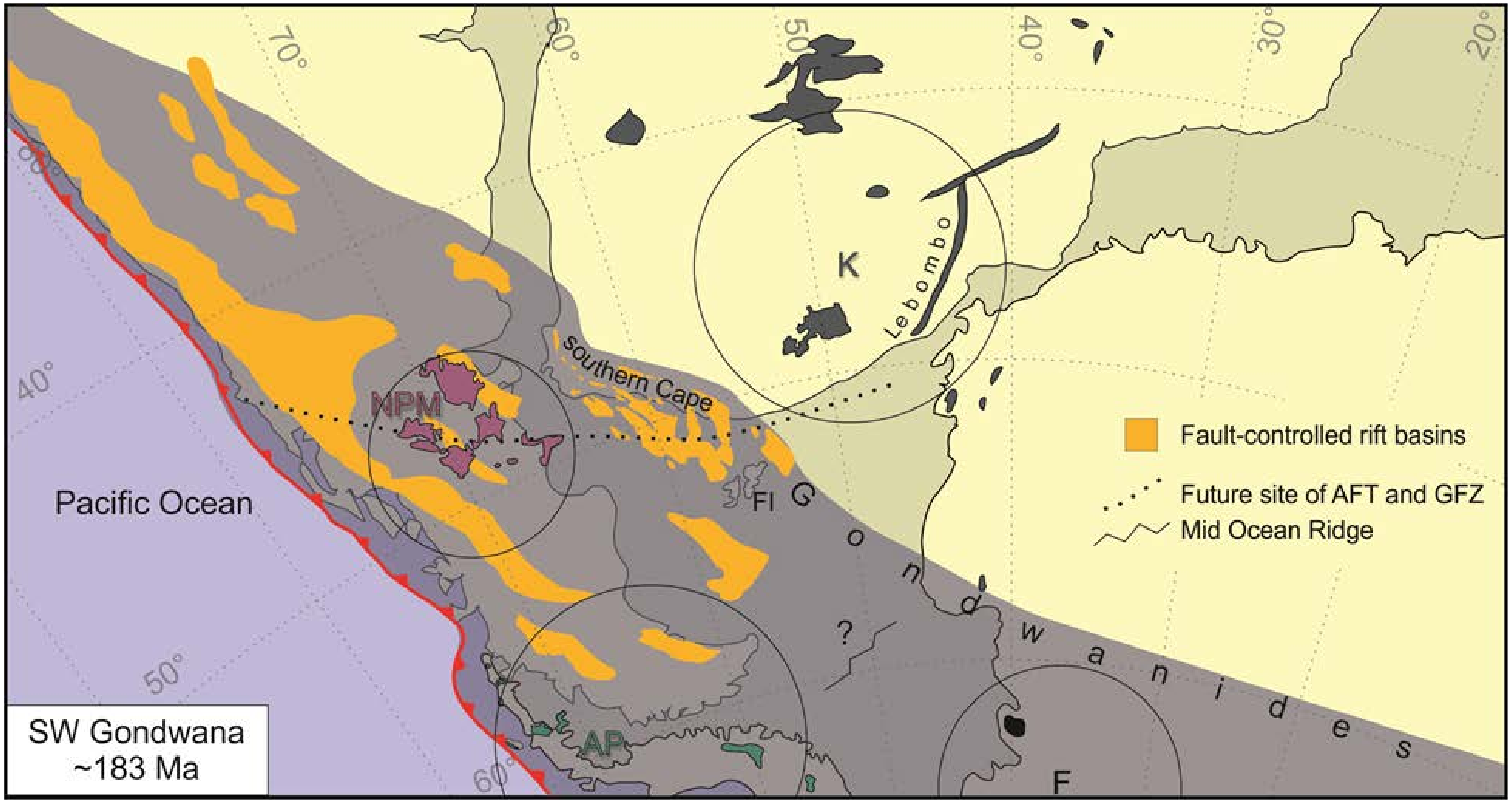

Fig. 5.77. Palaeogeographic reconstruction of the SW Gondwana in the Early Jurassic modified from Jokat et al. (2003) with additions from Gust et al. (1985), Pankhurst et al. (2000), Ghidella et al. (2002), Jourdan et al. (2005), Milani and de Wit (2008) and Hervé et al. (2006). Abbreviations and corresponding colours signify present-day distribution of Lower Jurassic extrusive rocks: AP, Antarctic Peninsula; K, Karoo LIP; F, Ferrar LIP; NPM, North Patagonian Massif. Circles highlight volcanic centres. FI, Falkland Islands.

Gravitational collapse of the Cape Orogeny

An explanation for varied orientation of strain during the rifting southern Cape in the Jurassic is that the Cape Orogeny itself, in the absence of the compressive stress regime that ceased in the Early Jurassic (Bordy et al., 2004) entered a phase of gravitational collapse largely independent of distal spreading centres (Dewey, 1988; Rey et al., 2001). In this case the Jurassic Cape Mountains were simply no longer held up by the compressive stresses and essentially relaxed into a setting of inversion. Numerous authors have indeed noted that the normal faults responsible for extension in the Cape Fold Belt are reactivated compressional thrust planes (Lock et al., 1975; Fouché et al., 1992), although offer no driving mechanism for this inversion. Such rejuvenation of compressional fault planes as extensional is regularly observed in the post-orogenic collapse of mountain belts (Dewey, 1988) and it is likely that extensional stress emplaced by gravity played a significant role, or was entirely responsible for the phenomenon during the Jurassic southern Cape, which may have had conditions suitable for collapse, as had other parts of the Gondwanides.

Much of SW Gondwana, particularly the southern Cape and contiguous terranes were a part of a compressive belt that was suitable for orogenic collapse in the Early Jurassic. Plate reconstructions of the Jurassic SW Gondwana are in close agreement and place the Falkland Islands adjacent to the southern Cape (e.g., Martin and Hartnady, 1986; Jokat et al., 2003; Macdonald et al., 2003; Torsvik & Cocks, 2013), which allowed several authors to infer a lateral connectivity between the Outeniqua, North Falkland and Falkland Plateau basins (e.g., Martin et al., 1981; Parsiegla et al., 2009; Richardson et al., 2017; Baby et al., 2018). Importantly, all of these once contiguous offshore basins and the exposed onshore rift basins covered in this study directly overlie the deformed Palaeozoic basement rocks of the Cape Fold Belt as evidenced by deep boreholes (McMillan et al., 1997) and crustal thickness estimates (Parsiegla et al., 2009) and in turn corresponds well with the location of the Cape Orogeny within the greater Gondwanides (Catuneanu et al., 1998; Pankhurst et al., 2006; Ramos, 2006; Milani and De Wit, 2008). This broad region of SW Gondwana, when reconstructed, can be envisioned as an elevated region with rugged, mountainous topography that arose during Late Carboniferous to Early Triassic compression (e.g., Pankhurst et al., 2006; Milani and De

Wit, 2008; Pángaro et al., 2015). An intensive perod of Permian – Triassic compression occurred in the Cape of south Africa that was driven by low angle subduction (Lock, 1980) or transpression (Johnston, 2000; Fig. 5.77) that gave rise to the Cape Fold Belt. During this time, the Cape Orogeny, the vast lithospheric load that accumulated by thrusting (Hälbich, 1992; Newton, 1992; Booth and Shone, 1999) and buckling (Cloetingh et al., 1992) had far reaching flexural effects on the southern margin of Gondwana (i.e., Namaqua-Natal Mobile Belt and Kaapvaal Craton further north) in generating the retroarc foreland Karoo Basin (Cole, 1992; De Beer, 1992; Catuneanu et al., 1998; Pysklywec and Mitrovica, 1999; Scheiber-Enslin, 2015). This region would had to have had a crustal thickness far greater than the present-day 42 km calculated using P-wave velocity models (Parsiegla et al., 2009) and seismic studies of the adjacent Namaqua-Natal terrane (Green and Durrheim, 1990). Reliable estimates of the maximum crustal thickness accumulated during the Cape Orogeny, which realistically fluctuated during periods of lithospheric loading and unloading, remain elusive although forward modeling suggests that at least 60 km of crust had accumulated by the Triassic (Cloetingh et al., 1992), an estimate corroborated by lithospheric flexural models of the Karoo Basin that incorporate a 80 km thick crust in the southern Cape Fold Belt (Scheiber-Enslin, 2015). Such an elevated crustal thickness certainly meets prerequisites for gravity-driven extensional stress and approaches that of the present-day Himalayas in which the phenomenon is well-documented (Dewey, 1988).

Gravitational collapse as an extensional phenomenon was not limited to the Cape Fold Belt. Palaeogeographic reconstructions of the Early Jurassic of SW Gondwana (Fig. 5.77) include a number of elongated grabens and half-grabens that follow a NNW – SSE orientations (Gust et al., 1985; Uliana and Biddle, 1988). Despite there being contemporaneous mechanisms that might have caused the Late Triassic – Jurassic extension that initiated these basins (Mosquera and Ramos, 2006; D'Elia et al., 2015; Lovecchio et al., 2018) such as: A mantle plume that caused uplift, extension and volcanism in Patagonia and the Antarctic Peninsula (e.g., Gust et al., 1985; Pankhurst and Rapela, 1995; Pankhurst et al., 2000; D'Elia et al., 2015); and the active margin arc in the SW of SW Gondwana (e.g., Gust et al., 1985, Howell et al., 2005; Fig. 5.77), there is also evidence for Late Triassic – Early Jurassic extension for which the gravitational collapse of the Palaeozoic Ventania orogenic belt is entirely responsible (Franzese and Spalletti, 2001). These basins (e.g., the Nuequen, San Jorge and Magallanes basins of southern Argentina) are filled with thick, diachronous syn-rift red beds, conglomerates and volcaniclastic deposits deposited in mostly continental settings (Stipanicic et al., 1968; Gust et al., 1985; Uliana et al., 1999) that broadly resemble the Enon and Kirkwood formations in South Africa, albeit with significantly more volcanic successions given their close proximity to sites of coeval silicic volcanism (see Franzese and Spalletti, 2001 fig 4 for a summary of stratigraphy). It therefore would not be an exceptional case if the phenomenon also occurred in parts of the Gondwanides that were not directly affected by extensive extensional volcanism, such as the southern Cape.

There are however some observations that do not fit the gravitational collapse model for rifting in the southern Cape. Thorough revisiting the chronology of compression of the Cape Orogeny suggests that there were perhaps only as few as two principal compressional events at ~270 Ma and ~250 Ma (Blewett and Phillips, 2016; Hansma et al., 2016) rather than the more complex episodic compressional history previously envisioned (e.g., Hälbich, 1983; Gresse and Theron, 1992; Catuneanu et al., 1998). If this new model of the compressional history is to be fully accepted – indeed there are numerous features of the Karoo Basin that still need to be explained within this new framework – it implies that the main phase of compression ended in the earliest Triassic, more than 50 Ma before the initiation off rifting in the southern Cape in the late Early Jurassic. If the cessation of compression alone allowed for relaxation and inversion of Cape Fold Belt structures under gravitational forces, then we expect Triassic strata hosted in the depocentres of the rift basins in the southern Cape, which is not observed. Instead the oldest deposits in the syn-rift southern Cape are no older than latest Pliensbachian – Toarcian (Lower Jurassic). The findings of these two recent studies are yet to be fully understood in the context of the Cape Orogeny and Karoo Basin flexural tectonics, nevertheless, investigating when compression of the Orogeny ended is encouraged because such investigations will further elucidate the tectonic history of Mesozoic southern Africa, including the rifting of the southern Cape. Secondly, the normal fault arrays that are seen in the Cape Fold Belt are not the only expression of extensional strain at this time, as there are some smaller, syn-depositional normal faults with 10s of m total displacement in the southern main Karoo Basin within the Lower Jurassic (Hettangian to Pliensbachian) upper Elliot and Clarens formations too (e.g., Bordy et al., 2004; Haupt, 2018). If gravitational collapse were the sole driver of extension, then the extension is expected to be somewhat restricted to the Cape Fold Belt and not in areas > 600 km to the northeast.

Geodynamically-derived extension

A second possible cause for extension in the Jurassic Southern Cape is derived from the upwelling and hot mantle asthenosphere across SW Gondwana. Thomson (1999) invokes a plume-model for extension in the Gamtoos Basin, although some of the views presented there are rather antiquated. In accordance with plume-generated continental breakup (White and McKenzie, 1989), he attributes the Early Jurassic Karoo flood basalts to a ‘Karoo mantle plume’ that was centered to the northeast of the southern Cape, beneath Mozambique (White and McKenzie, 1989; Cox, 1992; Thomson, 1999). Since neither the age of the Karoo LIP, nor the timing of rift initiation in the Gamtoos Basin were well-constrained until recently, he explains that the plume head that caused volcanism from 193 – 162 Ma (sic), generated a topographic anomaly that provided extension in the Gamtoos Basin immediately afterwards. Nowadays with the benefits of more robust geochronological constraints we know that the Karoo LIP emplacement was at ~183 Ma (Svensen et al., 2012; Burgess et al., 2015), with some minor volcanism occurring prior to this (Moulin et al., 2017), and that spreading between East and West Gondwana occurred soon thereafter at ~170 – 165 Ma (Gaina et al., 2013). Meanwhile the Gamtoos Basin probably initiated in the latest Pliensbachian – Toarcian (Early Jurassic), and not the Late Jurassic as described by Thomson (1999). Despite the chronology of these two events being entirely revised since their relationship was proposed, both the age of Karoo LIP and of the initiation of rifting in the southern Cape have been pushed back to the Early Jurassic, and are still roughly contemporaneous events. This is compatible with a geodynamically initiated rifting for the Jurassic southern Cape, because the intensive heat introduced by the impinging asthenosphere associated with the

Karoo-LIP, coupled with the inherent long-wavelength positive topographic anomaly that accompanied it (White and McKenzie, 1989) may have provided the extensional stresses in the southern Cape that prompted the reactivation of compressional structures. This seems especially likely since new geochronological evidence and palaeogeographic reconstructions places the locus of the Lower Jurassic Karoo and Farrar LIPs, and the contemporaneous silicic volcanism in Patagonia and Antarctica near the southern Cape, essentially surrounding the Cape Fold Belt in the Early Jurassic (Fig. 5.77). Further, there is evidence from some areas that these volcanic events were accompanied with regional uplift (Dopico et al., 2016). Since such vast areas of SW Gondwana experienced volcanism at this time, to the SW, S, E and NE of the Cape Fold Belt, it follows that the thick lithosphere accumulated during Permo-Triassic orogenesis (Lindeque, et al., 2011) would have experienced elevated heat too, which may have further weakened deep-seated structures and promoted extension. We therefore propose that during this time of elevated lithospheric geothermal gradients and raised topography, rifting began in the southern Cape. This model for rift initiation better fits the observed normal faulting in regions that do not correspond to the Cape Fold Belt, for instance in SW Lesotho (Haupt, 2018), and instead dictates simply that the southern Cape experienced an extensional stress regime for the first time in the Early Jurassic, roughly contemporaneous with widespread volcanism across SW Gondwana and due to elevated temperatures and associated uplift. Due to this stress regime change, reactivation of weaknesses in the Cape Fold Belt occurred, resulting in major displacement (at the km scale) at a variety of orientations, while areas that had less inherited weaknesses, such as in regions of the main Karoo Basin only accommodated a small amount of the extensional strain and resulted in just 10s of meters of displacement along normal faults there (Bordy et al., 2004; Haupt, 2018).

Extension in the Jurassic southern Cape and across SW Gondwana as a whole was likely caused by a combination of these two factors. Gravitational collapse certainly occurred in other parts of the Gondwanides (Franzese and Spelletti, 2001), and likely also occurred in the southern Cape, but the sudden introduction of heat and associated topographic uplift that occurred during the late Early Jurassic in various regions of southern Gondwana would undoubtedly have impacted the region significantly and at least partly triggered onset of rifting in the southern Cape. In summary, these conditions caused extension that began around the Pliensbachian-Toarcian boundary, contemporaneously with the Karoo and Ferrar LIP, and also with volcanic events to the SW, and drove localized reactivation of compressive structures, which correspond to the oldest depocentres of each basin. Onshore, these old strata are exposed in the Heidelberg and Mossel Bay basins, but chronostratigraphic correlatives are expected at depth in many of the other basins as well, including the Oudtshoorn, Roberson, Worcester basins onshore, and the Bredasdorp, Pletmos, Gamtoos, Algoa, Outeniqua, North Falklands and Falkland Plateau basins offshore. As normal faulting progressed through the Jurassic under this stress regime, faults grew through linkage (Gupta et al., 1998) and progressively younger strata were deposited in expanding accommodation space (Paton, 2006). Conceivably, once thermal gradients beneath the Cape Fold Belt normalized, there was a period of widespread subsidence, probably in the Late Jurassic. The data presented in this thesis do not lend insights into this time period except that we know accommodation space in the rift basins of the southern Cape were still being filled at this time (evidenced by vast Upper Jurassic deposits of the Uitenhage Group). This period of tectonic quiescence was finally disrupted in the Late Valanginian – Hauterivian, when there was renewed rifting along the same structures that now relate to the onset of movement along the AFT (e.g., Ben-Avraham et al., 1997; Parsiegla et al., 2009) during which syn-rift 2 strata of the Uitenhage Group were deposited across basins in the southern Cape. Although there are still many unanswered questions relating to the tectonic setting across the Jurassic SW Gondwana, these extensional mechanisms seem to better fit the observed history of rifting in the Jurassic of SW Gondwana that previous models, and it is hoped that the ideas presented here, along with the improved chronology of events, provide a framework upon which to build.

Chapter 6: Volcanic provenance considerations

6.1 Introduction

The focal point of many of the findings in this thesis hinges on the presence of volcaniclastic deposits in the Uitenhage and Suurberg Groups, however these rocks have never been traced back to their volcanic source. During this research, it has become clear that the distribution of the volcaniclastics throughout the onshore Mesozoic appears to be far greater than previously thought, with outcropping volcaniclastic units appearing in most rift basins of the southern Cape. Moreover, as demonstrated in the previous two chapters, these southern Cape volcaniclastics span the Lower Jurassic and Lower Cretaceous. This wide range of ages of ash beds means that ash-fall events punctuated clastic rift-basin sedimentation, but it remains unclear where the volcanic activity was centered during this time or even if there was a singular or multiple volcanic sources.

The new age data presented in Chapters 4 and 5 already allow constraints on the provenance of the volcaniclastic deposits in the Jurassic – Cretaceous strata of the southern Cape. One scenario that was first outlined by Dingle et al. (1983) is that all the volcaniclastics in the Uitenhage Group are equivalent in age and can be correlated to the volcaniclastics in the northern Algoa Basin (now referred to as the Coerney Formation of the Suurberg Group). This parsimonious scenario – of a single eruptive episode that draped the entire southern Cape with ash – is not supported by new U-Pb ages, which demonstrate that multiple eruptive episodes are responsible for the volcaniclastic deposits in the Uitenhage Group, all of which (except for a deposit at De Rust) are younger than the Suurberg Group. During the Early Cretaceous opening of the South Atlantic at 130 ± 5 Ma (Koopman et al., 2014) a number contemporaneous dyke swarms were emplaced in Namibia and the Western Cape of South Africa (Day, 1987; Reid et al., 1991, Will and Frimmel, 2013) but all of these postdate the youngest dated volcaniclastic deposit in the Uitenhage Group and are not responsible for the volcaniclastic deposits of the Uitenhage Group, a relationship tentatively proposed by Viljoen (1996). Clearly, the new ages reported reveal that none of the previously suggested and more localized volcanic sources are traceable to the volcaniclastic deposits considered in this study, which begs the question – *where was the volcanic source?* Investigating the petrogenesis of highly altered volcaniclastic deposits may help answer this question.

Petrological studies that attempt to understand the volcanic provenance of such deposits quote the grain size of minerals or lithic fragments within the volcaniclastic rock, or its thickness as measures of proximity to a volcano (Fischer and Schminchke, 1984; Pyle, 1989). Naturally, the presence of bombs that are derived from explosive volcanism is the consequence of extreme proximity to the volcanic source, but none of the volcaniclastics in this study contain any clasts that cannot be adequately explained by normal siliciclastic input during or after deposition of fine ash. The assessment of grain size and mineral densities of finer grained volcaniclastic deposits (tuffs and their altered equivalents, which are found in the Mesozoic southern Cape) have been used to constrain a maximum distance from a volcanic eruption based on transport medium-grain size relationships (Fischer and Schmincke, 1984; Pyle, 1989; Carey and Sigurdsson, 2000; Rocha-Campos et a1., 2011). However, these studies are often oversimplified because they generally fail to take into account the elevated winds and jet-stream conditions that volcanic ash may encounter in the stratosphere and overlook the unusual atmospheric conditions within a pyroclastic plume, in which there is a reduced particle-medium density differential and unusual particle motion (Fung, 1998; Barham et al., 2016). Further, the thickness of primary ash-fall deposits is also not a very reliable proxy for determining the distance from the source volcano, because heterogeneities in the depositional environment – both topographic and preservational – and small-scale syn-depositional faulting can cause localized thickness variations (Königer and Stollhofen, 2001). These factors were certainly at play during the deposition of volcanic ash in the Jurassic – Cretaceous southern Cape and therefore the thicknesses of preserved volcaniclastic beds in the Uitenhage Group, making it a poor indicator of source proximity.

Geochemical characterization is more widely used and is considered more reliable in constraining the volcanic source of the volcaniclastic deposit (Bohor and Triplehorn, 1993; Bangert et al., 1999; Jones et al., 2016); however, these methods are also not without their problems. Volcanic ash derived from an eruption is often exceptionally fine-grained consisting of various components including pulverized rock and usually very small juvenile magmatic crystals that crystallize in rapidly cooling ejected lava. This fine-grained groundmass, coupled with the generally chemically unstable minerals present in ash (e.g., volcanic glass), are highly susceptible to alteration and therefore the geochemical composition of the sampled volcaniclastic rock is rarely reflective of parental lava composition. Nevertheless, some trace elements that are fairly immobile and therefore least affected by alteration processes can be representative of the original magmatic conditions and are widely used to discriminate lava types (Winchester and Floyd, 1977) and their volcanic setting (Pearce et al., 1984). However, just slight reworking and inclusion of siliciclastic detritus into the volcaniclastic unit can greatly affect the trace element signature measured so whole rock trace element geochemistry only works for primary ash deposits. Trace elements of specific minerals in the volcaniclastic deposit, such as zircon, can also be applied although their usefulness in discerning between the broadly granitic magma types is limited and best used in conjunction with other methods (Belousova, 2002; Belousova et al., 2006).

An alternative to using geochemical techniques to discern petrogenesis is to assess the morphological appearance of zircon (Fig. 6.1), a common accessory mineral that is present in all the volcaniclastic deposits considered in this study. Pupin (1980) developed a classification system for common zircon habits found in igneous rocks based on empirical observations that the thermal and chemical characteristics of the magma, affects zircon crystal habit, or *typology*. Zircons that crystallized in peraluminous conditions have distinct {211} pyramids, whereas those grown in perialkaline magmas have well-developed {101} pyramids. Therefore the alkalinity, represented by the ratio Al/(Na + K) and termed ‘index A’, is responsible for the development of pyramids in zircons and is depicted as the X axis on the typological classification diagram (Fig. 1A). In this system, the temperature of the magma during which zircons crystallized is considered the principal factor controlling the relative development of various prisms and is plotted on the Y-axis in the typological classification. This geothermal and chemical compositional scheme is represented by a grid in which each constituent square contains a zircon crystal subtype (Fig. 6.1A). The distribution of zircon subtypes in a given granitic rock can be placed into the petrogenetic classification system that distinguishes its crustal, mixed crustal and mantle, or mantle origin (Fig. 6.1B) and is extended to several non-granitic rocks (Fig. 6.1C).

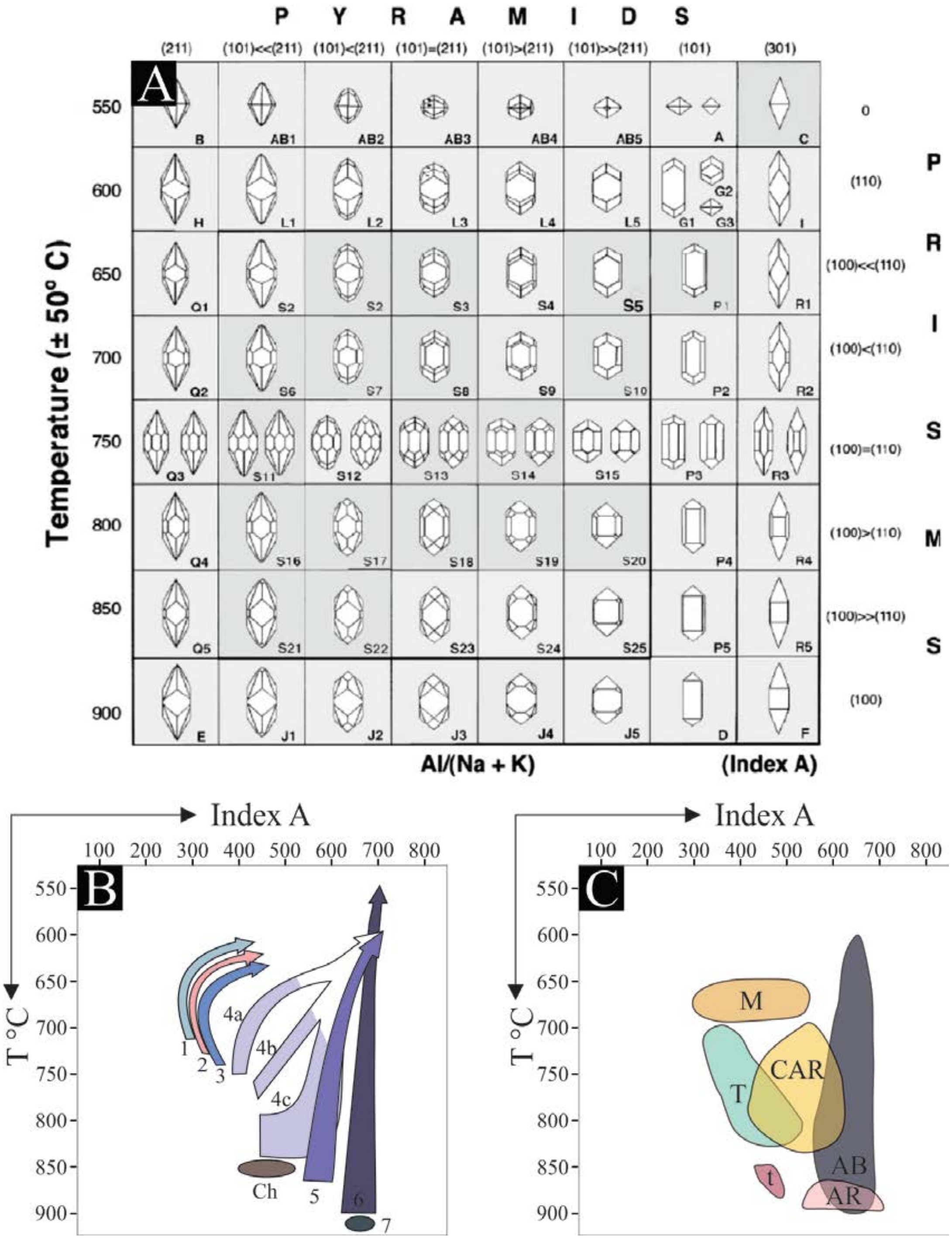

Fig. 6.1. A. Zircon typological classification system of Pupin (1980). Types (letters) and subtypes (numbers) of zircon crystals and corresponding geothermometric scale. Index A represents Al/Alkali ratio, which controls the development of pyramids, and temperature, which affects the development of prisms, follows the calibration of Pupin and Turco (1972). B. Zircon crystal morphological distributions for granites proposed by Pupin (1980). Granites of mainly crustal origin: (1) aluminous leucogranites; (2) (sub)autochthonous monzogranites and granodiorites; (3) intrusive aluminous monzogranites and granodiorites. Granites of mixed crustal and mantle origin: (4a – c, clear area) monzogranites and alkaline granites; (4a – c, shaded area) granodiorites and monzonites; (5) sub-alkaline series granites. Granites of mainly mantle origin: (6) alkaline series granites; (7) tholeiitic series granites. (Ch) Magmatic charnockite area; (Mu)

limit of muscovite granites (T < 725ºC). C. Zircon crystal morphological distributions for some non-granitic rocks after Pupin (1980): (AR) alkaline series rhyolites; (CAR) calc-alkalines series rhyolites; (M) migmatites; (t) trachyandesites; (T) tonalities.

In reality, assessing the volcanic source of volcaniclastic deposits is not straightforward and should best be attempted using multiple lines of evidence. Where geochemical techniques suffer from post-depositional alteration or reworking, zircon morphological assessments described by Pupin (1980) may be too simplistic (Varva, 1993; Benisek and Finger, 1993). Therefore, in the current study two independent methods, whole-rock trace element geochemistry and zircon typology, are used to assess the volcanic origin of the Mesozoic volcaniclastic deposits in the southern Cape. However, because a large number of such units are clearly of mixed detrital and volcanic origin (see Chapters 4 and 5), only pyroclastic deposits are assessed (Table 6.1) as they are most likely to best represent the volcanic source.

Table 6.1. Pyroclastic samples from Chapters 4 and 5 analysed for geochemical and zircon morphological characterization.

Sample name	Basin	Lithology	Geological age	Geochemical analysis	Zircon typological assessment
PLET	Plettenberg Bay	Bentonite	Lower Cretaceous	X	X
ROBE	Robertson	Bentonite	Upper Jurassic	X	X
OKT1	Oudtshoorn	Bentonite	Upper Jurassic	X	X
CALI	Oudtshoorn	Bentonite	Upper Jurassic	X	X
HBUP	Heidelberg	Bentonite	Upper Jurassic	X	X
HBMZ	Heidelberg	Zeolite	Middle Jurassic	X	
HBMB	Heidelberg	Bentonite	Middle Jurassic	X	X
HBMill	Heidelberg	Bentonite	Middle Jurassic	X	X
MATJ	Mossel Bay	Bentonite	Middle Jurassic	X	X
ASP1	N Algoa Basin	Tuffaceous sandstone	Lower Jurassic		X
ASLO	N Algoa Basin	Tuffaceous sandstone	Lower Jurassic		X

6.2 Analytical procedures

6.2.1 Trace element geochemistry

All trace element geochemical analyses were conducted at the Department of Geological Sciences, University of Cape Town in clean laboratory conditions using the following procedure outlined below. About 500 g from each of the nine samples (Table 6.1) was milled to a fine homogeneous powder using a swing mill. Following this, 50 mg of each sample powder was digested using a three-step dissolution procedure in a 4:1 HF/HNO_3 acid mixture in sealed Savilex beakers on a hotplate over a 48 h period. The sample solutions were then dried and each product taken up in a 5% HNO_3 solution containing 10 ppb Re, Rh, In and Bi, which were used as internal standards and calibration curves were obtained using artificial multi-element standards, from which standard solutions were made. Along with the nine samples, *JA-2* and *JR-2* rock standards and a blank (*TPB*) were analysed using a Thermo-Fisher X-Series II quadrupole ICP-MS with a solution autosampler in order to determine the precision and accuracy of analyses (Table 6.2). Compositional data are presented in Table 6.3.

6.2.2 Zircon morphological assessments

Zircons were picked from ten mineral separates attained following the protocols outlined in Chapters 4 and 5, and placed onto a circular disk mount coated with a carbon-glue paste. Roughly 90 zircons were picked per sample and placed side-by side onto the paste very lightly to prevent the zircons getting pressed into the soft paste, which helped to maximize the surface area exposed. The sample mounts and zircons were then coated with a fine film of gold before being loaded into the NovaNano Scanning Electron Microscope (SEM) at the Aaron Klug Centre for Imaging and Analysis, University of Cape Town. The magnification was adjusted so that each zircon filled most of the field of view before a secondary electron image of each was attained. This allowed for unobscured visualization of the crystal faces of most of the zircons and unambiguous typological classification.

Table 6.2. Immobile trace element values of JA-2 and JR-2 standards and total procedure blank (TPB) obtained by LA-ICPMS in this study compared to their recommended compositions outlined in Jochum et al. (2016) and Imai et al. (1995). %RSD = relative standard deviation in percent.

	JA-2 Recommended (ppm)	JA-2 Analysed (ppm)	%RSD	*JR-2 Recommended (ppm)*	JR-2 Analysed (ppm)	%RSD	TPB (ppb)
Ti	*4020*	3749	0.504	*400*	337.4	1.141	3.058
Rb	*69.8*	69.08	0.294	*303*	318.3	0.840	0.004
Y	*16.89*	15.15	0.156	*51.1*	43.25	0.397	0.001
Zr	*108.5*	107.2	0.348	*96.3*	83.43	0.358	0.176
Nb	*9.3*	8.830	0.887	*20.4*	16.67	0.925	0.024
La	*15.47*	14.76	0.499	*16.3*	13.73	0.549	0.002
Ce	*32.86*	30.53	0.207	*38.8*	33.99	0.667	0.002
Pr	*3.691*	3.520	0.704	*4.75*	4.410	0.477	0.001
Nd	*14.04*	13.17	0.664	*20.4*	17.72	0.481	0.002
Sm	*3.032*	2.891	0.811	*5.63*	5.034	0.708	0.001
Eu	*0.893*	0.841	1.341	*0.14*	0.095	0.628	0.001
Tb	*0.4786*	0.455	1.048	*1.1*	0.982	0.361	0.001
Gd	*3.013*	2.896	0.482	*5.83*	5.533	0.795	0.001
Dy	*2.851*	2.796	0.395	*6.63*	6.564	0.358	0.001
Ho	*0.591*	0.581	0.226	*1.39*	1.405	0.837	0.001
Er	*1.676*	1.688	0.987	*4.36*	4.459	0.240	0.001
Tm	*0.2546*	0.236	0.829	*0.74*	0.774	0.613	0.001
Yb	*1.645*	1.598	0.570	*5.33*	5.200	0.244	0.001
Lu	*0.2549*	0.253	0.872	*0.88*	0.857	0.574	0.001

6.3 Results and discussion

6.3.1 Trace element geochemistry

Relatively immobile trace elements including the REE, are presented for each of the nine pyroclastic units in the Kirkwood Formation (Table 6.3). There are fairly large variations in REE patterns across each of the nine samples with respect to the total elemental concentrations, Eu anomalies, and heavy REE when normalized to chondrite composition (Fig. 6.2). Sample CALI contains the lowest REE concentration, while PLET has the highest, with all samples having roughly parallel light REE patters that diverge at the medium and heavy REE. Strongly negative Eu anomalies exist for samples HBMZ and HBMill; Eu in samples ROBE, HBUP and HBMB are moderately anomalously negative and the remaining samples have very small negative Eu anomalies. This likely reflects the varied eruptive magmatic compositions and fractionation during the crystallization of plagioclase. In general, the samples exhibit a relative enrichment in the light REE compared to medium and heavy REE with respect to chondrite composition although sample ROBE is an exception and is enriched in TM, Yb and Lu. Overall there appears to be no trends through time expressed in REE patterns.

Ratios of immobile trace elements that are least likely to be affected by the alteration all the ash deposits experienced and can be used to discriminate the composition (Winchester and Floyd, 1977) and tectonic setting (Pearce et al., 1984) are preferred over conventional methods that rely on mobile elements (e.g., La Bas et al., 1986). Samples plot in the rhyodacite-dacite, rhyolite and commendite-pantellerite fields on the Zr/Ti-Nb/Y diagram (Fig. 6.3A), suggesting a predominantly felsic to intermediate parental magma composition for all bentonites. The youngest and only Cretaceous sample (PLET) has a lower Nb/Y ratio compared to other samples. All but two samples plot within the volcanic arc field in Rb-Y+Nb space (Fig. 6.3B), with one occupying the intersection of three fields and therefore impossible to confidently assign to a tectonomagmatic setting, and one sample, again the youngest, plotting within the ocean ridge field.

Table 6.3. Whole-rock trace element geochemistry values of nine pyroclastic deposits in the Uitenhage Group given in ppm.

	PLET	ROBE	CALI	OKT1	HBUP	HBMZ	MHMB	HBMill	MATJ
Ti	1361	1036	2119	1740	580.2	574.3	1447	688.3	1357
Rb	7.272	11.34	10.66	24.56	4.201	28.13	9.014	13.27	9.756
Y	57.17	19.79	12.52	37.74	17.24	10.65	18.10	14.79	37.08
Zr	151.7	205.2	203.0	117.8	154.0	99.20	181.4	151.2	187.4
Nb	5.182	14.22	7.864	14.64	11.04	11.70	16.05	16.19	17.46
La	88.40	39.31	14.17	46.78	40.06	24.53	34.51	23.83	37.74
Ce	191.1	84.97	27.32	100.5	92.96	49.55	81.12	60.03	105.4
Pr	24.97	10.15	3.569	10.86	10.19	6.216	9.177	7.139	13.91
Nd	100.8	37.20	13.49	40.62	38.76	23.29	34.90	26.98	61.44
Sm	21.87	7.491	2.882	8.741	8.409	5.126	7.248	5.831	13.36
Eu	4.259	0.862	0.513	1.749	0.832	0.389	1.165	0.345	2.653
Tb	2.779	0.900	0.433	1.226	0.985	0.638	0.846	0.672	1.658
Gd	20.11	5.782	2.864	8.395	6.915	4.498	5.908	4.269	12.43
Dy	14.69	5.026	2.489	6.992	5.364	3.349	4.448	4.022	8.955
Ho	2.516	0.901	0.474	1.367	0.874	0.564	0.798	0.759	1.550
Er	6.256	2.557	1.297	3.978	2.107	1.377	1.998	2.477	3.936
Tm	0.844	0.431	0.185	0.626	0.284	0.204	0.272	0.430	0.507
Yb	4.934	3.329	1.278	4.126	1.797	1.532	1.742	3.465	3.030
Lu	0.717	0.559	0.212	0.690	0.252	0.241	0.270	0.582	0.453

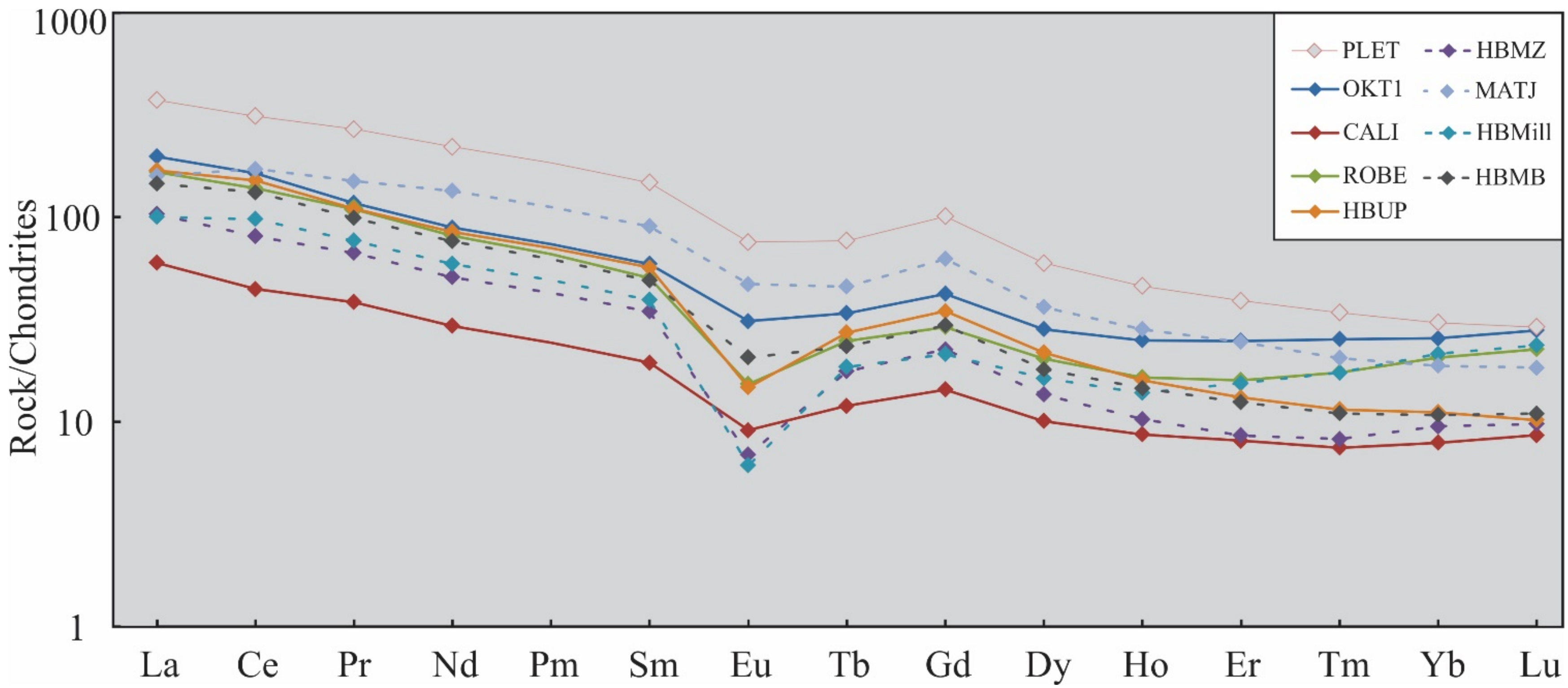

Fig. 6.2. Chondrite normalized rare earth element diagram of pyroclastic deposits. Dashed lines are Middle Jurassic deposits, solid lines are Upper Jurassic and open markers highlight the single Lower Cretaceous deposit. Chondrite normalization factors are taken from McDonough and Sun (1995).

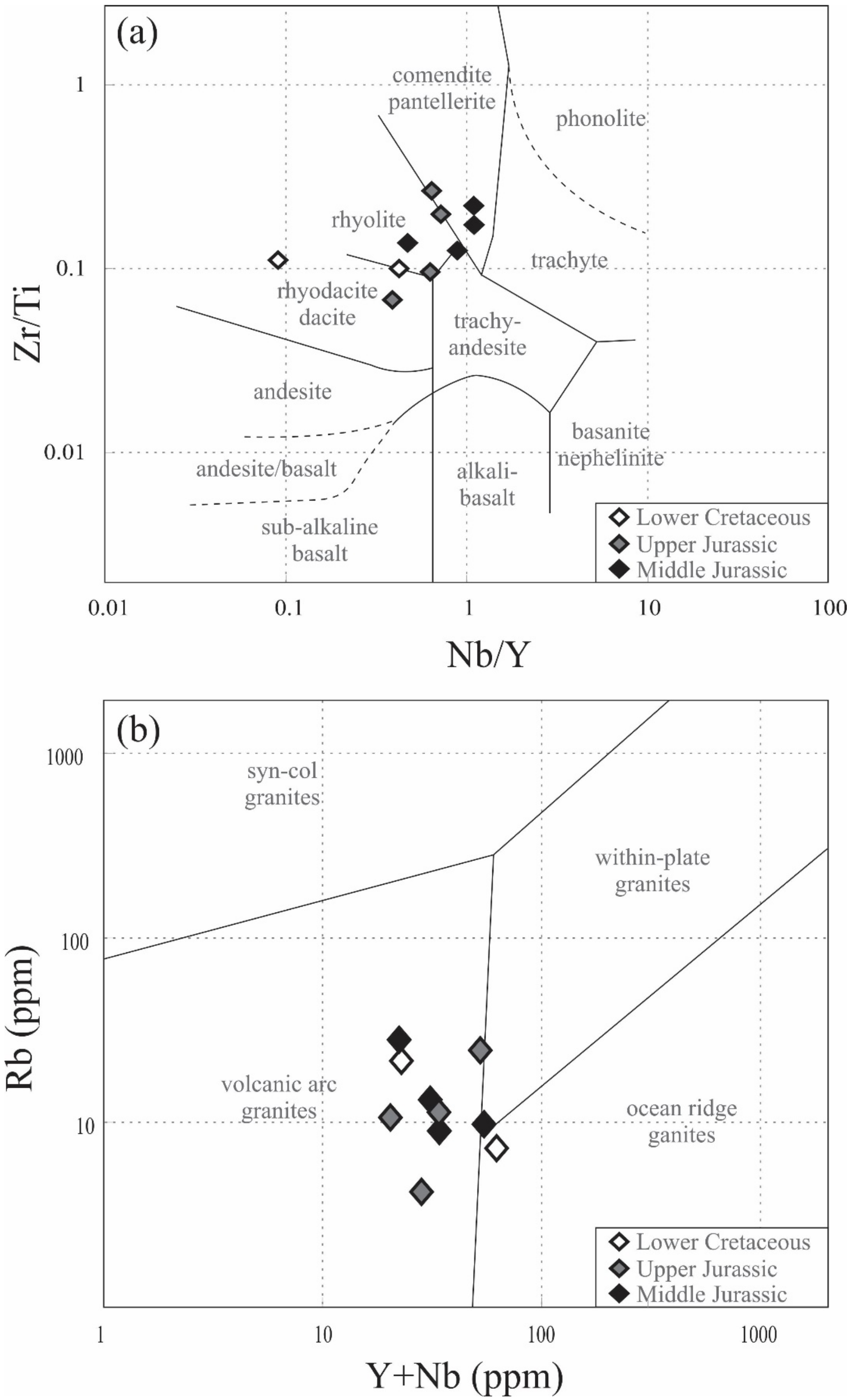

Fig. 6.3. Geochemical classification plots based on immobile element geochemistry. A) Composition of parental magma based on Zr/Ti-Nb/Y ratios of pyroclastic deposits after Winchester and Floyd (1977). B) Tectonomagmatic setting of volcanism based on Rb, Y and Nb concentrations after Pearce et al. (1984).

6.3.2 Zircon morphology

The majority of zircon crystals extracted from each of the four bentonitic Kirkwood Formation samples could be successfully categorized into subtypes based on secondary election SEM imagery. Almost all crystals were strongly euhedral and preserved the pyramidal and prismatic habits suitably for confident typological classification (Pupin, 1980) with the exception of some of the most fragile, elongated, needle-shaped grains that regularly preserved only one crystal termination.

Zircon typological distributions, when the size of the crystal is not considered, are very similar for samples PLET, CALI, ROBE, OKT1 and HBUP (Fig. 6.4). The majority of zircons are ‘S’-type, with S24 being the most represented subtype in these samples with the exception of OKT1, in which S17 is the commonest subtype. The respective distributions indicate that each of these pyroclastic deposits are derived from magmas of mixed mantle and crustal origin, corresponding to the calc-alkaline granodiorites and monzogranite fields or the tonalite (T), trachyandesite (t) and to a lesser degree the calc-alkaline rhyolite (CAR) fields for non-granitic rocks (Fig. 6.1A, B, C, 4). However, ROBE is less easily categorized because zircons display a bimodal distribution of subtypes, with ‘P’-type crystals forming a subordinate subpopulation along with the dominant ‘S’-types.

There is a significantly larger spread of zircon types in samples MATJ and HBMill than in in the other samples (Fig. 6.4) that cannot be simply be attributed to detritus because of the purely pyroclastic nature of the deposit. Most zircons are ‘S’-types, with S23 being the commonest subtype, although ‘J’, ‘P’ and ‘G’ types are also present in significant numbers. This diversity of zircon types makes assessing the characteristics of the parental magma nearly impossible. Nevertheless, because zircons are most commonly ‘S’ type, these two bentonites are probably derived from eruptions involving lavas of mixed mantle and crustal origin, corresponding to the calc-alkaline granodiorites and monzogranite fields or the tonalite (T), trachyandesite (t) and to a lesser degree the calc-alkaline rhyolite (CAR) fields for non-granitic rocks (Fig. 6.1A, B, C, 4). The complex zircon distribution may have arisen from rapid changes in the magma chamber prior to- or during eruption, sediment mixing and subtle detrital input during deposition of the volcanic ash, or zircon crystallization may have been affected by other parameters that are not accounted for by this classification (Benisek and Finger, 1993; Vavra, 1993).

Two of the samples, which are from the Lower Jurassic Suurberg Group, ASP1 and ASLO, are not pyroclastic in origin and contain a significant detrital component that is evidenced by a wide range of zircon ages, rounded quartz grains and rare quarzitic clasts (see Chapter 4 for details). Therefore the distributions of zircon morphologies in these samples are expectedly widespread (Fig. 6.4), as a reflection of the variety of zircon sources and both samples contain a significant proportion of grains that are too rounded for confident typological assessments, further corroborating a transported detrital origin. Nevertheless, most of the zircons in either samples are ‘S’-types, of which S19 is the commonest subtype in ASP1 and S24 the commonest in ASLO. ‘P’-type and ‘G’-type crystals are also common in both samples, with rare ‘Q’-type and ‘J’-type grains in ASLO. Due to the mixed origin of these units, it is not possible to attribute their morphological distributions to a specific parental magma source.

Fig. 6.4. (Following three pages). Zircon typological distributions and secondary electron image of common zircon subtypes, labelled in blue above each crystal image, for each respective sample.

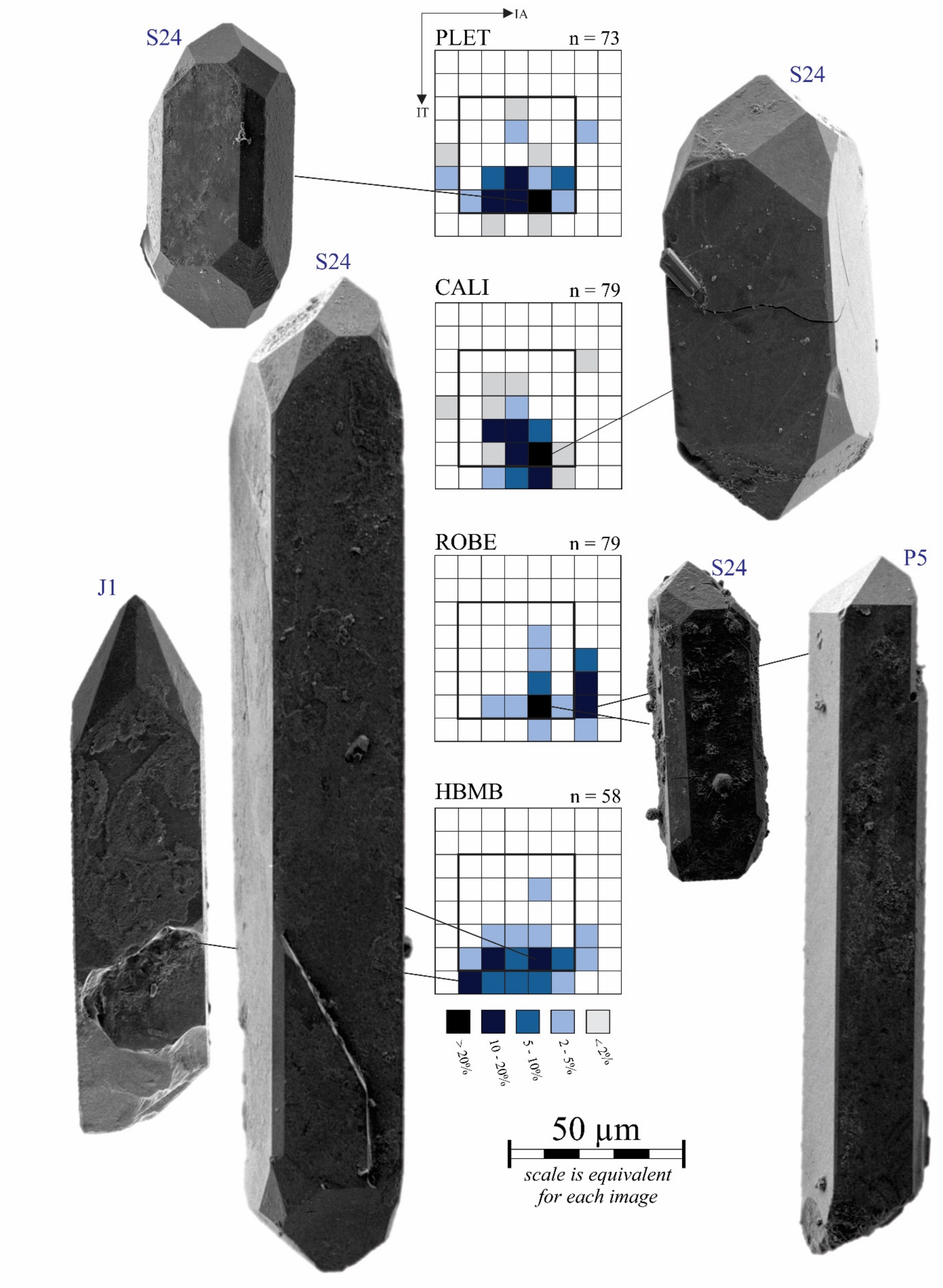
S24
IA
IT
PLET
n = 73
S24
S24
CALI
n = 79
ROBE
n = 79
S24
P5
J1
HBMB
n = 58
> 20%
10 - 20%
5 - 10%
2 - 5%
< 2%
50 μm
scale is equivalent
for each image

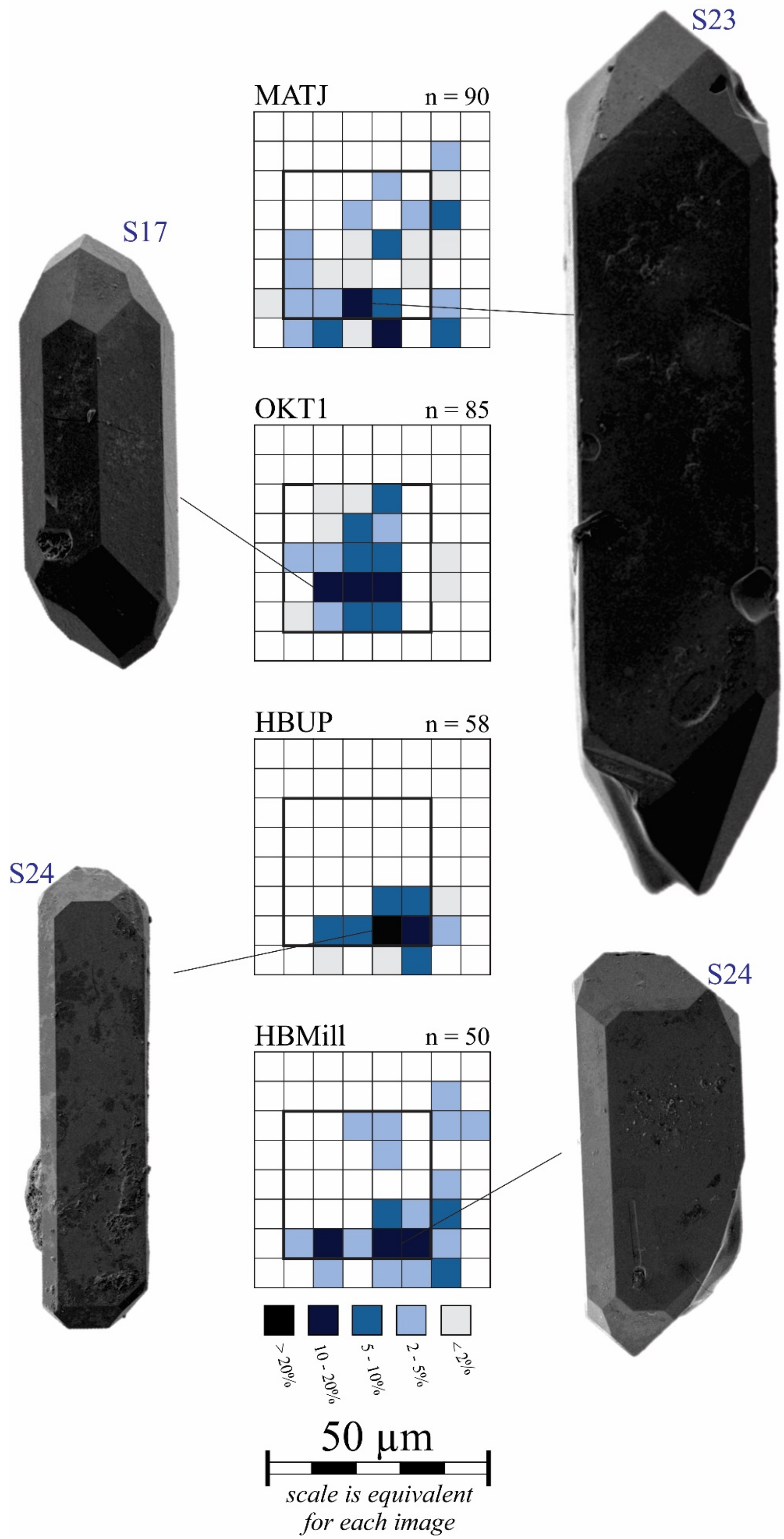
S23
MATJ
n = 90
S17
OKT1
n = 85
HBUP
n = 58
S24
S24
HBMill
n = 50
> 20%
10 - 20%
5 - 10%
2 - 5%
< 2%
50 µm
scale is equivalent for each image

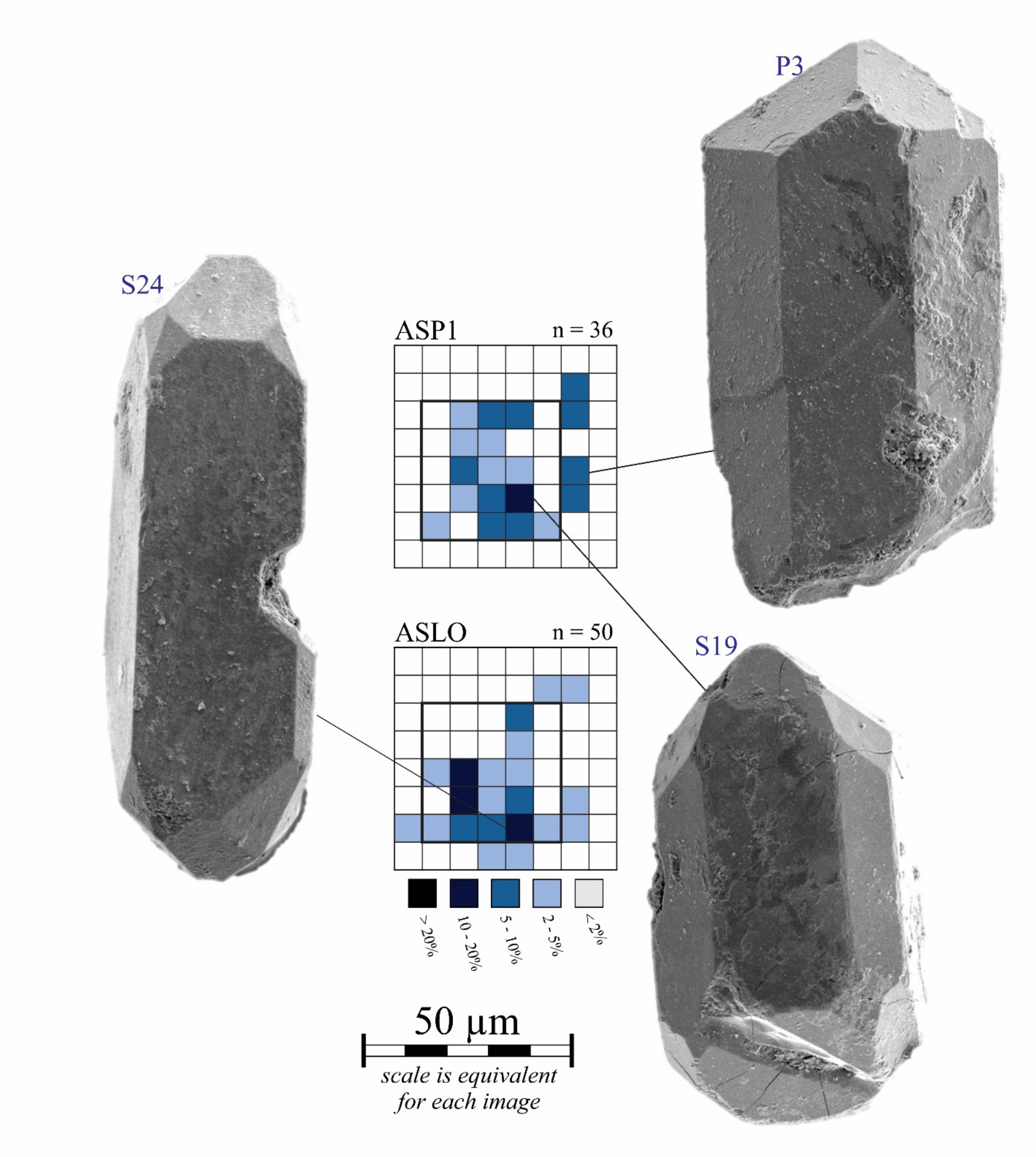
P3
S24
ASP1
n = 36
ASLO
n = 50
S19
> 20%
10 - 20%
5 - 10%
2 - 5%
< 2%
50 µm
scale is equivalent
for each image

6.3.3 Volcanic provenance

Both the trace element geochemical signature and zircon typological distributions indicate a felsic – intermediate parental magma for the pyroclastic deposits in the Uitenhage Group derived principally from a volcanic arc setting. This finding, coupled with new ages reported from pyroclastic beds in the Uitenhage Group, is strong evidence for a volcanic source to the SW of the southern Cape in modern-day Patagonia and the Antarctic Peninsula. Felsic to intermediate volcanic rocks are a common feature of Jurassic successions in these regions (Fig. 6.5), where they record a prolonged episodic period of silicic volcanism (Gust et al., 1985; Féraud et al., 1999; Pankhurst et al., 2000; González et al., 2019) with a volcanic arc geochemical signature, collectively referred to as the Chon Aike Large Igneous Province (Pankhurst et al., 1998; Riley et al., 2001). Additionally, comparatively minor silicic volcanism also occurred to the NE around the Lebombo region during the culmination of the Karoo LIP (Duncan et al., 1997; Riley et al., 2004; Miller and Harris, 2005), although it is unclear if this short-lived and laterally restricted, localized volcanism contributed at all to volcaniclastic deposition in the southern Cape. The collation of a large number of dated volcanic rocks and geochemical datasets has uncovered spatio-temporal trends in volcanic activity in the Jurassic SW Gondwana (Féraud et al., 1999; Pankhurst et al., 2000) that are relevant to volcanic provenance considerations.

Initially, silicic volcanism immediately followed the emplacement of the mostly mafic Karoo LIP through anatexis of the lower crust in South America (Pankhurst and Rapela, 1995), and magma underplating and re-melting of the shallow crust in the Lebombo region (Riley et al., 2004; Miller and Harris, 2005) during the Early Jurassic. Pankhurst et al. (2000) names this initial episode of silicic volcanism, lasting from 188 – 178 Ma, ‘V1’ (Fig. 6.6). The only volcaniclastic deposits dated to this period are those found in the Suurberg Group and the nature of their deposition remains rather unclear. Increasingly, evidence accumulates for a Karoo LIP affinity for the Suurberg Group, at least for its basaltic units (Marsh, 2016). Conceivably, the volcaniclastic deposits of the Suurberg Group may have been derived from the silicic volcanoes evidenced at Lebombo, ~1000 km to the N (Fig. 6.5). However, the contemporaneous volcaniclastics of the Group may equally have been derived from centres to the south on the modern-day Antarctic Peninsula, which was roughly equidistant from the southern Cape in the Early Jurassic (Fig. 6.5) A definitive provenancing of the volcanic zircons in the Suurberg Group remains elusive because all the units sampled are of resedimented volcaniclastic deposits and therefore provide unclear zircon typological distributions (ASP1 and ASLO) and are unsuitable for whole-rock geochemical characterization. Perhaps the analysis of the youngest volcanic zircons for trace elements or Hf isotopes would be useful and is recommended to future workers determined to resolve the matter.

Following this, southern Patagonia continued to experience crustal thinning and anatexis although volcanism began to migrate toward the proto-Pacific subducting margin in the SW (Féraud et al., 1999; Pankhurst et al., 2000), where volcanic rocks incorporate a subduction geochemical signature (Pankhurst et al., 2000). A particularly active period of volcanism occurred between 162 – 172 Ma (‘V2’ of Pankhurst et al., 2000; Fig. 6.6) in the Antarctic Peninsula and eastern Deseado Massif (Fig. 6.6) that would have provided suitable sources for the thick (> 1.5 m) bentonites and zeolites hosted in lacustrine deposits of the Kirkwood Formation in the Heidelberg and Mossel Bay basins of southern Cape (samples HBMB, HBMill and HBUP, MBMZ and MATJ). Following this, another peak of volcanic activity occurred in the Andean Cordilleras between 153 – 157 Ma evidenced by abundant ignimbrites of these ages (‘V3’ of Pankhurst et al., 2000; González et al., 2019). This pulse of Late Jurassic volcanism corresponds well with numerous bentonites dated in the Mossel Bay, Roberston and Oudtshoorn basins (samples VOEL, ROBE, CALI, OKT1). The precisely dated bentonite near Robertson (150.3 ± 0.2 Ma) postdates the youngest dated ignimbrite that corresponds to this volcanic episode (Pankhurst et al., 2000) from within the Ibáñez Formation (153 ± 1 Ma), but this unit has not been dated with the same level of accuracy or precision and a correlation cannot be ruled out based on these data.

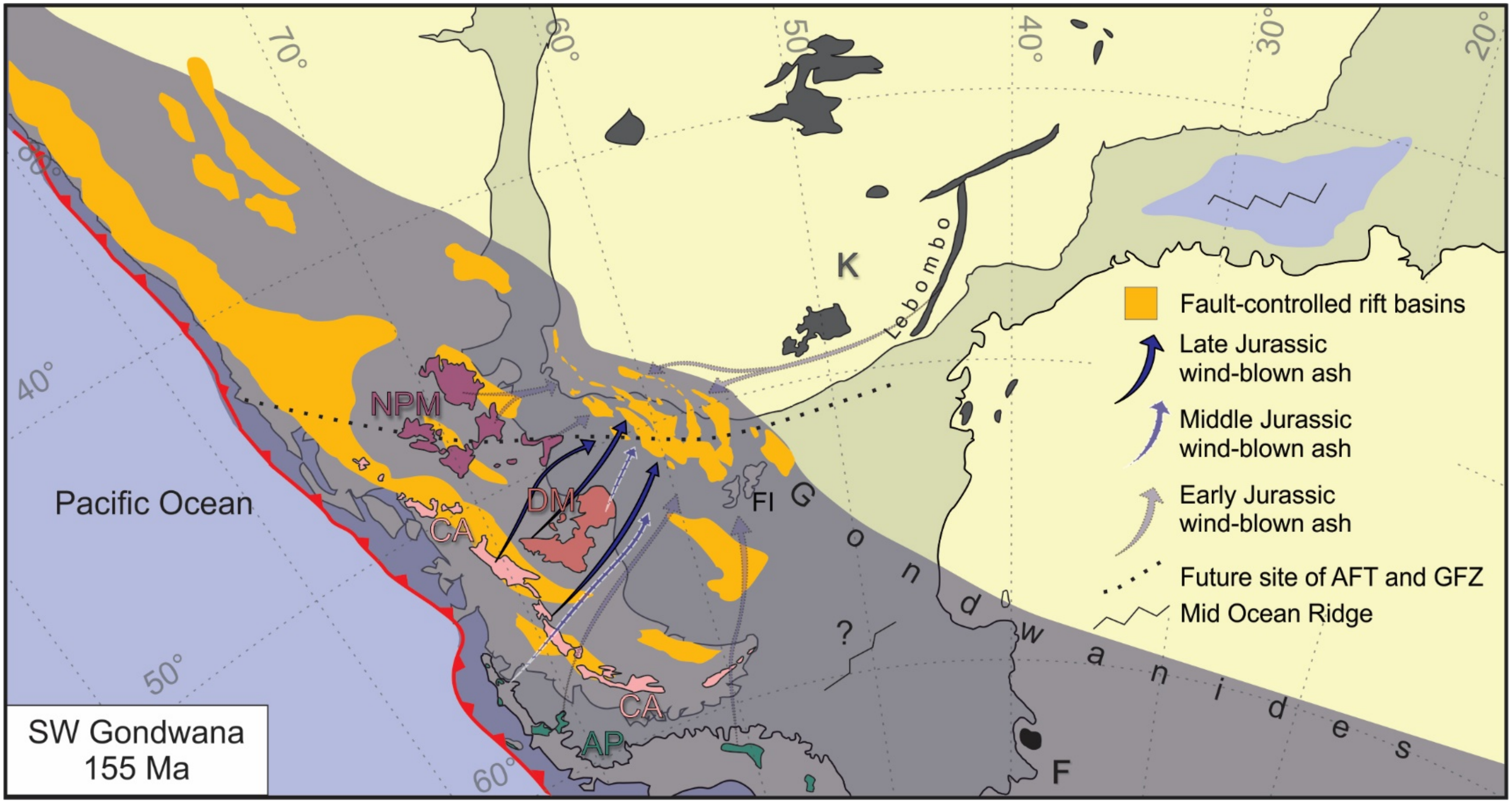

Fig. 6.5. Palaeogeocgraphic reconstruction of the Late Jurassic SW Gondwana. The proposed wind-blown ash transport directions from volcanic source areas in Patagonia, the Antarctic Peninsula and Lebombo, towards the modern-day southern Cape are shown. The distribution of fault-controlled Mesozoic basins and spreading centers are included. Abbreviations and colours signify present-day distribution of Jurassic extrusive rocks: AP, Antarctic Peninsula; CA, Andean Cordillera; DM, Deseado Massif; K, Karoo Igneous Province; NPM, North Patagonian Massif. Modified from Jokat et al. (2003) with additions from Gust et al. (1985), Pankhurst et al. (2000), Ghidella et al. (2002), Jourdan et al. (2005), Milani and de Wit (2008) and Hervé et al. (2006).

The youngest (140.2 ± 0.4 Ma) bentonite dated in from Plettenberg Bay (PLET) is not within error of any U-Pb dated volcanic rocks in Patagonia and cannot be attributed to any of the three periods of peak volcanism (Fig. 6.6). This bentonite is also the only one that has an ocean arc trace element geochemical signature (Fig. 6.3), which may indicate a different source area and tectonic setting entirely. Nevertheless, there are rhyolites dated to 144.2 ± 0.4 Ma in Patagonia by Ar-Ar techniques (Féraud et al.,1999) evidencing younger volcanism in the region that could account for Early Cretaceous volcaniclastics in the Uitenhage Group. Volcanics of the Paraná-Etendeka LIP, which predate the opening of the South Atlantic, are dated to between 131.7 ± 0.7 Ma and 132.3 ± 0.7 Ma (Renne et al., 1996) and because no volcaniclastic deposits of this age have been dated, either there was highly restricted delivery of ash from these volcanoes, or erosion has removed the associated volcaniclastic units from the Uitenhage Group. Indeed, the latter seems likely since the Early Cretaceous is poorly represented in the western parts of the onshore southern Cape, and where it is, the deposits are mostly coarse-grained (Buffelskloof Formation) and deposited in high energy conditions not suitable for ash preservation. Even its finer-grained distal correlative (Hartenbos Formation), which was deposited in low-energy conditions, contains no obvious volcaniclastic deposits nor any syn-depositional Early Cretaceous zircons.

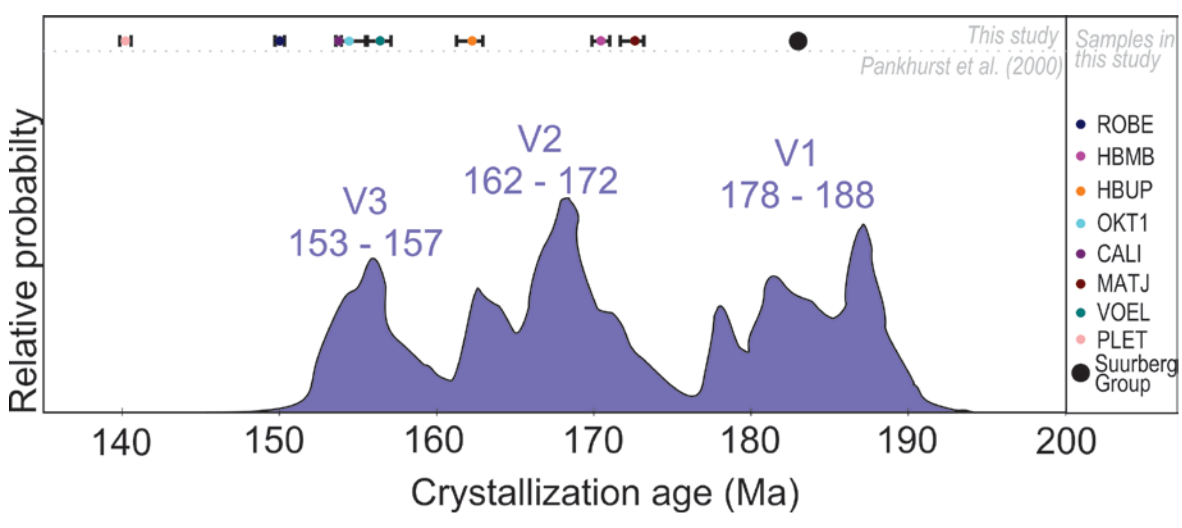

Fig. 6.6. Timing of Jurassic igneous activity in SW Gondwana compared to the age of robustly-dated primary ash beds of the Uitenhage Group. Three episodes of volcanism (V1 – 3) are identified in the probability density curve of crystallization ages reported by Pankhurst et al. (2000) for the Antarctic Peninsula and Patagonian silicic volcanics and subvolcanics and there are contemporaneous pyroclastic deposits for each. V1 episode corresponds to the Suurberg Group and correlatives, V2 weakly corresponds to middle Jurassic bentonites and V3 corresponds well with Late Jurassic bentonites.

The observed distribution of volcaniclastic deposits in the Jurassic – Cretaceous of the southern Cape, with more volcaniclastic material observed in the West compared to the East, supports a volcanic source to the W or SW of the southern Cape for most of the Jurassic. Although many volcaniclastic beds probably remain unmapped or entirely in the subsurface, making their distribution in space a rather weak line of argument for a source region, it is worth considering until proven otherwise. Perhaps future workers find volcaniclastic deposits in the Uitenhage Group of the Algoa or Gamtoos basins, the two most easterly basins in the southern Cape, but to date no such deposits have been found there. This contrasts with the western basins in which volcaniclastic deposits are a common feature (e.g., Robertson, Heidleberg and Mossel Bay basins). An overall pattern of eastward decreasing volcaniclastic occurrences in the Uitenhage Group seems to hold despite the Algoa Basin having by far the greatest areal extent and best quality exposures (not to mention considerable time spent unsuccessfully scouring outcrops and borehole cores for volcaniclastic deposits). Such a pattern is not unexpected considering a Patagonian and Antarctic Peninsula volcanic source, which was to the W and SW of the southern Cape in Jurassic plate reconstructions (Fig. 6.5). Further, wind patterns for the Late Jurassic and Early Cretaceous generated using global circulation models indicate that palaeowinds across the southern Cape region were seasonal from the SW, S and SE during December – February and from the W during June – August (Moore et al., 1992), which is strongly compatible with a Chon Aike LIP source. The absence of observed volcaniclastics in the Algoa and Gamtoos Basins may be because wind-blown volcanic ash did not reach these most distal basins. However, the oldest volcaniclastic material at De Rust in the Oudtshoorn Basin (DERU and DERC1) and in the Suurberg Group of the Algoa Basin both occur in the extreme north of their respective basins. It may not be a coincidence that these ~183 Ma strata only appear to occur in those regions closest to the contemporaneous Karoo LIP. If vast quantities of ash were ejected during Karoo LIP volcanism perhaps winds were unable to carry ejecta across Cape Mountains in the late Early Jurassic resulting in restricted Lower Jurassic volcaniclastic deposition in the northernmost basins of the southern Cape. Importantly, however the large majority of the extensive volcanism that constitutes the Karoo LIP is of mafic composition and the resulting volcanics very rarely contain any zircon as an accessory mineral constituent

(Svenson et al., 2012) raising doubts as to how zircon-rich ashes were distributed to the southern Cape. Rare silicic volcanism, zircon-bearing volcanism did occur at Lebombo at this time (Riley et al., 2004; Miller and Harris, 2005) and may be source for the lower Jurassic volcaniclastics of the Suurberg Group and at De Rust. Nevertheless, the volcaniclastic distribution patterns currently observed in the southern Cape could in the future be refined and adapted as new deposits are located. If significantly more volcaniclastic deposits are found in the east of the southern Cape that balance out the current skewed distribution, then this should not detract from the geochemical and zircon morphological arguments for a Patagonian and Antarctic Peninsula volcanic source during the Jurassic.

A distal origin for the volcaniclastics of the Uitenhage Group, and probably also for the Suurberg Group, is that the rifting of the southern Cape was not accompanied by volcanism at all. This is at odds with previous models of the rifting margin that incorporate incipient volcanism along structural weaknesses reactivated during extension (Lock et al., 1975; Dingle et al., 1983) and makes the setting quite unlike the Newark rift basins to which it is often compared (Lock et al., 1975). Instead, the Jurassic – Early Cretaceous rifting occurred at or closely after the Lower Jurassic Karoo and Ferrar LIPs, which were both centered near but not at the southern Cape site of rifting. Following this, volcanism picked up in the Antarctic Peninsula and Patagonia, on the opposite side of the Cape Fold Belt, in the Early–Middle Jurassic and migrated to the SW (Féraud et al., 1999; Pankhurst et al., 2000). The occurrence of volcanic centres on either side of the Cape Fold Belt but not evidenced in the basins of the southern Cape is probably because of the thickened lithosphere inherited from Permo-Triassic orogenesis-related compression (Lindeque, et al., 2011) prevented magma from rising to the surface (Marsh, 2016). Instead, the lithosphere below the Cape Fold Belt would have been heated, weakening lithosphere beneath the Cape Mountains in the Jurassic, and the presence of impinging asthenosphere probably also caused an uplifted topography (Thomson, 1999). These factors (detailed in section 5.4) may have contributed to the extensional regime experienced in the Jurassic long before the opening of the South Atlantic and initiation of the AFT.

In summary, the most likely provenance for the abundant volcaniclastics of the Uitenhage Group, especially in the western basins of the southern Cape, is the episodic Jurassic volcanism that occurred in the present-day Antarctic Peninsula and Patagonia. Wind-blow ejecta from these large eruptions supplied volcanic ash to the southern Cape during the deposition of the Uitenhage Group. However, the Lower Jurassic volcaniclastic beds in the Suurberg Group and near De Rust may equally have been delivered from the same distant source region or from silicic volcanism of the Karoo LIP. Cretaceous volcaniclastics of the Uitenhage Group predate the well-constrained Paraná-Etendeka LIP (Renne et al., 1996) and are more probably derived from the proto-Pacific subduction margin in southern Patagonia, which remained volcanically active into the Early Cretaceous (Féraud et al., 1999). It is likely that the volcanism that was common in the Jurassic of SW Gondwna affected the lithosphere in SW Gondwana and promoted an extensional stress regime, but there remains no evidence for incipient volcanism in the southern Cape during rifting and distal sources can adequately account for the numerous volcaniclastic deposits in the Uitenhage and Suurberg Groups.

Chapter 7: Conclusions

The findings presented in this thesis are a major contribution to the South African stratigraphic record and greatly improve understanding of the physical evolution of rifting during the breakup of Gondwana. This study also provides the first robust chronological framework upon which future investigations into the Jurassic – Cretaceous tectonics, landscape evolution and palaeoecology of SW Gondwana can be based. These contributions are each discussed in section 5.3, whereas in this short chapter the explicit assessment of whether the thesis achieves the aims stipulated in section 1.1 and its shortcomings. Following this, due to the time-sensitive nature of the data and findings presented throughout the thesis, a geological history of the Early Jurassic – Early Cretaceous is presented.

The first aim of this study is to locate and characterize the volcaniclastic deposits of the Uitenhage and Suurberg Groups. This was a successful endeavor, which builds on the previous work of Malan and Viljoen (1990), Viljoen (1992), who were the first geologists to map out the outcropping volcaniclastics in the Uitenhage Group during the 90's. These maps were used extensively but also several new deposits were located throughout the southern Cape. Volcaniclastic deposits are comparatively common in the Suurberg Group, although the limiting factor in locating adequate sampling locations there is the exposure quality. Fortunately, the work of Hill (1992) aided discoveries during fieldwork in the Algoa Basin. There also reports of volcaniclastic deposits in various historic literature, notably Rigassi and Dixon (1972) who claim that there are 'tuff bands' in the Lower Sundays River and in the lower parts of the Robberg Formation. On review of these sites no such deposits were found and neither field observations nor thin-sections produced from the suspected tuffaceous material yielded any sign of a volcanic origin and they were therefore not processed. Throughout the thesis, each sampled deposit is accompanied by a description of the outcrop and the nature of the volcaniclastic deposit. Where material was clearly mixed with clastic detritus (resedimented), the zircon age distribution was accordingly widespread, and therefore field observations were a good indication of whether the deposit was primary or not. Generally, but not always, the bentonites investigated in this study are of primary origin, while non-bentonitic units are resedimented.

Dating the zircons using the U-Pb system and LA-ICPMS and CA-TIMS techniques showed that both primary and mixed-origin volcaniclastics are common in the Uitenhage Group, and help establish the first ever ages for the syn-rift strata of the southern Cape (Chapter 5). Further, the age of the Suurberg Group was conclusively pinned to the Karoo and Ferrar LIPs at ~183 Ma for the first time based on the geochronological efforts detailed in Chapter 4. Not only is the Uitenhage Group considerably older than previous Late Jurassic – Early Cretaceous estimates (e.g., McMillan et al., 1997), but the group is long-lived, and spans a > 40 Ma depositional age range.

Finally, non-volcaniclastic deposits from key stratigraphic and fossiliferous deposits in the Uitenhage Group were sampled in an attempt to place the palaeontological findings in the Group into the U-Pb chronostratigraphic framework. This was moderately successful. In some instances, such as samples BRENS1 and OES1 in the Knysna and Oudtshoorn basins respectively, there were significant young zircons that helped pin-down constraints on the maximum depositional ages. This was not the case for the majority of terrigenous clastic deposits sampled, which instead contained no syn-depositional volcanic zircons and therefore had maximum depositional age constraints that were not useful beyond the already established Jurassic – Cretaceous ages established for the Uitenhage Group. The integration of these units into the chronostratigraphic framework has not been possible, although the new constraints established from the numerous primary volcaniclastics, and the new ages for the Suurberg Group do caution against a simple Late Jurassic – Early Cretaceous assumption for the age of the Kirkwood Formation in the Algoa Basin, because we know that rifting and deposition long-precedes this time.

7.1 Mesozoic geological history of the southern Cape:

180 – 170 Ma: There is new uncertainty with regard to the cessation of compression of the Cape Orogeny, the possibility that just one or two discrete periods of compression occurred (e.g., Blewett and Phillips, 2016; Hansma et al., 2016), which contrasts with the established episodic compressive regime (e.g., Hälbich, 1983; Gresse and Theron, 1992; Catuneanu et al., 1998). Nevertheless, by the late Early Jurassic Karoo and Ferrar Large igneous province events, SW Gondwana had switched into a regional extensional stress regime. This extension was probably caused by several combined factors: 1) the introduction of heat and topographic uplift during various volcanic events in SW Gondwana. Specifically, the large igneous provinces in the main Karoo Basin (Karoo LIP) and across Antarctica (Ferrar LIP), and silicic volcanic events in Patagonia and the Antarctic Peninsula (e.g., Féraud et al.,1999; Pankhurst et al., 2000; González et al., 2019); 2) the gravitational collapse of the Cape Orogeny; 3) possible far-field stress regime effects relating to the separation of East and West Gondwana. The extensional strain associated with this stress regime is centred at inherited weaknesses within the Cape Fold Belt that were reactivated as dip-slip normal faults, which followed the inherited structural orientations (Fouché et al., 1992; Paton, 2006). Initially, the faults were localized, and the first continental deposits (syn-rift 1) began to accumulate in the newly formed accommodation space (Fig. 7.1) overlying the basement rocks of principally the Cape Supergroup, but in places probably comprise the Karoo Supergroup (Dwyka Group in basement of the Robertson and Worcester basins) and the Suurberg Group in the northern Algoa Basin.

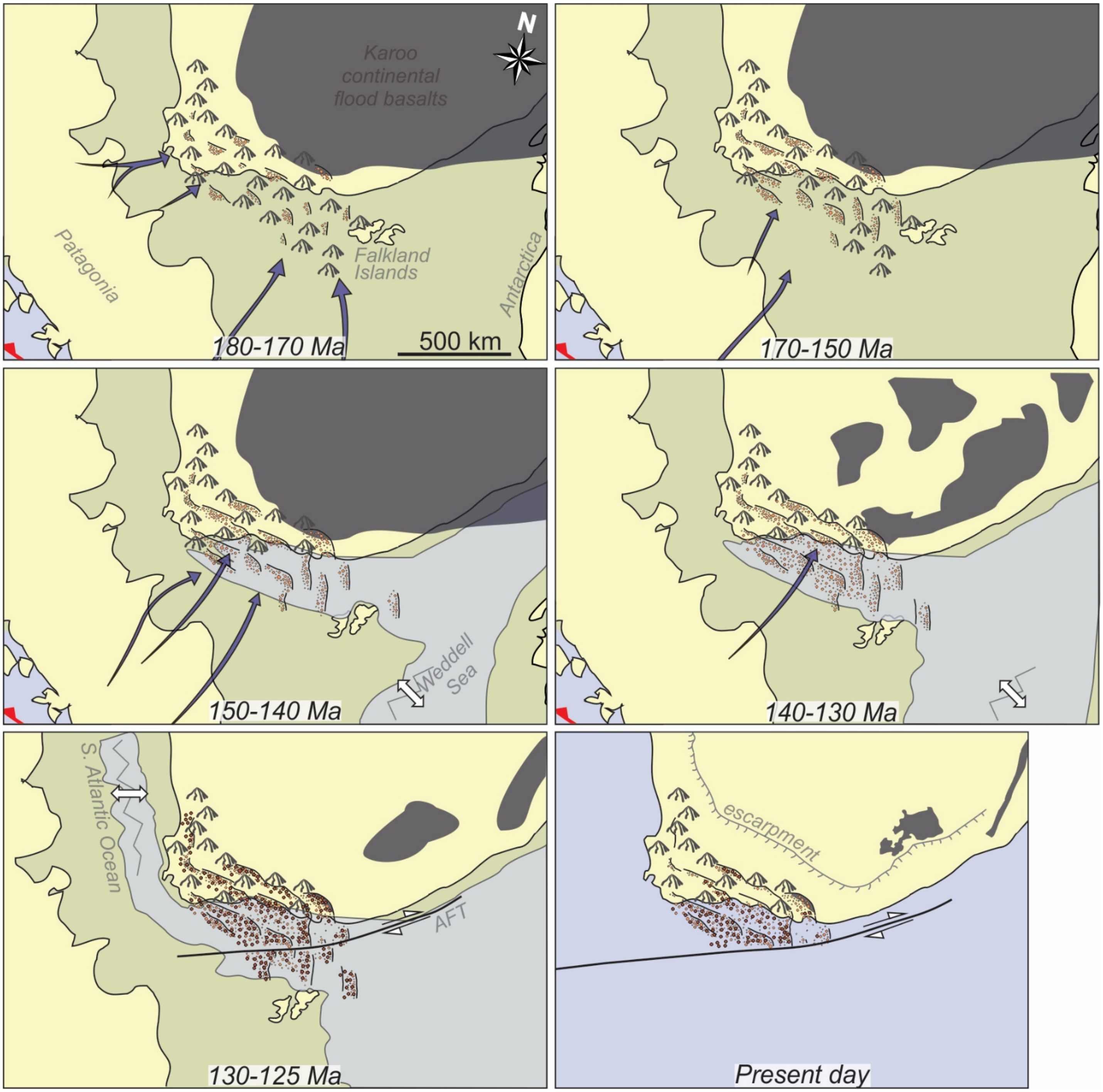

Fig. 7.1. Schematic illustration of the simplified geological evolution of the southern Cape in the Mesozoic from 180 Ma to present day. See text for details about each time period. Orange dots represent syn-rift 1 deposits and dark brown dots represent syn-rift 2 deposits. Blue arrows represent wind-blown ash input (see chapter 6 for details). Base map adopted from Jokat et al. (2013).

170 – 150 Ma: Normal faults continued to accumulate displacement and grew laterally resulting in vertical and lateral increases in accommodation space in which conglomerates, sandstones and mudstones of the Enon and Kirkwood formations were deposited (Fig. 7.1). Generally, steep gradients were maintained close to the scarp and therefore higher energy depositional environments existed there, whereas lower gradients and lower energy depositional environments were maintained distal from the fault scarps. Deposition in these settings was punctuated by wind-blown ash-fall deposition derived from violent silicic eruptions at volcanoes in Patagonia and the Antarctic Peninsula (e.g., Pankhurst et al., 2000).

150 – 140 Ma: As faults continued to grow through linkage (Paton, 2006) in the late Jurassic (Fig. 7.1), the first marine incursion events occurred in the southern Cape (Dingle, 1971; Jungslager, 1996), which caused the interruption of the purely continental deposition in the growing accommodation space. At this time the lowermost marine units in parts of the Bredasdorp Basin (Jungslager, 1996) and Bethelsdorp Member of the Kirkwood Formation in the Algoa Basin (McMillan, 2010; Muir et al., 2017b) were deposited. Marine deposition in other seaward basins also probably occurred at this time, such as the Pletmos, Gamtoos, Outeniqua, North Falkland and Falkland Plateau Basin. Conversely, continental deposition was maintained in the landward basins, in which the Enon and Kirkwood formations continued to be deposited. A second period of particularly large eruptions occurred in the region of Patagonia (e.g., Pankhurst et al., 2000), which supplied wind-blown ash across SW Gondwana and punctuated deposition in these basins – evidenced by the numerous Upper Jurassic volcaniclastic deposits in the Uitenhage Group. By the earliest Cretaceous the region was possiby in a period of tectonic quiescence (Jungslager, 1996).

140 Ma – 130 Ma: A second regional marine incursion occurred in which the Sundays River, Robberg and Brenton Formation sediments and their correlatives were deposited in the now large, interconnected rift basins (Fig. 7.1). It is unclear whether the same driving mechanisms that initiated extension were still causing fault-bound accommodation space to accumulate or if new extensional mechanisms had commenced (see Jungslager, 1996 and McMillan et al., 1997 for contrasting models).

~130 – 125 Ma: The South Atlantic began to open, which marks the separation of Africa from South America (Fig. 7.1). During this time movement along the AFT occurred and the southern Cape became a transverse margin. This new plate tectonic motion caused the reinvigoration of rifting in the southern Cape, renewed movement along preexisting boundary faults and increased denudation (e.g., Tinker et al., 2008b; Guillocheau; 2012; Wildman et al., 2015; Green et al., 2016). The sudden increase in accommodation space and steepened depositional gradients caused the shifting of depocentres (Paton and Underhill, 2004) and the deposition of Hauterivian deposits (syn-rift 2) atop the underlying, generally tilted Jurassic – Valanginian syn-rift 1 deposits. Deposition was marine where basins where inundated by the ocean (e.g., the southern Gamtoos Basin and the Bredasdorp Basin) and therefore syn-rift deposition was entirely marine there (Jungslager, 1996; McMillan et al., 1997; Paton and Underhill, 2004). Conversely, where basins were exposed on land, deposition of the Buffelskloof and Hartenbos formations occurred in continental and coastal/transitional marine settings.

post ~130 Ma: Subsequent to syn-rift 2 sedimentation, the basins of the southern Cape underwent periods of thermally-induced subsidence and deposition of sediments in what had become a passive margin setting. However, deposition was punctuated by periods of erosion or non-deposition controlled by relative sea level change and particularly intensive uplift in the Late Cretaceous (Tinker et al., 2008b; Guillocheau; 2012; Wildman et al., 2015; Green et al., 2016). Erosion of the southern Cape left remnants of once larger and probably continuous basins we have today, with varied stratigraphic levels of the syn-rift deposits exposed.

Chapter 8: References

Abebe, B., Acocella, V., Korme, T. and Ayalew, D., 2007. Quaternary faulting and volcanism in the Main Ethiopian Rift. Journal of African Earth Sciences, 48(2–3), 115–124.

Aide, R.J. ,1952. The position of the Falkland Islands in a reconstruction of Gondwananland. Geological Magazine 89, 401–410.

Almond, J.E., de Klerk,W.J. and Gess, R., 2009. Palaeontological heritage of the Eastern Cape. Interim SAHRA technical report, Natura Viva cc, Cape Town 51 p.

Alroy, J. (2010a). Geographical, environmental and intrinsic biotic controls on Phanerozoic marine diversification. Palaeontology 53, 1211–1235.

Andersen, T., Andersson, U.B., Graham, S., Åberg, G. and Simonsen, S.L., 2009. Granitic magmatism by melting of juvenile continental crust: new constraints on the source of Palaeoproterozoic granitoids in Fennoscandia from Hf isotopes in zircon. Journal of the Geological Society, 166(2), 233–247.

Baby, G., Guillocheau, F., Boulogne, C., Robin, C. and Dall'Asta, M., 2018. Uplift history of a transform continental margin revealed by the stratigraphic record: The case of the Agulhas transform margin along the Southern African Plateau. Tectonophysics, 731, 104–130.

Bamford, M.K., 1986. Aspects of the palaeoflora of the Kirkwood and Sundays River formations, Algoa Basin, South Africa. M.Sc. thesis, University of Witwatersrand, 160pp. (Unpublished).

Bangert, B., Stollhofen, H., Lorenz, V. and Armstrong, R., 1999. The geochronology and significance of ash-fall tuffs in the glaciogenic Carboniferous-Permian Dwyka Group of Namibia and South Africa. Journal of African Earth Sciences, 29 (1), 33–49.

Barham, M., Kirkland, C.L., Reynolds, S., O’Leary, M.J., Evans, N.J., Allen, H., Haines, P.W., Hocking, R.M., McDonald, B.J., Belousova, E. and Goodall, J., 2016. The answers are blowin’in the wind: Ultradistal ashfall zircons, indicators of Cretaceous super-eruptions in eastern Gondwana. Geology, 44(8), 643–646.

Belcher, C.M. and McElwain, J.C., 2008. Limits for combustion in low O2 redefine paleoatmospheric predictions for the Mesozoic. Science, 321(5893), 1197–1200.

Belcher, C.M., Yearsley, J.M., Hadden, R.M., McElwain, J.C. and Rein, G., 2010. Baseline intrinsic flammability of Earth's ecosystems estimated from paleoatmospheric oxygen over the past 350 million years. Proceedings of the National Academy of Sciences. DOI: 10.1073/pnas.1011974107

Belousova, E., Griffin, W.L., O'Reilly, S.Y. and Fisher, N.L., 2002. Igneous zircon: trace element composition as an indicator of source rock type. Contributions to mineralogy and petrology, 143(5), 602–622.

Belousova, E.A., Griffin, W.L. and O'reilly, S.Y., 2005. Zircon crystal morphology, trace element signatures and Hf isotope composition as a tool for petrogenetic modelling: examples from Eastern Australian granitoids. Journal of Petrology, 47(2), 329–353.

Ben-Avraham, Z., Hartnady, C.J.H. and Kitchin, K.A., 1997. Structure and tectonics of the Agulhas-Falkland fracture zone. Tectonophysics, 282(1–4), 83–98.

Ben-Avraham, Z., Hartnady, C.J.H. and Malan, J.A., 1993. Early tectonic extension between the Agulhas Bank and the Falkland Plate due to the rotation of the Lafonia microplate. Earth and Planetary Science Letters, 117, 43–58.

Benisek, A. and Finger, F., 1993. Factors controlling the development of prism faces in granite zircons: a microprobe study. Contributions to Mineralogy and Petrology, 114(4), 441–451.

Bergman, N.M., Lenton, T.M., Watson, A.J., 2004. COPSE: a new model of biogeochemical cycling over Phanerozoic time. American Journal of Science, 304, 397–437.

Berner, R.A., 2009. Phanerozoic atmospheric oxygen: new results using the GEOCARBSULF model. American Journal of Science, 309, 603–606.

Besse, J. and Courtillot, V., 2002. Apparent and true polar wander and the geometry of the geomagnetic field over the last 200 Myr. Journal of Geophysical Research: Solid Earth, 107(B11), pp. EPM-6.

Black L.P. and Gulson B.L., 1978. The age of the Mud Tank carbonatite, Strangways Range, Northern Territory. Bureau of Mineral Resources Journal of Australian Geology and Geophysics, 3, 227–232.

Blewett, S.C., Phillips, D., 2016. An overview of cape fold belt geochronology: implications for sediment provenance and the timing of orogenesis. In: Linol, B. and de Wit, M. (Eds.), Origin and Evolution of the Cape Mountains and Karoo Basin. Springer, pp. 45–55.

Bohor, B.F., Triplehorn, D.M., 1993. Tonsteins: altered volcanic-ash layers in coal-bearing sequences. Geological Society of America, Special Paper 285, 56 p.

Bond, W.J. and Scott, A.C., 2010. Fire and the spread of flowering plants in the Cretaceous. New Phytologist, 188(4), 1137–1150.

Booth, P.W.K., Shone, R.W., 1999. Complex thrusting at Uniondale, eastern sector of the Cape fold belt, Republic of South Africa: structural evidence for the need to revise the lithostratigraphy. Journal of African Earth Sciences 29, 125–133.

Bordy, E. M., America, T., 2016. Sedimentology of granite boulder conglomerates and associated clastics in the onshore section of the late Mesozoic Pletmos Basin (Western Cape, South Africa). Journal of African Earth Sciences 119, 67–77.

Bordy, E.M. and Abrahams, M., 2016. Geochemistry of the Pronksberg Bentonite of the Upper Elliot Formation (Early Jurassic), Eastern Cape, South Africa. In: Linol, B. and de Wit, M. (Eds.), Origin and Evolution of the Cape Mountains and Karoo Basin. Springer, pp. 119–127.

Bordy, E.M., Hancox, P.J. and Rubidge, B.S., 2004. Basin development during the deposition of the Elliot Formation (Late Triassic-Early Jurassic), Karoo Supergroup, South Africa. South African Journal of Geology, 107(3), 397–412.

Bowring, S.A. and Schmitz, M.D., 2003. High-precision U-Pb zircon geochronology and the stratigraphic record. Reviews in Mineralogy and Geochemistry, 53(1), 305–326.

Bowring, S.A., Erwin, D.H., Jin, Y.G., Martin, M.W., Davidek, K. and Wang, W., 1998. U/Pb zircon geochronology and tempo of the end-Permian mass extinction. Science, 280(5366), 1039–1045.

Bowring, S.A., Schoene, B., Crowley, J.L., Ramezani, J. and Condon, D.J., 2006. High-precision U-Pb zircon geochronology and the stratigraphic record: Progress and promise. The Paleontological Society Papers, 12, 25–45.

Broad, D.S., Jungslager, E.H.A., McLachlan, I.R., Roux, J. and Van der Spuy, D., 2012. South Africa's offshore Mesozoic basins. In: Roberts, D.G. and Bally, A.W. (Eds.), Regional Geology and Tectonics: Phanerozoic Passive Margins, Cratonic basins and Global Tectonic Maps, pp. 534–564.

Broom, R., 1904. V.—On the Occurrence of an Opisthocœlian Dinosaur (Algoasaurus Bauri) in the Cretaceous Beds of South Africa. Geological Magazine, 1(9), 445–447.

Brown, R.J., Bonadonna, C. and Durant, A.J., 2012. A review of volcanic ash aggregation. Physics and Chemistry of the Earth, Parts A/B/C, 45, 65–78.

Brown, S.A., Scott, A.C., Glasspool, I.J. and Collinson, M.E., 2012. Cretaceous wildfires and their impact on the Earth system. Cretaceous research, 36, 162–190.

Burgess, S. D., Bowring, S. A., Fleming, T. H., Elliot, D. H., 2015. High-precision geochronology links the Ferrar large igneous province with early-Jurassic ocean anoxia and biotic crisis. Earth and Planetary Science Letters 415, 90–99.

Burke, K., Steinberger, B., Torsvik, T.H. and Smethurst, M.A., 2008. Plume generation zones at the margins of large low shear velocity provinces on the core–mantle boundary. Earth and Planetary Science Letters, 265(1-2), 49–60.

Butler, R. J., Benson, R. B. J. & Barrett, P. M. (2013). Pterosaur diversity: untangling the influence of sampling biases, Lagerstätten, and genuine biodiversity signals. Palaeogeography, Palaeoclimatology, Palaeoecology 372, 78–87.

Carey, S. and Sigurdsson, H., 2000. Grain size of Miocene volcanic ash layers from Sites 998, 999, and 1000: Implications for source areas and dispersal. In Proceedings of the Ocean Drilling Program, Scientific Results, 165, 101–113.

Catuneanu, O., Hancox, P.J. and Rubidge, B.S., 1998. Reciprocal flexural behaviour and contrasting stratigraphies: a new basin development model for the Karoo retroarc foreland system, South Africa. Basin Research, 10(4), 417–439.

Catuneanu, O., Hancox, P.J. and Rubidge, B.S., 1998. Reciprocal flexural behaviour and contrasting stratigraphies: a new basin development model for the Karoo retroarc foreland system, South Africa. Basin Research, 10(4), 417–439.

Choiniere, J.N., Forster, C.A. and de Klerk, W.J., 2012. New information on Nqwebasaurus thwazi, a coelurosaurian theropod from the Early Cretaceous Kirkwood Formation in South Africa. Journal of African Earth Sciences, 71, 1–17.

Cloetingh, S.A.P.L., Lankreijer, A.C., de Wit, M.J. and Martinez, I., 1992. Subsidence history analysis and forward modelling of the Cape and Karoo Supergroups. In: De Wit, M.J., Ransome, I.G.D. (Eds.), Inversion Tectonics of the Cape Fold Belt. Karoo and Cretaceous basins of Southern Africa. A.A. Balkema, Rotterdam, pp. 239–249.

Cohen, K.M., Finney, S.C., Gibbard, P.L. and Fan, J.X., 2013 (updated). The ICS international chronostratigraphic chart. Episodes, 36(3), 199–204.

Cole, D.I., 1992. Evolution and development of the Karoo Basin. In: De Wit, M.J., Ransome, I.G.D. (Eds.), Inversion Tectonics of the Cape Fold Belt. A.A. Balkema, Rotterdam, pp. 87–99.

Cooper, M.R. 1983. The ammonite genus Umgazaniceras in the Sundays River Formation. Transactions of the Geological Society of South Africa, 86, 63–64.

Corfu, F., Hanchar, J.M., Hoskin, P.W. and Kinny, P., 2003. Atlas of zircon textures. Reviews in mineralogy and geochemistry, 53(1), 469–500.

Cox, K.G., 1992. Karoo igneous activity, and the early stages of the break-up of Gondwanaland. Geological Society, London, Special Publications, 68(1), 137–148.

Day, R.W., 1987. False Bay dolerites. Annals Geological Survey of South Africa, 21, 1-7.

de Assis Janasi, V., de Freitas, V.A. and Heaman, L.H., 2011. The onset of flood basalt volcanism, Northern Paraná Basin, Brazil: A precise U–Pb baddeleyite/zircon age for a Chapecó-type dacite. Earth and Planetary Science Letters, 302(1–2), 147–153.

De Beer, C.H., 1989. Structure of the Cape Fold Belt in the Ceres Syntaxis. Msc. Thesis, University of Stellenbosch (Unpublished).

De Beer, C.H., 1992. Structural evolution of the Cape Fold Belt syntaxis and its influence on syntectonic sedimentation in the SW Karoo Basin. In: De Wit, M.J., Ransome, I.G.D. (Eds.), Inversion Tectonics of the Cape Fold Belt. A.A. Balkema, Rotterdam, pp. 197–206.

De Klerk, W.J., Forster, C.A., Sampson, S.D., Chinsamy, A. and Ross, C.F., 2000. A new coelurosaurian dinosaur from the Early Cretaceous of South Africa. Journal of Vertebrate Paleontology, 20(2), 324–332.

D'Elia, L., Bilmes, A., Franzese, J.R., Veiga, G.D., Hernández, M. and Muravchik, M., 2015. Early evolution of the southern margin of the Neuquén Basin, Argentina: tectono-stratigraphic implications for rift evolution and exploration of hydrocarbon plays. Journal of South American Earth Sciences, 64, 42–57.

Dewey, J.F., 1988. Extensional collapse of orogens. Tectonics, 7(6), 1123–1139.

Dhuime, B., Hawkesworth, C.J., Cawood, P.A. and Storey, C.D., 2012. A change in the geodynamics of continental growth 3 billion years ago. Science, 335(6074), 1334–1336.

Dhuime, B., Wuestefeld, A. and Hawkesworth, C.J., 2015. Emergence of modern continental crust about 3 billion years ago. Nature Geoscience, 8(7), 552–555.

Dickinson, W.R. and Gehrels, G.E., 2009. Use of U–Pb ages of detrital zircons to infer maximum depositional ages of strata: a test against a Colorado Plateau Mesozoic database. Earth and Planetary Science Letters, 288(1-2), 115–125.

Dingle, R.V. and Klinger, H.C., 1971. Significance of Upper Jurassic sediments in the Knysna outlier (Cape Province) for timing of the breakup of Gondwanaland. Nature Physical Science, 232(28), 37.

Dingle, R.V., 1973. Mesozoic palaeogeography of the southern Cape, South Africa. Palaeogeography, Palaeoclimatology, Palaeoecology, 13(3), 203–213.

Dingle, R.V., Siesser, W.G. and Newton, A.R., 1983. Mesozoic and Tertiary geology of southern Africa. A.A. Balkema, Rotterdam, 375 pp.

Dinis, 2018. Sedimentology of the lower Uitenhage Group in the Middle to Late Mesozoic Oudtshoorn Basin, South Africa. MSc thesis, University of Cape Town (unpublished).

Dopico, C.I.M., Tohver, E., De Luchi, M.G.L., Wemmer, K., Rapalini, A.E. and Cawood, P.A., 2017. Jurassic cooling ages in Paleozoic to early Mesozoic granitoids of northeastern Patagonia: 40 Ar/39 Ar, 40 K–40 Ar mica and U–Pb zircon evidence. International Journal of Earth Sciences, 106(7), 2343–2357.

Du Plessis, P.G., 1947. Vlakteplaas Basin. Geological Survey of South Africa, unpublished report.

Du Preez, J.W., 1944. Lithology, structure and mode of deposition of the Cretaceous deposits in the Oudtshoorn area. Annals University of Stellenbosch 22A: 209-237.

Du Toit, 1974. Lithostratigraphy and correlation of rocks encountered in boreholes on the Agulhas Basnk, Republic of South Africa. Unpublished Soekor Report. 22 pp.

Du Toit, 1976. Mesozoic geology of the Agulhas Basnk, South Africa. PhD thesis, University of Cape Town, (Unpublished).

Duncan, R.A., Hooper, P.R., Rehacek, J., Marsh, J. and Duncan, A.R., 1997. The timing and duration of the Karoo igneous event, southern Gondwana. Journal of Geophysical Research: Solid Earth, 102(B8), 18,127–18,138.

Ebinger, C.J., Yemane, T., Woldegabriel, G., Aronson, J.L. and Walter, R.C., 1993. Late Eocene–Recent volcanism and faulting in the southern main Ethiopian rift. Journal of the Geological Society, 150(1), 99–108.

Encarnación, J., Fleming, T.H., Elliot, D.H. and Eales, H.V., 1996. Synchronous emplacement of Ferrar and Karoo dolerites and the early breakup of Gondwana. Geology, 24(6), 535–538.

Féraud, G., Alric, V., Fornari, M., Bertrand, H. and Haller, M., 1999. 40Ar/39Ar dating of the Jurassic volcanic province of Patagonia: migrating magmatism related to Gondwana break-up and subduction. Earth and Planetary Science Letters, 172(1–2), 83–96.

Fisher, R.V. and Schmincke, H.U., 1984. Submarine volcaniclastic rocks. In: Fisher, R.V. and Schmincke, H.U. (Eds.), Pyroclastic Rocks, Springer, pp. 265–296.

Föllmi, K.B., 2012. Early Cretaceous life, climate and anoxia. Cretaceous Research, 35, 230–257.

Forster, C. A., Farke, A. A., McCartney, J. A., De Klerk, W. J., Ross, C. F., 2009. A "basal" tetanuran from the Lower Cretaceous Kirkwood Formation of South Africa. Journal of Vertebrate Paleontology 29, 283–285.

Fouché, J., Bate, K.J. and Van de Merwe, R., 1992. Plate tectonic setting of the Mesozoic basins, southern offshore, South Africa: A review. In: De Wit, M.J., Ransome, I.G.D. (Eds.), Inversion Tectonics of the Cape Fold Belt. Karoo and Cretaceous basins of Southern Africa. A.A. Balkema, Rotterdam, pp. 33–48.

Franzese, J.R. and Spalletti, L.A., 2001. Late Triassic–early Jurassic continental extension in southwestern Gondwana: tectonic segmentation and pre-break-up rifting. Journal of South American Earth Sciences, 14(3), 257–270.

Fung, J.C.H., 1998. Effect of nonlinear drag on the settling velocity of particles in homogeneous isotropic turbulence. Journal of Geophysical Research: Oceans, 103(C12), 905–917.

Gaina, C., Torsvik, T.H., van Hinsbergen, D.J.J., Medvedev, S., Werner, S.C. and Labails, C., 2013. The African Plate: a history of oceanic crust accretion and subduction since the Jurassic. Tectonophysics, 604, 4–25.

Gehrels, G., 2011. Detrital zircon U-Pb geochronology: Current methods and new opportunities. In: Busby, C. and Azor, A. (Eds.), Tectonics of sedimentary basins: Recent advances, pp. 45–62.

Ghidella, M.E., Yáñez, G. and LaBrecque, J.L., 2002. Revised tectonic implications for the magnetic anomalies of the western Weddell Sea. Tectonophysics, 347(1–3), pp.65–86.

Glasspool, I.J. and Scott, A.C., 2010. Phanerozoic concentrations of atmospheric oxygen reconstructed from sedimentary charcoal. Nature Geoscience, 3(9), 627–630.

Gomez, B., Martxxnez-Delclos, X., Bamford, M. and Philippe, M., 2002. Taphonomy and palaeoecology of plant remains from the oldest African Early Cretaceous amber locality. Lethaia 35, 300–308.

González, V.R., Puigdomenech, C.G., Renda, E.M., Boltshauser, B., Somoza, R., Vizán, H., Zaffarana, C.B., Taylor, G.K., Haller, M. and Fernández, R., 2019. New paleomagnetic pole for the Upper Jurassic Chon Aike Formation of southern Argentina (South America): Testing the tectonic stability of Patagonia with respect to South America, and implications to Middle Jurassic-Early Cretaceous true polar wander. Tectonophysics, 750, 45–55.

Green, P.F., Duddy, I.R., Japsen, P., Bonow, J.M. and Malan, J.A., 2016. Post-breakup burial and exhumation of the southern margin of Africa. Basin Research, 29(1), 96–127.

Green, R.W.E. and Durrheim, R.J., 1990. A seismic refraction investigation of the Namaqualand Metamorphic Complex, South Africa. Journal of Geophysical Research: Solid Earth, 95(B12), 19927–19932.

Gresse, P.G. (compiler), 1997. Geological Map 3319 Worcester. 1:250 000 Geological Map Series, Geological Survey of South Africa.

Gresse, P.G. and Theron, J.N., 1992. Tectonic inversion and radiometric resetting of the basement in the Cape Fold Belt. In: De Wit, M.J., Ransome, I.G.D. (Eds.), Inversion tectonics of the Cape Fold Belt, Karoo and Cretaceous basins of Southern Africa. Balkema, Rotterdam, pp. 217 – 228.

Gröcke, D. R., Price, G. D., Ruffell, A. H., Mutterlose, J. and Baraboshkin, E., 2003. Isotopic evidence for Late Jurassic–Early Cretaceous climate change. Palaeogeography, Palaeoclimatology, Palaeoecology 202, 97–118.

Guillocheau, F., Rouby, D., Robin, C., Helm, C. and Rolland, N., 2012. Quantification and causes of the terrigeneous sediment budget at the scale of a continental margin: a new method applied to the Namibia-South Africa margin. Basin Research, 24(1), 3–30.

Gupta, S., Cowie, P.A., Dawers, N.H. and Underhill, J.R., 1998. A mechanism to explain rift-basin subsidence and stratigraphic patterns through fault-array evolution. Geology, 26(7), 595–598.

Gust, D.A., Biddle, K.T., Phelps, D.W. and Uliana, M.A., 1985. Associated Middle to Late Jurassic volcanism and extension in southern South America. Tectonophysics, 116(3-4), 223–253.

Hälbich, I.W., 1992. The Cape fold belt orogeny: State of the art 1970s–1980s. In: De Wit, M.J. and Ransome, I.G.D. (Eds.), Inversion tectonics of the Cape Fold Belt, Karoo and Cretaceous basins of southern Africa. Balkema, Rotterdam, pp. 141–158.

Hälbich, I.W., Fitch, F.J., Miller, J.A., 1983. Dating the Cape Orogeny. In: Söhnge, A.P.G. and Hälbich, I.W. (Eds.), Geodynamics of the Cape Fold Belt. The Geological Society of South Africa, Johannesburg, pp. 149–164.

Hallam, A., 1986. The Pliensbachian and Tithonian extinction events. Nature 319, 765–768.

Han, R., Ree, J.H., Cho, D.L., Kwon, S.T. and Armstrong, R., 2006. SHRIMP U–Pb zircon ages of pyroclastic rocks in the Bansong Group, Taebaeksan Basin, South Korea and their implication for the Mesozoic tectonics. Gondwana Research, 9(1–2), 106–117.

Hansma, J., Tohver, E., Schrank, C., Jourdan, F. and Adams, D., 2016. The timing of the Cape Orogeny: New $^{40}Ar/^{39}Ar$ age constraints on deformation and cooling of the Cape Fold Belt, South Africa. Gondwana Research, 32, 122–137.

Harley, S.L. and Kelly, N.M., 2007. Zircon tiny but timely. Elements, 3(1), 13–18.

Hart, R.J., Andreoli, M.A., Tredoux, M., Moser, D., Ashwal, L.D., Eide, E.A., Webb, S.J. and Brandt, D., 1997. Late Jurassic age for the Morokweng impact structure, southern Africa. Earth and Planetary Science Letters, 147(1–4), 25–35.

Haughton, S.H., 1928. The geology of the country between Grahamstown and Port Elizabeth: Explanation of Cape Sheet 9 (Port Elizabeth), Geological Survey of South Africa, 50 pp.

Haupt, T. 2018. Palaeoenvironmental change from the Hettangian to the Toarcian in Moyeni (Quthing District), southwestern Lesotho. MSc thesis, University of Cape Town (unpublished).

Hawkesworth, C.J. and Kemp, A.I.S., 2006. Using hafnium and oxygen isotopes in zircons to unravel the record of crustal evolution. Chemical Geology, 226(3–4), 144–162.

He, T., Lamont, B.B. and Manning, J., 2016. A Cretaceous origin for fire adaptations in the Cape flora. Scientific Reports, 6, 34880.

Hervé, F., Miller, H. and Pimpirev, C., 2006. Patagonia–Antarctica connections before Gondwana break-up. In: Fütterer, D.K., Damaske, D., Kleinschmidt, G., Miller, H. and Tessensohn, F. (Eds.), Antarctica. Springer, Berlin, Heidelberg, pp. 217–227.

Hiess, J., Condon, D.J., McLean, N. and Noble, S.R., 2012. $^{238}U/^{235}U$ systematics in terrestrial uranium-bearing minerals. Science, 335(6076), 1610–1614.

Hill, R.S., 1972. The Geology of the Northern Algoa Basin, Port Elizabeth. M.Sc. thesis. University of Stellenbosch (unpublished).

Hölzforster, F., 2007. Lithology and depositional environments of the Lower Jurassic Clarens Formation in the Eastern Cape, South Africa. South African Journal of Geology, 110(4), 543–560.

Horstwood, M.S.A., Košler, J., Gehrels, G., Jackson, S.E., McLean, N.M., Paton, C., Pearson, N.J., Sircombe, K., Sylvester, P., Vermeesch, P., Bowring, J.F., Condon, D.J., Schoene, B., 2016, Community-

Derived Standards for LA-ICP-MS U-(Th-)Pb Geochronology – Uncertainty Propagation, Age Interpretation and Data Reporting, Geostandards and Geoanalytical Research, 40, 3, 301–332.

Howell, J.A., Schwarz, E., Spalletti, L.A. and Veiga, G.D., 2005. The Neuquén basin: an overview. Geological Society, London, Special Publications, 252(1), 1–14.

Imai, N., Terashima, S., Itoh, S. and Ando, A., 1995. 1994 compilation values for GSJ reference samples, Igneous rock series. Geochemical Journal, 29(1), 91–95.

Ireland, T.R. and Williams, I.S., 2003. Considerations in zircon geochronology by SIMS. Reviews in mineralogy and geochemistry, 53(1), 215–241.

Jackson, S.E., Pearson, N.J., Griffin, W.L. and Belousova, E.A., 2004. The application of laser ablation-inductively coupled plasma-mass spectrometry to in situ U–Pb zircon geochronology. Chemical Geology, 211(1-2), 47–69.

Jackson, S.E., Pearson, N.J., Griffin, W.L., Belousova, E.A., 2004, The application of laser ablation-inductively coupled plasma-mass spectrometry to in situ U-Pb zircon geochronology, Chemical Geology, 211, 47–69.

Jaffey, A.H., Flynn, K.F., Glendenin, L.E., Bentley, W.T. and Essling, A.M., 1971. Precision measurement of half-lives and specific activities of U 235 and U 238. Physical Review C, 4(5), 1889–1906.

Jochum, K.P., Weis, U., Schwager, B., Stoll, B., Wilson, S.A., Haug, G.H., Andreae, M.O. and Enzweiler, J., 2016. Reference values following ISO guidelines for frequently requested rock reference materials. Geostandards and Geoanalytical Research, 40(3), 333–350.

Johnson, 1987. Guidelines for the standardized lithostratigraphic descriptions. South African Committee for stratigraphy (SACS). Circular 1, 19 pp.

Johnston, S.T., 2000. The Cape Fold Belt and Syntaxis and the rotated Falkland Islands: dextral transpressional tectonics along the southwest margin of Gondwana. Journal of African Earth Sciences, 31(1), 51–63.

Jokat, W., Boebel, T., König, M. and Meyer, U., 2003. Timing and geometry of early Gondwana breakup. Journal of Geophysical Research: Solid Earth, 108(B9).

Jones, M.T., Eliassen, G.T., Shephard, G.E., Svensen, H.H., Jochmann, M., Friis, B., Augland, L.E., Jerram, D.A. and Planke, S., 2016. Provenance of bentonite layers in the Palaeocene strata of the Central Basin, Svalbard: implications for magmatism and rifting events around the onset of the North Atlantic Igneous Province. Journal of Volcanology and Geothermal Research, 327, 571–584.

Joubert, P. and Johnson, M.R. 1998. Abridged lexicon of South African stratigraphy. South African Committee for Stratigraphy (SACS), Council for Geoscience, Pretoria, 160 pp.

Joubert, P. and Johnson, M.R., 1998. Abridged Lexicon of South African Stratigraphy. South African Committee for Stratigraphy, Council for Geosciences, Pretoria.

Jungslager, E.H.A., 1996. Geological evaluation of the remaining prospectivity for oil and gas of the pre-1At1 “synrift” succession in Block 9, Republic of South Africa. Unpubl. SOEKOR Rep.

Karlstrom, K., Hagadorn, J., Gehrels, G., Matthews, W., Schmitz, M., Madronich, L., Mulder, J., Pecha, M., Giesler, D. and Crossey, L., 2018. Cambrian Sauk transgression in the Grand Canyon region redefined by detrital zircons. Nature Geoscience, 438–443.

Kent, D.V. and Irving, E., 2010. Influence of inclination error in sedimentary rocks on the Triassic and Jurassic apparent pole wander path for North America and implications for Cordilleran tectonics. Journal of Geophysical Research: Solid Earth, 115(B10103).

Kent, D.V., Olsen, P.E. and Muttoni, G., 2017. Astrochronostratigraphic polarity time scale (APTS) for the Late Triassic and Early Jurassic from continental sediments and correlation with standard marine stages. Earth-Science Reviews, 166, 153–180.

Ketzer, J.M., Morad, S., Evans, R. and Al-Aasm, I.S., 2002. Distribution of diagenetic alterations in fluvial, deltaic, and shallow marine sandstones within a sequence stratigraphic framework: evidence from the Mullaghmore Formation (Carboniferous), NW Ireland. Journal of Sedimentary Research, 72(6), 760–774.

Kirstein, L.A., 1997. Magmatism in southern Uruguay and the early rifting of the South Atlantic. Ph.D. thesis, The Open University (unpublished).

Kitchin, F.L., 1908. The invertebrate fauna and palaeontological relations of the Uitenhage Series. Annuls of South African Museum, 7, 21–250.

Koeberl, C., Armstrong, R.A. and Uwe Reimold, W., 1997. Morokweng, South Africa: A large impact structure of Jurassic-Cretaceous boundary age. Geology, 25(8), 731–734.

Königer, S. and Stollhofen, H., 2001. Environmental and tectonic controls on preservation potential of distal fallout ashes in fluvio-lacustrine settings: the Carboniferous–Permian Saar–Nahe Basin, south-west Germany. In: White, J.D.L. and Riggs, N.R. (Eds.), Volcaniclastic sedimentation in lacustrine settings, Blackwell Science, pp. 263–284.

Koopmann, H., Franke, D., Schreckenberger, B., Schulz, H., Hartwig, A., Stollhofen, H. and di Primio, R., 2014. Segmentation and volcano-tectonic characteristics along the SW African continental margin, South Atlantic, as derived from multichannel seismic and potential field data. Marine and Petroleum Geology, 50, 22–39.

Košler, J. and Sylvester, P.J., 2003. Present trends and the future of zircon in geochronology: laser ablation ICPMS. Reviews in mineralogy and geochemistry, 53(1), 243–275.

Lamont, B.B. and He, T., 2012. Fire-adapted Gondwanan angiosperm floras evolved in the Cretaceous. BMC Evolutionary Biology, 12, 223.

Landing, E., Bowring, S.A., Davidek, K.L., Westrop, S.R., Geyer, G. and Heldmaier, W., 1998. Duration of the Early Cambrian: U-Pb ages of volcanic ashes from Avalon and Gondwana. Canadian Journal of Earth Sciences, 35(4), 329–338.

Landing, E., Bowring, S.A., Davidek, K.L., Westrop, S.R., Geyer, G. and Heldmaier, W., 1998. Duration of the Early Cambrian: U-Pb ages of volcanic ashes from Avalon and Gondwana. Canadian Journal of Earth Sciences, 35(4), 329–338.

Lawton, T.F. and Bradford, B.A., 2011. Correlation and provenance of Upper Cretaceous (Campanian) fluvial strata, Utah, USA, from zircon U-Pb geochronology and petrography. Journal of Sedimentary Research, 81(7), 495–512.

Le Bas, M.L., Maitre, R.L., Streckeisen, A. and Zanettin, B. 1986. A chemical classification of volcanic rocks based on the total alkali-silica diagram. Journal of Petrology, 27(3), 745–750.

Legarreta, L. and Uliana, M.A., 1999. El Jurásico y Cretácico de la Cordillera Principal y la Cuenca Neuquina. Geología Argentina (Caminos, R.; editor). Servicio Geológico Minero Argentino, Anales, 29(16), 399–416.

Lindeque, A., de Wit, M.J., Ryberg, T., Weber, M. and Chevallier, L., 2011. Deep crustal profile across the southern Karoo Basin and Beattie Magnetic Anomaly, South Africa: an integrated interpretation with tectonic implications. South African Journal of Geology, 114(3–4), 265–292.

Linol, B. and de Wit, M.J., 2016. Origin and Evolution of the Cape Mountains and Karoo Basin. Springer. pp. 193.

Lock, B.E., 1980. Flat-plate subduction and the Cape Fold belt of South Africa. Geology, 8(1), 35–39.

Lock, B.E., Shone, R., Coates, A.T. and Hatton, C.J., 1975. Mesozoic Newark-Type sedimentary basins within the Cape Fold Belt of South Africa. Proceedings of the 9th International Congress of Sedimentology, Nice, 2, 217–225.

Lovecchio, J.P., Rohais, S., Joseph, P., Bolatti, N.D., Kress, P.R., Gerster, R. and Ramos, V.A., 2018. Multistage rifting evolution of the Colorado basin (offshore Argentina): Evidence for extensional settings prior to the South Atlantic opening. Terra Nova, 30(5), 359–368.

Ludwig, K.R., 2000. Isoplot/Ex, A geochronological tool kit for Microsoft Excel version 2.2. Berkeley Geochronology Center, Special Publication 1a.

Maas, R., Kinny, P.D., Williams, I.S., Froude, D.O. and Compston, W., 1992. The Earth's oldest known crust: a geochronological and geochemical study of 3900–4200 Ma old detrital zircons from Mt. Narryer and Jack Hills, Western Australia. Geochimica et Cosmochimica Acta, 56(3), 1281–1300.

Macdonald, D., Gomez-Perez, I., Franzese, J., Spalletti, L., Lawver, L., Gahagan, L., Dalziel, I., Thomas, C., Trewin, N., Hole, M. and Paton, D., 2003. Mesozoic break-up of SW Gondwana: implications for regional hydrocarbon potential of the southern South Atlantic. Marine and Petroleum Geology, 20(3–4), 287–308.

Macdonald, D., Gomez-Perez, I., Franzese, J., Spalletti, L., Lawver, L., Gahagan, L., Dalziel, I., Thomas, C., Trewin, N., Hole, M. and Paton, D., 2003. Mesozoic break-up of SW Gondwana: implications for regional hydrocarbon potential of the southern South Atlantic. Marine and Petroleum Geology, 20(3–4), 287–308.

Makhubele, M.H and Bordy, E.M. 2018. Sequence stratigraphy of the post-Jurassic in the Algoa and Gamtoos basins: Implication for hydrocarbon potential in the Eastern Cape, South Africa. 2018 AAPG ICE Conference, Cape Town, Poster presentation.

Malan, J.A. (compiler), 1993. Geological Map 3420 Riversdale. 1:250 000 Geological Map Series, Geological Survey of South Africa.

Malan, J.A. and Viljoen, J.H.A., 1990. Mesozoic and Cenozoic geology of the Cape South Coast. Guidebook Geocongress '90, Geological Society of South Africa, PO3, 81 pp.

Malan, J.A. and Viljoen, J.H.A., 2016. Southern Cape Geology: Evolution of a rifted margin. Field Trip Guide, 35th International Geological Congress, Cape Town, Post11, 64 pp.

Malan, J.A., Viljoen, J.H.A., Siegfried, H.P. and Wickens, H. de V., 1994. Die geologie van die gebied Riversdale: Explanation of sheet 3420 Riversdale, Council for Geoscience, 63 pp.

Mannion, P.D., Upchurch, P., Carrano, M.T. and Barrett, P.M., 2011. Testing the effect of the rock record on diversity: a multidisciplinary approach to elucidating the generic richness of sauropodomorph dinosaurs through time. Biological Reviews, 86(1), 157–181.

Marsh, J.S., Lock, B.E. and Fuchter, W.H., 1979. New chemical analyses of the Suurberg volcanic rocks and their significance in relation to Mesozoic volcanism in southern Africa. South African Journal of Science, 75(5), 227–229.

Marsh, J.S., Lock, B.E. and Fuchter, W.H., 1979. New Chemical Analyses of the Suurberg Volcanic Rocks and Their Significance in Relation to Mesozoic Volcanism in Southern Africa. South African Journal of Science, 75, 227–229.

Marsh, J.S.G., 2016. New Evidence for the Correlation of Basalts of the Suurberg Group with the Upper Part of the Karoo Basalt Sequence of Lesotho. In: Linol, B. and de Wit, M. (Eds.) Origin and Evolution of the Cape Mountains and Karoo Basin, Springer, pp.59–65.

Marshall, J.E.A., 1994. The Falkland Islands: a key element in Gondwana paleogeography. Tectonics, 13(2), 499–514.

Martin, A.K. and Hartnady, C.J.H., 1986. Plate tectonic development of the South West Indian Ocean: a revised reconstruction of East Antarctica and Africa. Journal of Geophysical Research: Solid Earth, 91(B5), 4767–4786.

Martin, A.K., Hartnady, C.J. and Goodlad, S.W., 1981. A revised fit of South America and south central Africa. Earth and Planetary Science Letters, 54(2), 293–305.

Martin, U. and Nemeth, K., 2007. Practical volcanology-Lecture notes for understanding volcanic rocks from field based studies. Occasional Papers of the Geological Institute of Hungary, 207, pp. 221.

Mattinson, J.M., 2010. Analysis of the relative decay constants of 235U and 238U by multi-step CA-TIMS measurements of closed-system natural zircon samples. Chemical Geology, 275(3–4), 186–198.

McClintock, M., Marsh, J.S. and White, J.D., 2008. Compositionally diverse magmas erupted close together in space and time within a Karoo flood basalt crater complex. Bulletin of Volcanology, 70(8), 923–946.

McDonough, W.F. and Sun, S.S., 1995. The composition of the Earth. Chemical geology, 120(3–4), 223–253.

McKay, M.P., Weislogel, A.L., Fildani, A., Brunt, R.L., Hodgson, D.M. and Flint, S.S., 2015. U-PB zircon tuff geochronology from the Karoo Basin, South Africa: implications of zircon recycling on stratigraphic age controls. International Geology Review, 57(4), 393–410.

McLachlan, I.R. and McMillan, I.K., 1976. Review and stratigraphic significance of southern Cape Mesozoic palaeontology. Transactions of the Geological Society of South Africa, 79, 197–212.

McLachlan, I.R. and McMillan, I.K., 1979. Microfaunal biostratigraphy, chronostratigraphy and history of Mesozoic and Cenozoic deposits on the coastal margin of South Africa. Geological Society of South Africa Special Publication, 6, 161–181.

McLachlan, I.R., Brenner, P.W. and McMillan, I.K., 1976. The Stratigraphy and Micropalaeontology of the Cretaceous Brenton Formation and the PB-A/1 well, near Knysna, Cape Province. Transaction of the Geological Society of South Africa, 79, 341–370.

McMillan, I.K., 2003. The Foraminifera of the Late Valanginian to Hauterivian (Early Cretaceous) Sundays River Formation of the Algoa Basin, Eastern Cape Province, South Africa. Annals of the South Africa Museum, 106, 1–274.

McMillan, I.K., 2010. The Foraminifera of the Portlandian (Late Jurassic) Bethelsdorp Formation of the onshore Algoa Basin, Eastern Cape Province. Les Rosalines Press, Clovelly, 176 pp.

McMillan, I.K., Brink, G.I., Broad, D.S. and Maier, J.J., 1997. Late Mesozoic sedimentary basins off the south coast of South Africa. In: Selley, R.C. (Ed.), Sedimentary basins of the World, Elsevier, 3, pp. 319–376.

McPhee, B.W., Mannion, P.D., de Klerk, W.J. and Choiniere, J.N., 2016. High diversity in the sauropod dinosaur fauna of the Lower Cretaceous Kirkwood Formation of South Africa: implications for the Jurassic – Cretaceous transition. Cretaceous Research, 59, 228–248.

Milani, E.J. and De Wit, M.J., 2008. Correlations between the classic Paraná and Cape–Karoo sequences of South America and southern Africa and their basin infills flanking the Gondwanides: du Toit revisited. Geological Society, London, Special Publications, 294(1), 319–342.

Miller, J.A. and Harris, C., 2006. Petrogenesis of the Swaziland and northern Natal rhyolites of the Lebombo rifted volcanic margin, south east Africa. Journal of Petrology, 48(1), 185–218.

Moore, G.T., Hayashida, D.N., Ross, C.A. and Jacobson, S.R., 1992. Paleoclimate of the Kimmeridgian/Tithonian (Late Jurassic) world: I. Results using a general circulation model. Palaeogeography, Palaeoclimatology, Palaeoecology, 93(1–2), 113–150.

Mosquera, A. and Ramos, V.A., 2006. Intraplate deformation in the Neuquén Embayment. In: Kay, S.M. and Ramos, V.A. (Eds.), Evolution of an Andean margin: A tectonic and magmatic view from the Andies to the Neuquén Basin (35º–39ºS lat). Geological Society of America Special Paper 407, pp. 97–123.

Moulin, M., Fluteau, F., Courtillot, V., Marsh, J., Delpech, G., Quidelleur, X. and Gérard, M., 2017. Eruptive history of the Karoo lava flows and their impact on early Jurassic environmental change. Journal of Geophysical Research: Solid Earth, 122(2), 738–772.

Muir, R.A., Bordy, E.M. and Prevec, R., 2015. Lower Cretaceous deposit reveals first evidence of a post-wildfire debris flow in the Kirkwood Formation, Algoa Basin, Eastern Cape, South Africa. Cretaceous Research, 56, 161–179.

Muir, R.A., Bordy, E.M., Reddering, J.S.V. and Viljoen, J.H.A., 2017a. Lithostratigraphy of the Enon Formation (Uitenhage Group), South Africa. South African Journal of Geology 2017, 120(2), 273–280.

Muir, R.A., Bordy, E.M., Reddering, J.S.V. and Viljoen, J.H.A. 2017b. Lithostratigraphy of the Kirkwood Formation (Uitenhage Group), including the Bethelsdorp, Colchester and Swartkops members, South Africa. South African Journal of Geology 120(2), 281–293.

Mundil, R., Ludwig, K.R., Metcalfe, I. and Renne, P.R., 2004. Age and timing of the Permian mass extinctions: U/Pb dating of closed-system zircons. Science, 305(5691), 1760–1763.

Nasdala, L., Hofmeister, W., Norberg, N., Martinson, J.M., Corfu, F., Dörr, W., Kamo, S.L., Kennedy, A.K., Kronz, A., Reiners, P.W. and Frei, D., 2008. Zircon M257-a homogeneous natural reference material for the ion microprobe U-Pb analysis of zircon. Geostandards and Geoanalytical Research, 32(3), 247–265.

Navarrete, C., Gianni, G., Echaurren, A., Kingler, F.L. and Folguera, A., 2016. Episodic Jurassic to lower Cretaceous intraplate compression in Central Patagonia during Gondwana breakup. Journal of Geodynamics, 102, 185–201.

Newton, 1992. Thrusting on the northern margin of the Cape Fold Belt, near Laingsburg. In: e Wit, M.J. and Ransome, I.G.D. (Eds.), Inversion tectonics of the Cape Fold Belt, Karoo and Cretaceous basins of southern Africa, pp. 193–195.

Olsen, P.E., 1997. Stratigraphic record of the early Mesozoic breakup of Pangea in the Laurasia-Gondwana rift system. Annual Review of Earth and Planetary Sciences, 25(1), 337–401.

Olsen, P.E., Kent, D.V., Cornet, B., Witte, W.K. and Schlische, R.W., 1996. High-resolution stratigraphy of the Newark rift basin (early Mesozoic, eastern North America). Geological Society of America Bulletin, 108(1), 40–77.

Pángaro, F., Ramos, V.A. and Pazos, P.J., 2016. The Hesperides basin: a continental-scale upper Palaeozoic to Triassic basin in southern Gondwana. Basin Research, 28(5), 685–711.

Pankhurst, R.J. and Rapela, C.R., 1995. Production of Jurassic rhyolite by anatexis of the lower crust of Patagonia. Earth and Planetary Science Letters, 134(1–2) 23–36.

Pankhurst, R.J., Leat, P.T., Sruoga, P., Rapela, C.W., Márquez, M., Storey, B.C. and Riley, T.R., 1998. The Chon Aike province of Patagonia and related rocks in West Antarctica: a silicic large igneous province. Journal of volcanology and geothermal research, 81(1–2), 113–136.

Pankhurst, R.J., Rapela, C.W., Fanning, C.M. and Márquez, M., 2006. Gondwanide continental collision and the origin of Patagonia. Earth-Science Reviews, 76(3–4), 235–257.

Pankhurst, R.J., Riley, T.R., Fanning, C.M. and Kelley, S.P., 2000. Episodic silicic volcanism in Patagonia and the Antarctic Peninsula: chronology of magmatism associated with the break-up of Gondwana. Journal of Petrology, 41(5), 605–625.

Parrish, R.R., Parrish, R.R. and Noble, S.R., 2003. Zircon U-Th-Pb geochronology by isotope dilution—thermal ionization mass spectrometry (ID-TIMS). Reviews in Mineralogy and Geochemistry, 53(1), 183–213.

Parsiegla, N., Stankiewicz, J., Gohl, K., Ryberg, T. and Uenzelmann-Neben, G., 2009. Southern African continental margin: Dynamic processes of a transform margin. Geochemistry, Geophysics, Geosystems, 10(3).

Paton, C., Hellstrom, J., Paul, B., Woodhead, J., Hergt, J., 2011, Iolite: freeware for the visualisation and processing of mass spectrometric data, J. Anal. At. Spectrom., 26, 2508–2518.

Paton, D.A., 2006. Influence of crustal heterogeneity on normal fault dimensions and evolution: southern South Africa extensional system. Journal of Structural Geology, 28, 868–886.

Paton, D.A., Underhill, J.R., 2004. Role of crustal anisotropy inmodifying the structural and sedimentological evolution of extensional basins: the Gamtoos Basin, South Africa. Basin Res. 16, 339–359.

Pearce JA, Harris NBW, Tindle AG (1984) Trace element discrimination diagrams for the tectonic interpretation of granitic rocks. J Petrol 25:956–983.

Pearce, J.A., Harris, N.B. and Tindle, A.G., 1984. Trace element discrimination diagrams for the tectonic interpretation of granitic rocks. Journal of petrology, 25(4), 956–983.

Petrus, J.A., Kamber, B.S., 2012, VizualAge: A Novel Approach to Laser Ablation ICP-MS U-Pb Geochronology Data Reduction, Geostandards and Geoanalytical Research, 36, 247–270.

Pitts, B., Maher, M.J., De Beer, J.H., Gough, D.I., 1992. Interpretation of magnetic, gravity and magnetotelluric data across the Cape Fold Belt and Karoo Basin. In: De Wit, M.J. and Ransome, I.D.G. (Eds.) Inversion tectonics of the cape fold belt, Karoo and cretaceous basins of Southern Africa, 27–32.

Pupin, J.P. and Turco, G., 1972. Le zircon accessoire en géothermométrie. CR Acad. Sci. Paris, 274(2), 212-214.

Pupin, J.P., 1980. Zircon and granite petrology. Contributions to Mineralogy and Petrology, 73(3), 207-220.

Pyle, D.M., 1989. The thickness, volume and grainsize of tephra fall deposits. Bulletin of Volcanology, 51(1), pp.1-15.

Pysklywec, R.N. and Mitrovica, J.X., 1999. The role of subduction-induced subsidence in the evolution of the Karoo Basin. The Journal of geology, 107(2), 155–164.

Ramos, V.A., Mosquera, A., Folguera, A. and García Morabito, E., 2011. Evolución tectónica de los Andes y del Engolfamiento Neuquino adyacente. In Geología y Recursos Naturales de la Provincia de Neuquén. Relatorio del VXIII Congreso Geológico Argentino, Buenos Aires, 335–348.

Reddering, J.S.V., 2000. Sedimentary facies, sequences and depositional environments of the Mesozoic Robberg formation in its type area, South Africa. Council for Geoscience Bulletin 126, 212 pp.

Reddering, J.S.V., 2003. Lithostratigraphy of the Robberg formation(Uitenhage group), including the St Sebastian point member. Lithostratigraphic series. 18 pp.

Reid, M.R. and Coath, C.D., 2000. In situ U-Pb ages of zircons from the Bishop Tuff: No evidence for long crystal residence times. Geology, 28(5), 443–446.

Reid, M.R., Coath, C.D., Harrison, T.M. and McKeegan, K.D., 1997. Prolonged residence times for the youngest rhyolites associated with Long Valley Caldera: ^{230}Th–^{238}U ion microprobe dating of young zircons. Earth and Planetary Science Letters, 150(1), 27–39.

Reid., D.L., Erlank, A.J. and Rex, D.C, 1991. Age and correlation of the False Bay dolerite dyke swarm, south-western Cape, Cape Province. South African Journal of Geology, 94, 155–158.

Renne, P.R., Glen, J.M., Milner, S.C. and Duncan, A.R., 1996. Age of Etendeka flood volcanism and associated intrusions in southwestern Africa. Geology, 24 (7): 659–662.

Rex, D.C., 1991. Age and correlation of the False Bay dolerite dyke swarm, south-western Cape, Cape Province. South African Jounral of Geology, 94(2–3) 155–158.

Rey, P., Vanderhaeghe, O. and Teyssier, C., 2001. Gravitational collapse of the continental crust: definition, regimes and modes. Tectonophysics, 342(3–4), 435–449.

Rich, T.H.V., Molnar, R.E. and Rich, P.V., 1983. Fossil vertebrates from the Late Jurassic or Early Cretaceous Kirkwood Formation, Algoa Basin, Southern Africa. Transactions of the Geological Society of South Africa, 86(3), 281–291.

Richards, P.C., Gatliff, R.W., Quinn, M.F. and Fannin, N.G.T., 1996. Petroleum potential of the Falkland Islands offshore area. Journal of Petroleum Geology, 19(2), 161–182.

Richards, P.C., Stone, P., Kimbell, G.S., McIntosh, W.C. and Phillips, E.R., 2013. Mesozoic magmatism in the Falkland Islands (South Atlantic) and their offshore sedimentary basins. Journal of Petroleum Geology, 36(1), 61–73.

Richardson, J.C., Hodgson, D.M., Paton, D., Craven, B., Rawcliffe, A. and Lang, A., 2017. Where is my sink? Reconstruction of landscape development in southwestern Africa since the Late Jurassic. Gondwana Research 45, 43–64.

Riel, N., Jaillard, E., Martelat, J.E., Guillot, S. and Braun, J., 2018. Permian-Triassic Tethyan realm reorganization: Implications for the outward Pangea margin. Journal of South American Earth Sciences, 81, 78–86.

Rigassi, D.A. and Dixon, G.E., 1972. Cretaceous of the Cape Province, Republic of South Africa. In: Dessauvagie, T.F.J., Whiteman, A.J. (Eds.), African Geology. Geology Department, University of Ibadan, Nigeria, pp. 513–527

Riley, T.R., Leat, P.T., Pankhurst, R.J. and Harris, C., 2001. Origins of large volume rhyolitic volcanism in the Antarctic Peninsula and Patagonia by crustal melting. Journal of petrology, 42(6), 1043–1065.

Riley, T.R., Millar, I.L., Watkeys, M.K., Curtis, M.L., Leat, P.T., Klausen, M.B. and Fanning, C.M., 2004. U–Pb zircon (SHRIMP) ages for the Lebombo rhyolites, South Africa: refining the duration of Karoo volcanism. Journal of the Geological Society, 161(4), 547–550.

Roberts, E.M., Stevens, N.J., O'Connor, P.M., Dirks, P.H.G.M., Gottfried, M.D., Clyde, W.C., Armstrong, R.A., Kemp, A.I.S. and Hemming, S., 2012. Initiation of the western branch of the East African Rift coeval with the eastern branch. Nature Geoscience, 5(4), 289– 294.

Roby, D.J. and Johnson, M.R. (compiles), 1995. Geological Map 3326 Grahamstown. 1:250 000 Geological Map Series, Geological Survey of South Africa.

Rocha-Campos, A.C., Basei, M.A., Nutman, A.P., Kleiman, L.E., Varela, R., Llambias, E., Canile, F.M. and Da Rosa, O.D.C., 2011. 30 million years of Permian volcanism recorded in the Choiyoi igneous province (W Argentina) and their source for younger ash fall deposits in the Paraná Basin: SHRIMP U–Pb zircon geochronology evidence. Gondwana Research, 19(2), 509–523.

Rocher, S., Vallecillo, G., Castro de Machuca, B. and Alasino, P., 2015. El Grupo Choiyoi (Pérmico temprano-medio) en la Cordillera Frontal de Calingasta, San Juan, Argentina: volcanismo de arco asociado a extensión. Revista mexicana de ciencias geológicas, 32(3), 415–432.

Rocholl, A., Schaltegger, U., Gilg, H.A., Wijbrans, J. and Böhme, M., 2018. The age of volcanic tuffs from the Upper Freshwater Molasse (North Alpine Foreland Basin) and their possible use for tephrostratigraphic correlations across Europe for the Middle Miocene. International Journal of Earth Sciences, 107(2), 387–407.

Rogers, A.W. 1905. Geological survey of parts of the Divisions of Uitenhage and Alexandria. Annual report of the Geological Commission of the Cape of Good Hope, pp. 1–18.

Rogers, A.W. and Schwarz, E.H.L. 1901. Report on parts of the Uitenhage and Port Elizabeth Divisions. Annual report of the Geological Commission of the Cape of Good Hope, pp. 1–18.

Roux, J. and Davids, A., 2016. Structural Evolution of the Gamtoos Basin, based on 2D seismic data, 35th IGC Conference, Cape Town, Poster Abstract.

Scheiber-Enslin, 2015. Integrated geophysical investigation of the Karoo Basin, South Africa. PhD thesis, University of the Witwatersrand, (unpublished).

Schoene, B., 2014. 4.10-U–Th–Pb Geochronology. Treatise on geochemistry, 4, 341–378.

Schoene, B., Samperton, K.M., Eddy, M.P., Keller, G., Adatte, T., Bowring, S.A., Khadri, S.F. and Gertsch, B., 2015. U-Pb geochronology of the Deccan Traps and relation to the end-Cretaceous mass extinction. Science, 347(6218), 182–184.

Schwarz, E.H.L., 1915. New Cretaceous fossils from Brenton, Knysna. Records of the Albany Mus, pp. 120-126.

Seton, M., Müller, R.D., Zahirovic, S., Gaina, C., Torsvik, T., Shephard, G., Talsma, A., Gurnis, M., Turner, M., Maus, S. and Chandler, M., 2012. Global continental and ocean basin reconstructions since 200 Ma. Earth-Science Reviews, 113(3–4), 212–270.

Shone, R.W., 1976. The sedimentology of the Mesozoic Algoa Basin. MSc. thesis. University of Port Elizabeth (unpublished).

Shone, R.W., 1978. A case for lateral gradation between the Kirkwood and Sundays River formations, Algoa Basin. Transactions of the Geological Society of South Africa, 81, 319–326.

Shone, R.W., 2006. Onshore post-Karoo Mesozoic deposits. In: Johnson, M.R., Anhaeusser, C.R., and Thomas, R.J., (Eds.), The Geology of South Africa. Geological Society of South Africa, Johannesburg, and Council for Geoscience, Pretoria, 541–571.

Sláma, J., Košler, J., Condon, D.J., Crowley, J.L., Gerdes, A., Hanchar, J.M., Horstwood, M.S.A., Morris, G.A., Nasdala, L., Norberg, N.,Schaltegger, U., Schoene, B., Tubrett, M.N., Whitehouse, M.J., 2008, Plešovice zircon – a new natural reference material for U-Pb and Hf isotopic microanalysis, Chemical Geology, 241, 1–35.

Spath, L.F., 1930. On the Cephalopoda of the Uitenhage beds. Annuls of the South Arican Museum, 28, 131–157.

Spencer, C.J., Cawood, P.A., Hawkesworth, C.J., Raub, T.D., Prave, A.R. and Roberts, N.M., 2014. Proterozoic onset of crustal reworking and collisional tectonics: Reappraisal of the zircon oxygen isotope record. Geology, 42(5), 451–454.

Stacey, J.T. and Kramers, 1., 1975. Approximation of terrestrial lead isotope evolution by a two-stage model. Earth and planetary science letters, 26(2), 207–221.

Stipanicic, P.N., Rodrigo, F., Baulies, O.L. and Martínez, C.G., 1968. Las formaciones presenonianas en el denominado Macizo Nordpatagónico y regiones adyacentes. Revista de la Asociación Geológica Argentina, 23(2), 67–98.

Storey, B.C., 1995. The role of mantle plumes in continental breakup: case histories from Gondwanaland. Nature, 377(6547), 301–308.

Sutter, J.F., 1988. Innovative approaches to the dating of igneous events in the early Mesozoic basins of the eastern United States. US Geological Survey Bulletin, 1776, 194–200.

Svensen, H., Corfu, F., Polteau, S., Hammer, Ø. and Planke, S., 2012. Rapid magma emplacement in the Karoo large igneous province. Earth and Planetary Science Letters, 325, 1–9.

Tankard, A., Welsink, H., Aukes, P., Newton, R. and Stettler, E., 2012. Geodynamic interpretation of the Cape and Karoo basins, South Africa. In: Roberts, D.G. and Bally, A.W. (Eds.), Regional Geology and Tectonics: Phanerozoic Passive Margins, Cratonic basins and Global Tectonic Maps, pp. 869–945.

Tankard, A.J., Jackson, M.P.A., Eriksson, K.A., Hobday, D.K., Hunter, D.R. and Minter, W.E.L., 1982. Crustal Evolution of Southern Africa, Springer-Verlag, New York, 523 pp.

Tennant, J.P., Mannion, P.D., Upchurch, P., Sutton, M.D. and Price, G.D., 2017. Biotic and environmental dynamics through the Late Jurassic–Early Cretaceous transition: evidence for protracted faunal and ecological turnover. Biological Reviews, 92(2), 776–814.

Theron, J.N. (compiler), 1991. Geological Map 3320 Ladismith. 1:250 000 Geological Map Series, Geological Survey of South Africa.

Thomson, K., 1999. Role of continental break-up, mantle plume development and fault reactivation in the evolution of the Gamtoos Basin, South Africa. Marine and petroleum geology, 16(5), 409–429.

Tilton, G.R., Patterson, C., Brown, H., Inghram, M., Hayden, R., Hess, D. and Larsen Jr, E., 1955. Isotopic composition and distribution of lead, uranium, and thorium in a Precambrian granite. Geological Society of America Bulletin, 66(9), 1131–1148.

Tinker, J., de Wit, M. and Brown, R., 2008a. Mesozoic exhumation of the southern Cape, South Africa, quantified using apatite fission track thermochronology. Tectonophysics 455, 77–93.

Tinker, J., de Wit, M. and Brown, R., 2008b. Linking source and sink: Evaluating the balance between onshore erosion and offshore sediment accumulation since Gondwana break-up, South Africa. Tectonophysics, 455, 94–103.

Toerien, D.K. (compiler), 1991. Geological Map 3324 Port Elizabeth. 1:250 000 Geological Map Series, Geological Survey of South Africa.

Toerien, D.K. and Roby, D.J. (compilers), 1979. Geological Map 3322 Oudtshoorn. 1:250 000 Geological Map Series, Geological Survey of South Africa.

Torsvik, T.H. and Cocks, L.R.M., 2013. Gondwana from top to base in space and time. Gondwana Research, 24 (3): 999–1030.

Torsvik, T.H., Van der Voo, R., Preeden, U., Mac Niocaill, C., Steinberger, B., Doubrovine, P.V., Van Hinsbergen, D.J., Domeier, M., Gaina, C., Tohver, E. and Meert, J.G., 2012. Phanerozoic polar wander, palaeogeography and dynamics. Earth-Science Reviews, 114(3–4), pp. 325–368.

Tucker, R.T., Roberts, E.M., Hu, Y., Kemp, A.I. and Salisbury, S.W., 2013. Detrital zircon age constraints for the Winton Formation, Queensland: contextualizing Australia's Late Cretaceous dinosaur faunas. Gondwana Research, 24(2), 767–779.

Uliana, M.A., Biddle, K.T., 1987. Permian to Late Cenozoic evolution of Patagonia, main tectonic events, magmatic activity, and depositional trends. In: McKenzie, G.D. (Ed.), Gondwana Six: Structure, Tectonics, and Geophysics. AGU Monograph, Washington, D.C., pp. 271–286.

Uliana, M.A., Biddle, K.T., Cerdan, J., 1989. Mesozoic extension and the formation of Argentine sedimentary basins. In: Tankard, A.J., Balkwill, H.R. (Eds.), Extensional Tectonics and Stratigraphy of the North Atlantic Margins, AAPG Memoir, vol. 46. American Association of Petroleum Geologists, pp. 599–614.

Upchurch, P., Mannion, P. D., Benson, R. B. J., Butler, R. J. & Carrano, M. T., 2011. Geological and anthropogenic controls on the sampling of the terrestrial fossils record: a case study from the Dinosauria. In: Mcgowan, A.J. and Smith, A.B. (Eds.), Comparing the Geological and Fossil Records: Implications for Biodiversity Studies, Geological Society of London, Special Publications, pp. 209–240.

Van Bloemenstein, C.B., 2016. A tectonostratigraphic comparison of the eastern and western parts of the Gamtoos Basin, South Africa. Poster presentation at the 35th IGC Conference, Cape Town. DOI: 10.13140/RG.2.2.27227.77606.

Van Breda, I,K, 2017. Chronostratigraphy of the Mesozoic Uitenhage Group in the Robertson-Ashton rift basin, South Africa. BSc (hons) thesis, University of the Western Cape (unpublished).

Van der Linde, C., 2017. Sediment supply processes and platterns in the Enon Formation, Gamtoos Basin, Eastern Cape, South Africa. MSc. thesis, University of Cape Town (unpublished).

Vavra, G., 1993. A guide to quantitative morphology of accessory zircon. Chemical Geology, 110(1-3), 15–28.

Venter, J.J., 1972. Type stratigraphy of the Sundays River Formation: Report of the Southern Oil Exploration Corporation (SEOKOR) (unpublished).

Viljoen, J.H.A., 1992. The stratigraphy of the Heidelberg/Riversdale Mesozoic Basin. In: De Wit, M.J., Ransome, I.G.D. (Eds.), Inversion Tectonics of the Cape Fold Belt. Karoo and Cretaceous basins of Southern Africa. A.A. Balkema, Rotterdam, 77–84.

Viljoen, J.H.A., 2000. Transfer zones: main conduits for sedimentation of the Buffelskloof Formation in the Heidelberg and Mossel Bay Mesozoic basins, Western Cape, South Africa: Abstracts, Geocongress 2000, Geological Society of South Africa, University of Stellenbosch, Journal of African Earth Sciences, 31, 87–88.

Viljoen, J.H.A., 2009. Hartenbos Formation (Uitenhage Group) In: M.R. Johnson (Eds.), Catalogue of South African Lithostratigraphic Units. South African Committee for Stratigraphy, 10, 9–10.

Viljoen, J.H.A., Malan, J.A. (compilers), 1993. Geological Map 3422AA Mosselbaai. 1:50 000 Geological Map Series, Geological Survey of South Africa.

Viljoen, J.H.A., Stapelberg, F.D.J. and Cloete, M., 2010. Technical report on the geological storage of carbon dioxide in South Africa. Report, Council for Geoscience, 236 pp.

Viljoen., J.H.A., 1996. Geology of Heidelberg (Cape) and vicinity. Council for Geoscience Excursion Guide. 11 pp.

Wang, T., Ramezani, J., Wang, C., Wu, H., He, H. and Bowring, S.A., 2016. High-precision U–Pb geochronologic constraints on the Late Cretaceous terrestrial cyclostratigraphy and geomagnetic polarity from the Songliao Basin, Northeast China. Earth and Planetary Science Letters, 446, 37–44.

Weissert, H. and Erba, E., 2004. Volcanism, CO2 and palaeoclimate: a Late Jurassic–Early Cretaceous carbon and oxygen isotope record. Journal of the Geological Society 161, 695–702.

Wernicke, B. and Burchfiel, B.C., 1982. Modes of extensional tectonics. Journal of Structural Geology, 4(2), 105–115.

Wetherill, G.W., 1956. Discordant uranium-lead ages, I. Eos, Transactions American Geophysical Union, 37(3), 320–326.

White, J.D.L. and Houghton, B.F., 2006. Primary volcaniclastic rocks. Geology, 34(8), 677–680.

White, R. and McKenzie, D., 1989. Magmatism at rift zones: the generation of volcanic continental margins and flood basalts. Journal of Geophysical Research: Solid Earth, 94(B6), 7685–7729.

Wiedenbeck, M.A.P.C., Alle, P., Corfu, F., Griffin, W.L., Meier, M., Oberli, F.V., Quadt, A.V., Roddick, J.C. and Spiegel, W., 1995. Three natural zircon standards for U-Th-Pb, Lu-Hf, trace element and REE analyses. Geostandards newsletter, 19(1), 1–23.

Wildman, M., Brown, R., Watkins, R., Carter, A., Gleadow, A. and Summerfield, M., 2015. Post break-up tectonic inversion across the southwestern cape of South Africa: New insights from apatite and zircon fission track thermochronometry. Tectonophysics 654, 30–55.

Will, T.M. and Frimmel, H.E., 2013. The influence of inherited structures on dike emplacement during Gondwana breakup in southwestern Africa. The Journal of Geology, 121(5), 455–474.

Will, T.M. and Frimmel, H.E., 2018. Where does a continent prefer to break up? Some lessons from the South Atlantic margins. Gondwana Research, 53, 9–19.

Winchester, J.A. and Floyd, P.A., 1977. Geochemical discrimination of different magma series and their differentiation products using immobile elements. Chemical geology, 20, 325–343.

Winter, H. de la R., 1973. Geology of the Algoa Basin, South Africa, In: Blant, G. (Editor), Sedimentary basins of the African coasts, Part 2, South and East Coast. Association of African Geological Surveys, Paris, 17–48.

Winter, H. de la R., 1979. Application of basic principles of stratigraphy to the Jurassic-Cretaceous interval in southern Africa. In: A.M. Anderson and W.A. Van Biljon (Eds.), Geocongress 77: Some Sedimentary Ore Deposits in South Africa. Special Publication, Geological Society of South Africa, 6, 183–196.

Zerfass, H., Lavina, E.L., Schultz, C.L., Garcia, A.J.V., Faccini, U.F. and Chemale Jr, F., 2003. Sequence stratigraphy of continental Triassic strata of Southernmost Brazil: a contribution to Southwestern Gondwana palaeogeography and palaeoclimate. Sedimentary Geology, 161(1-2), 85–105.

Appendices

Appendices A–H are followed by two published papers referred to in section 2.2.2 and 2.2.3 of this thesis.

Appendix A. Isotopic data acquired by LA-ICPMS analysis of reference zircons

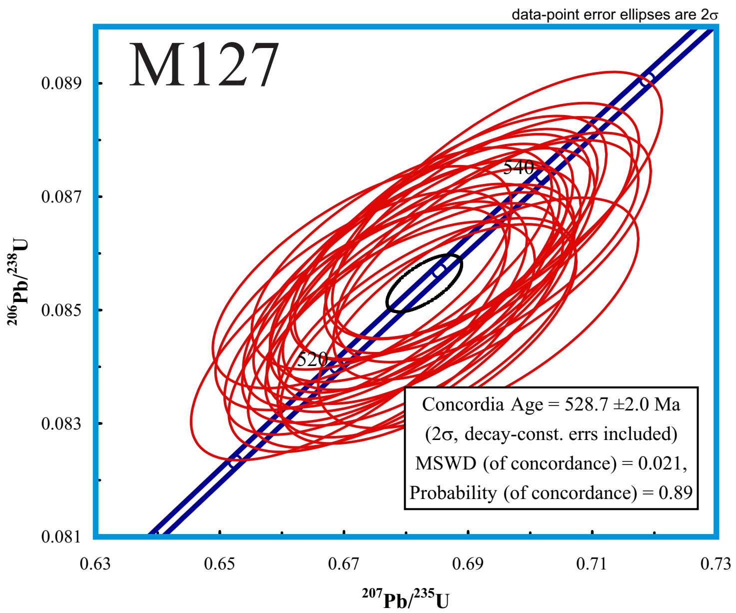

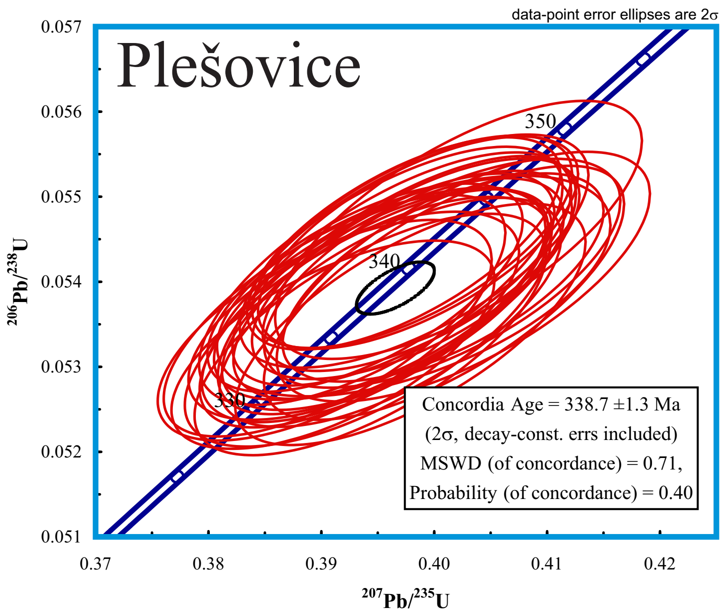

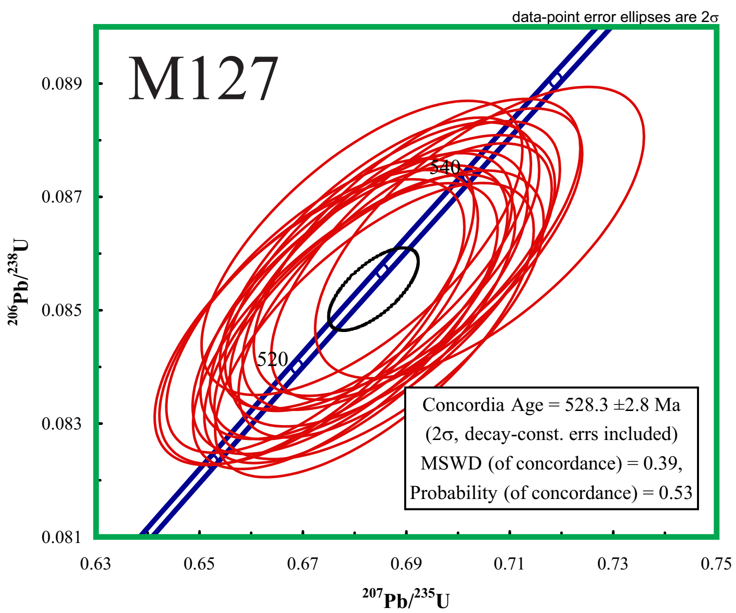

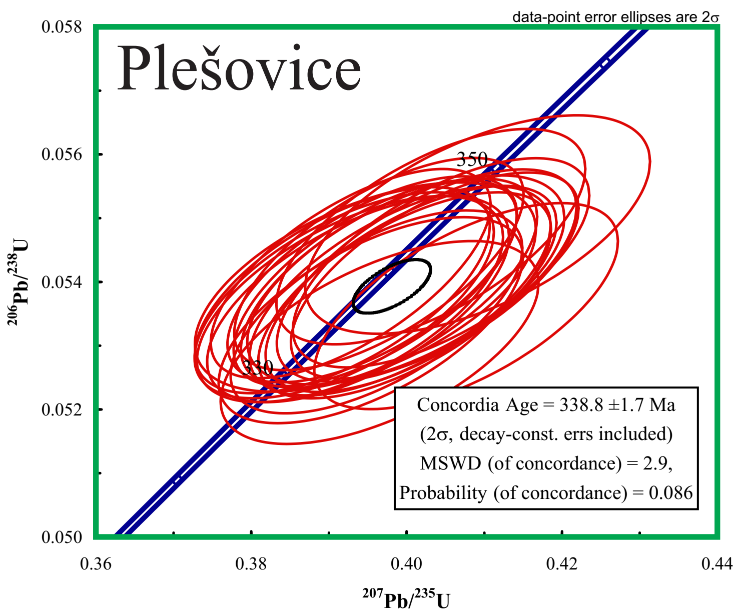

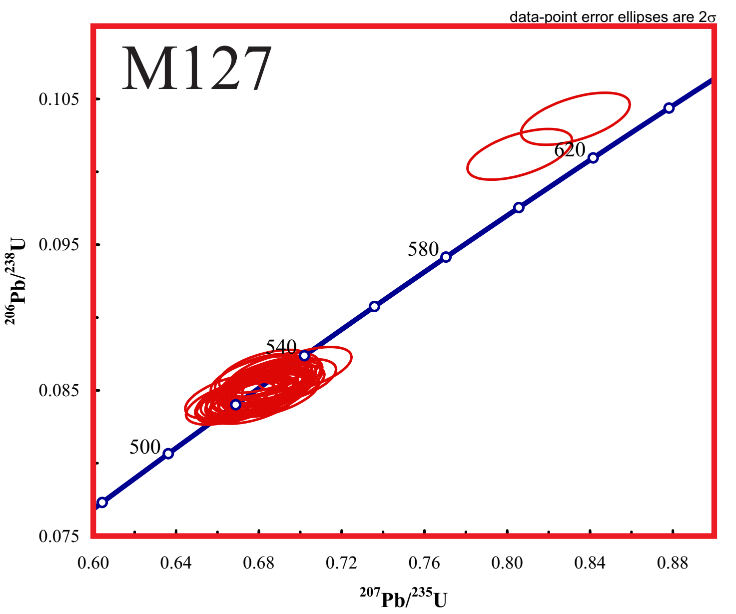

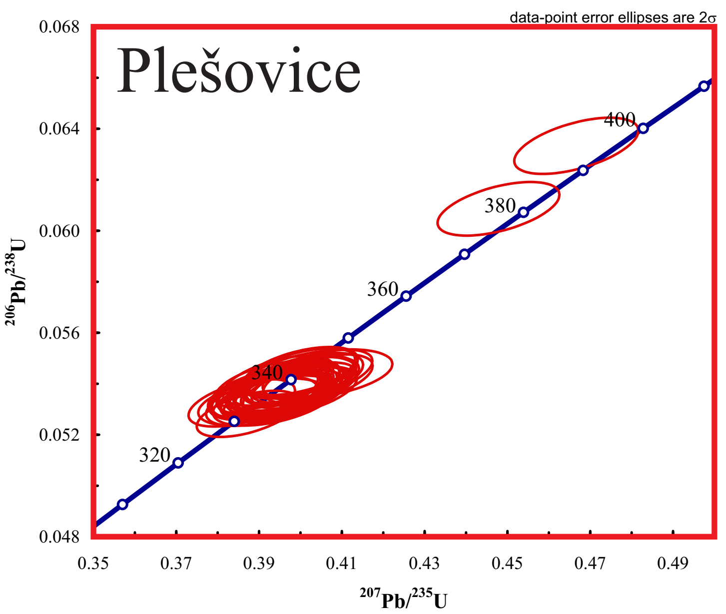

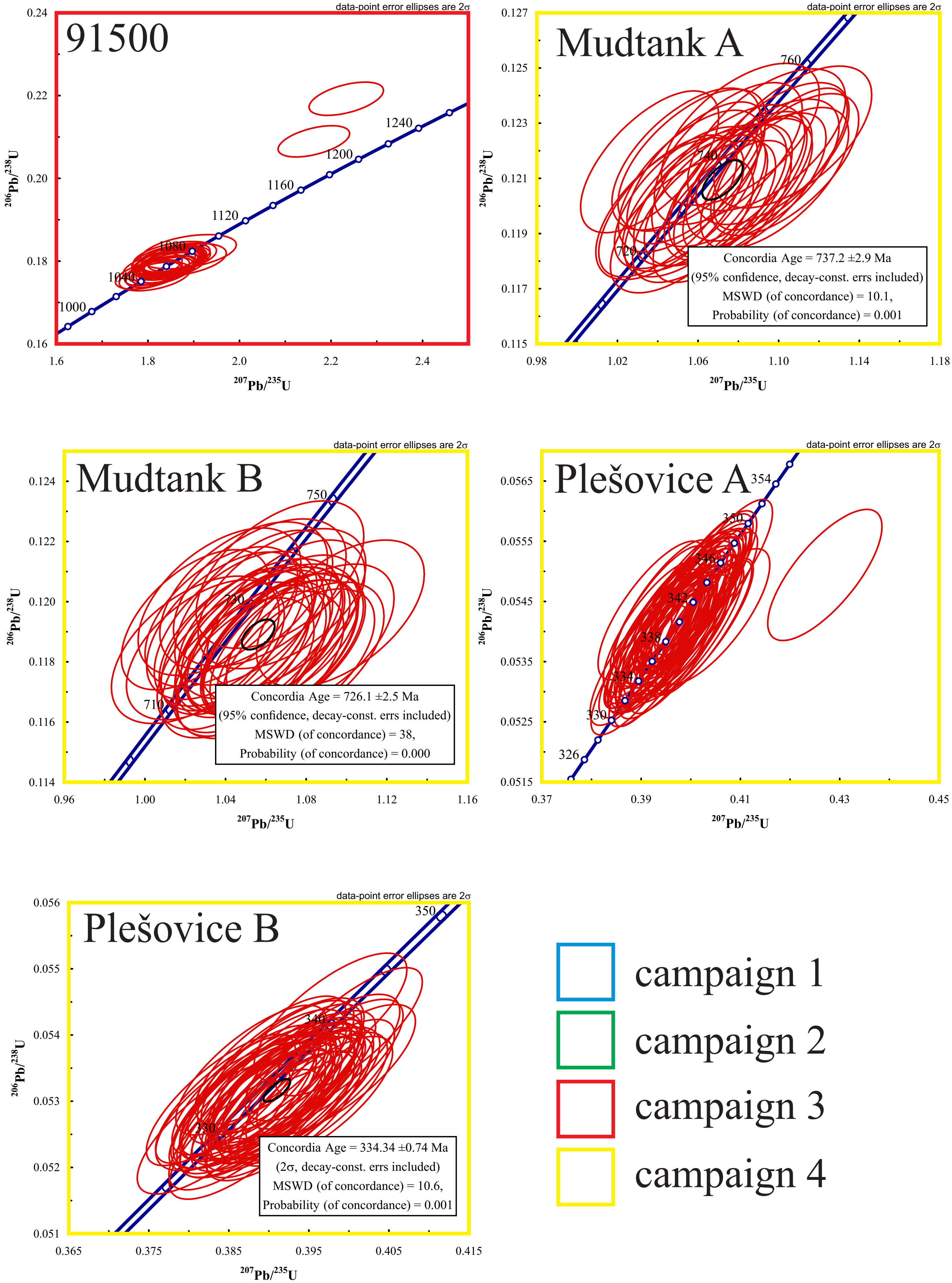

Fig. A1. Reference zircons M127, Mudtank, Plešovice and 91500 used across 4 analytical campaigns. Border colours indicate the respective campaign in which data were used to process unknowns. In the case of campaign 3, two analytical runs were conducted several weeks apart, run A and run B, and reference zircons are labeled accordingly.

Appendix B. LA-ICPMS isotopic data for samples from the Suurberg Group

Table B1. LA-ICPMS isotopic data for sample ASP1 from the Suurberg Group in the northern Algoa Basin

ASP1							RATIOS							AGES [Ma]						Conc.
Sample	Analysis	U [ppm][a]	Pb [ppm][a]	Th [ppm][a]	$^{206}Pb/^{204}Pb$	Th/U[a]	$^{207}Pb/^{235}U$[b]	2 σ[d]	$^{206}Pb/^{238}U$[b]	2 σ[d]	rho[c]	$^{207}Pb/^{206}Pb$	2 σ[d]	$^{207}Pb/^{235}U$	2 σ	$^{206}Pb/^{238}U$	2 σ	$^{207}Pb/^{206}Pb$	2 σ	%
ASP1	ASP1-1	181	25	46	1186	0.26	1.749	0.066	0.1359	0.0034	0.66	0.0934	0.0026	1027	39	821	20	1496	53	55
ASP1	ASP1-2	215	22	120	1460	0.56	0.834	0.033	0.1003	0.0025	0.63	0.0603	0.0019	616	24	616	15	615	67	100
ASP1	ASP1-3	142	7	69	668	0.49	0.333	0.020	0.0463	0.0012	0.44	0.0521	0.0028	291	17	292	8	290	123	101
ASP1	ASP1-4	532	26	148	7054	0.28	0.366	0.016	0.0495	0.0012	0.59	0.0537	0.0018	317	13	311	8	358	77	87
ASP1	ASP1-5	390	16	251	1728	0.64	0.281	0.013	0.0398	0.0010	0.56	0.0512	0.0019	251	11	252	6	248	86	102
ASP1	ASP1-6	193	64	52	15340	0.27	5.833	0.207	0.3304	0.0081	0.70	0.1280	0.0033	1951	69	1840	45	2071	45	89
ASP1	ASP1-7	50	4	26	457	0.53	0.699	0.055	0.0872	0.0025	0.37	0.0582	0.0042	538	42	539	16	535	160	101
ASP1	ASP1-8	161	16	168	1625	1.05	0.869	0.036	0.1007	0.0025	0.61	0.0626	0.0021	635	26	618	15	694	70	89
ASP1	ASP1-9	362	16	211	1517	0.58	0.307	0.015	0.0429	0.0011	0.53	0.0520	0.0021	272	13	271	7	284	93	95
ASP1	ASP1-10	302	22	65	1350	0.21	0.591	0.024	0.0729	0.0018	0.61	0.0588	0.0019	472	19	454	11	560	70	81
ASP1	ASP1-11	934	30	2409	2731	2.58	0.224	0.011	0.0324	0.0008	0.53	0.0503	0.0020	205	10	205	5	207	94	99
ASP1	ASP1-12	269	9	412	906	1.53	0.244	0.022	0.0341	0.0009	0.29	0.0521	0.0044	222	20	216	6	288	194	75
ASP1	ASP1-13	264	11	91	1434	0.35	0.316	0.017	0.0413	0.0011	0.48	0.0555	0.0026	278	15	261	7	431	105	60
ASP1	ASP1-14	231	19	219	1287	0.95	0.705	0.029	0.0818	0.0020	0.61	0.0626	0.0020	542	22	507	13	693	70	73
ASP1	ASP1-15	198	40	173	5883	0.88	2.203	0.080	0.2019	0.0050	0.68	0.0791	0.0021	1182	43	1186	29	1175	53	101
ASP1	ASP1-16	192	5	517	388	2.69	0.191	0.024	0.0274	0.0008	0.22	0.0506	0.0061	177	22	174	5	223	279	78
ASP1	ASP1-17	210	22	96	1378	0.46	0.880	0.075	0.1044	0.0026	0.29	0.0611	0.0050	641	54	640	16	643	175	100
ASP1	ASP1-18	447	13	349	1120	0.78	0.196	0.012	0.0284	0.0007	0.42	0.0500	0.0027	182	11	181	5	194	127	93
ASP1	ASP1-19	152	12	91	2523	0.60	0.631	0.040	0.0804	0.0022	0.43	0.0569	0.0032	497	31	499	14	488	125	102
ASP1	ASP1-20	517	21	314	881	0.61	0.315	0.017	0.0415	0.0011	0.47	0.0550	0.0027	278	15	262	7	411	108	64
ASP1	ASP1-21	75	2	89	285	1.17	0.212	0.042	0.0308	0.0008	0.14	0.0500	0.0099	196	39	196	5	195	460	101
ASP1	ASP1-22	180	18	41	2454	0.23	0.835	0.033	0.1003	0.0025	0.63	0.0604	0.0019	616	24	616	15	617	67	100
ASP1	ASP1-24	285	21	35	1286	0.12	0.582	0.027	0.0751	0.0019	0.55	0.0563	0.0022	466	22	467	12	462	86	101
ASP1	ASP1-25	584	40	665	4549	1.14	0.558	0.037	0.0679	0.0019	0.41	0.0596	0.0036	450	30	423	12	589	131	72
ASP1	ASP1-26	173	12	73	1618	0.42	0.552	0.025	0.0714	0.0018	0.56	0.0561	0.0021	446	20	445	11	456	85	98
ASP1	ASP1-27	620	23	490	3079	0.79	0.267	0.018	0.0378	0.0010	0.41	0.0513	0.0031	241	16	239	6	254	138	94
ASP1	ASP1-28	236	41	113	3799	0.48	1.734	0.064	0.1718	0.0043	0.67	0.0732	0.0020	1021	38	1022	25	1019	55	100
ASP1	ASP1-29	800	20	1306	1348	1.63	0.173	0.010	0.0252	0.0006	0.43	0.0499	0.0027	162	10	160	4	192	126	84
ASP1	ASP1-30	53	2	72	150	1.35	0.205	0.050	0.0288	0.0008	0.12	0.0518	0.0124	190	46	183	5	278	549	66
ASP1	ASP1-31	29	1	64	215	2.24	0.262	0.104	0.0282	0.0009	0.08	0.0675	0.0266	237	93	179	6	854	818	21
ASP1	ASP1-32	171	5	233	1232	1.37	0.208	0.014	0.0300	0.0008	0.38	0.0502	0.0032	192	13	191	5	206	146	92
ASP1	ASP1-33	288	13	184	1969	0.64	0.310	0.015	0.0436	0.0011	0.54	0.0515	0.0020	274	13	275	7	263	91	105
ASP1	ASP1-34	779	56	1357	4339	1.74	0.554	0.026	0.0718	0.0018	0.54	0.0559	0.0023	447	21	447	11	450	90	99
ASP1	ASP1-35	417	22	134	6067	0.32	0.385	0.020	0.0524	0.0014	0.49	0.0532	0.0025	331	18	329	9	339	105	97
ASP1	ASP1-36	183	19	159	44917	0.87	0.854	0.034	0.1022	0.0025	0.63	0.0606	0.0019	627	25	628	16	624	66	101
ASP1	ASP1-37	288	22	101	4355	0.35	0.591	0.023	0.0754	0.0019	0.64	0.0569	0.0017	472	18	468	12	488	67	96
ASP1	ASP1-38	150	11	163	1361	1.09	0.555	0.032	0.0719	0.0018	0.44	0.0560	0.0029	448	25	447	11	454	113	99
ASP1	ASP1-39	640	30	292	6788	0.46	0.338	0.015	0.0470	0.0012	0.56	0.0522	0.0019	296	13	296	7	292	84	101
ASP1	ASP1-40	381	18	150	3879	0.39	0.347	0.014	0.0479	0.0012	0.62	0.0525	0.0017	302	12	302	8	309	72	98
ASP1	ASP1-41	162	7	30	1010	0.19	0.312	0.021	0.0433	0.0012	0.41	0.0523	0.0032	276	18	273	7	299	140	91
ASP1	ASP1-42	288	13	230	2363	0.80	0.336	0.015	0.0466	0.0012	0.56	0.0523	0.0020	294	13	294	7	299	86	98
ASP1	ASP1-43	50	1	65	136	1.31	0.190	0.044	0.0276	0.0009	0.13	0.0498	0.0114	176	41	176	5	188	532	94
ASP1	ASP1-44	206	16	144	1413	0.70	0.593	0.024	0.0760	0.0019	0.61	0.0566	0.0018	473	19	472	12	474	71	100
ASP1	ASP1-45	136	14	76	1032	0.56	0.843	0.038	0.0999	0.0025	0.56	0.0612	0.0023	621	28	614	16	647	80	95
ASP1	ASP1-46	27	1	53	108	1.95	0.189	0.049	0.0275	0.0009	0.12	0.0497	0.0128	175	45	175	6	182	598	96
ASP1	ASP1-47	323	15	209	3328	0.65	0.334	0.014	0.0458	0.0011	0.60	0.0529	0.0018	293	12	288	7	326	76	89
ASP1	ASP1-48	568	61	231	5618	0.41	0.903	0.034	0.1069	0.0027	0.66	0.0613	0.0017	653	25	655	16	648	61	101
ASP1	ASP1-49	100	8	85	1289	0.85	0.628	0.031	0.0767	0.0020	0.53	0.0594	0.0025	495	24	476	12	583	91	82
ASP1	ASP1-50	1106	60	514	9019	0.46	0.398	0.021	0.0543	0.0014	0.49	0.0532	0.0024	340	18	341	9	336	104	101
ASP1	ASP1-51	272	12	166	1179	0.61	0.324	0.014	0.0445	0.0011	0.57	0.0527	0.0019	285	13	281	7	315	82	89
ASP1	ASP1-52	24	1	29	97	1.21	0.219	0.044	0.0316	0.0010	0.16	0.0504	0.0099	201	40	200	6	213	454	94
ASP1	ASP1-53	256	12	163	2856	0.64	0.347	0.015	0.0479	0.0012	0.58	0.0525	0.0018	302	13	302	8	306	80	99
ASP1	ASP1-54	832	23	1051	1461	1.26	0.192	0.008	0.0280	0.0007	0.59	0.0498	0.0017	178	8	178	4	185	80	96
ASP1	ASP1-55	33	1	60	291	1.84	0.215	0.068	0.0310	0.0009	0.10	0.0503	0.0158	198	62	197	6	209	727	94
ASP1	ASP1-56	350	10	277	2102	0.79	0.201	0.012	0.0291	0.0007	0.42	0.0500	0.0028	186	11	185	5	194	128	96
ASP1	ASP1-57	343	83	141	10179	0.41	3.030	0.110	0.2431	0.0060	0.68	0.0904	0.0024	1415	52	1403	35	1434	51	98
ASP1	ASP1-58	42	1	48	110	1.14	0.187	0.051	0.0266	0.0009	0.13	0.0509	0.0137	174	47	169	6	235	621	72

ASP1	ASP1-59	177	37	60	2916	0.34	2.356	0.087	0.2101	0.0052	0.67	0.0813	0.0022	1229	45	1229	31	1230	54	100
ASP1	ASP1-60	99	3	156	531	1.56	0.201	0.019	0.0289	0.0008	0.28	0.0505	0.0045	186	17	183	5	219	208	84
ASP1	ASP1-61	159	30	62	3179	0.39	2.635	0.100	0.1884	0.0047	0.66	0.1014	0.0029	1311	50	1113	28	1651	53	67
ASP1	ASP1-62	252	7	881	342	3.50	0.198	0.021	0.0264	0.0007	0.25	0.0545	0.0055	184	19	168	4	392	227	43
ASP1	ASP1-63	258	23	82	2430	0.32	0.721	0.028	0.0889	0.0022	0.64	0.0588	0.0018	551	22	549	14	559	66	98
ASP1	ASP1-64	43	1	61	187	1.41	0.228	0.057	0.0265	0.0010	0.15	0.0626	0.0155	209	52	168	6	695	527	24
ASP1	ASP1-65	351	55	33	7484	0.09	1.571	0.058	0.1569	0.0039	0.68	0.0726	0.0020	959	35	940	23	1003	55	94
ASP1	ASP1-66	45	1	57	478	1.25	0.212	0.032	0.0308	0.0009	0.19	0.0501	0.0074	196	29	195	6	200	343	98
ASP1	ASP1-67	322	13	196	3089	0.61	0.284	0.015	0.0400	0.0010	0.47	0.0514	0.0024	254	14	253	6	261	109	97
ASP1	ASP1-68	53	2	51	1512	0.96	0.282	0.081	0.0393	0.0012	0.10	0.0521	0.0148	252	72	248	7	290	649	86
ASP1	ASP1-69	134	10	105	690	0.79	0.612	0.039	0.0743	0.0020	0.43	0.0597	0.0034	485	31	462	13	592	124	78
ASP1	ASP1-70	181	5	258	733	1.43	0.188	0.013	0.0276	0.0007	0.37	0.0496	0.0032	175	12	175	5	174	151	101
ASP1	ASP1-71	74	6	48	974	0.65	0.706	0.034	0.0878	0.0023	0.53	0.0583	0.0024	542	26	542	14	541	90	100
ASP1	ASP1-72	734	21	1355	21349	1.85	0.196	0.014	0.0283	0.0007	0.36	0.0502	0.0033	181	13	180	5	205	152	88
ASP1	ASP1-73	263	20	133	3493	0.51	0.633	0.028	0.0757	0.0019	0.58	0.0607	0.0022	498	22	470	12	627	77	75
ASP1	ASP1-74	367	14	195	2404	0.53	0.276	0.012	0.0391	0.0010	0.57	0.0511	0.0019	247	11	247	6	246	84	100
ASP1	ASP1-75	443	12	646	1309	1.46	0.189	0.012	0.0275	0.0007	0.39	0.0499	0.0030	176	12	175	4	188	142	93
ASP1	ASP1-76	135	14	68	2203	0.51	0.906	0.037	0.1069	0.0027	0.61	0.0615	0.0020	655	27	654	16	656	70	100
ASP1	ASP1-77	48	1	42	3359	0.88	0.200	0.040	0.0292	0.0008	0.15	0.0498	0.0098	186	37	185	5	186	456	100
ASP1	ASP1-78	116	8	92	1085	0.80	0.548	0.026	0.0662	0.0017	0.54	0.0600	0.0024	444	21	413	11	605	87	68
ASP1	ASP1-79	70	3	74	205	1.06	0.286	0.060	0.0390	0.0011	0.14	0.0532	0.0111	255	54	247	7	335	475	74
ASP1	ASP1-80	89	3	126	139	1.42	0.220	0.040	0.0298	0.0009	0.16	0.0535	0.0096	202	37	189	5	350	405	54
ASP1	ASP1-81	220	10	145	2240	0.66	0.313	0.014	0.0438	0.0011	0.55	0.0520	0.0020	277	13	276	7	283	86	97
ASP1	ASP1-82	261	22	155	3326	0.59	0.661	0.026	0.0831	0.0021	0.63	0.0577	0.0018	515	20	515	13	518	68	99
ASP1	ASP1-83	574	98	157	12554	0.27	1.789	0.064	0.1700	0.0042	0.69	0.0763	0.0020	1041	38	1012	25	1103	52	92
ASP1	ASP1-84	90	3	127	280	1.41	0.198	0.027	0.0290	0.0008	0.20	0.0495	0.0065	183	25	184	5	171	308	108
ASP1	ASP1-85	217	38	58	2750	0.27	1.798	0.067	0.1760	0.0044	0.67	0.0741	0.0021	1045	39	1045	26	1044	56	100
ASP1	ASP1-86	110	19	42	1279	0.38	1.722	0.068	0.1709	0.0043	0.64	0.0731	0.0022	1017	40	1017	25	1016	62	100
ASP1	ASP1-87	331	150	195	5930	0.59	9.976	0.370	0.4529	0.0113	0.67	0.1598	0.0044	2433	90	2408	60	2453	46	98
ASP1	ASP1-89	88	3	118	319	1.34	0.198	0.027	0.0287	0.0008	0.20	0.0500	0.0066	183	25	182	5	196	307	93
ASP1	ASP1-90	233	23	263	5422	1.13	0.836	0.033	0.1002	0.0025	0.64	0.0605	0.0018	617	24	616	15	622	65	99
ASP1	ASP1-91	433	35	88	5638	0.20	0.646	0.025	0.0814	0.0020	0.65	0.0576	0.0017	506	19	504	13	513	64	98
ASP1	ASP1-92	458	39	288	3005	0.63	0.693	0.034	0.0857	0.0022	0.53	0.0587	0.0024	535	26	530	14	554	90	96
ASP1	ASP1-93	39	1	35	156	0.90	0.211	0.049	0.0295	0.0009	0.13	0.0521	0.0119	195	45	187	6	288	522	65
ASP1	ASP1-94	174	5	180	668	1.04	0.202	0.011	0.0294	0.0008	0.48	0.0499	0.0023	187	10	187	5	189	109	99
ASP1	ASP1-95	35	3	20	482	0.57	0.643	0.043	0.0729	0.0020	0.41	0.0640	0.0039	504	34	453	13	740	130	61
ASP1	ASP1-96	150	4	259	309	1.72	0.193	0.015	0.0283	0.0007	0.33	0.0497	0.0037	180	14	180	5	179	173	100
ASP1	ASP1-97	160	5	275	869	1.72	0.197	0.015	0.0287	0.0007	0.35	0.0500	0.0034	183	13	182	5	194	160	94
ASP1	ASP1-98	523	23	399	4415	0.76	0.309	0.013	0.0434	0.0011	0.61	0.0517	0.0017	274	11	274	7	274	74	100
ASP1	ASP1-99	350	10	429	578	1.22	0.201	0.014	0.0294	0.0007	0.36	0.0496	0.0032	186	13	187	5	178	150	105
ASP1	ASP1-100	275	11	163	614	0.59	0.358	0.015	0.0407	0.0010	0.59	0.0638	0.0022	311	13	257	6	735	73	35
ASP1	ASP1-102	956	182	242	4345	0.25	2.448	0.088	0.1901	0.0047	0.69	0.0934	0.0024	1257	45	1122	28	1496	49	75
ASP1	ASP1-103	236	21	217	2369	0.92	0.709	0.028	0.0880	0.0022	0.63	0.0585	0.0018	544	22	543	14	548	68	99
ASP1	ASP1-104	134	21	25	7670	0.18	1.613	0.070	0.1593	0.0041	0.58	0.0735	0.0026	975	43	953	24	1026	72	93
ASP1	ASP1-105	429	12	363	1427	0.85	0.194	0.009	0.0282	0.0007	0.57	0.0498	0.0018	180	8	179	5	187	85	96
ASP1	ASP1-106	74	2	115	98	1.54	0.206	0.018	0.0300	0.0008	0.31	0.0498	0.0041	191	17	191	5	188	193	102
ASP1	ASP1-107	285	49	113	5467	0.39	1.724	0.068	0.1705	0.0043	0.63	0.0733	0.0022	1018	40	1015	25	1023	62	99
ASP1	ASP1-108	250	7	218	414	0.87	0.196	0.010	0.0286	0.0007	0.49	0.0497	0.0023	182	10	182	5	182	109	100
ASP1	ASP1-109	458	35	49	5937	0.11	0.594	0.030	0.0757	0.0020	0.52	0.0570	0.0024	474	24	470	12	490	94	96
ASP1	ASP1-110	155	6	69	757	0.45	0.289	0.030	0.0409	0.0013	0.30	0.0512	0.0050	257	27	258	8	248	226	104
ASP1	ASP1-111	263	12	141	1044	0.54	0.334	0.019	0.0463	0.0012	0.46	0.0522	0.0027	292	17	292	8	295	116	99

[a] U and Pb concentrations and Th/U ratios are calculated relative to GJ-1 reference zircon

[b] Corrected for background and within-run Pb/U fractionation and normalised to reference zircon GJ-1 (ID-TIMS values/measured value); $^{207}Pb/^{235}U$ calculated using $(^{207}Pb/^{206}Pb)/(^{238}U/^{206}Pb * 1/137.88)$

[c] Rho is the error correlation defined as the quotient of the propagated errors of the $^{206}Pb/^{238}U$ and the $^{207}/^{235}U$ ratio

[d] Quadratic addition of within-run errors (2 SD) and daily reproducibility of GJ-1 (2 SD)

[e] Corrected for mass-bias by normalising to GJ-1 reference zircon (~0.6 per atomic mass unit) and common Pb using the model Pb composition of Stacey & Kramers (1975)

Table B2. LA-ICPMS isotopic data for sample ASP2 from the Suurberg Group in the northern Algoa Basin

ASP2						RATIOS							AGES [Ma]						Conc.
Sample	Analysis	U [ppm][a]	Pb [ppm][a]	$^{206}Pb/^{204}Pb$	Th/U[a]	$^{207}Pb/^{235}U$[b]	2 σ[d]	$^{206}Pb/^{238}U$[b]	2 σ[d]	rho[c]	$^{207}Pb/^{206}Pb$[c]	2 σ[d]	$^{207}Pb/^{235}U$	2 σ	$^{206}Pb/^{238}U$	2 σ	$^{207}Pb/^{206}Pb$	2 σ	%
ASP2	C4-1-1	264	26	1983	0.20	0.825	0.031	0.0973	0.0016	0.44	0.0615	0.0021	611	23	598	10	658	72	91
ASP2	C4-1-2	139	5	24340	0.39	0.232	0.015	0.0334	0.0007	0.32	0.0504	0.0030	212	13	211	4	213	133	99
ASP2	C4-1-3	109	4	1129	0.97	0.239	0.045	0.0335	0.0015	0.24	0.0518	0.0096	217	41	212	10	274	423	77
ASP2	C4-1-6	45	1	302	1.94	0.198	0.048	0.0292	0.0017	0.24	0.0493	0.0115	184	44	186	11	160	547	116
ASP2	C4-1-7	111	5	406	0.39	0.320	0.031	0.0408	0.0011	0.28	0.0570	0.0054	282	28	258	7	491	207	52
ASP2	C4-1-8	305	13	2933	0.60	0.316	0.015	0.0440	0.0008	0.37	0.0522	0.0023	279	13	277	5	293	102	95
ASP2	C4-1-9	138	11	576	0.57	0.629	0.031	0.0799	0.0015	0.37	0.0571	0.0026	496	25	496	9	495	102	100
ASP2	C4-1-10	465	21	1318	0.46	0.332	0.015	0.0463	0.0008	0.38	0.0521	0.0021	291	13	292	5	290	93	101
ASP2	C4-1-12	59	6	1439	0.50	0.861	0.041	0.1023	0.0019	0.38	0.0611	0.0027	631	30	628	11	642	95	98
ASP2	C4-1-13	77	8	43993	0.43	0.930	0.043	0.1086	0.0019	0.39	0.0621	0.0026	668	31	665	12	679	91	98
ASP2	C4-1-14	93	4	20677	0.93	0.314	0.037	0.0420	0.0013	0.27	0.0542	0.0062	277	33	265	8	381	257	70
ASP2	C4-1-15	78	3	17167	1.72	0.319	0.045	0.0416	0.0016	0.27	0.0556	0.0076	281	40	263	10	436	303	60
ASP2	C4-2-1	163	7	3053	0.82	0.295	0.035	0.0408	0.0014	0.28	0.0524	0.0060	262	31	258	9	301	261	86
ASP2	C4-2-2	581	16	1802	0.74	0.186	0.011	0.0274	0.0005	0.34	0.0494	0.0027	173	10	174	3	165	128	105
ASP2	C4-2-3	591	51	57153	0.25	0.692	0.021	0.0859	0.0016	0.62	0.0584	0.0014	534	16	531	10	545	52	98
ASP2	C4-2-4	375	64	262659	0.20	1.746	0.053	0.1703	0.0032	0.63	0.0744	0.0017	1026	31	1014	19	1051	47	96
ASP2	C4-2-5	617	18	73109	1.13	0.198	0.008	0.0289	0.0006	0.46	0.0497	0.0018	183	8	183	4	181	86	101
ASP2	C4-2-6	200	6	2056	1.27	0.197	0.016	0.0290	0.0006	0.26	0.0494	0.0038	183	15	184	4	164	181	112
ASP2	C4-2-7	232	21	1777	0.39	0.749	0.029	0.0925	0.0018	0.51	0.0587	0.0020	567	22	570	11	556	73	102
ASP2	C4-2-8	160	7	451	0.45	0.293	0.029	0.0411	0.0008	0.21	0.0518	0.0050	261	26	259	5	275	221	94
ASP2	C4-2-9	187	5	21290	0.50	0.192	0.020	0.0277	0.0006	0.21	0.0501	0.0051	178	19	176	4	200	235	88
ASP2	C4-2-10	211	23	94631	0.27	0.931	0.042	0.1090	0.0023	0.46	0.0620	0.0025	668	30	667	14	673	86	99
ASP2	C4-2-11	372	11	43352	1.09	0.194	0.016	0.0284	0.0006	0.25	0.0495	0.0039	180	14	180	4	171	182	105
ASP2	C4-2-12	475	33	2326	0.26	0.535	0.021	0.0669	0.0014	0.51	0.0564	0.0019	435	17	429	8	466	74	92
ASP2	C4-2-13	208	6	1310	0.75	0.195	0.012	0.0284	0.0006	0.34	0.0499	0.0030	181	11	180	4	191	135	94
ASP2	C4-2-14	580	17	27126	0.39	0.196	0.008	0.0285	0.0006	0.46	0.0499	0.0019	182	8	181	4	188	89	96
ASP2	C4-2-15	271	8	32032	0.45	0.197	0.020	0.0287	0.0006	0.19	0.0497	0.0051	182	19	183	4	179	233	102
ASP2	C4-2-16	269	7	2186	0.99	0.190	0.017	0.0276	0.0006	0.23	0.0499	0.0042	177	15	176	4	191	197	92
ASP2	C4-2-17	458	39	161646	0.19	0.691	0.025	0.0859	0.0017	0.54	0.0583	0.0018	533	19	531	10	541	67	98
ASP2	C4-2-18	162	7	28777	0.12	0.308	0.014	0.0432	0.0009	0.46	0.0517	0.0021	272	12	272	6	272	91	100
ASP2	C4-2-19	216	37	152012	0.31	1.751	0.057	0.1719	0.0033	0.59	0.0739	0.0020	1027	34	1023	20	1038	54	99
ASP2	C4-2-20	59	11	1178	0.36	2.024	0.083	0.1903	0.0040	0.49	0.0771	0.0029	1124	49	1123	24	1125	75	100
ASP2	C4-2-21	430	39	3256	0.27	0.709	0.025	0.0880	0.0017	0.55	0.0585	0.0017	544	19	544	11	547	64	99
ASP2	C4-2-22	375	11	43644	1.05	0.204	0.010	0.0203	0.0006	0.44	0.0522	0.0022	130	9	130	4	294	96	61
ASP2	C4-2-24	114	5	314	0.32	0.290	0.027	0.0411	0.0012	0.30	0.0512	0.0046	259	24	260	7	248	205	105
ASP2	C4-2-25	625	55	7264	0.11	0.712	0.022	0.0883	0.0017	0.61	0.0585	0.0014	546	17	545	10	549	53	99
ASP2	C4-2-26	533	46	6973	0.59	0.708	0.026	0.0871	0.0017	0.53	0.0589	0.0018	543	20	538	11	564	68	96
ASP2	C4-2-27	211	6	770	1.07	0.215	0.011	0.0283	0.0006	0.43	0.0551	0.0025	198	10	180	4	415	100	43
ASP2	C4-2-31	326	24	4388	0.43	0.673	0.043	0.0739	0.0013	0.38	0.0661	0.0039	523	33	459	11	809	123	57
ASP2	C4-2-33	375	32	3757	0.51	0.687	0.026	0.0843	0.0017	0.53	0.0591	0.0019	531	20	522	10	569	69	92
ASP2	C4-2-34	603	17	233	0.59	0.423	0.017	0.0281	0.0006	0.52	0.1094	0.0037	358	14	178	4	1789	62	10
ASP2	C4-2-35	727	62	255853	0.40	0.692	0.022	0.0856	0.0016	0.59	0.0586	0.0015	534	17	529	10	553	57	96
ASP2	C4-2-36	1094	109	5483	0.14	0.822	0.028	0.0992	0.0019	0.56	0.0601	0.0017	609	21	609	12	607	62	100
ASP2	C4-2-37	939	69	5997	0.38	0.568	0.019	0.0731	0.0014	0.58	0.0564	0.0015	457	15	455	9	469	59	97
ASP2	C4-2-38	682	20	1501[illegible]	0.77	0.196	0.010	0.0286	0.0006	0.40	0.0498	0.0023	182	9	182	4	186	105	98
ASP2	C4-2-39	456	39	7589	0.18	0.677	0.021	0.0851	0.0016	0.60	0.0577	0.0015	525	17	526	10	519	56	101
ASP2	C4-2-40	682	115	471684	0.17	1.776	0.059	0.1682	0.0032	0.58	0.0766	0.0021	1037	34	1002	19	1111	54	90
ASP2	C4-2-41	926	164	15413	0.11	1.841	0.054	0.1774	0.0033	0.64	0.0753	0.0017	1060	31	1053	20	1076	45	98
ASP2	C4-2-42	90	3	7258	1.26	0.189	0.026	0.0280	0.0007	0.17	0.0491	0.0066	176	24	178	4	151	317	118
ASP2	C4-2-43	372	15	63587	0.33	0.298	0.016	0.0416	0.0008	0.36	0.0521	0.0027	265	15	263	5	288	117	91
ASP2	C4-2-44	350	29	119355	0.16	0.667	0.025	0.0830	0.0016	0.53	0.0583	0.0018	519	19	514	10	541	68	95
ASP2	C4-2-45	125	5	887	0.52	0.303	0.045	0.0418	0.0009	0.14	0.0526	0.0078	269	40	264	6	312	338	84
ASP2	C4-2-46	142	11	46269	0.44	0.633	0.035	0.0795	0.0018	0.40	0.0577	0.0030	498	28	493	11	520	113	95
ASP2	C4-2-47	329	9	37661	1.22	0.190	0.011	0.0278	0.0006	0.34	0.0496	0.0027	177	10	177	4	175	129	101
ASP2	C4-2-48	452	33	136298	0.85	0.568	0.018	0.0733	0.0014	0.59	0.0562	0.0015	457	15	456	9	460	58	99
ASP2	C4-2-49	174	5	20039	0.30	0.193	0.018	0.0279	0.0006	0.23	0.0500	0.0045	179	17	178	4	196	203	91

ASP2	C4-2-50	90	3	5235	0.93	0.195	0.019	0.0286	0.0007	0.24	0.0495	0.0047	181	18	182	4	171	222	107
ASP2	C4-2-51	252	8	1106	1.44	0.214	0.011	0.0310	0.0007	0.40	0.0502	0.0024	197	10	197	4	202	113	97
ASP2	C4-2-52	543	24	641	0.76	0.313	0.016	0.0433	0.0008	0.36	0.0525	0.0026	277	14	273	5	306	111	89
ASP2	C4-2-53	52	2	193	0.84	0.282	0.035	0.0398	0.0010	0.19	0.0514	0.0063	253	32	252	6	259	283	97
ASP2	C4-2-54	284	11	44389	0.71	0.269	0.013	0.0380	0.0008	0.44	0.0513	0.0022	242	11	240	5	255	97	94
ASP2	C4-2-55	461	13	2181	0.45	0.197	0.011	0.0285	0.0006	0.37	0.0500	0.0025	182	10	181	4	195	116	93
ASP2	C4-2-56	665	28	681	0.37	0.314	0.019	0.0421	0.0008	0.32	0.0542	0.0031	278	17	266	5	378	128	70
ASP2	C4-2-57	538	92	5022	0.37	1.854	0.056	0.1701	0.0032	0.62	0.0790	0.0019	1065	32	1013	19	1173	47	86
ASP2	C4-2-58	290	24	99372	0.43	0.672	0.024	0.0833	0.0016	0.56	0.0585	0.0017	522	18	516	10	549	63	94
ASP2	C4-2-59	669	49	200394	0.19	0.571	0.018	0.0728	0.0014	0.60	0.0569	0.0014	459	15	453	9	487	56	93
ASP2	C4-2-60	440	19	3058	0.21	0.308	0.013	0.0429	0.0009	0.49	0.0522	0.0019	273	11	271	5	293	81	92
ASP2	C4-2-61	709	32	12031	0.74	0.284	0.012	0.0399	0.0008	0.47	0.0515	0.0019	253	11	252	5	263	86	96
ASP2	C4-2-62	163	31	2054	0.37	1.993	0.073	0.1800	0.0037	0.54	0.0769	0.0024	1113	41	1111	22	1119	61	99
ASP2	C4-2-63	1072	89	10517	0.10	0.684	0.021	0.0834	0.0016	0.62	0.0595	0.0014	529	16	517	10	584	53	89
ASP2	C4-2-64	409	15	60606	0.23	0.208	0.008	0.0301	0.0006	0.50	0.0500	0.0017	192	8	191	4	196	81	97
ASP2	C4-2-65	450	40	40389	0.29	0.722	0.023	0.0891	0.0017	0.59	0.0583	0.0015	552	18	550	10	560	56	98
ASP2	C4-2-66	213	18	1660	0.35	0.687	0.026	0.0856	0.0017	0.52	0.0582	0.0019	531	20	530	10	538	71	98
ASP2	C4-2-67	824	125	12543	0.17	1.536	0.047	0.1517	0.0029	0.61	0.0734	0.0018	945	29	911	17	1025	49	89
ASP2	C4-2-68	213	9	35470	0.74	0.287	0.022	0.0405	0.0008	0.27	0.0514	0.0038	256	19	256	5	259	163	99
ASP2	C4-2-69	308	27	9117	0.38	0.695	0.024	0.0865	0.0017	0.55	0.0583	0.0017	536	19	535	10	542	63	99
ASP2	C4-2-70	99	3	418	1.15	0.216	0.035	0.0286	0.0007	0.14	0.0548	0.0088	199	32	182	4	405	353	45
ASP2	C4-2-71	361	15	60687	0.49	0.290	0.019	0.0408	0.0008	0.31	0.0515	0.0031	259	17	258	5	263	140	98
ASP2	C4-2-72	213	6	2542	1.03	0.190	0.011	0.0277	0.0006	0.37	0.0499	0.0026	177	10	176	4	189	123	93
ASP2	C4-2-73	188	5	21667	0.34	0.192	0.011	0.0281	0.0006	0.37	0.0496	0.0027	178	10	179	4	174	127	102
ASP2	C4-2-74	248	15	2292	0.44	0.456	0.017	0.0588	0.0012	0.52	0.0562	0.0018	381	14	369	7	461	71	80
ASP2	C4-2-75	368	10	41157	1.18	0.190	0.009	0.0272	0.0006	0.42	0.0508	0.0023	177	9	173	4	231	104	75
ASP2	C4-2-76	2893	237	97315	0.11	0.655	0.021	0.0818	0.0016	0.59	0.0581	0.0015	512	17	507	10	535	57	95
ASP2	C4-2-77	708	27	3500	0.56	0.270	0.010	0.0384	0.0007	0.54	0.0510	0.0015	242	9	243	5	240	69	101
ASP2	C4-2-78	991	68	6469	0.52	0.572	0.018	0.0689	0.0013	0.60	0.0602	0.0015	459	14	430	8	611	53	70
ASP2	C4-2-79	351	13	2606	0.55	0.265	0.013	0.0374	0.0008	0.42	0.0513	0.0023	238	12	237	5	253	104	93
ASP2	C4-2-80	491	38	8843	0.35	0.634	0.025	0.0778	0.0015	0.50	0.0591	0.0020	499	20	483	10	570	74	85
ASP2	C4-2-81	634	24	100604	0.36	0.274	0.010	0.0386	0.0007	0.53	0.0515	0.0016	246	9	244	5	261	71	94
ASP2	C4-2-82	86	2	9776	1.51	0.191	0.033	0.0277	0.0007	0.14	0.0501	0.0086	178	31	176	4	201	393	88

[a] U and Pb concentrations and Th/U ratios are calculated relative to GJ-1 reference zircon

[b] Corrected for background and within-run Pb/U fractionation and normalised to reference zircon GJ-1 (ID-TIMS values/measured value); $^{207}Pb/^{235}U$ calculated using $(^{207}Pb/^{206}Pb)/(^{238}U/^{206}Pb * 1/137.88)$

[c] Rho is the error correlation defined as the quotient of the propagated errors of the $^{206}Pb/^{238}U$ and the $^{207}/^{235}U$ ratio

[d] Quadratic addition of within-run errors (2 SD) and daily reproducibility of GJ-1 (2 SD)

[e] Corrected for mass-bias by normalising to GJ-1 reference zircon (~0.6 per atomic mass unit) and common Pb using the model Pb composition of Stacey & Kramers (1975)

Table B3. LA-ICPMS isotopic data for sample ASC3 from the Suurberg Group in the northern Algoa Basin

ASC3						RATIOS							AGES [Ma]						Conc.
Sample	Analysis	U [ppm][a]	Pb [ppm][a]	$^{206}Pb/^{204}Pb$	Th/U[a]	$^{207}Pb/^{235}U$[b]	2 σ[d]	$^{206}Pb/^{238}U$[b]	2 σ[d]	rho[c]	$^{207}Pb/^{206}Pb$[e]	2 σ[d]	$^{207}Pb/^{235}U$	2 σ	$^{206}Pb/^{238}U$	2 σ	$^{207}Pb/^{206}Pb$	2 σ	%
ASC3	C3-1	216	18	77783	0.62	0.641	0.024	0.0811	0.0013	0.43	0.0574	0.0019	503	19	502	8	506	74	99
ASC3	C3-2	242	11	47564	1.51	0.320	0.014	0.0444	0.0007	0.39	0.0522	0.0021	282	12	280	5	296	90	95
ASC3	C3-3	53	10	45331	0.23	2.059	0.098	0.1921	0.0037	0.40	0.0777	0.0034	1135	54	1133	22	1140	86	99
ASC3	C3-4	224	18	81949	0.53	0.656	0.030	0.0824	0.0015	0.38	0.0578	0.0025	512	24	511	9	521	94	98
ASC3	C3-5	183	5	445	1.69	0.213	0.023	0.0294	0.0006	0.18	0.0527	0.0056	196	21	187	4	315	241	59
ASC3	C3-6	68	4	19868	0.75	0.507	0.028	0.0660	0.0013	0.35	0.0558	0.0029	417	23	412	8	443	115	93
ASC3	C3-7	188	6	4905	0.81	0.205	0.025	0.0297	0.0005	0.14	0.0502	0.0062	190	24	189	3	202	285	93
ASC3	C3-8	315	13	2838	0.99	0.291	0.011	0.0407	0.0007	0.41	0.0519	0.0019	260	10	257	4	282	82	91
ASC3	C3-9	338	43	188603	0.08	1.183	0.043	0.1259	0.0020	0.45	0.0682	0.0022	793	29	765	12	873	67	88
ASC3	C3-10	252	11	4434	0.51	0.313	0.013	0.0438	0.0007	0.41	0.0519	0.0019	276	11	276	5	279	84	99
ASC3	C3-11	279	20	89579	0.32	0.558	0.026	0.0726	0.0013	0.38	0.0557	0.0024	450	21	452	8	441	94	102
ASC3	C3-12	333	30	132346	0.52	0.728	0.022	0.0897	0.0014	0.51	0.0589	0.0015	555	17	554	8	562	56	99
ASC3	C3-13	60	11	47993	0.48	1.859	0.070	0.1802	0.0030	0.45	0.0748	0.0025	1067	40	1068	18	1064	68	100
ASC3	C3-15	133	13	58426	0.28	0.824	0.034	0.0993	0.0017	0.41	0.0602	0.0023	610	25	610	10	611	81	100
ASC3	C3-16	230	7	29524	1.06	0.209	0.009	0.0291	0.0005	0.39	0.0521	0.0021	192	8	185	3	288	90	64
ASC3	C3-17	162	23	100302	0.44	1.329	0.043	0.1398	0.0022	0.48	0.0690	0.0020	859	28	844	13	897	59	94
ASC3	C3-18	213	22	97345	0.37	0.862	0.029	0.1033	0.0016	0.46	0.0605	0.0018	631	21	634	10	622	65	102
ASC3	C3-19	108	3	138	2.01	0.269	0.056	0.0294	0.0007	0.11	0.0663	0.0137	242	50	187	4	816	432	23
ASC3	C3-20	166	15	6947	0.55	0.724	0.024	0.0872	0.0014	0.46	0.0602	0.0018	553	19	539	8	609	65	88
ASC3	C3-21	68	7	28926	0.02	0.803	0.034	0.0969	0.0017	0.40	0.0601	0.0024	599	26	596	10	608	85	98
ASC3	C3-22	140	13	5567	0.57	0.749	0.029	0.0920	0.0015	0.42	0.0591	0.0021	568	22	567	9	570	77	99
ASC3	C3-23	385	30	9375	0.37	0.631	0.044	0.0772	0.0017	0.32	0.0592	0.0039	497	34	480	11	576	142	83
ASC3	C3-24	242	25	7873	0.46	0.853	0.029	0.1013	0.0016	0.46	0.0610	0.0018	626	21	622	10	640	65	97
ASC3	C3-25	187	5	676	0.56	0.197	0.031	0.0286	0.0005	0.11	0.0500	0.0079	183	29	182	3	194	367	94
ASC3	C3-26	294	26	10713	0.48	0.716	0.022	0.0889	0.0014	0.49	0.0584	0.0016	549	17	549	8	546	59	101
ASC3	C3-27	163	5	450	0.89	0.205	0.022	0.0299	0.0005	0.16	0.0499	0.0054	190	21	190	3	190	251	100
ASC3	C3-28	118	7	723	0.41	0.496	0.036	0.0619	0.0014	0.31	0.0581	0.0040	409	30	387	9	534	152	72
ASC3	C3-29	186	16	1205	0.47	0.665	0.023	0.0835	0.0013	0.46	0.0577	0.0018	518	18	517	8	520	68	99
ASC3	C3-30	151	7	1295	0.39	0.317	0.063	0.0442	0.0007	0.08	0.0521	0.0104	280	56	279	5	292	455	96
ASC3	C3-32	142	11	50481	0.35	0.641	0.026	0.0808	0.0014	0.41	0.0576	0.0022	503	21	501	8	513	82	98
ASC3	C3-33	502	39	2946	0.15	0.674	0.023	0.0781	0.0012	0.46	0.0625	0.0019	523	18	485	8	693	65	70
ASC3	C3-34	246	10	3050	0.97	0.288	0.023	0.0402	0.0007	0.20	0.0520	0.0041	257	21	254	4	283	181	90
ASC3	C3-35	44	1	169	1.22	0.228	0.089	0.0300	0.0007	0.06	0.0552	0.0216	209	82	190	5	420	874	45
ASC3	C3-36	90	3	11776	1.58	0.203	0.038	0.0297	0.0006	0.10	0.0497	0.0093	188	35	189	4	180	436	105
ASC3	C3-37	60	2	318	1.20	0.207	0.035	0.0301	0.0007	0.15	0.0498	0.0083	191	32	191	5	187	386	103
ASC3	C3-38	177	25	5514	0.62	1.344	0.041	0.1434	0.0022	0.50	0.0680	0.0018	865	26	864	13	869	55	99
ASC3	C3-40	81	7	1127	0.39	0.960	0.082	0.0881	0.0025	0.33	0.0790	0.0064	683	59	544	16	1172	160	46
ASC3	C3-41	147	8	549	0.37	0.447	0.035	0.0565	0.0013	0.31	0.0574	0.0042	375	29	354	8	506	162	70
ASC3	C3-42	160	13	1769	0.57	0.686	0.059	0.0835	0.0022	0.31	0.0596	0.0049	530	45	517	13	589	177	88
ASC3	C3-43	116	11	902	0.73	0.746	0.034	0.0922	0.0016	0.39	0.0587	0.0025	566	26	569	10	554	92	103
ASC3	C3-44	220	18	3216	0.79	0.666	0.027	0.0831	0.0014	0.41	0.0581	0.0021	518	21	515	9	535	81	96
ASC3	C3-45	302	27	7426	0.28	0.729	0.023	0.0893	0.0014	0.49	0.0592	0.0016	556	17	552	8	573	59	96
ASC3	C3-46	58	2	77	1.29	0.410	0.125	0.0427	0.0010	0.07	0.0697	0.0213	349	107	269	6	919	628	29
ASC3	C3-47	103	3	442	1.08	0.200	0.030	0.0292	0.0007	0.16	0.0497	0.0074	185	28	185	5	180	345	103
ASC3	C3-49	251	21	2161	0.48	0.650	0.024	0.0821	0.0013	0.44	0.0574	0.0019	508	19	508	8	508	73	100
ASC3	C3-50	171	14	62656	0.47	0.670	0.030	0.0834	0.0015	0.39	0.0583	0.0024	521	24	516	9	540	92	96
ASC3	C3-51	151	12	407	0.29	0.777	0.072	0.0779	0.0023	0.32	0.0723	0.0063	584	54	484	14	993	178	49
ASC3	C3-52	257	44	192830	0.13	1.710	0.050	0.1705	0.0026	0.52	0.0728	0.0018	1012	30	1015	15	1007	51	101
ASC3	C3-53	174	5	439	0.67	0.198	0.040	0.0292	0.0005	0.09	0.0492	0.0100	183	37	185	3	155	474	120
ASC3	C3-55	225	20	86674	0.24	0.710	0.027	0.0876	0.0014	0.43	0.0588	0.0020	545	21	542	9	559	74	97

ASC3	C3-56	261	25	110974	0.69	0.797	0.030	0.0968	0.0016	0.43	0.0598	0.0021	595	23	596	10	595	75	100
ASC3	C3-57	102	4	13273	1.23	0.292	0.041	0.0407	0.0007	0.13	0.0519	0.0073	260	37	257	5	282	322	91
ASC3	C3-58	225	7	29034	0.73	0.203	0.025	0.0293	0.0005	0.15	0.0503	0.0062	188	23	186	3	208	284	90
ASC3	C3-59	558	43	610	0.07	0.809	0.029	0.0778	0.0013	0.46	0.0754	0.0024	602	21	483	8	1079	63	45

[a]U and Pb concentrations and Th/U ratios are calculated relative to GJ-1 reference zircon

[b]Corrected for background and within-run Pb/U fractionation and normalised to reference zircon GJ-1 (ID-TIMS values/measured value): $^{207}Pb/^{235}U$ calculated using $(^{207}Pb/^{206}Pb)/(^{238}U/^{206}Pb * 1/137.88)$

[c]Rho is the error correlation defined as the quotient of the propagated errors of the $^{206}Pb/^{238}U$ and the $^{207}/^{235}U$ ratio

[d]Quadratic addition of within-run errors (2 SD) and daily reproducibility of GJ-1 (2 SD)

[e]Corrected for mass-bias by normalising to GJ-1 reference zircon (~0.6 per atomic mass unit) and common Pb using the model Pb composition of Stacey & Kramers (1975)

Table B4. LA-ICPMS isotopic data for sample ASUP from the Suurberg Group in the northern Algoa Basin

ASUP							RATIOS							AGES [Ma]						Conc.
Sample	Analysis	U [ppm][a]	Pb [ppm][a]	Th [ppm][a]	$^{206}Pb/^{204}Pb$	Th/U[a]	$^{207}Pb/^{235}U$[b]	2 σ[d]	$^{206}Pb/^{238}U$[b]	2 σ[d]	rho[c]	$^{207}Pb/^{206}Pb$[e]	2 σ[d]	$^{207}Pb/^{235}U$	2 σ	$^{206}Pb/^{238}U$	2 σ	$^{207}Pb/^{206}Pb$	2 σ	%
ASUP	ASUP-2	304	23	96	188423	0.31	0.591	0.017	0.07511	0.00108	0.51	0.0571	0.0014	472	13	467	7	495	53	94
ASUP	ASUP-3	264	8	303	1679	1.15	0.210	0.008	0.02930	0.00046	0.43	0.0519	0.0017	193	7	186	3	282	76	66
ASUP	ASUP-4	380	15	182	126938	0.48	0.285	0.009	0.04043	0.00060	0.49	0.0511	0.0013	254	8	255	4	243	60	105
ASUP	ASUP-6	366	16	175	4477	0.48	0.329	0.019	0.04269	0.00082	0.33	0.0560	0.0030	289	17	269	5	451	121	60
ASUP	ASUP-8	261	20	29	4663	0.11	0.594	0.026	0.07559	0.00128	0.38	0.0570	0.0023	474	21	470	8	493	90	95
ASUP	ASUP-9	149	11	69	94200	0.46	0.622	0.039	0.07659	0.00158	0.33	0.0589	0.0035	491	31	476	10	562	129	85
ASUP	ASUP-12	395	12	233	2024	0.59	0.201	0.011	0.02920	0.00046	0.30	0.0499	0.0025	186	10	186	3	192	118	97
ASUP	ASUP-13	289	8	351	8480	1.21	0.196	0.008	0.02865	0.00044	0.38	0.0497	0.0018	182	7	182	3	182	86	100
ASUP	ASUP-14	135	4	167	878	1.24	0.203	0.011	0.02959	0.00050	0.32	0.0498	0.0025	188	10	188	3	185	117	101
ASUP	ASUP-15	396	15	311	11356	0.78	0.303	0.015	0.03874	0.00068	0.35	0.0567	0.0026	268	13	245	4	473	103	51
ASUP	ASUP-17	162	14	67	29812	0.41	0.712	0.021	0.08872	0.00132	0.49	0.0582	0.0015	546	16	548	8	537	57	102
ASUP	ASUP-18	126	12	94	99587	0.74	0.785	0.025	0.09545	0.00142	0.46	0.0596	0.0016	588	18	588	9	589	60	100
ASUP	ASUP-19	97	4	49	1325	0.51	0.272	0.037	0.03698	0.00132	0.26	0.0533	0.0070	244	33	234	8	342	296	68
ASUP	ASUP-20	210	6	225	983	1.07	0.203	0.011	0.02938	0.00048	0.31	0.0501	0.0025	188	10	187	3	200	117	94
ASUP	ASUP-21	79	15	22	122018	0.28	1.982	0.072	0.18762	0.00308	0.45	0.0766	0.0025	1109	40	1108	18	1111	65	100
ASUP	ASUP-22	156	28	50	227646	0.32	1.823	0.052	0.17750	0.00260	0.52	0.0745	0.0018	1054	30	1053	15	1055	49	100
ASUP	ASUP-23	110	3	96	27069	0.87	0.207	0.009	0.02983	0.00050	0.37	0.0504	0.0021	191	9	189	3	212	98	90
ASUP	ASUP-24	289	20	143	165290	0.49	0.589	0.026	0.06931	0.00118	0.39	0.0617	0.0025	471	21	432	7	663	87	65
ASUP	ASUP-25	138	7	119	566	0.86	0.409	0.030	0.05172	0.00116	0.31	0.0573	0.0040	348	25	325	7	504	153	65
ASUP	ASUP-26	234	16	178	1428	0.76	0.526	0.028	0.06858	0.00126	0.35	0.0556	0.0027	429	23	428	8	435	110	98
ASUP	ASUP-28	58	2	82	13998	1.41	0.205	0.023	0.02909	0.00060	0.18	0.0511	0.0057	189	21	185	4	244	255	76
ASUP	ASUP-29	281	23	84	465	0.30	0.878	0.038	0.08272	0.00146	0.40	0.0770	0.0031	640	28	512	9	1121	80	46
ASUP	ASUP-30	151	13	125	103303	0.83	0.666	0.028	0.08298	0.00140	0.40	0.0582	0.0023	518	22	514	9	537	86	96
ASUP	ASUP-32	330	13	230	17329	0.70	0.339	0.018	0.04014	0.00076	0.35	0.0612	0.0031	296	16	254	5	647	109	39
ASUP	ASUP-33	223	7	430	2956	1.93	0.207	0.013	0.02977	0.00046	0.25	0.0504	0.0030	191	12	189	3	215	136	88
ASUP	ASUP-34	226	12	133	414	0.59	0.440	0.030	0.05120	0.00112	0.32	0.0623	0.0040	370	25	322	7	684	136	47
ASUP	ASUP-35	166	14	107	115156	0.65	0.846	0.042	0.08434	0.00158	0.38	0.0727	0.0033	622	31	522	10	1006	93	52
ASUP	ASUP-37	113	3	136	27457	1.21	0.205	0.021	0.02961	0.00050	0.17	0.0501	0.0050	189	19	188	3	201	233	94
ASUP	ASUP-38	194	29	126	1069	0.65	1.573	0.058	0.14800	0.00242	0.44	0.0771	0.0025	959	35	890	15	1123	66	79
ASUP	ASUP-39	431	26	67	459	0.16	0.767	0.027	0.06093	0.00098	0.45	0.0913	0.0029	578	21	381	6	1454	60	26
ASUP	ASUP-42	147	6	93	40516	0.63	0.287	0.033	0.04013	0.00122	0.27	0.0518	0.0057	256	29	254	3	277	252	92
ASUP	ASUP-43	251	19	126	24822	0.50	0.634	0.030	0.07432	0.00152	0.34	0.0619	0.0035	499	30	462	9	670	121	69
ASUP	ASUP-44	457	13	200	687	0.44	0.203	0.012	0.02943	0.00044	0.26	0.0513	0.0029	192	11	187	3	255	130	73
ASUP	ASUP-46	334	25	143	3116	0.43	0.610	0.024	0.07601	0.00124	0.42	0.0582	0.0021	484	19	472	3	533	70	88
ASUP	ASUP-47	321	9	263	1840	0.82	0.209	0.013	0.02869	0.00044	0.24	0.0529	0.0033	193	12	182	3	323	142	56
ASUP	ASUP-49	212	16	121	120173	0.57	0.579	0.036	0.07345	0.00150	0.33	0.0572	0.0033	464	29	457	9	500	120	91
ASUP	ASUP-50	596	17	328	8420	0.55	0.199	0.006	0.02930	0.00044	0.50	0.0492	0.0013	184	6	186	3	155	61	120
ASUP	ASUP-51	118	22	105	12076	0.89	2.023	0.069	0.18333	0.00294	0.47	0.0800	0.0024	1125	33	1083	17	1196	59	91
ASUP	ASUP-52	374	18	209	1050	0.56	0.358	0.020	0.04881	0.00092	0.33	0.0532	0.0029	311	13	307	6	335	122	91
ASUP	ASUP-53	164	14	113	4830	0.69	0.813	0.042	0.08333	0.00160	0.37	0.0708	0.0034	607	31	519	10	951	98	55
ASUP	ASUP-54	243	20	105	1670	0.43	0.725	0.039	0.08405	0.00160	0.36	0.0625	0.0031	553	30	520	10	692	106	75
ASUP	ASUP-55	274	12	127	95697	0.46	0.314	0.022	0.04250	0.00090	0.31	0.0536	0.0035	277	19	268	6	355	147	75
ASUP	ASUP-56	408	15	223	1347	0.55	0.265	0.014	0.03645	0.00066	0.34	0.0527	0.0027	238	13	231	4	314	115	73
ASUP	ASUP-57	280	8	372	458	1.33	0.225	0.016	0.02917	0.00048	0.24	0.0560	0.0038	206	14	185	3	451	149	41
ASUP	ASUP-58	163	11	120	2015	0.74	0.572	0.032	0.06484	0.00128	0.35	0.0639	0.0034	459	26	405	8	733	112	55
ASUP	ASUP-59	194	39	59	994	0.30	2.159	0.063	0.20175	0.00292	0.50	0.0776	0.0020	1168	34	1185	17	1137	50	104
ASUP	ASUP 60	301	26	140	213670	0.46	0.689	0.020	0.08628	0.00126	0.50	0.0579	0.0015	532	16	533	8	527	55	101
ASUP	ASUP-62	361	17	109	13196	0.30	0.370	0.023	0.04712	0.00094	0.32	0.0569	0.0033	320	20	297	6	483	129	61
ASUP	ASUP 63	359	15	128	1442	0.36	0.355	0.023	0.04169	0.00090	0.33	0.0618	0.0039	309	20	263	6	668	134	39
ASUP	ASUP-65	125	24	27	198981	0.22	2.065	0.076	0.19298	0.00320	0.45	0.0776	0.0026	1137	42	1137	19	1137	66	100
ASUP	ASUP 66	442	31	47	5166	0.11	0.566	0.020	0.06993	0.00108	0.43	0.0587	0.0019	455	16	436	7	555	71	78
ASUP	ASUP-67	397	12	312	889	0.79	0.203	0.016	0.02927	0.00048	0.21	0.0503	0.0039	188	15	186	3	210	180	88
ASUP	ASUP-68	166	5	259	39194	1.56	0.197	0.014	0.02871	0.00048	0.23	0.0499	0.0035	183	13	182	3	183	164	97
ASUP	ASUP-69	300	12	341	352	1.14	0.368	0.022	0.03862	0.00078	0.34	0.0691	0.0038	318	19	244	5	902	113	27
ASUP	ASUP-70	405	12	387	2173	0.95	0.210	0.007	0.03051	0.00046	0.45	0.0499	0.0015	193	6	194	3	183	69	103
ASUP	ASUP-71	160	5	224	661	1.40	0.205	0.023	0.02990	0.00078	0.23	0.0497	0.0055	189	21	190	5	180	256	106

ASUP	ASUP-72	549	40	19	23032	0.03	0.559	0.021	0.07217	0.00116	0.42	0.0562	0.0019	451	17	449	7	461	76	97
ASUP	ASUP-73	215	18	93	611	0.43	0.790	0.032	0.08374	0.00140	0.42	0.0684	0.0025	591	24	518	9	880	76	59
ASUP	ASUP-74	207	15	129	126882	0.62	0.576	0.033	0.07438	0.00146	0.34	0.0562	0.0031	462	27	462	9	461	121	100
ASUP	ASUP-75	120	12	29	2457	0.24	0.856	0.052	0.09872	0.00204	0.34	0.0629	0.0036	628	38	607	13	705	120	86
ASUP	ASUP-78	307	13	188	1981	0.61	0.307	0.013	0.04285	0.00070	0.40	0.0519	0.0020	272	11	270	4	282	80	96
ASUP	ASUP-79	566	16	170	1635	0.30	0.202	0.008	0.02838	0.00042	0.38	0.0517	0.0019	187	7	180	3	270	83	67
ASUP	ASUP-80	112	19	66	1840	0.59	1.806	0.068	0.16654	0.00274	0.45	0.0813	0.0026	1009	39	993	16	1227	63	81
ASUP	ASUP-81	157	5	152	1526	0.97	0.206	0.010	0.02995	0.00050	0.35	0.0500	0.0022	191	9	190	3	194	104	98
ASUP	ASUP-82	247	7	282	60090	1.14	0.204	0.015	0.02957	0.00048	0.23	0.0501	0.0035	189	14	188	3	201	163	93
ASUP	ASUP-84	148	13	91	105521	0.62	0.735	0.048	0.08662	0.00186	0.33	0.0616	0.0038	560	36	536	11	659	132	81
ASUP	ASUP-85	574	13	391	143300	0.68	0.213	0.012	0.03050	0.00056	0.33	0.0519	0.0027	200	11	194	4	280	118	69

[a]U and Pb concentrations and Th/U ratios are calculated relative to GJ-1 reference zircon

[b]Corrected for background and within-run Pb/U fractionation and normalised to reference zircon GJ-1 (ID-TIMS values/measured value); ^{207}Pb/^{235}U calculated using (^{207}Pb/^{206}Pb)/(^{238}U/^{206}Pb * 1/137.88)

[c]Rho is the error correlation defined as the quotient of the propagated errors of the ^{206}Pb/^{238}U and the ^{207}/^{235}U ratio

[d]Quadratic addition of within-run errors (2 SD) and daily reproducibility of GJ-1 (2 SD)

[e]Corrected for mass-bias by normalising to GJ-1 reference zircon (~0.6 per atomic mass unit) and common Pb using the model Pb composition of Stacey & Kramers (1975)

Table B5. LA-ICPMS isotopic data for sample ASLO from the Suurberg Group in the northern Algoa Basin

ASLO							RATIOS							AGES [Ma]						Conc.
Sample	Analysis	U [ppm][a]	Pb [ppm][a]	Th [ppm][a]	$^{206}Pb/^{204}Pb$	Th/U[a]	$^{207}Pb/^{235}U$[b]	2 σ[d]	$^{206}Pb/^{238}U$[b]	2 σ[d]	rho[c]	$^{207}Pb/^{206}Pb$[e]	2 σ[d]	$^{207}Pb/^{235}U$	2 σ	$^{206}Pb/^{238}U$	2 σ	$^{207}Pb/^{206}Pb$	2 σ	%
ASLO	ASLO-1	189	6	265	53616	1.40	0.208	0.011	0.0303	0.0005	0.30	0.0499	0.0024	192	10	192	3	192	114	100
ASLO	ASLO-2	372	32	220	3120	0.59	0.741	0.023	0.0856	0.0012	0.47	0.0628	0.0017	563	17	529	8	702	58	75
ASLO	ASLO-3	270	10	111	4731	0.41	0.338	0.022	0.0353	0.0007	0.31	0.0694	0.0044	295	20	224	5	911	130	25
ASLO	ASLO-6	88	9	39	462	0.45	1.049	0.065	0.1047	0.0023	0.35	0.0726	0.0042	728	45	642	14	1004	118	64
ASLO	ASLO-7	161	29	68	275807	0.42	1.918	0.053	0.1829	0.0026	0.52	0.0761	0.0018	1087	30	1083	15	1097	47	99
ASLO	ASLO-9	26	1	61	7357	2.32	0.214	0.057	0.0301	0.0007	0.09	0.0516	0.0136	197	52	191	5	268	603	72
ASLO	ASLO-10	110	4	274	237	2.48	0.450	0.037	0.0354	0.0010	0.34	0.0921	0.0071	377	31	224	6	1470	147	15
ASLO	ASLO-11	291	12	134	114288	0.46	0.304	0.019	0.0420	0.0008	0.31	0.0525	0.0032	270	17	265	5	307	138	86
ASLO	ASLO-12	472	42	76	3208	0.16	0.731	0.026	0.0900	0.0014	0.43	0.0590	0.0019	557	20	555	9	565	70	98
ASLO	ASLO-13	481	20	379	185322	0.79	0.315	0.015	0.0412	0.0007	0.36	0.0555	0.0025	278	14	260	5	432	101	60
ASLO	ASLO-14	304	13	166	256	0.55	0.456	0.027	0.0415	0.0009	0.35	0.0797	0.0044	381	22	262	5	1189	108	22
ASLO	ASLO-15	216	40	39	371308	0.18	1.926	0.068	0.1837	0.0029	0.45	0.0761	0.0024	1090	38	1087	17	1097	63	99
ASLO	ASLO-16	281	15	114	2508	0.41	0.411	0.020	0.0552	0.0009	0.35	0.0540	0.0024	349	17	346	6	369	101	94
ASLO	ASLO-17	181	13	43	1087	0.24	0.713	0.032	0.0733	0.0013	0.39	0.0705	0.0029	547	25	456	8	943	85	48
ASLO	ASLO-18	221	11	92	12676	0.42	0.378	0.012	0.0519	0.0008	0.45	0.0528	0.0015	326	11	326	5	322	66	101
ASLO	ASLO-20	145	4	124	39366	0.86	0.203	0.014	0.0292	0.0005	0.24	0.0504	0.0033	188	13	186	3	213	151	87
ASLO	ASLO-21	158	16	127	12456	0.80	0.854	0.026	0.1024	0.0015	0.48	0.0605	0.0016	627	19	628	9	620	57	101
ASLO	ASLO-22	220	18	116	2272	0.53	0.663	0.032	0.0825	0.0015	0.37	0.0583	0.0026	516	25	511	9	540	98	95
ASLO	ASLO-23	182	5	184	4670	1.01	0.218	0.019	0.0281	0.0004	0.17	0.0563	0.0049	200	18	178	3	462	194	39
ASLO	ASLO-24	203	7	203	1817	1.00	0.298	0.025	0.0369	0.0009	0.30	0.0586	0.0046	265	22	234	6	553	172	42
ASLO	ASLO-26	271	24	200	2385	0.74	0.812	0.032	0.0892	0.0015	0.41	0.0661	0.0024	604	24	551	9	809	75	68
ASLO	ASLO-27	8	0	10	2856	1.26	0.394	0.154	0.0376	0.0042	0.29	0.0762	0.0284	338	132	238	27	1100	746	22
ASLO	ASLO-28	267	141	143	3834	0.54	13.826	0.342	0.5295	0.0074	0.56	0.1894	0.0039	2738	68	2739	38	2737	34	100
ASLO	ASLO-29	169	6	107	317	0.64	0.392	0.021	0.0362	0.0007	0.36	0.0786	0.0040	336	18	229	5	1163	101	20
ASLO	ASLO-30	169	6	96	1351	0.57	0.283	0.023	0.0383	0.0009	0.29	0.0536	0.0042	253	21	242	6	355	175	68
ASLO	ASLO-32	155	28	59	262259	0.38	1.913	0.052	0.1822	0.0026	0.52	0.0761	0.0018	1086	30	1079	15	1098	47	98
ASLO	ASLO-33	208	19	47	172328	0.23	0.720	0.020	0.0893	0.0013	0.51	0.0585	0.0014	551	16	551	8	549	53	100
ASLO	ASLO-34	288	49	162	2446	0.56	1.627	0.058	0.1695	0.0026	0.48	0.0782	0.0022	1055	33	1009	15	1151	55	88
ASLO	ASLO-35	208	25	63	667	0.30	1.353	0.051	0.1214	0.0020	0.43	0.0809	0.0028	869	33	738	12	1218	67	61
ASLO	ASLO-36	273	11	222	1081	0.81	0.336	0.020	0.0397	0.0008	0.33	0.0614	0.0034	294	17	251	5	652	120	39
ASLO	ASLO-38	542	42	218	3028	0.40	0.616	0.022	0.0772	0.0012	0.43	0.0578	0.0019	487	17	480	7	523	71	92
ASLO	ASLO-40	330	60	190	747	0.23	0.722	0.025	0.0711	0.0011	0.45	0.0737	0.0023	552	19	442	7	1034	62	43
ASLO	ASLO-41	412	16	263	667	0.64	0.361	0.020	0.0380	0.0007	0.35	0.0690	0.0035	313	17	240	5	893	105	27
ASLO	ASLO-42	254	23	129	12137	0.51	0.761	0.035	0.0904	0.0016	0.38	0.0611	0.0026	575	26	558	10	643	91	87
ASLO	ASLO-43	354	14	220	4954	0.62	0.390	0.019	0.0395	0.0007	0.37	0.0716	0.0033	334	17	249	5	975	95	26
ASLO	ASLO-44	111	3	124	30634	1.12	0.216	0.025	0.0299	0.0007	0.22	0.0526	0.0053	199	23	190	5	310	252	61
ASLO	ASLO-45	225	7	348	413	1.55	0.280	0.028	0.0293	0.0004	0.15	0.0692	0.0069	251	25	186	3	905	204	21
ASLO	ASLO-46	30	1	43	212	1.44	0.204	0.026	0.0295	0.0006	0.16	0.0502	0.0064	189	24	188	4	204	297	92
ASLO	ASLO-47	240	7	383	1816	1.60	0.202	0.010	0.0292	0.0004	0.30	0.0501	0.0024	187	9	186	3	201	110	93
ASLO	ASLO-48	177	5	124	48145	0.70	0.203	0.013	0.0294	0.0005	0.24	0.0500	0.0032	188	12	187	3	195	149	95
ASLO	ASLO-49	209	8	167	907	0.80	0.254	0.013	0.0360	0.0006	0.34	0.0511	0.0025	230	12	228	4	244	114	94
ASLO	ASLO-50	101	8	58	75749	0.58	0.710	0.058	0.0813	0.0021	0.31	0.0633	0.0049	545	44	504	13	719	164	70
ASLO	ASLO-54	204	6	191	402	0.94	0.250	0.015	0.0289	0.0004	0.26	0.0628	0.0035	227	13	184	3	701	120	26
ASLO	ASLO-55	64	3	36	244	0.55	0.315	0.035	0.0429	0.0013	0.27	0.0532	0.0057	278	31	271	8	337	241	80
ASLO	ASLO-56	761	21	277	643	0.36	0.251	0.014	0.0281	0.0004	0.26	0.0646	0.0034	227	12	179	3	761	110	24
ASLO	ASLO-57	221	9	98	29866	0.44	0.359	0.025	0.0411	0.0009	0.32	0.0633	0.0042	311	22	260	6	719	142	36
ASLO	ASLO-58	120	4	73	2059	0.61	0.228	0.026	0.0292	0.0005	0.15	0.0566	0.0064	208	24	185	3	475	250	39
ASLO	ASLO-60	193	15	86	4874	0.45	0.714	0.037	0.0778	0.0015	0.37	0.0665	0.0032	547	28	483	9	823	100	59
ASLO	ASLO-62	44	2	83	13864	1.89	0.212	0.027	0.0313	0.0010	0.27	0.0511	0.0055	220	24	217	6	247	247	88
ASLO	ASLO-63	278	8	286	1218	1.03	0.223	0.020	0.0293	0.0004	0.17	0.0551	0.0049	204	18	186	3	417	198	45
ASLO	ASLO-64	400	28	139	608	0.35	0.756	0.032	0.0709	0.0012	0.41	0.0773	0.0030	572	24	412	8	1130	77	39
ASLO	ASLO-66	366	13	241	752	0.66	0.318	0.012	0.0346	0.0005	0.42	0.0667	0.0022	281	10	219	3	829	70	26
ASLO	ASLO-67	461	17	189	158225	0.41	0.298	0.019	0.0374	0.0008	0.32	0.0579	0.0035	265	17	236	5	527	132	45
ASLO	ASLO-68	231	9	190	545	0.82	0.425	0.026	0.0405	0.0009	0.35	0.0761	0.0043	360	22	256	5	1099	114	23
ASLO	ASLO-70	460	35	66	3854	0.14	0.612	0.022	0.0768	0.0012	0.43	0.0578	0.0019	485	17	477	7	522	71	91
ASLO	ASLO-72	153	15	48	6152	0.31	0.789	0.057	0.0963	0.0022	0.32	0.0595	0.0041	591	43	593	14	584	148	101

ASLO	ASLO-73	78	14	23	3759	0.30	1.855	0.054	0.1795	0.0027	0.50	0.0750	0.0019	1065	31	1064	16	1067	51	100
ASLO	ASLO-74	576	25	97	1777	0.17	0.408	0.019	0.0430	0.0007	0.37	0.0690	0.0039	348	16	271	5	895	88	30
ASLO	ASLO-75	125	11	31	98560	0.25	0.698	0.033	0.0862	0.0015	0.38	0.0587	0.0025	538	25	533	9	557	94	96
ASLO	ASLO-76	431	12	341	680	0.79	0.207	0.015	0.0287	0.0004	0.21	0.0524	0.0036	191	13	182	3	302	157	60
ASLO	ASLO-77	275	8	267	422	0.97	0.213	0.020	0.0283	0.0004	0.16	0.0547	0.0049	196	18	180	3	400	202	45
ASLO	ASLO-78	241	32	50	1222	0.21	1.372	0.042	0.1343	0.0020	0.49	0.0741	0.0020	877	27	812	12	1044	54	78
ASLO	ASLO-81	165	5	90	501	0.54	0.208	0.016	0.0286	0.0005	0.22	0.0527	0.0038	192	14	182	3	315	166	58
ASLO	ASLO-82	182	18	30	715	0.44	1.251	0.052	0.0967	0.0017	0.42	0.0939	0.0036	824	35	595	11	1505	72	40
ASLO	ASLO-83	138	5	173	586	1.25	0.252	0.027	0.0360	0.0010	0.27	0.0509	0.0052	228	24	228	6	234	237	97
ASLO	ASLO-84	184	14	252	129405	1.37	0.684	0.030	0.0773	0.0013	0.39	0.0643	0.0026	529	23	480	8	750	85	64
ASLO	ASLO-85	232	13	39	1941	0.38	0.817	0.032	0.0783	0.0013	0.43	0.0752	0.0027	606	24	489	8	1073	71	46
ASLO	ASLO-86	315	70	277	7730	0.34	0.705	0.021	0.0859	0.0013	0.50	0.0595	0.0015	542	16	531	8	585	55	91
ASLO	ASLO-87	266	22	100	402	0.38	1.013	0.032	0.0828	0.0013	0.49	0.0893	0.0024	713	22	513	8	1410	52	36
ASLO	ASLO-88	153	4	137	333	0.90	0.296	0.021	0.0288	0.0005	0.23	0.0744	0.0051	263	18	183	3	1053	137	17
ASLO	ASLO-89	147	52	75	3126	0.51	6.217	0.191	0.3542	0.0056	0.52	0.1273	0.0033	2007	52	1955	31	2061	46	95
ASLO	ASLO-90	267	42	33	3433	0.13	1.712	0.049	0.1584	0.0023	0.51	0.0784	0.0019	1013	29	948	14	1157	49	82
ASLO	ASLO-91	141	4	130	624	0.92	0.285	0.024	0.0300	0.0005	0.19	0.0690	0.0056	255	21	191	3	897	169	21
ASLO	ASLO-92	191	14	128	8028	0.67	0.575	0.023	0.0716	0.0012	0.41	0.0583	0.0021	461	18	446	7	540	79	83
ASLO	ASLO-94	174	13	22	15644	0.12	0.641	0.032	0.0741	0.0014	0.36	0.0627	0.0030	503	25	461	8	699	100	66
ASLO	ASLO-95	157	16	80	953	0.51	0.927	0.038	0.1004	0.0017	0.41	0.0670	0.0025	666	27	617	10	838	77	74
ASLO	ASLO-96	382	44	144	1853	0.38	1.209	0.044	0.1146	0.0019	0.45	0.0765	0.0025	805	29	700	11	1108	65	63
ASLO	ASLO-97	188	27	55	5195	0.29	1.502	0.048	0.1437	0.0022	0.48	0.0758	0.0021	931	29	865	13	1091	55	79
ASLO	ASLO-99	145	13	51	2448	0.35	0.734	0.045	0.0901	0.0018	0.34	0.0591	0.0034	559	34	556	11	570	125	98
ASLO	ASLO-100	122	4	104	205	0.85	0.260	0.021	0.0298	0.0005	0.22	0.0633	0.0051	235	19	189	3	719	171	26
ASLO	ASLO-101	89	4	57	923	0.64	0.404	0.039	0.0415	0.0012	0.31	0.0707	0.0064	345	33	262	8	950	186	28
ASLO	ASLO-102	334	12	377	697	1.13	0.366	0.015	0.0359	0.0006	0.41	0.0739	0.0027	317	13	227	4	1039	75	22
ASLO	ASLO-103	164	21	40	1209	0.24	1.345	0.055	0.1283	0.0022	0.42	0.0760	0.0038	865	36	778	13	1096	75	71
ASLO	ASLO-104	151	12	51	416	0.34	0.911	0.047	0.0816	0.0016	0.38	0.0809	0.0038	658	34	506	10	1220	93	41
ASLO	ASLO-106	208	6	187	1184	0.90	0.215	0.015	0.0290	0.0005	0.23	0.0539	0.0037	198	14	184	3	368	157	50
ASLO	ASLO-107	283	64	121	1445	0.43	2.711	0.086	0.2275	0.0036	0.49	0.0865	0.0024	1332	42	1321	21	1348	54	98
ASLO	ASLO-109	320	13	231	998	0.72	0.388	0.018	0.0412	0.0007	0.39	0.0683	0.0029	333	15	260	5	878	88	30
ASLO	ASLO-112	262	20	58	183471	0.22	0.616	0.039	0.0772	0.0016	0.33	0.0579	0.0035	487	31	480	10	524	132	91
ASLO	ASLO-113	195	13	105	1282	0.54	0.707	0.023	0.0694	0.0011	0.47	0.0740	0.0022	543	18	432	7	1040	59	42
ASLO	ASLO-118	228	16	126	3357	0.55	0.620	0.034	0.0706	0.0014	0.35	0.0637	0.0032	490	27	440	8	732	108	60
ASLO	ASLO-118	38	1	69	116	1.83	0.471	0.065	0.0339	0.0015	0.33	0.1008	0.0131	392	54	215	10	1638	241	13

[a]U and Pb concentrations and Th/U ratios are calculated relative to GJ-1 reference zircon

[b]Corrected for background and within-run Pb/U fractionation and normalised to reference zircon GJ-1 (ID-TIMS values/measured value); $^{207}Pb/^{235}U$ calculated using $(^{207}Pb/^{206}Pb)/(^{238}U/^{206}Pb * 1/137.88)$

[c]Rho is the error correlation defined as the quotient of the propagated errors of the $^{206}Pb/^{238}U$ and the $^{207}/^{235}U$ ratio

[d]Quadratic addition of within-run errors (2 SD) and daily reproducibility of GJ-1 (2 SD)

[e]Corrected for mass-bias by normalising to GJ-1 reference zircon (~0.6 per atomic mass unit) and common Pb using the model Pb composition of Stacey & Kramers (1975)

Appendix C. LA-ICPMS detrital zircon isotopic data from samples in the Uitenhage Group plotted as concordia diagrams

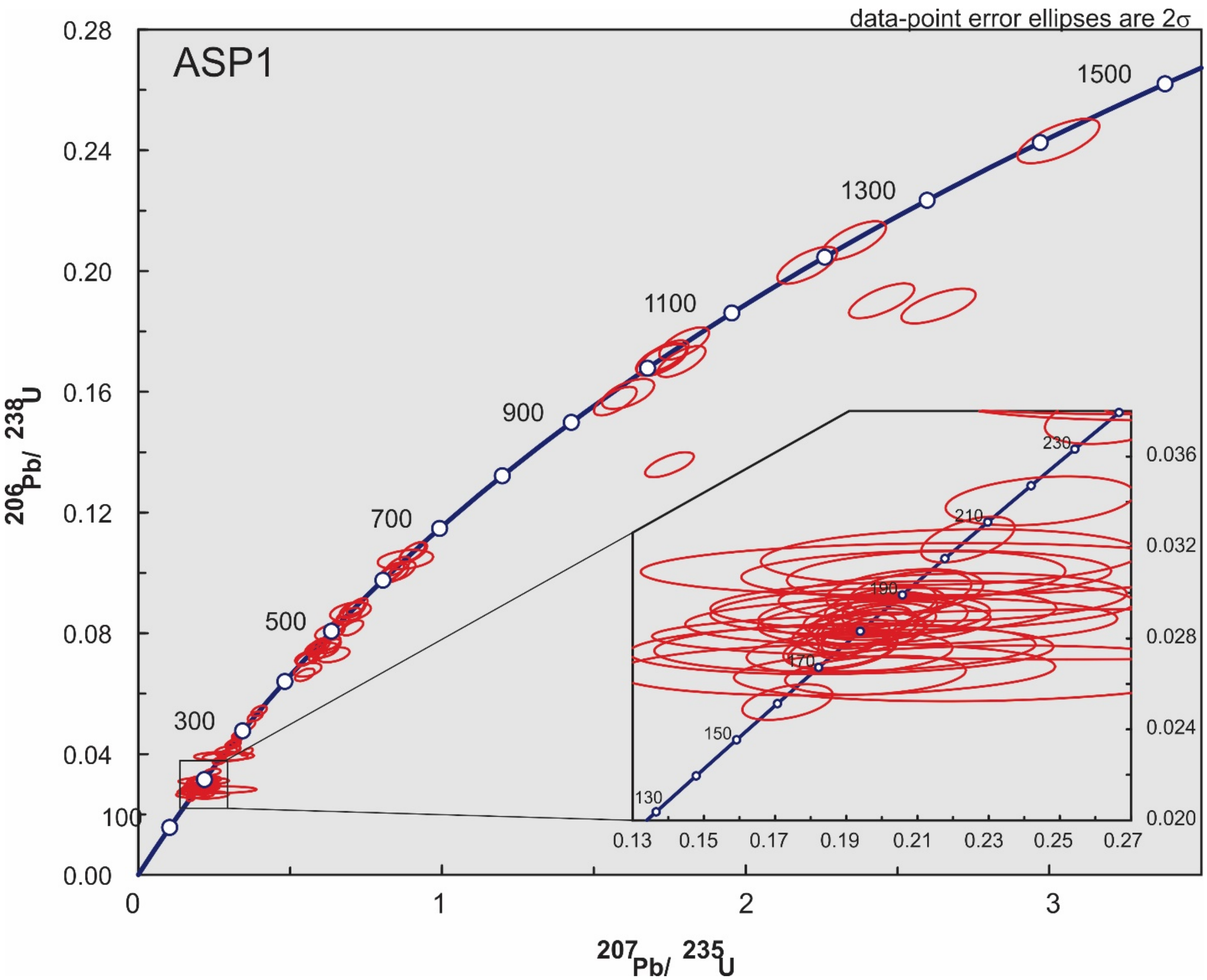

Fig. 1 Isotopic ratios for zircons analysed in sample ASP1, Algoa Basin

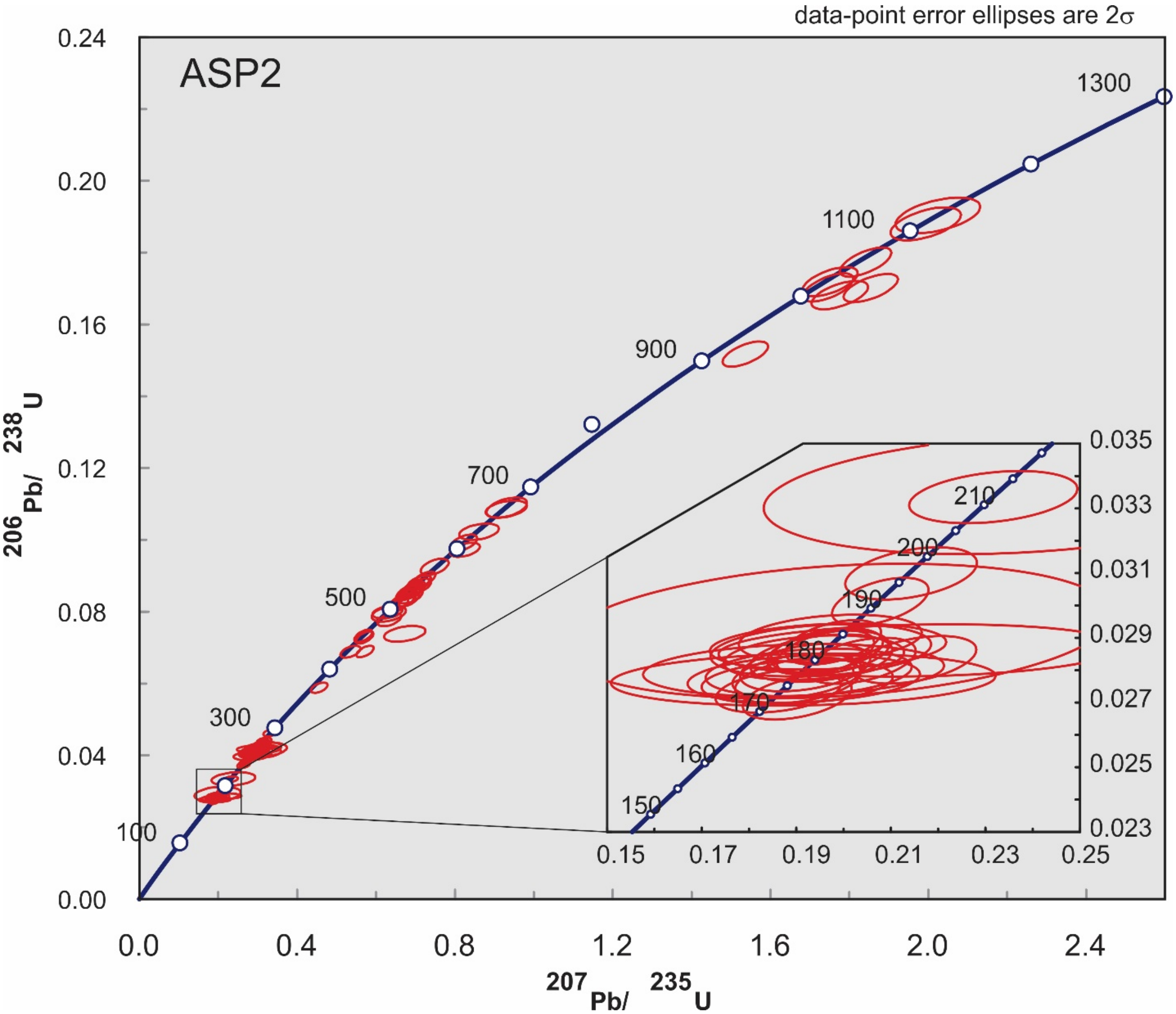

Fig. 2 Isotopic ratios for zircons analysed in sample ASP2, Algoa Basin

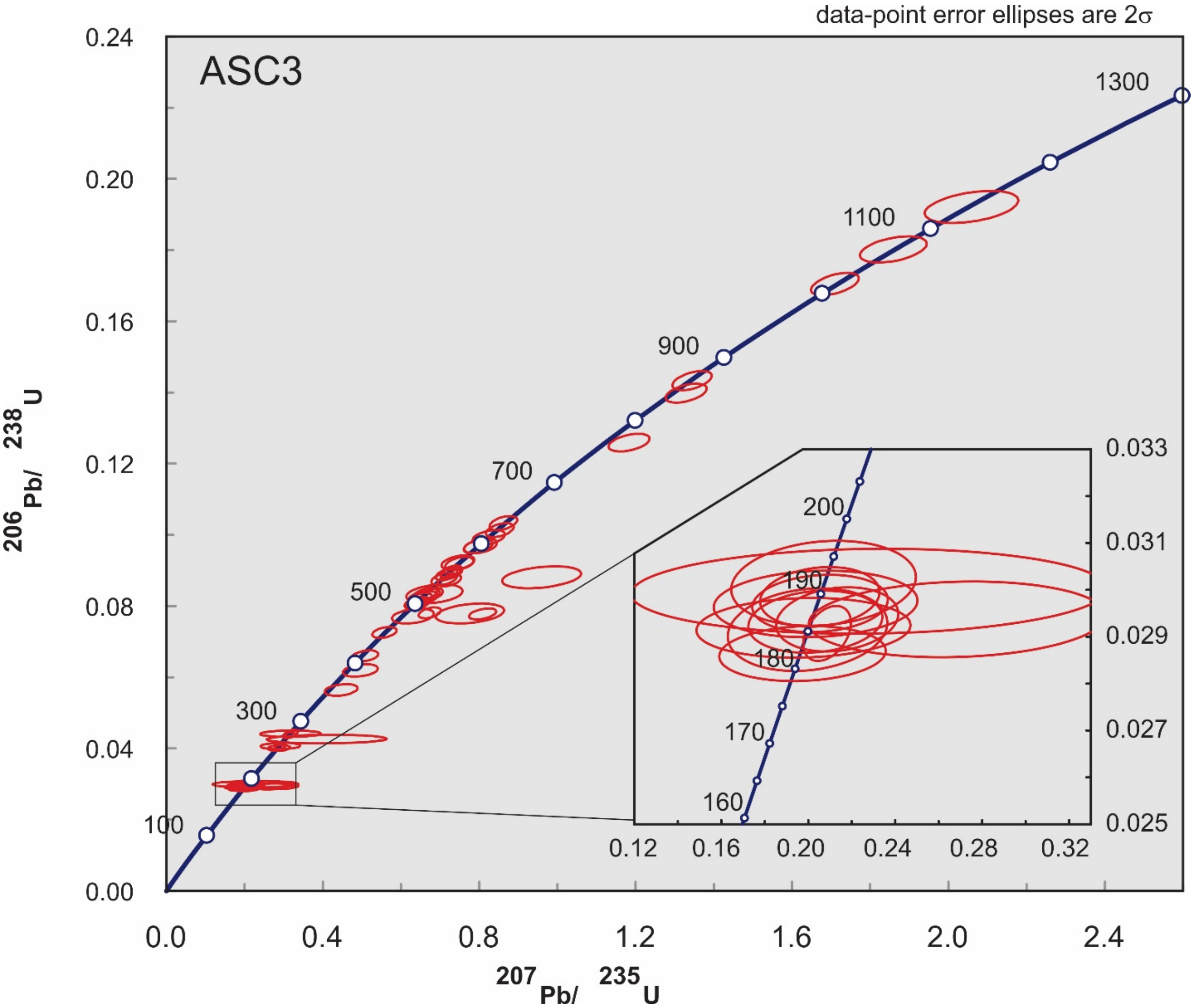

Fig. 3. Isotopic ratios for zircons analysed in sample ASC3, Algoa Basin

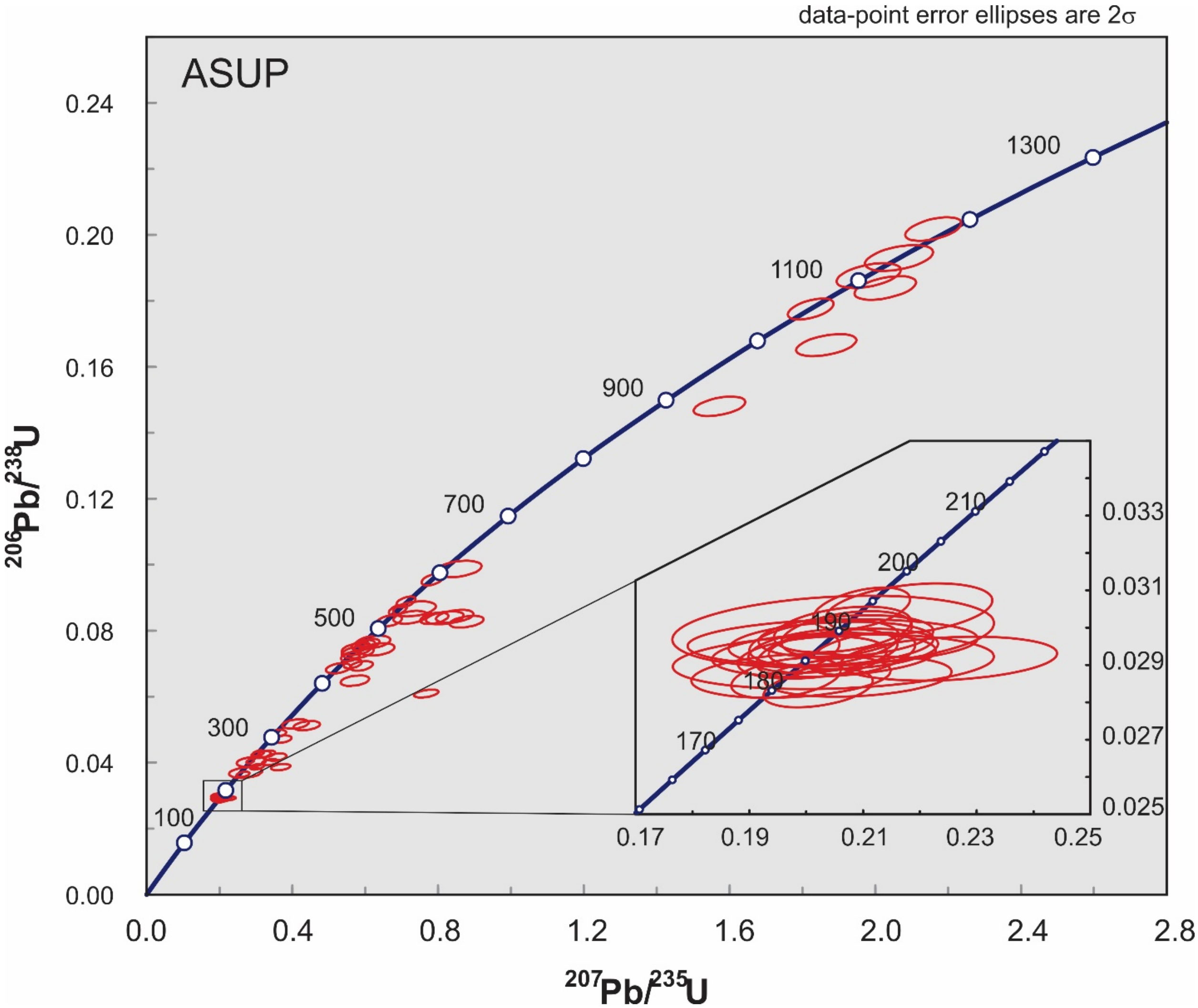

Fig. 4. Isotopic ratios for zircons analysed in sample ASUP, Algoa Basin

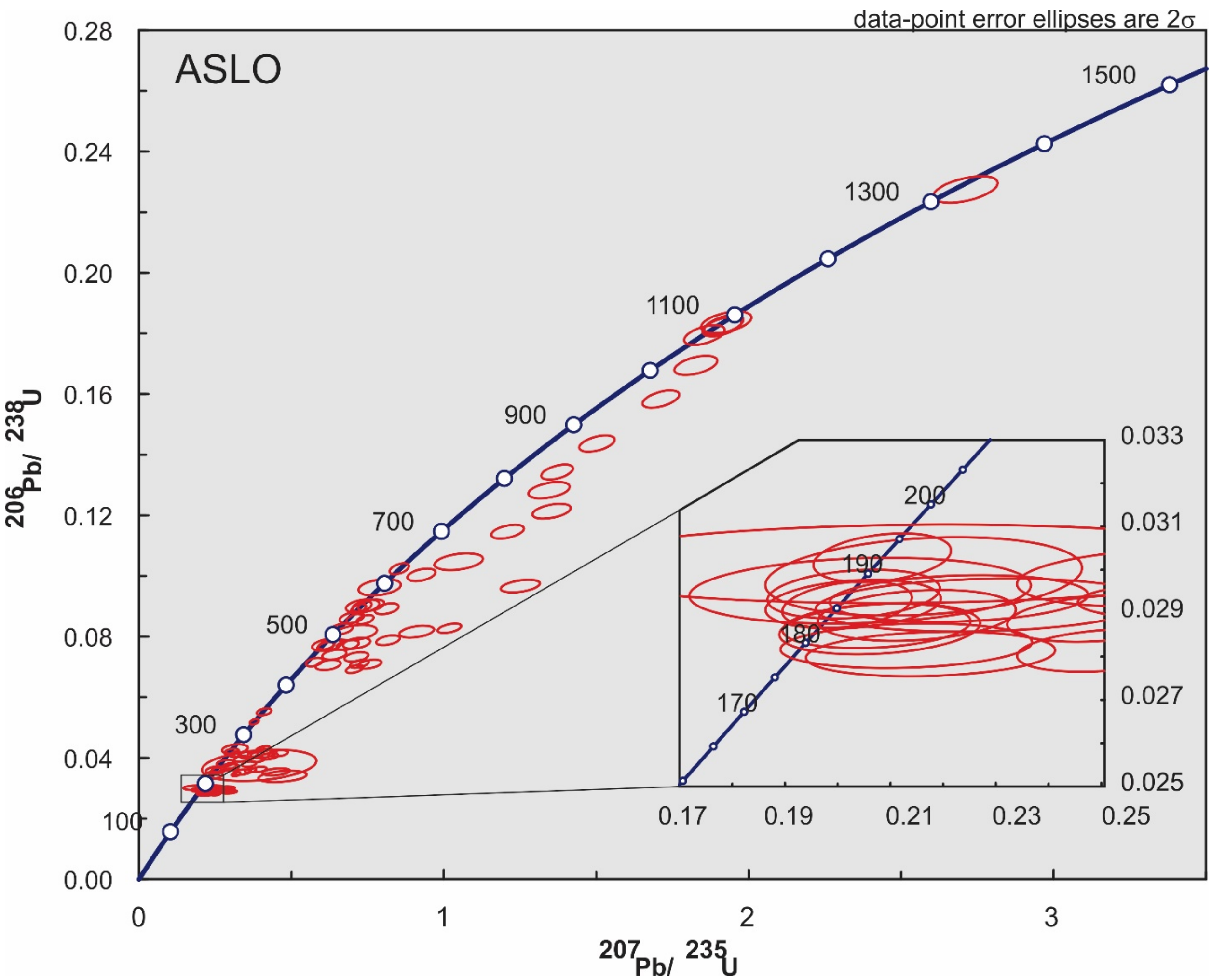

Fig. 5. Isotopic ratios for zircons analysed in sample ASLO, Algoa Basin

Appendix D. LA-ICPMS isotopic data for samples analysed during campaigns 1,2 and 3

Table D1. LA-ICPMS isotopic data for sample ROBE in the Robertson Basin

ROBE							RATIOS							AGES [Ma]						Conc.
Sample	Analysis	U [ppm][a]	Pb [ppm][a]	Th [ppm][a]	$^{206}Pb/^{204}Pb$	Th/U[a]	$^{207}Pb/^{235}U$[b]	2 σ[d]	$^{206}Pb/^{238}U$[b]	2 σ[d]	rho[c]	$^{207}Pb/^{206}Pb$[e]	2 σ[d]	$^{207}Pb/^{235}U$	2 σ	$^{206}Pb/^{238}U$	2 σ	$^{207}Pb/^{206}Pb$	2 σ	%
ROBE	BE-1	223	5	110	1411	0.49	0.163	0.007	0.02394	0.00050	0.49	0.0493	0.0018	153	6	153	3	160	86	95
ROBE	BE-2	264	6	168	799	0.64	0.171	0.015	0.02391	0.00050	0.23	0.0520	0.0045	161	14	152	3	284	199	54
ROBE	BE-3	449	11	260	98467	0.58	0.163	0.006	0.02344	0.00048	0.58	0.0503	0.0015	153	5	149	3	209	67	72
ROBE	BE-4	263	6	153	1972	0.58	0.158	0.006	0.02351	0.00048	0.50	0.0488	0.0017	149	6	150	3	140	83	107
ROBE	BE-5	386	9	175	2979	0.45	0.159	0.006	0.02351	0.00048	0.56	0.0490	0.0015	150	6	150	3	149	72	100
ROBE	BE-7	311	7	193	68638	0.62	0.161	0.008	0.02361	0.00048	0.43	0.0493	0.0021	151	7	150	3	164	99	92
ROBE	BE-8	334	8	181	6519	0.54	0.173	0.008	0.02536	0.00052	0.45	0.0495	0.0020	162	7	161	3	170	94	95
ROBE	BE-10	680	16	541	2167	0.80	0.159	0.009	0.02296	0.00046	0.34	0.0504	0.0028	150	9	146	3	211	130	69
ROBE	BE-11	863	20	670	7745	0.78	0.161	0.009	0.02295	0.00046	0.35	0.0508	0.0027	151	9	146	3	232	124	63
ROBE	BE-13	630	15	439	226	0.70	0.199	0.011	0.02386	0.00048	0.36	0.0604	0.0032	184	10	152	3	619	113	25
ROBE	BE-14	278	7	141	1320	0.51	0.159	0.011	0.02364	0.00050	0.30	0.0488	0.0033	150	11	151	3	138	161	109
ROBE	BE-15	624	15	440	7240	0.71	0.168	0.006	0.02401	0.00048	0.52	0.0507	0.0017	158	6	153	3	228	76	67
ROBE	BE-16	838	19	609	757	0.73	0.156	0.011	0.02244	0.00046	0.29	0.0505	0.0034	147	10	143	3	219	156	65
ROBE	BE-17	485	11	354	41985	0.73	0.161	0.006	0.02360	0.00048	0.57	0.0494	0.0015	151	5	150	3	165	69	91
ROBE	BE-18	559	13	417	8722	0.75	0.161	0.007	0.02351	0.00048	0.48	0.0495	0.0019	151	6	150	3	173	88	87
ROBE	BE-19	891	19	597	802	0.67	0.166	0.010	0.02086	0.00042	0.35	0.0578	0.0031	156	9	133	3	523	118	25
ROBE	BE-20	543	13	156	117633	0.29	0.157	0.005	0.02329	0.00048	0.59	0.0490	0.0014	148	5	148	3	146	66	101
ROBE	BE-21	267	6	114	1573	0.43	0.161	0.009	0.02338	0.00048	0.35	0.0500	0.0027	152	9	149	3	196	126	76
ROBE	BE-22	227	5	144	705	0.63	0.161	0.008	0.02394	0.00050	0.43	0.0489	0.0022	152	7	153	3	142	104	108
ROBE	BE-23	249	6	134	54569	0.54	0.159	0.008	0.02358	0.00050	0.44	0.0488	0.0021	150	7	150	3	138	101	109
ROBE	BE-25	232	5	162	1732	0.70	0.162	0.010	0.02338	0.00050	0.35	0.0503	0.0029	153	9	149	3	209	132	71
ROBE	BE-26	1068	24	561	3046	0.53	0.158	0.009	0.02226	0.00044	0.33	0.0514	0.0029	149	9	142	3	260	128	55
ROBE	BE-27	291	7	163	6756	0.56	0.159	0.006	0.02353	0.00048	0.52	0.0490	0.0016	150	6	150	3	146	78	102
ROBE	BE-28	316	7	198	232	0.63	0.175	0.014	0.02368	0.00050	0.27	0.0535	0.0041	164	13	151	3	352	171	43
ROBE	BE-31	208	5	122	485	0.59	0.169	0.020	0.02356	0.00050	0.18	0.0522	0.0060	159	19	150	3	292	262	51
ROBE	BE-33	726	17	482	160625	0.66	0.163	0.006	0.02390	0.00048	0.56	0.0496	0.0015	154	5	152	3	177	69	86
ROBE	BE-34	172	4	76	843	0.44	0.186	0.016	0.02324	0.00050	0.25	0.0581	0.0048	173	15	148	3	534	182	28
ROBE	BE-35	256	6	163	784	0.64	0.204	0.015	0.02358	0.00050	0.29	0.0626	0.0044	188	14	150	3	695	151	22
ROBE	BE-36	884	19	657	470	0.74	0.189	0.011	0.02100	0.00042	0.35	0.0654	0.0035	176	10	134	3	788	111	17
ROBE	BE-37	430	43	148	1518	0.34	0.973	0.034	0.10049	0.00204	0.58	0.0702	0.0020	690	24	617	13	935	59	66
ROBE	BE-38	325	8	188	71108	0.58	0.159	0.006	0.02365	0.00050	0.55	0.0488	0.0016	150	6	151	3	138	75	109
ROBE	BE-39	244	6	85	389	0.35	0.173	0.011	0.02386	0.00052	0.33	0.0526	0.0033	162	11	152	3	313	141	49
ROBE	BE-40	712	17	662	1449	0.93	0.171	0.010	0.02358	0.00048	0.35	0.0525	0.0029	160	9	150	3	308	124	49
ROBE	BE-41	303	7	201	1405	0.66	0.157	0.010	0.02310	0.00048	0.32	0.0492	0.0030	148	10	147	3	157	143	94
ROBE	BE-42	748	17	414	2025	0.55	0.156	0.009	0.02246	0.00046	0.34	0.0503	0.0028	147	9	143	3	210	131	68
ROBE	BE-43	268	6	164	1019	0.61	0.165	0.014	0.02401	0.00050	0.25	0.0497	0.0041	155	13	153	3	181	191	85
ROBE	BE-44	676	16	462	5396	0.68	0.160	0.007	0.02319	0.00048	0.49	0.0500	0.0019	150	6	148	3	193	87	77
ROBE	BE-45	353	8	223	382	0.63	0.165	0.018	0.02320	0.00048	0.19	0.0515	0.0054	155	16	148	3	264	240	56
ROBE	BE-46	365	9	259	492	0.71	0.190	0.011	0.02372	0.00050	0.38	0.0582	0.0030	177	10	151	3	538	113	28
ROBE	BE-47	283	7	150	1176	0.53	0.170	0.009	0.02374	0.00050	0.41	0.0519	0.0024	159	8	151	3	280	106	54
ROBE	BE-49	309	7	194	1916	0.63	0.161	0.008	0.02380	0.00050	0.45	0.0491	0.0020	152	7	152	3	151	97	100
ROBE	BE-50	730	17	441	2069	0.60	0.158	0.006	0.02318	0.00048	0.53	0.0495	0.0017	149	6	148	3	170	78	87
ROBE	BE-51	270	6	170	497	0.63	0.168	0.016	0.02312	0.00048	0.22	0.0526	0.0049	157	15	147	3	310	213	47
ROBE	BE-52	293	7	153	61825	0.52	0.156	0.006	0.02291	0.00048	0.51	0.0495	0.0018	147	6	146	3	169	83	86
ROBE	BE-53	250	6	127	54078	0.51	0.160	0.009	0.02348	0.00050	0.39	0.0495	0.0025	151	8	150	3	173	117	87
ROBE	BE-54	356	8	229	1008	0.64	0.165	0.008	0.02333	0.00048	0.42	0.0513	0.0023	155	8	149	3	252	102	59
ROBE	BE-55	295	7	175	690	0.59	0.167	0.009	0.02397	0.00050	0.39	0.0504	0.0025	157	8	153	3	215	115	71
ROBE	BE-56	339	8	111	74488	0.33	0.164	0.007	0.02391	0.00050	0.47	0.0497	0.0020	154	7	152	3	179	92	85
ROBE	BE-57	1052	25	453	1122	0.43	0.161	0.007	0.02342	0.00048	0.45	0.0498	0.0020	151	7	149	3	186	94	80
ROBE	BE-58	275	7	197	61033	0.72	0.163	0.007	0.02419	0.00050	0.47	0.0490	0.0019	154	7	154	3	149	90	104
ROBE	BE-59	772	18	498	2064	0.64	0.161	0.006	0.02377	0.00048	0.57	0.0492	0.0014	152	5	151	3	155	69	98
ROBE	BE-60	232	5	150	349	0.64	0.181	0.014	0.02326	0.00050	0.29	0.0566	0.0041	169	13	148	3	476	159	31
ROBE	BE-62	282	7	153	3651	0.54	0.162	0.010	0.02388	0.00050	0.35	0.0493	0.0027	153	9	152	3	160	129	95
ROBE	BE-63	451	11	190	98668	0.42	0.164	0.006	0.02394	0.00050	0.56	0.0496	0.0015	154	6	153	3	174	72	87
ROBE	BE-64	352	8	144	75185	0.41	0.158	0.006	0.02336	0.00048	0.54	0.0490	0.0016	149	6	149	3	146	75	102
ROBE	BE-65	279	7	200	1488	0.72	0.169	0.009	0.02362	0.00050	0.40	0.0520	0.0025	159	8	150	3	284	112	53

ROBE	BE-67	704	16	415	147872	0.59	0.152	0.005	0.02256	0.00046	0.60	0.0489	0.0013	144	5	144	3	143	63	101
ROBE	BE-68	308	7	251	1493	0.81	0.164	0.006	0.02408	0.00050	0.53	0.0494	0.0017	154	6	153	3	164	79	93
ROBE	BE-69	351	8	157	75614	0.45	0.161	0.009	0.02360	0.00050	0.38	0.0495	0.0025	151	8	150	3	169	120	89
ROBE	BE-70	321	7	164	1984	0.51	0.153	0.009	0.02189	0.00046	0.36	0.0507	0.0028	145	8	140	3	229	127	61
ROBE	BE-71	89	8	42	991	0.47	0.676	0.026	0.08466	0.00178	0.55	0.0579	0.0018	524	20	524	11	527	70	99
ROBE	BE-72	316	8	188	69789	0.59	0.164	0.006	0.02424	0.00052	0.55	0.0491	0.0016	154	6	154	3	153	76	101
ROBE	BE-73	300	7	201	3056	0.67	0.158	0.007	0.02329	0.00050	0.51	0.0492	0.0018	149	6	148	3	159	84	93
ROBE	BE-74	227	5	142	1281	0.62	0.163	0.016	0.02327	0.00050	0.22	0.0508	0.0048	153	15	148	3	232	216	64
ROBE	BE-75	257	6	146	1616	0.57	0.165	0.014	0.02359	0.00050	0.25	0.0507	0.0042	155	13	150	3	229	193	66
ROBE	BE-76	131	3	63	28473	0.48	0.168	0.013	0.02395	0.00054	0.29	0.0508	0.0037	158	12	153	3	234	169	65
ROBE	BE-77	693	17	270	204	0.39	0.204	0.015	0.02389	0.00050	0.28	0.0618	0.0044	188	14	152	3	668	152	23
ROBE	BE-78	366	24	145	986	0.40	0.631	0.025	0.06665	0.00142	0.54	0.0686	0.0023	497	20	416	9	888	69	47
ROBE	BE-79	278	78	199	7890	0.72	4.393	0.130	0.28230	0.00578	0.69	0.1129	0.0024	1711	51	1603	33	1846	39	87
ROBE	BE-80	338	8	218	180	0.64	0.202	0.013	0.02366	0.00050	0.33	0.0620	0.0038	187	12	151	3	672	131	22
ROBE	BE-81	350	8	133	75275	0.38	0.161	0.006	0.02367	0.00050	0.53	0.0494	0.0017	152	6	151	3	164	80	92
ROBE	BE-82	584	14	232	126557	0.40	0.162	0.006	0.02384	0.00050	0.60	0.0493	0.0014	153	5	152	3	163	65	93
ROBE	BE-83	364	9	217	1139	0.60	0.167	0.011	0.02413	0.00050	0.32	0.0503	0.0031	157	10	154	3	209	145	73
ROBE	BE-84	300	7	176	3042	0.58	0.167	0.007	0.02457	0.00052	0.49	0.0494	0.0019	157	7	156	3	167	88	94
ROBE	BE-85	740	17	522	155237	0.71	0.161	0.006	0.02311	0.00048	0.54	0.0507	0.0016	152	6	147	3	226	74	65
ROBE	BE-86	338	8	176	73439	0.52	0.163	0.011	0.02394	0.00050	0.31	0.0494	0.0032	153	10	153	3	164	152	93
ROBE	BE-87	392	9	168	2154	0.43	0.164	0.007	0.02424	0.00052	0.50	0.0491	0.0018	154	7	154	3	151	87	102
ROBE	BE-88	222	5	133	46951	0.60	0.161	0.007	0.02331	0.00050	0.48	0.0501	0.0020	152	7	149	3	198	91	75
ROBE	BE-89	222	5	118	2206	0.53	0.164	0.013	0.02389	0.00052	0.27	0.0497	0.0039	154	12	152	3	181	182	84
ROBE	BE-90	328	8	141	1790	0.43	0.163	0.007	0.02394	0.00050	0.50	0.0493	0.0018	153	6	153	3	162	84	94
ROBE	BE-91	654	15	201	2060	0.31	0.157	0.008	0.02318	0.00048	0.42	0.0491	0.0022	148	7	148	3	155	104	96
ROBE	BE-92	554	13	126	2287	0.23	0.163	0.011	0.02342	0.00052	0.32	0.0505	0.0033	153	11	149	3	216	152	69
ROBE	BE-93	494	12	309	1352	0.63	0.164	0.008	0.02376	0.00050	0.42	0.0500	0.0023	154	8	151	3	195	107	77
ROBE	BE-94	399	10	268	220	0.67	0.176	0.014	0.02397	0.00050	0.25	0.0532	0.0042	164	14	153	3	337	181	45
ROBE	BE-95	476	11	308	1024	0.65	0.162	0.008	0.02385	0.00050	0.42	0.0494	0.0022	153	8	152	3	165	106	92
ROBE	BE-96	436	10	213	1175	0.49	0.162	0.007	0.02388	0.00050	0.51	0.0491	0.0017	152	6	152	3	152	82	100
ROBE	BE-97	423	9	262	996	0.62	0.168	0.011	0.02229	0.00048	0.33	0.0546	0.0033	157	10	142	3	395	136	36
ROBE	BE-98	1960	40	2612	309	1.33	0.231	0.011	0.02041	0.00042	0.42	0.0820	0.0036	211	10	130	3	1246	87	10
ROBE	BE-99	279	7	181	317	0.65	0.234	0.016	0.02415	0.00052	0.31	0.0702	0.0047	213	15	154	3	935	137	16
ROBE	BE-100	450	11	134	5383	0.30	0.164	0.007	0.02420	0.00052	0.52	0.0493	0.0017	155	6	154	3	161	82	96
ROBE	BE-101	531	13	172	113551	0.32	0.161	0.006	0.02372	0.00050	0.55	0.0492	0.0016	151	6	151	3	157	74	96
ROBE	BE-102	335	8	214	2335	0.64	0.163	0.012	0.02415	0.00052	0.30	0.0489	0.0033	153	11	154	3	145	158	106
ROBE	BE-103	725	17	356	1946	0.49	0.166	0.007	0.02411	0.00050	0.48	0.0500	0.0019	156	7	154	3	195	89	79
ROBE	BE-104	621	15	494	1787	0.80	0.161	0.006	0.02370	0.00050	0.58	0.0492	0.0014	151	5	151	3	158	68	95
ROBE	BE-106	422	10	147	3083	0.35	0.164	0.006	0.02425	0.00052	0.57	0.0491	0.0015	154	6	154	3	151	72	102
ROBE	BE-107	519	12	200	110489	0.39	0.162	0.006	0.02366	0.00050	0.57	0.0495	0.0015	152	6	151	3	173	71	87
ROBE	BE-108	218	5	114	45904	0.52	0.168	0.010	0.02337	0.00052	0.37	0.0522	0.0029	158	10	149	3	292	129	51
ROBE	BE-109	74	5	30	42647	0.40	0.484	0.022	0.06383	0.00144	0.51	0.0551	0.0021	401	18	399	9	414	86	96
ROBE	BE-110	502	17	560	1422	1.11	0.241	0.010	0.03397	0.00072	0.51	0.0514	0.0019	219	9	215	5	257	83	84
ROBE	BE-111	208	5	92	44692	0.44	0.162	0.007	0.02396	0.00054	0.50	0.0490	0.0019	152	7	153	3	147	91	104
ROBE	BE-112	241	104	57	9702	0.24	15.784	0.471	0.42950	0.00892	0.70	0.2665	0.0057	2864	86	2303	48	3286	34	70
ROBE	BE-113	268	46	61	17679	0.23	1.741	0.054	0.17107	0.00356	0.67	0.0738	0.0017	1024	32	1018	21	1036	46	98
ROBE	BE-114	1393	123	22	794255	0.02	0.718	0.022	0.08850	0.00184	0.69	0.0588	0.0013	549	17	547	11	561	48	97
ROBE	BE-115	331	8	197	6905	0.60	0.162	0.009	0.02394	0.00052	0.38	0.0492	0.0026	153	9	153	3	158	125	97

[a] U and Pb concentrations and Th/U ratios are calculated relative to GJ-1 reference zircon

[b] Corrected for background and within-run Pb/U fractionation and normalised to reference zircon GJ-1 (ID-TIMS values/measured value); $^{207}Pb/^{235}U$ calculated using $(^{207}Pb/^{206}Pb)/(^{238}U/^{206}Pb * 1/137.88)$

[c] Rho is the error correlation defined as the quotient of the propagated errors of the $^{206}Pb/^{238}U$ and the $^{207}/^{235}U$ ratio

[d] Quadratic addition of within-run errors (2 SD) and daily reproducibility of GJ-1 (2 SD)

[e] Corrected for mass-bias by normalising to GJ-1 reference zircon (~0.6 per atomic mass unit) and common Pb using the model Pb composition of Stacey & Kramers (1975)

Table D2. LA-ICPMS isotopic data for sample Ak5 in the Robertson Basin

AK5						RATIOS							AGES [Ma]						Conc.
Sample	Analysis	U [ppm][a]	Pb [ppm][a]	$^{206}Pb/^{204}Pb$	Th/U[a]	$^{207}Pb/^{235}U$[b]	2 σ[d]	$^{206}Pb/^{238}U$[b]	2 σ[d]	rho[c]	$^{207}Pb/^{206}Pb$[e]	2 σ[d]	$^{207}Pb/^{235}U$	2 σ	$^{206}Pb/^{238}U$	2 σ	$^{207}Pb/^{206}Pb$	2 σ	%
AK5	AK5-1-1	124	21	96632	0.31	1.705	0.056	0.1698	0.0027	0.49	0.0728	0.0021	1010	33	1011	16	1009	58	100
AK5	AK5-1-3	122	10	1874	0.27	0.676	0.026	0.0849	0.0014	0.43	0.0578	0.0020	524	20	525	9	521	75	101
AK5	AK5-1-6	180	16	2693	0.47	0.705	0.024	0.0875	0.0014	0.47	0.0584	0.0017	542	18	541	9	546	64	99
AK5	AK5-1-7	97	9	40718	0.41	0.746	0.028	0.0921	0.0015	0.44	0.0588	0.0020	566	21	568	9	560	74	101
AK5	AK5-1-9	121	44	202541	0.65	6.277	0.173	0.3665	0.0056	0.55	0.1242	0.0029	2015	56	2013	31	2018	41	100
AK5	AK5-1-10	121	18	83342	0.91	1.555	0.068	0.1511	0.0027	0.42	0.0747	0.0030	952	42	907	16	1059	80	86
AK5	AK5-1-11	76	8	36654	0.31	0.889	0.036	0.1054	0.0018	0.42	0.0612	0.0022	646	26	646	11	646	79	100
AK5	AK5-1-12	80	8	37791	0.22	0.860	0.033	0.1032	0.0017	0.43	0.0605	0.0021	630	24	633	11	620	76	102
AK5	AK5-1-15	106	19	87305	1.64	1.837	0.057	0.1799	0.0028	0.50	0.0740	0.0020	1059	33	1067	17	1043	55	102
AK5	AK5-1-16	112	20	90184	0.63	1.797	0.056	0.1754	0.0027	0.50	0.0743	0.0020	1044	33	1042	16	1050	55	99
AK5	AK5-1-17	82	10	47908	0.23	1.140	0.042	0.1280	0.0021	0.45	0.0646	0.0021	773	28	777	13	761	69	102
AK5	AK5-1-18	215	6	565	0.60	0.189	0.017	0.0276	0.0007	0.28	0.0497	0.0043	176	16	175	4	180	202	97
AK5	AK5-1-19	180	14	1934	0.23	0.678	0.026	0.0778	0.0013	0.44	0.0632	0.0021	525	20	483	8	716	72	67
AK5	AK5-1-20	331	27	123096	0.58	0.644	0.021	0.0813	0.0013	0.48	0.0575	0.0016	505	16	504	8	510	63	99
AK5	AK5-1-21	327	23	103050	0.35	0.540	0.024	0.0690	0.0012	0.40	0.0568	0.0023	439	19	430	7	485	89	89
AK5	AK5-1-22	132	14	63451	0.32	0.885	0.030	0.1054	0.0017	0.46	0.0609	0.0019	644	22	646	10	636	66	102
AK5	AK5-1-23	135	11	51552	0.48	0.658	0.034	0.0833	0.0016	0.36	0.0573	0.0028	513	27	516	10	503	108	103
AK5	AK5-1-24	427	32	11809	0.80	0.599	0.019	0.0761	0.0012	0.49	0.0571	0.0016	477	15	473	7	496	60	95
AK5	AK5-1-25	263	27	122941	0.11	0.868	0.028	0.1021	0.0016	0.49	0.0617	0.0017	635	20	627	10	663	60	95
AK5	AK5-1-26	587	83	7784	0.35	1.336	0.037	0.1420	0.0021	0.54	0.0682	0.0016	862	24	856	13	876	49	98
AK5	AK5-1-28	147	27	7282	0.17	1.969	0.059	0.1846	0.0029	0.51	0.0774	0.0020	1105	33	1092	17	1131	51	97
AK5	AK5-1-29	191	13	1272	0.41	0.670	0.023	0.0692	0.0011	0.46	0.0702	0.0021	521	18	431	7	935	62	46
AK5	AK5-1-31	2596	181	8622	0.44	0.540	0.018	0.0697	0.0011	0.48	0.0563	0.0016	439	14	434	7	462	63	94
AK5	AK5-1-32	275	21	1676	0.25	0.583	0.034	0.0749	0.0015	0.34	0.0565	0.0031	467	28	466	9	471	123	99
AK5	AK5-1-33	225	18	17056	0.77	0.620	0.021	0.0791	0.0012	0.47	0.0569	0.0017	490	16	491	8	487	64	101
AK5	AK5-1-36	132	12	2056	0.47	0.883	0.042	0.0939	0.0017	0.39	0.0682	0.0030	642	30	578	11	875	90	66
AK5	AK5-1-38	49	16	72864	0.48	4.992	0.154	0.3253	0.0052	0.52	0.1113	0.0029	1818	56	1815	29	1821	48	100
AK5	AK5-2-1	418	32	13206	0.68	0.605	0.020	0.0764	0.0015	0.59	0.0575	0.0015	481	16	474	9	510	57	93
AK5	AK5-2-2	246	6	-848	0.49	0.154	0.010	0.0227	0.0005	0.36	0.0492	0.0029	146	9	145	3	159	139	91
AK5	AK5-2-3	254	52	433534	0.19	2.320	0.071	0.2058	0.0039	0.63	0.0818	0.0019	1218	37	1206	23	1240	46	97
AK5	AK5-2-4	252	19	2090	0.54	0.603	0.026	0.0755	0.0015	0.48	0.0580	0.0022	479	20	469	10	529	82	89
AK5	AK5-2-5	318	25	3211	0.77	0.619	0.022	0.0788	0.0015	0.55	0.0570	0.0017	489	17	489	10	493	65	99
AK5	AK5-2-6	441	37	13385	0.12	0.675	0.021	0.0845	0.0016	0.62	0.0580	0.0014	524	16	523	10	528	52	99
AK5	AK5-2-7	708	51	2658	0.20	0.601	0.019	0.0713	0.0014	0.59	0.0611	0.0016	478	15	444	8	642	56	69
AK5	AK5-2-8	355	21	5500	0.61	0.433	0.014	0.0582	0.0011	0.58	0.0540	0.0015	365	12	364	7	369	61	99
AK5	AK5-2-9	239	6	2332	0.87	0.162	0.013	0.0234	0.0005	0.26	0.0503	0.0038	153	12	149	3	209	173	71
AK5	AK5-2-10	541	40	3738	0.63	0.569	0.025	0.0731	0.0015	0.47	0.0564	0.0022	457	20	455	9	469	86	97
AK5	AK5-2-11	600	25	4844	0.41	0.295	0.010	0.0417	0.0008	0.59	0.0513	0.0013	262	9	263	5	256	60	103
AK5	AK5-2-12	481	46	6227	0.79	0.783	0.026	0.0951	0.0018	0.59	0.0597	0.0016	587	19	586	11	594	57	99
AK5	AK5-2-13	372	27	18165	0.33	0.568	0.020	0.0736	0.0014	0.55	0.0560	0.0017	457	16	458	9	453	67	101
AK5	AK5-2-14	114	11	1114	0.61	0.768	0.045	0.0935	0.0022	0.39	0.0596	0.0032	579	34	576	13	589	118	98
AK5	AK5-2-15	266	6	1765	0.40	0.157	0.022	0.0230	0.0005	0.14	0.0494	0.0069	148	21	147	3	168	324	87
AK5	AK5-2-16	341	30	3626	0.64	0.737	0.033	0.0894	0.0019	0.47	0.0598	0.0024	561	25	552	11	596	86	93
AK5	AK5-2-17	444	35	1773	0.61	0.658	0.022	0.0778	0.0015	0.58	0.0613	0.0017	513	17	483	9	649	58	74
AK5	AK5-2-18	387	9	724	0.86	0.164	0.021	0.0231	0.0005	0.16	0.0513	0.0064	154	19	147	3	256	287	58
AK5	AK5-2-19	501	86	8937	0.17	1.900	0.055	0.1713	0.0032	0.65	0.0804	0.0018	1081	31	1019	19	1208	43	84
AK5	AK5-2-20	453	33	15527	0.61	0.569	0.019	0.0733	0.0014	0.58	0.0563	0.0015	457	15	456	9	464	60	98
AK5	AK5-2-21	356	26	2505	0.56	0.553	0.025	0.0718	0.0015	0.46	0.0559	0.0022	447	20	447	9	447	88	100
AK5	AK5-2-22	510	37	183776	0.36	0.572	0.018	0.0731	0.0014	0.61	0.0568	0.0014	459	14	455	9	482	54	94
AK5	AK5-2-23	236	51	7076	0.14	2.415	0.090	0.2147	0.0044	0.54	0.0816	0.0026	1247	47	1254	25	1235	62	102
AK5	AK5-2-24	157	7	17172	0.78	0.300	0.020	0.0425	0.0009	0.30	0.0512	0.0033	266	18	268	5	252	148	107
AK5	AK5-2-25	297	63	7982	0.43	2.374	0.077	0.2110	0.0041	0.60	0.0816	0.0021	1235	40	1234	24	1236	51	100
AK5	AK5-2-26	211	9	1371	1.10	0.298	0.022	0.0412	0.0008	0.27	0.0524	0.0038	265	20	261	5	304	164	86
AK5	AK5-2-27	382	33	2437	0.44	0.764	0.031	0.0870	0.0018	0.49	0.0636	0.0023	576	24	538	11	730	76	74

AK5	AK5-2-28	215	16	76648	0.31	0.569	0.026	0.0723	0.0015	0.46	0.0571	0.0023	457	21	450	9	493	89	91
AK5	AK5-2-29	654	53	15150	0.54	0.656	0.026	0.0818	0.0016	0.51	0.0582	0.0020	512	20	507	10	538	74	94
AK5	AK5-2-30	716	52	1978	0.63	0.572	0.026	0.0724	0.0015	0.46	0.0573	0.0023	459	21	450	9	503	88	90
AK5	AK5-2-31	483	28	2111	0.34	0.461	0.020	0.0575	0.0012	0.48	0.0581	0.0022	385	16	361	7	535	81	67
AK5	AK5-2-32	557	37	672	0.38	0.731	0.026	0.0659	0.0013	0.54	0.0804	0.0024	557	20	412	8	1208	60	34
AK5	AK5-2-34	95	6	30776	1.92	0.582	0.049	0.0655	0.0018	0.34	0.0645	0.0051	466	39	409	11	757	166	54
AK5	AK5-2-35	244	16	80071	0.70	0.518	0.036	0.0664	0.0016	0.36	0.0565	0.0036	424	29	415	10	473	142	88
AK5	AK5-2-36	249	18	1192	1.97	0.566	0.030	0.0711	0.0016	0.41	0.0578	0.0028	456	24	443	10	522	107	85
AK5	AK5-2-37	830	132	4469	0.42	1.730	0.051	0.1586	0.0030	0.64	0.0791	0.0018	1020	30	949	18	1174	45	81
AK5	AK5-2-38	788	60	8352	0.46	0.595	0.020	0.0757	0.0015	0.58	0.0570	0.0016	474	16	471	9	490	60	96
AK5	AK5-2-39	282	25	123400	0.23	0.731	0.037	0.0886	0.0019	0.43	0.0599	0.0027	557	28	547	12	598	98	92
AK5	AK5-2-40	1050	66	967	0.12	0.594	0.025	0.0628	0.0013	0.48	0.0686	0.0026	473	20	392	8	888	78	44
AK5	AK5-2-41	390	22	1089	0.64	0.454	0.025	0.0575	0.0013	0.41	0.0572	0.0029	380	21	360	8	500	110	72
AK5	AK5-2-42	704	118	6949	0.50	1.808	0.052	0.1678	0.0031	0.65	0.0782	0.0017	1049	30	1000	19	1151	44	87
AK5	AK5-2-43	242	20	1271	0.36	0.638	0.025	0.0806	0.0016	0.51	0.0574	0.0019	501	20	500	10	506	74	99
AK5	AK5-2-44	784	55	50080	0.36	0.565	0.025	0.0705	0.0014	0.47	0.0581	0.0023	455	20	439	9	534	85	82
AK5	AK5-2-46	185	4	20845	0.47	0.155	0.009	0.0228	0.0005	0.38	0.0493	0.0025	146	8	145	3	160	121	91
AK5	AK5-2-47	275	48	238442	0.42	1.831	0.057	0.1757	0.0033	0.61	0.0756	0.0019	1057	33	1043	20	1085	49	96
AK5	AK5-2-48	84	6	1407	1.51	0.567	0.042	0.0707	0.0018	0.35	0.0582	0.0040	456	34	441	11	535	151	82
AK5	AK5-2-50	219	5	24955	0.48	0.158	0.013	0.0230	0.0005	0.25	0.0497	0.0040	149	12	147	3	179	189	82
AK5	AK5-2-51	479	35	4822	0.33	0.573	0.019	0.0732	0.0014	0.57	0.0568	0.0016	460	16	455	9	485	61	94
AK5	AK5-2-52	400	30	1973	0.47	0.584	0.022	0.0747	0.0015	0.53	0.0567	0.0018	467	17	464	9	479	69	97
AK5	AK5-2-53	189	5	400	1.16	0.189	0.020	0.0276	0.0006	0.21	0.0497	0.0050	176	18	175	4	182	236	96
AK5	AK5-2-54	473	34	3065	0.33	0.601	0.023	0.0716	0.0014	0.52	0.0609	0.0020	478	18	446	9	636	70	70
AK5	AK5-2-55	131	14	1957	0.68	0.876	0.032	0.1046	0.0021	0.54	0.0607	0.0019	639	23	642	13	630	67	102
AK5	AK5-2-56	195	15	2428	0.67	0.621	0.023	0.0787	0.0015	0.54	0.0572	0.0018	490	18	489	10	498	68	98
AK5	AK5-2-57	190	15	72549	0.57	0.608	0.028	0.0773	0.0016	0.45	0.0570	0.0024	482	22	480	10	492	91	98
AK5	AK5-2-58	322	24	2271	0.47	0.597	0.025	0.0752	0.0015	0.48	0.0576	0.0021	475	20	467	9	513	80	91
AK5	AK5-2-59	495	82	19381	0.06	1.659	0.050	0.1661	0.0031	0.63	0.0725	0.0017	993	30	991	19	999	48	99
AK5	AK5-2-60	265	23	112456	0.42	0.688	0.023	0.0856	0.0016	0.58	0.0583	0.0016	532	17	530	10	540	59	98
AK5	AK5-2-61	390	66	78093	0.55	1.691	0.051	0.1689	0.0032	0.62	0.0726	0.0017	1005	30	1006	19	1003	48	100
AK5	AK5-2-62	224	5	25876	0.54	0.159	0.011	0.0233	0.0005	0.29	0.0494	0.0034	150	11	149	3	166	161	90
AK5	AK5-2-63	570	41	3325	0.96	0.569	0.025	0.0719	0.0015	0.47	0.0575	0.0022	458	20	447	9	510	85	88
AK5	AK5-2-64	1218	219	8582	0.47	1.845	0.059	0.1795	0.0034	0.60	0.0746	0.0019	1062	34	1064	20	1056	51	101
AK5	AK5-2-65	543	94	9745	0.15	1.760	0.055	0.1728	0.0033	0.61	0.0739	0.0018	1031	32	1028	20	1037	50	99
AK5	AK5-2-66	392	33	66912	0.57	0.699	0.022	0.0829	0.0016	0.60	0.0612	0.0016	538	17	514	10	645	55	80
AK5	AK5-2-67	543	101	45707	0.26	1.979	0.059	0.1868	0.0035	0.63	0.0768	0.0018	1108	33	1104	21	1117	46	99
AK5	AK5-2-68	124	16	4371	0.31	1.188	0.041	0.1315	0.0025	0.56	0.0655	0.0019	795	27	796	15	791	60	101
AK5	AK5-2-70	179	29	143583	0.62	1.593	0.052	0.1620	0.0031	0.59	0.0713	0.0019	967	31	968	19	966	53	100
AK5	AK5-2-71	540	38	2130	0.60	0.584	0.026	0.0696	0.0014	0.46	0.0609	0.0024	467	21	434	9	636	86	68
AK5	AK5-2-72	417	10	1362	0.50	0.158	0.011	0.0232	0.0005	0.29	0.0495	0.0032	149	10	148	3	170	153	87
AK5	AK5-2-73	327	26	2007	0.44	0.638	0.026	0.0796	0.0016	0.49	0.0581	0.0021	501	20	494	10	535	78	92
AK5	AK5-2-75	123	22	17768	0.44	1.855	0.062	0.1791	0.0035	0.58	0.0751	0.0021	1065	36	1062	21	1072	55	99
AK5	AK5-2-76	179	39	27669	0.36	2.457	0.078	0.2156	0.0041	0.60	0.0826	0.0021	1259	40	1259	24	1261	50	100
AK5	AK5-2-77	622	53	261585	0.34	0.678	0.025	0.0849	0.0017	0.52	0.0580	0.0019	526	20	525	10	529	70	99
AK5	AK5-2-79	495	27	919	0.25	0.558	0.022	0.0545	0.0011	0.50	0.0742	0.0026	450	18	342	7	1047	70	33
AK5	AK5-2-81	406	30	5562	0.65	0.708	0.026	0.0750	0.0015	0.53	0.0685	0.0022	543	20	466	9	883	65	53

[a] U and Pb concentrations and Th/U ratios are calculated relative to GJ-1 reference zircon

[b] Corrected for background and within-run Pb/U fractionation and normalised to reference zircon GJ-1 (ID-TIMS values/measured value); $^{207}Pb/^{235}U$ calculated using $(^{207}Pb/^{206}Pb)/(^{238}U/^{206}Pb * 1/137.88)$

[c] Rho is the error correlation defined as the quotient of the propagated errors of the $^{206}Pb/^{238}U$ and the $^{207}/^{235}U$ ratio

[d] Quadratic addition of within-run errors (2 SD) and daily reproducibility of GJ-1 (2 SD)

[e] Corrected for mass-bias by normalising to GJ-1 reference zircon (~0.6 per atomic mass unit) and common Pb using the model Pb composition of Stacey & Kramers (1975)

Table D3. LA-ICPMS isotopic data for sample ASH1 in the Robertson Basin

ASH1						RATIOS							AGES [Ma]						Conc.
Sample	Analysis	U [ppm][a]	Pb [ppm][a]	$^{206}Pb/^{204}Pb$	Th/U[a]	$^{207}Pb/^{235}U$[b]	2 σ[d]	$^{206}Pb/^{238}U$[b]	2 σ[d]	rho[c]	$^{207}Pb/^{206}Pb$	2 σ[d]	$^{207}Pb/^{235}U$	2 σ	$^{206}Pb/^{238}U$	2 σ	$^{207}Pb/^{206}Pb$	2 σ	%
ASH1	ASH1-1	44	4	1198	0.50	0.746	0.045	0.0914	0.0019	0.34	0.0592	0.0034	566	34	564	12	576	123	98
ASH1	ASH1-2	66	12	52054	0.54	1.868	0.063	0.1803	0.0029	0.48	0.0752	0.0022	1070	36	1068	17	1073	59	100
ASH1	ASH1-3	77	8	910	0.87	0.806	0.036	0.0975	0.0017	0.40	0.0599	0.0024	600	27	600	11	601	88	100
ASH1	ASH1-4	35	4	17554	0.78	0.996	0.056	0.1140	0.0023	0.36	0.0634	0.0033	702	39	696	14	721	111	97
ASH1	ASH1-5	134	24	105069	0.69	1.835	0.056	0.1788	0.0028	0.51	0.0745	0.0020	1058	32	1060	17	1054	53	101
ASH1	ASH1-6	107	19	4069	0.36	1.772	0.073	0.1739	0.0031	0.43	0.0739	0.0028	1035	43	1033	18	1039	75	99
ASH1	ASH1-7	260	48	211063	0.70	1.941	0.054	0.1851	0.0028	0.54	0.0760	0.0018	1095	31	1095	17	1096	47	100
ASH1	ASH1-8	290	22	97460	0.33	0.599	0.019	0.0764	0.0012	0.49	0.0568	0.0015	477	15	475	7	485	60	98
ASH1	ASH1-9	77	15	9293	0.43	2.049	0.096	0.1921	0.0037	0.41	0.0774	0.0033	1132	53	1133	22	1130	85	100
ASH1	ASH1-10	193	19	5890	0.20	0.840	0.026	0.1006	0.0016	0.49	0.0606	0.0017	619	19	618	10	624	59	99
ASH1	ASH1-11	61	9	40698	0.46	1.451	0.053	0.1518	0.0025	0.46	0.0693	0.0022	910	33	911	15	909	67	100
ASH1	ASH1-12	33	4	16544	0.20	1.206	0.073	0.1296	0.0028	0.36	0.0675	0.0038	803	49	785	17	853	118	92
ASH1	ASH1-13	42	5	1485	0.46	1.137	0.051	0.1261	0.0023	0.40	0.0654	0.0027	771	34	765	14	787	85	97
ASH1	ASH1-14	183	13	771	0.60	0.575	0.043	0.0735	0.0017	0.31	0.0567	0.0041	461	35	457	11	480	158	95
ASH1	ASH1-15	247	19	85134	0.25	0.610	0.021	0.0782	0.0012	0.47	0.0566	0.0017	484	16	485	8	476	66	102
ASH1	ASH1-16	383	37	4660	0.13	0.817	0.042	0.0967	0.0018	0.37	0.0613	0.0029	606	31	595	11	648	102	92
ASH1	ASH1-17	247	26	114474	0.43	0.900	0.030	0.1054	0.0017	0.48	0.0619	0.0018	652	21	646	10	670	62	96
ASH1	ASH1-18	177	11	46564	0.48	0.443	0.019	0.0597	0.0010	0.40	0.0538	0.0021	372	16	374	6	362	89	103
ASH1	ASH1-19	223	20	88280	0.45	0.724	0.027	0.0897	0.0015	0.44	0.0586	0.0020	553	21	554	9	550	73	101
ASH1	ASH1-22	449	40	175928	0.09	0.714	0.021	0.0889	0.0013	0.52	0.0582	0.0014	547	16	549	8	538	54	102
ASH1	ASH1-23	239	39	6784	0.20	1.592	0.045	0.1615	0.0024	0.54	0.0715	0.0017	967	27	965	15	972	48	99
ASH1	ASH1-24	362	62	3063	0.40	1.842	0.056	0.1726	0.0027	0.51	0.0774	0.0020	1061	33	1026	16	1132	52	91
ASH1	ASH1-25	151	22	2102	0.26	1.372	0.049	0.1458	0.0024	0.46	0.0683	0.0022	877	32	877	14	876	66	100
ASH1	ASH1-26	240	51	5363	0.35	2.516	0.079	0.2111	0.0034	0.51	0.0864	0.0023	1277	40	1235	20	1348	52	92
ASH1	ASH1-27	83	15	5926	0.35	1.753	0.057	0.1738	0.0028	0.49	0.0731	0.0021	1028	33	1033	16	1018	57	101
ASH1	ASH1-29	87	12	1552	0.26	1.206	0.043	0.1326	0.0022	0.45	0.0660	0.0021	803	29	803	13	805	67	100
ASH1	ASH1-30	193	17	74453	0.48	0.697	0.023	0.0871	0.0014	0.48	0.0580	0.0017	537	18	539	8	530	63	102
ASH1	ASH1-31	419	25	3369	0.34	0.448	0.018	0.0601	0.0010	0.42	0.0541	0.0019	376	15	376	6	376	80	100
ASH1	ASH1-32	121	13	59535	0.38	0.955	0.032	0.1115	0.0018	0.47	0.0622	0.0018	681	23	681	11	680	63	100
ASH1	ASH1-33	48	4	19505	0.33	0.755	0.039	0.0920	0.0017	0.36	0.0595	0.0028	571	29	567	11	587	104	97
ASH1	ASH1-34	67	6	886	0.58	0.672	0.030	0.0843	0.0015	0.39	0.0579	0.0023	522	23	522	9	524	89	100
ASH1	ASH1-35	166	17	2594	1.05	0.868	0.029	0.1027	0.0016	0.48	0.0613	0.0018	634	21	630	10	650	62	97
ASH1	ASH1-36	181	31	138126	0.22	1.742	0.053	0.1720	0.0027	0.51	0.0734	0.0019	1024	31	1023	16	1026	53	100
ASH1	ASH1-37	243	25	111470	0.19	0.865	0.028	0.1035	0.0016	0.48	0.0606	0.0017	633	21	635	10	625	62	102
ASH1	ASH1-38	105	10	1337	0.52	0.783	0.030	0.0949	0.0016	0.43	0.0598	0.0021	587	23	585	10	598	75	98
ASH1	ASH1-39	54	6	1496	0.53	0.914	0.042	0.1072	0.0019	0.39	0.0618	0.0026	659	30	657	12	668	90	98
ASH1	ASH1-40	125	11	47739	0.45	0.701	0.040	0.0865	0.0017	0.35	0.0588	0.0031	539	31	535	11	560	116	96
ASH1	ASH1-41	217	27	120466	0.27	1.121	0.037	0.1255	0.0020	0.47	0.0648	0.0019	763	25	762	12	767	62	99
ASH1	ASH1-42	133	11	3132	0.41	0.628	0.044	0.0797	0.0018	0.32	0.0572	0.0038	495	35	494	11	498	147	99
ASH1	ASH1-43	130	25	54325	0.32	1.977	0.059	0.1882	0.0029	0.52	0.0762	0.0019	1108	33	1112	17	1100	51	101
ASH1	ASH1-44	36	7	32197	0.35	2.251	0.084	0.2040	0.0035	0.46	0.0801	0.0026	1197	44	1197	20	1198	65	100
ASH1	ASH1-45	79	14	17840	0.44	1.867	0.060	0.1813	0.0029	0.49	0.0747	0.0021	1070	34	1074	17	1060	57	101
ASH1	ASH1-46	131	11	1532	0.25	0.629	0.031	0.0804	0.0015	0.37	0.0567	0.0026	495	25	498	9	481	103	104
ASH1	ASH1-47	60	9	3605	0.33	1.421	0.053	0.1486	0.0025	0.44	0.0693	0.0023	898	34	893	15	909	70	98
ASH1	ASH1-48	110	19	5232	0.24	1.765	0.067	0.1712	0.0029	0.45	0.0748	0.0025	1033	39	1019	17	1063	68	96
ASH1	ASH1-49	34	6	26353	0.42	1.768	0.082	0.1733	0.0033	0.41	0.0740	0.0031	1034	48	1030	19	1041	85	99
ASH1	ASH1-50	133	17	77672	0.56	1.195	0.039	0.1313	0.0021	0.49	0.0660	0.0019	798	26	795	12	807	59	99
ASH1	ASH1-51	140	13	1857	0.36	0.718	0.024	0.0895	0.0014	0.46	0.0582	0.0018	549	19	553	9	536	66	103
ASH1	ASH1-52	115	12	1511	0.46	0.880	0.032	0.1038	0.0017	0.45	0.0615	0.0020	641	23	637	10	656	70	97
ASH1	ASH1-53	259	46	31829	0.16	1.823	0.051	0.1777	0.0027	0.53	0.0744	0.0018	1054	29	1054	16	1052	48	100
ASH1	ASH1-54	250	19	86281	0.39	0.607	0.020	0.0776	0.0012	0.48	0.0567	0.0016	481	16	482	7	479	63	101
ASH1	ASH1-55	86	7	1004	0.44	0.617	0.035	0.0787	0.0015	0.35	0.0569	0.0030	488	28	488	10	488	117	100
ASH1	ASH1-56	48	8	37453	1.17	1.776	0.065	0.1745	0.0029	0.46	0.0738	0.0024	1037	38	1037	17	1036	66	100
ASH1	ASH1-57	220	25	4281	0.35	1.076	0.033	0.1150	0.0018	0.50	0.0679	0.0018	742	23	702	11	865	55	81

ASH1	ASH1-58	277	23	1162	0.36	0.647	0.036	0.0815	0.0016	0.35	0.0576	0.0030	507	28	505	10	513	115	98
ASH1	ASH1-59	123	11	47341	0.46	0.696	0.026	0.0868	0.0014	0.44	0.0582	0.0019	537	20	536	9	538	73	100
ASH1	ASH1-60	37	3	1761	0.63	0.697	0.075	0.0869	0.0027	0.29	0.0582	0.0060	537	57	537	17	537	224	100
ASH1	ASH1-61	99	17	19413	0.35	0.867	0.044	0.1761	0.0027	0.30	0.0357	0.0017	634	32	1045	16	-654	134	-160
ASH1	ASH1-62	72	21	64330	0.28	4.102	0.122	0.2925	0.0045	0.52	0.1017	0.0026	1655	49	1654	26	1656	47	100
ASH1	ASH1-63	102	25	6622	0.54	3.056	0.093	0.2469	0.0039	0.51	0.0898	0.0024	1422	43	1422	22	1421	50	100
ASH1	ASH1-64	40	4	1144	0.62	0.931	0.046	0.1088	0.0020	0.38	0.0621	0.0028	668	33	665	12	678	98	98
ASH1	ASH1-65	155	29	128144	0.35	1.943	0.057	0.1858	0.0028	0.52	0.0758	0.0019	1096	32	1099	17	1090	50	101
ASH1	ASH1-66	91	16	72147	0.32	1.823	0.059	0.1777	0.0028	0.48	0.0744	0.0021	1054	34	1054	17	1053	57	100
ASH1	ASH1-67	259	47	19237	0.17	1.908	0.053	0.1831	0.0027	0.54	0.0756	0.0018	1084	30	1084	16	1084	47	100
ASH1	ASH1-68	263	43	192696	0.20	1.625	0.048	0.1642	0.0025	0.51	0.0718	0.0018	980	29	980	15	980	52	100
ASH1	ASH1-69	200	34	150338	0.42	1.704	0.049	0.1686	0.0025	0.52	0.0733	0.0018	1010	29	1004	15	1022	50	98
ASH1	ASH1-70	176	18	81056	0.64	0.864	0.028	0.1029	0.0016	0.48	0.0609	0.0017	632	20	632	10	635	61	99
ASH1	ASH1-71	119	9	1632	0.32	0.632	0.026	0.0799	0.0013	0.41	0.0573	0.0022	497	20	495	8	505	83	98
ASH1	ASH1-72	150	26	116104	0.44	1.731	0.052	0.1730	0.0026	0.51	0.0726	0.0019	1020	31	1029	16	1002	53	103
ASH1	ASH1-73	146	15	68504	0.29	0.877	0.032	0.1048	0.0017	0.44	0.0607	0.0020	639	23	643	10	628	71	102
ASH1	ASH1-74	311	56	77534	0.16	1.882	0.052	0.1804	0.0027	0.53	0.0756	0.0018	1075	30	1069	16	1086	47	99
ASH1	ASH1-75	118	22	97682	0.36	1.943	0.060	0.1855	0.0029	0.50	0.0760	0.0020	1096	34	1097	17	1094	53	100
ASH1	ASH1-76	133	11	1066	0.44	0.685	0.025	0.0859	0.0014	0.44	0.0579	0.0019	530	19	531	8	524	71	101
ASH1	ASH1-77	125	21	93690	0.55	1.672	0.052	0.1677	0.0026	0.50	0.0723	0.0019	998	31	999	15	994	55	101
ASH1	ASH1-78	273	29	11422	0.37	0.898	0.027	0.1057	0.0016	0.50	0.0616	0.0016	650	20	648	10	660	56	98
ASH1	ASH1-79	137	22	8757	0.96	1.517	0.048	0.1564	0.0024	0.49	0.0704	0.0019	937	30	937	14	939	57	100
ASH1	ASH1-80	159	29	128537	0.34	1.874	0.056	0.1809	0.0028	0.51	0.0751	0.0019	1072	32	1072	16	1072	52	100
ASH1	ASH1-81	155	14	61601	1.12	0.717	0.025	0.0888	0.0014	0.46	0.0586	0.0018	549	19	548	9	551	67	99
ASH1	ASH1-82	88	16	4870	1.31	1.957	0.075	0.1856	0.0031	0.44	0.0765	0.0026	1101	42	1097	19	1107	68	99
ASH1	ASH1-83	110	10	45736	0.42	0.761	0.043	0.0928	0.0018	0.35	0.0594	0.0031	574	32	572	11	583	115	98
ASH1	ASH1-84	118	22	2351	0.43	2.014	0.071	0.1879	0.0031	0.46	0.0777	0.0024	1120	39	1110	18	1140	62	97
ASH1	ASH1-85	107	9	3034	0.34	0.719	0.027	0.0891	0.0014	0.43	0.0585	0.0020	550	21	550	9	550	75	100
ASH1	ASH1-86	74	22	100312	0.15	4.380	0.138	0.3032	0.0048	0.51	0.1048	0.0028	1709	54	1707	27	1710	50	100
ASH1	ASH1-87	184	16	70664	0.36	0.686	0.027	0.0858	0.0014	0.41	0.0581	0.0021	531	21	530	9	532	80	100
ASH1	ASH1-88	311	56	3530	0.31	1.862	0.054	0.1794	0.0027	0.52	0.0753	0.0019	1068	31	1064	16	1075	50	99
ASH1	ASH1-89	61	5	22398	0.29	0.653	0.030	0.0820	0.0014	0.38	0.0578	0.0025	510	24	508	9	521	93	97
ASH1	ASH1-90	174	32	4233	0.26	1.979	0.059	0.1868	0.0028	0.51	0.0769	0.0020	1108	33	1104	17	1118	51	99
ASH1	ASH1-91	97	15	18049	0.41	1.537	0.053	0.1575	0.0025	0.46	0.0708	0.0022	945	33	943	15	950	63	99
ASH1	ASH1-92	186	31	140939	0.54	1.686	0.050	0.1684	0.0025	0.51	0.0726	0.0019	1003	30	1003	15	1003	52	100
ASH1	ASH1-93	230	31	138752	0.17	1.303	0.039	0.1341	0.0020	0.50	0.0705	0.0018	847	25	811	12	941	53	86
ASH1	ASH1-94	174	32	145871	0.39	1.964	0.061	0.1859	0.0029	0.50	0.0766	0.0021	1103	34	1099	17	1111	54	99
ASH1	ASH1-95	84	7	1301	0.52	0.687	0.028	0.0859	0.0014	0.41	0.0580	0.0022	531	22	531	9	529	82	100
ASH1	ASH1-96	163	91	32304	0.61	19.226	0.518	0.5607	0.0083	0.55	0.2487	0.0056	3053	82	2869	42	3177	36	90
ASH1	ASH1-97	189	24	106322	0.62	1.105	0.034	0.1250	0.0019	0.49	0.0641	0.0017	756	24	760	12	744	57	102
ASH1	ASH1-98	153	15	69789	0.30	0.864	0.033	0.1013	0.0017	0.43	0.0618	0.0021	632	24	622	10	669	74	93
ASH1	ASH1-99	387	57	14642	0.12	1.534	0.044	0.1466	0.0022	0.52	0.0759	0.0018	944	27	882	13	1093	49	81
ASH1	ASH1-100	125	12	51952	0.62	0.756	0.034	0.0926	0.0016	0.39	0.0592	0.0024	571	26	571	10	574	90	99
ASH1	ASH1-101	283	54	10554	0.39	2.032	0.059	0.1904	0.0028	0.52	0.0774	0.0019	1126	33	1124	17	1132	49	99
ASH1	ASH1-102	273	24	1886	0.33	0.708	0.022	0.0874	0.0013	0.48	0.0587	0.0016	543	17	540	8	556	61	97
ASH1	ASH1-103	125	12	54498	0.34	0.804	0.031	0.0971	0.0016	0.43	0.0601	0.0021	599	23	597	10	606	74	98
ASH1	ASH1-104	422	70	314294	0.55	1.652	0.050	0.1651	0.0025	0.50	0.0726	0.0019	990	30	985	15	1002	53	98
ASH1	ASH1-105	176	16	3692	0.58	0.713	0.025	0.0885	0.0014	0.44	0.0584	0.0019	546	19	547	9	545	70	100

[a]U and Pb concentrations and Th/U ratios are calculated relative to GJ-1 reference zircon

[b]Corrected for background and within-run Pb/U fractionation and normalised to reference zircon GJ-1 (ID-TIMS values/measured value); $^{207}Pb/^{235}U$ calculated using $(^{207}Pb/^{206}Pb)/(^{238}U/^{206}Pb * 1/137.88)$

[c]Rho is the error correlation defined as the quotient of the propagated errors of the $^{206}Pb/^{238}U$ and the $^{207}/^{235}U$ ratio

[d]Quadratic addition of within-run errors (2 SD) and daily reproducibility of GJ-1 (2 SD)

[e]Corrected for mass-bias by normalising to GJ-1 reference zircon (~0.6 per atomic mass unit) and common Pb using the model Pb composition of Stacey & Kramers (1975)

Table D4. LA-ICPMS isotopic data for sample RAE in the Robertson Basin

RAE						RATIOS							AGES [Ma]						Conc.
Sample	Analysis	U [ppm][a]	Pb [ppm][a]	$^{206}Pb/^{204}Pb$	Th/U[a]	$^{207}Pb/^{235}U$[b]	2 σ[d]	$^{206}Pb/^{238}U$[b]	2 σ[d]	rho[c]	$^{207}Pb/^{206}Pb$[e]	2 σ[d]	$^{207}Pb/^{235}U$	2 σ	$^{206}Pb/^{238}U$	2 σ	$^{207}Pb/^{206}Pb$	2 σ	%
RAE	RAE-1	938	80	366694	0.38	0.683	0.019	0.0857	0.0013	0.54	0.0578	0.0014	529	15	530	8	522	52	101
RAE	RAE-2	275	36	7494	0.13	1.170	0.034	0.1292	0.0020	0.51	0.0657	0.0017	787	23	783	12	796	53	98
RAE	RAE-3	93	9	1125	0.50	0.764	0.039	0.0937	0.0018	0.37	0.0591	0.0028	576	29	578	11	571	103	101
RAE	RAE-4	31	6	26621	1.40	2.051	0.094	0.1906	0.0036	0.42	0.0781	0.0032	1133	52	1125	21	1148	82	98
RAE	RAE-5	160	29	35762	0.79	1.888	0.054	0.1816	0.0028	0.53	0.0754	0.0018	1077	31	1075	16	1080	49	100
RAE	RAE-6	204	38	173757	0.40	1.963	0.055	0.1864	0.0028	0.54	0.0764	0.0018	1103	31	1102	17	1105	48	100
RAE	RAE-7	178	20	1615	0.39	0.957	0.040	0.1114	0.0019	0.41	0.0623	0.0024	682	29	681	12	685	82	99
RAE	RAE-8	57	8	1609	0.52	1.293	0.049	0.1397	0.0023	0.44	0.0671	0.0023	842	32	843	14	841	71	100
RAE	RAE-9	49	4	1605	0.63	0.674	0.034	0.0844	0.0016	0.37	0.0580	0.0027	523	26	522	10	528	101	99
RAE	RAE-10	65	6	25258	0.72	0.698	0.033	0.0854	0.0015	0.38	0.0593	0.0026	538	25	528	10	577	95	92
RAE	RAE-11	178	28	128387	1.33	1.539	0.050	0.1582	0.0025	0.49	0.0706	0.0020	946	31	946	15	946	58	100
RAE	RAE-12	44	4	17711	0.85	0.712	0.036	0.0881	0.0016	0.37	0.0586	0.0028	546	28	544	10	551	104	99
RAE	RAE-13	268	26	119899	0.48	0.807	0.024	0.0980	0.0015	0.52	0.0598	0.0015	601	18	603	9	595	55	101
RAE	RAE-14	105	12	30322	0.09	1.018	0.041	0.1167	0.0020	0.43	0.0633	0.0023	713	28	711	12	717	77	99
RAE	RAE-15	87	8	1955	0.37	0.732	0.030	0.0902	0.0015	0.41	0.0588	0.0022	557	23	557	10	561	82	99
RAE	RAE-16	314	28	128475	0.37	0.722	0.022	0.0896	0.0014	0.49	0.0584	0.0016	552	17	553	9	546	59	101
RAE	RAE-17	95	8	38263	0.36	0.717	0.028	0.0881	0.0015	0.42	0.0591	0.0021	549	22	544	9	570	78	95
RAE	RAE-18	30	6	25515	0.85	1.929	0.147	0.1839	0.0049	0.35	0.0761	0.0054	1091	83	1088	29	1097	143	99
RAE	RAE-19	29	5	24655	0.38	2.032	0.088	0.1880	0.0034	0.42	0.0784	0.0031	1126	49	1110	20	1157	77	96
RAE	RAE-20	88	16	8690	0.40	1.839	0.058	0.1789	0.0028	0.50	0.0745	0.0020	1059	33	1061	17	1056	55	100
RAE	RAE-21	220	19	84768	0.34	0.671	0.024	0.0844	0.0013	0.45	0.0577	0.0018	521	18	522	8	518	69	101
RAE	RAE-22	167	14	66040	0.50	0.694	0.023	0.0864	0.0014	0.47	0.0582	0.0017	535	18	534	8	538	65	99
RAE	RAE-23	61	5	23688	1.01	0.715	0.032	0.0853	0.0015	0.40	0.0609	0.0025	548	24	527	9	635	88	83
RAE	RAE-24	57	9	3189	0.17	1.643	0.059	0.1605	0.0027	0.46	0.0743	0.0024	987	36	959	16	1049	65	92
RAE	RAE-25	562	47	71766	0.01	0.660	0.019	0.0831	0.0012	0.53	0.0576	0.0014	515	15	515	8	514	53	100
RAE	RAE-26	219	19	84823	0.06	0.681	0.022	0.0848	0.0013	0.48	0.0583	0.0017	527	17	525	8	540	62	97
RAE	RAE-27	80	15	20858	0.60	2.072	0.067	0.1939	0.0031	0.49	0.0775	0.0022	1140	37	1143	18	1134	56	101
RAE	RAE-28	113	11	52460	0.29	0.845	0.031	0.1014	0.0017	0.44	0.0604	0.0020	622	23	623	10	619	71	101
RAE	RAE-29	462	38	8194	0.32	0.645	0.020	0.0815	0.0013	0.49	0.0574	0.0016	505	16	505	8	507	60	100
RAE	RAE-30	237	25	113102	0.14	0.879	0.026	0.1046	0.0016	0.51	0.0609	0.0016	640	19	641	10	637	56	101
RAE	RAE-31	268	53	241534	0.44	2.137	0.059	0.1975	0.0030	0.55	0.0785	0.0018	1161	32	1162	17	1159	45	100
RAE	RAE-32	108	9	1777	0.45	0.698	0.030	0.0864	0.0015	0.40	0.0586	0.0023	538	23	534	9	551	87	97
RAE	RAE-34	326	28	4707	0.36	0.700	0.021	0.0869	0.0013	0.50	0.0584	0.0015	539	16	537	8	544	57	99
RAE	RAE-35	34	7	29999	0.55	2.077	0.080	0.1929	0.0033	0.45	0.0781	0.0027	1141	44	1137	20	1148	69	99
RAE	RAE-36	239	24	111792	0.13	0.867	0.033	0.1024	0.0017	0.44	0.0614	0.0021	634	24	629	10	654	73	96
RAE	RAE-37	146	13	58521	0.38	0.710	0.025	0.0879	0.0014	0.46	0.0586	0.0018	545	19	543	9	550	67	99
RAE	RAE-38	71	12	3998	0.43	1.686	0.059	0.1676	0.0027	0.47	0.0730	0.0022	1003	35	999	16	1013	62	99
RAE	RAE-39	95	16	75097	0.15	1.754	0.062	0.1725	0.0028	0.46	0.0737	0.0023	1029	37	1026	17	1034	64	99
RAE	RAE-40	57	5	23631	0.40	0.737	0.042	0.0905	0.0018	0.35	0.0591	0.0032	561	32	558	11	570	117	98
RAE	RAE-41	146	22	2132	0.14	1.617	0.050	0.1539	0.0024	0.50	0.0762	0.0020	977	30	923	14	1100	54	84
RAE	RAE-42	151	13	24451	0.48	0.701	0.028	0.0867	0.0015	0.42	0.0587	0.0022	539	22	536	9	554	80	97
RAE	RAE-43	138	16	3504	0.70	1.093	0.035	0.1184	0.0018	0.49	0.0670	0.0019	750	24	721	11	838	58	86
RAE	RAE-44	183	32	146554	0.14	1.775	0.053	0.1749	0.0027	0.52	0.0736	0.0019	1036	31	1039	16	1031	52	101
RAE	RAE-45	657	54	4295	0.53	0.661	0.025	0.0826	0.0014	0.43	0.0580	0.0020	515	20	512	8	529	76	97
RAE	RAE-46	138	12	1373	0.52	0.686	0.024	0.0851	0.0014	0.45	0.0585	0.0019	531	19	526	8	550	69	96
RAE	RAE-47	66	6	26377	0.31	0.698	0.032	0.0869	0.0016	0.39	0.0582	0.0025	537	25	537	10	538	94	100
RAE	RAE-48	63	6	956	0.35	0.748	0.035	0.0907	0.0016	0.38	0.0598	0.0026	567	27	559	10	597	95	94
RAE	RAE-49	273	23	104734	0.44	0.666	0.021	0.0839	0.0013	0.49	0.0576	0.0016	518	16	519	8	514	60	101
RAE	RAE-50	71	12	53306	0.56	1.658	0.066	0.1639	0.0028	0.43	0.0734	0.0026	993	40	978	17	1025	73	95
RAE	RAE-51	79	14	65636	1.74	1.937	0.098	0.1828	0.0037	0.39	0.0769	0.0036	1094	55	1082	22	1118	93	97

[a]U and Pb concentrations and Th/U ratios are calculated relative to GJ-1 reference zircon

[b]Corrected for background and within-run Pb/U fractionation and normalised to reference zircon GJ-1 (ID-TIMS values/measured value); $^{207}Pb/^{235}U$ calculated using $(^{207}Pb/^{206}Pb)/(^{238}U/^{206}Pb * 1/137.88)$

[c]Rho is the error correlation defined as the quotient of the propagated errors of the $^{206}Pb/^{238}U$ and the $^{207}/^{235}U$ ratio

[d]Quadratic addition of within-run errors (2 SD) and daily reproducibility of GJ-1 (2 SD)

[e]Corrected for mass-bias by normalising to GJ-1 reference zircon (~0.6 per atomic mass unit) and common Pb using the model Pb composition of Stacey & Kramers (1975)

Table D5. LA-ICPMS isotopic data for sample HBUP in the Heidelberg Basin

HBUP							RATIOS							AGES [Ma]						Conc.
Sample	Analysis	U [ppm][a]	Pb [ppm][a]	Th [ppm][a]	$^{206}Pb/^{204}Pb$	Th/U[a]	$^{207}Pb/^{235}U$[b]	2 σ[d]	$^{206}Pb/^{238}U$[b]	2 σ[d]	rho[c]	$^{207}Pb/^{206}Pb$	2 σ[d]	$^{207}Pb/^{235}U$	2 σ	$^{206}Pb/^{238}U$	2 σ	$^{207}Pb/^{206}Pb$	2 σ	%
HBUP	HBUP-1	412	10	278	50576	0.68	0.170	0.007	0.02519	0.00048	0.43	0.0488	0.0019	159	7	160	3	140	93	115
HBUP	HBUP-2	374	10	241	2089	0.64	0.176	0.008	0.02552	0.00048	0.43	0.0499	0.0020	164	7	162	3	190	92	86
HBUP	HBUP-3	275	7	139	267	0.50	0.174	0.017	0.02500	0.00050	0.20	0.0505	0.0049	163	16	159	3	220	223	72
HBUP	HBUP-4	228	6	130	767	0.57	0.174	0.010	0.02579	0.00050	0.36	0.0491	0.0025	163	9	164	3	151	119	109
HBUP	HBUP-5	247	6	165	4248	0.67	0.174	0.010	0.02546	0.00050	0.34	0.0495	0.0027	163	9	162	3	170	128	96
HBUP	HBUP-6	203	5	93	54036	0.46	0.178	0.009	0.02586	0.00050	0.39	0.0499	0.0023	166	8	165	3	188	106	88
HBUP	HBUP-7	294	8	182	1324	0.62	0.179	0.010	0.02593	0.00050	0.34	0.0499	0.0026	167	9	165	3	192	122	86
HBUP	HBUP-8	271	7	127	573	0.47	0.179	0.013	0.02536	0.00048	0.27	0.0511	0.0035	167	12	161	3	245	157	66
HBUP	HBUP-9	765	52	73	532195	0.10	0.554	0.023	0.06740	0.00134	0.48	0.0597	0.0022	448	19	420	8	591	79	71
HBUP	HBUP-10	249	6	93	359	0.37	0.196	0.029	0.02612	0.00050	0.13	0.0544	0.0080	182	27	166	3	389	331	43
HBUP	HBUP-11	299	7	144	77108	0.48	0.170	0.008	0.02500	0.00048	0.42	0.0493	0.0020	159	7	159	3	160	97	100
HBUP	HBUP-12	97	2	43	25645	0.45	0.176	0.021	0.02567	0.00054	0.17	0.0498	0.0060	165	20	163	3	188	278	87
HBUP	HBUP-13	307	8	152	1030	0.50	0.184	0.027	0.02564	0.00054	0.14	0.0522	0.0077	172	25	163	3	293	335	56
HBUP	HBUP-14	342	9	99	31267	0.29	0.178	0.006	0.02598	0.00050	0.54	0.0496	0.0015	166	6	165	3	175	70	94
HBUP	HBUP-16	475	12	265	1360	0.56	0.175	0.007	0.02552	0.00048	0.45	0.0498	0.0018	164	7	162	3	183	86	89
HBUP	HBUP-17	677	18	247	292	0.37	0.191	0.016	0.02624	0.00050	0.23	0.0528	0.0042	177	15	167	3	318	181	52
HBUP	HBUP-18	2239	104	2517	29	1.12	0.580	0.031	0.04639	0.00086	0.34	0.0907	0.0046	465	25	292	5	1441	97	20
HBUP	HBUP-19	355	9	150	2171	0.42	0.174	0.009	0.02561	0.00048	0.37	0.0492	0.0023	163	8	163	3	156	110	104
HBUP	HBUP-20	200	5	135	52244	0.68	0.170	0.007	0.02540	0.00050	0.49	0.0486	0.0017	160	6	162	3	131	83	124
HBUP	HBUP-21	335	9	147	882	0.44	0.192	0.017	0.02556	0.00048	0.22	0.0544	0.0046	178	16	163	3	389	191	42
HBUP	HBUP-22	583	15	201	30297	0.35	0.176	0.006	0.02593	0.00048	0.58	0.0491	0.0013	164	5	165	3	153	61	108
HBUP	HBUP-23	25	5	15	777	0.62	2.121	0.151	0.19478	0.00512	0.37	0.0790	0.0052	1156	82	1147	30	1172	131	98
HBUP	HBUP-24	199	5	67	2745	0.34	0.178	0.007	0.02596	0.00050	0.47	0.0496	0.0018	166	7	165	3	178	84	93
HBUP	HBUP-25	358	9	264	13117	0.74	0.176	0.006	0.02605	0.00050	0.55	0.0491	0.0014	165	6	166	3	150	69	110
HBUP	HBUP-26	292	7	113	76244	0.39	0.173	0.006	0.02535	0.00048	0.52	0.0494	0.0015	162	6	161	3	168	73	96
HBUP	HBUP-27	157	4	84	40634	0.54	0.172	0.008	0.02506	0.00050	0.44	0.0498	0.0020	161	7	160	3	187	95	85
HBUP	HBUP-28	288	7	132	2766	0.46	0.176	0.007	0.02553	0.00050	0.47	0.0501	0.0019	165	7	163	3	199	86	82
HBUP	HBUP-29	374	10	255	4282	0.68	0.174	0.006	0.02577	0.00050	0.56	0.0490	0.0014	163	6	164	3	148	68	111
HBUP	HBUP-30	167	4	65	2105	0.39	0.173	0.011	0.02534	0.00050	0.31	0.0495	0.0030	162	10	161	3	171	143	94
HBUP	HBUP-31	335	8	195	218	0.58	0.180	0.021	0.02526	0.00048	0.16	0.0518	0.0060	168	20	161	3	276	266	58
HBUP	HBUP-32	237	6	94	1033	0.40	0.201	0.029	0.02590	0.00052	0.14	0.0564	0.0081	186	27	165	3	468	317	35
HBUP	HBUP-33	78	27	100	65037	1.28	5.479	0.159	0.34139	0.00642	0.65	0.1164	0.0026	1897	55	1893	36	1902	40	100
HBUP	HBUP-34	237	6	85	61640	0.36	0.173	0.007	0.02527	0.00048	0.49	0.0497	0.0017	162	6	161	3	179	78	90
HBUP	HBUP-35	193	5	72	1038	0.37	0.175	0.008	0.02568	0.00050	0.44	0.0495	0.0020	164	7	163	3	171	92	96
HBUP	HBUP-37	262	7	93	70402	0.36	0.179	0.007	0.02614	0.00050	0.49	0.0498	0.0017	168	7	166	3	185	80	90
HBUP	HBUP-39	84	2	44	717	0.52	0.178	0.036	0.02503	0.00052	0.10	0.0515	0.0103	166	34	159	3	261	461	61
HBUP	HBUP-40	279	7	151	3695	0.54	0.173	0.011	0.02520	0.00048	0.31	0.0497	0.0029	162	10	160	3	179	136	90
HBUP	HBUP-41	458	12	236	4614	0.51	0.178	0.010	0.02623	0.00050	0.34	0.0493	0.0026	167	9	167	3	164	125	102
HBUP	HBUP-42	217	6	87	141	0.40	0.250	0.030	0.02599	0.00056	0.18	0.0697	0.0083	226	27	165	4	920	245	18
HBUP	HBUP-43	416	10	157	9025	0.38	0.172	0.006	0.02513	0.00048	0.55	0.0496	0.0014	161	6	160	3	175	67	91
HBUP	HBUP-44	272	7	196	2660	0.72	0.173	0.007	0.02522	0.00050	0.47	0.0498	0.0018	162	7	161	3	185	86	87
HBUP	HBUP-45	227	6	155	2712	0.68	0.173	0.009	0.02546	0.00050	0.38	0.0493	0.0024	162	8	162	3	164	113	99
HBUP	HBUP-46	150	4	61	39570	0.41	0.174	0.010	0.02560	0.00050	0.35	0.0493	0.0026	163	9	163	3	160	122	102
HBUP	HBUP-47	312	8	173	2416	0.55	0.174	0.006	0.02552	0.00048	0.52	0.0493	0.0015	162	6	162	3	163	72	100
HBUP	HBUP-48	272	7	165	71735	0.61	0.173	0.006	0.02561	0.00050	0.52	0.0491	0.0016	162	6	163	3	154	74	106
HBUP	HBUP-49	299	8	134	3824	0.45	0.174	0.006	0.02586	0.00050	0.53	0.0488	0.0015	163	6	165	3	137	73	120
HBUP	HBUP-50	209	5	116	8616	0.55	0.173	0.011	0.02518	0.00050	0.32	0.0499	0.0029	162	10	160	3	189	135	85

HBUP	HBUP-51	283	7	121	3253	0.43	0.171	0.007	0.02512	0.00048	0.44	0.0495	0.0019	161	7	160	3	172	91	93
HBUP	HBUP-52	244	6	126	166	0.52	0.177	0.015	0.02613	0.00054	0.24	0.0491	0.0041	166	14	166	3	155	197	108
HBUP	HBUP-53	282	7	110	73395	0.39	0.174	0.006	0.02529	0.00048	0.51	0.0498	0.0016	163	6	161	3	185	74	87
HBUP	HBUP-54	257	7	136	69240	0.53	0.177	0.007	0.02623	0.00050	0.51	0.0489	0.0016	165	6	167	3	142	76	118
HBUP	HBUP-55	220	6	115	3317	0.52	0.178	0.008	0.02611	0.00050	0.43	0.0495	0.0020	166	7	166	3	170	93	98
HBUP	HBUP-56	208	5	153	9104	0.74	0.174	0.007	0.02557	0.00050	0.49	0.0495	0.0017	163	7	163	3	170	81	96
HBUP	HBUP-57	191	5	88	49329	0.46	0.170	0.007	0.02507	0.00050	0.48	0.0491	0.0018	159	7	160	3	152	86	105
HBUP	HBUP-58	248	6	111	1665	0.45	0.169	0.007	0.02497	0.00048	0.49	0.0491	0.0017	158	6	159	3	151	79	105
HBUP	HBUP-59	404	10	264	975	0.65	0.172	0.006	0.02511	0.00048	0.54	0.0496	0.0015	161	6	160	3	178	69	90
HBUP	HBUP-61	243	6	123	2542	0.51	0.174	0.007	0.02558	0.00050	0.47	0.0494	0.0018	163	7	163	3	167	85	97
HBUP	HBUP-62	231	6	100	774	0.43	0.174	0.007	0.02549	0.00050	0.47	0.0495	0.0018	163	7	162	3	173	85	94
HBUP	HBUP-64	119	3	53	1086	0.44	0.174	0.008	0.02549	0.00052	0.42	0.0494	0.0022	162	8	162	3	166	102	98
HBUP	HBUP-65	245	6	107	64599	0.44	0.177	0.007	0.02567	0.00050	0.49	0.0500	0.0017	165	7	163	3	193	80	85
HBUP	HBUP-67	333	8	99	1292	0.30	0.172	0.006	0.02501	0.00048	0.51	0.0499	0.0016	161	6	159	3	189	76	84
HBUP	HBUP-68	146	21	71	215845	0.48	1.345	0.041	0.14372	0.00270	0.62	0.0679	0.0016	866	26	866	16	865	49	100
HBUP	HBUP-69	751	19	216	21493	0.29	0.172	0.006	0.02514	0.00048	0.51	0.0496	0.0016	161	6	160	3	177	75	90
HBUP	HBUP-70	119	3	52	31142	0.43	0.172	0.012	0.02537	0.00052	0.29	0.0492	0.0033	161	11	162	3	158	158	102
HBUP	HBUP-71	250	6	115	65589	0.46	0.173	0.007	0.02549	0.00050	0.52	0.0491	0.0016	162	6	162	3	152	76	107
HBUP	HBUP-72	291	7	170	1564	0.59	0.174	0.008	0.02536	0.00048	0.42	0.0496	0.0020	162	7	161	3	177	95	91
HBUP	HBUP-73	438	11	151	1732	0.34	0.171	0.007	0.02515	0.00048	0.46	0.0494	0.0018	160	7	160	3	164	85	97
HBUP	HBUP-74	621	16	179	162086	0.29	0.175	0.006	0.02539	0.00048	0.58	0.0499	0.0013	163	5	162	3	188	62	86
HBUP	HBUP-76	361	9	174	2250	0.48	0.178	0.007	0.02623	0.00050	0.45	0.0493	0.0018	167	7	167	3	163	87	103
HBUP	HBUP-77	296	7	118	76677	0.40	0.172	0.008	0.02521	0.00048	0.41	0.0494	0.0021	161	7	160	3	164	99	98
HBUP	HBUP-78	434	11	311	953	0.72	0.177	0.013	0.02585	0.00050	0.26	0.0498	0.0036	166	12	165	3	186	169	89
HBUP	HBUP-79	177	5	106	890	0.60	0.176	0.009	0.02586	0.00052	0.39	0.0494	0.0023	165	8	165	3	165	110	99
HBUP	HBUP-80	340	9	178	87893	0.52	0.172	0.013	0.02520	0.00048	0.26	0.0495	0.0036	161	12	160	3	171	168	94
HBUP	HBUP-81	375	10	194	46989	0.52	0.174	0.006	0.02570	0.00050	0.55	0.0491	0.0014	163	6	164	3	152	69	108
HBUP	HBUP-82	337	8	145	685	0.43	0.180	0.017	0.02507	0.00048	0.20	0.0521	0.0049	168	16	160	3	288	217	55
HBUP	HBUP-83	216	6	91	56613	0.42	0.175	0.010	0.02549	0.00050	0.35	0.0497	0.0026	163	9	162	3	181	124	90
HBUP	HBUP-84	396	10	167	102579	0.42	0.172	0.006	0.02522	0.00048	0.55	0.0494	0.0014	161	6	161	3	165	68	97
HBUP	HBUP-85	171	4	63	44672	0.37	0.173	0.008	0.02541	0.00050	0.45	0.0494	0.0019	162	7	162	3	166	91	97
HBUP	HBUP-86	338	9	130	392	0.38	0.178	0.009	0.02607	0.00052	0.39	0.0496	0.0023	167	8	166	3	178	109	93
HBUP	HBUP-88	328	8	166	84531	0.51	0.172	0.010	0.02515	0.00048	0.32	0.0495	0.0028	161	10	160	3	173	131	93
HBUP	HBUP-89	368	9	127	1337	0.35	0.176	0.007	0.02569	0.00050	0.47	0.0497	0.0018	165	7	164	3	181	84	91
HBUP	HBUP-90	247	6	104	2057	0.42	0.174	0.007	0.02563	0.00050	0.46	0.0493	0.0019	163	7	163	3	161	89	102
HBUP	HBUP-91	557	14	203	4672	0.36	0.171	0.007	0.02510	0.00048	0.49	0.0493	0.0017	160	6	160	3	161	79	99
HBUP	HBUP-92	201	5	78	36359	0.39	0.169	0.008	0.02503	0.00050	0.43	0.0491	0.0021	159	7	159	3	153	98	104
HBUP	HBUP-94	307	8	154	7955	0.50	0.176	0.010	0.02550	0.00050	0.35	0.0500	0.0026	164	9	162	3	196	122	83
HBUP	HBUP-96	283	7	154	33708	0.54	0.172	0.009	0.02527	0.00048	0.38	0.0494	0.0023	161	8	161	3	165	107	98
HBUP	HBUP-98	593	15	196	410	0.33	0.172	0.016	0.02513	0.00048	0.21	0.0496	0.0044	161	15	160	3	178	208	90
HBUP	HBUP-99	355	23	252	2520	0.71	0.610	0.020	0.06334	0.00122	0.57	0.0698	0.0019	484	16	396	8	924	56	43
HBUP	HBUP-103	302	8	162	572	0.53	0.175	0.008	0.02551	0.00050	0.46	0.0496	0.0019	163	7	162	3	177	89	92
HBUP	HBUP-104	425	11	301	112320	0.71	0.175	0.008	0.02576	0.00050	0.45	0.0494	0.0019	164	7	164	3	165	90	99
HBUP	HBUP-105	446	113	226	12027	0.51	3.592	0.103	0.25328	0.00474	0.66	0.1029	0.0022	1548	44	1455	27	1676	40	87
HBUP	HBUP-106	258	7	106	2648	0.41	0.174	0.008	0.02562	0.00050	0.43	0.0491	0.0020	162	7	163	3	154	96	106
HBUP	HBUP-108	304	8	174	2876	0.57	0.176	0.009	0.02588	0.00050	0.38	0.0494	0.0023	165	8	165	3	165	109	100
HBUP	HBUP-109	421	11	304	2359	0.72	0.174	0.020	0.02536	0.00048	0.17	0.0498	0.0056	163	18	161	3	184	260	88
HBUP	HBUP-110	137	3	46	1309	0.34	0.174	0.010	0.02556	0.00052	0.37	0.0494	0.0026	163	9	163	3	165	121	99
HBUP	HBUP-111	86	2	38	22996	0.44	0.177	0.009	0.02596	0.00054	0.39	0.0494	0.0024	165	9	165	3	164	114	100

HBUP	HBUP-112	331	29	99	5928	0.30	0.705	0.024	0.08804	0.00168	0.57	0.0581	0.0016	542	18	544	10	533	60	102
HBUP	HBUP-113	242	6	97	358	0.40	0.182	0.016	0.02616	0.00050	0.22	0.0505	0.0042	170	15	166	3	218	194	76
HBUP	HBUP-114	315	8	180	961	0.57	0.181	0.016	0.02625	0.00050	0.22	0.0500	0.0042	169	15	167	3	193	197	87
HBUP	HBUP-115	118	3	63	409	0.53	0.176	0.017	0.02585	0.00052	0.21	0.0493	0.0047	164	16	165	3	160	224	103

[a]U and Pb concentrations and Th/U ratios are calculated relative to GJ-1 reference zircon

[b]Corrected for background and within-run Pb/U fractionation and normalised to reference zircon GJ-1 (ID-TIMS values/measured value); $^{207}Pb/^{235}U$ calculated using ($^{207}Pb/^{206}Pb$)/($^{238}U/^{206}Pb$ * 1/137.88)

[c]Rho is the error correlation defined as the quotient of the propagated errors of the $^{206}Pb/^{238}U$ and the $^{207}/^{235}U$ ratio

[d]Quadratic addition of within-run errors (2 SD) and daily reproducibility of GJ-1 (2 SD)

[e]Corrected for mass-bias by normalising to GJ-1 reference zircon (~0.6 per atomic mass unit) and common Pb using the model Pb composition of Stacey & Kramers (1975)

Table D6. LA-ICPMS isotopic data for sample HBMB in the Heidelberg Basin

HBMB							RATIOS							AGES [Ma]						Conc.
Sample	Analysis	U [ppm][a]	Pb [ppm][a]	Th [ppm][a]	$^{206}Pb/^{204}Pb$	Th/U[a]	$^{207}Pb/^{235}U$[b]	2 σ[d]	$^{206}Pb/^{238}U$[b]	2 σ[d]	rho[c]	$^{207}Pb/^{206}Pb$	2 σ[d]	$^{207}Pb/^{235}U$	2 σ	$^{206}Pb/^{238}U$	2 σ	$^{207}Pb/^{206}Pb$	2 σ	%
HBMB	MB-1	98	3	72	642	0.73	0.183	0.014	0.02682	0.00058	0.29	0.0495	0.0036	171	13	171	4	170	169	100
HBMB	MB-2	91	3	57	24083	0.63	0.192	0.014	0.02765	0.00060	0.30	0.0504	0.0035	178	13	176	4	214	162	82
HBMB	MB-3	407	11	285	771	0.70	0.198	0.013	0.02724	0.00054	0.29	0.0527	0.0034	183	12	173	3	315	147	55
HBMB	MB-5	389	11	214	634	0.55	0.188	0.022	0.02750	0.00054	0.17	0.0495	0.0057	175	20	175	3	171	267	102
HBMB	MB-6	445	12	312	341	0.70	0.185	0.013	0.02716	0.00054	0.29	0.0493	0.0033	172	12	173	3	162	156	107
HBMB	MB-7	258	7	181	3934	0.70	0.188	0.009	0.02694	0.00054	0.43	0.0506	0.0021	175	8	171	3	220	98	78
HBMB	MB-8	451	13	305	17385	0.68	0.190	0.008	0.02778	0.00056	0.47	0.0496	0.0019	177	8	177	4	175	88	101
HBMB	MB-9	255	7	147	4646	0.58	0.190	0.008	0.02761	0.00056	0.51	0.0499	0.0017	177	7	176	4	190	80	92
HBMB	MB-10	426	11	291	1157	0.68	0.210	0.012	0.02678	0.00054	0.37	0.0569	0.0029	194	11	170	3	487	113	35
HBMB	MB-11	395	11	255	1805	0.64	0.194	0.009	0.02768	0.00056	0.43	0.0509	0.0022	180	9	176	4	237	99	74
HBMB	MB-12	298	8	206	522	0.69	0.192	0.015	0.02751	0.00056	0.26	0.0506	0.0038	178	14	175	4	224	174	78
HBMB	MB-13	395	11	251	973	0.64	0.223	0.015	0.02769	0.00054	0.29	0.0584	0.0038	204	14	176	3	545	143	32
HBMB	MB-14	170	5	75	4033	0.44	0.189	0.008	0.02760	0.00056	0.46	0.0498	0.0019	176	8	176	4	184	91	95
HBMB	MB-16	313	8	236	152	0.76	0.237	0.021	0.02717	0.00056	0.23	0.0632	0.0054	216	19	173	4	716	182	24
HBMB	MB-17	249	7	146	290	0.59	0.234	0.023	0.02785	0.00056	0.20	0.0610	0.0059	214	21	177	4	640	207	28
HBMB	MB-18	295	8	181	241	0.61	0.303	0.015	0.02769	0.00056	0.40	0.0794	0.0037	269	14	176	4	1181	92	15
HBMB	MB-19	358	10	202	854	0.56	0.200	0.021	0.02778	0.00056	0.19	0.0523	0.0055	185	20	177	4	298	238	59
HBMB	MB-20	298	8	171	-3340	0.57	0.185	0.007	0.02712	0.00054	0.53	0.0495	0.0016	172	6	172	3	170	74	102
HBMB	MB-21	77	2	41	398	0.54	0.200	0.037	0.02690	0.00060	0.12	0.0540	0.0100	185	35	171	4	371	417	46
HBMB	MB-22	219	6	121	1010	0.55	0.193	0.008	0.02741	0.00056	0.51	0.0511	0.0017	179	7	174	4	243	79	72
HBMB	MB-23	188	5	88	306	0.47	0.190	0.010	0.02779	0.00058	0.40	0.0495	0.0024	176	9	177	4	172	113	103
HBMB	MB-25	437	12	250	16341	0.57	0.182	0.007	0.02664	0.00052	0.53	0.0495	0.0015	170	6	169	3	173	73	98
HBMB	MB-26	173	5	96	200	0.56	0.206	0.039	0.02716	0.00060	0.12	0.0549	0.0103	190	36	173	4	409	420	42
HBMB	MB-27	195	5	71	374	0.37	0.198	0.023	0.02685	0.00054	0.17	0.0534	0.0061	183	21	171	3	346	258	49
HBMB	MB-28	328	9	192	273	0.59	0.252	0.017	0.02705	0.00054	0.29	0.0677	0.0044	229	16	172	3	858	135	20
HBMB	MB-29	358	10	221	116	0.62	0.190	0.019	0.02719	0.00058	0.22	0.0508	0.0049	177	17	173	4	232	223	74
HBMB	MB-30	403	11	228	7532	0.57	0.192	0.014	0.02716	0.00054	0.27	0.0514	0.0037	179	13	173	3	259	165	67
HBMB	MB-31	276	8	188	123	0.68	0.254	0.027	0.02755	0.00056	0.19	0.0669	0.0070	230	25	175	4	835	219	21
HBMB	MB-32	441	12	288	2736	0.65	0.187	0.007	0.02724	0.00054	0.54	0.0497	0.0015	174	6	173	3	182	72	95
HBMB	MB-33	355	10	192	258	0.54	0.288	0.018	0.02764	0.00056	0.32	0.0756	0.0045	257	16	176	4	1084	118	16
HBMB	MB-34	114	3	64	262	0.56	0.238	0.040	0.02698	0.00058	0.13	0.0641	0.0106	217	36	172	4	745	351	23
HBMB	MB-37	130	4	102	33850	0.78	0.217	0.026	0.02713	0.00058	0.18	0.0579	0.0068	199	24	173	4	526	257	33
HBMB	MB-38	197	5	90	417	0.46	0.274	0.020	0.02744	0.00056	0.28	0.0725	0.0050	246	18	175	4	999	141	17
HBMB	MB-39	209	6	126	55719	0.60	0.191	0.008	0.02787	0.00058	0.49	0.0497	0.0019	178	8	177	4	181	87	98
HBMB	MB-40	50	1	20	12898	0.39	0.196	0.046	0.02699	0.00070	0.11	0.0527	0.0124	182	43	172	4	314	537	55
HBMB	MB-41	92	3	31	439	0.34	0.189	0.018	0.02764	0.00062	0.23	0.0495	0.0046	175	17	176	4	172	219	102
HBMB	MB-42	445	12	353	115960	0.79	0.191	0.009	0.02727	0.00054	0.41	0.0508	0.0022	178	9	173	3	233	101	75
HBMB	MB-43	143	4	61	243	0.43	0.249	0.024	0.02738	0.00060	0.23	0.0661	0.0061	226	21	174	4	808	193	22
HBMB	MB-44	341	9	236	5961	0.69	0.185	0.011	0.02682	0.00054	0.35	0.0500	0.0027	172	10	171	3	196	124	87
HBMB	MB-45	268	7	188	69777	0.70	0.189	0.010	0.02726	0.00056	0.39	0.0503	0.0024	176	9	173	4	208	112	83
HBMB	MB-46	241	6	118	3754	0.49	0.185	0.007	0.02686	0.00054	0.50	0.0499	0.0017	172	7	171	3	190	80	90
HBMB	MB-47	549	15	388	644	0.71	0.218	0.014	0.02673	0.00052	0.30	0.0592	0.0037	200	13	170	3	574	134	30
HBMB	MB-48	220	6	171	976	0.78	0.183	0.007	0.02673	0.00054	0.51	0.0495	0.0017	170	7	170	3	173	80	98
HBMB	MB-49	152	4	96	73465	0.63	0.196	0.016	0.02705	0.00056	0.25	0.0526	0.0042	182	15	172	4	310	183	55
HBMB	MB-50	366	10	207	94124	0.57	0.184	0.007	0.02690	0.00054	0.56	0.0495	0.0015	171	6	171	3	173	70	99
HBMB	MB-51	208	6	129	209	0.62	0.182	0.010	0.02654	0.00054	0.36	0.0496	0.0026	169	9	169	3	177	121	96
HBMB	MB-52	189	5	128	328	0.68	0.190	0.011	0.02779	0.00058	0.38	0.0497	0.0025	177	10	177	4	180	119	98

HBMB	MB-53	406	11	323	341	0.80	0.187	0.009	0.02657	0.00054	0.40	0.0509	0.0023	174	9	169	3	238	106	71
HBMB	MB-55	387	10	255	872	0.66	0.185	0.010	0.02694	0.00054	0.36	0.0498	0.0026	172	10	171	3	185	120	93
HBMB	MB-57	437	12	288	-7629	0.66	0.192	0.008	0.02767	0.00056	0.49	0.0504	0.0018	178	7	176	4	212	83	83
HBMB	MB-59	144	4	87	614	0.61	0.184	0.011	0.02692	0.00056	0.36	0.0494	0.0027	171	10	171	4	169	127	101
HBMB	MB-60	293	8	178	528	0.61	0.190	0.010	0.02762	0.00056	0.39	0.0499	0.0024	177	9	176	4	189	110	93
HBMB	MB-61	128	4	63	1602	0.49	0.193	0.013	0.02792	0.00058	0.31	0.0501	0.0032	179	12	178	4	201	149	88
HBMB	MB-62	184	5	104	553	0.56	0.181	0.009	0.02659	0.00054	0.40	0.0493	0.0023	169	8	169	3	160	107	106
HBMB	MB-63	187	5	125	1434	0.67	0.181	0.008	0.02649	0.00054	0.48	0.0497	0.0019	169	7	169	3	179	87	94
HBMB	MB-64	634	17	846	1616	1.33	0.188	0.009	0.02659	0.00052	0.42	0.0514	0.0022	175	8	169	3	258	97	65
HBMB	MB-66	155	4	88	804	0.57	0.204	0.022	0.02757	0.00058	0.20	0.0537	0.0056	189	20	175	4	359	236	49
HBMB	MB-68	356	10	241	357	0.68	0.253	0.015	0.02669	0.00054	0.33	0.0687	0.0039	229	14	170	3	889	119	19
HBMB	MB-69	339	9	151	257	0.45	0.258	0.019	0.02782	0.00056	0.28	0.0674	0.0047	233	17	177	4	849	146	21
HBMB	MB-70	309	19	119	182406	0.38	0.464	0.015	0.06177	0.00122	0.61	0.0545	0.0014	387	13	386	8	393	58	98
HBMB	MB-71	331	9	195	85390	0.59	0.186	0.007	0.02706	0.00054	0.52	0.0498	0.0016	173	7	172	3	187	77	92
HBMB	MB-73	184	5	92	548	0.50	0.205	0.018	0.02718	0.00056	0.24	0.0548	0.0045	190	16	173	4	404	185	43
HBMB	MB-74	407	11	264	103948	0.65	0.183	0.007	0.02676	0.00054	0.55	0.0496	0.0015	170	6	170	3	174	72	98
HBMB	MB-75	316	8	196	3255	0.62	0.183	0.008	0.02663	0.00054	0.45	0.0498	0.0020	170	8	169	3	184	93	92
HBMB	MB-76	365	10	204	13993	0.56	0.183	0.007	0.02675	0.00054	0.55	0.0496	0.0015	170	6	170	3	175	71	97
HBMB	MB-77	420	12	205	2740	0.49	0.189	0.010	0.02741	0.00054	0.39	0.0499	0.0023	176	9	174	3	192	109	91
HBMB	MB-79	313	8	198	611	0.63	0.187	0.009	0.02688	0.00054	0.43	0.0504	0.0021	174	8	171	3	215	96	80
HBMB	MB-80	429	11	315	8416	0.73	0.185	0.009	0.02675	0.00054	0.43	0.0501	0.0021	172	8	170	3	200	97	85
HBMB	MB-81	261	7	138	1887	0.53	0.188	0.009	0.02747	0.00056	0.44	0.0497	0.0020	175	8	175	4	179	96	98
HBMB	MB-82	282	7	151	70626	0.53	0.202	0.015	0.02622	0.00054	0.28	0.0560	0.0039	187	14	167	3	451	154	37
HBMB	MB-83	136	4	97	34034	0.71	0.180	0.008	0.02621	0.00056	0.46	0.0498	0.0021	168	8	167	4	186	97	90
HBMB	MB-85	320	9	160	36940	0.50	0.183	0.007	0.02672	0.00054	0.53	0.0496	0.0016	171	7	170	3	178	76	96
HBMB	MB-86	331	9	216	2237	0.65	0.183	0.012	0.02677	0.00054	0.32	0.0495	0.0030	171	11	170	3	173	139	98
HBMB	MB-88	327	9	185	512	0.56	0.182	0.008	0.02664	0.00054	0.47	0.0496	0.0019	170	7	169	3	174	89	97
HBMB	MB-91	119	3	59	810	0.49	0.185	0.014	0.02697	0.00058	0.27	0.0497	0.0037	172	13	172	4	179	176	96
HBMB	MB-92	68	2	21	17238	0.31	0.183	0.020	0.02671	0.00060	0.20	0.0496	0.0054	170	19	170	4	177	255	96
HBMB	MB-95	111	3	93	745	0.84	0.186	0.018	0.02697	0.00058	0.22	0.0500	0.0047	173	17	172	4	194	220	89
HBMB	MB-97	227	6	124	354	0.55	0.255	0.018	0.02793	0.00058	0.29	0.0662	0.0046	231	17	178	4	813	145	22
HBMB	MB-98	278	8	156	440	0.56	0.220	0.017	0.02705	0.00054	0.27	0.0590	0.0043	202	15	172	3	567	158	30
HBMB	MB-99	200	5	120	382	0.60	0.196	0.019	0.02729	0.00056	0.21	0.0520	0.0050	182	18	174	4	286	218	61
HBMB	MB-101	581	16	429	3002	0.74	0.184	0.008	0.02691	0.00054	0.48	0.0497	0.0018	172	7	171	3	181	84	94
HBMB	MB-102	380	10	208	2006	0.55	0.205	0.015	0.02740	0.00054	0.27	0.0542	0.0038	189	14	174	3	379	159	46
HBMB	MB-103	46	1	25	11697	0.56	0.188	0.024	0.02685	0.00064	0.19	0.0508	0.0064	175	22	171	4	231	289	74
HBMB	MB-104	381	10	259	162	0.68	0.193	0.021	0.02748	0.00056	0.18	0.0509	0.0056	179	20	175	4	236	252	74
HBMB	MB-105	522	14	301	634	0.58	0.206	0.017	0.02700	0.00054	0.24	0.0553	0.0044	190	16	172	3	422	179	41
HBMB	MB-108	266	7	95	291	0.36	0.213	0.019	0.02744	0.00058	0.23	0.0564	0.0049	196	18	175	4	467	194	37
HBMB	MB-109	561	15	426	181	0.76	0.265	0.020	0.02746	0.00054	0.26	0.0700	0.0052	239	18	175	3	929	151	19
HBMB	MB-110	453	12	278	1242	0.61	0.183	0.007	0.02671	0.00054	0.50	0.0496	0.0017	170	7	170	3	178	81	96
HBMB	MB-111	234	6	135	672	0.58	0.196	0.026	0.02764	0.00056	0.15	0.0513	0.0067	181	24	176	4	256	300	69
HBMB	MB-112	113	3	88	350	0.78	0.240	0.035	0.02727	0.00060	0.15	0.0639	0.0091	219	32	173	4	739	301	23
HBMB	MB-115	384	10	239	464	0.62	0.237	0.019	0.02718	0.00054	0.25	0.0633	0.0050	216	17	173	3	717	167	24

[a]U and Pb concentrations and Th/U ratios are calculated relative to GJ-1 reference zircon

[b]Corrected for background and within-run Pb/U fractionation and normalised to reference zircon GJ-1 (ID-TIMS values/measured value); $^{207}Pb/^{235}U$ calculated using ($^{207}Pb/^{206}Pb$)/($^{238}U/^{206}Pb$ * 1/137.88)

[c]Rho is the error correlation defined as the quotient of the propagated errors of the $^{206}Pb/^{238}U$ and the $^{207}/^{235}U$ ratio

[d]Quadratic addition of within-run errors (2 SD) and daily reproducibility of GJ-1 (2 SD)

[e]Corrected for mass-bias by normalising to GJ-1 reference zircon (~0.6 per atomic mass unit) and common Pb using the model Pb composition of Stacey & Kramers (1975)

Table D7. LA-ICPMS isotopic data for sample HMill in the Heidelberg Basin

HBMill							RATIOS							AGES [Ma]						Conc.
Sample	Analysis	U [ppm][a]	Pb [ppm][a]	Th [ppm][a]	$^{206}Pb/^{204}Pb$	Th/U[a]	$^{207}Pb/^{235}U$[b]	2 σ[d]	$^{206}Pb/^{238}U$[b]	2 σ[d]	rho[c]	$^{207}Pb/^{206}Pb$[e]	2 σ[d]	$^{207}Pb/^{235}U$	2 σ	$^{206}Pb/^{238}U$	2 σ	$^{207}Pb/^{206}Pb$	2 σ	%
HBMill	HBM-1	199	6	91	51178	0.46	0.190	0.007	0.0286	0.0004	0.41	0.0483	0.0016	177	7	182	3	115	80	157
HBMill	HBM-2	143	4	99	269	0.69	0.417	0.017	0.0271	0.0005	0.44	0.1116	0.0041	354	14	172	3	1825	66	9
HBMill	HBM-3	311	8	208	5804	0.67	0.185	0.011	0.0271	0.0004	0.26	0.0495	0.0027	172	10	172	3	171	129	101
HBMill	HBM-4	141	4	65	427	0.47	0.188	0.009	0.0275	0.0004	0.32	0.0496	0.0023	175	9	175	3	174	110	100
HBMill	HBM-5	341	9	205	747	0.60	0.200	0.017	0.0258	0.0004	0.18	0.0562	0.0047	185	16	164	3	461	185	36
HBMill	HBM-6	297	8	183	448	0.61	0.193	0.016	0.0281	0.0004	0.19	0.0500	0.0040	180	14	179	3	193	184	93
HBMill	HBM-7	569	16	296	986	0.52	0.218	0.018	0.0279	0.0004	0.17	0.0567	0.0047	201	17	178	3	481	182	37
HBMill	HBM-9	590	16	286	9599	0.48	0.188	0.005	0.0275	0.0004	0.50	0.0496	0.0012	175	5	175	3	175	58	100
HBMill	HBM-10	780	22	337	29558	0.43	0.192	0.005	0.0282	0.0004	0.51	0.0495	0.0012	179	5	179	3	173	57	103
HBMill	HBM-12	217	6	188	214	0.87	0.252	0.027	0.0271	0.0005	0.16	0.0674	0.0073	228	25	172	3	849	224	20
HBMill	HBM-13	220	6	99	3299	0.45	0.187	0.013	0.0273	0.0004	0.23	0.0496	0.0033	174	12	174	3	178	155	98
HBMill	HBM-14	224	6	134	238	0.60	0.215	0.015	0.0272	0.0004	0.23	0.0573	0.0040	198	14	173	3	503	153	34
HBMill	HBM-15	71	2	49	182	0.69	0.488	0.061	0.0292	0.0005	0.14	0.1211	0.0151	404	51	186	3	1973	222	9
HBMill	HBM-16	363	10	176	2943	0.48	0.203	0.018	0.0269	0.0004	0.17	0.0546	0.0047	187	16	171	3	394	192	43
HBMill	HBM-17	236	6	141	55282	0.60	0.176	0.018	0.0259	0.0004	0.16	0.0493	0.0049	165	17	165	3	162	232	102
HBMill	HBM-18	212	6	130	1991	0.61	0.190	0.011	0.0276	0.0004	0.27	0.0498	0.0027	176	10	175	3	187	124	94
HBMill	HBM-19	382	10	246	92631	0.64	0.182	0.006	0.0268	0.0004	0.47	0.0493	0.0014	170	5	170	3	162	65	105
HBMill	HBM-20	650	17	310	157563	0.48	0.182	0.005	0.0268	0.0004	0.49	0.0494	0.0012	170	5	170	2	166	59	102
HBMill	HBM-21	826	22	366	2218	0.44	0.187	0.005	0.0271	0.0004	0.48	0.0499	0.0013	174	5	173	2	188	59	92
HBMill	HBM-22	131	4	48	32817	0.36	0.188	0.009	0.0277	0.0004	0.32	0.0493	0.0023	175	9	176	3	163	110	108
HBMill	HBM-23	195	5	63	368	0.33	0.209	0.028	0.0258	0.0004	0.13	0.0589	0.0077	193	25	164	3	562	285	29
HBMill	HBM-24	219	6	100	56030	0.46	0.194	0.007	0.0283	0.0004	0.42	0.0498	0.0017	180	7	180	3	186	78	97
HBMill	HBM-25	372	10	202	1741	0.54	0.191	0.006	0.0279	0.0004	0.47	0.0496	0.0014	177	6	178	3	176	66	101
HBMill	HBM-27	257	7	153	569	0.60	0.191	0.021	0.0257	0.0004	0.14	0.0540	0.0058	178	19	164	3	369	242	44
HBMill	HBM-28	537	14	301	895	0.56	0.203	0.014	0.0260	0.0004	0.22	0.0566	0.0037	188	13	166	2	478	146	35
HBMill	HBM-29	372	11	124	573	0.33	0.207	0.018	0.0295	0.0004	0.17	0.0508	0.0043	191	16	188	3	232	195	81
HBMill	HBM-30	363	10	167	89673	0.46	0.183	0.014	0.0272	0.0004	0.19	0.0487	0.0038	170	13	173	3	131	183	132
HBMill	HBM-31	375	10	233	2621	0.62	0.181	0.012	0.0257	0.0004	0.24	0.0511	0.0032	169	11	164	3	247	143	66
HBMill	HBM-32	342	9	149	500	0.44	0.262	0.026	0.0275	0.0004	0.16	0.0691	0.0067	236	23	175	3	903	200	19
HBMill	HBM-33	526	15	257	446	0.49	0.243	0.020	0.0278	0.0004	0.18	0.0636	0.0051	221	18	177	3	728	169	24
HBMill	HBM-34	337	9	178	831	0.53	0.176	0.007	0.0259	0.0004	0.41	0.0494	0.0017	165	6	165	3	165	80	100
HBMill	HBM-35	524	14	329	678	0.63	0.200	0.017	0.0272	0.0004	0.18	0.0533	0.0043	185	15	173	3	343	184	51
HBMill	HBM-36	312	9	235	4795	0.75	0.197	0.009	0.0287	0.0004	0.31	0.0499	0.0022	183	9	182	3	190	104	96
HBMill	HBM-37	328	9	187	84726	0.57	0.195	0.007	0.0284	0.0004	0.39	0.0497	0.0017	181	7	181	3	180	81	101
HBMill	HBM-38	276	14	161	1595	0.58	0.388	0.024	0.0518	0.0010	0.31	0.0542	0.0032	333	20	326	6	380	131	86
HBMill	HBM-39	255	7	160	466	0.63	0.280	0.025	0.0286	0.0004	0.17	0.0711	0.0062	251	22	181	3	960	179	19
HBMill	HBM-40	223	6	133	592	0.59	0.224	0.017	0.0271	0.0004	0.21	0.0600	0.0044	206	15	172	3	605	159	29
HBMill	HBM-41	303	8	200	941	0.66	0.205	0.017	0.0270	0.0004	0.17	0.0550	0.0046	189	16	172	3	413	186	42
HBMill	HBM-42	129	4	80	68	0.62	0.879	0.063	0.0348	0.0006	0.22	0.1835	0.0129	641	46	220	4	2684	116	8
HBMill	HBM-43	338	9	238	748	0.70	0.186	0.008	0.0273	0.0004	0.35	0.0495	0.0019	173	7	174	3	170	92	102
HBMill	HBM-44	211	6	139	6205	0.66	0.190	0.010	0.0278	0.0004	0.28	0.0495	0.0026	177	10	177	3	172	122	103
HBMill	HBM-45	223	6	161	1674	0.72	0.194	0.016	0.0260	0.0004	0.18	0.0541	0.0044	180	15	165	3	374	185	44
HBMill	HBM-46	261	7	141	356	0.54	0.216	0.020	0.0261	0.0004	0.17	0.0600	0.0056	198	19	166	3	605	202	27
HBMill	HBM-47	341	9	184	377	0.54	0.198	0.019	0.0259	0.0004	0.16	0.0555	0.0052	184	18	165	3	432	210	38
HBMill	HBM-48	279	8	182	408	0.65	0.185	0.014	0.0272	0.0004	0.21	0.0495	0.0036	173	13	173	3	170	169	102
HBMill	HBM-49	344	10	171	1127	0.50	0.198	0.006	0.0287	0.0004	0.46	0.0500	0.0014	183	6	182	3	195	66	94
HBMill	HBM-50	521	14	335	2534	0.64	0.185	0.009	0.0270	0.0004	0.30	0.0497	0.0023	172	8	172	3	179	109	96

HBMiII	HBM-51	329	9	152	18582	0.46	0.189	0.008	0.0274	0.0004	0.33	0.0500	0.0021	176	8	174	3	195	99	89
HBMiII	HBM-52	194	5	106	5664	0.54	0.184	0.011	0.0268	0.0004	0.27	0.0498	0.0028	171	10	170	3	186	133	92
HBMiII	HBM-53	135	4	61	342	0.45	0.415	0.034	0.0295	0.0005	0.21	0.1020	0.0081	352	29	187	3	1661	147	11
HBMiII	HBM-54	190	5	104	299	0.55	0.252	0.022	0.0271	0.0004	0.17	0.0674	0.0059	228	20	172	3	850	181	20
HBMiII	HBM-55	156	4	62	254	0.40	0.304	0.037	0.0270	0.0004	0.13	0.0818	0.0099	270	33	171	3	1242	236	14
HBMiII	HBM-56	149	4	95	263	0.64	0.222	0.023	0.0260	0.0005	0.17	0.0621	0.0064	204	21	165	3	676	220	24
HBMiII	HBM-57	310	8	186	1139	0.60	0.178	0.010	0.0258	0.0004	0.27	0.0501	0.0028	167	10	164	3	199	131	83
HBMiII	HBM-58	300	8	142	6294	0.47	0.188	0.008	0.0273	0.0004	0.34	0.0501	0.0020	175	7	173	3	198	93	88
HBMiII	HBM-59	215	6	137	296	0.64	0.210	0.018	0.0283	0.0004	0.18	0.0539	0.0044	194	16	180	3	366	186	49
HBMiII	HBM-60	250	6	202	267	0.81	0.191	0.016	0.0259	0.0004	0.20	0.0534	0.0044	177	15	165	3	347	188	47
HBMiII	HBM-61	166	5	145	132	0.87	0.570	0.045	0.0289	0.0005	0.21	0.1432	0.0110	458	36	184	3	2267	132	8
HBMiII	HBM-63	420	11	229	1375	0.54	0.179	0.010	0.0260	0.0004	0.27	0.0498	0.0026	167	9	166	2	188	122	88
HBMiII	HBM-64	278	7	138	469	0.50	0.189	0.017	0.0268	0.0004	0.17	0.0514	0.0046	176	16	170	3	257	205	66
HBMiII	HBM-65	234	7	152	519	0.65	0.221	0.020	0.0280	0.0004	0.16	0.0573	0.0052	203	19	178	3	503	200	35
HBMiII	HBM-66	347	10	216	473	0.62	0.206	0.015	0.0282	0.0004	0.21	0.0531	0.0037	191	14	179	3	331	158	54
HBMiII	HBM-68	215	6	114	421	0.53	0.214	0.015	0.0267	0.0004	0.21	0.0581	0.0040	197	14	170	3	535	152	32
HBMiII	HBM-69	272	7	131	1953	0.48	0.182	0.015	0.0266	0.0004	0.19	0.0496	0.0039	170	14	169	3	178	183	95
HBMiII	HBM-70	276	8	160	598	0.58	0.182	0.013	0.0272	0.0004	0.21	0.0487	0.0034	170	12	173	3	131	164	131
HBMiII	HBM-71	165	5	88	290	0.53	0.301	0.027	0.0281	0.0004	0.17	0.0777	0.0069	268	24	179	3	1139	177	16
HBMiII	HBM-72	470	12	251	64626	0.54	0.177	0.008	0.0259	0.0004	0.32	0.0496	0.0022	166	8	165	2	175	103	94
HBMiII	HBM-73	350	9	330	791	0.94	0.218	0.018	0.0258	0.0004	0.18	0.0611	0.0050	200	17	164	2	642	175	26
HBMiII	HBM-74	206	6	104	406	0.51	0.183	0.008	0.0270	0.0004	0.35	0.0492	0.0021	171	8	172	3	156	98	110
HBMiII	HBM-75	545	14	285	4792	0.52	0.183	0.008	0.0259	0.0004	0.33	0.0514	0.0021	171	8	165	2	258	96	64
HBMiII	HBM-76	303	8	180	403	0.59	0.189	0.012	0.0258	0.0004	0.25	0.0532	0.0032	176	11	164	3	339	134	48
HBMiII	HBM-77	353	9	202	1883	0.57	0.187	0.011	0.0258	0.0004	0.25	0.0524	0.0030	174	10	164	2	304	130	54
HBMiII	HBM-78	382	10	331	2261	0.87	0.179	0.009	0.0261	0.0004	0.28	0.0497	0.0025	167	9	166	2	180	116	92
HBMiII	HBM-79	1219	40	425	82	0.35	0.498	0.020	0.0328	0.0005	0.34	0.1103	0.0042	411	17	208	3	1805	70	12
HBMiII	HBM-80	332	9	123	1763	0.37	0.203	0.015	0.0259	0.0004	0.21	0.0570	0.0042	188	14	165	3	490	163	34
HBMiII	HBM-81	248	7	99	62920	0.40	0.181	0.010	0.0266	0.0004	0.28	0.0493	0.0026	169	9	169	3	163	122	104
HBMiII	HBM-82	307	8	174	1231	0.57	0.182	0.008	0.0267	0.0004	0.35	0.0495	0.0020	170	7	170	3	170	94	100
HBMiII	HBM-84	351	10	133	472	0.38	0.224	0.012	0.0281	0.0004	0.28	0.0579	0.0030	205	11	179	3	527	112	34
HBMiII	HBM-86	302	8	159	435	0.53	0.240	0.022	0.0270	0.0005	0.19	0.0645	0.0057	218	20	172	3	757	186	23
HBMiII	HBM-87	196	6	80	576	0.41	0.194	0.008	0.0282	0.0004	0.36	0.0498	0.0020	180	8	179	3	188	94	96
HBMiII	HBM-88	212	6	122	1826	0.57	0.201	0.013	0.0289	0.0004	0.23	0.0503	0.0032	186	12	184	3	210	147	88
HBMiII	HBM-89	431	12	268	11157	0.62	0.190	0.008	0.0279	0.0004	0.35	0.0496	0.0019	177	7	177	3	175	88	101

[a]U and Pb concentrations and Th/U ratios are calculated relative to GJ-1 reference zircon

[b]Corrected for background and within-run Pb/U fractionation and normalised to reference zircon GJ-1 (ID-TIMS values/measured value); $^{207}Pb/^{235}U$ calculated using $(^{207}Pb/^{206}Pb)/(^{238}U/^{206}Pb * 1/137.88)$

[c]Rho is the error correlation defined as the quotient of the propagated errors of the $^{206}Pb/^{238}U$ and the $^{207}/^{235}U$ ratio

[d]Quadratic addition of within-run errors (2 SD) and daily reproducibility of GJ-1 (2 SD)

[e]Corrected for mass-bias by normalising to GJ-1 reference zircon (~0.6 per atomic mass unit) and common Pb using the model Pb composition of Stacey & Kramers (1975)

Table D8. LA-ICPMS isotopic data for sample HBUE1 in the Heidelberg Basin

HBUE1							RATIOS							AGES [Ma]						Conc.
Sample	Analysis	U [ppm][a]	Pb [ppm][a]	Th [ppm][a]	$^{206}Pb/^{204}Pb$	Th/U[a]	$^{207}Pb/^{235}U$[b]	2 σ[d]	$^{206}Pb/^{238}U$[b]	2 σ[d]	rho[c]	$^{207}Pb/^{206}Pb$[e]	2 σ[d]	$^{207}Pb/^{235}U$	2 σ	$^{206}Pb/^{238}U$	2 σ	$^{207}Pb/^{206}Pb$	2 σ	%
HBUE1	HBUE1-1	104	4	104	4711	1.00	0.296	0.015	0.0418	0.0008	0.36	0.0514	0.0024	263	13	264	5	258	109	102
HBUE1	HBUE1-2	276	13	197	2395	0.71	0.333	0.017	0.0462	0.0008	0.36	0.0523	0.0024	292	15	291	5	298	106	98
HBUE1	HBUE1-3	366	24	110	160370	0.30	0.512	0.016	0.0665	0.0010	0.49	0.0559	0.0015	420	13	415	6	447	59	93
HBUE1	HBUE1-4	407	48	85	317149	0.21	1.053	0.031	0.1182	0.0018	0.52	0.0646	0.0016	730	21	720	11	761	52	95
HBUE1	HBUE1-5	911	162	200	13969	0.22	1.837	0.047	0.1777	0.0026	0.57	0.0750	0.0016	1059	27	1054	15	1069	42	99
HBUE1	HBUE1-6	94	9	9	507	0.09	1.001	0.071	0.0980	0.0024	0.34	0.0741	0.0050	704	50	603	15	1043	135	58
HBUE1	HBUE1-7	511	23	254	151632	0.50	0.323	0.011	0.0449	0.0007	0.45	0.0521	0.0016	284	10	283	4	288	71	98
HBUE1	HBUE1-8	188	16	77	104816	0.41	0.691	0.021	0.0847	0.0013	0.50	0.0592	0.0016	533	16	524	8	573	57	91
HBUE1	HBUE1-9	324	21	109	3320	0.34	0.529	0.015	0.0635	0.0010	0.52	0.0604	0.0015	431	13	397	6	617	54	64
HBUE1	HBUE1-10	412	83	191	8738	0.46	2.207	0.057	0.2017	0.0029	0.57	0.0794	0.0017	1183	30	1184	17	1181	42	100
HBUE1	HBUE1-11	136	13	156	84695	1.15	0.773	0.024	0.0946	0.0014	0.49	0.0593	0.0016	581	18	582	9	577	59	101
HBUE1	HBUE1-12	167	8	111	50545	0.67	0.334	0.029	0.0458	0.0011	0.29	0.0529	0.0043	293	25	289	7	324	185	89
HBUE1	HBUE1-13	535	38	101	1774	0.19	0.576	0.018	0.0713	0.0011	0.48	0.0586	0.0016	462	15	444	7	551	61	81
HBUE1	HBUE1-14	129	12	138	2402	1.07	0.744	0.027	0.0908	0.0015	0.44	0.0594	0.0020	565	21	561	9	581	72	97
HBUE1	HBUE1-15	191	15	132	2754	0.69	0.619	0.019	0.0789	0.0012	0.49	0.0569	0.0016	489	15	489	7	489	60	100
HBUE1	HBUE1-16	499	20	286	1371	0.57	0.348	0.014	0.0406	0.0007	0.41	0.0621	0.0023	303	12	257	4	678	78	38
HBUE1	HBUE1-17	575	32	239	1933	0.42	0.524	0.015	0.0560	0.0008	0.51	0.0680	0.0017	428	13	351	5	868	52	40
HBUE1	HBUE1-18	406	34	39	2949	0.10	0.668	0.021	0.0841	0.0013	0.48	0.0576	0.0016	519	16	520	8	515	61	101
HBUE1	HBUE1-19	202	9	73	13994	0.36	0.314	0.017	0.0442	0.0008	0.35	0.0517	0.0026	278	15	279	5	270	115	103
HBUE1	HBUE1-20	216	6	158	39015	0.73	0.188	0.016	0.0273	0.0006	0.28	0.0500	0.0040	175	15	173	4	195	186	89
HBUE1	HBUE1-21	174	19	23	124435	0.13	0.912	0.027	0.1077	0.0016	0.51	0.0614	0.0015	658	19	659	10	654	54	101
HBUE1	HBUE1-22	602	30	66	4507	0.11	0.383	0.015	0.0491	0.0008	0.43	0.0566	0.0019	329	13	309	5	474	76	65
HBUE1	HBUE1-23	188	16	116	109402	0.62	0.706	0.022	0.0879	0.0013	0.49	0.0583	0.0016	543	17	543	8	541	59	100
HBUE1	HBUE1-24	405	17	172	110866	0.43	0.320	0.017	0.0413	0.0008	0.35	0.0563	0.0029	282	15	261	5	462	113	56
HBUE1	HBUE1-25	155	13	61	21960	0.40	0.656	0.022	0.0819	0.0013	0.46	0.0581	0.0017	512	17	507	8	533	66	95
HBUE1	HBUE1-26	269	26	173	6426	0.64	0.796	0.023	0.0964	0.0014	0.53	0.0599	0.0014	595	17	593	9	600	52	99
HBUE1	HBUE1-27	123	9	72	279	0.59	0.748	0.054	0.0694	0.0017	0.34	0.0782	0.0053	567	41	433	11	1151	135	38
HBUE1	HBUE1-28	256	11	242	74530	0.94	0.318	0.020	0.0438	0.0009	0.32	0.0527	0.0031	281	18	276	6	317	135	87
HBUE1	HBUE1-29	259	17	148	701	0.57	0.799	0.035	0.0657	0.0012	0.42	0.0882	0.0035	596	26	410	7	1387	76	30
HBUE1	HBUE1-30	533	36	126	649	0.24	0.784	0.031	0.0679	0.0012	0.43	0.0837	0.0030	587	23	423	7	1287	69	33
HBUE1	HBUE1-31	164	7	157	2024	0.96	0.361	0.022	0.0405	0.0008	0.35	0.0646	0.0036	313	19	256	5	761	119	34
HBUE1	HBUE1-32	224	9	81	62284	0.36	0.326	0.029	0.0418	0.0011	0.29	0.0565	0.0048	286	25	264	7	473	186	56
HBUE1	HBUE1-33	202	9	138	1342	0.69	0.311	0.011	0.0433	0.0007	0.44	0.0520	0.0017	275	10	273	4	287	74	95
HBUE1	HBUE1-34	426	19	235	123339	0.55	0.320	0.014	0.0436	0.0007	0.39	0.0532	0.0022	282	12	275	5	339	92	81
HBUE1	HBUE1-35	320	14	177	94498	0.55	0.323	0.016	0.0445	0.0008	0.36	0.0528	0.0024	285	14	280	5	319	104	88
HBUE1	HBUE1-36	939	29	678	193721	0.72	0.218	0.008	0.0310	0.0005	0.44	0.0510	0.0016	200	7	197	3	239	72	82
HBUE1	HBUE1-37	287	21	107	1370	0.37	0.601	0.030	0.0738	0.0013	0.37	0.0591	0.0027	478	23	459	8	570	99	81
HBUE1	HBUE1-38	227	39	103	2367	0.45	1.742	0.058	0.1699	0.0027	0.48	0.0743	0.0022	1024	34	1012	16	1050	59	96
HBUE1	HBUE1-39	140	11	92	488	0.66	0.685	0.043	0.0819	0.0017	0.34	0.0607	0.0036	530	33	507	11	629	126	81
HBUE1	HBUE1-40	80	3	56	429	0.70	0.309	0.022	0.0433	0.0009	0.30	0.0518	0.0034	274	19	274	6	276	152	99
HBUE1	HBUE1-41	102	18	23	122649	0.23	1.864	0.054	0.1798	0.0027	0.52	0.0752	0.0019	1068	31	1066	16	1074	50	99
HBUE1	HBUE1-43	418	30	140	1786	0.34	0.580	0.020	0.0722	0.0011	0.46	0.0582	0.0018	464	16	450	7	539	66	83
HBUE1	HBUE1-44	263	23	69	596	0.26	0.886	0.029	0.0861	0.0013	0.48	0.0746	0.0021	644	21	532	8	1059	58	50
HBUE1	HBUE1-45	559	37	121	2827	0.22	0.520	0.019	0.0663	0.0010	0.44	0.0570	0.0018	425	15	414	6	490	71	84
HBUE1	HBUE1-46	143	6	252	40963	1.76	0.308	0.024	0.0428	0.0010	0.30	0.0521	0.0038	273	21	270	6	292	168	93
HBUE1	HBUE1-47	69	3	82	1586	1.20	0.287	0.033	0.0370	0.0012	0.28	0.0563	0.0062	256	29	234	7	463	244	51
HBUE1	HBUE1-48	390	31	184	1691	0.47	0.632	0.026	0.0783	0.0013	0.40	0.0586	0.0022	498	21	486	8	552	83	88

HBUE1	HBUE1-49	511	37	297	876	0.58	0.818	0.031	0.0720	0.0012	0.45	0.0824	0.0028	607	23	448	7	1255	66	36
HBUE1	HBUE1-50	139	12	38	11613	0.27	0.770	0.047	0.0867	0.0018	0.34	0.0644	0.0037	580	35	536	11	755	121	71
HBUE1	HBUE1-51	782	111	440	5092	0.56	1.538	0.042	0.1425	0.0021	0.54	0.0783	0.0018	946	26	859	13	1154	46	74
HBUE1	HBUE1-52	115	5	85	34360	0.74	0.318	0.034	0.0446	0.0013	0.27	0.0518	0.0053	281	30	281	8	275	235	102
HBUE1	HBUE1-53	489	71	292	475467	0.60	1.482	0.044	0.1454	0.0022	0.51	0.0739	0.0019	923	28	875	13	1040	52	84
HBUE1	HBUE1-54	317	25	65	168840	0.21	0.626	0.019	0.0798	0.0012	0.50	0.0570	0.0015	494	15	495	7	490	58	101
HBUE1	HBUE1-55	94	3	159	17962	1.69	0.207	0.025	0.0285	0.0009	0.27	0.0526	0.0061	191	23	181	6	310	264	58
HBUE1	HBUE1-56	301	19	89	856	0.30	0.655	0.033	0.0641	0.0012	0.38	0.0741	0.0034	511	25	400	8	1045	93	38
HBUE1	HBUE1-57	366	20	210	2525	0.58	0.439	0.016	0.0554	0.0009	0.44	0.0574	0.0018	369	13	348	5	508	70	68
HBUE1	HBUE1-58	224	20	162	2461	0.72	0.743	0.039	0.0884	0.0017	0.36	0.0610	0.0030	564	30	546	10	638	105	86
HBUE1	HBUE1-59	143	6	147	42758	1.03	0.324	0.027	0.0448	0.0011	0.29	0.0525	0.0043	285	24	282	7	307	185	92
HBUE1	HBUE1-60	268	23	118	3260	0.44	0.686	0.026	0.0854	0.0014	0.42	0.0583	0.0020	530	20	528	9	541	77	98
HBUE1	HBUE1-61	159	7	83	45173	0.52	0.301	0.026	0.0424	0.0010	0.29	0.0515	0.0042	267	23	267	7	263	188	102
HBUE1	HBUE1-62	409	34	278	476	0.68	0.963	0.041	0.0843	0.0015	0.42	0.0828	0.0032	685	29	522	9	1264	76	41
HBUE1	HBUE1-63	259	11	107	6785	0.41	0.311	0.012	0.0437	0.0007	0.41	0.0516	0.0019	275	11	276	4	270	83	102
HBUE1	HBUE1-64	261	92	96	19118	0.37	5.869	0.152	0.3521	0.0051	0.56	0.1209	0.0026	1957	51	1945	28	1969	38	99
HBUE1	HBUE1-65	307	14	212	91928	0.69	0.321	0.012	0.0446	0.0007	0.42	0.0522	0.0018	282	11	281	4	292	77	96
HBUE1	HBUE1-66	67	7	151	44966	2.26	0.837	0.035	0.1001	0.0017	0.40	0.0607	0.0023	617	26	615	10	627	83	98
HBUE1	HBUE1-69	531	28	309	582	0.58	0.566	0.022	0.0534	0.0009	0.43	0.0768	0.0026	455	17	336	6	1116	69	30
HBUE1	HBUE1-70	50	5	24	34329	0.48	0.857	0.054	0.1016	0.0022	0.33	0.0612	0.0037	628	40	624	13	645	129	97
HBUE1	HBUE1-71	396	17	416	116426	1.05	0.313	0.012	0.0438	0.0007	0.42	0.0519	0.0018	277	10	276	4	282	78	98
HBUE1	HBUE1-72	77	13	46	5139	0.59	1.729	0.055	0.1690	0.0026	0.48	0.0742	0.0021	1019	33	1007	16	1046	57	96
HBUE1	HBUE1-73	319	28	155	24967	0.49	0.710	0.020	0.0884	0.0013	0.52	0.0582	0.0014	544	16	546	8	539	53	101
HBUE1	HBUE1-74	215	20	155	131272	0.72	0.743	0.022	0.0909	0.0014	0.50	0.0593	0.0015	564	17	561	8	579	56	97
HBUE1	HBUE1-75	137	7	102	45474	0.75	0.359	0.017	0.0494	0.0008	0.37	0.0528	0.0023	312	14	311	5	318	97	98
HBUE1	HBUE1-76	37	2	56	2121	1.52	0.296	0.053	0.0415	0.0019	0.25	0.0516	0.0089	263	47	262	12	269	397	98
HBUE1	HBUE1-77	133	5	60	627	0.45	0.285	0.016	0.0401	0.0008	0.34	0.0515	0.0027	254	14	253	5	264	122	96
HBUE1	HBUE1-78	345	26	32	172017	0.09	0.578	0.018	0.0741	0.0011	0.49	0.0566	0.0015	463	14	461	7	475	59	97
HBUE1	HBUE1-79	488	40	327	5375	0.67	0.698	0.025	0.0818	0.0013	0.44	0.0619	0.0020	537	19	507	8	670	68	76
HBUE1	HBUE1-80	328	32	51	13189	0.16	0.820	0.032	0.0984	0.0016	0.42	0.0604	0.0021	608	24	605	10	618	76	98
HBUE1	HBUE1-81	477	21	448	1687	0.94	0.314	0.015	0.0437	0.0007	0.37	0.0521	0.0022	277	13	276	5	288	98	96
HBUE1	HBUE1-82	210	8	150	796	0.71	0.269	0.019	0.0372	0.0008	0.30	0.0525	0.0036	242	17	236	5	308	156	76
HBUE1	HBUE1-84	138	23	44	5404	0.32	1.877	0.061	0.1671	0.0026	0.48	0.0815	0.0023	1073	35	996	16	1233	56	81
HBUE1	HBUE1-85	409	27	141	1574	0.35	0.607	0.023	0.0660	0.0011	0.43	0.0667	0.0023	482	18	412	7	828	71	50
HBUE1	HBUE1-86	200	18	124	120822	0.62	0.722	0.022	0.0895	0.0013	0.49	0.0585	0.0015	552	17	553	8	549	57	101
HBUE1	HBUE1-87	333	23	92	154005	0.28	0.528	0.015	0.0685	0.0010	0.50	0.0559	0.0014	430	13	427	6	448	56	95
HBUE1	HBUE1-88	207	14	71	1615	0.34	0.708	0.027	0.0678	0.0011	0.43	0.0757	0.0026	543	21	423	7	1087	69	39
HBUE1	HBUE1-89	356	18	236	121886	0.66	0.372	0.012	0.0508	0.0008	0.46	0.0531	0.0015	321	10	319	5	332	66	96
HBUE1	HBUE1-90	403	37	85	9498	0.21	0.736	0.022	0.0910	0.0013	0.50	0.0586	0.0015	560	17	562	8	553	56	101
HBUE1	HBUE1-91	249	135	77	908077	0.31	14.942	0.394	0.5403	0.0079	0.56	0.2006	0.0044	2812	74	2785	41	2831	36	98
HBUE1	HBUE1-92	80	3	59	20749	0.74	0.268	0.028	0.0383	0.0011	0.27	0.0508	0.0051	241	25	242	7	234	232	104
HBUE1	HBUE1-93	169	28	65	50087	0.38	1.709	0.057	0.1651	0.0026	0.47	0.0750	0.0022	1012	34	985	16	1070	59	92
HBUE1	HBUE1-94	228	17	54	1002	0.24	0.600	0.036	0.0761	0.0015	0.33	0.0572	0.0032	477	29	473	9	498	124	95
HBUE1	HBUE1-95	255	11	130	5983	0.51	0.324	0.011	0.0449	0.0007	0.45	0.0524	0.0016	285	10	283	4	304	69	93
HBUE1	HBUE1-96	246	19	43	1238	0.18	0.640	0.029	0.0775	0.0013	0.38	0.0599	0.0025	502	23	481	8	599	90	80
HBUE1	HBUE1-97	232	7	190	680	0.82	0.198	0.009	0.0287	0.0005	0.36	0.0500	0.0022	184	9	183	3	196	102	93
HBUE1	HBUE1-98	377	34	129	232487	0.34	0.763	0.023	0.0912	0.0014	0.49	0.0607	0.0016	576	18	562	8	630	57	89
HBUE1	HBUE1-99	244	22	194	6143	0.79	0.731	0.022	0.0898	0.0013	0.49	0.0590	0.0016	557	17	554	8	569	58	97
HBUE1	HBUE1-100	792	33	160	1449	0.20	0.362	0.015	0.0417	0.0007	0.40	0.0631	0.0024	314	13	263	4	712	79	37

HBUE1	HBUE1-101	300	25	253	7673	0.84	0.674	0.021	0.0844	0.0013	0.48	0.0579	0.0016	523	16	522	8	527	61	99
HBUE1	HBUE1-102	616	23	415	155857	0.67	0.270	0.014	0.0373	0.0007	0.34	0.0524	0.0026	242	13	236	4	303	115	78
HBUE1	HBUE1-104	216	9	141	13398	0.65	0.303	0.020	0.0414	0.0009	0.31	0.0531	0.0034	269	18	261	5	333	146	78
HBUE1	HBUE1-105	198	99	152	3535	0.77	12.285	0.323	0.4994	0.0072	0.55	0.1784	0.0039	2626	69	2611	38	2638	36	99
HBUE1	HBUE1-106	555	57	42	5327	0.08	0.861	0.028	0.1024	0.0016	0.47	0.0610	0.0018	630	21	628	10	638	62	99

[a]U and Pb concentrations and Th/U ratios are calculated relative to GJ-1 reference zircon

[b]Corrected for background and within-run Pb/U fractionation and normalised to reference zircon GJ-1 (ID-TIMS values/measured value); ^{207}Pb/^{235}U calculated using (^{207}Pb/^{206}Pb)/(^{238}U/^{206}Pb * 1/137.88)

[c]Rho is the error correlation defined as the quotient of the propagated errors of the ^{206}Pb/^{238}U and the ^{207}/^{235}U ratio

[d]Quadratic addition of within-run errors (2 SD) and daily reproducibility of GJ-1 (2 SD)

[e]Corrected for mass-bias by normalising to GJ-1 reference zircon (~0.6 per atomic mass unit) and common Pb using the model Pb composition of Stacey & Kramers (1975)

Table D9. LA-ICPMS isotopic data for sample KLIP in the Mossel Bay Basin

KLIP							RATIOS							AGES [Ma]						Conc.
Sample	Analysis	U [ppm][a]	Pb [ppm][a]	Th [ppm][a]	$^{206}Pb/^{204}Pb$	Th/U[a]	$^{207}Pb/^{235}U$[b]	2 σ[d]	$^{206}Pb/^{238}U$[b]	2 σ[d]	rho[c]	$^{207}Pb/^{206}Pb$[c]	2 σ[d]	$^{207}Pb/^{235}U$	2 σ	$^{206}Pb/^{238}U$	2 σ	$^{207}Pb/^{206}Pb$	2 σ	%
KLIP	KLIP-1	929	24	508	141407	0.55	0.177	0.008	0.0261	0.0006	0.58	0.0493	0.0017	166	7	166	4	162	81	103
KLIP	KLIP-2	484	86	214	18617	0.44	1.847	0.065	0.1787	0.0043	0.69	0.0750	0.0019	1062	37	1060	26	1068	51	99
KLIP	KLIP-3	329	14	65	101650	0.20	0.301	0.016	0.0422	0.0011	0.48	0.0518	0.0024	267	14	267	7	274	107	97
KLIP	KLIP-4	267	24	161	1737	0.60	0.706	0.034	0.0882	0.0022	0.53	0.0581	0.0023	543	26	545	14	532	88	102
KLIP	KLIP-5	310	8	151	13426	0.49	0.186	0.013	0.0274	0.0007	0.40	0.0494	0.0031	174	12	174	5	167	146	104
KLIP	KLIP-6	411	35	246	233223	0.60	0.725	0.037	0.0862	0.0022	0.50	0.0610	0.0027	554	29	533	14	639	96	83
KLIP	KLIP-7	278	19	209	38141	0.75	0.522	0.022	0.0678	0.0017	0.59	0.0558	0.0019	427	18	423	10	445	75	95
KLIP	KLIP-8	959	23	927	247	0.97	0.165	0.015	0.0235	0.0006	0.28	0.0508	0.0043	155	14	150	4	233	197	64
KLIP	KLIP-9	688	15	403	8264	0.59	0.151	0.009	0.0222	0.0005	0.41	0.0495	0.0027	143	9	142	3	170	127	83
KLIP	KLIP-10	183	28	46	201067	0.25	1.551	0.067	0.1505	0.0038	0.58	0.0747	0.0026	951	41	904	23	1060	71	85
KLIP	KLIP-11	252	7	80	51389	0.32	0.190	0.011	0.0279	0.0007	0.42	0.0495	0.0027	177	10	177	4	172	125	103
KLIP	KLIP-12	76	2	108	15743	1.42	0.199	0.023	0.0282	0.0008	0.23	0.0511	0.0057	184	21	180	5	245	259	73
KLIP	KLIP-14	118	18	37	132629	0.32	1.488	0.059	0.1536	0.0038	0.62	0.0702	0.0022	925	37	921	23	935	64	98
KLIP	KLIP-15	17	0	55	3553	3.27	0.212	0.101	0.0290	0.0011	0.08	0.0531	0.0253	195	93	184	7	333	1079	55
KLIP	KLIP-16	90	9	182	63068	2.02	0.788	0.063	0.0956	0.0028	0.36	0.0598	0.0045	590	47	589	17	597	162	99
KLIP	KLIP-17	317	19	213	3162	0.67	0.445	0.032	0.0585	0.0016	0.38	0.0551	0.0037	373	27	366	10	417	151	88
KLIP	KLIP-18	270	23	101	3190	0.37	0.739	0.043	0.0857	0.0023	0.46	0.0625	0.0032	562	32	530	14	693	110	77
KLIP	KLIP-19	296	8	138	14940	0.47	0.177	0.008	0.0260	0.0007	0.54	0.0494	0.0020	166	8	166	4	166	93	100
KLIP	KLIP-20	187	6	174	1248	0.93	0.211	0.020	0.0295	0.0007	0.26	0.0519	0.0048	194	19	187	5	281	212	67
KLIP	KLIP-21	862	19	733	2747	0.85	0.160	0.007	0.0225	0.0006	0.55	0.0514	0.0019	150	7	143	4	260	87	55
KLIP	KLIP-22	181	8	130	5239	0.72	0.313	0.018	0.0439	0.0011	0.45	0.0517	0.0027	276	16	277	7	271	120	102
KLIP	KLIP-23	418	10	255	6941	0.61	0.164	0.012	0.0232	0.0006	0.34	0.0513	0.0036	154	11	148	4	253	161	59
KLIP	KLIP-24	323	9	493	1169	1.53	0.194	0.013	0.0280	0.0007	0.36	0.0504	0.0032	180	12	178	4	214	149	83
KLIP	KLIP-25	394	16	371	2067	0.94	0.285	0.019	0.0395	0.0011	0.40	0.0523	0.0032	254	17	250	7	297	140	84
KLIP	KLIP-26	199	5	212	1095	1.07	0.161	0.015	0.0239	0.0006	0.27	0.0489	0.0043	152	14	152	4	145	208	105
KLIP	KLIP-27	276	7	194	1470	0.70	0.189	0.016	0.0272	0.0007	0.30	0.0505	0.0041	176	15	173	4	218	188	79
KLIP	KLIP-28	86	16	36	114237	0.41	1.923	0.089	0.1819	0.0046	0.55	0.0767	0.0030	1089	51	1077	27	1113	78	97
KLIP	KLIP-29	405	80	99	2860	0.25	2.137	0.084	0.1977	0.0049	0.63	0.0784	0.0024	1161	45	1163	29	1157	60	101
KLIP	KLIP-30	231	20	66	96261	0.29	0.690	0.035	0.0848	0.0022	0.50	0.0590	0.0026	533	27	524	13	568	97	92
KLIP	KLIP-31	518	48	246	1091	0.47	0.958	0.034	0.0934	0.0023	0.68	0.0744	0.0020	682	25	576	14	1052	53	55
KLIP	KLIP-32	359	45	126	10990	0.35	1.113	0.041	0.1250	0.0031	0.67	0.0646	0.0018	760	28	759	19	761	57	100
KLIP	KLIP-33	233	11	175	2190	0.75	0.338	0.021	0.0471	0.0012	0.43	0.0520	0.0029	296	18	297	8	287	127	103
KLIP	KLIP-34	383	18	305	129369	0.80	0.334	0.014	0.0464	0.0011	0.59	0.0522	0.0017	293	12	292	7	295	76	99
KLIP	KLIP-35	270	12	322	86080	1.19	0.313	0.018	0.0436	0.0011	0.45	0.0521	0.0027	277	16	275	7	289	118	95
KLIP	KLIP-36	121	3	113	1236	0.93	0.158	0.013	0.0235	0.0007	0.34	0.0488	0.0037	149	12	149	4	140	180	107
KLIP	KLIP-37	1164	33	687	242250	0.59	0.196	0.011	0.0285	0.0007	0.43	0.0498	0.0025	182	10	181	4	185	119	98
KLIP	KLIP-38	220	44	67	2265	0.30	2.392	0.111	0.2017	0.0052	0.55	0.0860	0.0033	1240	57	1184	30	1339	75	88
KLIP	KLIP-39	495	12	248	1181	0.50	0.160	0.011	0.0235	0.0006	0.37	0.0492	0.0030	150	10	150	4	159	144	94
KLIP	KLIP-40	443	31	373	1273	0.84	0.551	0.029	0.0706	0.0018	0.50	0.0567	0.0026	446	23	440	11	478	100	92
KLIP	KLIP-41	442	71	272	10085	0.61	1.791	0.074	0.1605	0.0040	0.60	0.0809	0.0027	1042	43	960	24	1220	65	79
KLIP	KLIP-43	483	11	399	741	0.83	0.154	0.010	0.0221	0.0005	0.39	0.0505	0.0030	145	9	141	3	218	136	65
KLIP	KLIP-44	217	6	266	43686	1.22	0.194	0.016	0.0276	0.0007	0.32	0.0511	0.0039	180	14	176	4	244	175	72
KLIP	KLIP-45	536	14	299	2370	0.56	0.172	0.007	0.0252	0.0006	0.59	0.0495	0.0017	161	7	161	4	173	79	93
KLIP	KLIP-46	242	11	266	2592	1.10	0.333	0.018	0.0460	0.0012	0.47	0.0524	0.0025	292	16	290	7	303	109	96
KLIP	KLIP-47	220	18	100	128763	0.46	0.631	0.025	0.0802	0.0020	0.61	0.0571	0.0018	497	20	497	12	496	70	100
KLIP	KLIP-48	132	4	202	27994	1.53	0.220	0.029	0.0291	0.0008	0.20	0.0548	0.0070	202	26	185	5	402	286	46
KLIP	KLIP-49	686	19	972	441	1.42	0.191	0.014	0.0280	0.0007	0.34	0.0493	0.0033	177	13	178	4	164	156	109

KLIP	KLIP-50	105	70	62	17256	0.59	24.726	0.885	0.6667	0.0165	0.69	0.2690	0.0069	3297	118	3293	82	3300	40	100
KLIP	KLIP-51	296	7	241	51862	0.81	0.163	0.010	0.0240	0.0006	0.43	0.0491	0.0026	153	9	153	4	152	124	101
KLIP	KLIP-52	282	26	81	189803	0.29	0.754	0.029	0.0926	0.0023	0.65	0.0591	0.0017	571	22	571	14	571	63	100
KLIP	KLIP-53	278	6	246	44719	0.89	0.151	0.012	0.0221	0.0006	0.32	0.0497	0.0037	143	11	141	4	181	174	78
KLIP	KLIP-54	403	19	272	135255	0.67	0.332	0.013	0.0461	0.0011	0.61	0.0523	0.0017	291	12	290	7	298	72	97
KLIP	KLIP-56	138	15	43	19305	0.31	0.933	0.039	0.1091	0.0027	0.59	0.0620	0.0021	669	28	667	17	675	72	99
KLIP	KLIP-57	185	16	173	113570	0.94	0.670	0.037	0.0845	0.0022	0.47	0.0576	0.0028	521	29	523	14	513	106	102
KLIP	KLIP-58	134	16	26	2054	0.19	1.024	0.041	0.1173	0.0029	0.62	0.0634	0.0020	716	29	715	18	720	66	99
KLIP	KLIP-59	180	4	109	1677	0.61	0.160	0.012	0.0236	0.0006	0.34	0.0490	0.0035	150	11	151	4	149	165	101
KLIP	KLIP-61	231	20	136	3836	0.59	0.704	0.029	0.0866	0.0021	0.61	0.0589	0.0019	541	22	536	13	564	70	95
KLIP	KLIP-62	321	30	75	215728	0.24	0.756	0.029	0.0925	0.0023	0.63	0.0593	0.0018	572	22	570	14	577	65	99
KLIP	KLIP-63	339	26	156	2365	0.46	0.608	0.040	0.0764	0.0021	0.42	0.0577	0.0034	482	32	475	13	517	131	92
KLIP	KLIP-64	156	5	100	568	0.64	0.238	0.019	0.0342	0.0010	0.35	0.0505	0.0038	217	18	217	6	216	176	100
KLIP	KLIP-65	348	8	141	58800	0.41	0.157	0.010	0.0232	0.0006	0.41	0.0491	0.0028	148	9	148	4	155	132	96
KLIP	KLIP-66	444	41	216	296308	0.49	0.745	0.032	0.0918	0.0023	0.58	0.0588	0.0021	565	24	566	14	561	77	101
KLIP	KLIP-67	365	64	219	17733	0.60	1.790	0.064	0.1751	0.0043	0.69	0.0741	0.0019	1042	37	1040	25	1045	52	100
KLIP	KLIP-68	643	59	383	7947	0.60	0.753	0.028	0.0921	0.0023	0.65	0.0593	0.0017	570	22	568	14	579	62	98
KLIP	KLIP-69	415	11	432	1082	1.04	0.187	0.015	0.0266	0.0007	0.30	0.0508	0.0040	174	14	169	4	233	183	73
KLIP	KLIP-71	294	7	180	50806	0.61	0.166	0.013	0.0238	0.0006	0.33	0.0505	0.0038	156	12	152	4	218	174	70
KLIP	KLIP-72	437	10	180	73755	0.41	0.157	0.008	0.0232	0.0006	0.47	0.0490	0.0023	148	8	148	4	146	110	101
KLIP	KLIP-73	293	7	208	3038	0.71	0.168	0.012	0.0248	0.0006	0.35	0.0491	0.0033	158	11	158	4	154	155	103
KLIP	KLIP-74	292	48	77	8626	0.26	1.651	0.070	0.1637	0.0041	0.59	0.0731	0.0025	990	42	977	25	1018	69	96
KLIP	KLIP-75	73	7	49	67	0.67	0.749	0.043	0.0915	0.0024	0.46	0.0594	0.0031	567	33	564	15	580	112	97
KLIP	KLIP-76	124	22	62	16220	0.50	1.790	0.068	0.1749	0.0043	0.65	0.0742	0.0021	1042	40	1039	26	1047	58	99
KLIP	KLIP-77	252	31	124	5751	0.49	1.081	0.041	0.1222	0.0030	0.65	0.0642	0.0018	744	28	743	18	747	60	100
KLIP	KLIP-78	353	20	461	147815	1.31	0.426	0.020	0.0576	0.0015	0.54	0.0537	0.0021	360	17	361	9	356	89	101
KLIP	KLIP-79	122	3	157	580	1.29	0.174	0.018	0.0248	0.0007	0.26	0.0511	0.0050	163	17	158	4	244	226	64
KLIP	KLIP-80	260	15	96	3509	0.37	0.440	0.019	0.0591	0.0015	0.58	0.0539	0.0019	370	16	370	9	369	79	100
KLIP	KLIP-81	603	14	264	4882	0.44	0.153	0.006	0.0227	0.0006	0.58	0.0489	0.0017	145	6	145	4	141	81	103
KLIP	KLIP-82	728	95	215	3573	0.29	1.380	0.051	0.1307	0.0032	0.67	0.0766	0.0021	881	32	792	20	1111	54	71
KLIP	KLIP-84	151	4	108	2474	0.72	0.192	0.012	0.0282	0.0007	0.44	0.0495	0.0027	179	11	179	5	172	126	104
KLIP	KLIP-85	195	18	37	27698	0.19	0.762	0.032	0.0927	0.0023	0.59	0.0597	0.0020	575	24	571	14	591	73	97
KLIP	KLIP-86	283	7	152	1329	0.54	0.163	0.022	0.0237	0.0006	0.18	0.0498	0.0067	153	21	151	4	188	315	80
KLIP	KLIP-87	286	23	166	2158	0.58	0.625	0.029	0.0794	0.0020	0.55	0.0570	0.0022	493	23	493	13	493	86	100
KLIP	KLIP-88	528	12	431	856	0.82	0.155	0.008	0.0230	0.0006	0.48	0.0489	0.0023	146	8	147	4	142	109	103
KLIP	KLIP-89	1045	23	424	1456	0.41	0.146	0.009	0.0216	0.0005	0.41	0.0493	0.0028	139	9	138	3	161	132	86
KLIP	KLIP-90	372	28	97	4870	0.26	0.596	0.023	0.0765	0.0019	0.63	0.0565	0.0017	475	19	475	12	473	67	100
KLIP	KLIP-91	243	23	110	10566	0.45	0.764	0.030	0.0937	0.0023	0.64	0.0592	0.0018	577	22	577	14	574	65	101
KLIP	KLIP-92	415	10	271	1344	0.65	0.169	0.008	0.0250	0.0006	0.49	0.0490	0.0021	158	8	159	4	146	103	109
KLIP	KLIP-93	151	25	157	17730	1.04	1.633	0.062	0.1648	0.0041	0.65	0.0719	0.0021	983	37	983	24	983	58	100
KLIP	KLIP-94	277	26	102	5935	0.37	0.763	0.031	0.0936	0.0023	0.61	0.0591	0.0019	576	23	577	14	572	70	101
KLIP	KLIP-96	214	38	38	25093	0.18	1.856	0.070	0.1789	0.0044	0.66	0.0753	0.0021	1066	40	1061	26	1075	57	99
KLIP	KLIP-97	1258	28	1435	147	1.14	0.188	0.014	0.0223	0.0006	0.34	0.0611	0.0043	175	13	142	4	642	151	22
KLIP	KLIP-98	365	8	264	6540	0.72	0.155	0.008	0.0227	0.0006	0.48	0.0495	0.0023	146	8	144	4	171	109	85
KLIP	KLIP-99	124	24	52	5011	0.42	2.042	0.091	0.1902	0.0048	0.57	0.0779	0.0028	1130	50	1122	29	1144	72	98
KLIP	KLIP-100	129	12	209	5408	1.62	0.737	0.034	0.0908	0.0023	0.55	0.0589	0.0023	561	26	560	14	563	84	100
KLIP	KLIP-101	305	7	456	1039	1.49	0.152	0.016	0.0224	0.0006	0.24	0.0493	0.0050	144	15	143	4	161	237	88
KLIP	KLIP-102	165	4	98	29404	0.59	0.168	0.015	0.0246	0.0006	0.28	0.0495	0.0043	158	14	157	4	171	205	92
KLIP	KLIP-104	157	8	73	1326	0.47	0.355	0.023	0.0484	0.0013	0.42	0.0532	0.0031	309	20	305	8	339	131	90

KLIP	KLIP-105	278	6	125	30122	0.45	0.168	0.014	0.0227	0.0006	0.32	0.0537	0.0043	157	13	144	4	356	180	41
KLIP	KLIP-106	373	9	194	2072	0.52	0.155	0.008	0.0229	0.0006	0.53	0.0490	0.0020	146	7	146	4	149	98	98
KLIP	KLIP-107	174	5	64	1217	0.37	0.197	0.021	0.0276	0.0007	0.25	0.0517	0.0053	183	19	176	5	271	235	65
KLIP	KLIP-108	157	4	151	1299	0.96	0.189	0.013	0.0277	0.0007	0.38	0.0496	0.0032	176	12	176	5	176	149	100
KLIP	KLIP-109	286	25	135	181029	0.47	0.703	0.030	0.0874	0.0022	0.58	0.0583	0.0020	540	23	540	13	542	76	100
KLIP	KLIP-110	457	36	244	2087	0.53	0.630	0.032	0.0784	0.0020	0.50	0.0583	0.0026	496	26	487	13	541	98	90
KLIP	KLIP-111	312	10	6	3229	0.02	0.244	0.026	0.0326	0.0010	0.29	0.0544	0.0054	222	23	207	6	387	225	53
KLIP	KLIP-112	53	1	21	333	0.40	0.166	0.044	0.0227	0.0008	0.13	0.0530	0.0140	156	41	145	5	327	598	44
KLIP	KLIP-113	174	29	54	212166	0.31	1.681	0.064	0.1679	0.0042	0.65	0.0727	0.0021	1001	38	1000	25	1004	58	100
KLIP	KLIP-114	316	57	245	346791	0.78	1.947	0.072	0.1818	0.0045	0.67	0.0777	0.0021	1097	40	1077	27	1138	54	95
KLIP	KLIP-115	1136	27	487	1452	0.43	0.177	0.009	0.0237	0.0006	0.50	0.0543	0.0023	166	8	151	4	385	95	39
KLIP	KLIP-116	159	15	81	1589	0.51	0.747	0.034	0.0918	0.0023	0.56	0.0590	0.0022	566	26	566	14	568	81	100
KLIP	KLIP-117	361	9	129	61772	0.36	0.160	0.007	0.0236	0.0006	0.56	0.0491	0.0019	150	7	150	4	150	89	100
KLIP	KLIP-118	582	14	208	1361	0.36	0.160	0.008	0.0237	0.0006	0.52	0.0491	0.0020	151	7	151	4	154	93	98
KLIP	KLIP-119	407	31	147	227055	0.36	0.609	0.043	0.0770	0.0021	0.40	0.0573	0.0037	483	34	478	13	505	142	95
KLIP	KLIP-120	197	39	49	280429	0.25	2.120	0.078	0.1964	0.0048	0.67	0.0783	0.0021	1155	43	1156	28	1154	54	100
KLIP	KLIP-121	312	30	201	5321	0.65	0.785	0.039	0.0958	0.0025	0.51	0.0594	0.0025	588	29	590	15	581	93	101
KLIP	KLIP-122	283	6	202	1085	0.71	0.152	0.015	0.0227	0.0006	0.27	0.0487	0.0047	144	14	145	4	131	226	110
KLIP	KLIP-123	562	25	403	49870	0.72	0.312	0.014	0.0436	0.0011	0.58	0.0519	0.0019	276	12	275	7	280	82	98
KLIP	KLIP-124	29	1	36	283	1.23	0.201	0.034	0.0287	0.0009	0.18	0.0507	0.0085	186	32	182	6	228	385	80
KLIP	KLIP-125	115	14	48	4877	0.42	1.067	0.044	0.1216	0.0030	0.61	0.0636	0.0021	737	30	740	18	729	69	102
KLIP	KLIP-126	1082	25	844	579	0.78	0.172	0.011	0.0229	0.0006	0.37	0.0544	0.0034	161	11	146	4	386	140	38
KLIP	KLIP-127	214	41	113	10170	0.53	2.082	0.083	0.1927	0.0048	0.63	0.0784	0.0024	1143	45	1136	28	1156	61	98
KLIP	KLIP-128	187	9	128	3721	0.68	0.360	0.017	0.0495	0.0013	0.55	0.0527	0.0020	312	14	312	8	318	88	98
KLIP	KLIP-129	215	5	311	1319	1.44	0.162	0.010	0.0239	0.0006	0.40	0.0493	0.0029	153	10	152	4	164	138	93
KLIP	KLIP-130	713	16	599	1544	0.84	0.154	0.008	0.0227	0.0006	0.46	0.0494	0.0024	146	8	145	4	164	113	88
KLIP	KLIP-131	201	14	62	100976	0.31	0.531	0.040	0.0693	0.0020	0.37	0.0555	0.0039	432	33	432	12	434	157	100
KLIP	KLIP-132	178	13	72	93043	0.40	0.564	0.033	0.0723	0.0019	0.45	0.0566	0.0030	454	27	450	12	476	116	94
KLIP	KLIP-133	549	82	70	592961	0.13	1.501	0.054	0.1491	0.0037	0.68	0.0730	0.0019	931	33	896	22	1014	53	88
KLIP	KLIP-134	495	13	269	93805	0.54	0.179	0.008	0.0262	0.0007	0.59	0.0496	0.0017	167	7	167	4	175	81	95
KLIP	KLIP-135	112	3	224	1839	2.00	0.201	0.017	0.0291	0.0008	0.32	0.0501	0.0039	186	15	185	5	201	181	92
KLIP	KLIP-136	244	10	200	1277	0.82	0.288	0.014	0.0407	0.0010	0.52	0.0514	0.0022	257	13	257	7	258	97	100
KLIP	KLIP-137	79	2	72	16146	0.91	0.196	0.016	0.0284	0.0008	0.34	0.0501	0.0038	181	15	180	5	198	174	91
KLIP	KLIP-138	172	5	69	6108	0.40	0.186	0.014	0.0269	0.0007	0.34	0.0500	0.0036	173	13	171	4	196	169	87

[a]U and Pb concentrations and Th/U ratios are calculated relative to GJ-1 reference zircon

[b]Corrected for background and within-run Pb/U fractionation and normalised to reference zircon GJ-1 (ID-TIMS values/measured value); $^{207}Pb/^{235}U$ calculated using ($^{207}Pb/^{206}Pb$)/($^{238}U/^{206}Pb$ * 1/137.88)

[c]Rho is the error correlation defined as the quotient of the propagated errors of the $^{206}Pb/^{238}U$ and the $^{207}/^{235}U$ ratio

[d]Quadratic addition of within-run errors (2 SD) and daily reproducibility of GJ-1 (2 SD)

[e]Corrected for mass-bias by normalising to GJ-1 reference zircon (~0.6 per atomic mass unit) and common Pb using the model Pb composition of Stacey & Kramers (1975)

Table D10. LA-ICPMS isotopic data for sample MATJ in the Mossel Bay Basin

MATJ							RATIOS							AGES [Ma]						Conc.
Sample	Analysis	U [ppm][a]	Pb [ppm][a]	Th [ppm][a]	^{206}Pb/^{204}Pb	Th/U[a]	^{207}Pb/^{235}U[b]	2 σ[d]	^{206}Pb/^{238}U[b]	2 σ[d]	rho[c]	^{207}Pb/^{206}Pb	2 σ[d]	^{207}Pb/^{235}U	2 σ	^{206}Pb/^{238}U	2 σ	^{207}Pb/^{206}Pb	2 σ	%
MATJ	MATJ-2	57	2	48	493	0.84	0.267	0.036	0.02673	0.00052	0.14	0.0725	0.0097	240	32	170	3	999	271	17
MATJ	MATJ-3	98	3	133	20137	1.35	0.187	0.013	0.02718	0.00048	0.26	0.0498	0.0032	174	12	173	3	187	150	93
MATJ	MATJ-4	32	1	49	6477	1.55	0.186	0.022	0.02718	0.00064	0.20	0.0497	0.0058	174	21	173	4	182	271	95
MATJ	MATJ-5	409	11	232	83309	0.57	0.185	0.009	0.02699	0.00042	0.30	0.0498	0.0024	173	9	172	3	184	113	93
MATJ	MATJ-6	869	24	373	2836	0.43	0.185	0.006	0.02723	0.00040	0.49	0.0494	0.0013	173	5	173	3	166	62	104
MATJ	MATJ-7	101	3	145	20793	1.43	0.189	0.024	0.02714	0.00048	0.14	0.0506	0.0063	176	22	173	3	222	286	78
MATJ	MATJ-8	198	5	105	2567	0.53	0.187	0.010	0.02712	0.00044	0.31	0.0499	0.0025	174	9	172	3	192	116	90
MATJ	MATJ-9	116	3	109	1237	0.93	0.193	0.027	0.02675	0.00046	0.12	0.0523	0.0071	179	25	170	3	297	312	57
MATJ	MATJ-10	109	3	59	22360	0.55	0.190	0.010	0.02724	0.00048	0.33	0.0506	0.0026	177	9	173	3	222	117	78
MATJ	MATJ-11	231	6	240	1050	1.04	0.189	0.015	0.02728	0.00044	0.21	0.0501	0.0038	175	14	174	3	201	177	86
MATJ	MATJ-12	89	2	61	17779	0.68	0.179	0.014	0.02626	0.00048	0.23	0.0495	0.0038	167	13	167	3	173	179	97
MATJ	MATJ-13	843	22	393	6593	0.47	0.182	0.006	0.02652	0.00040	0.49	0.0497	0.0013	169	5	169	3	180	62	94
MATJ	MATJ-14	113	3	137	7034	1.21	0.187	0.020	0.02728	0.00048	0.16	0.0497	0.0053	174	19	174	3	183	249	95
MATJ	MATJ-15	110	3	143	1248	1.31	0.188	0.018	0.02736	0.00048	0.19	0.0499	0.0046	175	17	174	3	190	216	91
MATJ	MATJ-16	240	7	206	1536	0.86	0.190	0.011	0.02767	0.00044	0.28	0.0499	0.0028	177	10	176	3	189	129	93
MATJ	MATJ-17	74	2	55	246	0.75	0.184	0.017	0.02684	0.00060	0.25	0.0498	0.0043	172	15	171	4	185	202	92
MATJ	MATJ-19	380	11	307	48581	0.81	0.194	0.009	0.02845	0.00044	0.34	0.0495	0.0021	180	8	181	3	171	100	106
MATJ	MATJ-20	113	3	173	1179	1.53	0.188	0.010	0.02738	0.00048	0.32	0.0498	0.0026	175	10	174	3	183	120	95
MATJ	MATJ-21	275	8	136	4319	0.49	0.193	0.011	0.02832	0.00044	0.27	0.0495	0.0027	179	10	180	3	173	127	104
MATJ	MATJ-22	228	6	142	47889	0.62	0.190	0.009	0.02768	0.00044	0.34	0.0497	0.0022	176	8	176	3	182	102	97
MATJ	MATJ-23	88	2	62	4687	0.70	0.186	0.010	0.02713	0.00048	0.34	0.0497	0.0024	173	9	173	3	179	115	97
MATJ	MATJ-24	71	2	70	8599	0.98	0.210	0.017	0.02813	0.00052	0.23	0.0541	0.0043	193	16	179	3	375	179	48
MATJ	MATJ-25	66	2	67	13330	1.02	0.184	0.021	0.02657	0.00050	0.17	0.0502	0.0056	172	19	169	3	206	258	82
MATJ	MATJ-26	29	1	38	5883	1.33	0.199	0.037	0.02701	0.00066	0.13	0.0533	0.0100	184	35	172	4	342	423	50
MATJ	MATJ-27	195	5	167	40194	0.86	0.185	0.014	0.02715	0.00044	0.22	0.0495	0.0036	173	13	173	3	171	171	101
MATJ	MATJ-28	552	15	199	114325	0.36	0.184	0.006	0.02723	0.00040	0.48	0.0491	0.0013	172	5	173	3	152	62	114
MATJ	MATJ-29	117	3	155	874	1.32	0.186	0.015	0.02721	0.00046	0.21	0.0497	0.0039	173	14	173	3	179	182	97
MATJ	MATJ-30	125	22	27	328645	0.22	1.833	0.053	0.17895	0.00268	0.52	0.0743	0.0018	1057	31	1061	16	1050	50	101
MATJ	MATJ-32	173	5	160	1161	0.92	0.195	0.015	0.02852	0.00046	0.21	0.0495	0.0037	181	14	181	3	173	174	105
MATJ	MATJ-33	147	4	91	31701	0.62	0.193	0.010	0.02821	0.00046	0.31	0.0495	0.0025	179	10	179	3	173	119	104
MATJ	MATJ-34	63	2	45	13881	0.71	0.197	0.017	0.02884	0.00054	0.21	0.0495	0.0042	182	16	183	3	172	199	107
MATJ	MATJ-35	461	13	261	98624	0.57	0.191	0.006	0.02805	0.00042	0.47	0.0493	0.0014	177	6	178	3	164	65	109
MATJ	MATJ-36	45	1	21	950	0.47	0.186	0.027	0.02692	0.00056	0.14	0.0500	0.0071	173	25	171	4	194	331	88
MATJ	MATJ-37	127	3	119	2065	0.93	0.190	0.010	0.02753	0.00046	0.33	0.0500	0.0024	177	9	175	3	196	110	89
MATJ	MATJ-39	137	4	117	393	0.86	0.185	0.015	0.02686	0.00044	0.20	0.0501	0.0040	173	14	171	3	198	187	86
MATJ	MATJ-40	323	9	221	66196	0.68	0.183	0.008	0.02682	0.00040	0.35	0.0495	0.0020	171	7	171	3	173	92	99
MATJ	MATJ-41	529	15	261	2944	0.49	0.195	0.007	0.02846	0.00042	0.42	0.0497	0.0016	181	6	181	3	182	74	99
MATJ	MATJ-44	125	3	181	9991	1.45	0.186	0.015	0.02736	0.00046	0.20	0.0493	0.0040	173	14	174	3	163	191	107
MATJ	MATJ-45	97	3	147	19673	1.52	0.181	0.009	0.02660	0.00046	0.34	0.0492	0.0023	169	9	169	3	159	111	106
MATJ	MATJ-50	58	2	55	675	0.95	0.199	0.017	0.02801	0.00054	0.23	0.0515	0.0042	184	16	178	3	261	188	68
MATJ	MATJ-52	145	4	150	31247	1.03	0.191	0.012	0.02804	0.00046	0.27	0.0494	0.0029	177	11	178	3	165	136	108
MATJ	MATJ-54	209	6	104	526	0.50	0.186	0.012	0.02735	0.00042	0.25	0.0494	0.0030	173	11	174	3	166	142	105
MATJ	MATJ-55	65	2	96	1010	1.48	0.198	0.018	0.02803	0.00052	0.20	0.0512	0.0046	183	17	178	3	252	205	71
MATJ	MATJ-57	323	20	130	19776	0.40	0.454	0.014	0.06067	0.00090	0.49	0.0543	0.0014	380	11	380	6	384	59	99
MATJ	MATJ-58	311	8	176	63929	0.57	0.183	0.007	0.02677	0.00042	0.41	0.0495	0.0017	170	7	170	3	169	82	101
MATJ	MATJ-60	270	7	215	56637	0.79	0.184	0.008	0.02724	0.00042	0.38	0.0490	0.0019	172	7	173	3	149	89	116
MATJ	MATJ-61	32	1	63	6553	2.00	0.185	0.032	0.02686	0.00062	0.13	0.0500	0.0087	173	30	171	4	195	403	87

MATJ	MATJ-63	141	4	138	1484	0.98	0.184	0.008	0.02684	0.00044	0.37	0.0498	0.0020	172	8	171	3	185	94	92
MATJ	MATJ-64	520	15	366	4008	0.70	0.192	0.006	0.02805	0.00042	0.46	0.0497	0.0014	179	6	178	3	181	67	98
MATJ	MATJ-65	264	7	267	2123	1.01	0.184	0.008	0.02688	0.00042	0.34	0.0497	0.0021	172	8	171	3	183	100	94
MATJ	MATJ-66	137	4	181	28417	1.33	0.184	0.010	0.02692	0.00044	0.31	0.0496	0.0025	171	9	171	3	174	117	98
MATJ	MATJ-67	56	2	58	11604	1.05	0.183	0.024	0.02692	0.00052	0.15	0.0493	0.0064	171	22	171	3	161	303	106
MATJ	MATJ-68	206	6	173	721	0.84	0.184	0.009	0.02703	0.00042	0.34	0.0495	0.0022	172	8	172	3	170	102	101
MATJ	MATJ-69	69	2	81	21879	1.17	0.182	0.019	0.02671	0.00054	0.20	0.0496	0.0050	170	17	170	3	174	234	98
MATJ	MATJ-70	112	3	100	841	0.89	0.185	0.015	0.02724	0.00046	0.21	0.0492	0.0038	172	14	173	3	156	180	111
MATJ	MATJ-74	251	7	162	4213	0.64	0.188	0.009	0.02719	0.00044	0.35	0.0501	0.0022	175	8	173	3	198	100	87
MATJ	MATJ-76	113	3	141	1388	1.25	0.191	0.014	0.02784	0.00046	0.23	0.0499	0.0035	178	13	177	3	188	164	94
MATJ	MATJ-77	84	2	122	358	1.45	0.183	0.013	0.02678	0.00048	0.25	0.0494	0.0035	170	12	170	3	168	164	101
MATJ	MATJ-83	333	9	285	1279	0.86	0.187	0.012	0.02704	0.00042	0.23	0.0503	0.0032	174	12	172	3	208	149	83
MATJ	MATJ-85	159	4	173	513	1.09	0.184	0.010	0.02703	0.00044	0.31	0.0495	0.0024	172	9	172	3	172	115	100
MATJ	MATJ-86	373	10	193	3288	0.52	0.188	0.006	0.02750	0.00040	0.44	0.0495	0.0015	175	6	175	3	173	70	101
MATJ	MATJ-88	91	3	85	1629	0.94	0.193	0.013	0.02829	0.00050	0.25	0.0494	0.0033	179	12	180	3	166	157	108
MATJ	MATJ-89	60	2	64	8998	1.08	0.186	0.019	0.02726	0.00052	0.19	0.0496	0.0050	174	18	173	3	175	235	99
MATJ	MATJ-90	163	4	98	2153	0.60	0.189	0.014	0.02717	0.00044	0.22	0.0505	0.0037	176	13	173	3	218	168	79
MATJ	MATJ-92	892	24	398	33753	0.45	0.186	0.005	0.02715	0.00040	0.50	0.0498	0.0013	173	5	173	3	183	59	94
MATJ	MATJ-93	410	11	241	3592	0.59	0.191	0.007	0.02794	0.00042	0.41	0.0496	0.0016	177	6	178	3	174	77	102
MATJ	MATJ-95	746	20	416	369	0.56	0.204	0.010	0.02665	0.00038	0.28	0.0555	0.0027	188	10	170	2	430	109	39
MATJ	MATJ-96	202	6	141	4012	0.70	0.195	0.011	0.02829	0.00044	0.26	0.0499	0.0028	181	11	180	3	192	132	94
MATJ	MATJ-97	153	4	106	11305	0.69	0.186	0.011	0.02706	0.00044	0.28	0.0498	0.0028	173	10	172	3	185	131	93
MATJ	MATJ-101	128	3	139	1180	1.09	0.186	0.010	0.02712	0.00044	0.31	0.0499	0.0025	174	9	172	3	189	115	91
MATJ	MATJ-102	60	2	59	325	0.99	0.191	0.021	0.02667	0.00050	0.17	0.0520	0.0056	178	19	170	3	283	247	60
MATJ	MATJ-104	348	10	360	4045	1.04	0.187	0.010	0.02738	0.00040	0.27	0.0495	0.0026	174	9	174	3	172	121	101

[a]U and Pb concentrations and Th/U ratios are calculated relative to GJ-1 reference zircon

[b]Corrected for background and within-run Pb/U fractionation and normalised to reference zircon GJ-1 (ID-TIMS values/measured value); $^{207}Pb/^{235}U$ calculated using $(^{207}Pb/^{206}Pb)/(^{238}U/^{206}Pb * 1/137.88)$

[c]Rho is the error correlation defined as the quotient of the propagated errors of the $^{206}Pb/^{238}U$ and the $^{207}/^{235}U$ ratio

[d]Quadratic addition of within-run errors (2 SD) and daily reproducibility of GJ-1 (2 SD)

[e]Corrected for mass-bias by normalising to GJ-1 reference zircon (~0.6 per atomic mass unit) and common Pb using the model Pb composition of Stacey & Kramers (1975)

Table D11. LA-ICPMS isotopic data for sample SITT2 in the Mossel Bay Basin

SITT2							**RATIOS**							**AGES [Ma]**						**Conc.**
Sample	**Analysis**	**U [ppm][a]**	**Pb [ppm][a]**	**Th [ppm][a]**	**$^{206}Pb/^{204}Pb$**	**Th/U[a]**	**$^{207}Pb/^{235}U$[b]**	**2 σ[d]**	**$^{206}Pb/^{238}U$[b]**	**2 σ[d]**	**rho[c]**	**$^{207}Pb/^{206}Pb$**	**2 σ[d]**	**$^{207}Pb/^{235}U$**	**2 σ**	**$^{206}Pb/^{238}U$**	**2 σ**	**$^{207}Pb/^{206}Pb$**	**2 σ**	**%**
SITT2	SITT2-1	441	35	125	1230	0.28	0.72	0.03	0.079	0.002	0.49	0.066	0.003	549	27	491	12	800	89	61
SITT2	SITT2-2	504	12	348	771	0.69	0.20	0.02	0.024	0.001	0.27	0.059	0.005	183	15	155	3	561	173	28
SITT2	SITT2-3	137	16	45	141840	0.33	0.98	0.06	0.114	0.003	0.39	0.062	0.004	691	46	695	18	681	131	102
SITT2	SITT2-4	426	76	173	10112	0.41	1.83	0.06	0.178	0.004	0.70	0.075	0.002	1056	33	1053	23	1060	45	99
SITT2	SITT2-5	407	35	76	28520	0.19	0.69	0.02	0.086	0.002	0.68	0.058	0.001	534	17	532	12	543	51	98
SITT2	SITT2-6	745	18	408	1819	0.55	0.17	0.01	0.024	0.001	0.47	0.050	0.002	159	7	155	3	215	96	72
SITT2	SITT2-7	227	42	79	12267	0.35	1.93	0.06	0.183	0.004	0.68	0.076	0.002	1091	35	1084	24	1106	47	98
SITT2	SITT2-8	326	8	153	2284	0.47	0.16	0.01	0.024	0.001	0.38	0.049	0.003	154	9	154	3	147	129	105
SITT2	SITT2-9	346	10	721	396	2.08	0.24	0.01	0.029	0.001	0.38	0.060	0.003	220	13	185	4	611	116	30
SITT2	SITT2-10	776	18	239	2634	0.31	0.17	0.01	0.024	0.001	0.38	0.051	0.003	156	9	150	3	253	122	59
SITT2	SITT2-11	284	19	133	172570	0.47	0.51	0.02	0.067	0.002	0.52	0.055	0.002	416	18	416	9	415	83	100
SITT2	SITT2-12	662	16	309	1748	0.47	0.17	0.01	0.024	0.001	0.44	0.052	0.002	162	8	154	3	288	105	53
SITT2	SITT2-13	759	18	391	1025	0.52	0.18	0.01	0.024	0.001	0.46	0.056	0.002	171	8	152	3	444	93	34
SITT2	SITT2-14	216	40	103	361682	0.48	1.93	0.06	0.184	0.004	0.70	0.076	0.002	1090	34	1090	24	1090	45	100
SITT2	SITT2-15	191	5	85	764	0.45	0.19	0.01	0.028	0.001	0.40	0.049	0.003	178	10	179	4	161	125	111
SITT2	SITT2-16	555	25	343	222586	0.62	0.32	0.01	0.044	0.001	0.59	0.052	0.002	280	11	279	6	288	69	97
SITT2	SITT2-17	544	24	191	45581	0.35	0.31	0.01	0.044	0.001	0.64	0.052	0.001	277	9	276	6	282	60	98
SITT2	SITT2-18	537	46	117	6865	0.22	0.69	0.02	0.085	0.002	0.66	0.058	0.001	532	18	529	12	547	55	97
SITT2	SITT2-19	476	11	159	1744	0.33	0.16	0.01	0.023	0.001	0.34	0.049	0.003	149	10	148	3	156	146	95
SITT2	SITT2-20	249	6	155	358	0.62	0.23	0.02	0.023	0.001	0.31	0.072	0.005	209	15	148	3	972	141	15
SITT2	SITT2-21	340	8	140	3394	0.41	0.16	0.02	0.023	0.001	0.24	0.051	0.005	149	15	144	3	230	218	63
SITT2	SITT2-22	452	10	156	1498	0.34	0.16	0.01	0.023	0.001	0.33	0.051	0.003	148	10	144	3	220	145	65
SITT2	SITT2-23	541	22	132	3323	0.24	0.29	0.01	0.041	0.001	0.49	0.052	0.002	259	12	257	6	278	95	92
SITT2	SITT2-24	428	11	173	310	0.41	0.20	0.02	0.026	0.001	0.20	0.055	0.006	182	21	164	4	424	252	39
SITT2	SITT2-25	362	8	344	1538	0.95	0.18	0.01	0.023	0.001	0.31	0.057	0.004	166	12	144	3	501	151	29
SITT2	SITT2-26	330	25	234	228481	0.71	0.62	0.03	0.077	0.002	0.44	0.059	0.003	491	27	475	12	564	107	84
SITT2	SITT2-30	1311	31	381	427	0.29	0.18	0.01	0.023	0.001	0.47	0.057	0.002	171	8	149	3	479	92	31
SITT2	SITT2-32	477	31	206	965	0.43	0.58	0.02	0.064	0.001	0.55	0.066	0.002	465	19	400	9	798	73	50
SITT2	SITT2-34	432	80	135	2798	0.31	1.92	0.07	0.185	0.004	0.63	0.075	0.002	1087	39	1094	25	1071	56	102
SITT2	SITT2-36	291	6	292	1903	1.00	0.15	0.01	0.022	0.001	0.42	0.049	0.002	142	8	141	3	161	115	88
SITT2	SITT2-37	652	15	380	3415	0.58	0.15	0.01	0.023	0.001	0.49	0.050	0.002	145	7	143	3	177	91	81
SITT2	SITT2-38	710	33	393	2003	0.55	0.34	0.01	0.046	0.001	0.57	0.053	0.002	295	12	290	7	339	73	85
SITT2	SITT2-39	289	7	122	6813	0.42	0.16	0.01	0.023	0.001	0.42	0.051	0.002	153	8	148	3	226	110	66
SITT2	SITT2-40	271	7	184	989	0.68	0.17	0.01	0.024	0.001	0.47	0.050	0.002	159	8	155	4	212	101	73
SITT2	SITT2-41	580	14	402	902	0.69	0.19	0.01	0.024	0.001	0.53	0.059	0.002	180	8	153	3	550	78	28
SITT2	SITT2-42	148	30	38	2490	0.26	2.29	0.10	0.205	0.005	0.56	0.081	0.003	1210	51	1205	28	1219	69	99
SITT2	SITT2-43	679	60	159	536674	0.23	0.71	0.02	0.088	0.002	0.68	0.058	0.001	543	18	542	12	545	52	99
SITT2	SITT2-44	553	15	449	1058	0.81	0.22	0.01	0.028	0.001	0.49	0.057	0.002	200	10	175	4	503	93	35
SITT2	SITT2-45	419	35	224	30829	0.53	0.67	0.02	0.084	0.002	0.61	0.058	0.002	523	19	521	12	535	64	97
SITT2	SITT2-46	405	10	392	456	0.97	0.19	0.01	0.024	0.001	0.45	0.058	0.003	176	9	150	3	531	100	28
SITT2	SITT2-47	263	26	156	2371	0.59	0.81	0.03	0.098	0.002	0.57	0.060	0.002	605	24	602	14	614	72	98
SITT2	SITT2-48	210	18	68	163377	0.32	0.70	0.03	0.087	0.002	0.61	0.059	0.002	539	20	536	12	550	65	97
SITT2	SITT2-49	110	3	134	317	1.22	0.24	0.03	0.029	0.001	0.20	0.059	0.007	215	26	182	4	583	254	31
SITT2	SITT2-50	207	18	191	158447	0.92	0.68	0.03	0.085	0.002	0.50	0.058	0.002	530	25	527	12	541	89	97
SITT2	SITT2-51	514	42	349	1492	0.68	0.70	0.04	0.082	0.002	0.48	0.062	0.003	541	27	510	12	670	93	76
SITT2	SITT2-52	599	13	184	120304	0.31	0.15	0.01	0.022	0.001	0.61	0.049	0.001	143	5	143	3	151	69	94
SITT2	SITT2-53	191	15	45	132106	0.23	0.60	0.02	0.077	0.002	0.60	0.057	0.002	477	18	478	11	473	67	101

SITT2	SITT2-55	1106	25	688	20609	0.62	0.16	0.01	0.023	0.001	0.65	0.050	0.001	148	5	146	3	188	60	77
SITT2	SITT2-56	421	9	298	3021	0.71	0.15	0.01	0.022	0.001	0.59	0.049	0.002	141	5	141	3	140	73	101
SITT2	SITT2-58	255	116	50	28630	0.20	9.71	0.30	0.455	0.010	0.72	0.155	0.003	2408	74	2416	54	2401	36	101
SITT2	SITT2-59	200	15	207	1273	1.03	0.59	0.03	0.075	0.002	0.43	0.057	0.003	474	27	469	12	497	114	94
SITT2	SITT2-60	237	23	134	3958	0.57	0.81	0.03	0.098	0.002	0.62	0.060	0.002	601	22	600	14	603	62	99
SITT2	SITT2-61	317	7	142	30974	0.45	0.16	0.01	0.024	0.001	0.56	0.049	0.002	151	6	151	3	155	80	97
SITT2	SITT2-62	109	5	81	2614	0.74	0.32	0.02	0.044	0.001	0.43	0.052	0.003	278	16	277	7	287	120	97
SITT2	SITT2-63	151	7	123	669	0.82	0.48	0.02	0.047	0.001	0.50	0.074	0.003	396	19	294	7	1043	83	28
SITT2	SITT2-64	344	8	216	845	0.63	0.17	0.01	0.024	0.001	0.39	0.052	0.003	162	10	155	4	265	125	59
SITT2	SITT2-65	294	8	157	989	0.53	0.18	0.01	0.026	0.001	0.41	0.050	0.003	169	9	165	4	217	117	76
SITT2	SITT2-66	171	4	50	570	0.29	0.20	0.02	0.026	0.001	0.25	0.056	0.005	184	17	164	4	452	202	36
SITT2	SITT2-67	677	267	159	4737	0.23	9.67	0.29	0.394	0.009	0.73	0.178	0.004	2404	73	2140	47	2636	35	81
SITT2	SITT2-68	545	39	541	720	0.99	0.75	0.03	0.072	0.002	0.67	0.075	0.002	566	19	447	10	1078	51	41
SITT2	SITT2-69	368	29	159	4874	0.43	0.61	0.02	0.078	0.002	0.57	0.057	0.002	486	20	483	11	499	73	97
SITT2	SITT2-70	520	12	201	1164	0.39	0.16	0.01	0.023	0.001	0.41	0.050	0.002	148	8	146	3	176	117	83
SITT2	SITT2-71	122	21	34	20402	0.28	1.80	0.07	0.173	0.004	0.61	0.075	0.002	1044	40	1031	24	1072	60	96
SITT2	SITT2-72	1237	29	1044	788	0.84	0.21	0.01	0.023	0.001	0.40	0.064	0.003	190	11	149	3	734	109	20
SITT2	SITT2-73	835	412	65	86005	0.08	11.79	0.36	0.493	0.011	0.72	0.173	0.004	2588	80	2585	58	2591	36	100
SITT2	SITT2-74	232	115	103	21388	0.45	12.19	0.37	0.498	0.011	0.72	0.178	0.004	2619	80	2604	58	2631	35	99
SITT2	SITT2-75	202	18	28	157378	0.14	0.71	0.03	0.088	0.002	0.63	0.058	0.002	542	20	542	12	542	61	100
SITT2	SITT2-76	225	9	318	13241	1.42	0.29	0.01	0.040	0.001	0.49	0.052	0.002	257	12	256	6	272	96	94
SITT2	SITT2-77	553	44	53	2802	0.10	0.65	0.02	0.079	0.002	0.64	0.059	0.002	506	18	490	11	577	59	85
SITT2	SITT2-78	635	14	278	655	0.44	0.18	0.01	0.022	0.001	0.34	0.059	0.004	167	11	141	3	556	138	25
SITT2	SITT2-79	689	16	1338	2450	1.94	0.16	0.01	0.023	0.001	0.44	0.051	0.002	149	8	145	3	223	108	65
SITT2	SITT2-80	720	15	522	467	0.73	0.16	0.01	0.021	0.000	0.39	0.055	0.003	152	9	136	3	419	119	32
SITT2	SITT2-81	373	29	248	1502	0.67	0.65	0.04	0.076	0.002	0.45	0.062	0.003	509	28	475	12	664	107	71
SITT2	SITT2-82	471	21	663	11937	1.41	0.33	0.01	0.045	0.001	0.52	0.052	0.002	286	13	286	7	285	88	100
SITT2	SITT2-83	590	13	212	1168	0.36	0.16	0.01	0.022	0.001	0.46	0.053	0.002	151	8	140	3	328	101	43
SITT2	SITT2-84	706	62	717	12696	1.02	0.71	0.02	0.089	0.002	0.68	0.058	0.001	547	18	547	12	548	52	100
SITT2	SITT2-85	222	10	164	434	0.74	0.46	0.03	0.045	0.001	0.41	0.074	0.005	386	26	286	8	1043	124	27
SITT2	SITT2-86	350	31	142	274821	0.41	0.72	0.02	0.089	0.002	0.67	0.059	0.001	550	19	548	12	562	55	97
SITT2	SITT2-87	608	27	319	3991	0.52	0.32	0.01	0.044	0.001	0.64	0.052	0.001	280	10	279	6	283	63	99
SITT2	SITT2-88	210	11	217	1221	1.03	0.55	0.03	0.053	0.001	0.42	0.075	0.004	444	28	332	9	1076	115	31
SITT2	SITT2-89	301	14	162	119834	0.54	0.32	0.01	0.045	0.001	0.63	0.052	0.001	282	10	283	6	274	64	103
SITT2	SITT2-90	366	9	126	1314	0.34	0.18	0.01	0.025	0.001	0.40	0.051	0.003	168	10	162	4	252	121	64
SITT2	SITT2-91	212	5	160	512	0.75	0.25	0.02	0.023	0.001	0.34	0.079	0.005	229	16	148	4	1168	132	13
SITT2	SITT2-92	272	21	98	2130	0.36	0.61	0.03	0.077	0.002	0.45	0.057	0.003	485	27	480	12	509	109	94
SITT2	SITT2-93	274	12	455	2367	1.66	0.30	0.01	0.042	0.001	0.49	0.052	0.002	268	13	267	6	272	99	98
SITT2	SITT2-94	399	34	131	44696	0.33	0.67	0.02	0.085	0.002	0.65	0.058	0.002	523	18	524	12	516	58	102
SITT2	SITT2-96	547	61	116	6457	0.21	0.97	0.04	0.111	0.003	0.55	0.063	0.002	689	30	681	16	714	77	95
SITT2	SITT2-97	434	19	232	4575	0.53	0.31	0.01	0.043	0.001	0.53	0.052	0.002	275	12	274	6	282	86	97
SITT2	SITT2-98	757	17	410	2644	0.54	0.16	0.01	0.023	0.001	0.57	0.052	0.002	153	6	146	3	267	76	55
SITT2	SITT2-99	162	4	78	2156	0.48	0.17	0.02	0.025	0.001	0.26	0.049	0.005	161	15	161	4	170	214	95
SITT2	SITT2-100	354	9	291	812	0.82	0.17	0.01	0.024	0.001	0.39	0.051	0.003	160	9	155	4	229	125	68
SITT2	SITT2-102	598	15	389	1585	0.65	0.18	0.01	0.024	0.001	0.39	0.052	0.003	166	10	156	4	306	122	51
SITT2	SITT2-103	197	27	76	8109	0.39	1.29	0.04	0.138	0.003	0.68	0.068	0.002	843	28	834	19	866	51	96
SITT2	SITT2-104	533	51	185	4076	0.35	0.84	0.03	0.095	0.002	0.66	0.064	0.002	618	21	588	13	732	54	80
SITT2	SITT2-105	62	5	25	40850	0.41	0.58	0.06	0.074	0.003	0.30	0.057	0.006	465	52	462	16	482	234	96
SITT2	SITT2-106	200	5	70	2143	0.35	0.16	0.01	0.024	0.001	0.47	0.049	0.002	150	8	150	4	146	103	103

SITT2	SITT2-107	192	6	73	383	0.38	0.22	0.02	0.029	0.001	0.24	0.055	0.005	202	19	186	4	393	207	47
SITT2	SITT2-108	179	9	78	2589	0.43	0.35	0.02	0.049	0.001	0.48	0.053	0.002	308	16	307	7	310	101	99
SITT2	SITT2-109	389	34	158	295856	0.41	0.70	0.02	0.086	0.002	0.68	0.058	0.001	536	18	534	12	544	53	98
SITT2	SITT2-110	417	36	55	8310	0.13	0.69	0.03	0.086	0.002	0.61	0.058	0.002	532	20	531	12	540	66	98
SITT2	SITT2-111	426	10	234	2449	0.55	0.16	0.01	0.023	0.001	0.51	0.050	0.002	151	7	148	3	200	91	74
SITT2	SITT2-112	379	28	228	1535	0.60	0.64	0.02	0.074	0.002	0.65	0.064	0.002	505	18	458	10	726	56	63
SITT2	SITT2-113	459	34	271	838	0.59	0.75	0.02	0.073	0.002	0.68	0.074	0.002	566	19	457	10	1033	49	44
SITT2	SITT2-114	252	6	127	49743	0.51	0.15	0.01	0.022	0.001	0.33	0.050	0.003	145	10	143	3	172	153	83
SITT2	SITT2-115	1139	180	23	18708	0.02	1.57	0.05	0.158	0.004	0.69	0.072	0.002	960	32	946	21	993	48	95

[a]U and Pb concentrations and Th/U ratios are calculated relative to GJ-1 reference zircon

[b]Corrected for background and within-run Pb/U fractionation and normalised to reference zircon GJ-1 (ID-TIMS values/measured value); $^{207}Pb/^{235}U$ calculated using ($^{207}Pb/^{206}Pb$)/($^{238}U/^{206}Pb$ * 1/137.88)

[c]Rho is the error correlation defined as the quotient of the propagated errors of the $^{206}Pb/^{238}U$ and the $^{207}/^{235}U$ ratio

[d]Quadratic addition of within-run errors (2 SD) and daily reproducibility of GJ-1 (2 SD)

[e]Corrected for mass-bias by normalising to GJ-1 reference zircon (~0.6 per atomic mass unit) and common Pb using the model Pb composition of Stacey & Kramers (1975)

Table D12. LA-ICPMS isotopic data for sample SITT3 in the Mossel Bay Basin

SITT3							RATIOS							AGES [Ma]						Conc.
Sample	Analysis	U [ppm][a]	Pb [ppm][a]	Th [ppm][a]	$^{206}Pb/^{204}Pb$	Th/U[a]	$^{207}Pb/^{235}U$[b]	2 σ[d]	$^{206}Pb/^{238}U$[b]	2 σ[d]	rho[c]	$^{207}Pb/^{206}Pb$	2 σ[d]	$^{207}Pb/^{235}U$	2 σ	$^{206}Pb/^{238}U$	2 σ	$^{207}Pb/^{206}Pb$	2 σ	%
SITT3	SITT3-1	270	79	199	2016	0.73	4.741	0.148	0.2931	0.0066	0.72	0.1173	0.0025	1775	56	1657	37	1916	39	86
SITT3	SITT3-2	264	11	223	769	0.85	0.315	0.024	0.0401	0.0011	0.36	0.0570	0.0041	278	22	254	7	492	159	52
SITT3	SITT3-3	360	14	228	1665	0.63	0.314	0.021	0.0394	0.0010	0.40	0.0578	0.0035	277	18	249	7	522	134	48
SITT3	SITT3-4	127	4	49	348	0.38	0.287	0.024	0.0281	0.0007	0.29	0.0740	0.0060	256	22	179	4	1041	164	17
SITT3	SITT3-5	146	4	221	903	1.51	0.189	0.015	0.0275	0.0007	0.31	0.0498	0.0036	176	14	175	4	186	170	94
SITT3	SITT3-6	378	71	87	20845	0.23	2.003	0.063	0.1870	0.0042	0.72	0.0777	0.0017	1116	35	1105	25	1138	43	97
SITT3	SITT3-7	960	62	61	539108	0.06	0.495	0.016	0.0649	0.0015	0.69	0.0553	0.0013	408	14	405	9	425	54	95
SITT3	SITT3-8	210	5	171	250	0.81	0.327	0.033	0.0238	0.0006	0.24	0.0997	0.0097	288	29	152	4	1619	182	9
SITT3	SITT3-9	220	5	170	442	0.77	0.192	0.025	0.0231	0.0006	0.19	0.0603	0.0076	178	23	147	4	613	273	24
SITT3	SITT3-10	199	4	101	1607	0.51	0.176	0.017	0.0226	0.0005	0.25	0.0566	0.0053	165	16	144	3	474	209	30
SITT3	SITT3-11	615	55	734	5047	1.19	0.738	0.031	0.0898	0.0021	0.56	0.0596	0.0021	561	23	554	13	589	75	94
SITT3	SITT3-12	415	29	475	1466	1.15	0.624	0.029	0.0702	0.0017	0.51	0.0645	0.0026	493	23	437	10	758	84	58
SITT3	SITT3-13	125	6	159	1579	1.27	0.362	0.045	0.0467	0.0017	0.29	0.0563	0.0067	314	39	294	10	466	263	63
SITT3	SITT3-14	244	30	60	4260	0.24	1.174	0.054	0.1246	0.0029	0.50	0.0684	0.0027	789	36	757	17	880	82	86
SITT3	SITT3-15	65	2	141	242	2.17	0.195	0.034	0.0286	0.0007	0.15	0.0494	0.0086	181	32	182	5	168	408	108
SITT3	SITT3-16	804	135	28	24086	0.03	1.702	0.055	0.1677	0.0038	0.70	0.0736	0.0017	1009	32	999	23	1031	46	97
SITT3	SITT3-17	2008	246	799	9835	0.40	1.120	0.036	0.1227	0.0028	0.70	0.0662	0.0015	763	25	746	17	813	49	92
SITT3	SITT3-18	429	36	453	493	1.06	0.878	0.044	0.0833	0.0021	0.49	0.0765	0.0034	640	32	516	13	1107	88	47
SITT3	SITT3-19	543	49	203	13305	0.37	0.746	0.025	0.0906	0.0021	0.69	0.0598	0.0014	566	19	559	13	595	52	94
SITT3	SITT3-20	330	23	217	30541	0.66	0.538	0.024	0.0700	0.0017	0.53	0.0558	0.0021	437	20	436	10	443	85	99
SITT3	SITT3-21	275	24	205	27210	0.75	0.729	0.027	0.0890	0.0021	0.62	0.0594	0.0018	556	21	550	13	581	64	95
SITT3	SITT3-22	179	10	154	719	0.86	0.488	0.042	0.0574	0.0013	0.26	0.0617	0.0052	404	35	360	8	663	179	54
SITT3	SITT3-23	511	25	150	319	0.29	0.610	0.027	0.0481	0.0012	0.55	0.0921	0.0034	484	22	303	7	1469	71	21
SITT3	SITT3-24	552	13	497	3815	0.90	0.163	0.008	0.0241	0.0006	0.50	0.0492	0.0020	154	7	153	4	159	95	96
SITT3	SITT3-25	39	3	13	324	0.33	0.610	0.086	0.0781	0.0031	0.28	0.0566	0.0077	483	68	485	19	477	301	102
SITT3	SITT3-26	254	6	124	1771	0.49	0.164	0.016	0.0243	0.0006	0.25	0.0491	0.0046	154	15	155	4	151	220	103
SITT3	SITT3-27	258	11	222	3067	0.86	0.318	0.017	0.0423	0.0010	0.46	0.0545	0.0026	280	15	267	7	393	107	68
SITT3	SITT3-28	417	12	472	887	1.13	0.206	0.012	0.0288	0.0007	0.40	0.0520	0.0027	191	11	183	4	286	120	64
SITT3	SITT3-29	307	24	34	1746	0.11	0.657	0.029	0.0780	0.0019	0.55	0.0610	0.0022	513	22	484	12	640	78	76
SITT3	SITT3-30	333	8	274	550	0.82	0.230	0.017	0.0242	0.0006	0.31	0.0688	0.0049	210	16	154	4	891	147	17
SITT3	SITT3-31	304	22	92	784	0.30	0.564	0.033	0.0729	0.0018	0.43	0.0561	0.0029	454	26	454	11	457	116	99
SITT3	SITT3-32	868	78	427	51132	0.49	0.723	0.023	0.0896	0.0020	0.71	0.0586	0.0013	553	18	553	13	552	50	100
SITT3	SITT3-33	358	13	406	7224	1.13	0.277	0.017	0.0376	0.0011	0.45	0.0534	0.0030	248	16	238	7	345	126	69
SITT3	SITT3-34	332	31	76	963	0.23	0.794	0.039	0.0929	0.0023	0.50	0.0620	0.0026	594	29	573	14	674	90	85
SITT3	SITT3-35	175	16	108	11594	0.61	0.721	0.037	0.0891	0.0022	0.48	0.0587	0.0026	551	28	550	14	557	98	99
SITT3	SITT3-36	314	7	156	644	0.50	0.180	0.013	0.0236	0.0006	0.32	0.0553	0.0038	168	12	151	4	425	154	35
SITT3	SITT3-37	287	7	229	236	0.80	0.223	0.019	0.0243	0.0006	0.28	0.0665	0.0054	204	17	155	4	821	170	19
SITT3	SITT3-41	300	7	205	802	0.68	0.150	0.009	0.0222	0.0005	0.40	0.0491	0.0026	142	8	141	3	154	126	92
SITT3	SITT3-42	132	6	102	5301	0.78	0.344	0.021	0.0472	0.0012	0.43	0.0528	0.0029	300	18	297	8	322	123	92
SITT3	SITT3-43	430	17	231	559	0.54	0.348	0.019	0.0405	0.0009	0.43	0.0623	0.0030	303	16	256	6	685	103	37
SITT3	SITT3-44	156	13	71	112405	0.46	0.678	0.025	0.0840	0.0019	0.63	0.0586	0.0017	526	19	520	12	551	62	94
SITT3	SITT3-45	1430	122	1012	22979	0.71	0.681	0.021	0.0851	0.0019	0.72	0.0581	0.0013	527	17	526	12	532	48	99
SITT3	SITT3-46	226	15	170	715	0.75	0.615	0.030	0.0644	0.0016	0.50	0.0693	0.0030	487	24	402	10	908	88	44
SITT3	SITT3-47	151	3	132	970	0.87	0.153	0.014	0.0225	0.0005	0.26	0.0493	0.0043	145	13	144	3	164	206	88
SITT3	SITT3-48	754	63	124	1824	0.16	0.771	0.025	0.0842	0.0019	0.71	0.0664	0.0015	580	19	521	12	819	48	64
SITT3	SITT3-49	349	31	214	4701	0.61	0.734	0.026	0.0900	0.0021	0.65	0.0592	0.0016	559	20	555	13	575	59	97
SITT3	SITT3-50	591	27	362	893	0.61	0.411	0.014	0.0449	0.0010	0.69	0.0664	0.0016	350	12	283	6	820	50	35

SITT3	SITT3-51	1009	80	558	6906	0.55	0.677	0.028	0.0796	0.0019	0.57	0.0617	0.0021	525	22	494	12	663	74	74
SITT3	SITT3-52	70	6	30	2258	0.42	0.746	0.043	0.0899	0.0023	0.44	0.0602	0.0031	566	33	555	14	610	112	91
SITT3	SITT3-53	127	11	52	7660	0.41	0.681	0.049	0.0833	0.0022	0.37	0.0593	0.0039	528	38	516	14	579	144	89
SITT3	SITT3-54	862	42	1136	5345	1.32	0.358	0.013	0.0493	0.0011	0.64	0.0526	0.0015	310	11	310	7	312	64	99
SITT3	SITT3-55	338	27	337	3265	1.00	0.634	0.025	0.0802	0.0019	0.59	0.0573	0.0018	498	20	497	12	503	71	99
SITT3	SITT3-56	261	42	107	2003	0.41	1.652	0.068	0.1608	0.0038	0.58	0.0745	0.0025	990	41	961	23	1056	68	91
SITT3	SITT3-57	158	4	92	761	0.59	0.184	0.018	0.0270	0.0008	0.31	0.0493	0.0046	171	17	172	5	161	219	107
SITT3	SITT3-58	730	33	341	2060	0.47	0.356	0.013	0.0455	0.0010	0.65	0.0567	0.0015	309	11	287	7	480	59	60
SITT3	SITT3-59	131	11	76	96717	0.58	0.685	0.026	0.0860	0.0020	0.62	0.0578	0.0017	530	20	532	12	522	65	102
SITT3	SITT3-60	891	22	336	11258	0.38	0.168	0.009	0.0246	0.0006	0.45	0.0497	0.0023	158	8	156	4	182	107	86
SITT3	SITT3-61	384	58	136	8072	0.36	1.463	0.050	0.1509	0.0035	0.67	0.0703	0.0018	915	31	906	21	937	52	97
SITT3	SITT3-62	902	20	389	264	0.43	0.153	0.008	0.0226	0.0005	0.42	0.0491	0.0025	145	8	144	3	152	117	95
SITT3	SITT3-63	319	7	124	2551	0.39	0.159	0.008	0.0234	0.0006	0.48	0.0493	0.0022	150	8	149	4	161	105	92
SITT3	SITT3-64	1266	28	552	5432	0.44	0.152	0.008	0.0222	0.0005	0.42	0.0496	0.0025	143	8	141	3	174	118	81
SITT3	SITT3-65	303	25	185	2026	0.61	0.714	0.032	0.0838	0.0020	0.53	0.0618	0.0024	547	25	518	13	667	82	78
SITT3	SITT3-66	441	86	70	193556	0.16	2.115	0.069	0.1947	0.0045	0.70	0.0788	0.0018	1154	38	1147	26	1167	46	98
SITT3	SITT3-67	213	10	332	7088	1.56	0.341	0.016	0.0474	0.0011	0.51	0.0521	0.0021	298	14	299	7	290	92	103
SITT3	SITT3-68	969	42	417	537	0.43	0.394	0.017	0.0431	0.0010	0.52	0.0664	0.0025	337	15	272	6	818	79	33
SITT3	SITT3-69	228	10	228	13624	1.00	0.333	0.020	0.0439	0.0011	0.42	0.0551	0.0031	292	18	277	7	416	124	67
SITT3	SITT3-70	390	9	257	779	0.66	0.171	0.010	0.0242	0.0006	0.41	0.0514	0.0027	160	9	154	4	259	119	59
SITT3	SITT3-71	392	16	437	2226	1.11	0.326	0.021	0.0413	0.0011	0.41	0.0573	0.0033	287	18	261	7	503	128	52
SITT3	SITT3-74	461	10	286	355	0.62	0.188	0.013	0.0226	0.0005	0.32	0.0602	0.0041	175	13	144	3	612	147	24
SITT3	SITT3-75	324	8	268	216	0.83	0.205	0.015	0.0246	0.0006	0.34	0.0606	0.0040	190	13	157	4	624	144	25
SITT3	SITT3-76	482	29	279	776	0.58	0.556	0.023	0.0591	0.0014	0.57	0.0682	0.0024	449	19	370	9	876	72	42
SITT3	SITT3-78	382	9	261	1251	0.68	0.182	0.012	0.0240	0.0006	0.36	0.0550	0.0033	169	11	153	4	413	136	37
SITT3	SITT3-80	609	39	84	3337	0.14	0.526	0.022	0.0635	0.0015	0.57	0.0601	0.0021	429	18	397	9	606	74	65
SITT3	SITT3-81	985	74	304	36460	0.31	0.606	0.026	0.0754	0.0018	0.55	0.0583	0.0021	481	21	468	11	541	79	87
SITT3	SITT3-82	361	9	260	790	0.72	0.187	0.015	0.0242	0.0006	0.30	0.0562	0.0042	174	14	154	4	459	165	34
SITT3	SITT3-83	399	17	148	148606	0.37	0.310	0.011	0.0436	0.0010	0.65	0.0516	0.0014	274	10	275	6	268	62	103
SITT3	SITT3-84	965	41	405	4725	0.42	0.304	0.010	0.0424	0.0010	0.70	0.0520	0.0012	269	9	267	6	287	54	93
SITT3	SITT3-85	434	30	415	1767	0.96	0.571	0.025	0.0696	0.0017	0.55	0.0595	0.0022	459	20	434	10	587	79	74
SITT3	SITT3-86	450	60	26	1859	0.06	1.312	0.047	0.1334	0.0031	0.65	0.0713	0.0019	851	30	807	19	966	55	84
SITT3	SITT3-87	236	9	191	435	0.81	0.296	0.030	0.0396	0.0013	0.31	0.0543	0.0053	263	27	250	8	384	218	65
SITT3	SITT3-88	728	29	685	1899	0.94	0.341	0.014	0.0404	0.0010	0.59	0.0611	0.0020	298	12	256	6	644	70	40
SITT3	SITT3-89	454	23	219	1295	0.48	0.453	0.026	0.0501	0.0012	0.42	0.0656	0.0034	379	21	315	8	794	107	40
SITT3	SITT3-90	137	18	80	1171	0.59	1.398	0.071	0.1332	0.0034	0.50	0.0762	0.0034	888	45	806	20	1099	88	73
SITT3	SITT3-91	381	30	135	5005	0.35	0.621	0.030	0.0779	0.0019	0.50	0.0578	0.0024	491	24	484	12	523	93	93
SITT3	SITT3-92	234	10	160	89069	0.69	0.321	0.012	0.0447	0.0010	0.61	0.0521	0.0016	283	11	282	7	289	69	98
SITT3	SITT3-93	218	19	95	1913	0.44	0.761	0.036	0.0894	0.0022	0.51	0.0618	0.0025	575	27	552	13	665	87	83
SITT3	SITT3-94	343	70	189	6488	0.55	3.009	0.102	0.2029	0.0047	0.69	0.1075	0.0026	1410	48	1191	28	1758	45	68
SITT3	SITT3-95	220	5	351	300	1.60	0.260	0.020	0.0243	0.0006	0.31	0.0775	0.0058	234	18	155	4	1133	149	14
SITT3	SITT3-96	614	55	160	10150	0.26	0.721	0.025	0.0890	0.0021	0.67	0.0588	0.0015	551	19	550	13	559	56	98
SITT3	SITT3-97	223	24	67	205467	0.30	0.920	0.031	0.1082	0.0025	0.68	0.0616	0.0015	662	23	662	15	662	54	100
SITT3	SITT3-98	446	38	86	9012	0.19	0.678	0.022	0.0855	0.0020	0.70	0.0575	0.0014	525	17	529	12	510	52	104
SITT3	SITT3-99	285	24	67	51359	0.24	0.682	0.023	0.0852	0.0020	0.68	0.0581	0.0015	528	18	527	12	534	55	99
SITT3	SITT3-100	331	29	58	11012	0.17	0.720	0.026	0.0884	0.0021	0.66	0.0591	0.0016	551	20	546	13	569	58	96
SITT3	SITT3-101	286	16	135	874	0.47	0.440	0.024	0.0554	0.0014	0.46	0.0576	0.0028	370	20	348	9	513	108	68
SITT3	SITT3-102	186	93	94	7807	0.50	12.363	0.394	0.5006	0.0115	0.72	0.1791	0.0039	2632	84	2616	60	2645	37	99
SITT3	SITT3-103	140	5	236	1354	1.68	0.300	0.039	0.0383	0.0013	0.27	0.0570	0.0071	267	35	242	8	490	275	49

SITT3	SITT3-104	225	18	75	152889	0.34	0.680	0.042	0.0798	0.0021	0.43	0.0618	0.0034	527	32	495	13	666	119	74
SITT3	SITT3-105	629	50	751	6576	1.19	0.625	0.021	0.0787	0.0018	0.69	0.0576	0.0014	493	16	488	11	515	53	95
SITT3	SITT3-106	1081	26	1257	1027	1.16	0.182	0.010	0.0240	0.0006	0.43	0.0552	0.0027	170	9	153	4	418	109	37
SITT3	SITT3-108	274	12	195	100513	0.71	0.308	0.012	0.0431	0.0010	0.62	0.0519	0.0015	273	10	272	6	280	68	97
SITT3	SITT3-109	225	10	154	40602	0.69	0.319	0.029	0.0441	0.0013	0.32	0.0525	0.0046	281	26	278	8	305	199	91
SITT3	SITT3-110	160	7	166	278	1.04	0.429	0.029	0.0415	0.0011	0.41	0.0750	0.0046	362	24	262	7	1068	122	25
SITT3	SITT3-111	281	12	282	5777	1.00	0.309	0.015	0.0433	0.0011	0.49	0.0519	0.0023	274	14	273	7	279	100	98
SITT3	SITT3-113	150	4	81	825	0.54	0.202	0.020	0.0276	0.0007	0.25	0.0530	0.0050	186	18	175	4	329	214	53
SITT3	SITT3-114	209	6	189	1386	0.90	0.194	0.015	0.0276	0.0007	0.31	0.0510	0.0038	180	14	176	4	239	170	74
SITT3	SITT3-115	352	19	215	815	0.61	0.463	0.021	0.0528	0.0013	0.54	0.0637	0.0024	386	17	331	8	731	79	45

[a]U and Pb concentrations and Th/U ratios are calculated relative to GJ-1 reference zircon

[b]Corrected for background and within-run Pb/U fractionation and normalised to reference zircon GJ-1 (ID-TIMS values/measured value); ^{207}Pb/^{235}U calculated using (^{207}Pb/^{206}Pb)/(^{238}U/^{206}Pb * 1/137.88)

[c]Rho is the error correlation defined as the quotient of the propagated errors of the ^{206}Pb/^{238}U and the ^{207}/^{235}U ratio

[d]Quadratic addition of within-run errors (2 SD) and daily reproducibility of GJ-1 (2 SD)

[e]Corrected for mass-bias by normalising to GJ-1 reference zircon (~0.6 per atomic mass unit) and common Pb using the model Pb composition of Stacey & Kramers (1975)

Table D13. LA-ICPMS isotopic data for sample VOEL in the Mossel Bay Basin

VOEL							RATIOS							AGES [Ma]						Conc.
Sample	Analysis	U [ppm][a]	Pb [ppm][a]	Th [ppm][a]	^{206}Pb/^{204}Pb	Th/U[a]	^{207}Pb/^{235}U[b]	2 σ[d]	^{206}Pb/^{238}U[b]	2 σ[d]	rho[c]	^{207}Pb/^{206}Pb	2 σ[d]	^{207}Pb/^{235}U	2 σ	^{206}Pb/^{238}U	2 σ	^{207}Pb/^{206}Pb	2 σ	%
VOEL	VOEL-1	591	14	180	477	0.30	0.206	0.016	0.0245	0.0005	0.27	0.0611	0.0047	190	15	156	3	643	165	24
VOEL	VOEL-2	315	8	143	1657	0.45	0.179	0.012	0.0248	0.0005	0.32	0.0522	0.0033	167	11	158	3	293	144	54
VOEL	VOEL-3	860	21	587	958	0.68	0.168	0.007	0.0247	0.0005	0.48	0.0493	0.0018	157	7	157	3	162	86	97
VOEL	VOEL-4	1070	26	919	239497	0.86	0.168	0.006	0.0243	0.0005	0.54	0.0501	0.0016	158	6	155	3	198	74	78
VOEL	VOEL-5	1179	28	1365	563	1.16	0.163	0.008	0.0236	0.0005	0.39	0.0502	0.0024	154	8	150	3	205	111	73
VOEL	VOEL-6	472	12	225	2651	0.48	0.169	0.007	0.0249	0.0005	0.48	0.0491	0.0019	158	7	158	3	154	90	103
VOEL	VOEL-7	413	10	221	26199	0.53	0.170	0.006	0.0249	0.0005	0.57	0.0493	0.0015	159	6	159	3	163	71	98
VOEL	VOEL-8	448	11	215	1365	0.48	0.173	0.008	0.0249	0.0005	0.43	0.0504	0.0022	162	8	158	3	211	103	75
VOEL	VOEL-9	840	20	541	1127	0.64	0.164	0.007	0.0241	0.0005	0.46	0.0495	0.0020	154	7	153	3	170	93	90
VOEL	VOEL-10	563	14	264	2514	0.47	0.166	0.008	0.0244	0.0005	0.44	0.0492	0.0021	156	7	155	3	158	99	98
VOEL	VOEL-11	703	17	572	1030	0.81	0.176	0.010	0.0240	0.0005	0.36	0.0531	0.0029	164	10	153	3	334	123	46
VOEL	VOEL-12	319	8	181	1231	0.57	0.164	0.010	0.0242	0.0005	0.35	0.0493	0.0029	155	10	154	3	160	136	97
VOEL	VOEL-13	1016	25	771	8156	0.76	0.167	0.006	0.0246	0.0005	0.62	0.0494	0.0013	157	5	156	3	167	61	94
VOEL	VOEL-14	614	16	326	2759	0.53	0.174	0.008	0.0256	0.0005	0.46	0.0494	0.0020	163	7	163	3	164	95	99
VOEL	VOEL-15	452	11	309	1972	0.68	0.168	0.007	0.0248	0.0005	0.47	0.0492	0.0019	158	7	158	3	156	91	101
VOEL	VOEL-16	485	12	355	3866	0.73	0.171	0.012	0.0241	0.0005	0.29	0.0515	0.0035	160	11	153	3	265	158	58
VOEL	VOEL-17	507	12	257	6594	0.51	0.169	0.012	0.0245	0.0005	0.31	0.0500	0.0033	158	11	156	3	195	152	80
VOEL	VOEL-18	524	13	306	4147	0.58	0.168	0.008	0.0243	0.0005	0.45	0.0502	0.0021	158	7	155	3	206	95	75
VOEL	VOEL-19	409	10	189	3184	0.46	0.170	0.007	0.0245	0.0005	0.49	0.0505	0.0019	160	7	156	3	218	87	71
VOEL	VOEL-20	646	16	300	7841	0.46	0.165	0.006	0.0243	0.0005	0.60	0.0493	0.0014	155	5	155	3	164	64	95
VOEL	VOEL-21	267	7	122	61642	0.46	0.171	0.007	0.0252	0.0005	0.51	0.0493	0.0018	160	7	160	3	163	84	99
VOEL	VOEL-22	712	17	573	1606	0.80	0.167	0.006	0.0243	0.0005	0.53	0.0498	0.0016	156	6	155	3	184	76	84
VOEL	VOEL-23	784	19	595	4114	0.76	0.172	0.007	0.0249	0.0005	0.50	0.0502	0.0018	161	7	158	3	206	85	77
VOEL	VOEL-24	527	13	336	120569	0.64	0.171	0.006	0.0250	0.0005	0.55	0.0496	0.0016	160	6	159	3	175	73	91
VOEL	VOEL-26	412	10	306	2481	0.74	0.171	0.009	0.0245	0.0005	0.39	0.0507	0.0025	161	9	156	3	228	116	68
VOEL	VOEL-27	626	15	422	2929	0.67	0.166	0.006	0.0242	0.0005	0.54	0.0497	0.0016	156	6	154	3	181	74	85
VOEL	VOEL-28	542	13	228	1124	0.42	0.183	0.012	0.0242	0.0005	0.32	0.0548	0.0033	170	11	154	3	404	136	38
VOEL	VOEL-31	335	8	293	1005	0.87	0.174	0.014	0.0243	0.0005	0.26	0.0520	0.0041	163	13	155	3	285	180	54
VOEL	VOEL-32	898	22	625	281	0.70	0.178	0.011	0.0249	0.0005	0.35	0.0519	0.0029	166	10	158	3	279	129	57
VOEL	VOEL-33	908	22	515	5507	0.57	0.165	0.005	0.0244	0.0005	0.63	0.0489	0.0012	155	5	155	3	144	59	108
VOEL	VOEL-34	408	10	212	3039	0.52	0.165	0.007	0.0245	0.0005	0.52	0.0490	0.0017	155	6	156	3	150	81	104
VOEL	VOEL-35	876	21	565	2309	0.65	0.162	0.007	0.0238	0.0005	0.49	0.0493	0.0019	152	7	151	3	162	88	93
VOEL	VOEL-36	675	17	473	153495	0.70	0.170	0.007	0.0249	0.0005	0.51	0.0495	0.0017	159	6	159	3	170	81	93
VOEL	VOEL-37	495	12	232	1619	0.47	0.174	0.009	0.0245	0.0005	0.43	0.0514	0.0023	163	8	156	3	257	103	61
VOEL	VOEL-38	774	19	511	5318	0.66	0.168	0.007	0.0247	0.0005	0.50	0.0493	0.0018	157	7	157	3	161	86	98
VOEL	VOEL-39	390	9	140	1784	0.36	0.166	0.007	0.0243	0.0005	0.52	0.0495	0.0017	156	6	155	3	170	81	91
VOEL	VOEL-40	978	24	565	12131	0.58	0.168	0.006	0.0248	0.0005	0.63	0.0492	0.0013	158	5	158	3	158	61	100
VOEL	VOEL-41	469	11	263	1415	0.56	0.170	0.011	0.0244	0.0005	0.34	0.0505	0.0030	159	10	155	3	219	136	71
VOEL	VOEL-42	412	10	370	545	0.90	0.186	0.016	0.0248	0.0005	0.25	0.0544	0.0044	173	14	158	3	387	182	41
VOEL	VOEL-43	573	14	302	2158	0.53	0.169	0.009	0.0248	0.0005	0.38	0.0496	0.0025	159	9	158	3	177	119	89
VOEL	VOEL-44	380	10	246	585	0.65	0.191	0.014	0.0252	0.0005	0.29	0.0550	0.0039	177	13	160	3	410	157	39
VOEL	VOEL-45	816	20	512	4674	0.63	0.177	0.007	0.0249	0.0005	0.55	0.0517	0.0016	166	6	159	3	271	73	58
VOEL	VOEL-46	972	24	527	221688	0.54	0.169	0.005	0.0250	0.0005	0.64	0.0492	0.0012	159	5	159	3	155	58	103
VOEL	VOEL-47	538	13	411	120323	0.76	0.172	0.010	0.0245	0.0005	0.38	0.0509	0.0026	161	9	156	3	236	120	66
VOEL	VOEL-48	1008	25	498	225386	0.49	0.168	0.006	0.0246	0.0005	0.64	0.0497	0.0013	158	5	156	3	183	60	86
VOEL	VOEL-49	443	11	228	1473	0.52	0.172	0.011	0.0245	0.0005	0.33	0.0510	0.0031	161	10	156	3	239	139	65
VOEL	VOEL-50	612	15	335	2446	0.55	0.173	0.008	0.0245	0.0005	0.49	0.0510	0.0019	162	7	156	3	241	88	65

VOEL	VOEL-51	570	14	294	124824	0.52	0.165	0.006	0.0240	0.0005	0.54	0.0498	0.0016	155	6	153	3	186	75	82
VOEL	VOEL-52	1186	29	502	5559	0.42	0.168	0.006	0.0243	0.0005	0.57	0.0502	0.0015	158	6	155	3	204	68	76
VOEL	VOEL-53	423	11	169	1596	0.40	0.172	0.010	0.0249	0.0005	0.38	0.0501	0.0027	161	9	158	3	197	124	80
VOEL	VOEL-54	467	12	237	105261	0.51	0.168	0.007	0.0248	0.0005	0.47	0.0492	0.0019	158	7	158	3	156	91	101
VOEL	VOEL-56	875	21	459	192153	0.52	0.164	0.006	0.0242	0.0005	0.62	0.0493	0.0013	154	5	154	3	162	62	95
VOEL	VOEL-57	787	19	465	4756	0.59	0.167	0.006	0.0245	0.0005	0.58	0.0495	0.0015	157	6	156	3	171	70	91
VOEL	VOEL-58	519	13	341	2159	0.66	0.167	0.006	0.0245	0.0005	0.58	0.0493	0.0015	156	6	156	3	161	69	97
VOEL	VOEL-59	609	15	370	1173	0.61	0.166	0.010	0.0239	0.0005	0.36	0.0503	0.0027	156	9	153	3	211	126	72
VOEL	VOEL-60	876	22	626	7350	0.71	0.168	0.006	0.0247	0.0005	0.63	0.0493	0.0013	157	5	157	3	162	61	97
VOEL	VOEL-61	780	19	443	1864	0.57	0.178	0.010	0.0242	0.0005	0.38	0.0533	0.0027	166	9	154	3	341	113	45
VOEL	VOEL-62	868	21	611	2529	0.70	0.166	0.007	0.0243	0.0005	0.49	0.0493	0.0018	156	6	155	3	164	84	95
VOEL	VOEL-63	686	17	423	792	0.62	0.182	0.009	0.0250	0.0005	0.43	0.0530	0.0023	170	8	159	3	330	99	48
VOEL	VOEL-64	871	21	540	1490	0.62	0.165	0.006	0.0244	0.0005	0.57	0.0492	0.0015	155	6	155	3	156	70	100
VOEL	VOEL-65	450	11	282	2676	0.63	0.171	0.010	0.0247	0.0005	0.35	0.0503	0.0028	161	10	157	3	208	129	75
VOEL	VOEL-66	872	21	572	194844	0.66	0.167	0.006	0.0246	0.0005	0.64	0.0491	0.0013	157	5	157	3	154	60	102
VOEL	VOEL-67	928	23	548	3237	0.59	0.167	0.006	0.0246	0.0005	0.61	0.0495	0.0014	157	5	156	3	171	64	92
VOEL	VOEL-68	626	15	259	1730	0.41	0.168	0.008	0.0241	0.0005	0.41	0.0504	0.0023	157	8	154	3	213	107	72
VOEL	VOEL-69	571	14	337	124892	0.59	0.165	0.009	0.0241	0.0005	0.36	0.0495	0.0026	155	9	154	3	173	123	89
VOEL	VOEL-70	1035	25	625	6652	0.60	0.165	0.008	0.0242	0.0005	0.43	0.0496	0.0022	155	8	154	3	177	102	87
VOEL	VOEL-71	1022	24	661	874	0.65	0.196	0.008	0.0239	0.0005	0.51	0.0595	0.0021	182	7	152	3	585	76	26
VOEL	VOEL-72	465	12	163	2274	0.35	0.174	0.010	0.0248	0.0005	0.38	0.0509	0.0026	163	9	158	3	237	119	67
VOEL	VOEL-73	798	19	353	8033	0.44	0.163	0.006	0.0238	0.0005	0.57	0.0499	0.0015	154	6	152	3	188	71	80
VOEL	VOEL-74	555	14	285	5202	0.51	0.166	0.006	0.0245	0.0005	0.60	0.0490	0.0014	156	6	156	3	148	67	105
VOEL	VOEL-75	999	24	538	3954	0.54	0.161	0.007	0.0236	0.0005	0.48	0.0495	0.0019	152	7	151	3	173	90	87
VOEL	VOEL-76	754	19	399	167625	0.53	0.166	0.007	0.0246	0.0005	0.48	0.0491	0.0019	156	7	157	3	152	92	103
VOEL	VOEL-77	1334	32	1265	3185	0.95	0.166	0.008	0.0242	0.0005	0.42	0.0495	0.0022	156	8	154	3	173	104	89
VOEL	VOEL-78	330	8	128	871	0.39	0.170	0.011	0.0249	0.0005	0.34	0.0495	0.0030	159	10	158	3	171	142	93
VOEL	VOEL-79	966	24	725	1356	0.75	0.167	0.008	0.0243	0.0005	0.47	0.0497	0.0020	156	7	155	3	179	95	87
VOEL	VOEL-80	873	21	515	191995	0.59	0.165	0.006	0.0243	0.0005	0.56	0.0493	0.0016	155	6	155	3	162	74	96
VOEL	VOEL-81	433	11	406	97503	0.94	0.171	0.011	0.0249	0.0005	0.33	0.0499	0.0030	160	10	159	3	188	142	84
VOEL	VOEL-82	394	10	155	1683	0.39	0.167	0.011	0.0241	0.0005	0.34	0.0501	0.0030	157	10	154	3	200	138	77
VOEL	VOEL-83	1072	25	681	1876	0.64	0.164	0.007	0.0237	0.0005	0.50	0.0502	0.0019	154	7	151	3	205	86	73
VOEL	VOEL-84	759	18	474	2445	0.62	0.162	0.009	0.0237	0.0005	0.38	0.0496	0.0026	152	9	151	3	174	121	87
VOEL	VOEL-85	501	12	265	1619	0.53	0.168	0.010	0.0240	0.0005	0.34	0.0510	0.0029	158	10	153	3	241	133	63
VOEL	VOEL-86	1149	27	621	667	0.54	0.173	0.010	0.0233	0.0005	0.37	0.0539	0.0028	162	9	149	3	367	115	40
VOEL	VOEL-87	501	12	239	1326	0.48	0.161	0.008	0.0233	0.0005	0.41	0.0501	0.0024	152	8	149	3	198	109	75
VOEL	VOEL-88	510	12	262	1764	0.51	0.164	0.010	0.0244	0.0005	0.36	0.0489	0.0027	154	9	155	3	143	130	109
VOEL	VOEL-89	239	6	122	3506	0.51	0.173	0.012	0.0242	0.0005	0.31	0.0520	0.0034	162	11	154	3	285	149	54
VOEL	VOEL-90	761	18	485	1719	0.64	0.165	0.007	0.0241	0.0005	0.50	0.0496	0.0018	155	6	153	3	176	85	87
VOEL	VOEL-91	691	16	521	2460	0.75	0.163	0.007	0.0238	0.0005	0.47	0.0497	0.0020	154	7	152	3	181	93	84
VOEL	VOEL-92	425	10	167	2443	0.39	0.172	0.008	0.0247	0.0005	0.43	0.0505	0.0022	161	8	157	3	217	102	72
VOEL	VOEL-93	599	15	451	131134	0.75	0.165	0.006	0.0243	0.0005	0.61	0.0491	0.0014	155	5	155	3	153	66	101
VOEL	VOEL-94	748	18	690	1141	0.92	0.169	0.008	0.0237	0.0005	0.45	0.0519	0.0022	159	8	151	3	281	97	54
VOEL	VOEL-95	570	14	332	1154	0.58	0.179	0.011	0.0244	0.0005	0.34	0.0532	0.0032	167	11	155	3	339	134	46
VOEL	VOEL-96	578	15	573	2261	0.99	0.172	0.007	0.0252	0.0005	0.50	0.0496	0.0018	161	7	160	3	175	86	92
VOEL	VOEL-97	741	18	372	4495	0.50	0.171	0.007	0.0239	0.0005	0.50	0.0519	0.0019	160	7	152	3	280	84	54
VOEL	VOEL-98	510	12	253	8337	0.50	0.165	0.006	0.0243	0.0005	0.56	0.0493	0.0016	155	6	155	3	163	74	95
VOEL	VOEL-100	1295	30	725	525	0.56	0.158	0.012	0.0232	0.0005	0.29	0.0495	0.0036	149	11	148	3	171	169	87
VOEL	VOEL-101	366	9	286	6316	0.78	0.169	0.007	0.0249	0.0005	0.49	0.0492	0.0019	158	7	158	3	159	90	99

VOEL	VOEL-102	635	15	328	3531	0.52	0.171	0.008	0.0239	0.0005	0.43	0.0521	0.0023	161	8	152	3	288	100	53
VOEL	VOEL-103	911	22	584	8934	0.64	0.169	0.006	0.0246	0.0005	0.60	0.0499	0.0014	159	6	157	3	189	66	83
VOEL	VOEL-104	759	18	475	2457	0.63	0.160	0.008	0.0233	0.0005	0.43	0.0498	0.0023	151	8	149	3	184	106	81
VOEL	VOEL-105	679	16	365	4923	0.54	0.164	0.006	0.0241	0.0005	0.58	0.0495	0.0015	154	6	153	3	171	71	90
VOEL	VOEL-106	1546	36	2393	730	1.55	0.175	0.010	0.0235	0.0005	0.39	0.0541	0.0028	164	9	150	3	377	115	40
VOEL	VOEL-107	1159	27	598	1602	0.52	0.164	0.007	0.0230	0.0005	0.49	0.0520	0.0019	155	7	146	3	285	84	51
VOEL	VOEL-108	458	11	191	101448	0.42	0.166	0.006	0.0246	0.0005	0.57	0.0490	0.0015	156	6	157	3	146	71	107
VOEL	VOEL-109	1099	26	1227	2045	1.12	0.161	0.006	0.0237	0.0005	0.55	0.0493	0.0016	152	6	151	3	162	74	93
VOEL	VOEL-110	431	11	171	1888	0.40	0.169	0.009	0.0246	0.0005	0.41	0.0498	0.0023	159	8	157	3	187	109	84
VOEL	VOEL-111	820	20	476	179489	0.58	0.165	0.006	0.0244	0.0005	0.63	0.0491	0.0013	155	5	155	3	150	62	103
VOEL	VOEL-112	758	19	502	5472	0.66	0.174	0.010	0.0254	0.0005	0.38	0.0496	0.0025	163	9	162	3	176	119	92
VOEL	VOEL-113	517	13	249	113789	0.48	0.166	0.006	0.0245	0.0005	0.56	0.0491	0.0015	156	6	156	3	153	73	102
VOEL	VOEL-114	225	5	116	834	0.51	0.171	0.013	0.0233	0.0005	0.29	0.0533	0.0039	161	12	149	3	343	165	43
VOEL	VOEL-115	567	14	248	890	0.44	0.172	0.012	0.0239	0.0005	0.31	0.0521	0.0035	161	11	152	3	289	154	53

[a]U and Pb concentrations and Th/U ratios are calculated relative to GJ-1 reference zircon

[b]Corrected for background and within-run Pb/U fractionation and normalised to reference zircon GJ-1 (ID-TIMS values/measured value); $^{207}Pb/^{235}U$ calculated using ($^{207}Pb/^{206}Pb$)/($^{238}U/^{206}Pb$ * 1/137.88)

[c]Rho is the error correlation defined as the quotient of the propagated errors of the $^{206}Pb/^{238}U$ and the $^{207}/^{235}U$ ratio

[d]Quadratic addition of within-run errors (2 SD) and daily reproducibility of GJ-1 (2 SD)

[e]Corrected for mass-bias by normalising to GJ-1 reference zircon (~0.6 per atomic mass unit) and common Pb using the model Pb composition of Stacey & Kramers (1975)

Table D14. LA-ICPMS isotopic data for sample CALI in the Oudsthoorn Basin

CALI								RATIOS							AGES [Ma]						Conc.
Sample	Analysis	Analysis	U [ppm][a]	Pb [ppm][a]	Th [ppm]	$^{206}Pb/^{204}Pb$	Th/U meas	$^{207}Pb/^{235}U$[b]	2 σ[d]	$^{206}Pb/^{238}U$[b]	2 σ[d]	rho[c]	$^{207}Pb/^{206}Pb$[e]	2 σ[d]	$^{207}Pb/^{235}U$	2 σ	$^{206}Pb/^{238}U$	2 σ	$^{207}Pb/^{206}Pb$	2 σ	%
CALI	LI-1	A_126	117	3	66	16403	0.56	0.165	0.032	0.02428	0.00064	0.14	0.0494	0.0093	155	30	155	4	164	441	94
CALI	LI-2	A_127	150	4	96	21379	0.64	0.168	0.017	0.02468	0.00064	0.25	0.0494	0.0049	158	16	157	4	165	232	95
CALI	LI-3	A_128	214	5	181	30426	0.84	0.167	0.015	0.02460	0.00062	0.27	0.0493	0.0044	157	14	157	4	163	207	96
CALI	LI-4	A_129	133	3	84	848	0.63	0.162	0.017	0.02375	0.00062	0.25	0.0495	0.0050	153	16	151	4	173	236	87
CALI	LI-9	A_134	130	3	83	986	0.63	0.164	0.032	0.02429	0.00064	0.13	0.0488	0.0096	154	31	155	4	139	462	111
CALI	LI-11	A_136	298	7	222	41662	0.75	0.165	0.012	0.02425	0.00060	0.35	0.0492	0.0032	155	11	154	4	158	153	98
CALI	LI-12	A_137	323	8	290	548	0.90	0.160	0.019	0.02371	0.00060	0.21	0.0489	0.0056	151	18	151	4	142	270	106
CALI	LI-13	A_140	177	4	120	1529	0.68	0.165	0.019	0.02400	0.00062	0.22	0.0498	0.0057	155	18	153	4	188	268	82
CALI	LI-14	A_141	178	4	157	24509	0.88	0.162	0.020	0.02392	0.00062	0.21	0.0492	0.0059	153	19	152	4	159	278	96
CALI	LI-15	A_142	404	10	332	56583	0.82	0.164	0.011	0.02431	0.00060	0.37	0.0489	0.0030	154	10	155	4	142	146	109
CALI	LI-16	A_143	327	8	386	4233	1.18	0.166	0.010	0.02457	0.00062	0.40	0.0491	0.0028	156	10	156	4	150	134	104
CALI	LI-18	A_145	160	4	137	1194	0.86	0.164	0.022	0.02409	0.00062	0.19	0.0493	0.0064	154	21	153	4	161	306	95
CALI	LI-19	A_146	170	4	143	1425	0.84	0.165	0.011	0.02414	0.00062	0.39	0.0495	0.0030	155	10	154	4	169	144	91
CALI	LI-20	A_147	888	22	835	124242	0.94	0.166	0.009	0.02427	0.00060	0.46	0.0496	0.0024	156	8	155	4	177	113	87
CALI	LI-21	A_148	87	2	74	12258	0.85	0.164	0.043	0.02433	0.00068	0.11	0.0490	0.0128	154	41	155	4	147	615	106
CALI	LI-22	A_149	131	3	91	17851	0.69	0.161	0.028	0.02359	0.00062	0.15	0.0494	0.0084	151	26	150	4	167	396	90
CALI	LI-23	A_150	144	3	102	19888	0.71	0.163	0.016	0.02401	0.00064	0.27	0.0493	0.0047	153	15	153	4	160	223	96
CALI	LI-24	A_151	138	3	111	18920	0.81	0.161	0.016	0.02377	0.00062	0.27	0.0491	0.0046	152	15	151	4	153	220	99
CALI	LI-25	A_152	126	3	74	324	0.59	0.160	0.025	0.02356	0.00062	0.17	0.0493	0.0076	151	24	150	4	160	361	94
CALI	LI-26	A_153	146	3	88	20111	0.60	0.163	0.014	0.02388	0.00062	0.30	0.0494	0.0041	153	13	152	4	166	195	91
CALI	LI-28	A_161	210	5	179	2946	0.85	0.163	0.012	0.02392	0.00062	0.34	0.0495	0.0036	154	12	152	4	173	168	88
CALI	LI-29	A_162	154	4	94	20997	0.61	0.162	0.017	0.02373	0.00062	0.25	0.0495	0.0050	152	16	151	4	172	234	88
CALI	LI-31	A_164	136	3	82	2166	0.60	0.163	0.015	0.02386	0.00064	0.30	0.0494	0.0042	153	14	152	4	168	200	91
CALI	LI-32	A_165	200	5	132	2016	0.66	0.161	0.014	0.02375	0.00062	0.30	0.0493	0.0042	152	13	151	4	162	197	93
CALI	LI-33	A_166	201	5	148	27311	0.74	0.162	0.010	0.02367	0.00060	0.42	0.0497	0.0028	153	9	151	4	182	129	83
CALI	LI-34	A_167	155	4	105	20542	0.68	0.157	0.016	0.02305	0.00060	0.25	0.0495	0.0050	148	15	147	4	171	236	86
CALI	LI-35	A_168	85	2	56	11696	0.65	0.161	0.023	0.02384	0.00066	0.20	0.0489	0.0067	151	21	152	4	141	324	108
CALI	LI-36	A_169	193	5	162	26528	0.84	0.164	0.012	0.02389	0.00062	0.34	0.0497	0.0036	154	12	152	4	181	167	84
CALI	LI-37	A_170	221	5	150	1100	0.68	0.163	0.012	0.02387	0.00062	0.34	0.0495	0.0035	153	12	152	4	169	165	90
CALI	LI-38	A_171	153	4	122	21147	0.80	0.164	0.015	0.02408	0.00064	0.29	0.0495	0.0044	154	14	153	4	171	209	90
CALI	LI-39	A_174	124	3	71	723	0.57	0.165	0.022	0.02440	0.00066	0.20	0.0492	0.0064	155	21	155	4	156	305	100
CALI	LI-41	A_176	118	3	70	16642	0.59	0.167	0.016	0.02454	0.00066	0.29	0.0493	0.0044	157	15	156	4	164	209	96
CALI	LI-42	A_177	167	4	112	3133	0.67	0.161	0.013	0.02367	0.00062	0.33	0.0493	0.0036	151	12	151	4	162	173	93
CALI	LI-43	A_178	490	12	439	26394	0.90	0.164	0.008	0.02413	0.00060	0.50	0.0493	0.0021	154	8	154	4	161	101	95
CALI	LI-49	A_184	135	3	85	778	0.63	0.160	0.015	0.02373	0.00062	0.28	0.0490	0.0044	151	14	151	4	147	212	103
CALI	LI-50	A_185	120	3	68	16498	0.57	0.163	0.013	0.02389	0.00064	0.33	0.0496	0.0039	154	13	152	4	177	181	86
CALI	LI-52	A_187	188	4	130	25640	0.69	0.162	0.015	0.02375	0.00062	0.28	0.0496	0.0045	153	14	151	4	174	211	87
CALI	LI-53	A_188	182	4	137	24670	0.75	0.161	0.018	0.02364	0.00062	0.24	0.0493	0.0053	151	17	151	4	160	251	94
CALI	LI-54	A_191	70	2	34	632	0.49	0.162	0.028	0.02392	0.00068	0.16	0.0490	0.0083	152	26	152	4	146	399	104
CALI	LI-55	A_192	100	2	76	140	0.76	0.155	0.029	0.02299	0.00064	0.15	0.0489	0.0091	146	28	147	4	144	437	102
CALI	LI-56	A_193	165	4	118	518	0.72	0.161	0.014	0.02376	0.00062	0.29	0.0493	0.0042	152	13	151	4	161	198	94
CALI	LI-57	A_194	177	4	120	24635	0.68	0.167	0.018	0.02424	0.00062	0.23	0.0498	0.0053	156	17	154	4	188	248	82
CALI	LI-58	A_195	206	5	166	28085	0.81	0.161	0.012	0.02380	0.00062	0.35	0.0491	0.0034	152	11	152	4	154	164	99
CALI	LI-59	A_196	125	3	74	866	0.59	0.165	0.012	0.02423	0.00064	0.38	0.0493	0.0032	155	11	154	4	160	152	97
CALI	LI-60	A_197	281	7	303	1594	1.08	0.168	0.011	0.02456	0.00062	0.38	0.0495	0.0030	157	10	156	4	173	143	90
CALI	LI-61	A_198	121	3	74	16320	0.62	0.160	0.016	0.02352	0.00064	0.28	0.0494	0.0047	151	15	150	4	168	220	89
CALI	LI-62	A_199	95	2	53	13114	0.56	0.164	0.017	0.02406	0.00066	0.26	0.0496	0.0050	155	16	153	4	175	234	87
CALI	LI-63	A_200	399	10	297	2377	0.74	0.171	0.009	0.02510	0.00062	0.47	0.0494	0.0023	160	9	160	4	166	110	96
CALI	LI-64	A_201	592	14	452	79601	0.76	0.161	0.007	0.02344	0.00058	0.53	0.0497	0.0020	151	7	149	4	180	92	83
CALI	LI-66	A_203	124	3	71	17258	0.57	0.166	0.015	0.02437	0.00066	0.30	0.0494	0.0042	156	14	155	4	165	200	94
CALI	LI-67	A_204	384	10	282	1898	0.73	0.166	0.020	0.02479	0.00062	0.20	0.0485	0.0058	156	19	158	4	124	283	128
CALI	LI-68	A_205	160	4	121	268	0.76	0.161	0.013	0.02371	0.00062	0.32	0.0493	0.0038	152	12	151	4	164	182	92
CALI	LI-69	A_212	151	4	100	20872	0.66	0.164	0.019	0.02415	0.00064	0.22	0.0492	0.0057	154	18	154	4	157	270	98
CALI	LI-79	A_222	172	4	119	1433	0.70	0.163	0.021	0.02376	0.00062	0.21	0.0499	0.0062	154	19	151	4	188	288	80
CALI	LI-83	A_228	122	3	78	386	0.64	0.166	0.029	0.02435	0.00066	0.16	0.0496	0.0085	156	27	155	4	174	402	89
CALI	LI-84	A_229	103	3	61	7246	0.59	0.169	0.016	0.02461	0.00066	0.28	0.0499	0.0046	159	15	157	4	188	213	83
CALI	LI-85	A_230	860	21	872	121654	1.01	0.168	0.008	0.02475	0.00062	0.52	0.0491	0.0020	157	8	158	4	153	96	103
CALI	LI-86	A_231	207	5	173	617	0.83	0.166	0.017	0.02460	0.00064	0.25	0.0490	0.0049	156	16	157	4	146	236	107
CALI	LI-90	A_235	101	2	64	336	0.63	0.166	0.017	0.02421	0.00066	0.26	0.0498	0.0050	156	16	154	4	184	236	84
CALI	LI-92	A_237	200	5	152	1209	0.76	0.165	0.010	0.02446	0.00064	0.45	0.0491	0.0026	155	9	156	4	150	123	104
CALI	LI-93	A_238	108	3	62	1403	0.58	0.163	0.013	0.02391	0.00066	0.35	0.0493	0.0037	153	12	152	4	164	175	93
CALI	LI-94	A_239	270	6	201	36492	0.74	0.161	0.015	0.02363	0.00060	0.27	0.0493	0.0044	151	14	151	4	162	210	93
CALI	LI-95	A_242	98	2	62	1373	0.63	0.160	0.024	0.02362	0.00066	0.19	0.0492	0.0071	151	22	150	4	158	339	95
CALI	LI-96	A_243	153	4	103	592	0.67	0.164	0.016	0.02373	0.00062	0.27	0.0501	0.0047	154	15	151	4	198	217	76
CALI	LI-97	A_244	247	6	177	34242	0.71	0.165	0.014	0.02427	0.00062	0.30	0.0492	0.0040	155	13	155	4	159	189	97
CALI	LI-99	A_246	115	3	72	1131	0.63	0.161	0.018	0.02376	0.00064	0.24	0.0493	0.0053	152	17	151	4	161	253	94

CALI	LI-100	A_247	154	4	109	20452	0.71	0.159	0.015	0.02333	0.00062	0.27	0.0493	0.0046	149	15	149	4	162	218	92
CALI	LI-101	A_248	122	3	69	16956	0.57	0.164	0.015	0.02430	0.00066	0.30	0.0490	0.0042	154	14	155	4	148	200	105
CALI	LI-102	A_249	122	3	79	560	0.65	0.165	0.015	0.02410	0.00064	0.30	0.0496	0.0042	155	14	154	4	175	198	88
CALI	LI-103	A_250	157	4	95	21578	0.61	0.165	0.018	0.02405	0.00064	0.24	0.0496	0.0053	155	17	153	4	177	248	86
CALI	LI-104	A_251	735	18	737	62518	1.00	0.165	0.009	0.02433	0.00060	0.48	0.0492	0.0022	155	8	155	4	157	107	98
CALI	LI-105	A_252	127	3	84	626	0.66	0.164	0.017	0.02373	0.00064	0.26	0.0500	0.0050	154	16	151	4	194	233	78
CALI	LI-106	A_253	236	6	201	32908	0.85	0.168	0.021	0.02444	0.00062	0.20	0.0497	0.0061	157	20	156	4	181	287	86
CALI	LI-108	A_255	107	3	62	671	0.58	0.162	0.022	0.02388	0.00066	0.20	0.0492	0.0066	153	21	152	4	158	312	96
CALI	LI-109	A_256	119	3	66	917	0.55	0.164	0.012	0.02413	0.00066	0.38	0.0494	0.0033	154	11	154	4	164	154	93
CALI	LI-110	A_262	123	3	78	16950	0.63	0.165	0.023	0.02409	0.00064	0.19	0.0495	0.0069	155	22	153	4	173	326	89
CALI	LI-111	A_263	207	5	160	28401	0.77	0.162	0.014	0.02405	0.00062	0.30	0.0489	0.0040	153	13	153	4	143	192	107
CALI	LI-114	A_266	119	3	70	487	0.59	0.160	0.013	0.02360	0.00064	0.33	0.0491	0.0038	151	12	150	4	154	183	98
CALI	LI-115	A_267	168	4	117	22173	0.70	0.157	0.011	0.02322	0.00062	0.38	0.0490	0.0031	148	10	148	4	148	150	100
CALI	LI-116	A_268	96	2	53	13249	0.55	0.166	0.020	0.02414	0.00066	0.23	0.0499	0.0058	156	19	154	4	189	271	81
CALI	LI-118	A_270	180	4	150	403	0.83	0.166	0.018	0.02432	0.00064	0.24	0.0496	0.0052	156	17	155	4	175	246	89
CALI	LI-119	A_271	143	3	94	19334	0.66	0.161	0.013	0.02380	0.00064	0.33	0.0491	0.0038	152	12	152	4	152	179	100
CALI	LI-120	A_272	148	3	107	779	0.73	0.158	0.023	0.02330	0.00062	0.18	0.0493	0.0070	149	22	148	4	163	331	91

[a]U and Pb concentrations and Th/U ratios are calculated relative to GJ-1 reference zircon

[b]Corrected for background and within-run Pb/U fractionation and normalised to reference zircon GJ-1 (ID-TIMS values/measured value); $^{207}Pb/^{235}U$ calculated using ($^{207}Pb/^{206}Pb$)/($^{238}U/^{206}Pb$ * 1/137.88)

[c]Rho is the error correlation defined as the quotient of the propagated errors of the $^{206}Pb/^{238}U$ and the $^{207}/^{235}U$ ratio

[d]Quadratic addition of within-run errors (2 SD) and daily reproducibility of GJ-1 (2 SD)

[e]Corrected for mass-bias by normalising to GJ-1 reference zircon (~0.6 per atomic mass unit) and common Pb using the model Pb composition of Stacey & Kramers (1975)

Table D15. LA-ICPMS isotopic data for sample DERU in the Oudsthoorn Basin

DERU							RATIOS							AGES [Ma]						Conc.
Sample	Analysis	U [ppm][a]	Pb [ppm][a]	Th [ppm][a]	$^{206}Pb/^{204}Pb$	Th/U[a]	$^{207}Pb/^{235}U$[b]	2 σ[d]	$^{206}Pb/^{238}U$[b]	2 σ[d]	rho[c]	$^{207}Pb/^{206}Pb$[e]	2 σ[d]	$^{207}Pb/^{235}U$	2 σ	$^{206}Pb/^{238}U$	2 σ	$^{207}Pb/^{206}Pb$	2 σ	%
DERU	DERU-1	117	3	69	1088	0.59	0.206	0.014	0.0291	0.0007	0.32	0.0515	0.0034	190	13	185	4	261	153	71
DERU	DERU-2	237	19	122	182887	0.51	0.659	0.024	0.0819	0.0018	0.60	0.0583	0.0017	514	19	508	11	542	64	94
DERU	DERU-3	238	7	120	1936	0.50	0.209	0.008	0.0304	0.0007	0.56	0.0498	0.0016	192	8	193	4	188	76	103
DERU	DERU-5	120	4	269	227	2.24	0.290	0.047	0.0304	0.0007	0.14	0.0691	0.0110	259	42	193	4	902	328	21
DERU	DERU-6	101	3	180	28429	1.78	0.210	0.026	0.0299	0.0007	0.18	0.0509	0.0062	193	24	190	4	234	280	81
DERU	DERU-7	148	4	282	40296	1.91	0.214	0.017	0.0290	0.0006	0.27	0.0536	0.0042	197	16	184	4	356	176	52
DERU	DERU-8	211	17	73	2666	0.35	0.647	0.033	0.0811	0.0019	0.46	0.0579	0.0026	507	26	503	12	525	99	96
DERU	DERU-9	121	4	248	1125	2.04	0.226	0.035	0.0303	0.0007	0.14	0.0540	0.0084	207	32	193	4	371	350	52
DERU	DERU-10	287	9	260	1011	0.91	0.214	0.012	0.0297	0.0006	0.39	0.0522	0.0026	197	11	189	4	292	116	65
DERU	DERU-11	684	32	483	28485	0.71	0.342	0.012	0.0464	0.0010	0.62	0.0534	0.0014	298	10	292	6	345	61	85
DERU	DERU-12	309	12	108	113777	0.35	0.276	0.017	0.0391	0.0010	0.39	0.0512	0.0030	247	16	247	6	251	134	99
DERU	DERU-13	463	14	251	1809	0.54	0.218	0.011	0.0298	0.0006	0.43	0.0531	0.0024	200	10	189	4	333	103	57
DERU	DERU-14	387	12	490	10176	1.27	0.210	0.014	0.0305	0.0007	0.34	0.0500	0.0030	194	13	194	4	195	141	99
DERU	DERU-15	95	4	48	1898	0.51	0.279	0.022	0.0392	0.0010	0.33	0.0517	0.0039	250	20	248	7	270	172	92
DERU	DERU-16	313	23	170	219332	0.55	0.611	0.028	0.0747	0.0017	0.50	0.0594	0.0023	484	22	464	11	580	85	80
DERU	DERU-17	254	13	192	55967	0.76	0.380	0.018	0.0512	0.0012	0.49	0.0539	0.0022	327	15	322	7	365	91	88
DERU	DERU-18	228	37	73	2085	0.32	1.747	0.061	0.1613	0.0035	0.63	0.0786	0.0021	1026	36	964	21	1161	54	83
DERU	DERU-19	225	7	86	62053	0.38	0.200	0.008	0.0294	0.0006	0.55	0.0494	0.0016	185	7	187	4	168	78	111
DERU	DERU-20	473	14	323	1706	0.68	0.201	0.010	0.0288	0.0006	0.43	0.0506	0.0023	186	9	183	4	221	104	83
DERU	DERU-22	289	8	127	2926	0.44	0.204	0.013	0.0294	0.0006	0.34	0.0505	0.0030	189	12	187	4	216	139	86
DERU	DERU-23	133	4	57	1491	0.43	0.214	0.012	0.0307	0.0007	0.38	0.0507	0.0027	197	11	195	4	227	124	86
DERU	DERU-24	632	25	436	234645	0.69	0.280	0.011	0.0396	0.0009	0.55	0.0513	0.0017	251	10	250	5	255	75	98
DERU	DERU-25	228	12	183	40910	0.80	0.416	0.022	0.0543	0.0013	0.44	0.0555	0.0027	353	19	341	8	433	107	79
DERU	DERU-26	129	4	224	1028	1.74	0.195	0.028	0.0288	0.0008	0.20	0.0491	0.0069	181	26	183	5	152	330	120
DERU	DERU-27	270	12	240	626	0.89	0.371	0.022	0.0443	0.0011	0.41	0.0608	0.0033	320	19	279	7	630	116	44
DERU	DERU-28	250	21	80	22674	0.32	0.660	0.022	0.0825	0.0018	0.66	0.0580	0.0014	515	17	511	11	531	54	96
DERU	DERU-29	331	9	165	609	0.50	0.210	0.018	0.0284	0.0006	0.25	0.0537	0.0045	194	17	181	4	359	187	50
DERU	DERU-30	273	17	456	157440	1.67	0.461	0.015	0.0616	0.0013	0.64	0.0543	0.0014	385	13	385	8	384	58	100
DERU	DERU-31	372	11	132	27042	0.36	0.209	0.012	0.0303	0.0007	0.39	0.0501	0.0026	193	11	192	4	198	119	97
DERU	DERU-32	417	37	38	43119	0.09	0.713	0.024	0.0881	0.0019	0.63	0.0587	0.0015	546	19	544	12	555	57	98
DERU	DERU-33	111	9	89	773	0.80	0.653	0.045	0.0804	0.0021	0.38	0.0589	0.0038	510	36	498	13	564	140	88
DERU	DERU-34	313	10	205	451	0.65	0.262	0.018	0.0305	0.0007	0.31	0.0622	0.0041	236	17	194	4	682	142	28
DERU	DERU-36	572	24	313	2022	0.55	0.334	0.016	0.0421	0.0010	0.48	0.0574	0.0025	292	14	266	6	508	94	52
DERU	DERU-37	65	3	55	10107	0.84	0.329	0.037	0.0461	0.0015	0.28	0.0518	0.0056	289	33	290	9	277	249	105
DERU	DERU-38	203	16	101	1679	0.50	0.616	0.030	0.0768	0.0018	0.47	0.0582	0.0025	487	24	477	11	538	95	89
DERU	DERU-39	469	20	253	183115	0.54	0.321	0.017	0.0418	0.0010	0.44	0.0556	0.0027	282	15	264	6	438	107	60
DERU	DERU-40	92	8	50	1373	0.54	0.666	0.047	0.0829	0.0022	0.37	0.0583	0.0038	518	36	514	13	540	143	95
DERU	DERU-43	59	5	25	614	0.42	0.762	0.046	0.0904	0.0022	0.41	0.0612	0.0034	575	35	558	14	645	118	87
DERU	DERU-44	393	27	178	1965	0.45	0.555	0.027	0.0685	0.0016	0.48	0.0588	0.0025	448	22	427	10	560	93	76
DERU	DERU-45	310	9	445	84162	1.43	0.202	0.010	0.0290	0.0006	0.44	0.0504	0.0022	186	9	185	4	211	103	87
DERU	DERU-46	415	18	138	5812	0.33	0.308	0.010	0.0432	0.0009	0.64	0.0516	0.0013	272	9	273	6	268	60	102
DERU	DERU-47	522	15	191	658	0.37	0.203	0.012	0.0290	0.0006	0.35	0.0507	0.0029	187	11	184	4	227	132	81
DERU	DERU-48	136	4	91	1027	0.67	0.216	0.025	0.0302	0.0007	0.20	0.0518	0.0058	198	23	192	4	277	256	69
DERU	DERU-49	419	18	248	860	0.59	0.336	0.015	0.0434	0.0010	0.49	0.0562	0.0022	294	13	274	6	459	88	60
DERU	DERU-50	156	7	108	22379	0.69	0.307	0.013	0.0429	0.0010	0.52	0.0518	0.0019	272	12	271	6	278	84	98
DERU	DERU-54	116	3	136	312	1.17	0.240	0.041	0.0301	0.0007	0.13	0.0577	0.0099	218	38	191	4	520	375	37
DERU	DERU-57	346	25	118	5385	0.34	0.554	0.020	0.0716	0.0016	0.60	0.0561	0.0016	447	16	446	10	455	65	98

DERU	DERU-60	242	11	158	106009	0.65	0.349	0.021	0.0472	0.0011	0.41	0.0536	0.0029	304	18	297	7	355	121	84
DERU	DERU-63	122	11	57	98427	0.47	0.701	0.036	0.0872	0.0021	0.46	0.0583	0.0027	539	28	539	13	539	100	100
DERU	DERU-64	154	13	88	117688	0.57	0.652	0.023	0.0825	0.0018	0.62	0.0574	0.0016	510	18	511	11	505	61	101
DERU	DERU-65	269	51	108	4779	0.40	2.011	0.063	0.1901	0.0041	0.69	0.0767	0.0017	1119	35	1122	24	1113	45	101
DERU	DERU-66	678	20	412	905	0.61	0.200	0.010	0.0291	0.0006	0.44	0.0499	0.0023	185	9	185	4	192	105	96
DERU	DERU-67	322	10	641	7090	1.99	0.211	0.019	0.0298	0.0007	0.25	0.0512	0.0044	194	17	189	4	250	200	76
DERU	DERU-70	263	8	97	10507	0.37	0.200	0.008	0.0292	0.0006	0.52	0.0498	0.0018	185	8	185	4	186	83	100
DERU	DERU-71	591	24	382	1555	0.65	0.324	0.016	0.0411	0.0010	0.47	0.0573	0.0025	285	14	259	6	502	97	52
DERU	DERU-74	289	9	88	1904	0.30	0.204	0.015	0.0296	0.0007	0.30	0.0499	0.0035	188	14	188	4	191	164	98
DERU	DERU-75	990	29	792	137	0.80	0.267	0.017	0.0295	0.0006	0.34	0.0657	0.0039	240	15	187	4	796	126	24
DERU	DERU-76	344	29	64	1874	0.19	0.719	0.028	0.0847	0.0019	0.58	0.0616	0.0019	550	21	524	12	660	67	79
DERU	DERU-77	164	7	66	65047	0.40	0.311	0.017	0.0428	0.0010	0.44	0.0527	0.0026	275	15	270	6	314	111	86
DERU	DERU-78	254	8	233	70471	0.92	0.207	0.010	0.0300	0.0007	0.44	0.0501	0.0022	191	10	191	4	198	104	96
DERU	DERU-79	128	4	214	882	1.67	0.212	0.018	0.0287	0.0007	0.28	0.0535	0.0043	195	16	182	4	350	180	52
DERU	DERU-83	306	15	194	135289	0.63	0.349	0.020	0.0478	0.0012	0.43	0.0529	0.0027	304	17	301	7	324	117	93
DERU	DERU-84	179	5	83	3212	0.46	0.205	0.010	0.0292	0.0007	0.45	0.0509	0.0023	189	10	185	4	234	104	79
DERU	DERU-86	683	85	121	11508	0.18	1.115	0.035	0.1252	0.0027	0.70	0.0646	0.0014	761	24	760	17	762	47	100
DERU	DERU-88	293	8	243	21032	0.83	0.198	0.008	0.0289	0.0006	0.56	0.0495	0.0016	183	7	184	4	173	76	106
DERU	DERU-89	260	14	131	1069	0.50	0.484	0.028	0.0520	0.0013	0.43	0.0675	0.0035	401	23	327	8	854	107	38
DERU	DERU-90	192	8	261	1944	1.36	0.302	0.024	0.0404	0.0011	0.35	0.0542	0.0040	268	21	255	7	379	166	67
DERU	DERU-92	201	6	55	1645	0.27	0.206	0.010	0.0299	0.0007	0.48	0.0500	0.0021	191	9	190	4	197	98	97
DERU	DERU-93	228	9	93	3903	0.41	0.308	0.025	0.0405	0.0011	0.34	0.0550	0.0042	272	22	256	7	414	170	62
DERU	DERU-94	427	13	692	1804	1.62	0.204	0.010	0.0293	0.0006	0.46	0.0504	0.0021	188	9	186	4	212	97	88
DERU	DERU-95	380	11	362	224	0.95	0.220	0.015	0.0287	0.0006	0.32	0.0556	0.0037	202	14	182	4	435	149	42
DERU	DERU-96	432	19	327	3178	0.76	0.318	0.011	0.0442	0.0010	0.62	0.0521	0.0015	280	10	279	6	289	64	97
DERU	DERU-98	455	14	241	607	0.53	0.233	0.014	0.0302	0.0007	0.37	0.0558	0.0031	212	13	192	4	445	123	43
DERU	DERU-99	284	19	117	4875	0.41	0.563	0.037	0.0663	0.0017	0.39	0.0616	0.0038	454	30	414	11	662	131	63
DERU	DERU-100	255	8	131	69041	0.51	0.207	0.012	0.0294	0.0007	0.37	0.0511	0.0029	191	12	187	4	246	129	76
DERU	DERU-101	432	13	367	874	0.85	0.204	0.011	0.0291	0.0006	0.40	0.0507	0.0026	188	10	185	4	228	118	81
DERU	DERU-102	379	15	175	2115	0.46	0.297	0.021	0.0404	0.0010	0.36	0.0533	0.0035	264	19	255	7	340	149	75
DERU	DERU-103	338	14	196	2281	0.58	0.285	0.013	0.0401	0.0009	0.50	0.0515	0.0021	254	12	253	6	264	92	96
DERU	DERU-104	92	3	163	719	1.77	0.229	0.029	0.0298	0.0007	0.19	0.0557	0.0069	209	26	189	4	440	274	43
DERU	DERU-105	118	3	208	1767	1.77	0.205	0.011	0.0295	0.0007	0.43	0.0505	0.0024	190	10	187	4	220	112	85
DERU	DERU-106	236	18	187	2956	0.79	0.604	0.026	0.0763	0.0017	0.53	0.0574	0.0021	479	21	474	11	507	81	93
DERU	DERU-107	324	10	717	376	2.22	0.209	0.018	0.0302	0.0007	0.26	0.0501	0.0042	193	17	192	4	201	193	95
DERU	DERU-109	195	38	171	349712	0.88	2.109	0.084	0.1951	0.0045	0.58	0.0784	0.0025	1152	46	1149	26	1158	64	99
DERU	DERU-110	260	8	341	1988	1.31	0.201	0.008	0.0295	0.0007	0.55	0.0495	0.0017	186	8	188	4	170	79	110
DERU	DERU-111	79	6	63	51908	0.80	0.561	0.053	0.0720	0.0022	0.32	0.0565	0.0050	452	42	448	13	474	196	95
DERU	DERU-113	89	3	99	4068	1.10	0.197	0.023	0.0284	0.0007	0.20	0.0503	0.0058	182	22	180	4	210	269	86
DERU	DERU-114	625	19	813	825	1.30	0.209	0.008	0.0304	0.0007	0.58	0.0499	0.0015	193	7	193	4	189	72	102
DERU	DERU-115	495	15	449	2649	0.91	0.206	0.009	0.0300	0.0007	0.49	0.0497	0.0019	190	8	191	4	182	90	105

[a]U and Pb concentrations and Th/U ratios are calculated relative to GJ-1 reference zircon

[b]Corrected for background and within-run Pb/U fractionation and normalised to reference zircon GJ-1 (ID-TIMS values/measured value); $^{207}Pb/^{235}U$ calculated using $(^{207}Pb/^{206}Pb)/(^{238}U/^{206}Pb * 1/137.88)$

[c]Rho is the error correlation defined as the quotient of the propagated errors of the $^{206}Pb/^{238}U$ and the $^{207}/^{235}U$ ratio

[d]Quadratic addition of within-run errors (2 SD) and daily reproducibility of GJ-1 (2 SD)

[e]Corrected for mass-bias by normalising to GJ-1 reference zircon (~0.6 per atomic mass unit) and common Pb using the model Pb composition of Stacey & Kramers (1975)

Table D16. LA-ICPMS isotopic data for sample DERC1 in the Oudsthoorn Basin

DERC1							RATIOS							AGES [Ma]						Conc.
Sample	Analysis	U [ppm][a]	Pb [ppm][a]	Th [ppm][a]	$^{206}Pb/^{204}Pb$	Th/U[a]	$^{207}Pb/^{235}U^{b}$	2 σ[d]	$^{206}Pb/^{238}U^{b}$	2 σ[d]	rho[c]	$^{207}Pb/^{206}Pb^{e}$	2 σ[d]	$^{207}Pb/^{235}U$	2 σ	$^{206}Pb/^{238}U$	2 σ	$^{207}Pb/^{206}Pb$	2 σ	%
DERC1	DERC1-2	146	26	47	4888	0.32	1.836	0.050	0.1779	0.0026	0.53	0.0749	0.0017	1058	29	1055	15	1064	47	99
DERC1	DERC1-3	212	7	389	651	1.84	0.218	0.008	0.0314	0.0005	0.42	0.0504	0.0017	201	8	200	3	212	80	94
DERC1	DERC1-4	242	10	223	83743	0.92	0.306	0.015	0.0426	0.0007	0.36	0.0521	0.0024	271	13	269	5	288	104	93
DERC1	DERC1-5	479	19	345	150689	0.72	0.307	0.017	0.0388	0.0007	0.31	0.0574	0.0030	272	15	245	4	508	113	48
DERC1	DERC1-6	101	3	67	344	0.66	0.231	0.032	0.0296	0.0005	0.12	0.0566	0.0077	211	29	188	3	475	303	40
DERC1	DERC1-7	399	12	314	3400	0.79	0.201	0.008	0.0292	0.0004	0.37	0.0498	0.0019	186	8	186	3	185	89	100
DERC1	DERC1-8	366	11	220	1329	0.60	0.197	0.010	0.0288	0.0004	0.30	0.0497	0.0025	183	9	183	3	183	115	100
DERC1	DERC1-9	111	5	127	26628	1.14	0.294	0.018	0.0416	0.0008	0.32	0.0513	0.0030	262	16	263	5	256	133	103
DERC1	DERC1-10	251	7	398	692	1.59	0.201	0.016	0.0292	0.0004	0.19	0.0499	0.0040	186	15	185	3	192	185	96
DERC1	DERC1-12	136	4	174	9536	1.28	0.219	0.015	0.0315	0.0005	0.23	0.0504	0.0034	201	14	200	3	214	157	93
DERC1	DERC1-13	67	6	16	2206	0.24	0.793	0.032	0.0967	0.0016	0.41	0.0595	0.0022	593	24	595	10	585	80	102
DERC1	DERC1-14	78	2	141	374	1.82	0.203	0.032	0.0290	0.0005	0.12	0.0508	0.0080	188	30	184	3	232	364	79
DERC1	DERC1-15	390	12	402	98029	1.03	0.215	0.008	0.0310	0.0005	0.41	0.0503	0.0017	198	7	197	3	209	77	94
DERC1	DERC1-17	464	13	275	78226	0.59	0.199	0.007	0.0290	0.0004	0.44	0.0497	0.0015	184	6	184	3	181	72	102
DERC1	DERC1-18	94	3	172	740	1.83	0.203	0.016	0.0294	0.0005	0.24	0.0500	0.0037	188	14	187	3	196	174	95
DERC1	DERC1-19	243	7	242	2006	0.99	0.207	0.012	0.0288	0.0004	0.25	0.0523	0.0030	191	12	183	3	299	133	61
DERC1	DERC1-20	69	2	76	17561	1.10	0.217	0.012	0.0313	0.0006	0.34	0.0502	0.0026	199	11	198	4	205	120	97
DERC1	DERC1-21	296	17	140	2707	0.47	0.432	0.014	0.0580	0.0009	0.46	0.0540	0.0016	364	12	364	6	369	67	99
DERC1	DERC1-22	126	5	115	1021	0.91	0.252	0.015	0.0360	0.0007	0.33	0.0509	0.0028	228	13	228	4	234	126	97
DERC1	DERC1-23	79	2	88	2511	1.10	0.199	0.017	0.0289	0.0005	0.21	0.0501	0.0043	184	16	183	3	197	198	93
DERC1	DERC1-25	733	27	349	219176	0.48	0.262	0.012	0.0369	0.0006	0.36	0.0516	0.0022	236	11	233	4	266	100	88
DERC1	DERC1-26	346	10	348	236	1.01	0.237	0.022	0.0294	0.0004	0.16	0.0585	0.0055	216	20	187	3	549	204	34
DERC1	DERC1-27	214	6	254	51416	1.19	0.208	0.013	0.0297	0.0005	0.24	0.0509	0.0032	192	12	188	3	235	143	80
DERC1	DERC1-28	322	13	252	759	0.78	0.347	0.028	0.0401	0.0006	0.19	0.0628	0.0050	302	24	253	4	702	169	36
DERC1	DERC1-29	109	3	139	3398	1.28	0.202	0.017	0.0294	0.0005	0.21	0.0498	0.0040	187	15	187	3	186	186	101
DERC1	DERC1-30	280	8	295	713	1.05	0.198	0.015	0.0287	0.0004	0.20	0.0500	0.0037	184	14	183	3	195	172	94
DERC1	DERC1-31	60	2	79	14415	1.32	0.205	0.030	0.0297	0.0006	0.13	0.0502	0.0073	190	28	189	4	203	338	93
DERC1	DERC1-32	270	9	362	405	1.34	0.222	0.014	0.0319	0.0005	0.24	0.0506	0.0030	204	13	202	3	220	139	92
DERC1	DERC1-34	381	11	515	90232	1.35	0.200	0.008	0.0292	0.0004	0.38	0.0498	0.0018	186	7	186	3	186	85	100
DERC1	DERC1-35	165	5	296	41812	1.79	0.216	0.013	0.0312	0.0005	0.26	0.0501	0.0030	198	12	198	3	200	140	99
DERC1	DERC1-36	202	6	363	923	1.80	0.198	0.011	0.0289	0.0005	0.28	0.0498	0.0027	184	10	184	3	187	127	98
DERC1	DERC1-37	122	4	190	1239	1.55	0.218	0.012	0.0313	0.0005	0.29	0.0507	0.0027	201	11	199	3	225	121	88
DERC1	DERC1-40	228	17	151	134895	0.66	0.592	0.032	0.0730	0.0011	0.29	0.0589	0.0031	472	26	454	7	563	114	81
DERC1	DERC1-42	210	6	329	3262	1.56	0.200	0.011	0.0293	0.0005	0.30	0.0496	0.0025	186	10	186	3	175	118	107
DERC1	DERC1-44	167	5	295	7590	1.77	0.217	0.010	0.0313	0.0005	0.34	0.0503	0.0022	199	9	198	3	209	101	95
DERC1	DERC1-45	145	4	224	531	1.55	0.213	0.016	0.0296	0.0005	0.21	0.0522	0.0039	196	15	188	3	295	170	64
DERC1	DERC1-46	165	5	134	889	0.81	0.204	0.023	0.0295	0.0005	0.14	0.0502	0.0056	188	21	187	3	203	260	92
DERC1	DERC1-47	109	3	171	26027	1.57	0.202	0.026	0.0294	0.0005	0.13	0.0498	0.0062	187	24	187	3	187	291	100
DERC1	DERC1-48	494	15	415	1960	0.84	0.208	0.009	0.0302	0.0004	0.34	0.0498	0.0020	191	8	192	3	184	94	104
DERC1	DERC1-49	237	23	59	23325	0.25	0.797	0.024	0.0973	0.0014	0.50	0.0594	0.0015	595	18	599	9	580	56	103
DERC1	DERC1-51	242	8	231	400	0.95	0.252	0.021	0.0322	0.0005	0.19	0.0569	0.0046	229	19	204	3	489	177	42
DERC1	DERC1-52	108	3	263	2127	2.44	0.204	0.025	0.0295	0.0005	0.14	0.0501	0.0061	188	23	187	3	198	284	95
DERC1	DERC1-53	268	8	402	5202	1.50	0.201	0.007	0.0293	0.0004	0.43	0.0498	0.0016	186	6	186	3	183	73	101
DERC1	DERC1-54	45	1	69	9854	1.54	0.207	0.024	0.0303	0.0006	0.17	0.0496	0.0057	191	22	193	4	176	269	109
DERC1	DERC1-55	309	23	92	796	0.30	0.700	0.031	0.0745	0.0011	0.34	0.0681	0.0029	539	24	463	7	872	87	53
DERC1	DERC1-56	269	21	12	1843	0.04	0.685	0.029	0.0792	0.0013	0.40	0.0627	0.0024	530	22	491	8	698	82	70
DERC1	DERC1-57	99	3	147	24166	1.48	0.206	0.012	0.0300	0.0005	0.31	0.0497	0.0027	190	11	191	3	180	128	106

DERC1	DERC1-58	137	4	167	953	1.22	0.206	0.012	0.0301	0.0005	0.28	0.0498	0.0028	190	11	191	3	186	133	103
DERC1	DERC1-59	192	21	102	249262	0.53	0.921	0.054	0.1076	0.0022	0.35	0.0621	0.0034	663	39	659	13	678	116	97
DERC1	DERC1-60	186	6	176	44803	0.94	0.205	0.015	0.0297	0.0005	0.22	0.0501	0.0037	189	14	189	3	198	171	95
DERC1	DERC1-61	44	1	63	11212	1.44	0.219	0.017	0.0314	0.0006	0.26	0.0505	0.0037	201	15	199	4	219	169	91
DERC1	DERC1-62	62	2	86	14762	1.38	0.201	0.017	0.0293	0.0005	0.22	0.0499	0.0040	186	15	186	3	188	189	99
DERC1	DERC1-65	363	14	294	109340	0.81	0.260	0.017	0.0372	0.0008	0.31	0.0507	0.0032	235	15	236	5	227	145	104
DERC1	DERC1-66	144	4	175	1673	1.21	0.216	0.009	0.0312	0.0005	0.39	0.0501	0.0019	198	8	198	3	200	87	99
DERC1	DERC1-67	402	18	235	3285	0.58	0.332	0.010	0.0460	0.0007	0.48	0.0523	0.0014	291	9	290	4	300	61	97
DERC1	DERC1-68	76	2	106	7852	1.39	0.208	0.026	0.0298	0.0005	0.14	0.0507	0.0064	192	24	189	3	228	291	83
DERC1	DERC1-71	483	32	263	4950	0.54	0.504	0.021	0.0659	0.0011	0.39	0.0555	0.0021	414	17	411	7	430	85	96
DERC1	DERC1-72	450	14	412	115307	0.92	0.219	0.010	0.0317	0.0005	0.38	0.0501	0.0020	201	9	201	3	201	94	100
DERC1	DERC1-74	348	17	359	1532	1.03	0.392	0.025	0.0486	0.0010	0.33	0.0585	0.0036	336	22	306	6	549	133	56
DERC1	DERC1-75	268	22	79	52108	0.29	0.667	0.019	0.0836	0.0012	0.51	0.0578	0.0014	519	15	518	8	524	54	99
DERC1	DERC1-76	153	5	383	922	2.50	0.210	0.012	0.0300	0.0005	0.27	0.0508	0.0029	193	11	190	3	232	131	82
DERC1	DERC1-77	49	2	87	626	1.77	0.222	0.035	0.0318	0.0006	0.12	0.0506	0.0078	204	32	202	4	224	357	90
DERC1	DERC1-78	537	16	543	128107	1.01	0.202	0.008	0.0295	0.0004	0.40	0.0496	0.0017	187	7	187	3	177	80	106
DERC1	DERC1-79	238	10	203	21086	0.85	0.300	0.010	0.0423	0.0006	0.46	0.0513	0.0015	266	9	267	4	256	67	105
DERC1	DERC1-80	137	13	61	105890	0.44	0.785	0.027	0.0957	0.0015	0.46	0.0595	0.0018	588	20	589	9	585	66	101
DERC1	DERC1-81	74	7	43	53722	0.58	0.723	0.025	0.0895	0.0014	0.45	0.0585	0.0018	552	19	553	9	550	69	100
DERC1	DERC1-82	432	32	25	260853	0.06	0.583	0.019	0.0746	0.0011	0.46	0.0567	0.0017	467	16	464	7	479	66	97
DERC1	DERC1-85	74	2	111	484	1.50	0.225	0.039	0.0298	0.0005	0.10	0.0548	0.0095	206	36	189	3	405	387	47
DERC1	DERC1-87	110	3	159	874	1.45	0.206	0.024	0.0297	0.0005	0.14	0.0503	0.0058	190	22	189	3	209	268	90
DERC1	DERC1-88	125	10	22	732	0.18	0.622	0.035	0.0779	0.0015	0.35	0.0579	0.0031	491	28	484	9	525	116	92
DERC1	DERC1-89	179	5	179	654	1.00	0.217	0.024	0.0297	0.0005	0.15	0.0529	0.0057	199	22	189	3	325	246	58
DERC1	DERC1-90	74	2	78	381	1.06	0.198	0.015	0.0288	0.0005	0.24	0.0499	0.0037	184	14	183	3	192	172	95
DERC1	DERC1-91	88	4	57	31387	0.64	0.315	0.021	0.0440	0.0009	0.31	0.0520	0.0033	278	19	277	6	287	147	97
DERC1	DERC1-92	12	0	19	3380	1.59	0.251	0.038	0.0358	0.0014	0.25	0.0510	0.0075	228	34	226	9	239	338	95
DERC1	DERC1-94	271	25	176	714	0.65	0.934	0.044	0.0929	0.0017	0.39	0.0730	0.0032	670	32	573	11	1013	89	57
DERC1	DERC1-95	158	5	205	546	1.30	0.237	0.016	0.0291	0.0005	0.24	0.0591	0.0039	216	15	185	3	570	143	32
DERC1	DERC1-96	74	6	99	45283	1.34	0.622	0.044	0.0758	0.0017	0.32	0.0596	0.0040	491	35	471	11	588	145	80
DERC1	DERC1-97	76	3	49	23573	0.65	0.275	0.042	0.0382	0.0015	0.26	0.0522	0.0077	246	38	242	9	292	336	83
DERC1	DERC1-99	186	20	115	891	0.62	1.149	0.043	0.1062	0.0018	0.44	0.0785	0.0026	777	29	651	11	1159	67	56
DERC1	DERC1-100	301	27	56	2048	0.19	0.793	0.040	0.0892	0.0017	0.37	0.0645	0.0030	593	30	551	10	758	98	73
DERC1	DERC1-101	386	13	458	949	1.19	0.237	0.019	0.0341	0.0008	0.29	0.0505	0.0039	216	17	216	5	217	178	100
DERC1	DERC1-102	97	3	181	23505	1.87	0.205	0.019	0.0300	0.0005	0.19	0.0496	0.0045	190	18	191	3	174	212	109
DERC1	DERC1-104	289	21	195	2835	0.67	0.659	0.032	0.0728	0.0013	0.37	0.0657	0.0030	514	25	453	8	795	96	57
DERC1	DERC1-105	262	23	79	21089	0.30	0.699	0.021	0.0871	0.0013	0.50	0.0582	0.0015	538	16	539	8	536	57	100
DERC1	DERC1-107	225	18	151	7766	0.67	0.650	0.045	0.0806	0.0018	0.32	0.0585	0.0039	509	36	500	11	549	145	91
DERC1	DERC1-108	393	18	214	144481	0.54	0.327	0.010	0.0455	0.0007	0.48	0.0521	0.0014	287	9	287	4	290	62	99
DERC1	DERC1-109	126	4	139	494	1.10	0.220	0.022	0.0292	0.0005	0.17	0.0547	0.0054	202	20	186	3	398	223	47
DERC1	DERC1-110	163	7	136	34197	0.84	0.315	0.012	0.0441	0.0007	0.42	0.0517	0.0018	278	11	278	4	274	80	102

[a]U and Pb concentrations and Th/U ratios are calculated relative to GJ-1 reference zircon

[b]Corrected for background and within-run Pb/U fractionation and normalised to reference zircon GJ-1 (ID-TIMS values/measured value); $^{207}Pb/^{235}U$ calculated using $(^{207}Pb/^{206}Pb)/(^{238}U/^{206}Pb * 1/137.88)$

[c]Rho is the error correlation defined as the quotient of the propagated errors of the $^{206}Pb/^{238}U$ and the $^{207}/^{235}U$ ratio

[d]Quadratic addition of within-run errors (2 SD) and daily reproducibility of GJ-1 (2 SD)

[e]Corrected for mass-bias by normalising to GJ-1 reference zircon (~0.6 per atomic mass unit) and common Pb using the model Pb composition of Stacey & Kramers (1975)

Table D17. LA-ICPMS isotopic data for sample OKT1 in the Oudsthoorn Basin

OKT1							RATIOS							AGES [Ma]						Conc.
Sample	Analysis	U [ppm][a]	Pb [ppm][a]	Th [ppm][a]	^{206}Pb/^{204}Pb	Th/U[a]	^{207}Pb/^{235}U[b]	2 σ[d]	^{206}Pb/^{238}U[b]	2 σ[d]	rho[c]	^{207}Pb/^{206}Pb[e]	2 σ[d]	^{207}Pb/^{235}U	2 σ	^{206}Pb/^{238}U	2 σ	^{207}Pb/^{206}Pb	2 σ	%
OKT1	OKT1-1	688	17	567	147123	0.83	0.163	0.010	0.0241	0.0004	0.24	0.0490	0.0029	153	9	154	2	150	139	103
OKT1	OKT1-2	164	4	158	342	0.96	0.191	0.016	0.0250	0.0004	0.19	0.0553	0.0046	177	15	159	3	423	187	38
OKT1	OKT1-3	155	4	89	252	0.58	0.183	0.013	0.0249	0.0004	0.23	0.0532	0.0035	170	12	159	3	336	151	47
OKT1	OKT1-4	277	7	224	7462	0.81	0.170	0.009	0.0248	0.0004	0.28	0.0498	0.0026	160	9	158	2	183	124	86
OKT1	OKT1-5	402	10	279	304	0.69	0.173	0.012	0.0242	0.0004	0.22	0.0520	0.0034	162	11	154	2	284	150	54
OKT1	OKT1-6	312	8	121	303	0.39	0.228	0.016	0.0251	0.0004	0.22	0.0658	0.0044	208	14	160	2	799	140	20
OKT1	OKT1-7	64	2	36	4978	0.57	0.178	0.037	0.0240	0.0005	0.10	0.0538	0.0111	166	34	153	3	363	464	42
OKT1	OKT1-8	458	11	281	1055	0.61	0.178	0.016	0.0238	0.0004	0.17	0.0544	0.0049	167	15	151	2	387	203	39
OKT1	OKT1-10	201	5	197	855	0.98	0.168	0.016	0.0241	0.0004	0.17	0.0505	0.0047	157	15	153	2	219	216	70
OKT1	OKT1-11	250	6	234	349	0.94	0.169	0.010	0.0249	0.0004	0.27	0.0493	0.0027	159	9	159	2	162	129	98
OKT1	OKT1-12	307	7	270	3288	0.88	0.160	0.011	0.0236	0.0004	0.22	0.0490	0.0034	150	11	150	2	150	161	100
OKT1	OKT1-14	153	4	68	706	0.44	0.175	0.023	0.0243	0.0004	0.13	0.0523	0.0068	164	21	155	3	298	297	52
OKT1	OKT1-15	356	9	203	1257	0.57	0.170	0.013	0.0241	0.0004	0.19	0.0512	0.0039	159	12	153	2	249	175	61
OKT1	OKT1-16	277	6	309	708	1.12	0.149	0.013	0.0220	0.0003	0.17	0.0490	0.0043	141	13	140	2	147	207	95
OKT1	OKT1-17	281	7	247	589	0.88	0.170	0.012	0.0240	0.0004	0.21	0.0515	0.0036	160	11	153	2	263	160	58
OKT1	OKT1-18	505	12	425	2887	0.84	0.166	0.009	0.0242	0.0004	0.26	0.0498	0.0027	156	9	154	2	186	128	83
OKT1	OKT1-19	350	8	232	882	0.66	0.175	0.010	0.0243	0.0004	0.25	0.0525	0.0030	164	10	155	2	306	132	51
OKT1	OKT1-20	329	8	211	35376	0.64	0.165	0.007	0.0244	0.0004	0.37	0.0491	0.0019	155	7	155	2	154	93	101
OKT1	OKT1-22	289	7	298	938	1.03	0.175	0.014	0.0249	0.0004	0.19	0.0509	0.0040	163	13	158	2	234	183	68
OKT1	OKT1-23	577	14	453	122248	0.79	0.165	0.006	0.0240	0.0004	0.41	0.0499	0.0017	155	6	153	2	188	78	81
OKT1	OKT1-24	437	10	340	836	0.78	0.170	0.011	0.0237	0.0004	0.23	0.0519	0.0033	159	10	151	2	281	144	54
OKT1	OKT1-25	457	12	311	2387	0.68	0.173	0.011	0.0252	0.0004	0.24	0.0498	0.0031	162	10	160	2	184	145	87
OKT1	OKT1-26	387	9	191	6941	0.50	0.164	0.008	0.0243	0.0004	0.30	0.0489	0.0023	154	8	155	2	142	110	109
OKT1	OKT1-28	180	4	67	2361	0.37	0.167	0.020	0.0241	0.0004	0.14	0.0503	0.0061	157	19	153	3	210	280	73
OKT1	OKT1-29	498	12	349	107216	0.70	0.168	0.007	0.0244	0.0004	0.34	0.0501	0.0021	158	7	155	2	199	96	78
OKT1	OKT1-30	244	6	160	1948	0.65	0.174	0.018	0.0243	0.0004	0.15	0.0518	0.0052	162	17	155	2	274	231	56
OKT1	OKT1-31	238	6	220	399	0.93	0.180	0.023	0.0240	0.0004	0.12	0.0542	0.0069	168	22	153	2	379	287	40
OKT1	OKT1-32	156	4	60	733	0.39	0.163	0.018	0.0237	0.0004	0.15	0.0497	0.0056	153	17	151	3	179	262	85
OKT1	OKT1-33	177	4	97	1735	0.55	0.163	0.008	0.0238	0.0004	0.34	0.0497	0.0022	153	7	151	2	181	102	84
OKT1	OKT1-34	193	5	150	5728	0.78	0.165	0.012	0.0244	0.0004	0.21	0.0490	0.0035	155	11	155	2	150	167	104
OKT1	OKT1-35	824	20	502	961	0.61	0.166	0.009	0.0244	0.0004	0.27	0.0494	0.0026	156	9	156	2	164	125	95
OKT1	OKT1-36	409	10	231	609	0.56	0.165	0.011	0.0240	0.0004	0.23	0.0500	0.0033	155	11	153	2	195	155	78
OKT1	OKT1-37	341	8	214	1978	0.63	0.175	0.011	0.0233	0.0004	0.24	0.0547	0.0034	164	11	148	2	401	140	37
OKT1	OKT1-38	246	6	159	11502	0.65	0.165	0.012	0.0232	0.0004	0.22	0.0516	0.0035	155	11	148	2	268	156	55
OKT1	OKT1-39	338	8	259	1910	0.77	0.170	0.012	0.0230	0.0004	0.23	0.0535	0.0036	159	11	147	2	349	150	42
OKT1	OKT1-40	510	12	413	4040	0.81	0.161	0.008	0.0236	0.0004	0.32	0.0495	0.0022	152	7	150	2	173	105	87
OKT1	OKT1-41	184	4	108	816	0.59	0.180	0.014	0.0236	0.0004	0.21	0.0555	0.0042	168	13	150	2	431	169	35
OKT1	OKT1-42	153	4	135	1471	0.88	0.168	0.015	0.0235	0.0005	0.22	0.0517	0.0046	157	14	150	3	273	202	55
OKT1	OKT1-44	270	7	191	1576	0.71	0.167	0.013	0.0247	0.0004	0.20	0.0490	0.0036	157	12	157	2	147	172	107
OKT1	OKT1-46	167	4	101	20516	0.60	0.163	0.013	0.0242	0.0004	0.20	0.0489	0.0039	153	12	154	3	143	187	108
OKT1	OKT1-47	476	11	262	467	0.55	0.164	0.018	0.0241	0.0004	0.14	0.0492	0.0053	154	17	154	2	157	251	98
OKT1	OKT1-48	209	5	138	364	0.66	0.179	0.020	0.0259	0.0004	0.14	0.0500	0.0055	167	18	165	3	195	254	84
OKT1	OKT1-50	401	9	305	452	0.76	0.181	0.015	0.0234	0.0004	0.18	0.0561	0.0046	169	14	149	2	455	183	33
OKT1	OKT1-51	298	7	195	1168	0.66	0.160	0.012	0.0237	0.0004	0.21	0.0491	0.0037	151	12	151	2	152	178	99
OKT1	OKT1-52	116	3	55	3599	0.47	0.185	0.027	0.0236	0.0004	0.12	0.0570	0.0083	172	25	150	3	492	319	30
OKT1	OKT1-53	251	6	133	4205	0.53	0.168	0.007	0.0246	0.0004	0.40	0.0497	0.0018	158	6	157	2	180	84	87
OKT1	OKT1-56	229	6	112	59079	0.49	0.167	0.009	0.0246	0.0004	0.28	0.0492	0.0026	156	9	156	2	156	124	100

OKT1	OKT1-57	585	14	240	2343	0.41	0.159	0.007	0.0236	0.0004	0.33	0.0490	0.0021	150	7	150	2	145	103	103
OKT1	OKT1-58	197	5	142	1421	0.72	0.163	0.007	0.0240	0.0004	0.39	0.0493	0.0019	154	6	153	2	162	88	95
OKT1	OKT1-59	153	4	96	3013	0.63	0.169	0.012	0.0251	0.0004	0.23	0.0488	0.0034	158	11	160	3	140	162	114
OKT1	OKT1-60	448	11	258	4309	0.58	0.161	0.005	0.0237	0.0004	0.45	0.0492	0.0015	151	5	151	2	156	71	96
OKT1	OKT1-61	715	18	424	1641	0.59	0.173	0.008	0.0251	0.0004	0.33	0.0500	0.0022	162	8	160	2	195	102	82
OKT1	OKT1-62	230	6	116	671	0.50	0.209	0.012	0.0240	0.0004	0.27	0.0633	0.0035	193	11	153	2	719	119	21
OKT1	OKT1-63	150	4	102	257	0.68	0.264	0.021	0.0265	0.0004	0.21	0.0724	0.0056	238	19	168	3	996	157	17
OKT1	OKT1-64	185	4	138	15399	0.75	0.183	0.013	0.0233	0.0004	0.23	0.0570	0.0039	171	12	148	2	491	152	30
OKT1	OKT1-66	388	9	192	82652	0.50	0.164	0.005	0.0242	0.0004	0.46	0.0491	0.0014	154	5	154	2	151	68	102
OKT1	OKT1-68	358	8	233	73254	0.65	0.158	0.006	0.0233	0.0004	0.44	0.0492	0.0016	149	5	148	2	159	74	93
OKT1	OKT1-70	555	13	318	114967	0.57	0.163	0.006	0.0236	0.0004	0.42	0.0501	0.0016	153	6	150	2	199	76	75
OKT1	OKT1-71	388	10	259	3256	0.67	0.175	0.009	0.0257	0.0004	0.32	0.0493	0.0023	164	8	164	3	163	108	100
OKT1	OKT1-73	189	4	114	359	0.60	0.174	0.020	0.0233	0.0004	0.15	0.0542	0.0062	163	19	149	3	380	255	39
OKT1	OKT1-74	224	5	124	45744	0.55	0.178	0.016	0.0232	0.0004	0.19	0.0554	0.0048	166	15	148	2	429	193	35
OKT1	OKT1-76	851	20	378	465	0.44	0.167	0.011	0.0239	0.0004	0.23	0.0505	0.0033	156	10	153	2	217	150	70
OKT1	OKT1-77	576	14	377	2616	0.65	0.165	0.011	0.0237	0.0004	0.23	0.0504	0.0033	155	10	151	2	215	150	70
OKT1	OKT1-79	168	4	184	1170	1.10	0.169	0.010	0.0249	0.0004	0.26	0.0490	0.0029	158	10	159	3	149	140	106
OKT1	OKT1-80	243	6	233	527	0.96	0.162	0.018	0.0236	0.0005	0.19	0.0497	0.0054	152	17	151	3	180	253	84
OKT1	OKT1-81	147	4	73	1176	0.50	0.182	0.013	0.0259	0.0004	0.23	0.0511	0.0037	170	13	165	3	244	165	68
OKT1	OKT1-82	181	4	96	807	0.53	0.191	0.016	0.0234	0.0004	0.20	0.0591	0.0048	177	15	149	2	572	176	26
OKT1	OKT1-83	247	6	242	956	0.98	0.176	0.019	0.0239	0.0004	0.15	0.0533	0.0056	165	18	152	2	343	238	44
OKT1	OKT1-84	262	6	146	3960	0.56	0.171	0.014	0.0236	0.0004	0.20	0.0524	0.0041	160	13	151	2	304	178	50
OKT1	OKT1-85	188	5	97	39485	0.52	0.161	0.016	0.0239	0.0004	0.16	0.0489	0.0047	152	15	152	2	141	225	108
OKT1	OKT1-88	264	7	140	506	0.53	0.176	0.014	0.0258	0.0004	0.19	0.0496	0.0040	165	13	164	3	177	187	93
OKT1	OKT1-90	252	6	128	990	0.51	0.171	0.011	0.0252	0.0004	0.25	0.0493	0.0030	160	10	160	3	161	141	100
OKT1	OKT1-91	154	4	91	417	0.59	0.188	0.018	0.0235	0.0004	0.16	0.0579	0.0056	175	17	150	2	527	213	28
OKT1	OKT1-92	224	5	192	1891	0.86	0.178	0.012	0.0237	0.0004	0.24	0.0544	0.0036	166	11	151	2	386	147	39
OKT1	OKT1-93	75	2	47	212	0.62	0.264	0.021	0.0254	0.0006	0.31	0.0756	0.0057	238	19	161	4	1084	150	15

[a] U and Pb concentrations and Th/U ratios are calculated relative to GJ-1 reference zircon

[b] Corrected for background and within-run Pb/U fractionation and normalised to reference zircon GJ-1 (ID-TIMS values/measured value); $^{207}Pb/^{235}U$ calculated using $(^{207}Pb/^{206}Pb)/(^{238}U/^{206}Pb * 1/137.88)$

[c] Rho is the error correlation defined as the quotient of the propagated errors of the $^{206}Pb/^{238}U$ and the $^{207}/^{235}U$ ratio

[d] Quadratic addition of within-run errors (2 SD) and daily reproducibility of GJ-1 (2 SD)

[e] Corrected for mass-bias by normalising to GJ-1 reference zircon (~0.6 per atomic mass unit) and common Pb using the model Pb composition of Stacey & Kramers (1975)

Table D18. LA-ICPMS isotopic data for sample BREN2 in the Knysna Basin

Bren2

Sample	Analysis	U [ppm][a]	Pb [ppm][a]	Th [ppm][a]	$^{206}Pb/^{204}Pb$	Th/U[a]	RATIOS $^{207}Pb/^{235}U$ [b]	2 σ[d]	$^{206}Pb/^{238}U$ [b]	2 σ[d]	rho[c]	$^{207}Pb/^{206}Pb$ [e]	2 σ[d]	AGES [Ma] $^{207}Pb/^{235}U$	2 σ	$^{206}Pb/^{238}U$	2 σ	$^{207}Pb/^{206}Pb$	2 σ	Conc. %
Bren2	Bren2-1	33	5	11	887	0.33	1.305	0.053	0.1404	0.0023	0.41	0.0674	0.0025	848	34	847	14	850	76	100
Bren2	Bren2-2	604	49	150	1231	0.25	0.680	0.029	0.0805	0.0013	0.39	0.0613	0.0024	527	22	499	8	649	84	77
Bren2	Bren2-3	91	11	23	73428	0.25	1.147	0.066	0.1248	0.0025	0.36	0.0667	0.0036	776	44	758	15	827	111	92
Bren2	Bren2-5	202	14	132	88413	0.65	0.550	0.033	0.0674	0.0014	0.33	0.0591	0.0034	445	27	421	8	572	124	74
Bren2	Bren2-6	202	9	170	55905	0.84	0.318	0.025	0.0427	0.0010	0.29	0.0540	0.0041	280	22	270	6	372	169	72
Bren2	Bren2-7	672	31	120	1842	0.18	0.437	0.017	0.0462	0.0007	0.41	0.0686	0.0025	368	14	291	5	887	74	33
Bren2	Bren2-8	863	37	24	6622	0.03	0.325	0.016	0.0424	0.0007	0.35	0.0557	0.0026	286	14	267	5	440	105	61
Bren2	Bren2-9	717	51	144	330467	0.20	0.544	0.025	0.0710	0.0012	0.37	0.0556	0.0024	441	20	442	8	437	96	101
Bren2	Bren2-10	371	35	51	11351	0.14	0.778	0.021	0.0948	0.0013	0.52	0.0595	0.0014	585	16	584	8	587	50	100
Bren2	Bren2-11	236	20	52	449	0.22	0.673	0.021	0.0850	0.0012	0.47	0.0575	0.0016	523	16	526	8	509	60	103
Bren2	Bren2-12	487	21	299	3254	0.61	0.300	0.009	0.0424	0.0006	0.48	0.0513	0.0013	266	8	267	4	254	59	105
Bren2	Bren2-13	486	34	97	10632	0.20	0.547	0.015	0.0706	0.0010	0.52	0.0562	0.0013	443	12	440	6	460	52	96
Bren2	Bren2-14	251	19	117	121954	0.47	0.582	0.018	0.0749	0.0011	0.48	0.0563	0.0015	466	14	466	7	466	59	100
Bren2	Bren2-15	121	4	82	24392	0.68	0.215	0.012	0.0311	0.0006	0.33	0.0502	0.0026	198	11	197	4	205	119	96
Bren2	Bren2-16	655	107	369	4282	0.56	1.702	0.050	0.1630	0.0024	0.50	0.0757	0.0019	1009	30	973	14	1087	51	90
Bren2	Bren2-17	282	21	42	2601	0.15	0.569	0.028	0.0736	0.0013	0.36	0.0561	0.0025	457	22	458	8	456	100	100
Bren2	Bren2-18	307	7	277	1603	0.90	0.161	0.008	0.0237	0.0004	0.34	0.0491	0.0024	151	8	151	3	154	116	98
Bren2	Bren2-19	432	78	324	506801	0.75	1.937	0.054	0.1807	0.0026	0.52	0.0777	0.0018	1094	30	1071	15	1140	47	94
Bren2	Bren2-21	266	20	191	126816	0.72	0.573	0.020	0.0733	0.0011	0.44	0.0566	0.0018	460	16	456	7	478	69	96
Bren2	Bren2-22	222	19	103	125846	0.47	0.703	0.026	0.0874	0.0014	0.42	0.0584	0.0020	541	20	540	9	543	74	99
Bren2	Bren2-23	286	23	75	1848	0.26	0.680	0.033	0.0809	0.0014	0.37	0.0609	0.0028	527	26	502	9	637	97	79
Bren2	Bren2-24	206	17	201	111767	0.98	0.667	0.024	0.0836	0.0013	0.43	0.0579	0.0018	519	18	517	8	524	70	99
Bren2	Bren2-25	388	17	427	109397	1.10	0.312	0.011	0.0433	0.0007	0.45	0.0523	0.0016	276	9	274	4	298	70	92
Bren2	Bren2-26	313	13	190	1567	0.60	0.307	0.015	0.0400	0.0007	0.35	0.0557	0.0025	272	13	253	4	441	100	57
Bren2	Bren2-27	525	19	443	1866	0.84	0.259	0.016	0.0357	0.0007	0.31	0.0525	0.0031	234	15	226	4	309	134	73
Bren2	Bren2-28	411	148	205	22680	0.50	6.082	0.153	0.3601	0.0050	0.55	0.1225	0.0026	1988	50	1983	28	1993	37	99
Bren2	Bren2-29	244	6	202	37986	0.83	0.181	0.024	0.0239	0.0008	0.26	0.0548	0.0071	169	23	153	5	405	289	38
Bren2	Bren2-30	719	17	581	1278	0.81	0.180	0.013	0.0243	0.0005	0.30	0.0538	0.0037	168	12	155	3	363	155	43
Bren2	Bren2-31	166	14	57	976	0.35	0.675	0.033	0.0838	0.0015	0.36	0.0584	0.0026	524	25	519	9	545	99	95
Bren2	Bren2-32	729	29	483	3320	0.66	0.318	0.020	0.0404	0.0008	0.32	0.0570	0.0034	280	18	255	5	492	131	52
Bren2	Bren2-33	181	17	58	4612	0.32	0.755	0.027	0.0924	0.0014	0.43	0.0593	0.0019	571	21	570	9	578	71	98
Bren2	Bren2-34	292	7	119	1052	0.41	0.163	0.008	0.0239	0.0004	0.35	0.0494	0.0022	153	7	152	3	167	104	91
Bren2	Bren2-35	360	21	95	133529	0.26	0.423	0.020	0.0571	0.0010	0.36	0.0537	0.0024	358	17	358	6	359	99	100
Bren2	Bren2-36	251	20	30	3765	0.12	0.643	0.019	0.0814	0.0012	0.49	0.0573	0.0015	504	15	504	7	504	57	100
Bren2	Bren2-37	234	10	188	51603	0.80	0.302	0.010	0.0423	0.0006	0.44	0.0518	0.0016	268	9	267	4	276	70	97
Bren2	Bren2-38	77	12	36	80154	0.47	1.563	0.067	0.1594	0.0028	0.41	0.0712	0.0028	956	41	953	17	962	80	99
Bren2	Bren2-39	355	30	109	26806	0.31	0.666	0.019	0.0835	0.0012	0.51	0.0579	0.0014	518	15	517	7	526	54	98
Bren2	Bren2-40	470	41	197	15580	0.42	0.708	0.019	0.0877	0.0012	0.52	0.0585	0.0014	543	15	542	8	549	51	99
Bren2	Bren2-41	121	10	55	753	0.45	0.668	0.032	0.0833	0.0015	0.37	0.0582	0.0026	520	25	516	9	538	97	96
Bren2	Bren2-42	274	7	104	44512	0.38	0.171	0.015	0.0250	0.0006	0.28	0.0496	0.0041	160	14	159	4	177	191	90
Bren2	Bren2-43	177	19	66	3637	0.37	0.880	0.031	0.1047	0.0016	0.43	0.0609	0.0020	641	23	642	10	637	69	101
Bren2	Bren2-44	518	12	403	792	0.78	0.155	0.007	0.0229	0.0004	0.35	0.0491	0.0022	146	7	146	2	152	105	96
Bren2	Bren2-46	175	5	314	29831	1.79	0.178	0.019	0.0262	0.0007	0.26	0.0494	0.0050	166	18	167	5	165	239	101
Bren2	Bren2-47	251	18	62	116533	0.25	0.548	0.023	0.0713	0.0012	0.39	0.0558	0.0021	444	18	444	7	442	85	100
Bren2	Bren2-48	357	9	570	56247	1.60	0.165	0.012	0.0242	0.0005	0.29	0.0494	0.0035	155	12	154	3	165	168	94
Bren2	Bren2-49	169	5	101	32213	0.60	0.205	0.033	0.0294	0.0012	0.25	0.0506	0.0079	189	31	187	7	222	362	84
Bren2	Bren2-50	182	7	120	48775	0.66	0.292	0.020	0.0412	0.0009	0.30	0.0514	0.0034	260	18	261	5	257	151	102
Bren2	Bren2-51	114	22	42	144095	0.37	2.075	0.058	0.1939	0.0028	0.52	0.0776	0.0019	1140	32	1143	16	1136	48	101
Bren2	Bren2-52	330	28	100	4893	0.30	0.673	0.023	0.0845	0.0013	0.44	0.0578	0.0018	523	18	523	8	521	68	100
Bren2	Bren2-53	434	17	182	4610	0.42	0.282	0.011	0.0398	0.0006	0.40	0.0514	0.0019	252	10	251	4	257	83	98
Bren2	Bren2-54	184	7	219	47205	1.19	0.278	0.022	0.0395	0.0009	0.29	0.0511	0.0038	249	19	249	6	247	172	101
Bren2	Bren2-55	46	1	41	96	0.89	0.199	0.041	0.0292	0.0015	0.24	0.0495	0.0098	185	38	186	9	171	463	109
Bren2	Bren2-56	273	24	192	153400	0.70	0.695	0.021	0.0863	0.0013	0.48	0.0584	0.0016	536	16	534	8	546	58	98
Bren2	Bren2-57	534	14	365	90273	0.68	0.178	0.009	0.0260	0.0004	0.35	0.0496	0.0023	166	8	165	3	176	107	94
Bren2	Bren2-58	268	14	241	50539	0.90	0.370	0.012	0.0509	0.0007	0.46	0.0527	0.0015	319	10	320	5	317	64	101
Bren2	Bren2-59	209	10	202	63344	0.97	0.337	0.012	0.0465	0.0007	0.44	0.0525	0.0016	295	10	293	4	308	70	95

Bren2	Bren2-60	303	17	103	107500	0.34	0.399	0.019	0.0545	0.0009	0.36	0.0531	0.0024	341	16	342	6	331	102	103
Bren2	Bren2-61	516	23	218	5970	0.42	0.317	0.010	0.0442	0.0006	0.45	0.0521	0.0015	280	9	279	4	288	65	97
Bren2	Bren2-62	299	24	169	6146	0.57	0.640	0.023	0.0804	0.0012	0.43	0.0577	0.0019	502	18	498	8	519	72	96
Bren2	Bren2-63	424	34	195	1311	0.46	0.788	0.027	0.0807	0.0012	0.45	0.0708	0.0022	590	20	500	8	952	62	53
Bren2	Bren2-64	291	25	283	3973	0.97	0.690	0.025	0.0855	0.0013	0.43	0.0586	0.0019	533	19	529	8	550	70	96
Bren2	Bren2-65	339	48	42	4673	0.12	1.335	0.037	0.1416	0.0020	0.51	0.0683	0.0016	861	24	854	12	879	50	97
Bren2	Bren2-66	169	27	70	175939	0.41	1.573	0.046	0.1601	0.0023	0.50	0.0713	0.0018	960	28	957	14	966	52	99
Bren2	Bren2-67	536	32	304	6571	0.57	0.444	0.019	0.0595	0.0010	0.39	0.0541	0.0021	373	16	372	6	375	87	99
Bren2	Bren2-68	566	104	155	677571	0.27	1.930	0.050	0.1840	0.0026	0.55	0.0761	0.0016	1092	28	1089	15	1097	43	99
Bren2	Bren2-69	406	10	226	1839	0.56	0.166	0.011	0.0243	0.0005	0.30	0.0495	0.0032	156	11	155	3	172	150	90
Bren2	Bren2-70	423	20	214	130901	0.51	0.349	0.023	0.0476	0.0010	0.31	0.0531	0.0033	304	20	300	6	334	140	90
Bren2	Bren2-71	241	19	49	121879	0.20	0.608	0.024	0.0777	0.0012	0.41	0.0567	0.0020	482	19	482	8	481	78	100
Bren2	Bren2-72	364	31	72	200308	0.20	0.672	0.019	0.0846	0.0012	0.50	0.0576	0.0014	522	15	523	7	515	53	102
Bren2	Bren2-73	373	66	105	426538	0.28	1.805	0.048	0.1757	0.0025	0.54	0.0745	0.0017	1047	28	1043	15	1055	45	99
Bren2	Bren2-74	160	16	57	4121	0.35	0.823	0.043	0.0987	0.0018	0.35	0.0605	0.0030	610	32	607	11	622	106	98
Bren2	Bren2-75	286	8	124	239	0.44	0.179	0.017	0.0263	0.0007	0.27	0.0494	0.0044	168	16	168	4	167	208	100
Bren2	Bren2-76	602	15	464	1600	0.77	0.167	0.008	0.0244	0.0004	0.36	0.0498	0.0021	157	7	155	3	187	98	83
Bren2	Bren2-77	193	11	166	2780	0.86	0.408	0.014	0.0549	0.0008	0.44	0.0539	0.0017	347	12	344	5	368	71	94
Bren2	Bren2-78	472	19	369	124201	0.78	0.287	0.021	0.0404	0.0009	0.29	0.0515	0.0037	256	19	255	6	265	163	97
Bren2	Bren2-79	697	31	482	3870	0.69	0.324	0.009	0.0452	0.0006	0.50	0.0520	0.0013	285	8	285	4	286	56	100
Bren2	Bren2-80	258	121	83	12545	0.32	11.371	0.315	0.4707	0.0071	0.54	0.1752	0.0041	2554	71	2487	37	2608	39	95
Bren2	Bren2-81	74	7	28	44546	0.38	0.898	0.038	0.0928	0.0016	0.40	0.0702	0.0027	651	28	572	10	933	80	61
Bren2	Bren2-82	118	6	56	674	0.47	0.387	0.019	0.0527	0.0009	0.35	0.0532	0.0025	332	16	331	6	339	105	98
Bren2	Bren2-83	252	21	160	3104	0.63	0.668	0.036	0.0836	0.0016	0.35	0.0580	0.0029	520	28	518	10	528	111	98
Bren2	Bren2-84	74	6	35	2935	0.48	0.668	0.030	0.0839	0.0014	0.38	0.0577	0.0024	519	23	519	9	520	91	100
Bren2	Bren2-85	580	31	449	15331	0.77	0.395	0.015	0.0538	0.0008	0.42	0.0532	0.0018	338	13	338	5	339	77	100
Bren2	Bren2-86	381	17	147	6088	0.39	0.330	0.011	0.0460	0.0007	0.46	0.0521	0.0015	290	9	290	4	291	65	99
Bren2	Bren2-87	146	11	42	72022	0.29	0.594	0.035	0.0759	0.0015	0.33	0.0568	0.0031	474	28	471	9	485	122	97
Bren2	Bren2-88	217	80	164	5957	0.76	6.322	0.163	0.3673	0.0052	0.55	0.1248	0.0027	2022	52	2017	28	2027	38	100
Bren2	Bren2-89	1098	46	556	5369	0.51	0.302	0.016	0.0424	0.0007	0.34	0.0518	0.0025	268	14	267	5	275	111	97
Bren2	Bren2-90	748	18	358	485	0.48	0.221	0.012	0.0241	0.0005	0.36	0.0664	0.0033	203	11	154	3	819	104	19
Bren2	Bren2-91	402	16	154	9214	0.38	0.290	0.009	0.0408	0.0006	0.47	0.0516	0.0014	259	8	258	4	266	64	97
Bren2	Bren2-92	59	8	29	2275	0.48	1.304	0.045	0.1397	0.0022	0.45	0.0677	0.0021	848	29	843	13	860	63	98
Bren2	Bren2-93	297	24	136	5835	0.46	0.662	0.025	0.0823	0.0013	0.42	0.0584	0.0020	516	19	510	8	543	75	94
Bren2	Bren2-94	84	31	67	8075	0.80	6.444	0.176	0.3719	0.0054	0.53	0.1257	0.0029	2038	56	2038	30	2038	41	100
Bren2	Bren2-95	98	4	47	26988	0.48	0.299	0.036	0.0423	0.0013	0.26	0.0513	0.0060	266	32	267	8	253	267	106
Bren2	Bren2-96	365	15	325	99259	0.89	0.299	0.016	0.0417	0.0008	0.34	0.0519	0.0026	265	14	264	5	280	115	94
Bren2	Bren2-97	176	14	162	4252	0.92	0.628	0.027	0.0797	0.0013	0.39	0.0571	0.0023	495	21	494	8	497	87	99
Bren2	Bren2-98	466	38	71	3958	0.15	0.646	0.018	0.0814	0.0012	0.51	0.0576	0.0014	506	14	504	7	514	53	98
Bren2	Bren2-99	305	122	125	87849	0.41	7.498	0.193	0.4005	0.0056	0.54	0.1358	0.0029	2173	56	2171	30	2174	38	100
Bren2	Bren2-100	224	20	117	130334	0.52	0.725	0.022	0.0893	0.0013	0.48	0.0589	0.0016	554	17	551	8	564	58	98
Bren2	Bren2-101	230	6	51	406	0.22	0.182	0.018	0.0269	0.0007	0.27	0.0492	0.0046	170	17	171	4	157	221	109
Bren2	Bren2-102	125	3	142	337	1.14	0.177	0.015	0.0260	0.0006	0.27	0.0494	0.0040	165	14	165	4	166	189	100
Bren2	Bren2-103	741	20	499	3079	0.67	0.182	0.009	0.0267	0.0004	0.35	0.0496	0.0022	170	8	170	3	174	103	98
Bren2	Bren2-104	303	7	209	47103	0.69	0.162	0.012	0.0238	0.0005	0.29	0.0493	0.0035	153	11	152	3	163	166	93
Bren2	Bren2-105	696	31	565	14257	0.81	0.318	0.011	0.0441	0.0007	0.43	0.0523	0.0017	280	10	278	4	298	74	94
Bren2	Bren2-106	503	82	30	7328	0.06	1.678	0.049	0.1640	0.0024	0.50	0.0742	0.0019	1000	29	979	14	1047	51	94
Bren2	Bren2-107	113	4	201	2343	1.78	0.226	0.023	0.0320	0.0009	0.27	0.0512	0.0050	207	21	203	6	248	227	82
Bren2	Bren2-109	186	17	172	108432	0.92	0.722	0.047	0.0895	0.0019	0.32	0.0585	0.0036	552	36	553	12	549	136	101
Bren2	Bren2-110	339	24	110	155507	0.32	0.540	0.018	0.0704	0.0011	0.45	0.0557	0.0017	439	15	439	7	439	67	100
Bren2	Bren2-111	422	38	192	234030	0.46	0.742	0.022	0.0910	0.0013	0.49	0.0592	0.0015	564	17	561	8	573	57	98
Bren2	Bren2-112	329	19	71	2373	0.21	0.490	0.019	0.0582	0.0009	0.41	0.0611	0.0022	405	16	365	6	642	77	57
Bren2	Bren2-113	332	8	271	22589	0.82	0.177	0.011	0.0256	0.0005	0.31	0.0502	0.0030	166	10	163	3	206	137	79
Bren2	Bren2-114	679	54	104	1800	0.15	0.748	0.020	0.0794	0.0011	0.52	0.0683	0.0016	567	15	492	7	879	48	56
Bren2	Bren2-115	159	4	154	28628	0.96	0.189	0.018	0.0276	0.0007	0.27	0.0498	0.0045	176	17	175	4	186	212	94
Bren2	Bren2-116	110	11	72	34215	0.66	0.808	0.028	0.0976	0.0015	0.44	0.0600	0.0019	601	21	600	9	604	68	99
Bren2	Bren2-117	442	25	354	1485	0.80	0.416	0.018	0.0563	0.0009	0.39	0.0536	0.0021	353	15	353	6	353	88	100
Bren2	Bren2-118	369	19	202	1520	0.55	0.399	0.025	0.0527	0.0011	0.32	0.0548	0.0033	341	21	331	7	405	133	82
Bren2	Bren2-119	442	18	256	2531	0.58	0.293	0.017	0.0408	0.0008	0.33	0.0520	0.0028	261	15	258	5	286	122	90
Bren2	Bren2-120	869	90	116	586860	0.13	0.865	0.028	0.1036	0.0015	0.46	0.0606	0.0017	633	20	635	9	625	61	102
Bren2	Bren2-121	154	7	55	44982	0.36	0.329	0.017	0.0448	0.0008	0.34	0.0534	0.0025	289	15	282	5	344	108	82

[a]U and Pb concentrations and Th/U ratios are calculated relative to GJ-1 reference zircon

[b]Corrected for background and within-run Pb/U fractionation and normalised to reference zircon GJ-1 (ID-TIMS values/measured value); $^{207}Pb/^{235}U$ calculated using $(^{207}Pb/^{206}Pb)/(^{238}U/^{206}Pb * 1/137.88)$

[c]Rho is the error correlation defined as the quotient of the propagated errors of the $^{206}Pb/^{238}U$ and the $^{207}/^{235}U$ ratio

[d]Quadratic addition of within-run errors (2 SD) and daily reproducibility of GJ-1 (2 SD)

[e]Corrected for mass-bias by normalising to GJ-1 reference zircon (~0.6 per atomic mass unit) and common Pb using the model Pb composition of Stacey & Kramers (1975)

Table D19. LA-ICPMS isotopic data for sample PLETT in the Plettenberg Bay Basin

PLETT							RATIOS							AGES [Ma]						Conc.
Sample	Analysis	U [ppm][a]	Pb [ppm][a]	Th [ppm][a]	$^{206}Pb/^{204}Pb$	Th/U[a]	$^{207}Pb/^{235}U$[b]	2 σ[d]	$^{206}Pb/^{238}U$[b]	2 σ[d]	rho[c]	$^{207}Pb/^{206}Pb$[e]	2 σ[d]	$^{207}Pb/^{235}U$	2 σ	$^{206}Pb/^{238}U$	2 σ	$^{207}Pb/^{206}Pb$	2 σ	%
PLETT	TT-1	441	10	278	3275	0.63	0.163	0.009	0.02259	0.00046	0.37	0.052	0.003	153	9	144	3	302	118	48
PLETT	TT-2	210	5	83	15230	0.40	0.150	0.012	0.02155	0.00044	0.26	0.051	0.004	142	11	137	3	223	178	62
PLETT	TT-5	523	12	344	657	0.66	0.156	0.013	0.02297	0.00046	0.24	0.049	0.004	147	12	146	3	163	189	90
PLETT	TT-6	245	5	145	796	0.59	0.151	0.009	0.02233	0.00046	0.33	0.049	0.003	143	9	142	3	152	136	94
PLETT	TT-7	296	6	183	910	0.62	0.145	0.007	0.02147	0.00044	0.43	0.049	0.002	137	7	137	3	141	101	97
PLETT	TT-8	169	4	61	3285	0.36	0.158	0.010	0.02291	0.00048	0.33	0.050	0.003	149	9	146	3	196	139	74
PLETT	TT-9	173	4	47	638	0.27	0.150	0.023	0.02161	0.00046	0.14	0.050	0.008	142	22	138	3	207	350	66
PLETT	TT-10	183	4	81	146	0.44	0.157	0.018	0.02325	0.00048	0.18	0.049	0.006	148	17	148	3	150	271	99
PLETT	TT-11	189	4	72	375	0.38	0.150	0.010	0.02199	0.00046	0.30	0.049	0.003	142	10	140	3	164	154	86
PLETT	TT-12	280	6	147	326	0.53	0.159	0.016	0.02270	0.00046	0.21	0.051	0.005	149	15	145	3	226	222	64
PLETT	TT-13	279	6	149	937	0.53	0.150	0.009	0.02211	0.00046	0.36	0.049	0.003	142	8	141	3	161	126	88
PLETT	TT-14	295	6	188	5185	0.64	0.147	0.007	0.02183	0.00044	0.43	0.049	0.002	139	7	139	3	142	100	98
PLETT	TT-15	358	8	216	72732	0.60	0.145	0.006	0.02140	0.00044	0.48	0.049	0.002	137	6	136	3	150	87	91
PLETT	TT-17	270	6	147	2541	0.54	0.147	0.006	0.02187	0.00044	0.50	0.049	0.002	139	6	139	3	137	82	102
PLETT	TT-18	293	6	165	764	0.56	0.160	0.010	0.02168	0.00044	0.33	0.054	0.003	151	9	138	3	354	133	39
PLETT	TT-19	346	7	198	188095	0.57	0.143	0.008	0.02136	0.00044	0.38	0.049	0.002	136	7	136	3	134	119	101
PLETT	TT-20	333	7	213	428	0.64	0.149	0.010	0.02194	0.00044	0.31	0.049	0.003	141	9	140	3	154	144	91
PLETT	TT-21	607	13	413	336	0.68	0.185	0.009	0.02198	0.00044	0.40	0.061	0.003	173	9	140	3	645	100	22
PLETT	TT-24	157	3	57	41348	0.37	0.148	0.011	0.02184	0.00046	0.28	0.049	0.004	140	11	139	3	156	172	89
PLETT	TT-25	194	4	67	39800	0.35	0.148	0.010	0.02165	0.00044	0.30	0.049	0.003	140	9	138	3	169	149	82
PLETT	TT-28	300	6	160	2413	0.53	0.169	0.013	0.02130	0.00044	0.27	0.058	0.004	159	12	136	3	518	164	26
PLETT	TT-30	120	3	35	4396	0.29	0.150	0.016	0.02216	0.00048	0.20	0.049	0.005	141	15	141	3	144	246	98
PLETT	TT-31	293	7	152	63431	0.52	0.154	0.008	0.02291	0.00046	0.38	0.049	0.002	146	8	146	3	141	114	103
PLETT	TT-33	546	13	357	2164	0.65	0.162	0.007	0.02367	0.00048	0.48	0.050	0.002	152	6	151	3	176	87	86
PLETT	TT-34	240	5	120	271	0.50	0.163	0.016	0.02221	0.00046	0.21	0.053	0.005	153	15	142	3	339	214	42
PLETT	TT-35	269	6	135	55128	0.50	0.158	0.015	0.02163	0.00044	0.21	0.053	0.005	149	14	138	3	325	214	43
PLETT	TT-36	186	4	62	37263	0.33	0.143	0.006	0.02120	0.00044	0.46	0.049	0.002	135	6	135	3	137	94	99
PLETT	TT-37	291	6	148	465	0.51	0.179	0.016	0.02163	0.00044	0.23	0.060	0.005	168	15	138	3	609	185	23
PLETT	TT-38	372	8	210	1355	0.57	0.146	0.006	0.02171	0.00044	0.51	0.049	0.002	138	6	138	3	132	81	105
PLETT	TT-39	231	5	111	47665	0.48	0.147	0.006	0.02180	0.00046	0.49	0.049	0.002	140	6	139	3	148	89	94
PLETT	TT-40	346	7	227	568	0.66	0.153	0.011	0.02140	0.00044	0.28	0.052	0.004	144	11	136	3	277	163	49
PLETT	TT-42	162	4	50	198	0.31	0.154	0.024	0.02190	0.00046	0.14	0.051	0.008	145	22	140	3	234	354	60
PLETT	TT-44	244	5	131	181	0.53	0.230	0.029	0.02240	0.00046	0.17	0.075	0.009	210	26	143	3	1056	247	14
PLETT	TT-45	198	4	88	144	0.44	0.235	0.031	0.02170	0.00046	0.16	0.078	0.010	214	28	138	3	1159	259	12
PLETT	TT-46	177	4	79	226	0.45	0.197	0.025	0.02221	0.00046	0.17	0.064	0.008	183	23	142	3	752	261	19
PLETT	TT-47	204	5	80	253	0.39	0.169	0.021	0.02244	0.00048	0.18	0.055	0.007	159	19	143	3	400	269	36
PLETT	TT-48	225	5	124	260	0.55	0.189	0.028	0.02216	0.00046	0.14	0.062	0.009	176	26	141	3	669	319	21
PLETT	TT-49	200	4	97	401	0.48	0.219	0.022	0.02152	0.00044	0.20	0.074	0.007	201	20	137	3	1032	200	13
PLETT	TT-53	263	6	139	230	0.53	0.221	0.019	0.02210	0.00046	0.25	0.073	0.006	203	17	141	3	1003	167	14
PLETT	TT-54	230	5	170	46905	0.74	0.145	0.008	0.02163	0.00044	0.36	0.049	0.003	138	8	138	3	136	125	101
PLETT	TT-56	259	6	143	633	0.55	0.189	0.016	0.02188	0.00046	0.25	0.063	0.005	176	15	140	3	700	172	20
PLETT	TT-57	291	6	155	185	0.53	0.150	0.009	0.02187	0.00044	0.32	0.050	0.003	142	9	139	3	187	136	75
PLETT	TT-58	230	5	131	46804	0.57	0.145	0.013	0.02156	0.00044	0.23	0.049	0.004	138	12	138	3	140	199	98
PLETT	TT-59	248	5	136	280	0.55	0.196	0.028	0.02134	0.00044	0.14	0.066	0.009	181	26	136	3	821	297	17
PLETT	TT-60	615	14	422	507	0.69	0.188	0.011	0.02216	0.00044	0.34	0.061	0.003	175	10	141	3	655	119	22
PLETT	TT-61	230	5	123	331	0.54	0.215	0.020	0.02211	0.00046	0.23	0.071	0.006	198	18	141	3	943	184	15
PLETT	TT-62	227	5	116	171	0.51	0.245	0.018	0.02222	0.00046	0.28	0.080	0.006	222	16	142	3	1194	139	12
PLETT	TT-63	452	10	264	336	0.58	0.151	0.009	0.02241	0.00046	0.35	0.049	0.003	143	8	143	3	140	131	102
PLETT	TT-64	286	6	155	284	0.54	0.196	0.014	0.02144	0.00044	0.28	0.066	0.005	182	13	137	3	813	145	17
PLETT	TT-65	285	6	149	722	0.52	0.149	0.017	0.02166	0.00044	0.18	0.050	0.006	141	16	138	3	195	257	71
PLETT	TT-66	256	6	126	195	0.49	0.299	0.021	0.02209	0.00046	0.30	0.098	0.007	266	19	141	3	1591	125	9
PLETT	TT-68	297	6	233	3728	0.79	0.146	0.006	0.02170	0.00044	0.51	0.049	0.002	138	5	138	3	139	80	99
PLETT	TT-72	161	4	60	922	0.37	0.164	0.026	0.02290	0.00048	0.13	0.052	0.008	154	24	146	3	281	355	52
PLETT	TT-73	318	7	145	63171	0.46	0.143	0.007	0.02112	0.00044	0.40	0.049	0.002	135	7	135	3	145	113	93
PLETT	TT-75	363	8	185	293	0.51	0.151	0.012	0.02231	0.00046	0.26	0.049	0.004	143	11	142	3	150	179	95
PLETT	TT-77	532	12	309	332	0.58	0.155	0.015	0.02176	0.00044	0.21	0.052	0.005	147	14	139	3	277	221	50

PLETT	TT-79	200	4	70	41378	0.35	0.149	0.012	0.02205	0.00048	0.27	0.049	0.004	141	11	141	3	141	180	100
PLETT	TT-81	448	10	269	477	0.60	0.150	0.011	0.02164	0.00044	0.28	0.050	0.004	142	10	138	3	209	164	66
PLETT	TT-84	292	6	199	7186	0.68	0.149	0.006	0.02204	0.00046	0.48	0.049	0.002	141	6	141	3	142	88	99
PLETT	TT-85	412	9	257	704	0.62	0.186	0.011	0.02178	0.00044	0.34	0.062	0.003	173	10	139	3	670	119	21
PLETT	TT-87	200	4	94	89	0.47	0.232	0.038	0.02207	0.00046	0.13	0.076	0.012	212	34	141	3	1098	322	13
PLETT	TT-88	382	8	273	321	0.72	0.204	0.015	0.02171	0.00044	0.27	0.068	0.005	188	14	138	3	868	151	16
PLETT	TT-89	200	4	119	237	0.60	0.219	0.025	0.02159	0.00046	0.18	0.073	0.008	201	23	138	3	1027	229	13
PLETT	TT-92	193	4	94	576	0.49	0.147	0.010	0.02172	0.00046	0.33	0.049	0.003	139	9	139	3	154	144	90
PLETT	TT-93	518	11	305	104799	0.59	0.146	0.005	0.02160	0.00044	0.56	0.049	0.001	138	5	138	3	142	71	97
PLETT	TT-94	203	4	87	444	0.43	0.197	0.025	0.02145	0.00046	0.17	0.067	0.008	183	23	137	3	826	258	17
PLETT	TT-96	297	6	174	149114	0.59	0.144	0.007	0.02132	0.00044	0.44	0.049	0.002	136	6	136	3	140	99	97
PLETT	TT-97	264	6	164	2547	0.62	0.144	0.010	0.02149	0.00044	0.29	0.049	0.003	137	10	137	3	136	161	101
PLETT	TT-98	193	4	111	226	0.57	0.165	0.013	0.02130	0.00044	0.27	0.056	0.004	155	12	136	3	462	162	29
PLETT	TT-99	170	4	54	174	0.32	0.161	0.016	0.02243	0.00048	0.22	0.052	0.005	151	15	143	3	284	219	50
PLETT	TT-101	322	7	135	604	0.42	0.219	0.024	0.02222	0.00048	0.20	0.072	0.008	201	22	142	3	976	221	15
PLETT	TT-103	199	4	90	4153	0.45	0.146	0.009	0.02154	0.00046	0.34	0.049	0.003	139	9	137	3	159	138	86
PLETT	TT-107	370	8	217	197	0.59	0.149	0.014	0.02196	0.00044	0.21	0.049	0.005	141	13	140	3	161	214	87
PLETT	TT-108	213	5	94	856	0.44	0.152	0.014	0.02175	0.00048	0.25	0.051	0.004	144	13	139	3	232	199	60
PLETT	TT-109	88	9	31	82195	0.35	0.835	0.030	0.09990	0.00204	0.56	0.061	0.002	616	22	614	13	625	65	98
PLETT	TT-110	143	3	60	145	0.42	0.248	0.039	0.02242	0.00050	0.14	0.080	0.012	225	35	143	3	1200	304	12
PLETT	TT-111	323	7	192	257	0.60	0.199	0.014	0.02132	0.00044	0.29	0.068	0.005	184	13	136	3	855	144	16
PLETT	TT-112	350	8	146	739	0.42	0.146	0.008	0.02159	0.00044	0.40	0.049	0.002	138	7	138	3	149	111	92
PLETT	TT-113	237	5	118	2458	0.50	0.148	0.010	0.02167	0.00046	0.30	0.050	0.003	140	10	138	3	177	155	78
PLETT	TT-114	202	4	75	470	0.37	0.149	0.012	0.02136	0.00046	0.26	0.051	0.004	141	12	136	3	220	182	62
PLETT	TT-115	162	3	60	224	0.37	0.249	0.027	0.02153	0.00046	0.19	0.084	0.009	226	25	137	3	1290	210	11

[a]U and Pb concentrations and Th/U ratios are calculated relative to GJ-1 reference zircon

[b]Corrected for background and within-run Pb/U fractionation and normalised to reference zircon GJ-1 (ID-TIMS values/measured value); $^{207}Pb/^{235}U$ calculated using $(^{207}Pb/^{206}Pb)/(^{238}U/^{206}Pb * 1/137.88)$

[c]Rho is the error correlation defined as the quotient of the propagated errors of the $^{206}Pb/^{238}U$ and the $^{207}/^{235}U$ ratio

[d]Quadratic addition of within-run errors (2 SD) and daily reproducibility of GJ-1 (2 SD)

[e]Corrected for mass-bias by normalising to GJ-1 reference zircon (~0.6 per atomic mass unit) and common Pb using the model Pb composition of Stacey & Kramers (1975)

Table D20. LA-ICPMS isotopic data for sample AECOCS in the Algoa Basin

AECOC							RATIOS							AGES [Ma]						Conc.
Sample	Analysis	U [ppm][a]	Pb [ppm][a]	Th [ppm][a]	$^{206}Pb/^{204}Pb$	Th/U[a]	$^{207}Pb/^{235}U^{b}$	2 σ[d]	$^{206}Pb/^{238}U^{b}$	2 σ[d]	rho[c]	$^{207}Pb/^{206}Pb^{e}$	2 σ[d]	$^{207}Pb/^{235}U$	2 σ	$^{206}Pb/^{238}U$	2 σ	$^{207}Pb/^{206}Pb$	2 σ	%
AECOC	AECOC-1	159	7	89	47661	0.56	0.315	0.012	0.0425	0.0007	0.42	0.0538	0.0018	278	10	268	4	362	75	74
AECOC	AECOC-2	526	22	136	8127	0.26	0.304	0.009	0.0427	0.0006	0.50	0.0517	0.0013	270	8	269	4	272	58	99
AECOC	AECOC-3	194	18	58	129688	0.30	0.780	0.025	0.0950	0.0014	0.48	0.0595	0.0016	585	18	585	9	585	60	100
AECOC	AECOC-4	292	13	107	3144	0.37	0.309	0.013	0.0435	0.0007	0.39	0.0516	0.0020	274	12	275	5	266	90	103
AECOC	AECOC-5	166	7	57	52779	0.34	0.323	0.018	0.0451	0.0008	0.33	0.0519	0.0027	284	16	285	5	281	121	101
AECOC	AECOC-6	76	11	28	1963	0.36	1.523	0.047	0.1386	0.0021	0.49	0.0797	0.0022	940	29	837	13	1190	53	70
AECOC	AECOC-8	195	8	97	3124	0.50	0.299	0.011	0.0418	0.0007	0.43	0.0518	0.0017	265	10	264	4	276	75	96
AECOC	AECOC-9	71	7	33	606	0.46	0.762	0.051	0.0932	0.0020	0.33	0.0592	0.0037	575	38	575	13	576	137	100
AECOC	AECOC-10	150	11	57	1092	0.38	0.572	0.020	0.0710	0.0011	0.44	0.0585	0.0018	460	16	442	7	549	69	81
AECOC	AECOC-11	152	9	105	64991	0.69	0.464	0.022	0.0607	0.0011	0.37	0.0555	0.0025	387	18	380	7	433	99	88
AECOC	AECOC-12	401	17	248	117687	0.62	0.299	0.009	0.0417	0.0006	0.48	0.0519	0.0014	265	8	263	4	283	62	93
AECOC	AECOC-13	361	63	82	9645	0.23	1.886	0.061	0.1747	0.0027	0.48	0.0783	0.0022	1076	35	1038	16	1155	56	90
AECOC	AECOC-14	213	10	49	69991	0.23	0.336	0.016	0.0467	0.0008	0.36	0.0522	0.0024	294	14	294	5	294	104	100
AECOC	AECOC-15	306	18	156	3776	0.51	0.425	0.013	0.0578	0.0009	0.50	0.0533	0.0014	360	11	362	5	342	59	106
AECOC	AECOC-16	210	9	123	61340	0.59	0.296	0.019	0.0417	0.0008	0.31	0.0515	0.0031	263	16	263	5	262	137	100
AECOC	AECOC-17	471	21	27	2559	0.06	0.319	0.011	0.0447	0.0007	0.44	0.0518	0.0016	281	10	282	4	277	71	102
AECOC	AECOC-18	289	13	83	1513	0.29	0.344	0.017	0.0461	0.0008	0.36	0.0542	0.0025	300	15	290	5	377	103	77
AECOC	AECOC-19	320	13	276	19851	0.86	0.296	0.010	0.0416	0.0006	0.44	0.0516	0.0016	263	9	262	4	267	71	98
AECOC	AECOC-20	361	15	137	108740	0.38	0.305	0.017	0.0429	0.0008	0.34	0.0516	0.0028	271	15	271	5	266	123	102
AECOC	AECOC-21	321	56	31	26183	0.10	1.765	0.046	0.1737	0.0025	0.55	0.0737	0.0016	1033	27	1033	15	1033	44	100
AECOC	AECOC-22	189	15	42	105815	0.22	0.627	0.019	0.0797	0.0012	0.49	0.0570	0.0015	494	15	494	7	492	59	101
AECOC	AECOC-23	112	5	60	2782	0.53	0.306	0.018	0.0428	0.0008	0.33	0.0519	0.0028	271	16	270	5	280	124	96
AECOC	AECOC-24	173	7	94	1008	0.55	0.304	0.013	0.0424	0.0007	0.40	0.0519	0.0020	269	11	268	4	280	86	96
AECOC	AECOC-25	733	29	136	200170	0.19	0.276	0.010	0.0389	0.0006	0.43	0.0514	0.0017	247	9	246	4	259	75	95
AECOC	AECOC-26	265	10	175	73180	0.66	0.279	0.009	0.0394	0.0006	0.45	0.0514	0.0015	250	8	249	4	257	69	97
AECOC	AECOC-27	423	18	147	126175	0.35	0.300	0.009	0.0425	0.0006	0.50	0.0511	0.0013	266	8	268	4	246	60	109
AECOC	AECOC-28	180	8	116	56235	0.64	0.318	0.018	0.0445	0.0008	0.33	0.0520	0.0028	281	16	280	5	283	124	99
AECOC	AECOC-29	107	5	34	294	0.31	0.478	0.025	0.0462	0.0009	0.37	0.0750	0.0037	396	21	291	6	1069	99	27
AECOC	AECOC-30	517	39	143	274269	0.28	0.588	0.016	0.0757	0.0011	0.53	0.0564	0.0013	470	13	470	7	467	51	101
AECOC	AECOC-31	401	19	175	1102	0.44	0.367	0.015	0.0464	0.0008	0.40	0.0574	0.0022	317	13	292	5	505	85	58
AECOC	AECOC-32	191	19	92	134640	0.48	0.838	0.025	0.1003	0.0015	0.51	0.0606	0.0015	618	18	616	9	626	55	98
AECOC	AECOC-33	718	30	209	213287	0.29	0.305	0.010	0.0424	0.0006	0.46	0.0522	0.0015	270	9	268	4	294	66	91
AECOC	AECOC-34	275	13	208	1308	0.75	0.333	0.022	0.0465	0.0010	0.31	0.0520	0.0033	292	19	293	6	286	145	102
AECOC	AECOC-35	195	14	75	99966	0.39	0.569	0.023	0.0732	0.0012	0.41	0.0563	0.0021	457	18	455	7	466	82	98
AECOC	AECOC-36	179	7	82	1095	0.46	0.276	0.018	0.0390	0.0008	0.31	0.0515	0.0033	248	17	246	5	261	146	94
AECOC	AECOC-37	100	7	55	1793	0.55	0.582	0.022	0.0742	0.0012	0.43	0.0569	0.0019	466	17	461	7	486	74	95
AECOC	AECOC-38	231	10	140	72384	0.61	0.326	0.013	0.0447	0.0007	0.41	0.0529	0.0019	287	11	282	5	324	82	87
AECOC	AECOC-39	286	25	40	174356	0.14	0.696	0.020	0.0870	0.0013	0.51	0.0580	0.0015	536	16	538	8	530	55	102
AECOC	AECOC-41	241	10	104	68943	0.43	0.292	0.010	0.0409	0.0006	0.45	0.0519	0.0016	260	9	258	4	279	70	92
AECOC	AECOC-42	356	15	113	9629	0.32	0.302	0.009	0.0425	0.0006	0.49	0.0516	0.0014	268	8	268	4	266	62	101
AECOC	AECOC-44	555	30	197	261890	0.35	0.402	0.011	0.0541	0.0008	0.52	0.0539	0.0013	343	10	339	5	368	55	92
AECOC	AECOC-45	455	23	103	163821	0.23	0.378	0.011	0.0515	0.0008	0.49	0.0532	0.0014	325	10	324	5	338	59	96
AECOC	AECOC-46	334	15	202	4482	0.61	0.319	0.012	0.0445	0.0007	0.42	0.0520	0.0018	281	11	281	5	287	81	98
AECOC	AECOC-47	446	23	412	630	0.92	0.533	0.021	0.0520	0.0009	0.43	0.0744	0.0027	434	17	327	6	1051	73	31
AECOC	AECOC-48	385	16	174	3589	0.45	0.295	0.009	0.0418	0.0006	0.48	0.0512	0.0014	263	8	264	4	251	62	105
AECOC	AECOC-49	63	3	55	212	0.87	0.289	0.028	0.0405	0.0011	0.28	0.0516	0.0048	257	25	256	7	270	213	95
AECOC	AECOC-50	525	21	458	1394	0.87	0.345	0.015	0.0399	0.0007	0.40	0.0628	0.0024	301	13	252	4	700	83	36

AECOC	AECOC-51	472	26	207	179627	0.44	0.404	0.013	0.0545	0.0008	0.47	0.0537	0.0016	344	11	342	5	360	65	95
AECOC	AECOC-52	131	6	71	41304	0.54	0.324	0.017	0.0453	0.0008	0.35	0.0518	0.0025	285	15	286	5	278	112	103
AECOC	AECOC-53	476	28	137	15581	0.29	0.480	0.019	0.0594	0.0010	0.41	0.0586	0.0022	398	16	372	6	553	80	67
AECOC	AECOC-54	301	14	84	3225	0.28	0.324	0.010	0.0452	0.0007	0.47	0.0520	0.0015	285	9	285	4	286	65	99
AECOC	AECOC-55	174	14	24	98072	0.14	0.640	0.020	0.0810	0.0012	0.48	0.0573	0.0016	502	16	502	8	503	60	100
AECOC	AECOC-56	140	8	120	3374	0.86	0.420	0.024	0.0561	0.0011	0.34	0.0544	0.0029	356	20	352	7	387	120	91
AECOC	AECOC-57	169	7	172	51930	1.02	0.355	0.022	0.0442	0.0009	0.33	0.0584	0.0034	309	19	279	6	544	126	51
AECOC	AECOC-58	304	13	172	88489	0.57	0.297	0.010	0.0418	0.0006	0.47	0.0515	0.0015	264	9	264	4	263	66	100
AECOC	AECOC-60	323	26	190	178324	0.59	0.625	0.018	0.0794	0.0012	0.51	0.0571	0.0014	493	14	492	7	495	55	99
AECOC	AECOC-61	329	13	243	93179	0.74	0.289	0.009	0.0407	0.0006	0.46	0.0514	0.0015	258	8	257	4	260	67	99
AECOC	AECOC-62	385	17	260	119332	0.68	0.319	0.010	0.0445	0.0007	0.48	0.0520	0.0015	281	9	281	4	286	64	98
AECOC	AECOC-63	151	6	115	1181	0.77	0.300	0.023	0.0417	0.0010	0.29	0.0522	0.0039	266	21	263	6	294	171	90
AECOC	AECOC-64	415	26	147	181892	0.35	0.472	0.021	0.0629	0.0011	0.38	0.0544	0.0022	392	17	393	7	388	91	101
AECOC	AECOC-65	451	28	143	195061	0.32	0.465	0.017	0.0621	0.0010	0.43	0.0544	0.0018	388	14	388	6	387	75	100
AECOC	AECOC-66	376	16	132	108267	0.35	0.295	0.009	0.0414	0.0006	0.48	0.0517	0.0014	262	8	262	4	271	63	97
AECOC	AECOC-67	169	7	50	49474	0.30	0.300	0.021	0.0421	0.0009	0.31	0.0517	0.0034	266	19	266	6	271	153	98
AECOC	AECOC-68	263	12	217	80796	0.82	0.338	0.016	0.0441	0.0008	0.37	0.0556	0.0024	295	14	278	5	434	96	64
AECOC	AECOC-70	226	9	189	65348	0.83	0.295	0.012	0.0415	0.0007	0.40	0.0516	0.0020	263	11	262	4	266	87	99
AECOC	AECOC-71	167	16	125	9168	0.75	0.814	0.025	0.0980	0.0015	0.49	0.0603	0.0016	605	19	602	9	613	59	98
AECOC	AECOC-72	68	3	36	468	0.53	0.335	0.034	0.0462	0.0013	0.27	0.0526	0.0052	293	30	291	8	311	224	94
AECOC	AECOC-73	219	9	83	63858	0.38	0.300	0.011	0.0420	0.0007	0.45	0.0519	0.0016	267	9	265	4	280	71	95
AECOC	AECOC-74	370	64	97	21277	0.26	1.764	0.047	0.1720	0.0025	0.54	0.0744	0.0017	1032	28	1023	15	1052	46	97
AECOC	AECOC-75	515	21	150	146391	0.29	0.293	0.012	0.0409	0.0007	0.39	0.0519	0.0020	261	11	259	4	279	90	93
AECOC	AECOC-76	595	30	226	28985	0.38	0.403	0.018	0.0509	0.0009	0.39	0.0575	0.0023	344	15	320	6	509	90	63
AECOC	AECOC-77	424	26	121	16608	0.29	0.464	0.015	0.0620	0.0009	0.47	0.0543	0.0015	387	12	387	6	385	64	101
AECOC	AECOC-78	307	14	123	97326	0.40	0.340	0.022	0.0456	0.0009	0.32	0.0540	0.0033	297	19	288	6	371	136	78
AECOC	AECOC-79	151	11	96	79848	0.64	0.591	0.023	0.0762	0.0012	0.42	0.0563	0.0020	472	18	474	8	463	77	102
AECOC	AECOC-80	229	20	127	6757	0.55	0.720	0.025	0.0892	0.0014	0.45	0.0585	0.0018	551	19	551	9	550	67	100
AECOC	AECOC-81	155	8	117	52582	0.75	0.356	0.017	0.0488	0.0009	0.37	0.0529	0.0024	309	15	307	5	326	101	94
AECOC	AECOC-83	248	11	120	3089	0.48	0.307	0.013	0.0430	0.0007	0.40	0.0518	0.0020	272	11	271	4	277	87	98
AECOC	AECOC-84	198	29	60	4202	0.30	1.430	0.040	0.1452	0.0022	0.53	0.0714	0.0017	901	25	874	13	969	49	90
AECOC	AECOC-85	118	5	74	33209	0.62	0.288	0.012	0.0405	0.0007	0.40	0.0516	0.0020	257	11	256	4	270	88	95
AECOC	AECOC-86	154	11	111	1570	0.72	0.580	0.038	0.0716	0.0015	0.33	0.0587	0.0036	464	30	446	9	556	134	80
AECOC	AECOC-87	142	22	45	2211	0.32	1.633	0.047	0.1537	0.0023	0.52	0.0770	0.0019	983	28	922	14	1122	49	82
AECOC	AECOC-88	80	3	76	11676	0.95	0.301	0.034	0.0423	0.0013	0.27	0.0516	0.0056	267	30	267	8	266	251	100
AECOC	AECOC-89	160	8	98	35419	0.61	0.342	0.013	0.0475	0.0008	0.43	0.0523	0.0018	299	11	299	5	296	77	101
AECOC	AECOC-90	661	26	226	181458	0.34	0.283	0.015	0.0396	0.0007	0.35	0.0518	0.0026	253	14	251	5	278	116	90
AECOC	AECOC-91	160	7	156	49766	0.97	0.319	0.014	0.0448	0.0008	0.38	0.0516	0.0021	281	13	283	5	266	95	106
AECOC	AECOC-92	39	7	15	46615	0.39	1.763	0.062	0.1733	0.0028	0.46	0.0738	0.0023	1032	37	1030	17	1036	64	99
AECOC	AECOC-94	278	11	155	78530	0.56	0.295	0.011	0.0409	0.0007	0.43	0.0523	0.0018	262	10	258	4	297	78	87
AECOC	AECOC-95	294	12	142	2223	0.48	0.286	0.018	0.0404	0.0008	0.32	0.0513	0.0031	255	16	255	5	256	137	100
AECOC	AECOC-96	843	42	235	292731	0.28	0.363	0.015	0.0502	0.0008	0.40	0.0525	0.0019	315	13	316	5	307	84	103
AECOC	AECOC-97	60	11	36	77284	0.59	1.951	0.063	0.1851	0.0029	0.49	0.0765	0.0021	1099	35	1095	17	1107	56	99
AECOC	AECOC-98	104	19	37	3080	0.35	1.876	0.056	0.1808	0.0028	0.51	0.0753	0.0019	1073	32	1071	16	1075	51	100

[a]U and Pb concentrations and Th/U ratios are calculated relative to GJ-1 reference zircon

[b]Corrected for background and within-run Pb/U fractionation and normalised to reference zircon GJ-1 (ID-TIMS values/measured value); $^{207}Pb/^{235}U$ calculated using $(^{207}Pb/^{206}Pb)/(^{238}U/^{206}Pb * 1/137.88)$

[c]Rho is the error correlation defined as the quotient of the propagated errors of the $^{206}Pb/^{238}U$ and the $^{207}/^{235}U$ ratio

[d]Quadratic addition of within-run errors (2 SD) and daily reproducibility of GJ-1 (2 SD)

[e]Corrected for mass-bias by normalising to GJ-1 reference zircon (~0.6 per atomic mass unit) and common Pb using the model Pb composition of Stacey & Kramers (1975)

Table D21. LA-ICPMS isotopic data for sample AKIRK in the Algoa Basin

AKIRK							RATIOS							AGES [Ma]						Conc.
Sample	Analysis	U [ppm][a]	Pb [ppm][a]	Th [ppm][a]	$^{206}Pb/^{204}Pb$	Th/U[a]	$^{207}Pb/^{235}U$[b]	2 σ[d]	$^{206}Pb/^{238}U$[b]	2 σ[d]	rho[c]	$^{207}Pb/^{206}Pb$[e]	2 σ[d]	$^{207}Pb/^{235}U$	2 σ	$^{206}Pb/^{238}U$	2 σ	$^{207}Pb/^{206}Pb$	2 σ	%
AKIRK	AKIRK-1	257	46	139	317637	0.54	1.860	0.051	0.1803	0.0027	0.54	0.0748	0.0017	1067	29	1069	16	1064	46	100
AKIRK	AKIRK-2	576	17	200	119101	0.35	0.208	0.008	0.0302	0.0005	0.42	0.0500	0.0016	192	7	192	3	196	76	98
AKIRK	AKIRK-3	745	33	436	228837	0.59	0.324	0.013	0.0449	0.0007	0.40	0.0524	0.0019	285	11	283	5	303	83	93
AKIRK	AKIRK-4	127	7	100	1767	0.78	0.417	0.018	0.0562	0.0010	0.39	0.0538	0.0022	354	15	353	6	364	90	97
AKIRK	AKIRK-5	292	9	228	2805	0.78	0.203	0.018	0.0292	0.0005	0.19	0.0504	0.0044	188	17	186	3	214	204	87
AKIRK	AKIRK-6	233	11	124	2319	0.53	0.342	0.014	0.0474	0.0008	0.41	0.0522	0.0019	298	12	299	5	296	84	101
AKIRK	AKIRK-8	117	5	75	3322	0.65	0.327	0.019	0.0459	0.0009	0.33	0.0518	0.0028	288	17	289	6	275	126	105
AKIRK	AKIRK-9	406	17	153	4273	0.38	0.301	0.012	0.0422	0.0007	0.42	0.0518	0.0018	267	10	266	4	275	80	97
AKIRK	AKIRK-10	279	27	160	19866	0.57	0.780	0.022	0.0952	0.0014	0.52	0.0594	0.0015	585	17	586	9	581	53	101
AKIRK	AKIRK-11	205	20	95	140420	0.46	0.830	0.024	0.0997	0.0015	0.51	0.0604	0.0015	614	18	613	9	618	54	99
AKIRK	AKIRK-12	747	43	168	21215	0.23	0.449	0.014	0.0581	0.0009	0.50	0.0561	0.0015	376	11	364	6	456	58	80
AKIRK	AKIRK-13	188	19	49	2445	0.26	0.836	0.025	0.1002	0.0015	0.51	0.0605	0.0016	617	18	616	9	620	56	99
AKIRK	AKIRK-14	227	25	62	174658	0.27	0.969	0.031	0.1123	0.0017	0.48	0.0626	0.0018	688	22	686	11	693	61	99
AKIRK	AKIRK-15	373	16	321	1630	0.86	0.322	0.010	0.0433	0.0007	0.48	0.0540	0.0015	283	9	273	4	371	63	74
AKIRK	AKIRK-16	229	43	132	296724	0.58	2.029	0.055	0.1888	0.0028	0.55	0.0780	0.0018	1125	30	1115	16	1146	45	97
AKIRK	AKIRK-17	352	14	128	96121	0.36	0.281	0.014	0.0399	0.0007	0.35	0.0512	0.0024	252	13	252	4	251	108	100
AKIRK	AKIRK-18	155	27	65	184157	0.42	1.745	0.049	0.1733	0.0026	0.53	0.0730	0.0017	1025	29	1030	15	1015	48	102
AKIRK	AKIRK-19	267	14	183	5305	0.69	0.379	0.026	0.0524	0.0011	0.31	0.0525	0.0035	326	23	329	7	306	150	107
AKIRK	AKIRK-20	560	24	199	163137	0.36	0.303	0.009	0.0425	0.0006	0.51	0.0518	0.0013	269	8	268	4	277	57	97
AKIRK	AKIRK-21	393	23	171	159777	0.43	0.441	0.013	0.0593	0.0009	0.50	0.0540	0.0014	371	11	371	6	369	58	101
AKIRK	AKIRK-22	396	22	116	148522	0.29	0.403	0.012	0.0546	0.0008	0.49	0.0535	0.0014	344	10	343	5	349	60	98
AKIRK	AKIRK-23	329	15	319	100478	0.97	0.320	0.011	0.0445	0.0007	0.45	0.0521	0.0016	282	10	281	4	290	69	97
AKIRK	AKIRK-24	145	13	56	14550	0.39	0.698	0.022	0.0864	0.0013	0.48	0.0586	0.0016	537	17	534	8	552	61	97
AKIRK	AKIRK-25	223	9	142	575	0.64	0.297	0.015	0.0415	0.0007	0.36	0.0519	0.0024	264	13	262	5	279	107	94
AKIRK	AKIRK-26	131	6	97	338	0.73	0.344	0.034	0.0468	0.0013	0.28	0.0533	0.0051	300	30	295	8	342	216	86
AKIRK	AKIRK-27	156	13	146	3362	0.94	0.659	0.024	0.0827	0.0013	0.44	0.0579	0.0019	514	18	512	8	524	71	98
AKIRK	AKIRK-28	475	18	339	126532	0.71	0.275	0.010	0.0388	0.0006	0.42	0.0513	0.0018	246	9	245	4	256	80	96
AKIRK	AKIRK-29	160	7	156	931	0.98	0.294	0.012	0.0410	0.0007	0.40	0.0519	0.0020	261	11	259	4	281	86	92
AKIRK	AKIRK-30	246	38	138	3188	0.56	1.460	0.041	0.1530	0.0023	0.53	0.0692	0.0017	914	26	917	14	905	49	101
AKIRK	AKIRK-31	407	12	407	81309	1.00	0.200	0.012	0.0291	0.0004	0.24	0.0499	0.0030	185	12	185	3	189	141	98
AKIRK	AKIRK-32	237	20	60	2047	0.25	0.663	0.021	0.0835	0.0013	0.48	0.0576	0.0016	517	16	517	8	516	61	100
AKIRK	AKIRK-33	236	10	186	2497	0.79	0.294	0.012	0.0413	0.0007	0.39	0.0516	0.0020	261	11	261	4	268	88	97
AKIRK	AKIRK-34	276	49	63	17424	0.23	1.850	0.052	0.1782	0.0027	0.53	0.0753	0.0018	1064	30	1057	16	1077	47	98
AKIRK	AKIRK-35	205	6	367	41181	1.79	0.200	0.012	0.0292	0.0005	0.27	0.0495	0.0029	185	11	186	3	173	135	107
AKIRK	AKIRK-36	99	6	40	40993	0.41	0.453	0.017	0.0605	0.0010	0.42	0.0542	0.0019	379	15	379	6	381	78	100
AKIRK	AKIRK-37	446	21	196	6670	0.44	0.340	0.012	0.0470	0.0007	0.44	0.0524	0.0017	297	11	296	5	303	72	98
AKIRK	AKIRK-38	291	12	131	1023	0.45	0.282	0.014	0.0396	0.0007	0.36	0.0516	0.0023	252	12	250	4	269	104	93
AKIRK	AKIRK-39	93	9	120	62885	1.28	0.817	0.034	0.0978	0.0017	0.40	0.0606	0.0023	606	26	602	10	623	83	97
AKIRK	AKIRK-40	175	15	102	60239	0.58	0.711	0.025	0.0880	0.0014	0.45	0.0586	0.0018	545	19	544	9	552	68	98
AKIRK	AKIRK-41	244	46	102	2084	0.42	1.975	0.059	0.1875	0.0029	0.51	0.0764	0.0020	1107	33	1108	17	1105	51	100
AKIRK	AKIRK-42	476	19	164	4778	0.34	0.278	0.011	0.0392	0.0006	0.40	0.0515	0.0019	249	10	248	4	263	85	94
AKIRK	AKIRK-43	578	42	304	1467	0.53	0.757	0.022	0.0723	0.0011	0.51	0.0759	0.0019	572	17	450	7	1092	51	41
AKIRK	AKIRK-44	137	6	137	42284	1.00	0.320	0.018	0.0448	0.0008	0.33	0.0518	0.0028	282	16	282	5	277	123	102
AKIRK	AKIRK-45	247	45	30	307644	0.12	1.872	0.053	0.1806	0.0027	0.53	0.0752	0.0018	1071	30	1070	16	1073	48	100
AKIRK	AKIRK-46	153	25	102	172626	0.67	1.639	0.050	0.1643	0.0025	0.50	0.0724	0.0019	985	30	980	15	996	54	98
AKIRK	AKIRK-47	347	50	45	3553	0.13	1.381	0.043	0.1438	0.0022	0.49	0.0696	0.0019	881	27	866	13	917	56	94
AKIRK	AKIRK-48	157	13	64	1418	0.41	0.733	0.023	0.0823	0.0013	0.49	0.0646	0.0017	558	17	510	8	761	57	67

AKIRK	AKIRK-49	317	53	47	19638	0.15	1.755	0.049	0.1673	0.0025	0.54	0.0761	0.0018	1029	28	997	15	1098	47	91
AKIRK	AKIRK-50	412	67	174	3543	0.42	1.672	0.047	0.1625	0.0024	0.53	0.0746	0.0018	998	28	971	14	1058	49	92
AKIRK	AKIRK-51	402	79	223	4651	0.56	2.166	0.058	0.1965	0.0029	0.55	0.0800	0.0018	1170	31	1156	17	1196	44	97
AKIRK	AKIRK-52	525	39	304	10836	0.58	0.587	0.018	0.0741	0.0011	0.49	0.0575	0.0015	469	14	461	7	510	59	90
AKIRK	AKIRK-53	181	9	153	781	0.85	0.341	0.017	0.0476	0.0008	0.36	0.0520	0.0024	298	15	300	5	287	105	104
AKIRK	AKIRK-54	211	9	103	61387	0.49	0.315	0.020	0.0421	0.0009	0.32	0.0542	0.0033	278	18	266	6	381	138	70
AKIRK	AKIRK-55	441	19	447	130746	1.01	0.309	0.009	0.0430	0.0006	0.48	0.0520	0.0014	273	8	272	4	285	62	95
AKIRK	AKIRK-56	118	3	155	10385	1.31	0.198	0.011	0.0288	0.0005	0.32	0.0498	0.0025	184	10	183	3	187	118	98
AKIRK	AKIRK-57	367	15	374	103742	1.02	0.294	0.010	0.0411	0.0006	0.45	0.0520	0.0015	262	9	259	4	286	68	91
AKIRK	AKIRK-58	525	24	334	8239	0.64	0.329	0.010	0.0459	0.0007	0.48	0.0520	0.0014	289	9	289	4	287	62	101
AKIRK	AKIRK-59	574	21	189	148032	0.33	0.268	0.013	0.0374	0.0006	0.37	0.0520	0.0023	241	11	237	4	286	99	83
AKIRK	AKIRK-60	280	12	137	6694	0.49	0.295	0.010	0.0416	0.0006	0.45	0.0515	0.0016	263	9	263	4	262	70	100
AKIRK	AKIRK-62	504	21	244	6917	0.48	0.299	0.009	0.0422	0.0006	0.50	0.0514	0.0013	266	8	267	4	261	59	102
AKIRK	AKIRK-63	466	23	267	159747	0.57	0.364	0.013	0.0496	0.0008	0.44	0.0531	0.0017	315	11	312	5	333	72	94
AKIRK	AKIRK-64	166	7	105	577	0.63	0.300	0.016	0.0420	0.0008	0.34	0.0518	0.0026	267	14	265	5	278	114	95
AKIRK	AKIRK-65	344	46	69	2461	0.20	1.365	0.037	0.1329	0.0019	0.54	0.0745	0.0017	874	23	804	12	1056	45	76
AKIRK	AKIRK-66	213	36	32	57959	0.15	1.692	0.055	0.1682	0.0026	0.48	0.0730	0.0021	1006	33	1002	16	1013	58	99
AKIRK	AKIRK-67	496	15	433	101617	0.87	0.205	0.007	0.0297	0.0004	0.46	0.0499	0.0014	189	6	189	3	192	66	98
AKIRK	AKIRK-68	448	37	360	2616	0.80	0.660	0.023	0.0829	0.0013	0.45	0.0578	0.0018	514	18	513	8	520	67	99
AKIRK	AKIRK-70	645	57	387	1378	0.60	0.873	0.023	0.0892	0.0013	0.54	0.0710	0.0016	637	17	551	8	958	46	57
AKIRK	AKIRK-71	354	14	248	51001	0.70	0.285	0.009	0.0401	0.0006	0.47	0.0516	0.0015	255	8	253	4	267	65	95
AKIRK	AKIRK-72	221	12	79	82400	0.36	0.396	0.020	0.0539	0.0010	0.35	0.0533	0.0025	339	17	339	6	341	107	99
AKIRK	AKIRK-73	481	19	257	131749	0.53	0.282	0.012	0.0397	0.0007	0.40	0.0515	0.0020	252	11	251	4	264	88	95
AKIRK	AKIRK-74	364	16	308	1117	0.85	0.311	0.011	0.0434	0.0007	0.44	0.0520	0.0016	275	10	274	4	284	72	97
AKIRK	AKIRK-75	304	54	95	374986	0.31	1.856	0.051	0.1787	0.0026	0.54	0.0753	0.0017	1066	29	1060	16	1077	46	98
AKIRK	AKIRK-76	191	34	122	169167	0.64	1.849	0.051	0.1787	0.0026	0.53	0.0751	0.0018	1063	29	1060	16	1070	47	99
AKIRK	AKIRK-77	224	7	241	45697	1.08	0.203	0.014	0.0295	0.0005	0.23	0.0498	0.0032	188	13	188	3	188	151	100
AKIRK	AKIRK-78	126	4	172	1871	1.36	0.200	0.011	0.0291	0.0005	0.31	0.0499	0.0027	185	10	185	3	188	124	98
AKIRK	AKIRK-79	159	16	153	113332	0.96	0.865	0.029	0.1028	0.0016	0.47	0.0610	0.0018	633	21	631	10	640	63	99
AKIRK	AKIRK-80	330	63	111	10797	0.34	2.017	0.054	0.1902	0.0028	0.54	0.0769	0.0017	1121	30	1122	16	1119	45	100
AKIRK	AKIRK-81	566	23	263	2846	0.46	0.296	0.011	0.0415	0.0007	0.42	0.0518	0.0018	263	10	262	4	275	78	95
AKIRK	AKIRK-82	317	26	119	14171	0.37	0.635	0.018	0.0805	0.0012	0.51	0.0572	0.0014	499	14	499	7	499	55	100
AKIRK	AKIRK-83	243	17	95	1307	0.39	0.548	0.020	0.0713	0.0011	0.43	0.0557	0.0018	444	16	444	7	441	73	101
AKIRK	AKIRK-84	185	17	102	117403	0.56	0.751	0.026	0.0920	0.0014	0.45	0.0592	0.0018	569	20	567	9	574	68	99
AKIRK	AKIRK-85	313	50	58	14893	0.19	1.642	0.046	0.1587	0.0023	0.53	0.0751	0.0018	987	28	949	14	1071	48	89
AKIRK	AKIRK-86	1043	47	521	651	0.50	0.468	0.015	0.0448	0.0007	0.48	0.0757	0.0021	389	12	283	4	1087	56	26
AKIRK	AKIRK-87	195	16	141	5686	0.72	0.654	0.020	0.0815	0.0012	0.49	0.0582	0.0016	511	16	505	8	539	59	94
AKIRK	AKIRK-88	171	15	111	6566	0.65	0.703	0.032	0.0870	0.0015	0.38	0.0586	0.0025	541	25	538	9	554	93	97
AKIRK	AKIRK-89	209	9	63	61950	0.30	0.308	0.012	0.0428	0.0007	0.41	0.0522	0.0019	273	11	270	4	295	83	91
AKIRK	AKIRK-90	427	14	123	1995	0.29	0.302	0.010	0.0320	0.0005	0.45	0.0683	0.0021	268	9	203	3	878	64	23
AKIRK	AKIRK-91	115	55	55	9514	0.48	11.945	0.348	0.4786	0.0076	0.55	0.1810	0.0044	2600	76	2521	40	2662	40	95
AKIRK	AKIRK-92	400	12	437	2877	1.09	0.199	0.009	0.0290	0.0004	0.34	0.0497	0.0021	184	8	184	3	182	99	101
AKIRK	AKIRK-93	384	15	134	3462	0.35	0.295	0.018	0.0400	0.0008	0.32	0.0535	0.0030	262	16	253	5	349	129	72
AKIRK	AKIRK-94	110	33	33	227809	0.31	4.406	0.149	0.3002	0.0050	0.49	0.1065	0.0031	1713	58	1692	28	1740	54	97
AKIRK	AKIRK-95	88	7	32	574	0.37	0.621	0.031	0.0786	0.0014	0.37	0.0573	0.0026	491	24	488	9	505	101	97
AKIRK	AKIRK-96	72	6	36	42599	0.50	0.687	0.030	0.0851	0.0015	0.39	0.0585	0.0024	531	23	527	9	550	89	96
AKIRK	AKIRK-97	551	25	116	170231	0.21	0.322	0.010	0.0446	0.0007	0.50	0.0524	0.0013	284	8	281	4	304	58	93
AKIRK	AKIRK-98	146	13	40	1450	0.28	0.688	0.027	0.0854	0.0014	0.42	0.0585	0.0021	532	21	528	9	547	78	97
AKIRK	AKIRK-99	441	18	239	124344	0.54	0.287	0.009	0.0407	0.0006	0.48	0.0511	0.0014	256	8	257	4	245	62	105

AKIRK	AKIRK-100	244	10	117	83955	0.48	0.305	0.011	0.0427	0.0007	0.44	0.0518	0.0016	270	9	269	4	275	72	98
AKIRK	AKIRK-101	240	14	88	98528	0.37	0.442	0.014	0.0591	0.0009	0.48	0.0543	0.0015	372	12	370	6	383	63	97
AKIRK	AKIRK-102	143	7	49	45839	0.34	0.332	0.013	0.0461	0.0007	0.42	0.0523	0.0018	291	11	291	5	296	79	98
AKIRK	AKIRK-103	214	9	115	441	0.54	0.312	0.018	0.0424	0.0008	0.33	0.0533	0.0029	276	16	268	5	341	125	79
AKIRK	AKIRK-104	82	14	22	1500	0.27	1.859	0.080	0.1759	0.0031	0.42	0.0767	0.0030	1067	46	1044	19	1112	78	94
AKIRK	AKIRK-105	140	12	62	82592	0.44	0.683	0.026	0.0851	0.0014	0.42	0.0582	0.0020	529	20	526	9	537	76	98
AKIRK	AKIRK-106	146	14	40	4246	0.27	0.807	0.029	0.0974	0.0015	0.45	0.0601	0.0019	601	21	599	9	606	68	99
AKIRK	AKIRK-107	266	11	129	4501	0.49	0.317	0.013	0.0426	0.0007	0.40	0.0540	0.0020	280	12	269	4	369	85	73
AKIRK	AKIRK-108	134	25	31	8585	0.23	1.935	0.055	0.1848	0.0027	0.52	0.0759	0.0019	1093	31	1093	16	1093	49	100
AKIRK	AKIRK-109	325	14	128	99195	0.39	0.315	0.011	0.0440	0.0007	0.45	0.0518	0.0016	278	9	278	4	278	70	100
AKIRK	AKIRK-110	128	6	249	392	1.95	0.484	0.029	0.0480	0.0010	0.35	0.0732	0.0041	401	24	302	6	1019	113	30
AKIRK	AKIRK-111	173	8	169	1683	0.98	0.331	0.019	0.0462	0.0009	0.33	0.0520	0.0028	290	17	291	6	285	124	102
AKIRK	AKIRK-112	61	2	75	328	1.23	0.200	0.030	0.0289	0.0006	0.13	0.0501	0.0074	185	28	184	4	198	344	93
AKIRK	AKIRK-113	540	23	365	156608	0.68	0.295	0.009	0.0418	0.0006	0.49	0.0512	0.0013	262	8	264	4	250	60	105
AKIRK	AKIRK-114	195	18	63	6060	0.32	0.771	0.023	0.0941	0.0014	0.49	0.0595	0.0016	581	18	580	9	584	58	99

[a]U and Pb concentrations and Th/U ratios are calculated relative to GJ-1 reference zircon

[b]Corrected for background and within-run Pb/U fractionation and normalised to reference zircon GJ-1 (ID-TIMS values/measured value); $^{207}Pb/^{235}U$ calculated using ($^{207}Pb/^{206}Pb$)/($^{238}U/^{206}Pb$ * 1/137.88)

[c]Rho is the error correlation defined as the quotient of the propagated errors of the $^{206}Pb/^{238}U$ and the $^{207}/^{235}U$ ratio

[d]Quadratic addition of within-run errors (2 SD) and daily reproducibility of GJ-1 (2 SD)

[e]Corrected for mass-bias by normalising to GJ-1 reference zircon (~0.6 per atomic mass unit) and common Pb using the model Pb composition of Stacey & Kramers (1975)

Table D22. LA-ICPMS isotopic data for sample AKSTR in the Algoa Basin

AKSTR							RATIOS							AGES [Ma]						Conc.
Sample	Analysis	U [ppm][a]	Pb [ppm][a]	Th [ppm][a]	^{206}Pb/^{204}Pb	Th/U[a]	^{207}Pb/^{235}U[b]	2 σ[d]	^{206}Pb/^{238}U[b]	2 σ[d]	rho[c]	^{207}Pb/^{206}Pb	2 σ[d]	^{207}Pb/^{235}U	2 σ	^{206}Pb/^{238}U	2 σ	^{207}Pb/^{206}Pb	2 σ	%
AKSTR	AKSTR-1	159	5	146	571	0.92	0.207	0.030	0.0298	0.0005	0.11	0.0504	0.0071	191	27	189	3	213	328	89
AKSTR	AKSTR-2	879	57	339	490	0.39	0.727	0.023	0.0648	0.0010	0.49	0.0813	0.0023	555	18	405	6	1229	55	33
AKSTR	AKSTR-3	495	91	171	644106	0.35	1.923	0.050	0.1830	0.0027	0.56	0.0762	0.0016	1089	28	1084	16	1101	43	98
AKSTR	AKSTR-4	776	122	207	4776	0.27	1.729	0.050	0.1568	0.0024	0.52	0.0800	0.0020	1019	30	939	14	1197	49	78
AKSTR	AKSTR-5	227	19	97	2433	0.43	0.805	0.027	0.0848	0.0013	0.46	0.0688	0.0021	600	20	525	8	894	62	59
AKSTR	AKSTR-6	484	35	265	1600	0.55	0.621	0.024	0.0717	0.0012	0.42	0.0628	0.0022	490	19	446	7	702	76	64
AKSTR	AKSTR-7	557	40	158	2712	0.28	0.569	0.024	0.0725	0.0012	0.40	0.0569	0.0022	457	19	451	8	487	86	93
AKSTR	AKSTR-8	145	12	67	85303	0.47	0.660	0.022	0.0830	0.0013	0.47	0.0577	0.0017	515	17	514	8	518	65	99
AKSTR	AKSTR-9	282	52	106	9700	0.37	1.968	0.052	0.1861	0.0027	0.55	0.0767	0.0017	1104	29	1100	16	1113	44	99
AKSTR	AKSTR-10	573	51	93	1455	0.16	0.984	0.035	0.0889	0.0015	0.46	0.0803	0.0026	696	25	549	9	1204	63	46
AKSTR	AKSTR-12	508	41	213	6611	0.42	0.645	0.018	0.0813	0.0012	0.54	0.0575	0.0013	505	14	504	7	512	50	98
AKSTR	AKSTR-13	707	64	93	17321	0.13	0.730	0.019	0.0903	0.0013	0.55	0.0586	0.0013	557	15	557	8	554	48	101
AKSTR	AKSTR-14	463	79	93	40389	0.20	1.742	0.046	0.1707	0.0025	0.56	0.0740	0.0016	1024	27	1016	15	1042	44	97
AKSTR	AKSTR-15	80	13	26	4175	0.32	1.615	0.053	0.1617	0.0025	0.48	0.0725	0.0021	976	32	966	15	999	58	97
AKSTR	AKSTR-16	150	26	43	16751	0.29	1.850	0.053	0.1771	0.0027	0.53	0.0758	0.0018	1064	30	1051	16	1090	49	96
AKSTR	AKSTR-17	98	8	51	54280	0.52	0.608	0.034	0.0777	0.0015	0.35	0.0568	0.0030	482	27	482	9	483	117	100
AKSTR	AKSTR-18	554	45	93	5745	0.17	0.650	0.023	0.0818	0.0013	0.45	0.0576	0.0018	509	18	507	8	516	69	98
AKSTR	AKSTR-19	69	11	76	76299	1.10	1.617	0.082	0.1550	0.0031	0.39	0.0757	0.0035	977	49	929	18	1086	93	86
AKSTR	AKSTR-20	136	15	48	103956	0.35	0.908	0.042	0.1073	0.0019	0.39	0.0614	0.0026	656	30	657	12	653	91	101
AKSTR	AKSTR-21	314	38	123	25238	0.39	1.068	0.029	0.1215	0.0018	0.54	0.0637	0.0015	738	20	739	11	732	49	101
AKSTR	AKSTR-22	57	10	22	2747	0.38	1.728	0.063	0.1683	0.0028	0.45	0.0745	0.0024	1019	37	1003	17	1055	66	95
AKSTR	AKSTR-23	359	10	453	1254	1.26	0.197	0.007	0.0287	0.0004	0.42	0.0497	0.0016	183	7	183	3	183	77	100
AKSTR	AKSTR-24	262	38	83	2376	0.32	1.556	0.047	0.1459	0.0022	0.50	0.0774	0.0020	953	29	878	13	1130	53	78
AKSTR	AKSTR-25	177	30	179	3401	1.01	1.802	0.054	0.1690	0.0026	0.51	0.0774	0.0020	1046	31	1007	15	1130	51	89
AKSTR	AKSTR-26	200	21	71	1349	0.36	0.992	0.028	0.1042	0.0016	0.52	0.0690	0.0017	700	20	639	10	898	50	71
AKSTR	AKSTR-27	61	16	74	7728	1.20	4.401	0.168	0.2565	0.0047	0.48	0.1245	0.0042	1713	65	1472	27	2021	59	73
AKSTR	AKSTR-28	271	28	131	197769	0.48	0.856	0.024	0.1024	0.0015	0.53	0.0607	0.0015	628	18	628	9	628	52	100
AKSTR	AKSTR-29	61	10	23	72377	0.37	1.657	0.053	0.1666	0.0026	0.49	0.0721	0.0020	992	32	993	16	989	57	100
AKSTR	AKSTR-30	385	42	77	4391	0.20	0.919	0.027	0.1086	0.0016	0.51	0.0614	0.0016	662	20	665	10	652	55	102
AKSTR	AKSTR-31	234	23	22	1919	0.09	0.970	0.027	0.0996	0.0015	0.53	0.0706	0.0017	688	19	612	9	946	49	65
AKSTR	AKSTR-32	368	40	135	8619	0.37	0.988	0.030	0.1083	0.0016	0.50	0.0662	0.0017	698	21	663	10	812	55	82
AKSTR	AKSTR-33	221	6	220	3263	0.99	0.201	0.015	0.0292	0.0005	0.20	0.0499	0.0038	186	14	185	3	189	175	98
AKSTR	AKSTR-34	283	30	55	5149	0.19	0.884	0.026	0.1049	0.0016	0.51	0.0612	0.0015	643	19	643	10	645	53	100
AKSTR	AKSTR-35	360	37	77	263263	0.21	0.856	0.026	0.1027	0.0015	0.50	0.0605	0.0016	628	19	630	9	621	56	101
AKSTR	AKSTR-36	299	12	129	8611	0.43	0.273	0.012	0.0386	0.0006	0.38	0.0512	0.0021	245	11	244	4	249	94	98
AKSTR	AKSTR-37	549	51	65	13156	0.12	0.763	0.021	0.0935	0.0014	0.53	0.0591	0.0014	576	16	576	9	572	51	101
AKSTR	AKSTR-38	249	26	186	9387	0.75	0.869	0.027	0.1028	0.0016	0.49	0.0613	0.0017	635	20	631	10	650	58	97
AKSTR	AKSTR-39	111	18	36	8238	0.33	1.643	0.056	0.1647	0.0026	0.47	0.0724	0.0022	987	33	983	16	997	61	99
AKSTR	AKSTR-40	108	3	113	6468	1.05	0.200	0.015	0.0293	0.0005	0.23	0.0497	0.0037	185	14	186	3	179	175	104
AKSTR	AKSTR-41	243	48	130	339445	0.54	2.119	0.056	0.1956	0.0029	0.55	0.0786	0.0017	1155	31	1152	17	1162	44	99
AKSTR	AKSTR-42	101	18	32	124847	0.31	1.759	0.055	0.1735	0.0027	0.50	0.0736	0.0020	1031	32	1031	16	1029	54	100
AKSTR	AKSTR-43	292	24	101	5621	0.35	0.694	0.026	0.0829	0.0013	0.44	0.0608	0.0020	535	20	513	8	631	72	81
AKSTR	AKSTR-44	638	67	77	13193	0.12	0.889	0.025	0.1051	0.0015	0.53	0.0613	0.0014	646	18	644	9	650	50	99
AKSTR	AKSTR-45	135	25	85	4380	0.63	1.961	0.115	0.1814	0.0040	0.38	0.0784	0.0043	1102	65	1075	24	1157	108	93
AKSTR	AKSTR-47	432	34	207	2974	0.48	0.708	0.024	0.0789	0.0012	0.46	0.0651	0.0020	543	19	489	8	776	64	63
AKSTR	AKSTR-48	227	18	170	126005	0.75	0.609	0.019	0.0778	0.0012	0.48	0.0569	0.0016	483	15	483	7	486	61	99
AKSTR	AKSTR-49	188	23	47	4783	0.25	1.317	0.048	0.1244	0.0020	0.45	0.0768	0.0025	853	31	756	12	1115	64	68

AKSTR	AKSTR-50	490	31	263	17052	0.54	0.480	0.016	0.0634	0.0010	0.47	0.0549	0.0016	398	13	396	6	407	65	97
AKSTR	AKSTR-51	533	39	234	276047	0.44	0.561	0.021	0.0727	0.0012	0.42	0.0560	0.0019	452	17	452	7	452	77	100
AKSTR	AKSTR-52	399	34	119	3909	0.30	0.716	0.025	0.0851	0.0013	0.44	0.0610	0.0019	548	19	526	8	641	68	82
AKSTR	AKSTR-53	88	9	21	3033	0.23	0.800	0.029	0.0970	0.0016	0.44	0.0598	0.0020	597	22	597	10	597	72	100
AKSTR	AKSTR-54	170	16	88	116066	0.52	0.944	0.041	0.0959	0.0017	0.41	0.0714	0.0028	675	29	590	10	968	80	61
AKSTR	AKSTR-55	198	17	30	16491	0.15	0.668	0.021	0.0837	0.0013	0.49	0.0579	0.0016	520	16	518	8	525	60	99
AKSTR	AKSTR-56	24	2	8	218	0.35	0.833	0.062	0.0999	0.0024	0.32	0.0605	0.0043	616	46	614	15	623	152	98
AKSTR	AKSTR-57	201	35	155	20271	0.77	1.799	0.062	0.1726	0.0028	0.47	0.0756	0.0023	1045	36	1026	17	1084	60	95
AKSTR	AKSTR-58	272	28	35	196801	0.13	0.842	0.025	0.1012	0.0015	0.51	0.0603	0.0015	620	18	621	9	615	54	101
AKSTR	AKSTR-59	430	37	147	267527	0.34	0.705	0.020	0.0873	0.0013	0.51	0.0586	0.0015	542	16	539	8	551	54	98
AKSTR	AKSTR-60	331	27	108	1301	0.33	0.764	0.021	0.0820	0.0012	0.53	0.0676	0.0016	576	16	508	7	857	49	59
AKSTR	AKSTR-61	173	16	120	111063	0.69	0.730	0.035	0.0899	0.0016	0.38	0.0589	0.0026	556	27	555	10	563	96	99
AKSTR	AKSTR-62	557	34	189	2205	0.34	0.552	0.020	0.0613	0.0010	0.44	0.0653	0.0021	446	16	384	6	784	68	49
AKSTR	AKSTR-63	503	38	350	8017	0.70	0.582	0.017	0.0754	0.0011	0.52	0.0560	0.0014	466	13	469	7	452	54	104
AKSTR	AKSTR-64	175	31	79	14442	0.45	1.855	0.057	0.1772	0.0027	0.50	0.0759	0.0020	1065	32	1052	16	1093	53	96
AKSTR	AKSTR-65	205	34	46	241422	0.22	1.651	0.051	0.1649	0.0025	0.50	0.0726	0.0020	990	31	984	15	1004	55	98
AKSTR	AKSTR-66	318	9	271	853	0.85	0.206	0.018	0.0296	0.0005	0.18	0.0506	0.0042	191	16	188	3	223	194	84
AKSTR	AKSTR-67	284	50	154	359239	0.54	1.831	0.049	0.1774	0.0026	0.54	0.0749	0.0017	1057	29	1053	15	1064	46	99
AKSTR	AKSTR-68	199	30	76	211538	0.38	1.492	0.042	0.1490	0.0022	0.53	0.0727	0.0017	927	26	895	13	1004	48	89
AKSTR	AKSTR-69	240	41	56	2833	0.23	1.715	0.060	0.1690	0.0027	0.46	0.0736	0.0023	1014	36	1006	16	1031	63	98
AKSTR	AKSTR-70	175	33	80	235606	0.46	1.998	0.060	0.1890	0.0029	0.51	0.0767	0.0020	1115	33	1116	17	1113	52	100
AKSTR	AKSTR-71	336	24	146	4182	0.43	0.563	0.027	0.0719	0.0013	0.38	0.0569	0.0025	454	22	447	8	487	97	92
AKSTR	AKSTR-72	299	29	61	210055	0.21	0.814	0.023	0.0983	0.0015	0.52	0.0600	0.0015	605	17	605	9	605	53	100
AKSTR	AKSTR-73	79	9	32	61356	0.41	0.942	0.040	0.1094	0.0019	0.41	0.0624	0.0024	674	29	669	12	689	83	97
AKSTR	AKSTR-74	352	34	85	4053	0.24	0.797	0.024	0.0966	0.0014	0.50	0.0599	0.0015	595	18	594	9	600	56	99
AKSTR	AKSTR-75	119	12	35	85897	0.30	0.842	0.046	0.1013	0.0020	0.36	0.0603	0.0031	621	34	622	12	614	110	101
AKSTR	AKSTR-76	360	10	426	2722	1.18	0.198	0.008	0.0288	0.0005	0.41	0.0500	0.0018	184	7	183	3	195	83	94
AKSTR	AKSTR-77	453	37	115	266955	0.25	0.653	0.018	0.0826	0.0012	0.52	0.0574	0.0014	510	14	511	8	506	53	101
AKSTR	AKSTR-78	604	47	99	1040	0.16	0.711	0.023	0.0774	0.0012	0.48	0.0667	0.0019	546	17	481	7	827	58	58
AKSTR	AKSTR-80	488	31	139	756	0.28	0.643	0.021	0.0640	0.0010	0.48	0.0729	0.0021	504	16	400	6	1011	58	40
AKSTR	AKSTR-81	402	30	97	1570	0.24	0.651	0.022	0.0754	0.0012	0.46	0.0627	0.0019	509	18	468	7	697	65	67
AKSTR	AKSTR-82	381	15	288	107785	0.75	0.281	0.009	0.0396	0.0006	0.47	0.0515	0.0015	252	8	250	4	264	65	95
AKSTR	AKSTR-83	367	62	52	621115	0.14	1.690	0.045	0.1684	0.0025	0.54	0.0728	0.0016	1005	27	1003	15	1009	46	99
AKSTR	AKSTR-84	253	19	62	22303	0.24	0.578	0.021	0.0748	0.0012	0.44	0.0561	0.0018	463	17	465	7	455	72	102
AKSTR	AKSTR-85	190	19	70	134504	0.37	0.825	0.036	0.0991	0.0017	0.40	0.0604	0.0024	611	26	609	10	616	86	99
AKSTR	AKSTR-86	608	105	203	19970	0.33	1.767	0.047	0.1729	0.0025	0.55	0.0741	0.0017	1033	28	1028	15	1044	45	98
AKSTR	AKSTR-87	179	15	84	107063	0.47	0.670	0.026	0.0836	0.0014	0.42	0.0581	0.0020	521	20	518	8	534	77	97
AKSTR	AKSTR-88	376	39	48	280942	0.13	0.886	0.025	0.1045	0.0015	0.53	0.0615	0.0015	644	18	640	9	658	51	97
AKSTR	AKSTR-89	169	30	238	5013	1.40	1.909	0.065	0.1753	0.0028	0.47	0.0790	0.0024	1084	37	1041	17	1172	59	89
AKSTR	AKSTR-90	68	6	25	41226	0.37	0.684	0.036	0.0846	0.0016	0.36	0.0586	0.0029	529	28	524	10	553	108	95
AKSTR	AKSTR-91	168	13	57	695	0.34	0.638	0.046	0.0790	0.0018	0.32	0.0586	0.0040	501	36	490	11	551	150	89
AKSTR	AKSTR-92	247	45	55	318739	0.22	1.879	0.051	0.1802	0.0026	0.54	0.0757	0.0017	1074	29	1068	16	1086	46	98
AKSTR	AKSTR-93	273	28	64	6946	0.24	0.867	0.025	0.1032	0.0015	0.51	0.0610	0.0015	634	18	633	9	637	54	99
AKSTR	AKSTR-94	177	28	109	201880	0.61	1.549	0.045	0.1594	0.0024	0.52	0.0705	0.0018	950	28	953	14	942	51	101
AKSTR	AKSTR-95	243	20	106	139907	0.44	0.639	0.019	0.0806	0.0012	0.50	0.0576	0.0015	502	15	499	7	513	57	97
AKSTR	AKSTR-96	200	14	96	1578	0.48	0.593	0.027	0.0715	0.0013	0.38	0.0601	0.0026	472	22	445	8	606	92	73
AKSTR	AKSTR-97	300	13	218	1627	0.73	0.308	0.015	0.0432	0.0008	0.37	0.0517	0.0023	273	13	273	5	273	102	100
AKSTR	AKSTR-98	382	17	386	119370	1.01	0.313	0.021	0.0436	0.0009	0.31	0.0521	0.0032	277	18	275	6	288	142	96
AKSTR	AKSTR-100	94	18	78	15521	0.82	1.980	0.059	0.1860	0.0028	0.51	0.0772	0.0020	1109	33	1099	17	1127	52	98

AKSTR	AKSTR-101	67	7	18	53592	0.27	0.966	0.084	0.1124	0.0031	0.31	0.0623	0.0052	686	60	687	19	685	177	100
AKSTR	AKSTR-103	488	81	125	3551	0.26	1.805	0.052	0.1670	0.0025	0.52	0.0784	0.0019	1047	30	996	15	1157	49	86
AKSTR	AKSTR-104	182	34	47	10560	0.26	2.021	0.067	0.1894	0.0030	0.48	0.0774	0.0023	1123	37	1118	18	1132	58	99
AKSTR	AKSTR-105	156	12	71	86806	0.45	0.647	0.039	0.0777	0.0016	0.34	0.0604	0.0034	506	30	482	10	617	121	78
AKSTR	AKSTR-106	160	6	245	510	1.53	0.316	0.036	0.0396	0.0012	0.28	0.0579	0.0063	279	31	250	8	525	237	48
AKSTR	AKSTR-107	107	9	28	2343	0.27	0.713	0.044	0.0885	0.0018	0.34	0.0584	0.0034	546	33	547	11	545	126	100
AKSTR	AKSTR-108	254	23	56	1989	0.22	0.753	0.022	0.0921	0.0014	0.51	0.0593	0.0015	570	17	568	9	576	55	99
AKSTR	AKSTR-109	324	58	57	417417	0.18	1.871	0.051	0.1801	0.0026	0.54	0.0754	0.0017	1071	29	1068	16	1078	46	99
AKSTR	AKSTR-110	332	10	385	1737	1.16	0.201	0.013	0.0292	0.0005	0.25	0.0499	0.0030	186	12	185	3	188	141	98
AKSTR	AKSTR-111	159	23	161	8678	1.02	1.498	0.080	0.1441	0.0029	0.38	0.0754	0.0037	930	49	868	18	1079	98	80
AKSTR	AKSTR-112	475	103	98	10845	0.21	2.488	0.071	0.2176	0.0032	0.53	0.0829	0.0020	1269	36	1269	19	1267	47	100
AKSTR	AKSTR-113	241	43	53	307781	0.22	1.846	0.051	0.1784	0.0026	0.53	0.0750	0.0018	1062	29	1058	16	1069	47	99
AKSTR	AKSTR-114	543	51	440	817	0.81	0.958	0.027	0.0930	0.0014	0.52	0.0747	0.0018	682	19	573	9	1060	49	54
AKSTR	AKSTR-115	68	6	24	41677	0.35	0.687	0.037	0.0851	0.0016	0.36	0.0585	0.0029	531	28	526	10	550	109	96
AKSTR	AKSTR-116	208	16	97	6952	0.47	0.661	0.020	0.0763	0.0011	0.49	0.0628	0.0017	515	16	474	7	702	57	67

[a] U and Pb concentrations and Th/U ratios are calculated relative to GJ-1 reference zircon

[b] Corrected for background and within-run Pb/U fractionation and normalised to reference zircon GJ-1 (ID-TIMS values/measured value); $^{207}Pb/^{235}U$ calculated using $(^{207}Pb/^{206}Pb)/(^{238}U/^{206}Pb * 1/137.88)$

[c] Rho is the error correlation defined as the quotient of the propagated errors of the $^{206}Pb/^{238}U$ and the $^{207}/^{235}U$ ratio

[d] Quadratic addition of within-run errors (2 SD) and daily reproducibility of GJ-1 (2 SD)

[e] Corrected for mass-bias by normalising to GJ-1 reference zircon (~0.6 per atomic mass unit) and common Pb using the model Pb composition of Stacey & Kramers (1975)

Table D23. LA-ICPMS isotopic data for sample KDUNS in the Algoa Basin

KDUNS							RATIOS							AGES [Ma]						Conc.
Sample	Analysis	U [ppm][a]	Pb [ppm][a]	Th [ppm][a]	^{206}Pb/^{204}Pb	Th/U[a]	^{207}Pb/^{235}U[b]	2 σ[d]	^{206}Pb/^{238}U[b]	2 σ[d]	rho[c]	^{207}Pb/^{206}Pb	2 σ[d]	^{207}Pb/^{235}U	2 σ	^{206}Pb/^{238}U	2 σ	^{207}Pb/^{206}Pb	2 σ	%
KDUNS	KDUNS-1	599	32	46	216401	0.08	0.401	0.011	0.0538	0.0008	0.51	0.0541	0.0013	342	9	338	5	374	53	90
KDUNS	KDUNS-2	605	33	47	5401	0.08	0.398	0.011	0.0544	0.0008	0.52	0.0530	0.0013	340	9	342	5	328	54	104
KDUNS	KDUNS-3	853	72	328	486725	0.38	0.682	0.018	0.0849	0.0012	0.53	0.0582	0.0013	528	14	525	7	538	48	98
KDUNS	KDUNS-4	77	3	32	20826	0.41	0.356	0.050	0.0405	0.0016	0.28	0.0638	0.0086	309	44	256	10	734	287	35
KDUNS	KDUNS-5	529	43	69	286733	0.13	0.644	0.018	0.0806	0.0011	0.51	0.0579	0.0014	504	14	500	7	525	52	95
KDUNS	KDUNS-6	132	7	32	1799	0.24	0.376	0.020	0.0517	0.0009	0.34	0.0527	0.0027	324	17	325	6	316	115	103
KDUNS	KDUNS-7	444	19	120	9167	0.27	0.307	0.011	0.0428	0.0007	0.42	0.0521	0.0017	272	10	270	4	291	75	93
KDUNS	KDUNS-9	523	24	152	163042	0.29	0.334	0.013	0.0464	0.0007	0.40	0.0522	0.0019	293	12	293	5	296	83	99
KDUNS	KDUNS-10	142	11	35	75607	0.25	0.620	0.020	0.0790	0.0012	0.46	0.0569	0.0016	490	16	490	7	487	64	101
KDUNS	KDUNS-11	290	14	290	5706	1.00	0.341	0.012	0.0472	0.0007	0.42	0.0523	0.0017	298	11	297	5	298	75	100
KDUNS	KDUNS-12	222	9	225	1247	1.01	0.302	0.011	0.0427	0.0007	0.41	0.0513	0.0018	268	10	270	4	256	80	105
KDUNS	KDUNS-13	328	14	249	93406	0.76	0.301	0.009	0.0424	0.0006	0.46	0.0514	0.0014	267	8	268	4	261	64	103
KDUNS	KDUNS-14	591	26	358	866	0.61	0.393	0.016	0.0439	0.0007	0.41	0.0649	0.0024	336	14	277	5	770	77	36
KDUNS	KDUNS-15	243	18	123	6699	0.51	0.575	0.022	0.0739	0.0012	0.41	0.0565	0.0020	462	18	460	7	471	77	98
KDUNS	KDUNS-16	235	11	119	4373	0.51	0.321	0.011	0.0447	0.0007	0.44	0.0520	0.0016	282	10	282	4	285	71	99
KDUNS	KDUNS-17	222	9	107	980	0.48	0.285	0.015	0.0399	0.0007	0.34	0.0517	0.0025	254	13	252	4	273	110	92
KDUNS	KDUNS-18	478	20	506	3985	1.06	0.300	0.011	0.0414	0.0006	0.43	0.0526	0.0017	267	10	262	4	313	74	84
KDUNS	KDUNS-19	170	7	61	4714	0.36	0.285	0.016	0.0394	0.0007	0.33	0.0524	0.0028	254	14	249	5	302	122	82
KDUNS	KDUNS-20	128	6	116	594	0.90	0.316	0.020	0.0440	0.0009	0.31	0.0520	0.0031	278	17	278	5	286	135	97
KDUNS	KDUNS-21	255	14	155	18986	0.61	0.401	0.015	0.0548	0.0008	0.41	0.0531	0.0018	342	13	344	5	332	77	103
KDUNS	KDUNS-22	384	13	221	26914	0.57	0.244	0.012	0.0346	0.0006	0.35	0.0512	0.0023	222	11	220	4	249	103	88
KDUNS	KDUNS-23	152	13	56	86996	0.37	0.689	0.028	0.0855	0.0014	0.40	0.0584	0.0021	532	21	529	9	546	80	97
KDUNS	KDUNS-24	247	7	334	46204	1.35	0.191	0.014	0.0279	0.0006	0.29	0.0497	0.0035	177	13	177	4	179	166	99
KDUNS	KDUNS-25	189	17	76	1468	0.40	0.718	0.022	0.0885	0.0013	0.48	0.0589	0.0016	550	17	546	8	563	59	97
KDUNS	KDUNS-26	537	25	267	165237	0.50	0.340	0.010	0.0458	0.0007	0.50	0.0538	0.0013	297	9	289	4	361	56	80
KDUNS	KDUNS-27	119	6	94	39911	0.79	0.364	0.020	0.0499	0.0009	0.34	0.0529	0.0027	315	17	314	6	324	116	97
KDUNS	KDUNS-28	114	14	37	5102	0.33	1.109	0.036	0.1217	0.0018	0.47	0.0661	0.0019	758	24	741	11	809	60	92
KDUNS	KDUNS-29	296	11	202	72741	0.68	0.259	0.021	0.0367	0.0009	0.29	0.0512	0.0040	234	19	232	5	251	181	92
KDUNS	KDUNS-30	165	7	121	902	0.73	0.296	0.021	0.0416	0.0009	0.30	0.0516	0.0034	263	18	263	6	269	152	98
KDUNS	KDUNS-31	59	10	69	69850	1.17	1.812	0.062	0.1767	0.0028	0.46	0.0744	0.0023	1050	36	1049	16	1052	61	100
KDUNS	KDUNS-32	367	15	259	994	0.71	0.286	0.020	0.0397	0.0008	0.30	0.0522	0.0036	255	18	251	5	295	156	85
KDUNS	KDUNS-33	131	16	74	108005	0.56	1.109	0.034	0.1228	0.0018	0.48	0.0655	0.0018	758	23	747	11	791	57	94
KDUNS	KDUNS-34	512	92	237	618612	0.46	1.882	0.048	0.1801	0.0025	0.55	0.0758	0.0016	1075	27	1068	15	1089	43	98
KDUNS	KDUNS-35	302	13	323	1080	1.07	0.318	0.011	0.0443	0.0007	0.44	0.0520	0.0016	280	9	280	4	287	69	98
KDUNS	KDUNS-36	73	7	28	3003	0.38	0.785	0.038	0.0953	0.0017	0.37	0.0597	0.0027	588	28	587	10	593	97	99
KDUNS	KDUNS-37	171	35	87	5173	0.51	2.230	0.067	0.2021	0.0030	0.50	0.0800	0.0021	1191	36	1187	18	1198	51	99
KDUNS	KDUNS-38	160	7	132	1873	0.83	0.337	0.018	0.0466	0.0009	0.34	0.0524	0.0027	295	16	294	5	302	117	97
KDUNS	KDUNS-39	97	19	48	85695	0.49	2.123	0.064	0.1944	0.0029	0.49	0.0792	0.0021	1156	35	1145	17	1177	51	97
KDUNS	KDUNS-40	221	18	65	2505	0.30	0.653	0.021	0.0823	0.0012	0.47	0.0575	0.0016	510	16	510	8	512	61	100
KDUNS	KDUNS-41	501	20	444	3250	0.89	0.287	0.011	0.0407	0.0006	0.41	0.0512	0.0018	256	10	257	4	250	80	103
KDUNS	KDUNS-42	170	14	272	11042	1.61	0.680	0.021	0.0846	0.0012	0.47	0.0583	0.0016	527	16	524	8	541	60	97
KDUNS	KDUNS-43	381	17	199	113162	0.52	0.318	0.010	0.0443	0.0006	0.47	0.0521	0.0014	281	9	279	4	290	61	96
KDUNS	KDUNS-44	197	8	233	53058	1.18	0.284	0.010	0.0402	0.0006	0.43	0.0512	0.0017	254	9	254	4	250	76	102
KDUNS	KDUNS-45	327	9	252	1700	0.77	0.188	0.011	0.0278	0.0005	0.32	0.0493	0.0026	175	10	176	3	160	125	110
KDUNS	KDUNS-46	158	27	83	177768	0.53	1.695	0.049	0.1683	0.0025	0.51	0.0731	0.0018	1007	29	1003	15	1016	50	99
KDUNS	KDUNS-47	710	24	531	1650	0.75	0.242	0.011	0.0336	0.0006	0.37	0.0522	0.0022	220	10	213	4	293	95	73
KDUNS	KDUNS-48	212	12	59	77391	0.28	0.406	0.015	0.0546	0.0008	0.43	0.0540	0.0017	346	12	342	5	370	73	93

KDUNS	KDUNS-49	168	7	107	1716	0.64	0.304	0.031	0.0427	0.0012	0.27	0.0517	0.0051	270	28	270	8	270	228	100
KDUNS	KDUNS-50	324	14	179	5170	0.55	0.322	0.010	0.0448	0.0007	0.46	0.0521	0.0015	283	9	282	4	291	66	97
KDUNS	KDUNS-51	936	25	531	1154	0.57	0.182	0.015	0.0264	0.0006	0.28	0.0501	0.0039	170	14	168	4	198	182	85
KDUNS	KDUNS-52	292	50	71	5590	0.24	1.743	0.051	0.1698	0.0025	0.50	0.0745	0.0019	1025	30	1011	15	1054	51	96
KDUNS	KDUNS-53	124	5	43	1866	0.35	0.260	0.018	0.0369	0.0008	0.30	0.0511	0.0034	235	16	234	5	247	152	95
KDUNS	KDUNS-54	463	20	204	132348	0.44	0.304	0.009	0.0426	0.0006	0.48	0.0516	0.0014	269	8	269	4	270	60	100
KDUNS	KDUNS-55	105	12	37	11073	0.36	0.958	0.035	0.1119	0.0018	0.43	0.0621	0.0020	682	25	684	11	677	70	101
KDUNS	KDUNS-56	150	13	66	1474	0.44	0.762	0.031	0.0844	0.0014	0.40	0.0655	0.0025	575	24	523	9	789	79	66
KDUNS	KDUNS-57	450	81	118	543928	0.26	1.921	0.056	0.1804	0.0026	0.50	0.0772	0.0019	1088	32	1069	16	1127	50	95
KDUNS	KDUNS-58	233	44	63	292020	0.27	1.952	0.052	0.1868	0.0027	0.53	0.0758	0.0017	1099	29	1104	16	1090	45	101
KDUNS	KDUNS-59	48	8	12	53665	0.25	1.692	0.079	0.1675	0.0031	0.39	0.0733	0.0031	1005	47	998	18	1021	87	98
KDUNS	KDUNS-60	205	9	108	5619	0.53	0.333	0.012	0.0462	0.0007	0.42	0.0524	0.0017	292	10	291	4	302	74	96
KDUNS	KDUNS-61	281	23	146	11687	0.52	0.632	0.026	0.0802	0.0013	0.40	0.0571	0.0021	497	20	497	8	497	83	100
KDUNS	KDUNS-62	412	17	221	3247	0.54	0.294	0.009	0.0415	0.0006	0.47	0.0515	0.0015	262	8	262	4	261	65	100
KDUNS	KDUNS-63	199	18	85	117846	0.43	0.723	0.023	0.0885	0.0013	0.47	0.0592	0.0017	552	18	547	8	574	61	95
KDUNS	KDUNS-64	425	18	281	2721	0.66	0.305	0.010	0.0428	0.0006	0.46	0.0518	0.0015	271	9	270	4	277	65	97
KDUNS	KDUNS-65	188	17	119	3574	0.64	0.754	0.023	0.0926	0.0014	0.49	0.0591	0.0016	570	17	571	8	569	57	100
KDUNS	KDUNS-66	526	23	216	153833	0.41	0.313	0.009	0.0437	0.0006	0.48	0.0519	0.0014	276	8	276	4	281	61	98
KDUNS	KDUNS-67	94	8	36	4460	0.38	0.721	0.034	0.0889	0.0016	0.37	0.0588	0.0026	551	26	549	10	560	96	98
KDUNS	KDUNS-68	523	23	231	154688	0.44	0.317	0.009	0.0442	0.0006	0.49	0.0521	0.0013	280	8	279	4	290	59	96
KDUNS	KDUNS-69	141	26	126	173742	0.89	1.922	0.054	0.1839	0.0027	0.52	0.0758	0.0018	1089	31	1088	16	1089	48	100
KDUNS	KDUNS-70	73	2	128	16086	1.75	0.231	0.019	0.0329	0.0008	0.28	0.0508	0.0041	211	18	209	5	234	187	89
KDUNS	KDUNS-71	700	105	85	591817	0.12	1.489	0.042	0.1507	0.0022	0.51	0.0717	0.0018	926	26	905	13	977	50	93
KDUNS	KDUNS-72	206	42	83	281464	0.40	2.257	0.061	0.2043	0.0029	0.53	0.0801	0.0018	1199	32	1199	17	1199	45	100
KDUNS	KDUNS-73	610	43	82	1449	0.14	0.786	0.024	0.0710	0.0011	0.49	0.0804	0.0022	589	18	442	7	1206	53	37
KDUNS	KDUNS-74	156	6	254	1467	1.62	0.279	0.018	0.0393	0.0008	0.31	0.0515	0.0032	250	16	248	5	261	142	95
KDUNS	KDUNS-75	250	39	58	259184	0.23	1.595	0.051	0.1547	0.0023	0.48	0.0748	0.0021	968	31	927	14	1062	56	87
KDUNS	KDUNS-76	128	8	80	605	0.62	0.685	0.034	0.0657	0.0012	0.38	0.0756	0.0035	530	27	410	8	1086	93	38
KDUNS	KDUNS-77	186	8	164	528	0.88	0.442	0.021	0.0442	0.0008	0.38	0.0726	0.0032	372	18	279	5	1002	89	28
KDUNS	KDUNS-79	239	11	188	18535	0.79	0.331	0.011	0.0461	0.0007	0.45	0.0520	0.0016	290	10	291	4	285	69	102
KDUNS	KDUNS-80	125	6	230	37937	1.83	0.323	0.023	0.0453	0.0010	0.30	0.0518	0.0035	284	20	285	6	277	153	103
KDUNS	KDUNS-81	404	17	145	111195	0.36	0.290	0.009	0.0411	0.0006	0.47	0.0511	0.0014	258	8	260	4	246	63	106
KDUNS	KDUNS-82	130	23	59	26115	0.45	1.795	0.052	0.1753	0.0026	0.51	0.0743	0.0018	1044	30	1041	15	1049	50	99
KDUNS	KDUNS-84	265	11	102	55489	0.39	0.303	0.012	0.0425	0.0007	0.40	0.0516	0.0019	269	11	269	4	268	83	100
KDUNS	KDUNS-85	231	8	126	1685	0.54	0.248	0.012	0.0346	0.0006	0.36	0.0519	0.0023	225	11	219	4	281	103	78
KDUNS	KDUNS-86	562	68	262	1337	0.47	1.220	0.039	0.1201	0.0018	0.48	0.0737	0.0021	810	26	731	11	1032	57	71
KDUNS	KDUNS-87	243	9	137	4217	0.56	0.271	0.012	0.0384	0.0006	0.36	0.0511	0.0022	243	11	243	4	246	99	99
KDUNS	KDUNS-88	881	29	487	2639	0.55	0.230	0.016	0.0327	0.0007	0.30	0.0511	0.0034	210	15	207	4	245	153	85
KDUNS	KDUNS-89	394	60	76	398610	0.19	1.448	0.041	0.1513	0.0022	0.51	0.0694	0.0017	909	26	908	13	911	50	100
KDUNS	KDUNS-90	459	19	218	18705	0.48	0.302	0.009	0.0425	0.0006	0.48	0.0516	0.0014	268	8	268	4	269	61	100
KDUNS	KDUNS-91	325	25	26	14178	0.08	0.614	0.018	0.0781	0.0011	0.49	0.0570	0.0015	486	14	485	7	490	57	99
KDUNS	KDUNS-92	910	36	280	1759	0.31	0.293	0.013	0.0398	0.0007	0.38	0.0533	0.0021	261	11	252	4	343	91	73
KDUNS	KDUNS-93	189	11	142	1037	0.75	0.412	0.015	0.0560	0.0009	0.42	0.0534	0.0018	350	13	351	5	344	75	102
KDUNS	KDUNS-94	513	21	151	138546	0.29	0.287	0.011	0.0404	0.0006	0.40	0.0515	0.0019	256	10	255	4	262	84	97
KDUNS	KDUNS-95	316	16	107	107396	0.34	0.377	0.012	0.0509	0.0007	0.46	0.0537	0.0015	325	10	320	5	358	63	89
KDUNS	KDUNS-96	91	8	31	50223	0.34	0.673	0.026	0.0828	0.0013	0.42	0.0589	0.0020	522	20	513	8	563	75	91
KDUNS	KDUNS-97	611	25	390	168386	0.64	0.294	0.009	0.0412	0.0006	0.49	0.0518	0.0013	262	8	260	4	277	59	94
KDUNS	KDUNS-98	216	10	300	9296	1.39	0.320	0.013	0.0441	0.0007	0.40	0.0527	0.0019	282	11	278	4	315	82	88
KDUNS	KDUNS-99	127	5	120	36647	0.94	0.308	0.013	0.0431	0.0007	0.38	0.0518	0.0021	272	12	272	4	277	92	98

KDUNS	KDUNS-100	227	15	96	730	0.42	0.513	0.024	0.0672	0.0012	0.37	0.0554	0.0024	421	20	419	7	427	97	98
KDUNS	KDUNS-101	506	38	87	7042	0.17	0.589	0.017	0.0752	0.0011	0.51	0.0569	0.0014	471	13	467	7	487	54	96
KDUNS	KDUNS-102	211	40	117	42082	0.56	2.058	0.057	0.1911	0.0028	0.52	0.0781	0.0018	1135	31	1127	16	1150	47	98
KDUNS	KDUNS-103	258	41	53	3430	0.20	1.654	0.045	0.1580	0.0023	0.52	0.0759	0.0018	991	27	946	14	1093	47	87
KDUNS	KDUNS-104	520	33	212	11471	0.41	0.505	0.024	0.0640	0.0011	0.37	0.0572	0.0025	415	19	400	7	500	96	80
KDUNS	KDUNS-105	228	38	90	2999	0.39	1.634	0.047	0.1644	0.0024	0.51	0.0721	0.0018	983	28	981	14	988	50	99
KDUNS	KDUNS-106	982	106	29	709212	0.03	0.922	0.025	0.1081	0.0015	0.53	0.0618	0.0014	663	18	662	9	668	49	99
KDUNS	KDUNS-107	154	9	77	2694	0.50	0.413	0.023	0.0560	0.0010	0.33	0.0535	0.0028	351	20	351	7	351	119	100
KDUNS	KDUNS-108	484	79	54	530617	0.11	1.660	0.048	0.1643	0.0024	0.50	0.0733	0.0018	994	29	980	14	1023	51	96
KDUNS	KDUNS-109	143	6	124	39362	0.86	0.319	0.025	0.0412	0.0010	0.30	0.0561	0.0042	281	22	260	6	454	166	57
KDUNS	KDUNS-110	403	29	145	191389	0.36	0.543	0.022	0.0711	0.0011	0.40	0.0554	0.0020	441	18	443	7	430	82	103
KDUNS	KDUNS-111	265	13	112	3053	0.42	0.349	0.013	0.0483	0.0007	0.42	0.0524	0.0017	304	11	304	5	302	75	101
KDUNS	KDUNS-112	206	8	107	1292	0.52	0.280	0.013	0.0398	0.0007	0.36	0.0511	0.0022	251	11	251	4	246	98	102
KDUNS	KDUNS-113	294	15	168	100142	0.57	0.375	0.020	0.0509	0.0009	0.34	0.0534	0.0027	323	17	320	6	347	113	92
KDUNS	KDUNS-114	299	12	200	82988	0.67	0.297	0.010	0.0416	0.0006	0.45	0.0519	0.0015	264	9	263	4	280	68	94
KDUNS	KDUNS-115	337	15	155	791	0.46	0.316	0.030	0.0434	0.0011	0.28	0.0529	0.0048	279	26	274	7	323	204	85
KDUNS	KDUNS-116	78	2	101	12979	1.30	0.171	0.032	0.0250	0.0012	0.24	0.0495	0.0091	160	30	159	7	170	429	94
KDUNS	KDUNS-117	101	21	43	1822	0.43	2.255	0.068	0.2042	0.0030	0.50	0.0801	0.0021	1198	36	1198	18	1199	51	100

[a]U and Pb concentrations and Th/U ratios are calculated relative to GJ-1 reference zircon

[b]Corrected for background and within-run Pb/U fractionation and normalised to reference zircon GJ-1 (ID-TIMS values/measured value); ^{207}Pb/^{235}U calculated using (^{207}Pb/^{206}Pb)/(^{238}U/^{206}Pb * 1/137.88)

[c]Rho is the error correlation defined as the quotient of the propagated errors of the ^{206}Pb/^{238}U and the ^{207}/^{235}U ratio

[d]Quadratic addition of within-run errors (2 SD) and daily reproducibility of GJ-1 (2 SD)

[e]Corrected for mass-bias by normalising to GJ-1 reference zircon (~0.6 per atomic mass unit) and common Pb using the model Pb composition of Stacey & Kramers (1975)

Table D24. LA-ICPMS isotopic data for sample SRFS1 in the Algoa Basin

SRFS1							RATIOS							AGES [Ma]						Conc.
Sample	Analysis	U [ppm][a]	Pb [ppm][a]	Th [ppm][a]	$^{206}Pb/^{204}Pb$	Th/U[a]	$^{207}Pb/^{235}U$[b]	2 σ[d]	$^{206}Pb/^{238}U$[b]	2 σ[d]	rho[c]	$^{207}Pb/^{206}Pb$[e]	2 σ[d]	$^{207}Pb/^{235}U$	2 σ	$^{206}Pb/^{238}U$	2 σ	$^{207}Pb/^{206}Pb$	2 σ	%
SRFS1	SRFS1-1	141	7	121	46975	0.86	0.384	0.026	0.0481	0.0010	0.32	0.0578	0.0037	330	22	303	7	523	142	58
SRFS1	SRFS1-2	240	10	141	9421	0.59	0.310	0.010	0.0434	0.0006	0.45	0.0517	0.0015	274	9	274	4	272	67	101
SRFS1	SRFS1-3	301	13	82	1166	0.27	0.303	0.011	0.0425	0.0007	0.43	0.0517	0.0017	269	10	268	4	274	75	98
SRFS1	SRFS1-4	1100	43	431	9783	0.39	0.277	0.009	0.0392	0.0006	0.44	0.0513	0.0015	248	8	248	4	256	69	97
SRFS1	SRFS1-5	255	11	116	73025	0.46	0.295	0.026	0.0414	0.0010	0.28	0.0518	0.0044	263	23	261	7	277	195	94
SRFS1	SRFS1-6	291	12	227	83097	0.78	0.291	0.009	0.0411	0.0006	0.46	0.0513	0.0015	260	8	260	4	256	65	101
SRFS1	SRFS1-7	214	9	181	63836	0.85	0.305	0.011	0.0429	0.0007	0.44	0.0515	0.0016	270	9	271	4	264	72	103
SRFS1	SRFS1-8	300	57	220	12226	0.73	2.005	0.054	0.1894	0.0027	0.54	0.0768	0.0017	1117	30	1118	16	1115	45	100
SRFS1	SRFS1-9	69	6	23	44589	0.34	0.791	0.048	0.0928	0.0019	0.34	0.0618	0.0035	592	36	572	12	668	123	86
SRFS1	SRFS1-10	144	13	103	1627	0.72	0.708	0.027	0.0868	0.0014	0.42	0.0592	0.0021	544	21	537	9	574	76	93
SRFS1	SRFS1-11	197	19	61	134625	0.31	0.825	0.024	0.0983	0.0014	0.50	0.0608	0.0015	611	18	605	9	634	54	95
SRFS1	SRFS1-12	902	49	107	338419	0.12	0.396	0.011	0.0540	0.0008	0.52	0.0532	0.0012	339	9	339	5	337	52	101
SRFS1	SRFS1-13	875	74	333	17979	0.38	0.671	0.018	0.0849	0.0012	0.54	0.0574	0.0013	521	14	525	7	506	48	104
SRFS1	SRFS1-14	224	11	174	955	0.78	0.353	0.016	0.0487	0.0008	0.38	0.0527	0.0022	307	14	306	5	315	94	97
SRFS1	SRFS1-15	358	67	147	464121	0.41	1.967	0.052	0.1868	0.0027	0.54	0.0764	0.0017	1104	29	1104	16	1105	45	100
SRFS1	SRFS1-17	309	13	158	89435	0.51	0.298	0.014	0.0416	0.0007	0.36	0.0519	0.0023	265	12	263	4	280	100	94
SRFS1	SRFS1-18	324	14	145	98839	0.45	0.313	0.014	0.0439	0.0007	0.37	0.0517	0.0021	277	12	277	5	273	95	101
SRFS1	SRFS1-19	378	14	231	6968	0.61	0.265	0.014	0.0378	0.0007	0.34	0.0508	0.0025	239	13	239	4	232	115	103
SRFS1	SRFS1-20	389	27	125	3066	0.32	0.552	0.021	0.0698	0.0011	0.42	0.0574	0.0020	446	17	435	7	507	75	86
SRFS1	SRFS1-21	281	11	476	24202	1.70	0.272	0.020	0.0384	0.0008	0.30	0.0514	0.0035	245	18	243	5	257	158	94
SRFS1	SRFS1-22	235	10	221	68248	0.94	0.301	0.016	0.0418	0.0008	0.34	0.0523	0.0026	267	14	264	5	300	115	88
SRFS1	SRFS1-23	239	9	102	66006	0.43	0.298	0.019	0.0397	0.0008	0.32	0.0545	0.0032	265	17	251	5	391	133	64
SRFS1	SRFS1-24	417	24	173	169224	0.41	0.438	0.016	0.0584	0.0009	0.41	0.0544	0.0018	369	14	366	6	388	76	94
SRFS1	SRFS1-25	799	31	284	11837	0.36	0.272	0.008	0.0385	0.0006	0.48	0.0513	0.0014	244	7	243	4	254	61	96
SRFS1	SRFS1-26	357	16	199	2576	0.56	0.312	0.015	0.0438	0.0008	0.36	0.0518	0.0024	276	13	276	5	275	104	100
SRFS1	SRFS1-27	325	42	36	9793	0.11	1.213	0.033	0.1300	0.0019	0.53	0.0677	0.0016	806	22	788	11	859	48	92
SRFS1	SRFS1-28	191	8	54	382	0.28	0.301	0.020	0.0423	0.0009	0.31	0.0517	0.0032	267	18	267	5	270	144	99
SRFS1	SRFS1-29	296	13	109	93729	0.37	0.326	0.010	0.0455	0.0007	0.47	0.0519	0.0014	286	9	287	4	281	63	102
SRFS1	SRFS1-30	347	13	170	90551	0.49	0.264	0.011	0.0375	0.0006	0.40	0.0511	0.0019	238	9	237	4	245	84	97
SRFS1	SRFS1-31	310	12	169	4240	0.54	0.275	0.009	0.0390	0.0006	0.46	0.0511	0.0015	247	8	247	4	247	66	100
SRFS1	SRFS1-32	409	17	98	48658	0.24	0.316	0.017	0.0414	0.0008	0.34	0.0553	0.0028	279	15	262	5	425	112	62
SRFS1	SRFS1-34	690	37	323	255267	0.47	0.393	0.013	0.0531	0.0008	0.46	0.0537	0.0016	337	11	334	5	357	66	93
SRFS1	SRFS1-37	145	23	46	3374	0.32	1.711	0.055	0.1587	0.0024	0.48	0.0782	0.0022	1013	33	949	15	1152	56	82
SRFS1	SRFS1-38	367	36	64	251430	0.17	0.811	0.022	0.0982	0.0014	0.53	0.0599	0.0014	603	16	604	9	599	50	101
SRFS1	SRFS1-39	247	20	130	135868	0.53	0.621	0.019	0.0789	0.0012	0.49	0.0571	0.0015	491	15	490	7	495	58	99
SRFS1	SRFS1-40	735	27	512	186590	0.70	0.262	0.009	0.0365	0.0006	0.43	0.0521	0.0017	236	8	231	4	289	73	80
SRFS1	SRFS1-41	513	39	133	2470	0.26	0.646	0.026	0.0762	0.0012	0.41	0.0614	0.0022	506	20	474	8	654	78	72
SRFS1	SRFS1-42	351	15	177	102274	0.50	0.298	0.016	0.0418	0.0008	0.34	0.0516	0.0026	264	14	264	5	268	116	98
SRFS1	SRFS1-43	481	22	217	27957	0.45	0.333	0.010	0.0462	0.0007	0.49	0.0524	0.0014	292	9	291	4	301	60	97
SRFS1	SRFS1-44	790	43	427	5583	0.54	0.405	0.013	0.0539	0.0008	0.45	0.0546	0.0016	345	11	338	5	394	66	86
SRFS1	SRFS1-45	228	27	59	4919	0.26	1.134	0.039	0.1201	0.0019	0.45	0.0685	0.0021	770	27	731	11	882	64	83
SRFS1	SRFS1-46	840	44	73	2396	0.09	0.391	0.012	0.0523	0.0008	0.47	0.0543	0.0015	335	10	329	5	381	62	86
SRFS1	SRFS1-47	654	28	404	193435	0.62	0.309	0.015	0.0424	0.0007	0.36	0.0528	0.0024	273	13	268	5	319	103	84
SRFS1	SRFS1-48	313	12	228	85014	0.73	0.300	0.013	0.0390	0.0006	0.37	0.0559	0.0023	267	12	246	4	448	91	55
SRFS1	SRFS1-49	764	32	302	6634	0.40	0.311	0.013	0.0425	0.0007	0.39	0.0532	0.0020	275	11	268	4	336	86	80
SRFS1	SRFS1-50	179	7	203	50169	1.14	0.286	0.014	0.0402	0.0007	0.35	0.0516	0.0023	255	12	254	4	267	102	95
SRFS1	SRFS1-52	474	18	334	2526	0.70	0.269	0.010	0.0376	0.0006	0.41	0.0518	0.0018	242	9	238	4	275	79	87

SRFS1	SRFS1-53	534	265	46	15655	0.09	12.486	0.321	0.4952	0.0071	0.56	0.1829	0.0039	2642	68	2593	37	2679	35	97
SRFS1	SRFS1-55	230	12	94	86192	0.41	0.393	0.017	0.0538	0.0009	0.38	0.0529	0.0022	336	15	338	6	326	93	104
SRFS1	SRFS1-56	636	25	261	176681	0.41	0.283	0.009	0.0398	0.0006	0.46	0.0515	0.0015	253	8	252	4	263	65	96
SRFS1	SRFS1-57	445	20	158	2123	0.36	0.381	0.015	0.0440	0.0007	0.41	0.0629	0.0022	328	13	277	4	704	74	39
SRFS1	SRFS1-58	266	93	140	71749	0.52	7.316	0.191	0.3482	0.0050	0.55	0.1524	0.0033	2151	56	1926	28	2373	37	81
SRFS1	SRFS1-59	201	40	89	282692	0.44	2.214	0.066	0.2018	0.0030	0.50	0.0796	0.0021	1185	35	1185	18	1187	51	100
SRFS1	SRFS1-60	331	12	184	87074	0.56	0.269	0.019	0.0377	0.0008	0.30	0.0517	0.0036	242	17	238	5	273	158	87
SRFS1	SRFS1-61	305	13	97	3855	0.32	0.310	0.010	0.0435	0.0006	0.47	0.0517	0.0014	274	9	274	4	273	64	100
SRFS1	SRFS1-62	776	28	235	2208	0.30	0.310	0.010	0.0365	0.0005	0.48	0.0617	0.0017	274	8	231	3	663	58	35
SRFS1	SRFS1-63	925	119	240	1399	0.26	1.521	0.040	0.1290	0.0018	0.54	0.0855	0.0019	939	25	782	11	1328	43	59
SRFS1	SRFS1-64	333	63	140	2493	0.42	2.059	0.058	0.1900	0.0028	0.51	0.0786	0.0019	1135	32	1121	16	1162	48	97
SRFS1	SRFS1-65	607	24	347	7615	0.57	0.283	0.009	0.0399	0.0006	0.46	0.0515	0.0015	253	8	252	4	262	65	96
SRFS1	SRFS1-66	236	20	134	7075	0.57	0.695	0.025	0.0850	0.0013	0.43	0.0593	0.0019	536	19	526	8	578	70	91
SRFS1	SRFS1-67	217	18	87	1301	0.40	0.700	0.028	0.0844	0.0014	0.40	0.0601	0.0022	539	22	522	9	609	81	86
SRFS1	SRFS1-68	799	33	383	232946	0.48	0.297	0.010	0.0417	0.0006	0.45	0.0517	0.0015	264	9	263	4	273	67	97
SRFS1	SRFS1-69	250	22	108	155020	0.43	0.722	0.028	0.0886	0.0014	0.41	0.0592	0.0021	552	21	547	9	573	76	96
SRFS1	SRFS1-70	370	15	178	1446	0.48	0.305	0.012	0.0408	0.0006	0.39	0.0543	0.0020	270	11	258	4	383	83	67
SRFS1	SRFS1-71	476	17	470	1583	0.99	0.276	0.011	0.0367	0.0006	0.40	0.0545	0.0020	247	10	232	4	393	81	59
SRFS1	SRFS1-72	228	9	78	2040	0.34	0.291	0.025	0.0408	0.0010	0.29	0.0517	0.0043	259	22	258	6	273	189	94
SRFS1	SRFS1-73	363	25	141	175931	0.39	0.543	0.026	0.0693	0.0012	0.36	0.0568	0.0025	440	21	432	7	483	99	89
SRFS1	SRFS1-74	327	14	201	2096	0.61	0.303	0.012	0.0423	0.0007	0.40	0.0519	0.0019	269	11	267	4	281	83	95
SRFS1	SRFS1-75	129	13	25	87913	0.20	0.806	0.031	0.0974	0.0016	0.42	0.0601	0.0021	600	23	599	10	605	75	99
SRFS1	SRFS1-76	377	17	199	3816	0.53	0.331	0.011	0.0462	0.0007	0.45	0.0520	0.0016	290	10	291	4	285	70	102
SRFS1	SRFS1-77	226	36	36	10201	0.16	1.601	0.045	0.1608	0.0023	0.51	0.0722	0.0018	971	27	961	14	992	50	97
SRFS1	SRFS1-78	239	9	131	62400	0.55	0.278	0.012	0.0373	0.0006	0.38	0.0540	0.0022	249	11	236	4	371	92	64
SRFS1	SRFS1-79	404	15	181	108497	0.45	0.307	0.013	0.0383	0.0006	0.39	0.0582	0.0023	272	12	242	4	535	87	45
SRFS1	SRFS1-80	222	10	118	1799	0.53	0.306	0.011	0.0430	0.0006	0.43	0.0517	0.0016	271	10	271	4	272	73	100
SRFS1	SRFS1-81	332	14	172	5808	0.52	0.295	0.010	0.0415	0.0006	0.46	0.0516	0.0015	263	9	262	4	266	67	98
SRFS1	SRFS1-82	323	27	158	188656	0.49	0.720	0.021	0.0834	0.0012	0.49	0.0626	0.0016	551	16	516	8	695	55	74
SRFS1	SRFS1-83	285	11	186	79938	0.65	0.282	0.010	0.0400	0.0006	0.44	0.0512	0.0016	252	9	253	4	250	70	101
SRFS1	SRFS1-84	235	19	106	4572	0.45	0.637	0.026	0.0806	0.0013	0.40	0.0573	0.0021	501	20	500	8	504	81	99
SRFS1	SRFS1-85	224	10	232	66580	1.04	0.302	0.018	0.0424	0.0008	0.32	0.0516	0.0029	268	16	268	5	268	127	100
SRFS1	SRFS1-86	481	30	198	10446	0.41	0.466	0.022	0.0626	0.0011	0.36	0.0540	0.0024	388	18	391	7	372	98	105
SRFS1	SRFS1-87	369	19	232	54660	0.63	0.372	0.015	0.0507	0.0008	0.40	0.0531	0.0019	321	13	319	5	335	82	95
SRFS1	SRFS1-88	349	16	121	133617	0.35	0.328	0.011	0.0457	0.0007	0.46	0.0521	0.0015	288	9	288	4	290	66	99
SRFS1	SRFS1-89	364	16	197	112482	0.54	0.316	0.010	0.0441	0.0006	0.47	0.0520	0.0014	279	9	278	4	285	62	97
SRFS1	SRFS1-90	257	31	81	4975	0.32	1.163	0.032	0.1190	0.0017	0.52	0.0709	0.0017	783	21	725	10	954	48	76
SRFS1	SRFS1-91	808	31	458	218201	0.57	0.273	0.009	0.0385	0.0006	0.46	0.0515	0.0014	245	8	244	4	263	64	93
SRFS1	SRFS1-92	180	28	88	1823	0.49	1.527	0.050	0.1568	0.0024	0.47	0.0706	0.0020	941	31	939	14	947	59	99
SRFS1	SRFS1-93	121	11	49	1023	0.41	0.802	0.039	0.0925	0.0017	0.37	0.0629	0.0028	598	29	570	10	704	95	81
SRFS1	SRFS1-94	419	17	216	1227	0.52	0.296	0.012	0.0400	0.0006	0.40	0.0537	0.0020	263	11	253	4	357	83	71
SRFS1	SRFS1-95	330	15	137	18267	0.41	0.315	0.010	0.0442	0.0006	0.47	0.0517	0.0014	278	9	279	4	272	63	102
SRFS1	SRFS1-96	183	7	210	696	1.14	0.300	0.019	0.0406	0.0008	0.32	0.0535	0.0031	266	16	257	5	350	133	73
SRFS1	SRFS1-97	146	27	36	4601	0.25	1.984	0.062	0.1869	0.0028	0.48	0.0770	0.0021	1110	35	1105	17	1121	54	99
SRFS1	SRFS1-98	202	8	167	59528	0.83	0.311	0.017	0.0420	0.0008	0.33	0.0537	0.0028	275	15	265	5	356	120	74
SRFS1	SRFS1-100	181	31	45	218296	0.25	1.819	0.061	0.1721	0.0027	0.46	0.0767	0.0023	1052	36	1023	16	1112	60	92
SRFS1	SRFS1-101	384	17	402	1980	1.05	0.340	0.018	0.0444	0.0008	0.34	0.0557	0.0028	297	16	280	5	438	112	64
SRFS1	SRFS1-103	494	20	596	142089	1.21	0.289	0.012	0.0409	0.0006	0.38	0.0512	0.0019	258	10	259	4	249	86	104
SRFS1	SRFS1-104	292	25	99	21326	0.34	0.683	0.020	0.0858	0.0012	0.50	0.0578	0.0014	529	15	530	8	522	55	102

SRFS1	SRFS1-105	62	8	40	58977	0.64	1.280	0.052	0.1349	0.0023	0.41	0.0688	0.0026	837	34	816	14	893	77	91
SRFS1	SRFS1-106	266	11	201	75687	0.76	0.287	0.010	0.0406	0.0006	0.44	0.0513	0.0015	256	9	256	4	254	69	101
SRFS1	SRFS1-107	164	6	117	43990	0.71	0.288	0.030	0.0382	0.0011	0.27	0.0546	0.0055	257	27	242	7	398	226	61
SRFS1	SRFS1-108	343	15	109	102086	0.32	0.303	0.010	0.0423	0.0006	0.46	0.0518	0.0015	268	9	267	4	278	65	96
SRFS1	SRFS1-109	309	13	220	816	0.71	0.329	0.022	0.0422	0.0009	0.32	0.0565	0.0035	288	19	266	6	471	139	57
SRFS1	SRFS1-110	611	62	68	1169	0.11	1.046	0.036	0.1006	0.0016	0.45	0.0754	0.0023	727	25	618	10	1079	61	57
SRFS1	SRFS1-111	388	17	208	121678	0.54	0.317	0.014	0.0446	0.0007	0.37	0.0516	0.0021	280	12	281	5	266	94	106
SRFS1	SRFS1-112	160	13	107	1433	0.67	0.619	0.023	0.0781	0.0012	0.42	0.0575	0.0020	489	18	485	8	511	75	95
SRFS1	SRFS1-113	45	8	36	57691	0.80	1.844	0.063	0.1804	0.0028	0.46	0.0741	0.0023	1061	36	1069	17	1045	62	102
SRFS1	SRFS1-114	198	16	71	2286	0.36	0.652	0.022	0.0822	0.0012	0.45	0.0575	0.0017	509	17	509	8	510	67	100

[a]U and Pb concentrations and Th/U ratios are calculated relative to GJ-1 reference zircon

[b]Corrected for background and within-run Pb/U fractionation and normalised to reference zircon GJ-1 (ID-TIMS values/measured value); ^{207}Pb/^{235}U calculated using (^{207}Pb/^{206}Pb)/(^{238}U/^{206}Pb * 1/137.88)

[c]Rho is the error correlation defined as the quotient of the propagated errors of the ^{206}Pb/^{238}U and the ^{207}/^{235}U ratio

[d]Quadratic addition of within-run errors (2 SD) and daily reproducibility of GJ-1 (2 SD)

[e]Corrected for mass-bias by normalising to GJ-1 reference zircon (~0.6 per atomic mass unit) and common Pb using the model Pb composition of Stacey & Kramers (1975)

Appendix E. LA-ICPMS isotopic data for samples analysed during campaign 4

Table E1. LA-ICPMS isotopic data for samples in the Mossel Bay, Oudtshoorn, Knysna, Plet, Gamtoos and Algoa Basins that were analysed during campaign 4. .

						Data for Tera-Wasserburg plot a				Data for Wetherill plot a					Dates (Ma) a									Concordance b	
Identifier	^{206}Pb (CPS)	^{204}Pb (CPS)	$^{206}Pb/^{204}Pb$	U (µg g^{-1})	Th/U	$^{238}U/^{206}Pb$	2 s	$^{207}Pb/^{206}Pb$	2 s	$^{207}Pb/^{235}U$	2 s	$^{206}Pb/^{238}U$	2 s	rho	$^{207}Pb/^{206}Pb$	2 s	2s $_{sys}$	$^{206}Pb/^{238}U$	2 s	2s $_{sys}$	$^{207}Pb/^{235}U$	2 s	2s $_{sys}$	6/38 - 7/35	6/38 - 7/6
GES3 - 1	3.7.E+05	b.d.	b.d	396	0.31	5.95	0.10	0.0759	0.0008	1.7610	0.0300	0.1680	0.0027	0.94	1088	19	24	1001	15	23	1031	11	17	97	92
GES3 - 2	1.7.E+05	b.d.	b.d	214	0.31	6.68	0.13	0.0766	0.0012	1.5820	0.0360	0.1497	0.0029	0.85	1103	30	33	899	16	22	961	15	20	94	82
GES3 - 3	3.2.E+04	b.d.	b.d	82	0.54	13.77	0.30	0.0626	0.0029	0.6310	0.0310	0.0726	0.0016	0.45	642	95	99	452	9	13	492	19	25	92	70
GES3 - 4	3.3.E+04	b.d.	b.d	75	0.79	12.41	0.23	0.0598	0.0016	0.6620	0.0200	0.0806	0.0015	0.62	543	60	61	499	9	13	513	13	17	97	92
GES3 - 5	3.6.E+05	b.d.	b.d	687	0.25	11.29	0.31	0.0698	0.0007	0.8550	0.0230	0.0886	0.0024	0.90	915	21	24	547	14	17	626	13	16	87	60
GES3 - 6	2.7.E+05	b.d.	b.d	367	0.32	7.19	0.16	0.0712	0.0008	1.3610	0.0300	0.1390	0.0030	0.98	955	20	25	839	17	22	872	14	17	96	88
GES3 - 7	2.5.E+04	b.d.	b.d	60	0.53	12.58	0.28	0.0697	0.0021	0.7580	0.0270	0.0795	0.0018	0.64	850	71	72	493	11	14	570	17	20	86	58
GES3 - 10	3.5.E+05	b.d.	b.d	392	0.23	5.80	0.09	0.0782	0.0008	1.8520	0.0320	0.1724	0.0028	0.94	1144	20	23	1025	16	23	1063	12	18	96	90
GES3 - 11	3.7.E+04	b.d.	b.d	74	1.04	10.78	0.19	0.0680	0.0017	0.8670	0.0250	0.0927	0.0016	0.60	810	55	56	572	10	14	629	14	21	91	71
GES3 - 12	1.5.E+05	b.d.	b.d	195	0.25	7.06	0.13	0.0755	0.0010	1.4660	0.0330	0.1417	0.0027	0.85	1072	26	29	854	16	21	914	14	20	93	80
GES3 - 13	5.2.E+05	b.d.	b.d	620	0.19	6.27	0.11	0.0759	0.0008	1.6660	0.0310	0.1596	0.0029	0.98	1089	16	24	954	16	23	996	12	17	96	88
GES3 - 14	1.2.E+05	b.d.	b.d	272	0.43	11.79	0.21	0.0595	0.0013	0.6970	0.0180	0.0848	0.0015	0.69	566	40	49	525	9	13	536	10	14	98	93
GES3 - 15	4.6.E+05	b.d.	b.d	611	0.10	7.37	0.14	0.0726	0.0008	1.3570	0.0260	0.1357	0.0025	0.96	1002	17	25	820	14	20	870	11	16	94	82
GES3 - 16	6.4.E+04	b.d.	b.d	156	0.47	13.08	0.22	0.0582	0.0012	0.6120	0.0150	0.0764	0.0013	0.69	498	44	47	475	8	11	483	10	14	98	95
GES3 - 17	1.1.E+05	b.d.	b.d	288	0.45	14.10	0.26	0.0590	0.0010	0.5750	0.0130	0.0709	0.0013	0.81	544	39	40	442	8	11	460	9	12	96	81
GES3 - 18	8.6.E+04	b.d.	b.d	148	0.22	9.15	0.22	0.0684	0.0019	1.0330	0.0320	0.1093	0.0026	0.77	858	55	58	669	15	19	718	17	21	93	78
GES3 - 19	2.7.E+05	b.d.	b.d	272	0.39	5.47	0.09	0.0752	0.0008	1.8920	0.0330	0.1828	0.0030	0.94	1069	20	24	1082	17	25	1078	12	17	100	101
GES3 - 20	8.2.E+04	b.d.	b.d	94	0.44	6.08	0.19	0.0764	0.0014	1.7240	0.0600	0.1644	0.0051	0.89	1090	38	39	981	29	33	1017	26	37	96	90
GES3 - 21	1.8.E+05	b.d.	b.d	204	0.38	6.11	0.10	0.0719	0.0008	1.6240	0.0290	0.1636	0.0026	0.89	981	22	25	977	15	22	978	11	17	100	100
GES3 - 22	7.4.E+05	b.d.	b.d	756	1.34	5.39	0.09	0.0779	0.0009	1.9910	0.0340	0.1855	0.0031	0.98	1140	16	25	1097	17	25	1112	11	18	99	96
GES3 - 23	2.1.E+05	b.d.	b.d	452	0.42	11.74	0.21	0.0632	0.0008	0.7420	0.0140	0.0852	0.0015	0.93	708	27	30	527	9	13	563	8	12	94	74
GES3 - 24	1.5.E+05	b.d.	b.d	196	0.37	6.53	0.22	0.0740	0.0014	1.5620	0.0530	0.1532	0.0051	0.98	1036	40	41	919	29	32	954	27	28	96	89
GES3 - 25	1.5.E+05	b.d.	b.d	444	0.40	15.50	0.31	0.0650	0.0009	0.5750	0.0120	0.0645	0.0013	0.97	760	30	32	403	8	11	460	8	11	88	53
GES3 - 27	1.6.E+05	b.d.	b.d	329	0.35	10.92	0.18	0.0600	0.0008	0.7560	0.0150	0.0916	0.0015	0.83	586	30	31	565	9	13	571	9	13	99	96
GES3 - 29	9.6.E+04	b.d.	b.d	246	0.48	13.26	0.25	0.0598	0.0016	0.6200	0.0170	0.0754	0.0014	0.68	572	57	59	469	9	12	489	11	14	96	82
GES3 - 30	1.3.E+05	b.d.	b.d	369	0.54	14.65	0.28	0.0694	0.0013	0.6520	0.0160	0.0683	0.0013	0.78	895	37	40	426	8	11	509	10	13	84	48
GES3 - 31	9.6.E+04	b.d.	b.d	209	0.46	11.69	0.21	0.0641	0.0012	0.7550	0.0180	0.0855	0.0015	0.74	720	42	43	529	9	13	570	10	14	93	73
GES3 - 32	1.4.E+05	b.d.	b.d	172	0.49	6.36	0.17	0.0767	0.0012	1.6560	0.0470	0.1572	0.0041	0.92	1096	33	34	941	23	28	990	21	23	95	86
GES3 - 33	7.0.E+04	b.d.	b.d	111	0.55	8.52	0.17	0.0725	0.0014	1.1590	0.0270	0.1174	0.0023	0.84	978	37	41	715	14	18	781	14	17	92	73
GES3 - 35	6.1.E+04	b.d.	b.d	113	0.50	9.54	0.22	0.0633	0.0020	0.9110	0.0370	0.1048	0.0024	0.56	674	68	69	642	14	18	654	18	25	98	95
GES3 - 37	1.4.E+05	b.d.	b.d	188	0.22	7.55	0.32	0.0720	0.0017	1.3150	0.0710	0.1325	0.0057	0.80	974	47	49	802	33	35	851	33	34	94	82
GES3 - 39	2.5.E+05	b.d.	b.d	396	0.54	7.96	0.13	0.0667	0.0008	1.1520	0.0210	0.1256	0.0021	0.92	819	24	26	763	12	18	777	11	15	98	93
GES3 - 40	7.4.E+04	b.d.	b.d	174	0.58	12.70	0.23	0.0574	0.0010	0.6240	0.0140	0.0788	0.0014	0.79	489	40	41	489	8	12	491	9	13	100	100
GES3 - 41	2.7.E+05	b.d.	b.d	362	0.57	6.64	0.26	0.0761	0.0020	1.5740	0.0640	0.1506	0.0059	0.96	1091	61	62	904	34	37	959	32	33	94	83
GES3 - 42	3.4.E+04	b.d.	b.d	75	0.66	11.88	0.21	0.0582	0.0016	0.6730	0.0210	0.0841	0.0015	0.57	480	60	61	521	9	13	520	13	17	100	108
GES3 - 43	9.4.E+04	b.d.	b.d	108	0.28	6.02	0.11	0.0744	0.0011	1.6980	0.0390	0.1662	0.0031	0.81	1042	30	32	991	18	24	1007	15	20	98	95
GES3 - 44	8.4.E+04	b.d.	b.d	164	0.01	10.37	0.26	0.0612	0.0013	0.8120	0.0270	0.0964	0.0024	0.75	620	44	47	593	13	18	603	13	18	98	96
GES3 - 46	3.8.E+05	b.d.	b.d	737	0.29	10.28	0.20	0.0626	0.0010	0.8386	0.0240	0.0973	0.0019	0.68	687	32	36	599	11	15	619	11	16	97	87
GES3 - 47	1.1.E+05	b.d.	b.d	285	0.41	13.35	0.27	0.0578	0.0011	0.5930	0.0140	0.0749	0.0015	0.85	507	42	43	466	9	12	473	9	11	98	92
GES3 - 48	1.8.E+05	b.d.	b.d	210	0.49	6.28	0.11	0.0781	0.0011	1.7160	0.0370	0.1593	0.0027	0.79	1140	29	30	954	15	21	1014	13	19	94	84
GES3 - 50	1.1.E+05	b.d.	b.d	290	0.54	13.20	0.23	0.0590	0.0009	0.6150	0.0130	0.0758	0.0013	0.81	545	33	35	471	8	11	486	8	12	97	86
GES3 - 52	9.6.E+04	b.d.	b.d	212	0.88	11.71	0.54	0.0638	0.0019	0.7520	0.0640	0.0854	0.0039	0.54	720	58	64	528	19	25	567	23	40	93	73
GES3 - 53	1.4.E+05	b.d.	b.d	160	0.32	5.85	0.26	0.0752	0.0023	1.7650	0.0820	0.1710	0.0077	0.97	1060	60	62	1017	45	46	1030	40	41	99	96
GES3 - 54	2.4.E+05	b.d.	b.d	320	0.12	6.57	0.12	0.0744	0.0013	1.5550	0.0340	0.1521	0.0027	0.81	1044	36	37	912	15	22	951	14	19	96	87
GES3 - 55	1.2.E+05	b.d.	b.d	159	0.60	7.09	0.12	0.0674	0.0010	1.3060	0.0270	0.1410	0.0024	0.82	834	31	32	850	14	20	847	12	17	100	102
GES3 - 57	7.0.E+04	b.d.	b.d	138	0.77	10.12	0.37	0.0628	0.0031	0.8530	0.0510	0.0988	0.0036	0.61	685	98	106	608	21	23	626	23	29	97	89
GES3 - 58	7.9.E+04	b.d.	b.d	202	1.09	13.97	0.23	0.0597	0.0011	0.5910	0.0140	0.0716	0.0012	0.71	583	38	41	446	7	11	470	9	13	95	76
GES3 - 59	1.9.E+05	b.d.	b.d	202	0.28	5.60	0.09	0.0760	0.0008	1.8680	0.0330	0.1785	0.0028	0.89	1085	22	24	1059	16	23	1069	12	18	99	98
GES3 - 61	5.2.E+04	b.d.	b.d	116	0.58	12.06	0.22	0.0624	0.0016	0.7140	0.0220	0.0829	0.0015	0.59	662	56	57	514	9	13	546	13	16	94	78
GES3 - 62	1.2.E+05	b.d.	b.d	178	0.69	7.84	0.14	0.0713	0.0010	1.2480	0.0240	0.1275	0.0022	0.90	961	28	29	773	12	18	822	11	16	94	80
GES3 - 63	1.3.E+05	b.d.	b.d	238	0.52	9.88	0.17	0.0611	0.0009	0.8540	0.0170	0.1012	0.0017	0.84	630	33	35	622	10	15	626	9	13	99	99
GES3 - 64	1.2.E+05	b.d.	b.d	257	0.60	12.10	0.19	0.0577	0.0009	0.6575	0.0130	0.0827	0.0013	0.80	499	34	35	512	8	12	513	8	11	100	103
GES3 - 65	1.1.E+06	b.d.	b.d	665	1.62	3.11	0.05	0.1209	0.0029	5.3300	0.1500	0.3213	0.0054	0.60	1961	34	44	1796	26	39	1870	21	32	96	92
GES3 - 66	2.9.E+05	b.d.	b.d	302	0.28	5.56	0.09	0.0754	0.0008	1.8700	0.0320	0.1798	0.0030	0.98	1077	19	24	1066	17	24	1069	12	18	100	99
GES3 - 68	3.0.E+05	b.d.	b.d	553	0.30	9.61	0.20	0.0620	0.0011	0.8860	0.0250	0.1040	0.0022	0.75	662	30	40	638	13	17	644	12	17	99	96
GES3 - 69	1.3.E+05	b.d.	b.d	247	0.15	9.84	0.15	0.0628	0.0010	0.8810	0.0180	0.1017	0.0016	0.77	692	33	35	624	10	14	640	10	14	97	90
GES3 - 70	5.0.E+04	b.d.	b.d	96	0.26	10.19	0.18	0.0604	0.0014	0.8150	0.0220	0.0981	0.0017	0.64	581	50	51	603	10	15	604	12	16	100	104
GES3 - 71	2.4.E+05	b.d.	b.d	333	0.28	7.00	0.15	0.0724	0.0010	1.4220	0.0340	0.1429	0.0030	0.88	990	27	29	861	17	22	897	16	19	96	87
GES3 - 72	1.0.E+05	b.d.	b.d	190	0.10	9.99	0.18	0.0609	0.0010	0.8390	0.0190	0.1001	0.0018	0.79	609	35	37	615	10	15	618	10	15	100	101
GES3 - 74	7.8.E+04	b.d.	b.d	128	0.89	8.19	0.28	0.0755	0.0022	1.2700	0.0540	0.1221	0.0042	0.81	1059	65	66	743	25	27	829	28	29	90	70
GES3 - 75	1.5.E+05	b.d.	b.d	128	0.56	4.50	0.07	0.0917	0.0011	2.8100	0.0550	0.2223	0.0036	0.83	1450	23	25	1294	19	29	1357	15	21	95	89
GES3 - 76	1.4.E+05	b.d.	b.d	156	0.68	6.27	0.11	0.0754	0.0009	1.6580	0.0360	0.1595	0.0029	0.84	1073	26	27	954	16	23	992	15	19	96	89
GES3 - 77	1.1.E+05	b.d.	b.d	114	0.46	5.51	0.22	0.0752	0.0015	1.8660	0.0870	0.1814	0.0071	0.84	1057	40	41	1074	39	43	1068	33	34	101	102
GES3 - 78	1.9.E+05	b.d.	b.d	318	0.25	9.13	0.15	0.0662	0.0008	1.0000	0.0200	0.1095	0.0018	0.82	801	26	28	670	10	16	702	10	15	95	84
GES3 - 79	1.1.E+05	b.d.	b.d	263	0.77	12.49	0.22	0.0769	0.0024	0.8510	0.0310	0.0800	0.0014	0.48	1067	60	63	496	8	12	623	17	21	80	47
KBEZS2 - 1	5.2.E+04	b.d.	b.d	240	0.93	24.20	0.41	0.0570	0.0015	0.3228	0.0094	0.0413	0.0007	0.58	439	58	59	261	4	6	284	7	8	92	59
KBEZS2 - 2	9.9.E+04	b.d.	b.d	230	0.18	12.05	0.20	0.0580	0.0010	0.6640	0.0140	0.0830	0.0014	0.80	507	36	38	515	8	12	516	9	13	100	101
KBEZS2 - 3	7.4.E+04	b.d.	b.d	345	0.37	24.43	0.41	0.0522	0.0010	0.2943	0.0071	0.0409	0.0007	0.69	267	42	45	259	4	6	261	6	8	99	97
KBEZS2 - 5	1.1.E+05	b.d.	b.d	311	0.39	14.80	0.31	0.0565	0.0011	0.5280	0.0140	0.0676	0.0014	0.78	455	45	46	421	9	11	429	10	13	98	93
KBEZS2 - 7	6.3.E+04	b.d.	b.d	308	0.58	24.36	0.41	0.0531	0.0014	0.3004	0.0082	0.0411	0.0007	0.62	315	54	61	259	4	6	266	6	8	97	82
KBEZS2 - 8	2.8.E+04	b.d.	b.d	131	1.08	23.88	0.42	0.0571	0.0020	0.3310	0.0130	0.0419	0.0007	0.45	429	76	78	264	5	7	288	10	14	92	62
KBEZS2 - 10	6.2.E+04	b.d.	b.d	310	0.64	25.49	0.46	0.0549	0.0012	0.2961	0.0074	0.0392	0.0007	0.72	381	47	50	248	4	6	263	6	8	94	65
KBEZS2 - 11	7.3.E+04	b.d.	b.d	346	0.96	24.35	0.40	0.0533	0.0011	0.3017	0.0074	0.0411	0.0007	0.68	312	44	48	259	4	6	267	6	8	97	83
KBEZS2 - 14	6.0.E+04	b.d.	b.d	301	0.83	24.41	0.54	0.0564	0.0028	0.3191	0.0190	0.0410	0.0009	0.37	443	87	111	259	6	7	281	12	16	92	58
KBEZS2 - 15	3.7.E+04	b.d.	b.d	179	0.81	24.56	0.51	0.0548	0.0026	0.3072	0.0180	0.0407	0.0009	0.36	368	80	107	257	5	7	271	12	16	95	70
KBEZS2 - 16	3.1.E+04	b.d.	b.d	156	0.70	25.17	0.48	0.0576	0.0028	0.3140	0.0140	0.0397	0.0008	0.42	463	86	107	251	5	6	276	10	13	91	54
KBEZS2 - 17	8.5.E+04	b.d.	b.d	588	1.19	36.21	0.60	0.0534	0.0011	0.2034	0.0052	0.0276	0.0005	0.65	331	44	48	176	3	4	188	4	6	94	53
KBEZS2 - 19	6.2.E+04	b.d.	b.d	314	0.93	25.73	0.46	0.0586	0.0036	0.3117	0.0180	0.0389	0.0007	0.31	507	93	135	246	4	6	275	12	16	90	48
KBEZS2 - 20	1.3.E+05	b.d.	b.d	622	0.71	23.61	0.40	0.0528	0.0010	0.3064	0.0070	0.0424	0.0007	0.74	301	43	45	267	5	6	271	6	7	99	89
KBEZS2 - 22	5.3.E+04	b.d.	b.d	178	0.83	16.86	0.48	0.0589	0.0037	0.4810	0.0240	0.0593	0.0017	0.57	529	95	137	371	10	12	400	15	16	93	70
KBEZS2 - 24	6.0.E+04	b.d.	b.d	296	0.82	25.40	0.45	0.0571	0.0016	0.3104	0.0098	0.0394	0.0007	0.56	468	61	63	249	4	6	275	8	9	91	53
KBEZS2 - 27	6.4.E+04	b.d.	b.d	286	0.56	22.53	0.45	0.0552	0.0018	0.3369	0.0140	0.0444	0.0009	0.48	384	64	74	280	6	7	294	9	13	95	73
KBEZS2 - 28	6.2.E+04	b.d.	b.d	303	0.96	24.82	0.44	0.0600	0.0013	0.3330	0.0088	0.0403	0.0007	0.68	579	48	49	255	4	6	291	7	9	87	44
KBEZS2 - 29	7.1.E+04	b.d.	b.d	318	0.77	23.06	0.39	0.0514	0.0010	0.3076	0.0071	0.0434	0.0007	0.74	242	41	44	274	5	7	272	6	8	101	113
KBEZS2 - 31	5.6.E+04	b.d.	b.d	289	1.38	25.87	0.46	0.0526	0.0017	0.2793	0.0092	0.0387	0.0007	0.53	280	64	74	244	4	6	249	7	9	98	87
KBEZS2 - 32	7.7.E+04	b.d.	b.d	359	0.56	24.10	0.41	0.0516	0.0010	0.2952	0.0073	0.0415	0.0007	0.69	250	45	46	262	4	6	262	6	8	100	105

KBEZS2 - 33	1.1.E+05	b.d.	b.d	538	0.45	23.72	0.41	0.0534	0.0011	0.3096	0.0073	0.0422	0.0007	0.72	331	45	48	266	5	7	273	6	8	97	80
KBEZS2 - 36	5.0.E+04	b.d.	b.d	248	0.77	24.72	0.42	0.0552	0.0014	0.3082	0.0085	0.0405	0.0007	0.62	385	56	58	256	4	6	272	7	9	94	66
KBEZS2 - 37	3.6.E+04	b.d.	b.d	181	0.49	24.56	0.48	0.0549	0.0023	0.3052	0.0130	0.0407	0.0008	0.46	373	84	94	257	5	7	270	10	12	95	69
KBEZS2 - 38	3.3.E+04	b.d.	b.d	163	1.04	24.85	0.46	0.0552	0.0016	0.3070	0.0094	0.0402	0.0008	0.61	380	62	66	254	5	6	271	7	9	94	67
KBEZS2 - 39	2.0.E+04	b.d.	b.d	100	0.91	25.98	0.52	0.0595	0.0026	0.3160	0.0140	0.0385	0.0008	0.45	524	91	96	243	5	7	276	10	14	88	46
KBEZS2 - 40	1.1.E+05	b.d.	b.d	517	0.53	24.22	0.40	0.0560	0.0011	0.3163	0.0068	0.0413	0.0007	0.78	425	41	45	261	4	6	279	5	7	93	61
KBEZS2 - 41	5.5.E+04	b.d.	b.d	263	0.75	24.64	0.42	0.0533	0.0011	0.2985	0.0077	0.0406	0.0007	0.66	314	47	48	256	4	6	264	6	8	97	82
KBEZS2 - 43	4.5.E+04	b.d.	b.d	200	0.66	23.03	0.40	0.0513	0.0013	0.3071	0.0087	0.0434	0.0008	0.61	226	55	59	274	5	7	271	7	9	101	121
KBEZS2 - 44	9.1.E+04	b.d.	b.d	271	0.25	14.45	0.27	0.0572	0.0012	0.5470	0.0130	0.0692	0.0013	0.79	471	46	48	431	8	11	443	9	11	97	92
KBEZS2 - 45	1.2.E+05	b.d.	b.d	571	0.29	24.52	0.41	0.0525	0.0010	0.2956	0.0071	0.0408	0.0007	0.70	297	44	45	258	4	6	263	6	7	98	87
KBEZS2 - 49	5.5.E+04	b.d.	b.d	140	0.51	13.25	0.23	0.0561	0.0012	0.5810	0.0140	0.0755	0.0013	0.71	421	46	49	469	8	11	464	9	13	101	111
KBEZS2 - 50	2.8.E+04	b.d.	b.d	132	0.58	23.72	0.46	0.0600	0.0020	0.3470	0.0120	0.0422	0.0008	0.56	547	70	73	266	5	7	303	9	10	88	49
KBEZS2 - 51	2.1.E+05	b.d.	b.d	930	0.31	22.92	0.37	0.0544	0.0007	0.3258	0.0061	0.0436	0.0007	0.86	373	29	31	275	4	7	286	5	7	96	74
KBEZS2 - 53	5.1.E+04	b.d.	b.d	243	1.07	23.60	0.51	0.0628	0.0027	0.3680	0.0210	0.0424	0.0009	0.38	662	74	92	268	6	7	318	14	17	84	40
KBEZS2 - 55	9.0.E+04	b.d.	b.d	324	0.53	17.27	0.36	0.0554	0.0011	0.4400	0.0110	0.0579	0.0012	0.83	395	44	46	363	7	10	369	8	11	98	92
KBEZS2 - 56	4.2.E+04	b.d.	b.d	206	0.84	24.80	0.45	0.0548	0.0013	0.3037	0.0090	0.0403	0.0007	0.61	365	53	54	255	5	6	269	7	8	95	70
KBEZS2 - 57	8.6.E+04	b.d.	b.d	417	0.95	25.03	0.41	0.0515	0.0009	0.2840	0.0066	0.0400	0.0007	0.71	247	40	44	253	4	6	254	5	7	100	102
KBEZS2 - 58	7.7.E+04	b.d.	b.d	383	0.49	24.33	0.47	0.0562	0.0030	0.3184	0.0150	0.0411	0.0008	0.41	438	85	119	260	5	7	281	11	12	93	59
KBEZS2 - 61	4.3.E+04	b.d.	b.d	200	0.91	23.65	0.45	0.0520	0.0016	0.3022	0.0110	0.0423	0.0008	0.52	245	67	71	267	5	7	267	8	11	100	109
KBEZS2 - 63	8.1.E+04	b.d.	b.d	397	1.00	24.81	0.55	0.0530	0.0018	0.2939	0.0170	0.0403	0.0009	0.39	299	62	78	255	6	7	261	12	15	98	85
KBEZS2 - 65	3.6.E+04	b.d.	b.d	184	0.77	24.46	0.55	0.0674	0.0035	0.3770	0.0180	0.0409	0.0009	0.47	802	95	108	258	6	7	323	12	16	80	32
KBEZS2 - 68	7.4.E+04	b.d.	b.d	350	0.34	23.87	0.48	0.0540	0.0024	0.3109	0.0100	0.0419	0.0008	0.62	341	71	101	265	5	7	274	8	10	97	78
KBEZS2 - 73	9.0.E+04	b.d.	b.d	434	0.50	23.65	0.49	0.0605	0.0026	0.3510	0.0160	0.0423	0.0009	0.46	579	80	93	267	5	7	306	11	13	87	46
KBEZS2 - 74	7.1.E+04	b.d.	b.d	317	0.58	22.94	0.38	0.0517	0.0011	0.3101	0.0078	0.0436	0.0007	0.67	246	47	50	275	5	7	274	6	8	100	112
KBEZS2 - 75	4.2.E+04	b.d.	b.d	214	1.03	26.13	0.50	0.0610	0.0017	0.3199	0.0088	0.0383	0.0007	0.69	603	57	61	242	5	6	282	7	8	86	40
KBEZS2 - 76	8.2.E+04	b.d.	b.d	416	0.68	25.18	0.62	0.0532	0.0018	0.2933	0.0170	0.0397	0.0010	0.43	327	65	78	251	6	8	261	10	15	96	77
KBEZS2 - 77	8.5.E+04	b.d.	b.d	373	0.53	21.89	0.40	0.0527	0.0015	0.3313	0.0140	0.0457	0.0008	0.44	295	54	66	288	5	7	290	8	12	99	98
KWAS2 - 1	3.8.E+05	b.d.	b.d	395	0.17	5.31	0.15	0.0775	0.0014	2.0090	0.0810	0.1882	0.0052	0.69	1129	30	37	1112	26	34	1118	18	30	99	98
KWAS2 - 2	1.2.E+05	b.d.	b.d	293	0.66	12.12	0.51	0.0616	0.0014	0.7020	0.0310	0.0825	0.0035	0.96	645	51	52	511	20	23	538	14	21	95	79
KWAS2 - 3	1.3.E+05	b.d.	b.d	205	0.44	7.98	0.19	0.0645	0.0017	1.1100	0.0370	0.1253	0.0030	0.72	745	49	57	761	17	21	757	16	22	101	102
KWAS2 - 4	6.3.E+04	b.d.	b.d	150	0.64	12.05	0.23	0.0579	0.0018	0.6600	0.0250	0.0830	0.0016	0.51	488	64	69	514	10	13	512	15	20	100	105
KWAS2 - 5	1.3.E+05	b.d.	b.d	238	0.39	9.81	0.16	0.0615	0.0008	0.8660	0.0170	0.1019	0.0017	0.85	645	31	32	626	10	15	633	9	13	99	97
KWAS2 - 6	1.4.E+05	b.d.	b.d	252	0.33	9.43	0.16	0.0623	0.0009	0.9090	0.0180	0.1060	0.0018	0.86	667	31	32	649	10	15	655	10	14	99	97
KWAS2 - 7	6.7.E+04	b.d.	b.d	146	0.61	11.53	0.20	0.0577	0.0012	0.6900	0.0170	0.0867	0.0015	0.70	488	47	48	536	9	13	531	10	15	101	110
KWAS2 - 9	4.3.E+05	b.d.	b.d	875	0.19	10.62	0.18	0.0604	0.0006	0.7837	0.0140	0.0942	0.0016	0.95	612	23	25	580	9	14	588	8	11	99	95
KWAS2 - 10	1.4.E+05	b.d.	b.d	218	0.33	7.97	0.13	0.0656	0.0009	1.1300	0.0220	0.1255	0.0021	0.86	775	29	30	762	12	18	766	11	16	99	98
KWAS2 - 11	3.1.E+05	b.d.	b.d	408	0.79	6.85	0.12	0.0693	0.0008	1.3910	0.0260	0.1459	0.0026	0.95	897	23	26	878	15	21	884	11	17	99	98
KWAS2 - 12	1.8.E+05	b.d.	b.d	386	0.92	11.29	0.18	0.0583	0.0008	0.7101	0.0130	0.0886	0.0014	0.86	528	29	32	547	9	13	544	8	12	101	104
KWAS2 - 13	6.9.E+04	b.d.	b.d	155	0.57	11.87	0.21	0.0578	0.0010	0.6740	0.0150	0.0842	0.0015	0.80	502	40	41	521	9	13	522	9	13	100	104
KWAS2 - 14	1.5.E+05	b.d.	b.d	335	0.29	11.92	0.20	0.0567	0.0008	0.6567	0.0130	0.0839	0.0014	0.84	463	32	34	519	8	12	512	8	12	101	112
KWAS2 - 16	9.7.E+04	b.d.	b.d	180	0.40	9.82	0.16	0.0605	0.0010	0.8480	0.0190	0.1018	0.0017	0.75	597	37	38	625	10	15	622	10	15	101	105
KWAS2 - 17	1.6.E+05	b.d.	b.d	320	0.38	10.80	0.17	0.0587	0.0008	0.7480	0.0140	0.0926	0.0015	0.87	540	29	30	571	9	13	566	8	12	101	106
KWAS2 - 18	6.2.E+04	b.d.	b.d	141	0.56	12.15	0.21	0.0569	0.0011	0.6470	0.0150	0.0823	0.0014	0.73	463	43	44	510	8	12	506	9	13	101	110
KWAS2 - 19	1.3.E+05	b.d.	b.d	150	0.48	5.85	0.10	0.0741	0.0024	1.7360	0.0540	0.1708	0.0029	0.55	1036	53	66	1016	16	24	1023	19	22	99	98
KWAS2 - 21	6.3.E+04	b.d.	b.d	66	0.54	5.32	0.10	0.0757	0.0014	1.9560	0.0430	0.1880	0.0034	0.82	1060	36	38	1110	18	27	1097	15	23	101	105
KWAS2 - 22	4.9.E+05	b.d.	b.d	549	0.46	5.58	0.17	0.0764	0.0010	1.8780	0.0600	0.1791	0.0056	0.98	1099	25	28	1062	32	35	1072	23	26	99	97
KWAS2 - 23	2.1.E+05	b.d.	b.d	237	0.29	5.88	0.10	0.0736	0.0008	1.7250	0.0320	0.1702	0.0030	0.95	1020	22	25	1013	16	24	1017	12	18	100	99
KWAS2 - 24	1.5.E+05	b.d.	b.d	168	0.44	5.55	0.13	0.0794	0.0020	1.9630	0.0660	0.1801	0.0041	0.68	1167	52	53	1067	23	29	1100	23	28	97	91
KWAS2 - 25	1.6.E+05	b.d.	b.d	375	0.64	12.33	0.20	0.0575	0.0008	0.6422	0.0130	0.0811	0.0013	0.79	502	31	33	503	8	12	504	8	11	100	100
KWAS2 - 26	5.0.E+04	b.d.	b.d	94	0.26	10.01	0.17	0.0606	0.0013	0.8370	0.0220	0.1000	0.0017	0.65	586	47	48	614	10	15	614	12	18	100	105
KWAS2 - 27	2.2.E+05	b.d.	b.d	405	0.37	9.74	0.15	0.0679	0.0007	0.9620	0.0170	0.1027	0.0016	0.88	861	22	24	630	9	14	683	9	14	92	73
KWAS2 - 30	1.5.E+05	b.d.	b.d	343	0.36	12.16	0.21	0.0578	0.0008	0.6540	0.0130	0.0823	0.0014	0.86	503	32	34	510	9	12	510	8	12	100	101
KWAS2 - 31	7.4.E+04	b.d.	b.d	174	0.61	12.22	0.21	0.0574	0.0011	0.6440	0.0150	0.0818	0.0014	0.73	480	43	44	507	8	12	504	9	12	101	106
KWAS2 - 32	3.8.E+04	b.d.	b.d	38	0.65	5.26	0.09	0.0776	0.0017	2.0350	0.0520	0.1902	0.0034	0.70	1109	45	46	1122	18	27	1124	18	25	100	101
KWAS2 - 33	1.3.E+05	b.d.	b.d	329	0.51	13.06	0.26	0.0585	0.0014	0.6170	0.0170	0.0766	0.0015	0.71	526	53	54	475	9	12	487	11	14	98	90
KWAS2 - 34	1.0.E+05	b.d.	b.d	234	0.68	12.30	0.21	0.0570	0.0009	0.6390	0.0130	0.0813	0.0014	0.85	470	36	37	504	8	12	501	8	12	101	107
KWAS2 - 35	6.4.E+04	b.d.	b.d	110	0.62	9.24	0.17	0.0606	0.0012	0.9070	0.0230	0.1082	0.0020	0.73	604	45	46	662	11	17	653	12	18	101	110
KWAS2 - 36	1.2.E+05	b.d.	b.d	213	0.36	9.58	0.16	0.0609	0.0009	0.8740	0.0180	0.1043	0.0017	0.79	614	33	34	640	10	15	636	10	14	101	104
KWAS2 - 38	1.1.E+05	b.d.	b.d	240	0.54	11.44	0.20	0.0587	0.0010	0.7060	0.0150	0.0874	0.0015	0.81	536	39	40	540	9	13	541	9	13	100	101
KWAS2 - 39	8.4.E+04	b.d.	b.d	172	0.42	11.08	0.20	0.0632	0.0011	0.7870	0.0170	0.0903	0.0016	0.82	692	38	39	557	9	14	589	10	13	95	80
KWAS2 - 40	1.9.E+05	b.d.	b.d	203	0.28	5.40	0.10	0.0756	0.0010	1.9190	0.0390	0.1853	0.0035	0.93	1072	25	28	1096	19	26	1087	13	19	101	102
KWAS2 - 41	6.6.E+04	b.d.	b.d	122	0.47	9.30	0.19	0.0696	0.0012	1.0280	0.0250	0.1075	0.0022	0.84	900	36	37	658	13	17	716	13	18	92	73
KWAS2 - 42	8.7.E+04	b.d.	b.d	202	0.56	12.25	0.21	0.0579	0.0010	0.6530	0.0150	0.0817	0.0014	0.75	499	39	40	506	8	12	509	9	13	99	101
KWAS2 - 43	1.4.E+05	b.d.	b.d	153	0.39	5.60	0.09	0.0748	0.0009	1.8380	0.0350	0.1785	0.0030	0.88	1054	24	27	1059	16	24	1058	12	19	100	101
KWAS2 - 44	3.6.E+05	b.d.	b.d	388	0.34	5.70	0.09	0.0759	0.0008	1.8370	0.0320	0.1754	0.0029	0.95	1085	19	24	1042	16	24	1058	11	18	98	96
KWAS2 - 45	1.9.E+05	b.d.	b.d	213	0.73	5.72	0.09	0.0784	0.0013	1.8840	0.0400	0.1749	0.0029	0.78	1145	30	34	1039	16	24	1074	14	20	97	91
KWAS2 - 46	3.1.E+05	b.d.	b.d	502	0.47	8.17	0.13	0.0662	0.0007	1.1170	0.0190	0.1225	0.0020	0.96	805	21	24	745	11	17	761	9	14	98	92
KWAS2 - 47	7.8.E+04	b.d.	b.d	214	0.42	14.27	0.35	0.0648	0.0017	0.6250	0.0210	0.0701	0.0017	0.72	752	53	56	437	10	13	492	13	16	89	58
KWAS2 - 48	3.2.E+05	b.d.	b.d	524	0.05	8.22	0.16	0.0681	0.0008	1.1410	0.0260	0.1216	0.0024	0.87	865	25	26	739	14	19	772	13	17	96	85
KWAS2 - 49	4.0.E+05	b.d.	b.d	403	0.32	5.19	0.09	0.0783	0.0009	2.0750	0.0360	0.1925	0.0032	0.96	1147	19	25	1135	17	26	1139	12	19	100	99
KWAS2 - 50	1.6.E+05	b.d.	b.d	401	0.50	12.48	0.22	0.0673	0.0009	0.7400	0.0150	0.0801	0.0014	0.86	832	26	28	497	8	12	562	9	12	88	60
KWAS2 - 51	1.1.E+05	b.d.	b.d	230	0.56	11.00	0.18	0.0584	0.0009	0.7320	0.0150	0.0909	0.0015	0.81	521	35	36	561	9	13	557	9	13	101	108
KWAS2 - 52	1.3.E+05	b.d.	b.d	150	0.34	5.67	0.10	0.0741	0.0010	1.7970	0.0360	0.1764	0.0031	0.88	1036	28	29	1047	17	24	1043	13	19	100	101
KWAS2 - 54	5.7.E+04	b.d.	b.d	117	0.70	10.52	0.20	0.0639	0.0013	0.8360	0.0220	0.0951	0.0018	0.72	697	44	45	585	11	15	614	12	18	95	84
KWAS2 - 55	3.6.E+05	b.d.	b.d	576	0.20	8.51	0.14	0.0653	0.0007	1.0570	0.0180	0.1175	0.0019	0.95	777	20	25	716	11	17	732	9	13	98	92
KWAS2 - 56	2.7.E+05	b.d.	b.d	286	0.40	5.56	0.09	0.0757	0.0008	1.8750	0.0320	0.1798	0.0029	0.95	1082	20	24	1066	16	23	1072	11	17	99	99
KWAS2 - 58	9.6.E+04	b.d.	b.d	180	0.48	9.74	0.17	0.0603	0.0010	0.8530	0.0190	0.1027	0.0018	0.79	594	37	38	630	10	15	624	10	15	101	106
KWAS2 - 59	4.7.E+04	b.d.	b.d	77	0.73	8.71	0.15	0.0635	0.0014	1.0020	0.0250	0.1148	0.0020	0.70	690	48	49	700	12	17	704	13	17	99	101
KWAS2 - 60	2.7.E+05	b.d.	b.d	265	0.89	5.19	0.09	0.0782	0.0009	2.0720	0.0380	0.1926	0.0034	0.96	1148	22	24	1135	18	27	1138	13	19	100	99
KWAS2 - 61	4.2.E+05	b.d.	b.d	931	0.01	11.63	0.19	0.0584	0.0006	0.6934	0.0120	0.0860	0.0014	0.94	535	23	25	532	8	12	534	8	11	100	99
KWAS2 - 62	9.1.E+04	b.d.	b.d	204	0.40	11.28	0.19	0.0595	0.0011	0.7260	0.0170	0.0887	0.0015	0.72	565	40	42	548	9	13	553	10	14	99	97
KWAS2 - 63	1.0.E+05	b.d.	b.d	160	0.13	7.73	0.18	0.0703	0.0015	1.2460	0.0350	0.1293	0.0030	0.83	922	48	49	783	18	23	821	17	19	95	85
KWAS2 - 64	1.0.E+05	b.d.	b.d	243	0.71	12.15	0.19	0.0571	0.0010	0.6470	0.0140	0.0823	0.0013	0.73	469	37	39	510	8	12	505	9	13	101	109
KWAS2 - 65	8.5.E+04	b.d.	b.d	196	0.36	11.96	0.20	0.0585	0.0010	0.6720	0.0150	0.0836	0.0014	0.75	523	38	39	517	8	12	521	9	13	99	99
KWAS2 - 66	3.2.E+05	b.d.	b.d	347	0.35	5.33	0.11	0.0759	0.0008	1.9570	0.0400	0.1876	0.0039	0.90	1086	21	23	1108	21	28	1099	15	20	101	102
KWAS2 - 67	7.0.E+05	b.d.	b.d	405	0.55	3.03	0.05	0.1158	0.0013	5.2770	0.0850	0.3305	0.0053	0.90	1888	15	22	1840	26	39	1865	14	21	99	97
KWAS2 - 68	2.2.E+05	b.d.	b.d	405	0.30	9.74	0.16	0.0613	0.0008	0.8652	0.0160	0.1027	0.0017	0.90	636	28	29	630	10	15	633	9	13	100	99
KWAS2 - 69	2.6.E+05	b.d.	b.d	609	0.30	12.07	0.20	0.0582	0.0007	0.6619	0.0120	0.0828	0.0014	0.93	529	25	27	513	8	12	516	7	10	99	97
KWAS2 - 70	7.6.E+04	b.d.	b.d	149	0.33	9.96	0.17	0.0629	0.0011	0.8650	0.0190	0.1004	0.0017	0.77	676	39	40	617	10	15	631	11	15	98	91
KWAS2 - 71	1.4.E+05	b.d.	b.d	257	0.34	9.62	0.16	0.0613	0.0009	0.8790	0.0180	0.1039	0.0017	0.80	631	31	33	637	10	15	639	10	15	100	101
KWAS2 - 72	3.4.E+04	b.d.	b.d	85	0.60	13.99	0.29	0.0628	0.0016	0.6170	0.0220	0.0715	0.0015	0.59	645	54	55	445	9	12	485	13	18	92	69

KWAS2 - 73	4.7.E+05	b.d.	b.d	485	0.33	5.46	0.09	0.0761	0.0008	1.9220	0.0330	0.1832	0.0031	0.99	1100	19	23	1085	17	24	1088	12	18	100	99
KWAS2 - 74	2.4.E+05	b.d.	b.d	283	0.36	5.87	0.12	0.0750	0.0013	1.7580	0.0430	0.1705	0.0034	0.82	1060	33	36	1015	19	26	1029	16	21	99	96
KWAS2 - 75	1.6.E+05	b.d.	b.d	171	0.77	5.54	0.09	0.0781	0.0011	1.9380	0.0370	0.1805	0.0030	0.87	1141	27	30	1070	16	24	1092	13	20	98	94
KWAS2 - 76	9.6.E+04	b.d.	b.d	128	0.56	6.93	0.12	0.0683	0.0011	1.3530	0.0280	0.1442	0.0024	0.80	855	35	36	868	13	20	867	13	18	100	102
KWAS2 - 77	2.5.E+05	b.d.	b.d	278	0.53	5.81	0.09	0.0748	0.0009	1.7740	0.0320	0.1720	0.0028	0.90	1054	23	25	1023	16	23	1036	12	17	99	97
KWAS2 - 78	1.3.E+05	b.d.	b.d	161	0.29	6.13	0.12	0.0749	0.0011	1.6720	0.0350	0.1632	0.0031	0.91	1046	30	31	974	17	24	996	14	20	98	93
KWAS2 - 79	2.5.E+05	b.d.	b.d	266	0.54	5.49	0.09	0.0773	0.0009	1.9420	0.0340	0.1820	0.0030	0.94	1123	19	25	1077	16	25	1094	12	18	98	96
KWAS2 - 80	2.9.E+05	b.d.	b.d	546	0.29	9.80	0.16	0.0608	0.0007	0.8579	0.0160	0.1020	0.0017	0.89	623	25	27	626	10	15	628	9	13	100	101
KWAS2 - 81	9.3.E+04	b.d.	b.d	178	0.34	9.97	0.17	0.0611	0.0010	0.8440	0.0180	0.1004	0.0017	0.79	618	37	38	616	10	15	621	10	14	99	100
KWAS2 - 83	4.0.E+05	b.d.	b.d	420	0.56	5.38	0.09	0.0782	0.0009	1.9960	0.0370	0.1860	0.0032	0.93	1141	22	25	1100	17	24	1114	12	18	99	96
KWAS2 - 84	1.8.E+05	b.d.	b.d	279	0.15	8.19	0.13	0.0648	0.0009	1.0900	0.0220	0.1221	0.0020	0.81	758	30	32	742	12	17	747	10	16	99	98
KWAS2 - 86	1.3.E+05	b.d.	b.d	238	0.53	9.66	0.17	0.0615	0.0009	0.8760	0.0180	0.1035	0.0018	0.85	644	33	35	635	10	15	638	10	14	100	99
KWAS2 - 87	4.7.E+04	b.d.	b.d	105	0.83	11.73	0.21	0.0584	0.0014	0.6870	0.0190	0.0852	0.0015	0.64	519	52	54	527	9	13	529	11	15	100	102
KWAS2 - 88	4.5.E+05	b.d.	b.d	494	0.62	5.62	0.09	0.0781	0.0008	1.9250	0.0320	0.1780	0.0029	0.98	1149	16	23	1056	16	24	1089	11	18	97	92
KWAS2 - 89	1.1.E+05	b.d.	b.d	182	0.13	9.00	0.22	0.0633	0.0013	0.9720	0.0320	0.1111	0.0027	0.74	701	41	45	679	15	19	688	15	20	99	97
KWAS2 - 90	3.2.E+05	b.d.	b.d	366	0.33	6.01	0.10	0.0762	0.0008	1.7540	0.0300	0.1665	0.0027	0.95	1093	19	23	993	15	22	1028	11	17	97	91
KWAS2 - 91	1.0.E+05	b.d.	b.d	242	0.51	12.30	0.21	0.0574	0.0010	0.6430	0.0140	0.0813	0.0014	0.79	484	37	39	504	8	12	503	9	12	100	104
RBGS1 - 2	1.7.E+05	b.d.	b.d	598	0.25	18.15	0.33	0.0548	0.0011	0.4160	0.0100	0.0551	0.0010	0.75	388	45	46	346	6	9	352	8	10	98	89
RBGS1 - 3	5.3.E+04	b.d.	b.d	237	0.77	24.32	0.40	0.0523	0.0012	0.2963	0.0080	0.0411	0.0007	0.61	264	51	54	260	4	6	263	6	8	99	98
RBGS1 - 6	4.6.E+04	b.d.	b.d	216	0.78	24.10	0.51	0.0564	0.0017	0.3210	0.0150	0.0415	0.0009	0.45	425	72	73	262	5	7	282	10	13	93	62
RBGS1 - 7	8.0.E+04	b.d.	b.d	355	0.60	23.96	0.40	0.0525	0.0011	0.3024	0.0073	0.0417	0.0007	0.69	286	45	49	264	4	6	268	6	8	98	92
RBGS1 - 8	2.1.E+04	b.d.	b.d	32	0.87	8.22	0.21	0.0966	0.0034	1.6100	0.0610	0.1216	0.0031	0.67	1518	66	67	739	18	23	970	23	30	76	49
RBGS1 - 9	8.2.E+04	b.d.	b.d	339	0.67	22.59	0.37	0.0526	0.0010	0.3211	0.0073	0.0443	0.0007	0.72	296	42	43	279	4	7	283	6	7	99	94
RBGS1 - 10	1.5.E+05	b.d.	b.d	682	0.70	23.83	0.39	0.0533	0.0008	0.3083	0.0062	0.0420	0.0007	0.82	328	32	35	265	4	6	273	5	7	97	81
RBGS1 - 11	6.3.E+04	b.d.	b.d	269	0.83	23.12	0.38	0.0525	0.0011	0.3128	0.0078	0.0433	0.0007	0.66	275	46	49	273	4	6	276	6	8	99	99
RBGS1 - 13	1.2.E+05	b.d.	b.d	322	0.76	14.38	0.25	0.0645	0.0037	0.6190	0.0380	0.0695	0.0012	0.28	745	72	122	433	7	10	488	19	26	89	58
RBGS1 - 14	5.4.E+04	b.d.	b.d	260	1.45	24.36	0.42	0.0541	0.0016	0.3080	0.0096	0.0411	0.0007	0.55	347	66	68	259	4	6	271	8	10	96	75
RBGS1 - 15	7.3.E+04	b.d.	b.d	333	0.84	24.10	0.40	0.0541	0.0012	0.3099	0.0084	0.0415	0.0007	0.61	347	47	51	262	4	6	273	7	9	96	76
RBGS1 - 16	1.0.E+05	b.d.	b.d	447	0.53	22.96	0.36	0.0519	0.0009	0.3110	0.0067	0.0436	0.0007	0.74	259	37	41	275	4	6	275	5	7	100	106
RBGS1 - 17	3.1.E+04	b.d.	b.d	157	1.09	25.21	0.53	0.0575	0.0040	0.3120	0.0180	0.0397	0.0008	0.37	468	110	153	251	5	7	275	13	16	91	54
RBGS1 - 18	7.5.E+04	b.d.	b.d	330	0.63	22.94	0.51	0.0536	0.0015	0.3209	0.0240	0.0436	0.0010	0.29	324	59	64	275	6	8	282	10	20	98	85
RBGS1 - 19	7.4.E+04	b.d.	b.d	331	0.51	23.88	0.40	0.0521	0.0010	0.3011	0.0073	0.0419	0.0007	0.69	269	43	45	264	4	6	267	6	8	99	98
RBGS1 - 20	2.5.E+04	b.d.	b.d	171	1.31	36.14	0.68	0.0529	0.0024	0.2019	0.0088	0.0277	0.0005	0.43	286	83	104	176	3	5	186	7	9	95	62
RBGS1 - 21	2.4.E+04	b.d.	b.d	113	1.81	24.93	0.45	0.0566	0.0020	0.3110	0.0110	0.0401	0.0007	0.51	398	75	79	254	5	6	273	9	11	93	64
RBGS1 - 22	6.3.E+04	b.d.	b.d	303	0.66	24.39	0.59	0.0563	0.0027	0.3180	0.0270	0.0410	0.0010	0.29	424	78	107	259	6	8	279	16	22	93	61
RBGS1 - 23	2.8.E+04	b.d.	b.d	133	0.85	25.34	0.52	0.0535	0.0025	0.2950	0.0150	0.0395	0.0008	0.40	312	80	106	250	5	7	261	10	14	96	80
RBGS1 - 24	9.2.E+04	b.d.	b.d	402	0.49	22.83	0.40	0.0559	0.0012	0.3364	0.0089	0.0438	0.0008	0.66	414	48	49	276	5	7	294	7	9	94	67
RBGS1 - 25	6.5.E+04	b.d.	b.d	288	0.57	23.90	0.42	0.0526	0.0012	0.3038	0.0081	0.0418	0.0007	0.65	280	49	53	264	5	7	269	6	8	98	94
RBGS1 - 28	5.1.E+04	b.d.	b.d	228	0.52	24.00	0.40	0.0531	0.0012	0.3044	0.0082	0.0417	0.0007	0.62	305	50	53	263	4	6	270	6	8	97	86
RBGS1 - 29	2.3.E+05	b.d.	b.d	712	0.45	16.75	0.28	0.0545	0.0007	0.4481	0.0083	0.0597	0.0010	0.89	382	29	31	374	6	9	376	6	8	99	98
RBGS1 - 31	5.2.E+04	b.d.	b.d	227	0.57	23.45	0.40	0.0518	0.0011	0.3041	0.0078	0.0427	0.0007	0.67	249	47	50	269	5	7	269	6	8	100	108
RBGS1 - 32	4.8.E+05	b.d.	b.d	226	0.06	2.38	0.07	0.1637	0.0016	9.4300	0.2900	0.4197	0.0120	0.93	2493	17	19	2257	60	66	2379	40	41	95	91
RBGS1 - 33	6.0.E+04	b.d.	b.d	270	0.70	23.12	0.42	0.0561	0.0016	0.3335	0.0094	0.0433	0.0008	0.64	429	56	64	273	5	7	292	7	9	93	64
RBGS1 - 35	1.1.E+05	b.d.	b.d	499	0.81	22.66	0.39	0.0622	0.0045	0.3790	0.0290	0.0441	0.0008	0.23	630	98	155	278	5	7	325	19	23	86	44
RBGS1 - 36	8.1.E+04	b.d.	b.d	380	0.69	24.99	0.41	0.0528	0.0010	0.2912	0.0067	0.0400	0.0007	0.72	296	42	44	253	4	6	259	5	7	98	85
RBGS1 - 39	9.1.E+04	b.d.	b.d	402	0.59	23.44	0.39	0.0523	0.0010	0.3077	0.0076	0.0427	0.0007	0.67	274	42	45	269	4	6	272	6	8	99	98
RBGS1 - 40	5.0.E+04	b.d.	b.d	237	0.86	24.83	0.43	0.0524	0.0013	0.2907	0.0084	0.0403	0.0007	0.59	274	53	58	255	4	6	259	6	8	98	93
RBGS1 - 41	3.7.E+04	b.d.	b.d	186	0.52	27.00	0.47	0.0608	0.0017	0.3103	0.0092	0.0370	0.0006	0.58	589	59	61	234	4	6	273	7	10	86	40
RBGS1 - 42	2.2.E+04	b.d.	b.d	106	1.21	24.81	0.48	0.0785	0.0044	0.4340	0.0220	0.0403	0.0008	0.38	1072	89	112	255	5	7	363	15	19	70	24
RBGS1 - 43	7.3.E+04	b.d.	b.d	352	0.85	24.10	0.55	0.0559	0.0031	0.3190	0.0210	0.0415	0.0010	0.35	416	91	124	262	6	8	280	13	18	94	63
RBGS1 - 44	8.7.E+04	b.d.	b.d	392	0.59	24.17	0.39	0.0526	0.0009	0.3002	0.0066	0.0414	0.0007	0.74	293	37	39	261	4	6	267	5	7	98	89
RBGS1 - 45	4.3.E+04	b.d.	b.d	199	1.30	24.35	0.42	0.0516	0.0014	0.2929	0.0088	0.0411	0.0007	0.57	245	58	63	260	4	6	260	7	9	100	106
RBGS1 - 46	1.5.E+04	b.d.	b.d	97	1.24	33.00	0.68	0.0523	0.0030	0.2170	0.0120	0.0303	0.0006	0.37	220	100	131	192	4	5	198	10	12	97	87
RBGS1 - 47	4.5.E+04	b.d.	b.d	214	0.58	24.04	0.47	0.0597	0.0038	0.3400	0.0220	0.0416	0.0008	0.30	542	92	138	263	5	7	296	15	18	89	48
RBGS1 - 48	2.3.E+04	b.d.	b.d	105	0.65	24.86	0.45	0.0604	0.0021	0.3340	0.0120	0.0402	0.0007	0.50	530	73	76	254	5	6	290	9	13	88	48
RBGS1 - 49	7.9.E+04	b.d.	b.d	344	0.79	23.39	0.39	0.0517	0.0010	0.3059	0.0073	0.0428	0.0007	0.70	252	43	46	270	4	7	270	6	8	100	107
RBGS1 - 51	5.2.E+04	b.d.	b.d	224	0.82	22.86	0.40	0.0538	0.0014	0.3226	0.0089	0.0437	0.0008	0.64	327	56	60	276	5	7	284	7	9	97	84
RBGS1 - 52	2.5.E+04	b.d.	b.d	59	0.78	12.31	0.21	0.0596	0.0019	0.6620	0.0220	0.0812	0.0014	0.52	532	64	70	503	9	12	513	13	18	98	95
RBGS1 - 53	3.6.E+04	b.d.	b.d	156	0.78	23.29	0.41	0.0531	0.0014	0.3129	0.0089	0.0429	0.0008	0.62	295	55	61	271	5	7	276	7	9	98	92
RBGS1 - 54	6.3.E+04	b.d.	b.d	261	0.54	20.95	0.42	0.0596	0.0021	0.3920	0.0130	0.0477	0.0010	0.60	566	67	77	301	6	8	334	9	12	90	53
RBGS1 - 55	4.2.E+04	b.d.	b.d	195	0.77	24.44	0.42	0.0547	0.0015	0.3090	0.0094	0.0409	0.0007	0.56	363	58	63	258	4	6	272	7	10	95	71
RBGS1 - 56	7.5.E+04	b.d.	b.d	254	0.82	17.66	0.29	0.0577	0.0013	0.4480	0.0120	0.0566	0.0009	0.62	494	50	51	355	6	8	375	9	11	95	72
RBGS1 - 57	3.8.E+04	b.d.	b.d	182	0.70	24.44	0.44	0.0637	0.0035	0.3580	0.0170	0.0409	0.0007	0.38	667	88	117	259	5	7	309	12	15	84	39
RBGS1 - 58	9.0.E+04	b.d.	b.d	391	0.44	23.21	0.39	0.0528	0.0010	0.3130	0.0073	0.0431	0.0007	0.73	299	40	43	272	5	7	276	6	7	98	91
RBGS1 - 59	1.5.E+05	b.d.	b.d	375	0.59	12.92	0.22	0.0590	0.0008	0.6260	0.0120	0.0774	0.0013	0.88	549	31	32	480	8	12	493	8	11	97	87
RBGS1 - 60	4.2.E+04	b.d.	b.d	192	0.54	24.00	0.49	0.0575	0.0027	0.3320	0.0160	0.0417	0.0009	0.42	470	77	104	263	5	7	290	11	15	91	56
RBGS1 - 61	8.5.E+04	b.d.	b.d	260	0.77	17.53	0.29	0.0565	0.0012	0.4447	0.0110	0.0571	0.0009	0.67	453	43	48	358	6	9	373	7	10	96	79
RBGS1 - 62	4.9.E+04	b.d.	b.d	230	0.93	24.61	0.42	0.0533	0.0013	0.2969	0.0082	0.0406	0.0007	0.61	301	53	56	257	4	6	264	7	8	97	85
RBGS1 - 63	9.0.E+04	b.d.	b.d	151	0.68	8.60	0.20	0.0780	0.0022	1.2560	0.0290	0.1163	0.0027	0.90	1136	50	57	709	16	20	823	13	20	86	62
RBGS1 - 64	8.5.E+04	b.d.	b.d	365	0.79	23.16	0.39	0.0528	0.0010	0.3139	0.0071	0.0432	0.0007	0.75	298	41	44	273	4	7	278	6	7	98	91
RBGS1 - 65	3.6.E+04	b.d.	b.d	172	0.64	24.22	0.52	0.0596	0.0027	0.3370	0.0170	0.0413	0.0009	0.42	523	85	99	261	5	7	293	13	15	89	50
RBGS1 - 67	1.2.E+05	b.d.	b.d	562	0.65	24.62	1.27	0.0543	0.0013	0.3038	0.0310	0.0406	0.0021	0.51	361	43	55	257	13	14	269	13	25	95	71
GKT1 - 1	3.7.E+05	b.d.	b.d	438	0.34	5.80	0.18	0.0743	0.0012	1.7840	0.0640	0.1724	0.0054	0.87	1039	36	37	1025	30	35	1037	27	29	99	99
GKT1 - 3	1.7.E+05	b.d.	b.d	188	0.46	5.66	0.09	0.0780	0.0012	1.8950	0.0390	0.1768	0.0029	0.80	1129	32	33	1049	16	24	1079	14	19	97	93
GKT1 - 5	1.1.E+05	b.d.	b.d	229	0.69	10.06	0.24	0.0615	0.0014	0.8460	0.0260	0.0994	0.0024	0.79	636	47	50	611	14	18	622	14	17	98	96
GKT1 - 6	2.5.E+05	b.d.	b.d	281	0.65	5.66	0.10	0.0763	0.0010	1.8600	0.0350	0.1766	0.0030	0.90	1095	28	29	1048	17	25	1065	13	19	98	96
GKT1 - 9	5.8.E+04	b.d.	b.d	144	0.39	12.33	0.23	0.0588	0.0013	0.6580	0.0170	0.0811	0.0015	0.72	532	47	49	503	9	13	512	10	14	98	94
GKT1 - 12	1.1.E+05	b.d.	b.d	215	1.56	9.85	0.37	0.0617	0.0024	0.8680	0.0590	0.1015	0.0038	0.55	640	64	84	623	22	25	632	21	35	99	97
GKT1 - 14	8.7.E+04	b.d.	b.d	100	0.47	5.79	0.10	0.0744	0.0015	1.7780	0.0420	0.1727	0.0031	0.76	1030	41	42	1027	17	25	1033	16	24	99	100
GKT1 - 15	1.5.E+05	b.d.	b.d	393	0.36	12.50	0.30	0.0568	0.0024	0.6300	0.0240	0.0800	0.0019	0.62	467	66	94	496	11	14	495	13	18	100	106
GKT1 - 18	1.4.E+05	b.d.	b.d	350	0.66	12.50	0.20	0.0565	0.0010	0.6249	0.0130	0.0800	0.0013	0.78	459	38	40	496	8	12	493	8	11	101	108
GKT1 - 19	6.0.E+05	b.d.	b.d	655	0.17	5.37	0.11	0.0778	0.0010	2.0030	0.0400	0.1863	0.0037	0.90	1134	26	28	1102	20	26	1115	14	20	99	97
GKT1 - 26	7.9.E+04	b.d.	b.d	87	0.37	5.53	0.17	0.0763	0.0018	1.8960	0.0690	0.1808	0.0057	0.87	1081	48	50	1071	32	36	1076	29	31	100	99
GKT1 - 31	1.2.E+05	b.d.	b.d	245	0.58	10.07	0.35	0.0614	0.0023	0.8430	0.0380	0.0993	0.0035	0.78	631	67	81	610	17	23	619	17	24	99	97
GKT1 - 32	5.1.E+04	b.d.	b.d	127	0.52	12.13	0.54	0.0589	0.0028	0.6690	0.0510	0.0824	0.0037	0.59	529	83	104	511	19	24	519	23	33	98	97
GKT1 - 35	1.3.E+05	b.d.	b.d	149	0.21	5.54	0.16	0.0752	0.0015	1.8710	0.0620	0.1806	0.0051	0.85	1061	39	41	1070	28	33	1068	26	28	100	101
GKT1 - 38	1.9.E+05	b.d.	b.d	381	0.57	9.97	0.18	0.0607	0.0010	0.8430	0.0180	0.1003	0.0018	0.84	610	37	38	616	11	15	620	10	14	99	101
GKT1 - 41	1.6.E+05	b.d.	b.d	183	0.34	5.76	0.10	0.0760	0.0012	1.8250	0.0370	0.1737	0.0030	0.85	1080	33	35	1032	16	24	1052	13	20	98	96
GKT1 - 42	1.4.E+05	b.d.	b.d	157	0.74	5.34	0.21	0.0771	0.0015	1.9930	0.0940	0.1871	0.0074	0.84	1117	40	41	1105	37	45	1111	21	36	99	99
GKT1 - 43	5.5.E+04	b.d.	b.d	139	0.66	12.05	0.30	0.0609	0.0021	0.6980	0.0240	0.0830	0.0021	0.74	596	66	75	514	12	15	536	13	18	96	86

GKT1 - 46	8.0.E+05	b.d.	b.d	1173	0.33	6.90	0.17	0.0779	0.0011	1.5570	0.0370	0.1450	0.0036	0.90	1137	26	30	872	21	26	952	16	20	92	77
GKT1 - 49	1.0.E+05	b.d.	b.d	170	0.76	8.02	0.14	0.0658	0.0011	1.1280	0.0250	0.1247	0.0021	0.76	777	36	37	758	12	18	765	12	18	99	98
GKT1 - 50	1.6.E+05	b.d.	b.d	388	0.47	12.19	0.22	0.0574	0.0009	0.6500	0.0130	0.0820	0.0015	0.91	492	33	36	508	9	13	508	8	12	100	103
GKT1 - 52	5.5.E+04	b.d.	b.d	114	0.79	9.90	0.27	0.0634	0.0023	0.8840	0.0360	0.1010	0.0028	0.68	688	66	78	620	16	20	640	18	24	97	90
GKT1 - 54	9.4.E+04	b.d.	b.d	135	0.20	6.84	0.20	0.0720	0.0017	1.4500	0.0450	0.1461	0.0043	0.95	966	47	49	879	24	28	907	19	24	97	91
GKT1 - 55	6.6.E+05	b.d.	b.d	929	0.05	6.46	0.18	0.0750	0.0012	1.6040	0.0520	0.1548	0.0043	0.86	1061	37	38	929	25	27	972	24	25	96	88
GKT1 - 56	9.4.E+04	b.d.	b.d	106	0.26	5.59	0.10	0.0760	0.0014	1.8730	0.0400	0.1788	0.0032	0.84	1073	36	38	1060	17	25	1069	14	21	99	99
GKT1 - 60	7.5.E+04	b.d.	b.d	195	0.56	12.66	0.26	0.0579	0.0014	0.6320	0.0190	0.0790	0.0016	0.67	493	49	54	490	9	13	496	11	15	99	99
GKT1 - 61	1.4.E+05	b.d.	b.d	343	0.06	11.55	0.21	0.0606	0.0012	0.7190	0.0150	0.0866	0.0016	0.89	603	40	44	535	10	13	549	9	13	97	89
GKT1 - 63	6.8.E+04	b.d.	b.d	140	0.70	9.67	0.23	0.0633	0.0020	0.9040	0.0370	0.1034	0.0025	0.59	687	64	68	634	15	18	651	18	24	97	92
GKT1 - 65	4.1.E+04	b.d.	b.d	104	0.81	12.22	0.54	0.0584	0.0022	0.6630	0.0480	0.0818	0.0036	0.61	490	77	83	508	21	22	512	22	34	99	104
GKT1 - 66	6.7.E+04	b.d.	b.d	170	0.51	12.26	0.21	0.0580	0.0013	0.6510	0.0160	0.0816	0.0014	0.70	494	48	50	505	9	12	508	10	13	99	102
GKT1 - 67	2.1.E+05	b.d.	b.d	264	0.33	6.09	0.10	0.0725	0.0010	1.6450	0.0310	0.1642	0.0028	0.90	990	29	30	980	15	23	986	12	18	99	99
GKT1 - 68	9.0.E+04	b.d.	b.d	232	0.53	12.77	0.33	0.0578	0.0016	0.6280	0.0260	0.0783	0.0020	0.62	498	56	62	486	11	15	494	14	18	98	98
GKT1 - 69	9.1.E+04	b.d.	b.d	169	0.52	8.87	0.18	0.0613	0.0013	0.9560	0.0270	0.1127	0.0023	0.72	619	44	47	688	14	18	678	14	20	102	111
																				0			0		
KBCS2 - 1	2.3.E+05	b.d.	b.d	247	0.67	5.63	0.10	0.0757	0.0012	1.8530	0.0390	0.1776	0.0031	0.83	1076	33	34	1054	17	24	1063	14	20	99	98
KBCS2 - 2	1.8.E+05	b.d.	b.d	525	0.09	15.13	0.25	0.0548	0.0010	0.5020	0.0110	0.0661	0.0011	0.76	389	41	42	413	7	10	412	8	10	100	106
KBCS2 - 3	2.2.E+05	b.d.	b.d	965	0.58	22.58	0.38	0.0624	0.0012	0.3804	0.0082	0.0443	0.0007	0.78	672	42	43	279	5	7	327	6	8	85	42
KBCS2 - 5	1.9.E+05	b.d.	b.d	467	0.45	12.85	0.25	0.0612	0.0011	0.6590	0.0130	0.0778	0.0015	0.98	625	38	40	483	9	12	513	8	12	94	77
KBCS2 - 6	1.1.E+05	b.d.	b.d	275	0.33	13.10	0.22	0.0581	0.0013	0.6130	0.0150	0.0763	0.0013	0.70	511	48	50	474	8	11	484	10	13	98	93
KBCS2 - 7	1.3.E+05	b.d.	b.d	602	0.53	24.47	0.42	0.0519	0.0010	0.2940	0.0071	0.0409	0.0007	0.71	270	45	46	258	4	6	262	5	7	99	96
KBCS2 - 8	2.1.E+05	b.d.	b.d	931	0.36	24.08	0.39	0.0545	0.0010	0.3116	0.0065	0.0415	0.0007	0.79	376	40	42	262	4	6	275	5	7	95	70
KBCS2 - 9	2.1.E+05	b.d.	b.d	523	0.12	12.56	0.24	0.0580	0.0013	0.6380	0.0170	0.0796	0.0015	0.71	516	51	52	494	9	12	500	10	14	99	96
KBCS2 - 10	1.3.E+05	b.d.	b.d	620	0.52	23.63	0.49	0.0529	0.0015	0.3091	0.0092	0.0423	0.0009	0.69	305	62	65	267	5	7	273	7	9	98	88
KBCS2 - 11	3.1.E+05	b.d.	b.d	342	0.87	5.90	0.10	0.0755	0.0012	1.7690	0.0370	0.1694	0.0029	0.82	1073	32	34	1010	17	22	1033	14	19	98	94
KBCS2 - 12	2.3.E+04	b.d.	b.d	86	0.77	19.86	0.38	0.0569	0.0026	0.3950	0.0180	0.0503	0.0010	0.42	405	97	101	317	6	8	336	13	16	94	78
KBCS2 - 13	5.3.E+04	b.d.	b.d	248	0.98	24.02	0.43	0.0541	0.0016	0.3116	0.0093	0.0416	0.0007	0.60	352	62	68	263	5	7	275	7	9	96	75
KBCS2 - 14	3.3.E+04	b.d.	b.d	304	0.61	48.22	0.98	0.0562	0.0024	0.1600	0.0062	0.0207	0.0004	0.52	395	89	95	132	3	4	151	6	7	88	33
KBCS2 - 15	2.6.E+04	b.d.	b.d	176	1.96	34.93	0.73	0.0600	0.0037	0.2320	0.0150	0.0286	0.0006	0.32	500	120	134	182	4	5	210	12	15	87	36
KBCS2 - 16	5.0.E+04	b.d.	b.d	238	0.99	25.08	0.42	0.0537	0.0015	0.2948	0.0092	0.0399	0.0007	0.54	325	62	64	252	4	6	262	7	9	96	78
KBCS2 - 17	8.2.E+04	b.d.	b.d	401	0.50	25.21	0.46	0.0540	0.0015	0.2958	0.0085	0.0397	0.0007	0.64	341	60	64	251	5	6	263	7	8	95	74
KBCS2 - 18	9.1.E+04	b.d.	b.d	314	0.34	17.80	0.38	0.0602	0.0015	0.4670	0.0130	0.0562	0.0012	0.77	595	55	56	352	7	10	388	9	12	91	59
KBCS2 - 19	1.4.E+05	b.d.	b.d	399	0.39	15.93	0.25	0.0552	0.0010	0.4769	0.0099	0.0628	0.0010	0.76	399	38	40	392	6	9	396	7	9	99	98
KBCS2 - 20	1.0.E+05	b.d.	b.d	463	0.57	23.31	0.54	0.0620	0.0019	0.3670	0.0130	0.0429	0.0010	0.66	644	65	66	271	6	8	317	10	12	86	42
KBCS2 - 21	2.1.E+04	b.d.	b.d	93	1.11	24.28	0.46	0.0544	0.0021	0.3080	0.0120	0.0412	0.0008	0.49	324	80	87	261	5	6	273	10	11	96	80
KBCS2 - 22	1.0.E+05	b.d.	b.d	433	0.43	23.23	0.36	0.0524	0.0010	0.3105	0.0068	0.0430	0.0007	0.71	286	42	44	272	4	6	274	5	7	99	95
KBCS2 - 23	3.5.E+04	b.d.	b.d	150	0.66	24.00	0.41	0.0521	0.0017	0.2981	0.0099	0.0417	0.0007	0.52	239	67	75	263	4	6	264	8	10	100	110
KBCS2 - 24	1.7.E+05	b.d.	b.d	904	0.35	27.50	0.46	0.0707	0.0012	0.3558	0.0072	0.0364	0.0006	0.83	942	37	38	230	4	6	309	5	8	75	24
KBCS2 - 25	3.4.E+04	b.d.	b.d	70	0.38	11.92	0.20	0.0584	0.0017	0.6760	0.0200	0.0839	0.0014	0.56	498	63	65	519	9	12	521	12	18	100	104
KBCS2 - 26	5.6.E+04	b.d.	b.d	255	0.88	24.30	0.57	0.0536	0.0020	0.3030	0.0150	0.0412	0.0010	0.48	315	71	85	260	6	8	268	11	13	97	83
KBCS2 - 27	7.2.E+04	b.d.	b.d	148	0.38	11.67	0.19	0.0590	0.0012	0.6970	0.0160	0.0857	0.0014	0.71	539	44	46	530	8	12	535	10	14	99	98
KBCS2 - 28	1.0.E+05	b.d.	b.d	440	0.48	24.59	0.42	0.0523	0.0012	0.2927	0.0074	0.0407	0.0007	0.67	277	46	54	257	4	6	260	6	8	99	93
KBCS2 - 30	1.3.E+05	b.d.	b.d	510	0.59	22.76	0.36	0.0519	0.0008	0.3152	0.0066	0.0439	0.0007	0.75	269	36	39	277	4	7	278	5	7	100	103
KBCS2 - 31	6.7.E+04	b.d.	b.d	290	0.40	23.21	0.42	0.0527	0.0012	0.3128	0.0082	0.0431	0.0008	0.69	280	50	53	272	5	7	276	6	9	99	97
KBCS2 - 32	5.5.E+04	b.d.	b.d	250	1.08	24.93	0.46	0.0529	0.0022	0.2924	0.0140	0.0401	0.0007	0.39	290	80	95	254	5	6	260	10	13	98	87
KBCS2 - 33	8.3.E+04	b.d.	b.d	353	0.49	24.10	0.39	0.0512	0.0010	0.2934	0.0070	0.0415	0.0007	0.68	229	44	47	262	4	6	261	6	8	101	114
KBCS2 - 34	7.1.E+04	b.d.	b.d	296	0.60	24.06	0.41	0.0523	0.0011	0.3008	0.0074	0.0416	0.0007	0.68	282	48	49	263	4	6	267	6	7	98	93
KBCS2 - 35	3.5.E+04	b.d.	b.d	155	1.91	25.47	0.44	0.0526	0.0014	0.2847	0.0083	0.0393	0.0007	0.59	282	57	62	248	4	6	254	7	9	98	88
KBCS2 - 36	9.3.E+04	b.d.	b.d	437	0.87	26.10	0.42	0.0587	0.0011	0.3100	0.0071	0.0383	0.0006	0.71	529	43	44	242	4	6	274	6	8	89	46
KBCS2 - 37	9.8.E+04	b.d.	b.d	727	0.52	39.79	0.78	0.0508	0.0017	0.1753	0.0057	0.0251	0.0005	0.60	212	73	78	160	3	4	164	5	6	98	75
KBCS2 - 39	4.6.E+04	b.d.	b.d	212	0.49	26.24	0.44	0.0519	0.0013	0.2728	0.0077	0.0381	0.0006	0.59	261	56	59	241	4	6	244	6	8	99	92
KBCS2 - 40	4.7.E+04	b.d.	b.d	190	0.65	22.90	0.38	0.0548	0.0014	0.3287	0.0090	0.0437	0.0007	0.60	360	55	58	276	4	7	288	7	9	96	77
KBCS2 - 41	4.6.E+04	b.d.	b.d	205	0.78	24.96	0.43	0.0526	0.0016	0.2907	0.0092	0.0401	0.0007	0.54	274	65	70	253	4	6	258	7	9	98	92
KBCS2 - 42	5.1.E+04	b.d.	b.d	212	0.73	24.17	0.40	0.0517	0.0012	0.2956	0.0081	0.0414	0.0007	0.61	243	53	55	261	4	6	262	6	9	100	108
KBCS2 - 44	2.5.E+05	b.d.	b.d	612	0.81	12.94	0.22	0.0574	0.0009	0.6139	0.0120	0.0773	0.0013	0.86	495	34	37	480	8	11	486	7	11	99	97
KBCS2 - 45	5.9.E+04	b.d.	b.d	264	0.53	24.72	0.55	0.0582	0.0023	0.3236	0.0170	0.0405	0.0009	0.42	483	76	87	256	6	7	284	11	15	90	53
KBCS2 - 46	1.4.E+05	b.d.	b.d	656	0.66	24.93	0.41	0.0522	0.0011	0.2887	0.0066	0.0401	0.0007	0.72	272	45	50	254	4	6	257	5	7	99	93
KBCS2 - 47	4.6.E+04	b.d.	b.d	102	0.67	12.41	0.20	0.0584	0.0015	0.6500	0.0180	0.0806	0.0013	0.58	499	56	57	499	8	12	505	11	17	99	100
KBCS2 - 48	9.0.E+04	b.d.	b.d	417	0.80	25.06	0.46	0.0582	0.0017	0.3197	0.0110	0.0399	0.0007	0.53	501	59	65	252	5	6	281	8	10	90	50
KBCS2 - 49	4.4.E+05	b.d.	b.d	416	0.68	5.14	0.08	0.0769	0.0009	2.0710	0.0360	0.1947	0.0032	0.95	1112	22	25	1147	17	26	1139	12	18	101	103
KBCS2 - 51	5.1.E+04	b.d.	b.d	223	0.83	23.88	0.40	0.0523	0.0014	0.3004	0.0085	0.0419	0.0007	0.60	265	57	62	264	4	6	266	7	8	99	100
KBCS2 - 52	1.9.E+05	b.d.	b.d	377	0.61	10.43	0.17	0.0645	0.0010	0.8500	0.0160	0.0958	0.0016	0.89	742	33	34	590	10	14	624	9	13	95	80
KBCS2 - 54	5.2.E+04	b.d.	b.d	238	0.86	24.80	0.40	0.0519	0.0013	0.2890	0.0083	0.0403	0.0007	0.56	247	54	59	255	4	6	257	7	9	99	103
KBCS2 - 55	5.0.E+04	b.d.	b.d	221	0.71	23.53	0.41	0.0527	0.0013	0.3083	0.0082	0.0425	0.0007	0.65	280	53	57	268	5	7	272	6	9	99	96
KBCS2 - 56	1.0.E+05	b.d.	b.d	488	0.76	24.63	0.45	0.0571	0.0015	0.3196	0.0078	0.0406	0.0008	0.76	468	53	59	257	5	7	281	6	8	91	55
KBCS2 - 57	1.8.E+05	b.d.	b.d	818	0.42	23.51	0.40	0.0542	0.0009	0.3183	0.0069	0.0425	0.0007	0.79	366	37	38	269	5	7	280	5	7	96	73
KBCS2 - 58	2.9.E+04	b.d.	b.d	143	0.60	25.33	0.51	0.0557	0.0051	0.3030	0.0290	0.0395	0.0008	0.21	385	120	204	250	5	7	267	18	25	94	65
KBCS2 - 60	3.7.E+04	b.d.	b.d	186	0.70	25.83	0.47	0.0542	0.0019	0.2905	0.0100	0.0387	0.0007	0.53	337	70	80	245	4	6	258	8	10	95	73
KBCS2 - 62	1.0.E+05	b.d.	b.d	507	0.71	24.25	0.39	0.0523	0.0010	0.2970	0.0065	0.0412	0.0007	0.73	280	40	43	261	4	6	264	5	7	99	93
KBCS2 - 63	4.9.E+04	b.d.	b.d	234	0.76	24.80	0.41	0.0529	0.0013	0.2937	0.0083	0.0403	0.0007	0.58	296	54	57	255	4	6	262	7	8	97	86
KBCS2 - 65	7.9.E+04	b.d.	b.d	385	0.90	24.73	0.40	0.0516	0.0012	0.2879	0.0075	0.0404	0.0007	0.63	246	49	55	256	4	6	256	6	8	100	104
KBCS2 - 66	3.5.E+04	b.d.	b.d	253	1.06	34.97	0.99	0.0529	0.0032	0.2082	0.0150	0.0286	0.0008	0.39	277	96	138	182	5	6	192	11	13	95	66
KBCS2 - 70	6.1.E+04	b.d.	b.d	284	0.65	24.50	0.40	0.0534	0.0012	0.3015	0.0076	0.0408	0.0007	0.65	326	47	52	258	4	6	267	6	8	96	79
KBCS2 - 71	7.0.E+04	b.d.	b.d	339	0.82	24.53	0.40	0.0528	0.0013	0.2981	0.0082	0.0408	0.0007	0.60	284	56	57	258	4	6	264	6	9	98	91
KBCS2 - 72	5.9.E+04	b.d.	b.d	287	0.82	24.49	0.42	0.0517	0.0013	0.2906	0.0080	0.0408	0.0007	0.62	242	56	59	258	4	6	258	6	8	100	107
KBCS2 - 74	8.6.E+04	b.d.	b.d	397	0.49	23.92	0.39	0.0540	0.0010	0.3118	0.0071	0.0418	0.0007	0.72	346	42	43	264	4	6	275	6	8	96	76
KBCS2 - 75	7.2.E+04	b.d.	b.d	167	0.47	11.81	0.20	0.0580	0.0013	0.6790	0.0170	0.0847	0.0014	0.66	502	46	50	524	8	12	525	10	14	100	104
KBCS2 - 76	7.4.E+04	b.d.	b.d	353	0.81	24.14	0.40	0.0516	0.0012	0.2956	0.0075	0.0414	0.0007	0.65	245	51	55	262	4	6	262	6	8	100	107
KBCS2 - 77	2.8.E+04	b.d.	b.d	208	0.53	37.88	0.66	0.0556	0.0021	0.2038	0.0084	0.0264	0.0005	0.42	407	74	85	168	3	4	188	7	8	89	41
KBCS2 - 78	3.4.E+04	b.d.	b.d	170	0.48	25.64	0.46	0.0521	0.0015	0.2795	0.0091	0.0390	0.0007	0.55	247	63	67	247	4	6	249	7	10	99	100
KBCS2 - 79	4.8.E+04	b.d.	b.d	242	0.91	24.90	0.47	0.0524	0.0017	0.2892	0.0091	0.0402	0.0008	0.59	262	65	75	254	5	6	257	7	9	99	97
KBCS2 - 80	1.4.E+05	b.d.	b.d	345	0.41	12.83	0.20	0.0573	0.0009	0.6171	0.0120	0.0780	0.0012	0.79	493	34	36	484	7	11	487	8	11	99	98
KBCS2 - 81	3.6.E+04	b.d.	b.d	170	1.36	24.54	0.43	0.0621	0.0025	0.3450	0.0150	0.0408	0.0007	0.40	592	78	87	257	4	6	300	11	13	86	43
KBCS2 - 83	6.0.E+04	b.d.	b.d	283	0.30	23.42	0.52	0.0548	0.0022	0.3210	0.0089	0.0427	0.0010	0.80	379	68	91	270	6	8	283	7	8	95	71
KBCS2 - 84	3.7.E+04	b.d.	b.d	178	0.60	24.67	0.44	0.0578	0.0025	0.3230	0.0130	0.0405	0.0007	0.45	464	75	96	256	5	6	283	10	12	91	55
KBCS2 - 89	1.2.E+05	b.d.	b.d	560	0.36	24.02	0.40	0.0525	0.0009	0.3031	0.0065	0.0416	0.0007	0.77	289	40	42	263	4	6	268	5	7	98	91
KBCS2 - 91	7.9.E+04	b.d.	b.d	386	1.21	25.32	0.45	0.0557	0.0018	0.3048	0.0096	0.0395	0.0007	0.56	413	62	73	250	4	6	269	7	9	93	60
KBCS2 - 93	9.7.E+04	b.d.	b.d	449	0.69	23.96	0.57	0.0533	0.0019	0.3075	0.0130	0.0417	0.0010	0.57	318	64	82	264	6	8	272	9	12	97	83
KBCS2 - 96	1.3.E+05	b.d.	b.d	634	0.44	24.11	0.64	0.0551	0.0026	0.3155	0.0220	0.0415	0.0011	0.38	394	85	106	262	7	8	278	12	18	94	66
MBHF - 1	8.4.E+04	b.d.	b.d	190	0.41	12.19	0.21	0.0576	0.0012	0.6520	0.0150	0.0820	0.0014	0.74	489	44	47	508	9	12	508	9	14	100	104

MBHF - 3	1.0.E+05	b.d.	b.d	531	0.64	27.01	0.58	0.0731	0.0017	0.3744	0.0088	0.0370	0.0008	0.92	996	55	57	234	5	6	322	7	9	73	24
MBHF - 4	2.1.E+05	b.d.	b.d	243	0.25	5.87	0.14	0.0771	0.0011	1.8050	0.0390	0.1705	0.0040	0.90	1115	28	30	1015	22	28	1045	15	21	97	91
MBHF - 5	3.3.E+04	b.d.	b.d	76	0.61	12.36	0.23	0.0580	0.0017	0.6450	0.0200	0.0809	0.0015	0.60	475	63	65	501	9	13	504	12	16	99	106
MBHF - 6	1.8.E+05	b.d.	b.d	214	0.52	6.62	0.11	0.0719	0.0011	1.4970	0.0290	0.1511	0.0026	0.89	971	31	33	907	14	22	927	12	18	98	93
MBHF - 7	6.5.E+05	b.d.	b.d	404	0.24	3.23	0.06	0.1093	0.0011	4.6670	0.0820	0.3095	0.0054	0.90	1787	19	21	1738	27	38	1761	15	22	99	97
MBHF - 8	1.6.E+05	b.d.	b.d	386	0.53	12.88	0.22	0.0573	0.0009	0.6127	0.0120	0.0776	0.0013	0.86	489	33	35	482	8	12	486	7	10	99	99
MBHF - 9	9.8.E+04	b.d.	b.d	223	0.45	12.07	0.20	0.0584	0.0011	0.6640	0.0150	0.0829	0.0014	0.75	517	42	43	513	8	12	516	9	13	100	99
MBHF - 10	2.2.E+04	b.d.	b.d	95	0.96	23.42	0.44	0.0580	0.0021	0.3410	0.0130	0.0427	0.0008	0.50	443	78	80	270	5	7	296	10	13	91	61
MBHF - 11	5.0.E+04	b.d.	b.d	227	0.83	24.12	0.45	0.0569	0.0016	0.3258	0.0100	0.0415	0.0008	0.61	435	60	63	262	5	7	285	8	10	92	60
MBHF - 12	1.8.E+05	b.d.	b.d	779	0.57	22.22	0.37	0.0761	0.0013	0.4721	0.0098	0.0450	0.0008	0.80	1080	34	36	284	5	7	392	7	10	72	26
MBHF - 13	2.5.E+05	b.d.	b.d	465	0.25	9.90	0.16	0.0609	0.0008	0.8470	0.0160	0.1010	0.0016	0.84	625	30	32	620	10	14	622	9	13	100	99
MBHF - 14	1.5.E+05	b.d.	b.d	204	0.51	7.05	0.17	0.0671	0.0011	1.3150	0.0390	0.1418	0.0034	0.81	833	36	37	856	20	23	850	18	22	101	103
MBHF - 15	5.8.E+04	b.d.	b.d	76	0.21	6.58	0.17	0.0711	0.0016	1.4900	0.0500	0.1519	0.0039	0.77	934	48	49	911	22	27	921	23	28	99	98
MBHF - 16	1.6.E+05	b.d.	b.d	391	0.53	12.71	0.21	0.0562	0.0009	0.6082	0.0120	0.0787	0.0013	0.84	443	36	39	488	8	12	482	8	11	101	110
MBHF - 17	4.9.E+04	b.d.	b.d	122	0.30	13.16	0.23	0.0575	0.0014	0.6040	0.0170	0.0760	0.0013	0.61	473	53	55	472	8	11	478	10	15	99	100
MBHF - 18	2.0.E+04	b.d.	b.d	50	0.70	12.81	0.23	0.0596	0.0020	0.6400	0.0220	0.0781	0.0014	0.52	522	74	75	484	9	12	500	14	18	97	93
MBHF - 19	1.1.E+04	b.d.	b.d	12	0.54	5.77	0.12	0.0792	0.0034	1.8630	0.0800	0.1732	0.0037	0.50	1050	90	92	1028	20	28	1054	28	45	98	98
MBHF - 20	1.7.E+04	b.d.	b.d	31	0.68	10.00	0.19	0.0612	0.0023	0.8460	0.0340	0.1000	0.0019	0.47	572	81	82	614	11	16	617	19	26	100	107
MBHF - 21	1.3.E+04	b.d.	b.d	25	0.38	10.00	0.20	0.0620	0.0025	0.8470	0.0340	0.1000	0.0020	0.50	582	86	87	614	12	16	616	19	27	100	105
MBHF - 22	1.9.E+05	b.d.	b.d	413	0.19	11.76	0.19	0.0623	0.0010	0.7320	0.0150	0.0851	0.0014	0.80	674	34	36	526	8	12	557	9	13	95	78
MBHF - 23	3.2.E+04	b.d.	b.d	148	0.67	24.56	0.43	0.0536	0.0017	0.2990	0.0094	0.0407	0.0007	0.55	307	66	73	257	4	6	265	7	9	97	84
MBHF - 24	5.4.E+04	b.d.	b.d	59	0.36	5.54	0.16	0.0766	0.0017	1.9100	0.0600	0.1806	0.0051	0.90	1084	43	46	1070	29	33	1081	23	28	99	99
MBHF - 25	8.0.E+04	b.d.	b.d	151	0.48	10.04	0.17	0.0680	0.0014	0.9340	0.0230	0.0996	0.0017	0.69	841	44	45	612	10	15	667	13	18	92	73
MBHF - 26	5.1.E+04	b.d.	b.d	108	0.60	11.35	0.21	0.0605	0.0014	0.7310	0.0200	0.0881	0.0016	0.66	585	52	53	544	9	14	556	11	15	98	93
MBHF - 27	1.4.E+05	b.d.	b.d	338	0.61	12.77	0.21	0.0573	0.0009	0.6205	0.0130	0.0783	0.0013	0.79	489	34	36	486	8	12	489	8	12	99	99
MBHF - 28	7.0.E+04	b.d.	b.d	157	0.49	12.05	0.20	0.0577	0.0012	0.6610	0.0150	0.0830	0.0014	0.74	501	45	47	514	8	12	514	10	13	100	103
MBHF - 29	3.0.E+04	b.d.	b.d	34	0.90	5.90	0.11	0.0754	0.0019	1.7620	0.0520	0.1694	0.0031	0.62	1038	53	54	1008	17	25	1025	20	29	98	97
MBHF - 30	6.5.E+04	b.d.	b.d	66	0.51	5.51	0.09	0.0760	0.0014	1.8990	0.0430	0.1816	0.0031	0.75	1079	37	39	1076	17	24	1078	15	22	100	100
MBHF - 31	1.4.E+04	b.d.	b.d	66	1.21	25.13	0.51	0.0540	0.0025	0.2950	0.0130	0.0398	0.0008	0.46	302	90	105	252	5	7	261	11	13	96	83
MBHF - 33	1.3.E+05	b.d.	b.d	287	0.34	11.38	0.19	0.0595	0.0011	0.7200	0.0160	0.0878	0.0015	0.77	562	39	42	543	9	12	549	9	14	99	97
MBHF - 34	3.2.E+04	b.d.	b.d	219	0.82	35.61	0.63	0.0502	0.0018	0.1914	0.0071	0.0281	0.0005	0.48	164	72	84	179	3	4	178	6	7	100	109
MBHF - 36	3.8.E+04	b.d.	b.d	69	0.42	9.19	0.30	0.0620	0.0031	0.9340	0.0420	0.1088	0.0035	0.72	632	95	108	666	21	23	665	23	28	100	105
MBHF - 37	2.1.E+04	b.d.	b.d	27	0.37	6.74	0.19	0.0745	0.0023	1.5160	0.0620	0.1484	0.0042	0.69	984	69	70	891	24	29	929	28	35	96	91
MBHF - 38	3.5.E+04	b.d.	b.d	79	0.59	12.02	0.22	0.0590	0.0016	0.6760	0.0200	0.0832	0.0015	0.61	513	61	62	515	9	13	521	12	18	99	100
MBHF - 41	1.8.E+05	b.d.	b.d	596	0.66	17.50	0.28	0.0542	0.0009	0.4267	0.0085	0.0571	0.0009	0.81	366	36	37	358	6	8	361	6	8	99	98
MBHF - 42	1.5.E+05	b.d.	b.d	367	0.47	12.39	0.20	0.0587	0.0012	0.6520	0.0150	0.0807	0.0013	0.70	533	41	46	500	8	12	509	9	13	98	94
MBHF - 43	5.4.E+04	b.d.	b.d	334	1.28	33.84	0.58	0.0517	0.0013	0.2101	0.0058	0.0296	0.0005	0.63	246	53	59	188	3	5	194	5	6	97	76
MBHF - 44	2.4.E+05	b.d.	b.d	260	0.35	5.83	0.10	0.0749	0.0010	1.7680	0.0310	0.1715	0.0028	0.93	1054	27	29	1020	15	23	1033	12	18	99	97
MBHF - 46	4.2.E+04	b.d.	b.d	97	0.44	12.49	0.22	0.0585	0.0016	0.6460	0.0190	0.0801	0.0014	0.59	507	60	61	497	8	12	505	12	15	98	98
MBHF - 48	1.3.E+05	b.d.	b.d	191	0.22	7.83	0.23	0.0659	0.0017	1.1620	0.0390	0.1277	0.0037	0.86	782	51	55	775	21	25	780	18	24	99	99
MBHF - 49	1.1.E+05	b.d.	b.d	122	0.54	5.99	0.16	0.0739	0.0014	1.7010	0.0490	0.1669	0.0045	0.94	1020	38	40	995	25	30	1006	20	25	99	98
MBHF - 50	1.6.E+05	b.d.	b.d	189	0.43	5.95	0.12	0.0758	0.0012	1.7650	0.0440	0.1681	0.0035	0.84	1074	33	34	1002	19	25	1030	17	23	97	93
MBHF - 51	2.5.E+05	b.d.	b.d	281	0.31	6.10	0.10	0.0732	0.0010	1.6560	0.0300	0.1639	0.0027	0.91	1013	27	29	978	15	22	991	12	18	99	97
MBHF - 53	1.2.E+05	b.d.	b.d	274	0.37	12.11	0.22	0.0596	0.0011	0.6770	0.0150	0.0826	0.0015	0.82	564	39	42	511	9	13	523	9	13	98	91
MBHF - 54	6.9.E+04	b.d.	b.d	301	0.44	23.39	0.39	0.0533	0.0011	0.3151	0.0078	0.0428	0.0007	0.68	312	46	48	270	5	7	277	6	8	97	86
MBHF - 55	1.5.E+05	b.d.	b.d	679	0.48	24.04	0.40	0.0512	0.0008	0.2939	0.0060	0.0416	0.0007	0.81	234	35	38	263	4	6	261	5	7	101	112
MBHF - 56	1.8.E+04	b.d.	b.d	112	1.82	34.07	0.63	0.0537	0.0021	0.2168	0.0088	0.0294	0.0005	0.45	288	82	89	186	3	5	198	7	9	94	65
MBHF - 57	4.8.E+05	b.d.	b.d	609	0.13	6.37	0.15	0.0732	0.0011	1.5800	0.0420	0.1569	0.0036	0.86	1009	31	32	941	20	24	961	18	21	98	93
MBHF - 59	3.5.E+04	b.d.	b.d	74	0.41	11.12	0.20	0.0621	0.0018	0.7680	0.0240	0.0900	0.0016	0.57	620	64	65	555	9	14	576	14	19	96	90
MBHF - 61	6.5.E+04	b.d.	b.d	150	0.39	12.06	0.20	0.0598	0.0013	0.6840	0.0170	0.0829	0.0014	0.68	572	47	48	513	9	12	528	10	14	97	90
MBHF - 62	4.6.E+04	b.d.	b.d	191	1.30	21.45	0.46	0.0537	0.0017	0.3450	0.0100	0.0466	0.0010	0.74	318	66	72	294	6	8	300	8	10	98	92
MBHF - 63	5.5.E+04	b.d.	b.d	122	0.74	11.63	0.20	0.0602	0.0015	0.7120	0.0200	0.0860	0.0015	0.62	572	56	57	532	9	13	543	12	17	98	93
MBHF - 65	7.0.E+04	b.d.	b.d	193	0.71	14.43	0.25	0.0567	0.0012	0.5430	0.0130	0.0693	0.0012	0.72	464	45	48	432	7	11	439	8	12	98	93
MBHF - 66	1.9.E+05	b.d.	b.d	197	0.52	5.59	0.09	0.0761	0.0010	1.8820	0.0340	0.1790	0.0029	0.90	1090	28	39	1061	16	24	1073	12	19	99	97
MBHF - 67	3.2.E+04	b.d.	b.d	132	0.58	21.77	0.38	0.0534	0.0017	0.3380	0.0110	0.0459	0.0008	0.54	300	65	73	290	5	7	295	8	10	98	97
MBHF - 70	1.5.E+05	b.d.	b.d	162	0.45	5.46	0.10	0.0773	0.0012	1.9560	0.0420	0.1832	0.0032	0.81	1115	31	33	1084	18	25	1097	15	23	99	97
MBHF - 71	1.8.E+05	b.d.	b.d	207	0.37	5.77	0.17	0.0741	0.0013	1.7750	0.0610	0.1732	0.0050	0.84	1034	39	41	1030	28	32	1034	27	28	100	100
MBHF - 73	4.0.E+04	b.d.	b.d	92	0.41	12.12	0.22	0.0596	0.0016	0.6760	0.0190	0.0825	0.0015	0.65	536	58	59	511	9	13	522	11	17	98	95
MBHF - 74	2.8.E+04	b.d.	b.d	146	0.80	26.71	0.60	0.0541	0.0026	0.2790	0.0140	0.0374	0.0008	0.45	308	91	109	237	5	7	249	11	13	95	77
MBHF - 75	8.9.E+04	b.d.	b.d	97	0.24	5.61	0.11	0.0763	0.0013	1.8820	0.0450	0.1782	0.0036	0.84	1091	35	36	1057	20	27	1073	17	22	99	97
MBHF - 76	5.0.E+04	b.d.	b.d	240	0.98	24.25	0.41	0.0532	0.0014	0.3020	0.0085	0.0412	0.0007	0.60	308	55	61	260	4	6	268	7	8	97	85
MBHF - 77	1.7.E+05	b.d.	b.d	769	0.39	23.54	0.40	0.0525	0.0009	0.3071	0.0063	0.0425	0.0007	0.84	288	36	40	268	5	7	272	5	7	99	93
MBHF - 79	3.0.E+04	b.d.	b.d	148	0.70	24.72	1.16	0.0531	0.0026	0.2970	0.0200	0.0405	0.0019	0.70	289	90	112	256	10	13	262	14	18	98	88
MBHF - 80	9.6.E+04	b.d.	b.d	436	0.49	22.28	0.55	0.0530	0.0014	0.3312	0.0130	0.0449	0.0011	0.62	316	58	61	283	7	8	290	9	11	98	90
MBHF - 81	4.8.E+04	b.d.	b.d	116	0.71	12.73	0.23	0.0649	0.0018	0.6990	0.0200	0.0785	0.0014	0.62	730	59	60	487	8	12	535	13	17	91	67
MBHF - 82	6.5.E+04	b.d.	b.d	79	1.02	6.06	0.15	0.0737	0.0016	1.6740	0.0540	0.1649	0.0041	0.77	1003	45	46	983	24	29	994	23	28	99	98
MBHF - 83	8.9.E+04	b.d.	b.d	101	0.32	5.72	0.11	0.0726	0.0013	1.7530	0.0400	0.1747	0.0033	0.83	983	37	38	1038	18	25	1025	15	22	101	106
MBHF - 84	8.9.E+04	b.d.	b.d	224	0.59	12.58	0.24	0.0587	0.0013	0.6440	0.0160	0.0795	0.0015	0.76	529	48	50	493	9	13	503	10	14	98	93
MBHF - 85	4.3.E+04	b.d.	b.d	100	0.43	11.49	0.22	0.0595	0.0016	0.7120	0.0190	0.0870	0.0017	0.73	537	56	59	537	10	14	543	11	17	99	100
																				0			0		
OES1 - 1	2.1.E+05	b.d.	b.d	310	0.27	6.70	0.24	0.0723	0.0024	1.4910	0.0630	0.1493	0.0053	0.84	981	65	68	896	32	34	925	29	40	97	91
OES1 - 2	7.5.E+04	b.d.	b.d	117	0.58	7.75	0.13	0.0646	0.0013	1.1490	0.0260	0.1290	0.0021	0.72	732	43	44	782	12	18	776	13	17	101	107
OES1 - 3	1.8.E+05	b.d.	b.d	206	2.11	5.62	0.10	0.0766	0.0011	1.8710	0.0360	0.1778	0.0031	0.91	1099	29	30	1055	17	24	1070	13	19	99	96
OES1 - 4	4.1.E+04	b.d.	b.d	279	0.93	33.91	0.59	0.0513	0.0014	0.2089	0.0065	0.0295	0.0005	0.56	228	58	64	187	3	5	193	5	6	97	82
OES1 - 5	3.2.E+04	b.d.	b.d	240	1.19	34.54	1.31	0.0533	0.0040	0.2145	0.0190	0.0290	0.0011	0.43	305	140	170	184	7	8	197	15	17	94	60
OES1 - 6	2.5.E+05	b.d.	b.d	269	0.89	5.00	0.09	0.0792	0.0011	2.1900	0.0420	0.1999	0.0036	0.94	1165	27	29	1174	19	28	1175	14	21	100	101
OES1 - 7	8.4.E+04	b.d.	b.d	105	1.09	6.15	0.11	0.0719	0.0014	1.6180	0.0370	0.1626	0.0028	0.75	969	39	41	971	16	23	974	14	22	100	100
OES1 - 8	1.3.E+04	b.d.	b.d	96	1.29	34.35	0.72	0.0537	0.0029	0.2150	0.0110	0.0291	0.0006	0.41	270	100	122	185	4	5	196	9	12	95	68
OES1 - 9	2.3.E+05	b.d.	b.d	143	1.05	3.13	0.05	0.1143	0.0014	5.0310	0.0880	0.3198	0.0052	0.93	1863	22	24	1788	26	39	1825	15	21	98	96
OES1 - 10	6.1.E+04	b.d.	b.d	151	0.45	12.18	0.21	0.0579	0.0014	0.6580	0.0180	0.0821	0.0014	0.62	497	50	54	509	8	12	513	11	14	99	102
OES1 - 11	6.4.E+04	b.d.	b.d	134	0.40	9.78	0.20	0.0609	0.0023	0.8600	0.0220	0.1022	0.0021	0.80	596	65	82	627	13	17	627	12	18	100	105
OES1 - 12	1.8.E+04	b.d.	b.d	43	0.68	11.96	0.23	0.0633	0.0023	0.7290	0.0280	0.0836	0.0016	0.50	622	78	79	518	9	13	549	16	25	94	83
OES1 - 14	8.0.E+04	b.d.	b.d	193	0.20	11.45	0.21	0.0590	0.0014	0.7070	0.0200	0.0873	0.0016	0.65	539	50	53	540	9	13	542	11	15	99	100
OES1 - 15	1.0.E+05	b.d.	b.d	219	0.43	9.92	0.43	0.0607	0.0019	0.8450	0.0430	0.1008	0.0044	0.86	609	58	68	619	25	28	622	19	25	99	102
OES1 - 16	1.3.E+05	b.d.	b.d	175	0.05	6.11	0.18	0.0743	0.0013	1.6790	0.0550	0.1637	0.0049	0.91	1035	35	37	977	26	32	997	19	27	98	94
OES1 - 18	1.6.E+05	b.d.	b.d	179	0.27	5.52	0.09	0.0768	0.0011	1.9220	0.0370	0.1813	0.0030	0.86	1105	29	30	1074	16	25	1087	13	20	99	97
OES1 - 19	1.5.E+05	b.d.	b.d	235	0.72	7.75	0.14	0.0659	0.0026	1.1720	0.0340	0.1290	0.0023	0.61	794	62	83	782	14	19	787	15	20	99	99
OES1 - 20	2.6.E+05	b.d.	b.d	454	0.09	9.41	0.35	0.0653	0.0010	0.9510	0.0460	0.1063	0.0039	0.76	776	29	33	651	22	25	679	20	25	96	84
OES1 - 21	7.5.E+04	b.d.	b.d	154	0.99	9.84	0.18	0.0611	0.0016	0.8550	0.0220	0.1016	0.0019	0.73	613	52	57	624	11	15	625	12	17	100	102
OES1 - 22	8.8.E+03	b.d.	b.d	63	1.38	34.03	0.72	0.0547	0.0029	0.2210	0.0110	0.0294	0.0006	0.42	290	110	119	187	4	5	200	10	12	93	64
OES1 - 23	4.7.E+04	b.d.	b.d	114	0.43	11.54	0.20	0.0590	0.0014	0.7030	0.0190	0.0867	0.0015	0.64	522	52	53	536	9	13	539	11	15	99	103
OES1 - 26	6.9.E+03	b.d.	b.d	48	1.20	34.16	0.76	0.0545	0.0036	0.2190	0.0140	0.0293	0.0007	0.35	210	130	149	186	4	5	197	12	16	94	89

OES1 - 27	9.2.E+04	b.d.	b.d	238	0.64	12.72	0.21	0.0576	0.0011	0.6220	0.0140	0.0786	0.0013	0.73	494	42	43	488	8	12	491	9	11	99	99
OES1 - 28	1.2.E+05	b.d.	b.d	151	0.21	5.80	0.15	0.0722	0.0014	1.7170	0.0630	0.1723	0.0046	0.73	970	40	41	1024	25	31	1012	18	29	101	106
OES1 - 29	3.3.E+05	b.d.	b.d	570	0.13	8.41	0.13	0.0640	0.0010	1.0510	0.0210	0.1189	0.0019	0.80	731	31	34	724	11	16	728	10	15	99	99
OES1 - 30	7.2.E+04	b.d.	b.d	151	0.25	9.99	0.36	0.0607	0.0026	0.8420	0.0250	0.1001	0.0036	0.90	615	68	93	615	22	24	618	14	18	99	100
OES1 - 31	2.0.E+05	b.d.	b.d	234	0.36	5.61	0.14	0.0766	0.0013	1.8850	0.0450	0.1782	0.0043	0.90	1103	32	35	1057	24	29	1074	17	22	98	96
OES1 - 32	1.4.E+05	b.d.	b.d	170	0.23	5.82	0.09	0.0773	0.0012	1.8280	0.0370	0.1718	0.0028	0.81	1114	30	33	1022	15	23	1054	13	19	97	92
OES1 - 33	7.8.E+04	b.d.	b.d	116	0.54	7.13	0.12	0.0690	0.0027	1.3370	0.0540	0.1402	0.0023	0.41	874	65	81	845	13	20	858	22	29	99	97
OES1 - 34	3.9.E+04	b.d.	b.d	79	0.42	9.87	0.18	0.0634	0.0016	0.8870	0.0240	0.1014	0.0018	0.66	677	55	56	622	10	15	643	14	17	97	92
OES1 - 35	7.5.E+04	b.d.	b.d	91	0.27	5.84	0.10	0.0739	0.0013	1.7480	0.0390	0.1712	0.0030	0.79	1016	36	37	1018	17	24	1023	14	22	100	100
OES1 - 36	1.1.E+05	b.d.	b.d	166	0.87	7.08	0.15	0.0682	0.0013	1.3300	0.0340	0.1412	0.0029	0.80	856	40	41	852	16	22	858	15	19	99	99
OES1 - 37	2.7.E+04	b.d.	b.d	252	0.75	44.13	1.85	0.0507	0.0035	0.1578	0.0130	0.0227	0.0010	0.51	180	130	160	144	5	7	148	11	12	97	80
OES1 - 38	2.1.E+04	b.d.	b.d	51	1.57	11.67	0.30	0.0644	0.0030	0.7580	0.0420	0.0857	0.0022	0.46	660	94	99	530	13	16	566	23	32	94	80
OES1 - 39	3.0.E+04	b.d.	b.d	213	1.75	34.15	0.72	0.0535	0.0028	0.2162	0.0140	0.0293	0.0006	0.33	294	92	119	186	4	5	198	11	13	94	63
OES1 - 41	3.2.E+05	b.d.	b.d	801	0.49	11.58	0.24	0.0579	0.0008	0.6880	0.0140	0.0864	0.0018	0.90	514	29	32	534	10	14	531	9	12	101	104
OES1 - 45	3.8.E+04	b.d.	b.d	306	0.47	36.58	1.87	0.0544	0.0042	0.2037	0.0250	0.0273	0.0014	0.42	347	150	174	174	8	9	189	17	21	92	50
OES1 - 46	8.0.E+04	b.d.	b.d	211	0.27	11.82	0.28	0.0587	0.0014	0.6910	0.0150	0.0846	0.0020	0.90	539	47	53	524	12	15	532	9	13	98	97
OES1 - 48	9.2.E+04	b.d.	b.d	239	0.90	12.00	0.24	0.0709	0.0027	0.8150	0.0320	0.0833	0.0017	0.52	894	66	79	515	10	14	600	15	25	86	58
OES1 - 50	3.1.E+04	b.d.	b.d	230	1.09	33.60	1.11	0.0519	0.0033	0.2119	0.0180	0.0298	0.0010	0.39	232	130	146	189	6	7	195	14	15	97	81
OES1 - 51	1.4.E+05	b.d.	b.d	162	0.34	5.59	0.09	0.0759	0.0012	1.8690	0.0370	0.1789	0.0030	0.85	1076	32	33	1062	16	23	1068	13	20	99	99
OES1 - 52	2.3.E+05	b.d.	b.d	270	0.21	5.67	0.09	0.0755	0.0010	1.8360	0.0340	0.1764	0.0029	0.89	1079	28	29	1047	16	24	1057	12	19	99	97
OES1 - 53	6.1.E+05	b.d.	b.d	1224	0.62	9.24	0.20	0.0812	0.0009	1.2120	0.0250	0.1082	0.0023	0.90	1219	23	25	662	13	18	805	12	16	82	54
OES1 - 54	1.1.E+05	b.d.	b.d	142	0.66	5.98	0.15	0.0737	0.0018	1.7070	0.0440	0.1673	0.0041	0.95	1022	44	50	997	23	28	1010	17	21	99	98
OES1 - 55	3.3.E+05	b.d.	b.d	420	0.27	5.89	0.10	0.0763	0.0009	1.7810	0.0310	0.1697	0.0028	0.95	1096	24	26	1010	15	23	1037	12	18	97	92
OES1 - 56	6.3.E+04	b.d.	b.d	90	0.39	6.64	0.11	0.0708	0.0014	1.4650	0.0350	0.1506	0.0026	0.72	923	40	42	905	15	20	913	15	21	99	98
OES1 - 57	6.2.E+04	b.d.	b.d	137	0.77	10.24	0.18	0.0615	0.0013	0.8290	0.0210	0.0977	0.0017	0.69	619	47	48	601	10	15	610	11	17	98	97
OES1 - 58	1.5.E+05	b.d.	b.d	187	0.28	5.43	0.16	0.0770	0.0015	1.9550	0.0710	0.1840	0.0055	0.82	1115	46	47	1088	31	36	1098	31	32	99	98
OES1 - 60	1.7.E+05	b.d.	b.d	196	1.19	5.50	0.09	0.0800	0.0011	2.0060	0.0380	0.1817	0.0030	0.87	1184	27	29	1077	16	24	1115	13	20	97	91
OES1 - 63	3.6.E+04	b.d.	b.d	332	0.56	42.07	1.95	0.0511	0.0029	0.1680	0.0160	0.0238	0.0011	0.49	216	120	131	151	7	7	158	12	14	96	70
OES1 - 66	2.1.E+05	b.d.	b.d	340	0.10	7.33	0.23	0.0687	0.0022	1.3060	0.0370	0.1365	0.0043	0.90	878	55	67	824	25	29	846	18	22	97	94
OES1 - 67	1.1.E+04	b.d.	b.d	74	1.24	33.06	0.70	0.0818	0.0056	0.3460	0.0250	0.0303	0.0006	0.29	910	140	142	192	4	5	291	18	30	66	21
OES1 - 68	3.0.E+05	b.d.	b.d	184	0.68	2.90	0.05	0.1212	0.0014	5.7670	0.1000	0.3446	0.0055	0.92	1969	22	23	1908	27	40	1940	16	24	98	97
OES1 - 70	6.0.E+04	b.d.	b.d	73	0.47	5.97	0.10	0.0750	0.0016	1.7300	0.0420	0.1675	0.0029	0.71	1047	45	46	998	16	24	1019	16	20	98	95
OES1 - 71	2.2.E+05	b.d.	b.d	365	0.44	7.78	0.14	0.0679	0.0009	1.2010	0.0250	0.1286	0.0023	0.86	855	30	31	780	13	19	801	12	15	97	91
OES1 - 72	1.4.E+05	b.d.	b.d	162	0.46	5.38	0.09	0.0773	0.0012	1.9830	0.0410	0.1860	0.0031	0.81	1114	30	33	1099	17	25	1107	14	21	99	99
OES1 - 74	1.7.E+05	b.d.	b.d	196	0.37	5.43	0.16	0.0764	0.0015	1.9490	0.0590	0.1843	0.0054	0.97	1090	38	41	1090	30	35	1095	22	27	100	100
OES1add - 2	8.3.E+05	b.d.	b.d	1207	0.99	11.67	0.41	0.1299	0.0041	1.5300	0.0460	0.0857	0.0030	0.90	2097	55	56	530	18	20	942	18	22	56	25
OES1add - 3	7.0.E+04	b.d.	b.d	101	0.85	11.98	0.26	0.0631	0.0026	0.7240	0.0240	0.0835	0.0018	0.65	712	88	88	517	11	14	553	14	16	93	73
OES1add - 4	2.0.E+05	b.d.	b.d	368	0.64	16.01	0.26	0.0590	0.0011	0.5077	0.0120	0.0625	0.0010	0.68	567	41	42	391	6	9	417	8	10	94	69
OES1add - 5	6.5.E+05	b.d.	b.d	510	0.47	6.81	0.14	0.0880	0.0014	1.7800	0.0390	0.1469	0.0031	0.96	1383	31	32	884	17	23	1038	14	19	85	64
KNYE - 2	5.5.E+05	b.d.	b.d	681	0.21	10.38	0.16	0.0607	0.0009	0.8035	0.0240	0.0964	0.0015	0.52	627	32	34	593	9	13	599	13	16	99	95
KNYE - 3	7.3.E+05	b.d.	b.d	698	0.48	7.94	0.22	0.0654	0.0013	1.1320	0.0330	0.1259	0.0035	0.95	787	42	43	764	20	24	769	16	19	99	97
KNYE - 4	2.4.E+05	b.d.	b.d	131	0.25	5.18	0.08	0.0786	0.0010	2.1000	0.0460	0.1929	0.0029	0.69	1162	25	27	1137	16	24	1149	15	20	99	98
KNYE - 5	5.5.E+04	b.d.	b.d	71	0.57	11.84	0.24	0.0581	0.0019	0.6780	0.0350	0.0845	0.0017	0.39	534	72	72	523	10	14	526	21	22	99	98
KNYE - 6	1.4.E+05	b.d.	b.d	187	0.48	11.51	0.49	0.0777	0.0036	0.9430	0.0680	0.0869	0.0037	0.59	1139	92	93	537	22	24	674	35	36	80	47
KNYE - 7	4.6.E+05	b.d.	b.d	198	0.89	3.60	0.11	0.1060	0.0016	4.0410	0.1300	0.2777	0.0081	0.91	1732	28	29	1580	41	48	1642	26	30	96	91
KNYE - 9	2.7.E+05	b.d.	b.d	166	0.97	5.44	0.08	0.0766	0.0010	1.9340	0.0440	0.1839	0.0026	0.62	1110	25	27	1088	14	23	1093	15	20	100	98
KNYE - 10	2.3.E+05	b.d.	b.d	256	0.18	9.28	0.31	0.0621	0.0019	0.9210	0.0290	0.1077	0.0036	0.90	678	65	66	660	21	24	663	15	18	99	97
KNYE - 11	6.7.E+05	b.d.	b.d	411	0.38	5.40	0.10	0.0764	0.0008	1.9500	0.0450	0.1851	0.0033	0.77	1105	21	24	1095	18	26	1098	15	20	100	99
KNYE - 16	3.4.E+04	b.d.	b.d	45	0.72	11.24	0.21	0.0601	0.0028	0.7360	0.0330	0.0890	0.0017	0.43	607	101	101	550	10	14	560	19	21	98	91
KNYE - 20	4.4.E+05	b.d.	b.d	275	0.27	5.73	0.12	0.0744	0.0009	1.7940	0.0500	0.1746	0.0038	0.78	1051	24	26	1037	21	27	1043	18	22	99	99
KNYE - 25	7.3.E+04	b.d.	b.d	85	0.65	10.47	0.21	0.0612	0.0019	0.8070	0.0320	0.0955	0.0019	0.50	646	67	68	588	11	15	601	18	20	98	91
KNYE - 29	2.8.E+05	b.d.	b.d	351	0.54	11.52	0.73	0.0594	0.0010	0.7120	0.0600	0.0868	0.0055	0.75	582	35	37	537	33	34	546	35	36	98	92
KNYE - 30	9.0.E+05	b.d.	b.d	722	0.64	7.09	0.50	0.0800	0.0009	1.5560	0.1300	0.1411	0.0099	0.84	1196	23	25	851	56	57	953	50	52	89	71
KNYE - 35	8.6.E+05	b.d.	b.d	184	0.75	1.93	0.04	0.1865	0.0036	13.3000	0.4500	0.5169	0.0120	0.69	2712	32	33	2686	51	64	2701	31	36	99	99
KNYE - 36	1.9.E+05	b.d.	b.d	113	0.71	5.72	0.08	0.0746	0.0010	1.8030	0.0400	0.1748	0.0023	0.59	1058	27	29	1039	13	21	1047	14	19	99	98
KNYE - 37	2.7.E+05	b.d.	b.d	190	0.71	6.39	0.20	0.0739	0.0011	1.5950	0.0570	0.1566	0.0050	0.89	1039	30	32	938	28	32	968	22	25	97	90
KNYE - 38	2.0.E+05	b.d.	b.d	238	0.87	10.82	0.15	0.0597	0.0010	0.7610	0.0190	0.0924	0.0013	0.56	592	36	38	570	8	12	575	11	14	99	96
KNYE - 40	2.5.E+05	b.d.	b.d	260	0.24	9.38	0.16	0.0615	0.0010	0.9070	0.0220	0.1066	0.0018	0.70	658	35	37	653	10	15	655	12	15	100	99
KNYE - 43	2.3.E+05	b.d.	b.d	318	0.72	12.85	0.21	0.0624	0.0011	0.6700	0.0160	0.0778	0.0013	0.70	688	38	39	483	8	11	521	10	12	93	70
KNYE - 46	6.1.E+05	b.d.	b.d	348	0.58	5.15	0.08	0.0775	0.0008	2.0860	0.0440	0.1943	0.0029	0.71	1135	20	22	1145	16	25	1144	14	19	100	101
KNYE - 47	1.2.E+05	b.d.	b.d	139	0.41	10.21	0.18	0.0617	0.0017	0.8340	0.0260	0.0980	0.0017	0.56	664	59	60	603	10	14	616	14	17	98	91
KNYE - 48	2.7.E+05	b.d.	b.d	377	0.31	11.57	0.25	0.0598	0.0015	0.7120	0.0200	0.0865	0.0019	0.78	595	54	56	535	11	15	546	12	14	98	90
KNYE - 49	2.4.E+05	b.d.	b.d	150	0.31	5.41	0.09	0.0817	0.0014	2.0850	0.0540	0.1850	0.0030	0.63	1238	34	35	1094	16	24	1144	18	22	96	88
KNYE - 50	9.4.E+05	b.d.	b.d	593	0.27	5.49	0.10	0.0768	0.0008	1.9310	0.0430	0.1821	0.0032	0.79	1116	20	22	1078	17	25	1092	15	19	99	97
KNYE - 52	1.5.E+05	b.d.	b.d	181	0.18	10.01	0.22	0.0610	0.0018	0.8420	0.0240	0.0999	0.0022	0.77	639	63	64	614	13	17	620	13	16	99	96
KNYE - 53	8.4.E+04	b.d.	b.d	118	0.80	11.66	0.26	0.0633	0.0022	0.7470	0.0250	0.0858	0.0019	0.66	718	74	75	531	11	15	566	14	17	94	74
KNYE - 54	5.5.E+05	b.d.	b.d	300	0.46	5.03	0.07	0.0784	0.0008	2.1560	0.0440	0.1988	0.0026	0.64	1157	20	23	1169	14	24	1167	14	19	100	101
KNYE - 55	7.1.E+04	b.d.	b.d	58	1.83	6.91	0.25	0.0727	0.0028	1.4450	0.0460	0.1447	0.0053	0.90	1006	78	79	871	30	33	908	19	22	96	87
KNYE - 56	7.3.E+05	b.d.	b.d	246	0.48	3.01	0.10	0.1131	0.0031	5.1910	0.1800	0.3321	0.0110	0.96	1849	50	50	1849	53	60	1851	29	33	100	100
KNYE - 57	3.9.E+05	b.d.	b.d	224	0.31	4.95	0.09	0.0790	0.0010	2.2040	0.0530	0.2021	0.0036	0.74	1172	25	27	1187	19	27	1182	17	21	100	101
KNYE - 58	4.6.E+05	b.d.	b.d	317	0.31	5.85	0.14	0.0736	0.0013	1.7360	0.0480	0.1710	0.0042	0.89	1030	36	37	1018	23	29	1022	18	21	100	99
KNYE - 63	1.6.E+05	b.d.	b.d	184	1.47	10.18	0.18	0.0610	0.0014	0.8300	0.0230	0.0982	0.0017	0.62	639	49	51	604	10	14	614	13	15	98	94
KNYE - 65	3.7.E+05	b.d.	b.d	374	1.18	9.53	0.13	0.0610	0.0007	0.8857	0.0190	0.1049	0.0014	0.62	641	25	27	643	8	14	644	10	14	100	100
KNYE - 66	1.3.E+05	b.d.	b.d	79	0.67	5.66	0.08	0.0755	0.0013	1.8420	0.0460	0.1766	0.0025	0.57	1082	35	36	1048	14	22	1061	16	20	99	97
KNYE - 68	2.0.E+05	b.d.	b.d	184	0.36	8.04	0.21	0.0649	0.0012	1.1160	0.0360	0.1244	0.0032	0.80	771	39	40	756	18	22	761	17	20	99	98
KNYE - 69	3.5.E+05	b.d.	b.d	266	0.29	6.34	0.17	0.0720	0.0011	1.5680	0.0550	0.1578	0.0043	0.78	986	31	33	945	24	29	958	22	24	99	96
KNYE - 70	5.3.E+05	b.d.	b.d	368	0.21	5.78	0.20	0.0738	0.0014	1.7570	0.0750	0.1729	0.0061	0.83	1035	38	40	1028	33	38	1030	27	30	100	99

Uncertainties quoted without components related to systematic error unless otherwise stated. Total systematic uncertainties (s sys): $^{206}Pb/^{238}U$ = 1.8 %; $^{207}Pb/^{206}Pb$ = 0.5 % (2s).

[a] Data not corrected for common Pb

[b] Concordance calculated as: (^{206}Pb-^{238}U date/^{207}Pb-^{235U} date)*100 and (^{206}Pb-^{238}U date/^{207}Pb-^{206}Pb date)*100

Appendix F. LA-ICPMS detrital zircon isotopic data from samples in the Uitenhage Group plotted as concordia diagrams

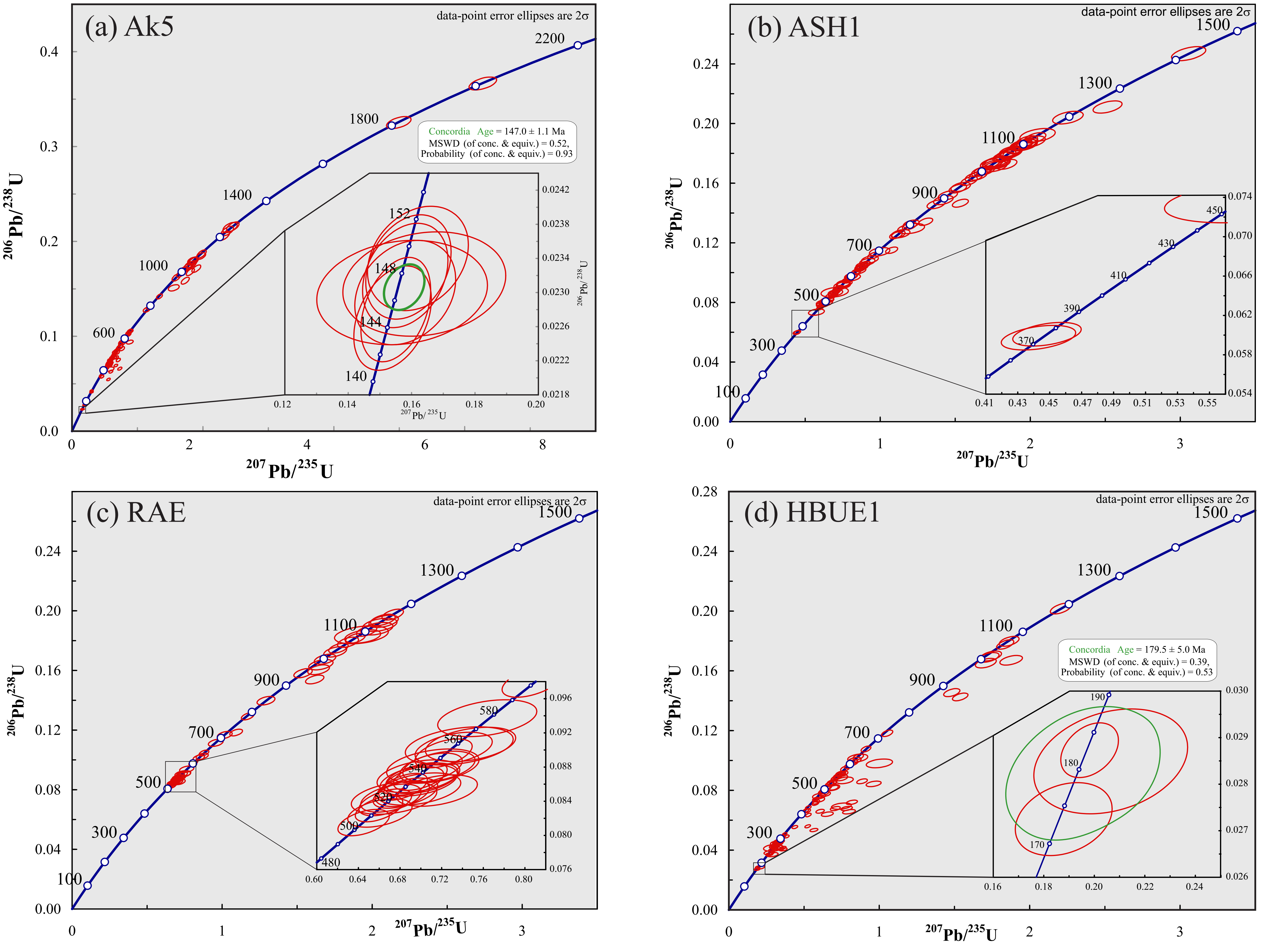

Fig. F1. Isotopic data for all detrital deposits in the Robertson and Heidelberg Basins plotted as concordia diagrams. a) Sample Ak5 from the Robertson Basin, a concordia age of 147.0 ± 1.1 Ma (95 % confidence) is calculated for the youngest age component, which is comprised of concordant and equivalent dates (Ludwig, 2000). b) Sample ASH1 from the Robertson Basin. c) RAE from the Robertson Basin. d) Sample HBUE1 from the Heidelberg Basin, a concordia age of 179 ± 5.0 Ma (95 % confidence) is calculated for the youngest age component, which is comprised of concordant and equivalent dates (Ludwig, 2000) Dates older than 1500 are omitted.

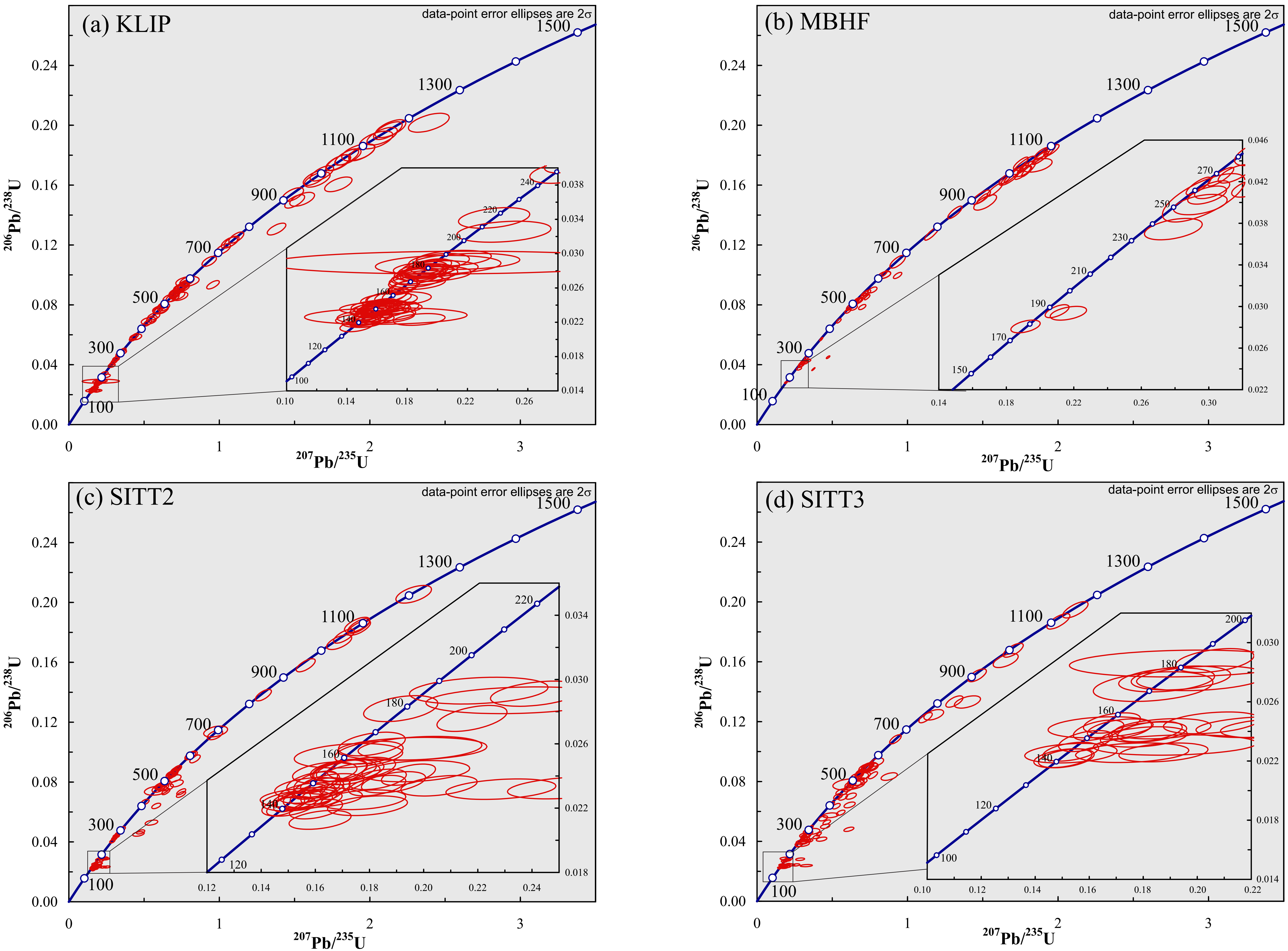

Fig. F2. Isotopic data from detrital zircon samples in the Mossel Bayt Basin plotted as concordia diagrams. a) Resedimented volcaniclastic sample KLIP; b) Siliciclastic sample MBHF; c) Resedimented volcaniclastic sample SITT2; d) Resedimented volcaniclastic sample SITT3. Dates older than 1500 are omitted.

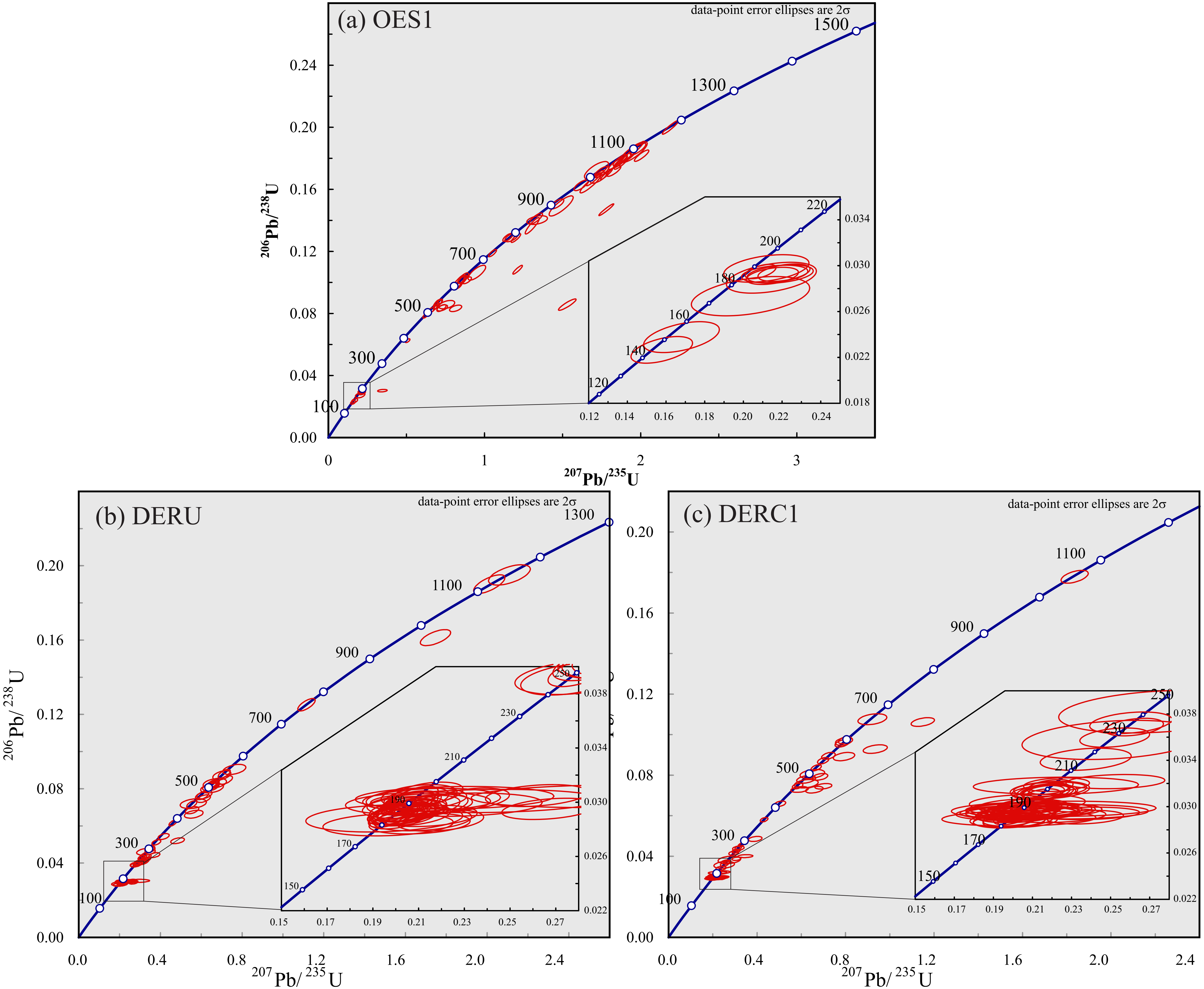

Fig. F3. Isotopic data for all detrital deposits in the Oudtshoorn Basin plotted as concordia diagrams. a) Siliciclastic sample OES1. b) Resedimented volcaniclastic sample DERU. c) Residemented volcaniclastic sample DERC1. Dates older than 1500 are omitted.

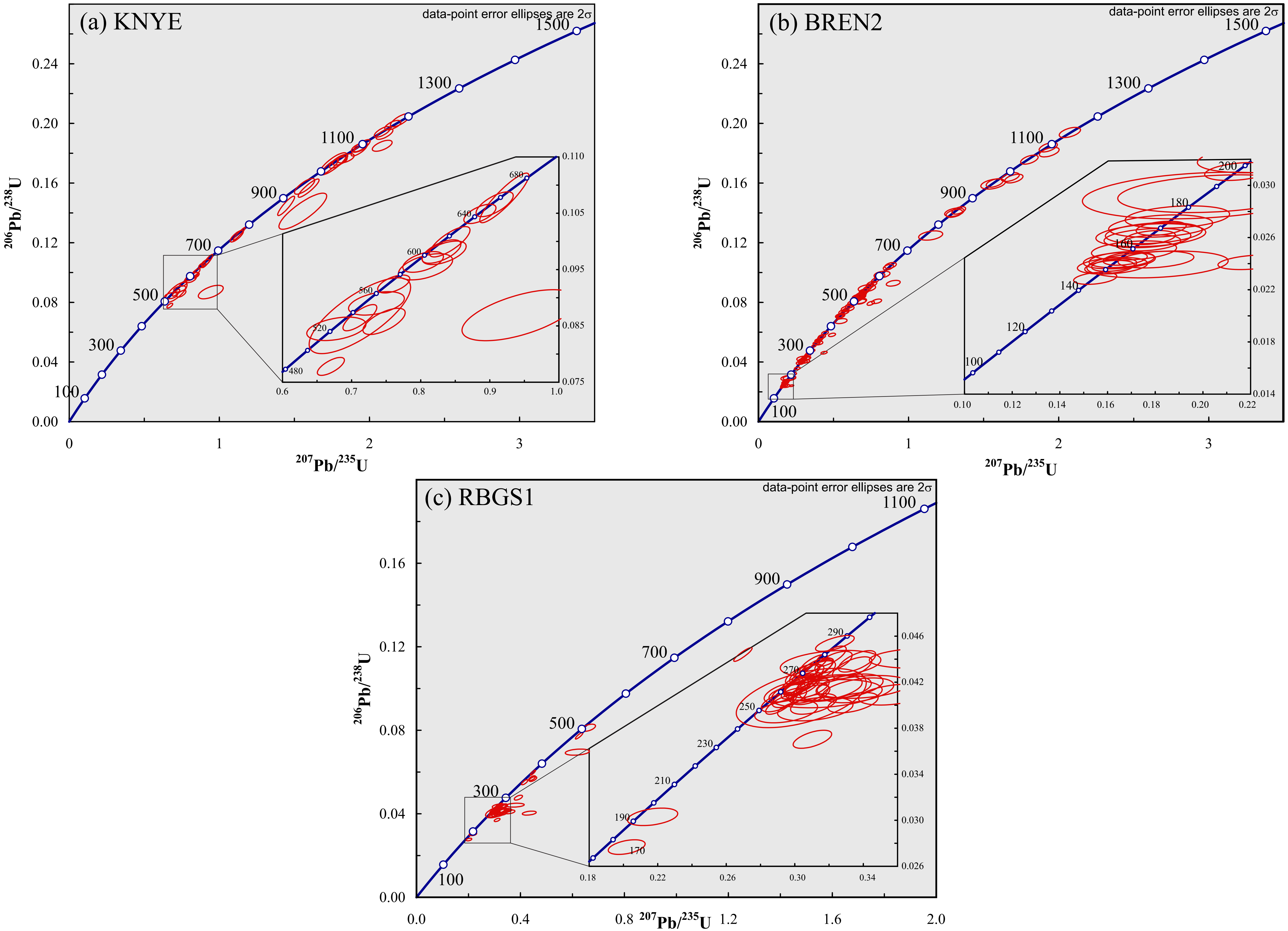

Fig. F4. Isotopic data from detrital samples in the Knysna and Plettenberg Bay Basins plotted as concordia diagrams. a) Siliciclastic sample KNYE from the Knysna Basin; b) Siliciclastic sample BREN2 from the Knysna Basin; c) Siliciclastic sample RBGS1 from the Plettenberg Bay Basin. Dates older than 1500 are omitted.

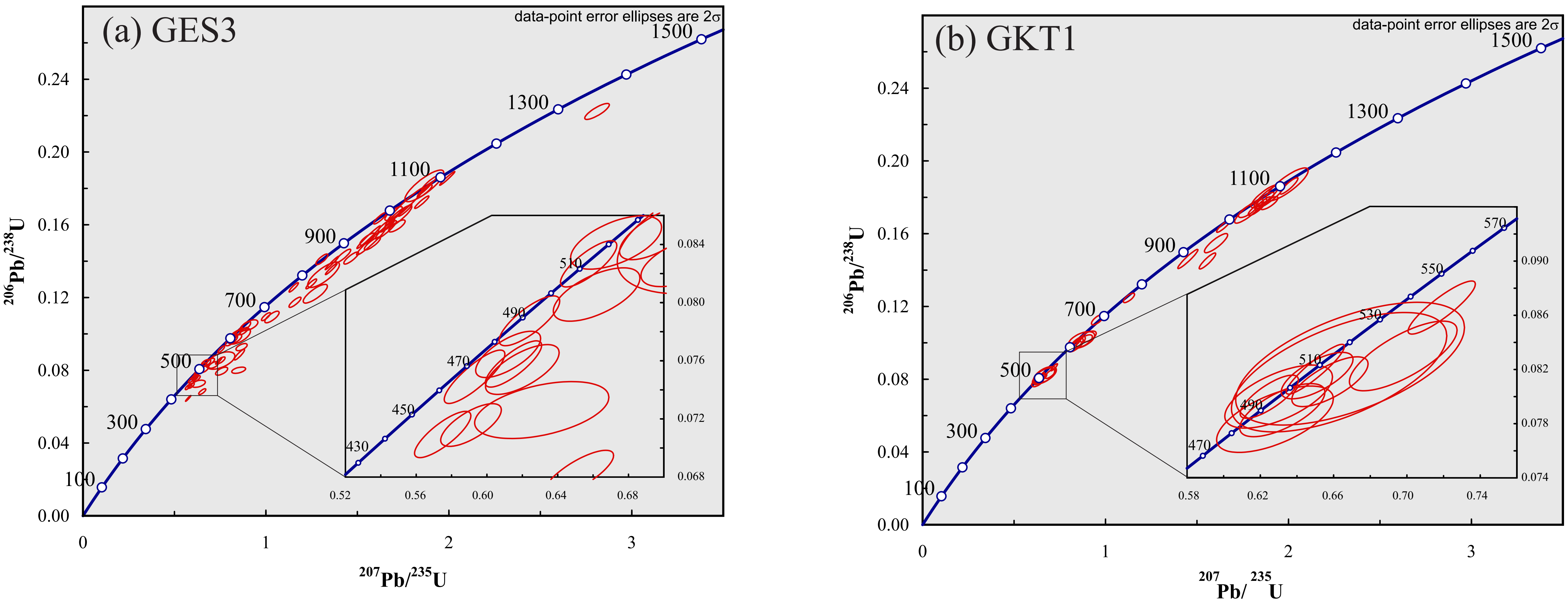

Fig. F5. Isotopic data from detrital samples in the Gamtoos Basin plotted as concordia diagrams. a) Siliciclastic sample GKT1; b) Siliciclastic sample GES3. Dates older than 1500 are omitted.

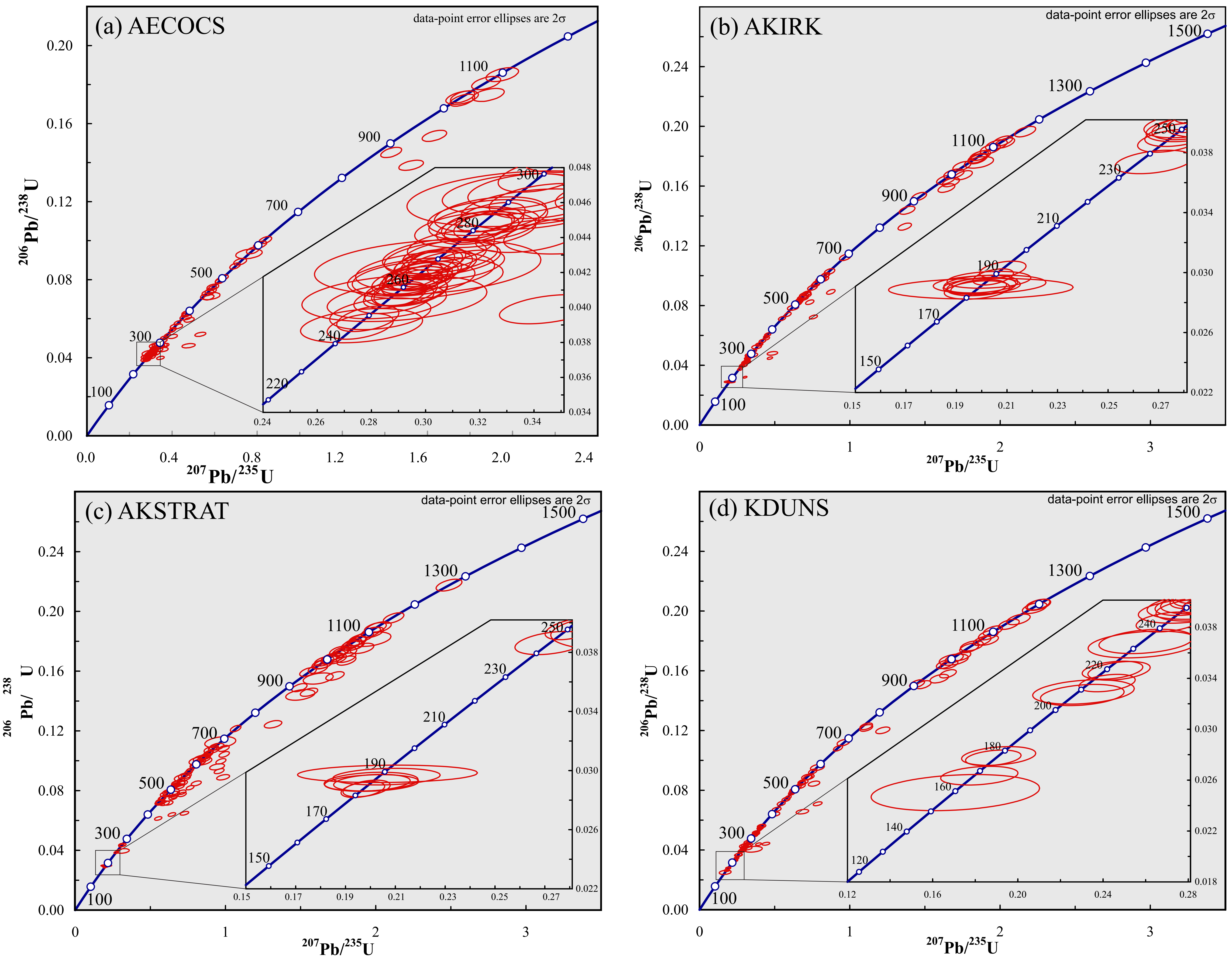

Figure continues on following page

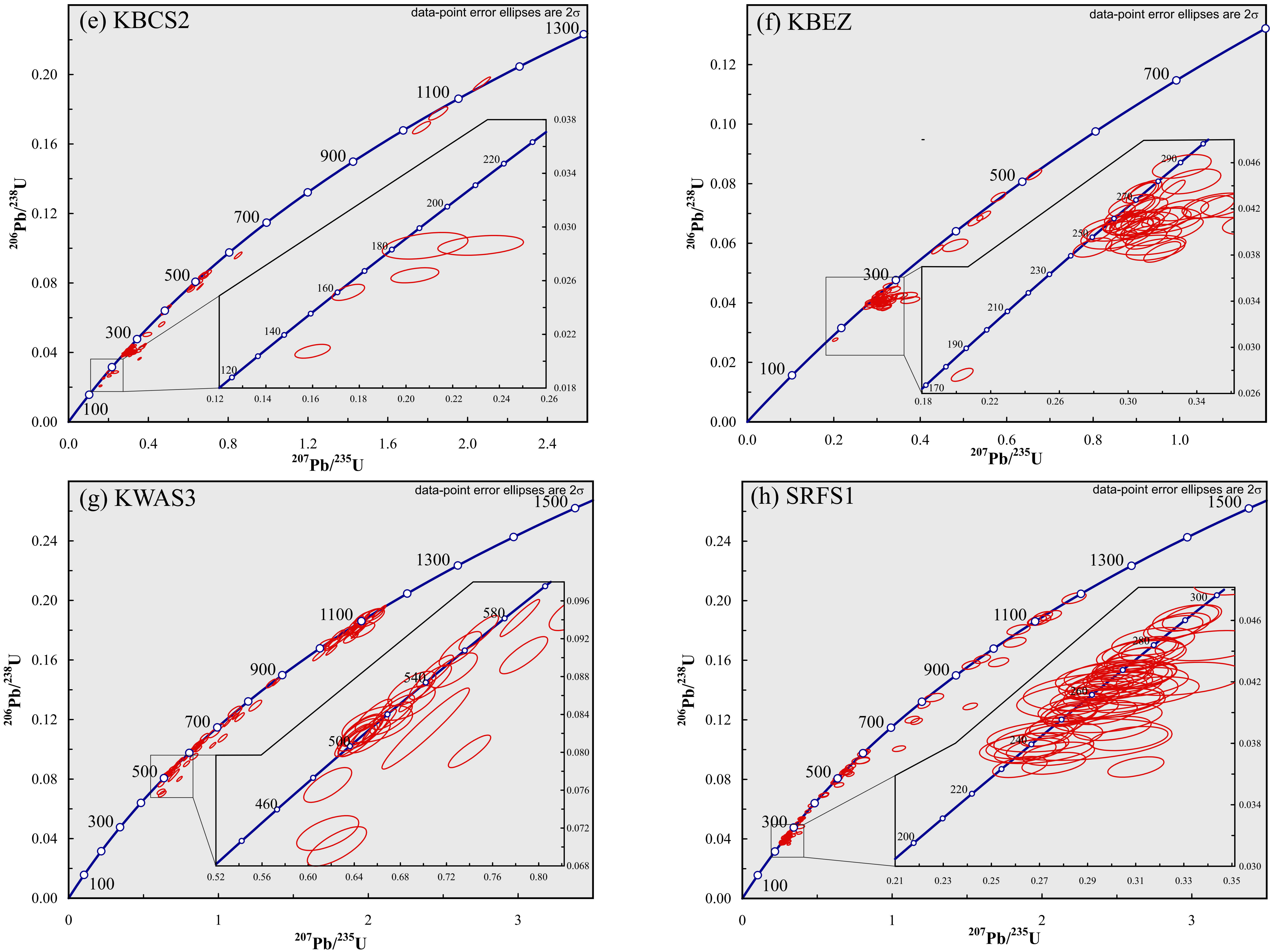

Fig. F6. Isotopic data of detrital samples from the Algoa Basin plotted as concordia diagrams. a) Silciclastic sample AECOCS; b) Silciclastic sample AKIRK; c) Silciclastic sample AKSTR; d) Siliciclastic sample KDUNS; e) Silciclastic sample KBCS2; f) Silciclastic sample KBEZS1; g) Silciclastic sample KWAS3; Silciclastic sample SRFS1. Dates older than 1500 are omitted.

Appendix G. CA-TIMS isotopic data

Table G1. Zircon isotopic data for four samples that were analysed by CA-TIMS at the Berkeley Geochronology Center

Sample	diseq.corr. $^{206}Pb^*/^{238}U$		$^{207}Pb^*/^{235}U$		diseq.corr. $^{207}Pb^*/^{206}Pb^*$		cm.Pb (pg)	Th/U	$^{207}Pb/^{235}U$	2σ %er	diseq.corr. $^{206}Pb/^{238}U$	2s %er	ρ	diseq.corr. $^{206}Pb/^{204}Pb$	corr. $^{206}Pb/^{204}Pb$	corr. $^{207}Pb/^{204}Pb$	corr. $^{208}Pb/^{204}Pb$	diseq.corr. $^{238}U/^{206}Pb$	2σ %er	diseq.corr. $^{207}Pb/^{206}Pb$	2σ %er	tot.diseq.corr. $^{238}U/^{206}Pb$	2σ %er	tot.diseq.corr. $^{207}Pb/^{206}Pb$	2σ %er	diseq.corr. $^{204}Pb/^{206}Pb$	2σ %er	tot.diseq.corr. $^{238}U/^{206}Pb$	2σ %er
CALI.Z03	153.84	0.24	153.8	0.76	153	±10.3	0.7	0.92	0.1635	0.49	0.024152	0.16	.46	1549	1548	90.8	485.0	41.40	0.16	0.04911	0.44	40.91	0.20	0.05862	0.09	0.00065	1.9	40.91	0.20
CALI.Z06	153.67	0.42	155.2	4.14	178	±59.9	0.8	0.90	0.1651	2.67	0.024124	0.28	.41	230	230	26.1	98.2	41.45	0.28	0.04964	2.57	38.13	0.22	0.11372	0.60	0.00435	0.6	38.13	0.22
CALI.Z05	153.98	0.48	155.3	5.26	176	±75.9	0.7	0.79	0.1653	3.39	0.024174	0.31	.46	189	189	24.1	80.8	41.37	0.31	0.04959	3.26	37.34	0.18	0.12748	0.60	0.00529	0.8	37.34	0.18
CALI.Z12	153.64	0.57	149.0	3.90	77	±59.2	1.0	0.58	0.1581	2.62	0.024119	0.37	.40	260	260	27.1	82.3	41.46	0.37	0.04754	2.49	38.53	0.41	0.10427	0.33	0.00384	1.3	38.53	0.41
CALI.Z02	153.56	0.71	154.1	5.86	162	±83.9	0.6	0.79	0.1639	3.80	0.024107	0.46	.51	280	280	28.5	103.0	41.48	0.46	0.04930	3.59	38.75	0.50	0.10194	0.53	0.00357	3.4	38.75	0.50
~~CALI.Z10~~	~~155.92~~	~~0.96~~	~~154.7~~	~~8.16~~	~~136~~	~~±117.6~~	~~1.2~~	~~0.93~~	~~0.1646~~	~~5.28~~	~~0.024483~~	~~0.62~~	~~.49~~	~~157~~	~~157~~	~~22.4~~	~~78.7~~	~~40.85~~	~~0.62~~	~~0.04875~~	~~5.00~~	~~36.04~~	~~0.61~~	~~0.14287~~	~~0.23~~	~~0.00639~~	~~2.1~~	~~36.04~~	~~0.61~~
CALI.Z09	152.75	1.34	149.1	16.40	92	±246.8	0.6	0.76	0.1582	10.99	0.023979	0.88	.67	118	118	20.4	61.8	41.70	0.88	0.04785	10.42	35.20	0.68	0.17289	0.51	0.00847	3.8	35.20	0.68
CALI.Z04	153.27	2.84	153.2	44.34	151	±642.6	1.6	0.82	0.1628	28.95	0.024061	1.85	.83	83	83	18.8	54.9	41.56	1.85	0.04907	27.43	32.38	0.95	0.22591	1.71	0.01200	7.1	32.38	0.95
CALI.Z11	152.08	3.03	165.4	22.77	360	±292.9	0.7	0.79	0.1769	13.77	0.023872	2.00	.45	73	73	18.6	51.7	41.89	2.00	0.05374	12.98	31.34	2.20	0.25403	0.84	0.01367	2.4	31.34	2.20
~~CALI.Z08~~	~~141.27~~	~~3.06~~	~~-7.2~~	~~-46.08~~	~~#NUM!~~	~~#NUM!~~	~~2.8~~	~~0.30~~	~~-0.0071~~	~~638.62~~	~~0.022156~~	~~2.16~~	~~-.71~~	~~134~~	~~134~~	~~15.4~~	~~49.1~~	~~45.13~~	~~2.16~~	~~-0.00232~~	~~640.16~~	~~38.94~~	~~1.79~~	~~0.11453~~	~~4.01~~	~~0.00745~~	~~13.3~~	~~38.94~~	~~1.79~~
CALI.Z07	151.55	3.18	124.9	35.23	-357	±699.0	2.1	0.73	0.1309	28.21	0.023787	2.10	.58	232	232	24.2	87.4	42.04	2.10	0.03990	27.04	38.70	2.21	0.10415	5.79	0.00431	18.2	38.70	2.21
CALI.Z01	153.74	5.45	154.5	6.80	167	±58.4	0.8	0.95	0.1644	4.40	0.024136	3.55	.82	311	311	30.1	125.8	41.43	3.55	0.04939	2.50	38.98	4.61	0.09675	0.70	0.00322	2.1	38.98	4.61
CALI.Z13	153.42	1.47	153.9	18.43	160	±267.3	0.8	0.69	0.1636	11.98	0.024085	0.96	.60	80	80	18.7	51.5	41.52	0.96	0.04926	11.43	32.02	0.49	0.23229	0.70	0.01242	2.1	32.02	0.49
CALI.Z13	151.09	0.68	140.4	5.65	-36	±93.2	1.3	0.80	0.1483	4.02	0.023714	0.45	.44	222	222	24.9	89.3	42.17	0.45	0.04537	3.84	38.67	0.47	0.11199	0.70	0.00450	2.1	38.67	0.47
CALI.Z13	306.20	19.35	35.4	281.22	#NUM!	#NUM!	63.4	0.70	0.0355	793.78	0.048646	6.32	.63	27	27	15.7	40.0	20.56	6.32	0.00529	789.79	6.60	0.47	0.57851	0.70	0.03689	2.1	6.60	0.47
CALI.Z13	153.46	2.31	167.3	30.07	367	±385.0	0.9	0.63	0.1791	17.98	0.024091	1.51	.62	56	56	17.7	45.6	41.51	1.51	0.05390	17.09	27.90	0.51	0.31466	0.70	0.01780	2.1	27.90	0.51
CALI.Z13	157.15	2.42	209.2	31.05	845	±289.8	4.4	0.87	0.2288	14.84	0.024677	1.54	.62	55	55	18.1	48.1	40.52	1.54	0.06724	13.93	26.98	0.47	0.32861	0.70	0.01815	2.1	26.98	0.47
HBMB.83	171.87	2.85	172.8	18.92	186	±241.5	1.5	0.85	0.1855	10.95	0.027020	1.66	.41	93	93	19.4	58.0	37.01	1.66	0.04980	10.37	29.68	1.91	0.20814	1.00	0.01076	2.3	29.68	1.91
HBMB.92	171.84	1.01	175.6	8.98	226	±112.8	1.3	0.52	0.1888	5.11	0.027015	0.59	.45	139	139	21.7	57.7	37.02	0.59	0.05068	4.88	32.10	0.54	0.15679	0.59	0.00722	1.3	32.10	0.54
HBMB.01	171.78	0.99	162.2	9.58	25	±134.0	1.5	0.79	0.1733	5.91	0.027005	0.57	.59	236	236	25.8	92.4	37.03	0.57	0.04653	5.59	34.14	0.58	0.10908	0.31	0.00423	4.5	34.14	0.58
HBMB.82	171.75	1.02	176.8	11.38	244	±142.5	1.3	0.72	0.1902	6.44	0.027000	0.59	.46	105	105	20.1	57.9	37.04	0.59	0.05107	6.19	30.54	0.29	0.19104	0.69	0.00952	0.8	30.54	0.29
HBMB.74	171.06	0.79	172.0	7.74	184	±100.5	2.1	0.74	0.1845	4.50	0.026891	0.46	.44	136	136	21.5	65.5	37.19	0.46	0.04977	4.32	32.14	0.30	0.15835	0.37	0.00738	0.5	32.14	0.30
HBMB.47	170.78	1.35	174.0	15.32	218	±196.4	1.8	0.71	0.1869	8.81	0.026846	0.79	.44	83	83	18.9	52.4	37.25	0.79	0.05049	8.48	28.94	0.38	0.22865	0.78	0.01211	0.7	28.94	0.38
HBMB.108	170.74	0.79	172.4	5.55	195	±71.3	1.9	0.70	0.1850	3.22	0.026839	0.46	.39	181	181	23.8	73.8	37.26	0.46	0.04999	3.07	33.47	0.47	0.13136	0.16	0.00553	0.6	33.47	0.47
HBMB.53	170.57	1.70	170.8	19.43	173	±255.1	0.9	1.06	0.1832	11.38	0.026813	1.00	.48	68	68	18.1	54.8	37.30	1.00	0.04954	10.93	27.27	0.36	0.26459	0.60	0.01460	0.8	27.27	0.36
HBMB.64	170.40	1.16	171.1	13.20	181	±173.5	1.5	1.38	0.1835	7.71	0.026785	0.68	.43	95	95	19.4	71.4	37.33	0.68	0.04969	7.45	30.08	0.37	0.20503	0.88	0.01055	0.7	30.08	0.37
HBMB.48	170.14	1.40	173.5	15.39	219	±196.7	2.2	0.57	0.1863	8.87	0.026744	0.82	.48	77	77	18.6	48.6	37.39	0.82	0.05052	8.50	28.43	0.22	0.24195	0.27	0.01302	0.6	28.43	0.22
HBMB.85	169.79	1.14	174.7	11.23	241	±141.8	1.8	0.66	0.1877	6.43	0.026689	0.67	.45	101	101	19.9	55.3	37.47	0.67	0.05101	6.15	30.67	0.45	0.19588	0.40	0.00986	0.8	30.67	0.45
HBMB.07	169.63	0.59	169.2	6.99	162	±91.7	1.4	0.73	0.1813	4.13	0.026662	0.35	.64	237	237	26.4	88.3	37.51	0.35	0.04931	3.92	34.59	0.25	0.11149	0.47	0.00422	3.0	34.59	0.25
HBMB.82	169.45	2.21	162.1	17.80	56	±248.0	1.0	0.67	0.1731	10.98	0.026634	1.30	.49	146	146	21.6	65.2	37.55	1.30	0.04712	10.40	32.81	1.47	0.14832	1.28	0.00685	4.8	32.81	1.47
HBMB.80	169.06	0.75	169.9	4.12	182	±52.7	1.5	0.72	0.1822	2.42	0.026572	0.44	.45	510	510	40.1	149.2	37.63	0.44	0.04972	2.26	36.28	0.54	0.07857	0.42	0.00196	4.3	36.28	0.54
HBMB.99	149.87	0.82	145.7	5.91	78	±91.8	1.2	0.65	0.1543	4.06	0.023520	0.55	.41	177	177	23.2	70.7	42.52	0.55	0.04757	3.86	38.09	0.58	0.13106	0.43	0.00566	1.3	38.09	0.58
LETT.Z112	151.32	40.23	134.8	445.22	-163	±7896.9	23.8	1.03	0.1419	330.34	0.023752	26.60	.48	20	20	15.7	38.6	42.10	26.60	0.04309	318.50	3.66	1.26	0.77906	0.08	0.04958	0.2	3.66	1.26
PLETT.Z22	137.50	7.96	161.0	88.60	519	±1149.0	16.7	0.83	0.1718	55.03	0.021558	5.80	.50	27	27	16.1	40.2	46.39	5.80	0.05773	52.39	14.26	0.43	0.60587	0.10	0.03761	0.6	14.26	0.43
PLETT.Z38	138.34	5.83	143.9	64.53	234	±991.1	12.8	0.67	0.1522	44.85	0.021692	4.21	.48	30	30	16.2	40.4	46.10	4.21	0.05085	42.97	17.43	0.58	0.54735	0.16	0.03377	0.4	17.43	0.58
PLETT.Z98	144.40	7.84	153.4	87.12	291	±1241.0	10.3	0.83	0.1630	56.81	0.022652	5.43	.49	27	27	16.1	40.3	44.15	5.43	0.05213	54.37	14.12	0.28	0.59428	0.15	0.03694	0.5	14.12	0.28
PLETT.Z58	145.96	10.81	105.2	161.37	-746	±4185.4	6.7	0.70	0.1092	153.33	0.022901	7.41	.54	26	26	15.9	39.6	43.67	7.41	0.03453	149.44	12.29	1.09	0.61983	1.35	0.03901	1.8	12.29	1.09
PLETT.Z39	142.63	3.04	144.0	33.51	166	±521.5	4.2	0.60	0.1524	23.27	0.022372	2.13	.48	40	40	16.7	42.2	44.70	2.13	0.04937	22.33	24.32	0.22	0.41394	0.11	0.02475	0.3	24.32	0.22
~~PLETT.Z15~~	~~170.92~~	~~1.95~~	~~177.1~~	~~13.81~~	~~261~~	~~±169.5~~	~~0.9~~	~~0.81~~	~~0.1906~~	~~7.80~~	~~0.026869~~	~~1.14~~	~~.43~~	~~185~~	~~185~~	~~24.2~~	~~80.6~~	~~37.22~~	~~1.14~~	~~0.05144~~	~~7.38~~	~~33.51~~	~~1.35~~	~~0.13087~~	~~1.86~~	~~0.00541~~	~~4.4~~	~~33.51~~	~~1.35~~
PLETT.Z02	141.41	1.59	158.9	22.45	428	±298.2	0.9	0.68	0.1694	14.12	0.022179	1.13	.69	79	79	19.0	51.1	45.09	1.13	0.05539	13.38	34.64	0.53	0.23933	1.07	0.01258	3.1	34.64	0.53
PLETT.Z73	140.85	1.63	151.0	24.34	313	±345.4	1.5	0.59	0.1604	16.12	0.022090	1.16	.82	90	90	19.4	51.4	45.27	1.16	0.05264	15.19	36.04	0.45	0.21508	0.55	0.01107	4.6	36.04	0.45
PLETT.Z97	140.68	1.60	144.8	26.07	213	±402.6	1.8	0.56	0.1533	18.00	0.022063	1.14	.57	77	77	18.6	48.5	45.32	1.14	0.05038	17.38	34.51	0.56	0.24089	2.18	0.01295	2.9	34.51	0.56
~~PLETT.Z19~~	~~140.68~~	~~0.57~~	~~149.3~~	~~6.03~~	~~289~~	~~±88.4~~	~~0.6~~	~~0.59~~	~~0.1584~~	~~4.04~~	~~0.022062~~	~~0.40~~	~~.46~~	~~148~~	~~148~~	~~22.4~~	~~62.1~~	~~45.33~~	~~0.40~~	~~0.05207~~	~~3.87~~	~~39.68~~	~~0.23~~	~~0.15140~~	~~0.45~~	~~0.00677~~	~~0.7~~	~~39.68~~	~~0.23~~
PLETT.Z36	140.34	0.67	144.8	7.22	218	±110.0	1.8	0.67	0.1533	4.99	0.022008	0.48	.52	138	138	21.7	63.2	45.44	0.48	0.05050	4.75	39.38	0.29	0.15704	0.29	0.00724	1.4	39.38	0.29
LETT.Z111	140.31	3.16	147.0	37.17	255	±554.9	1.5	0.76	0.1558	25.29	0.022005	2.26	.54	40	40	16.8	43.3	45.44	2.26	0.05131	24.14	24.69	0.34	0.41575	0.23	0.02480	1.1	24.69	0.34
PLETT.Z61	140.24	1.19	141.6	13.16	165	±208.2	1.2	0.64	0.1497	9.29	0.021993	0.85	.48	75	75	18.4	49.5	45.47	0.85	0.04935	8.91	34.32	0.24	0.24554	0.21	0.01332	0.6	34.32	0.24
PLETT.Z28	140.09	1.34	143.1	14.84	193	±231.1	1.5	0.65	0.1513	10.37	0.021969	0.95	.48	69	69	18.2	48.5	45.52	0.95	0.04995	9.94	33.38	0.27	0.26300	0.28	0.01448	0.6	33.38	0.27
PLETT.Z54	139.81	1.95	138.2	23.48	110	±383.5	3.2	0.77	0.1458	16.99	0.021926	1.40	.56	58	58	17.5	47.7	45.61	1.40	0.04822	16.25	31.06	0.63	0.30373	0.55	0.01732	1.6	31.06	0.63
PLETT.Z24	139.67	0.63	138.4	7.39	117	±123.0	0.8	0.64	0.1460	5.34	0.021903	0.45	.30	170	170	23.0	68.9	45.66	0.45	0.04835	5.22	40.71	0.42	0.13517	1.77	0.00589	0.9	40.71	0.42
PLETT.Z07	138.48	0.74	137.2	6.56	116	±107.7	1.0	0.66	0.1447	4.78	0.021714	0.54	.44	139	139	21.5	63.2	46.05	0.54	0.04834	4.57	39.94	0.46	0.15467	0.19	0.00721	1.0	39.94	0.46
ROBE.Z89	170.37	14.99	236.9	179.55	959	±1476.5	66.4	0.95	0.2628	75.78	0.026780	8.80	.45	24	24	16.0	39.6	37.34	8.80	0.07105	72.30	8.44	0.35	0.67348	0.91	0.04204	0.6	8.44	0.35
ROBE.Z22	156.01	13.69	168.5	151.58	343	±1943.3	49.4	0.90	0.1805	89.96	0.024496	8.78	.50	24	24	15.9	39.6	40.82	8.78	0.05334	85.95	9.24	0.57	0.66909	0.07	0.04201	0.6	9.24	0.57
ROBE.Z84	152.04	3.27	173.8	12.42	481	±146.3	0.4	0.66	0.1867	7.15	0.023866	2.15	.39	741	741	56.6	189.5	41.90	2.15	0.05672	6.62	40.86	2.77	0.07641	5.20	0.00135	15.5	40.86	2.77
ROBE.Z50	150.71	0.86	154.6	9.34	214	±133.8	1.0	0.67	0.1644	6.04	0.023654	0.57	.50	115	115	20.5	58.4	42.28	0.57	0.05041	5.78	35.50	0.34	0.17835	0.40	0.00870	1.2	35.50	0.34
ROBE.Z85	150.32	0.55	151.6	3.01	172	±43.6	0.8	0.87	0.1611	1.99	0.023592	0.37	.41	384	384	33.8	138.9	42.39	0.37	0.04951	1.87	40.36	0.44	0.08784	0.33	0.00260	2.0	40.36	0.44
ROBE.Z44	150.32	0.41	151.9	4.16	176	±61.5	1.7	0.87	0.1614	2.74	0.023592	0.27	.42	223	223	25.8	94.5	42.39	0.27	0.04960	2.64	38.88	0.20	0.11571	0.57	0.00449	0.6	38.88	0.20
ROBE.Z42	150.28	0.37	151.8	3.10	176	±45.6	1.4	0.45	0.1613	2.04	0.023586	0.25	.42	281	281	28.7	75.1	42.40	0.25	0.04959	1.95	39.62	0.22	0.10194	0.23	0.00355	0.7	39.62	0.22
ROBE.Z2	149.57	1.19	153.7	8.70	218	±125.0	0.8	0.71	0.1635	5.66	0.023474	0.80	.39	114	114	20.5	59.6	42.60	0.80	0.05051	5.40	35.74	0.81	0.17912	0.48	0.00874	0.7	35.74	0.81
ROBE.Z70	141.82	1.26	152.8	14.05	326	±199.3	0.9	0.54	0.1624	9.20	0.022244	0.89	.50	73	73	18.5	47.3	44.96	0.89	0.05294	8.79	33.63	0.25	0.25354	0.20	0.01368	0.7	33.63	0.25

Appendix H. Isotopic data aquired by TIMS

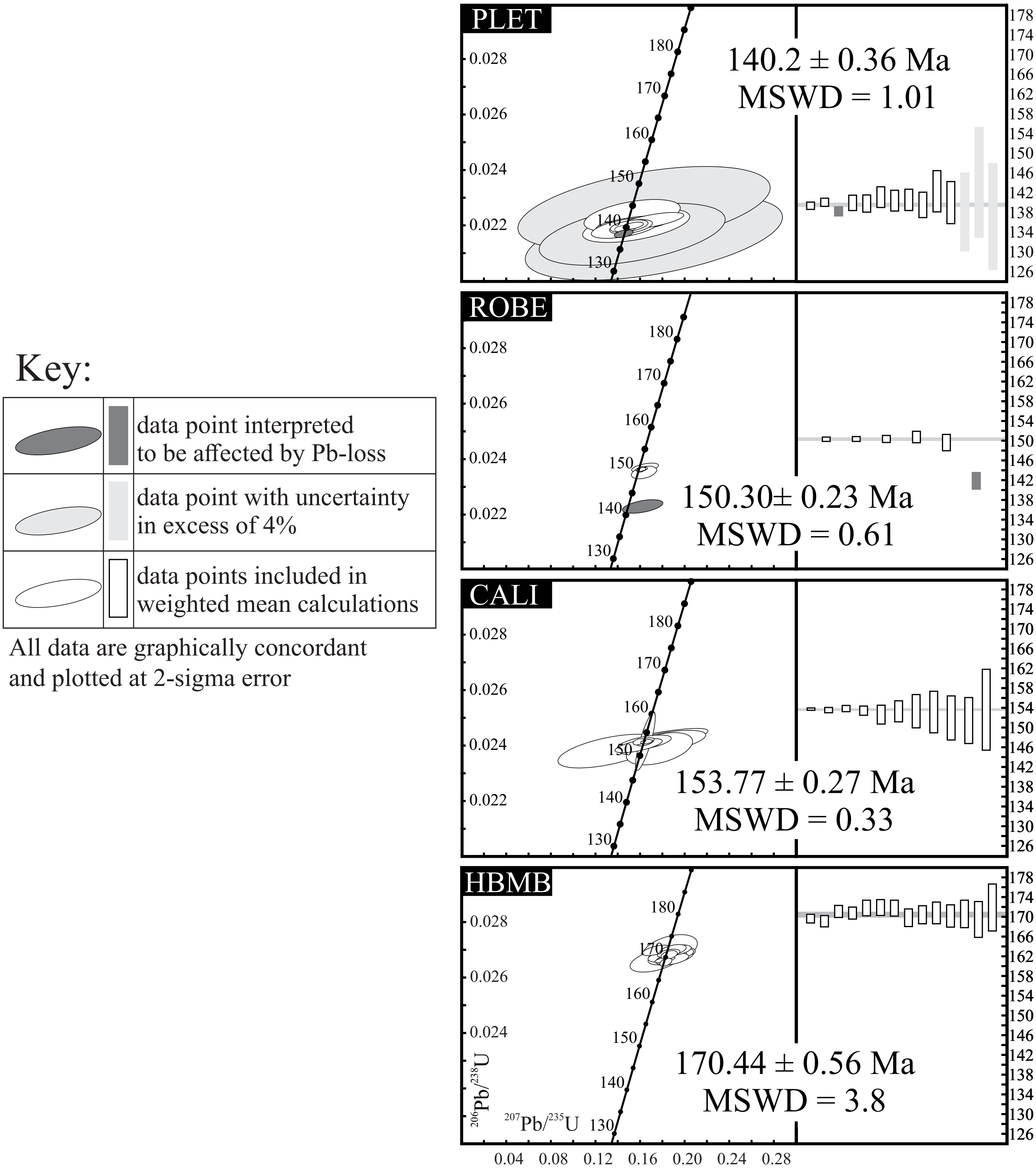

Fig. H1. All concordant isotopic data aquired by TIMS analysis of selected zircons from four pyroclastic deposits. Concordia diagrams (left) and correspongind $^{206}Pb/^{238}U$ dates ranked by uncertainties (right).

Lithostratigraphy of the Enon Formation (Uitenhage Group), South Africa

R.A. Muir
Department of Geological Sciences, University of Cape Town, Private Bag X3,
Rondebosch 7701, South Africa
e-mail: mrxrob009@myuct.ac.za

E.M. Bordy
Department of Geological Sciences, University of Cape Town, Private Bag X3,
Rondebosch 7701, South Africa
e-mail: emese.bordy@uct.ac.za

J.S.V. Reddering
Council for Geoscience, P.O. Box 5347, Walmer 6065, South Africa
(Deceased)

J.H.A. Viljoen
Council for Geoscience, P.O. Box 572, Bellville 7535, South Africa
e-mail: jviljoen@geocience.org.za

Abstract

The Uitenhage Group represents the earliest deposits that filled Mesozoic rift basins in the southern Cape of South Africa during the fragmentation of the supercontinent Gondwana. The sedimentology of the Enon Formation records the development of alluvial systems that drained the region since the onset of Gondwanan rifting, and therefore plays an important role in our understanding of early landscape evolution along the southern African continental margin. The mostly coarse conglomeratic unit was deposited continuously in actively subsiding, but separated, rift basins. As a result, the deposits are diachronous between basins and display highly varied thicknesses of up to well over 2000 m.

Introduction

The Jurassic – Cretaceous Enon Formation exists in several onshore and offshore Mesozoic rift basins that formed during the breakup of Gondwana (Lock et al., 1975; Dingle et al., 1983; Fouché et al., 1992) in the Western and Eastern Cape Provinces of South Africa. This description addresses only the onshore exposures of the Enon, which is the basal unit of the Uitenhage Group. It is very well exposed in road, river and railway cuttings in the Algoa Basin, but also displays discontinuous outcrops along the Worcester-Pletmos and Oudtshoorn-Gamtoos basin lines, and in the isolated Haasvlakte, Jubilee and Soutpansvlakte Basins near Bredasdorp (Figure 1). The unit is significant because it provides a record of landscape evolution during the breakup of Gondwana that has aided development of basin models used in hydrocarbon exploration in the offshore regions of the southern African continental margin.

Atherstone (1857) first used the name 'conglomerate of Enon' to describe the coarse clastic deposits in the vicinity of Enon, a village in the Sundays River Valley (Algoa Basin), roughly 60 km north of Port Elizabeth. It remains the type locality for the Formation (Figure 1), albeit for historic reasons only, because

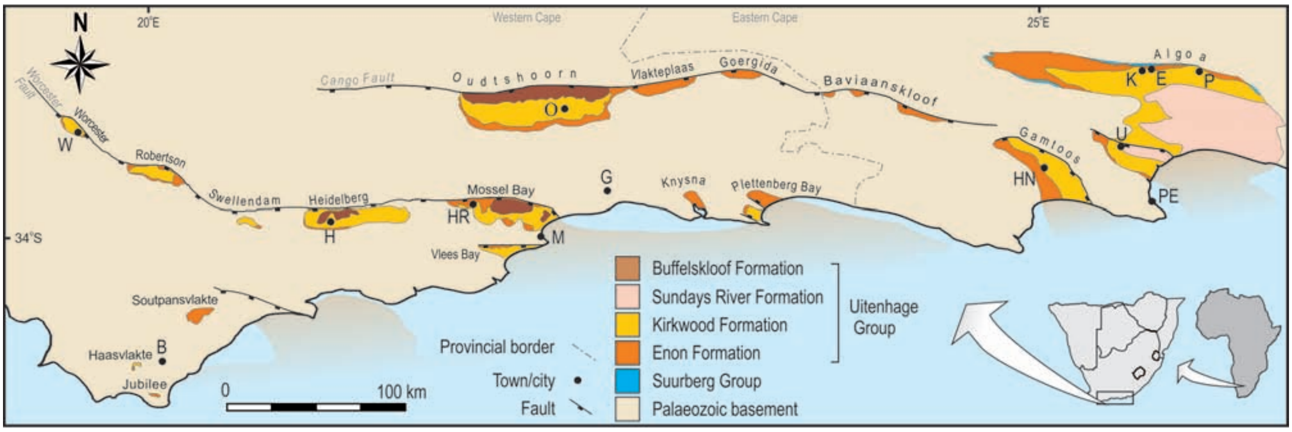

Figure 1. *Mesozoic rift basins of the Eastern and Western Cape provinces of South Africa and the major units of the onshore Uitenhage Group. The offshore extension of the Uitenhage Group is only shown schematically. The Worcester-Pletmos basin line comprises the Worcester, Robertson, Swellendam, Heidelberg, Mossel Bay, Knysna and Plettenberg Bay Basins, whereas the Gamtoos-Oudtshoorn Basin line contains the Oudtshoorn, Vlakteplaas, Georginda, Baviaanskloof and Gamtoos Basins. These exceptionally long, parallel fault arrays exploit pre-existing weaknesses in the Cape Fold Belt (Fouché et al., 1992; Paton, 2006). The Jurassic Suurberg Group is shown in the Algoa Basin, but the contentious Suurberg Fault, supposedly bounding the Algoa Basin to the north, is not included (Toerien, 1991). The exact extent of the Robberg, Hartenbos and Brenton Formations, which are also constituents of the Uitenhage Group, cannot be shown at this scale. Abbreviations: E = Enon; B = Bredasdorp; BT = Bethelsdorp; C = Colchester; G = George; H = Heidelberg; HN = Hankey; HR = Herbertsdale; K = Kirkwood; M = Mossel Bay; O = Oudtshoorn; P = Paterson; PE = Port Elizabeth; U = Uitenhage; W = Worcester.*

good exposures are found in all the other basins. Later workers similarly referred to the deposits as 'Enon Beds', 'Enon Conglomerate' and 'Enon Stage' (Rogers, 1905; Haughton, 1928; Engelbrecht et al., 1962; Joubert and Johnson, 1998). Truswell (1967), in a paper promoting the modern lithostratigraphic classification now in use by SACS, recommended the term 'Enon Conglomerate Formation'. Use of the lithological adjective in lithostratigraphic names was, however, cumbersome and soon fell into general disuse, with Winter (1973, 1979) being the first to use the shortened name 'Enon Formation'. Although most workers studying the Enon have done so in the Algoa Basin, where it was first described and is widely distributed, clear lithological correlatives in the other Mesozoic rift basins in the southern Cape are given the same name (SACS, 1980). We support this pragmatic trend based on the shared similarity of lithological traits, stratigraphic position, genesis and the likelihood that the deposits were once laterally connected.

Stratigraphic position and age

The Enon Formation is both the oldest and most proximal formation occupying the Mesozoic rift basins of South Africa (Figure 1). In the northern Algoa Basin, it overlies volcanic and volcaniclastic deposits of the Suurberg Group dated at 162 ± 7 Ma (K-Ar) by McLachlan and McMillan (1976) and 194 ± 11.9 Ma using the latest Ar-Ar dating methods (Kirstein, 1997; Marsh, 2016). The magnitude of the time gap that separates them from the Enon, however, remains unresolved. If the hiatus is negligible, as Hill (1972) suggests, the Enon could be Early Jurassic in age, but if the time gap is large (as suggested by Rogers et al., 1929), the deposits may be much younger. It is also thought that deposition of the Enon Formation was diachronous between basins, occurring at different stages from the Jurassic until the Early Cretaceous (Winter, 1973; McLachlan and McMillan, 1976). Dingle et al. (1983) support the contemporaneity of deposition of the Enon and Kirkwood Formations, the latter of which has been constrained to Tithonian – Valanginian in the Algoa Basin and by inference suggests a Cretaceous age for at least parts of the Enon Formation in that area. The Kirkwood Formation hosts datable volcaniclastic layers which may provide the best means to infer the age range of the Enon, but preliminary U-Pb analysis of zircon from these layers have yielded ages ranging from Middle Jurassic to Early Cretaceous (Muir and Brody, 2016).

Geological description

Basic unifying features

The Enon Formation primarily comprises thickly bedded, poorly sorted, pebble to cobble conglomerate with sub- and well-rounded clasts, together with subordinate sandstone and mudstone. Beds are commonly structureless internally, with local clast imbrication. The Enon Formation was derived from the erosion of the Cape Fold Belt thus is often characterized by clasts that contrast strongly with the immediate Palaeozoic basement rocks. The latter are most commonly from the Cape Supergroup but in places include the Karoo Supergroup, Cape Granite Suite (Maalgaten Granite) or Suurberg Group. It is separated from underlying strata by an unconformity almost everywhere, except when underlain by the Suurberg Group, with which it may locally be conformable. The mudstone-and-sandstone-dominated Kirkwood Formation generally conformably overlies, but locally interfingers with the Enon.

Thickness

The highly variable thickness of the Enon Formation in the various basins renders it impractical to provide an average thickness. A maximum measured thickness of 480 m is in evidence at the type locality in the Algoa Basin (Dingle, et al., 1983), whereas thinner packages crop out in most other onshore basins (Rigassi and Dixon, 1972). Theron et al. (1991) reported 3000 m of conglomerates in the Oudtshoorn Basin, but this estimate most probably includes the informally named, younger Buffelskloof Formation. In the Gamtoos Basin, boreholes have intersected very thick (>2000 m) accumulations, with a further 7 km of undrilled section below (McMillan et al., 1997), much of which is postulated to be Enon Formation. In contrast, several boreholes drilled in the Algoa Basin intercepted less than 200 m of the Enon Formation and in places the unit was entirely absent (Winter 1973). A borehole drilled in the Robertson Basin intersected 31 m of Enon Formation, but drilling ceased before basement was reached and this figure therefore represents a minimum thickness. The Enon Formation thus appears to have an extremely varied thickness and is likely to be much thicker in proximal regions of rift basins and thinner in distal regions. Outcrops suggest extensive erosion and are therefore unlikely to represent indications of true original thickness. In addition, accurate thickness determination is complicated by numerous intra-basinal normal faults (Tankard et al., 1982).

Lithology

Conglomerate (75-100%)

Immature to mature, thickly- to very thickly-bedded conglomerates (Figures 2A, B and C) dominate the Enon

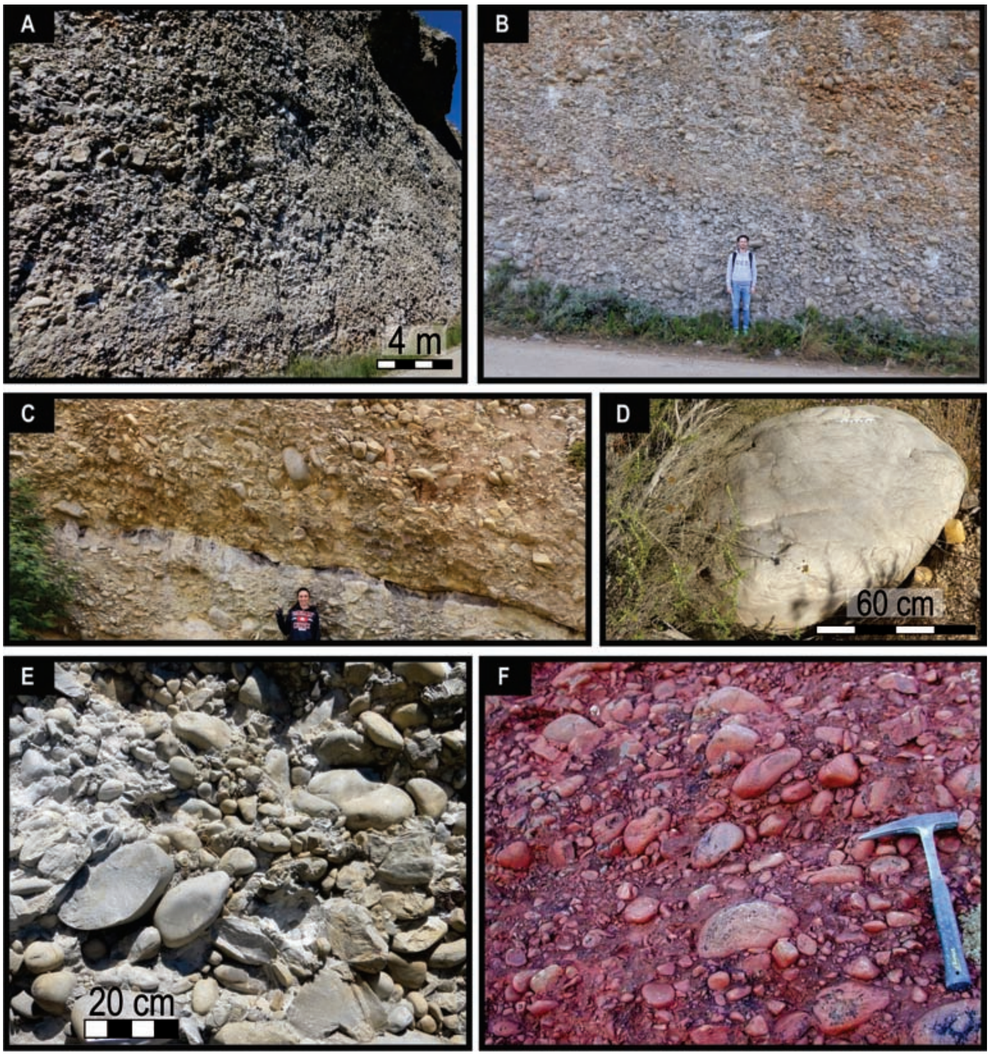

Figure 2. *(**A**) Very thickly bedded monomictic orthoconglomerate at Andrieskraal, Gamtoos Basin. (**B**) Crudely bedded conglomerates with bedding vaguely defined by vertical clast size variation, clast alignments (orange staining is a secondary feature) at Andrieskraal, Gamtoos Basin. (**C**) Upward fining, poorly sorted conglomerate bed overlain by massive conglomerate bed with an erosive base and abundant imbrication, Mossel Bay Basin. (**D**) This large quartzite boulder from the Enon Formation in the Gamtoos Basin was derived from the Table Mountain Group and exhibits chatter-marks. (**E**) Imbricated, white quartzite clasts (no secondary staining), in the Enon Formation, Gamtoos Basin. (**F**) Heavily stained, imbricated quartzite clasts giving an overall red appearance to the conglomerates near Enon, Algoa Basin (Photo courtesy of Dr. Billy de Klerk).*

Formation with isolated, interbedded, commonly white but also yellow, red or green fine- to medium-grained sandstone lenses and very rare mudstone units. Conglomerates are moderately to poorly sorted and commonly white (Figures 2A and E) but also exhibit an orange-red surface hue (Winter, 1973, Figure 2B and F). Clasts consist of quartzite, sheared quartzite, shale, and rarely of slate or granite, derived from the Cape and Karoo Supergroups, Cape Granite Suite and Suurberg Group. Clast diameter falls predominantly in the pebble size range but reach 1 m in places (Figure 2D) while matrix varies from pebbly sand to sandy mud. All the clasts are derived from the Cape Fold Belt and the quartzite clasts are typically rounded and spherical (Shone, 1976) whereas clasts of shale and slate are angular with low sphericity (Figures 3A and 3B).Rounded granitic boulders are present in the Mossel Bay and Robertson Basins (Figure 3C). Imbrication is generally well-developed and indicates a palaeocurrent direction from the south and southwest in the northern Algoa Basin (Shone, 1976). Although highly varied, a general northward imbrication orientation is discerned in the southern Oudtshoorn Basin (Du Preez, 1944) and is generally southeastward in the Gamtoos (van der Linde, 2017) and Worcester (Richardson et al., 2017) Basins.

Sandstone (0-20%)
Isolated interbedded, commonly white but also yellow, red or pale green, fine- to medium-grained sandstone lenses are common (Figures 4A to F). Larger lenses frequently exhibit cross-bedding or horizontal lamination (Figures 4B and C), rarely preserve soft sediment deformation (Figure 4E), are occasionally pebbly and display granule to pebble size lag linings.

Mudstone (0-5%)
Isolated lenses of white, yellow, red or pale green massive or horizontally laminated siltstones and mudstones are rare and weather preferentially.

Palaeontology

Abraded bone fragments, silicified fossil wood and charcoalified wood fragments are present (Figure 4G), but poorly preserved (McLachlan and McMillan, 1976; Shone 1976). Unfortunately no diagnostic age or positive identification can be made from these fossils (McLachlan and McMillan, 1976).

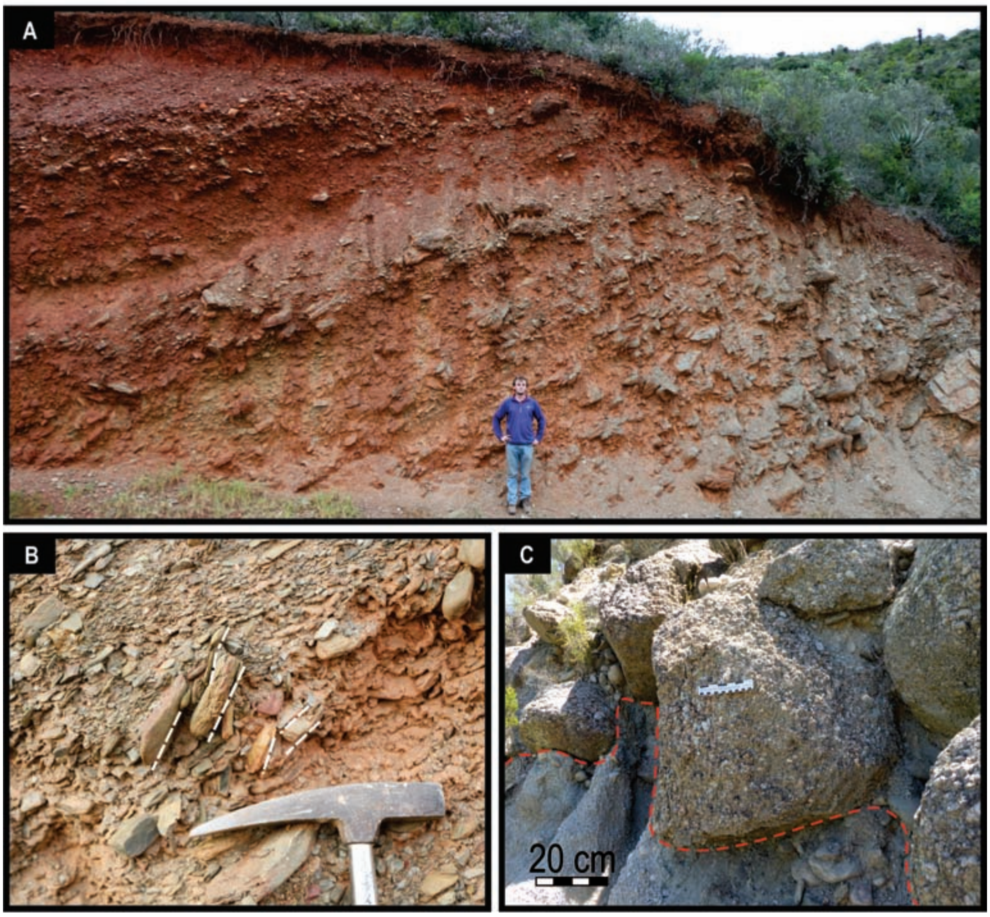

Figure 3. ***(A)*** *Upward fining package of bedded Enon Formation with predominantly shale clasts from the Bokkeveld Group near Herbertsdale, Mossel Bay Basin.* ***(B)*** *Imbricated disk-shaped shale pebbles and cobbles from the Mossel Bay Basin.* ***(C)*** *Large boulder conglomerate, Mossel Bay Basin. Red dashed line indicates an erosive contact.*

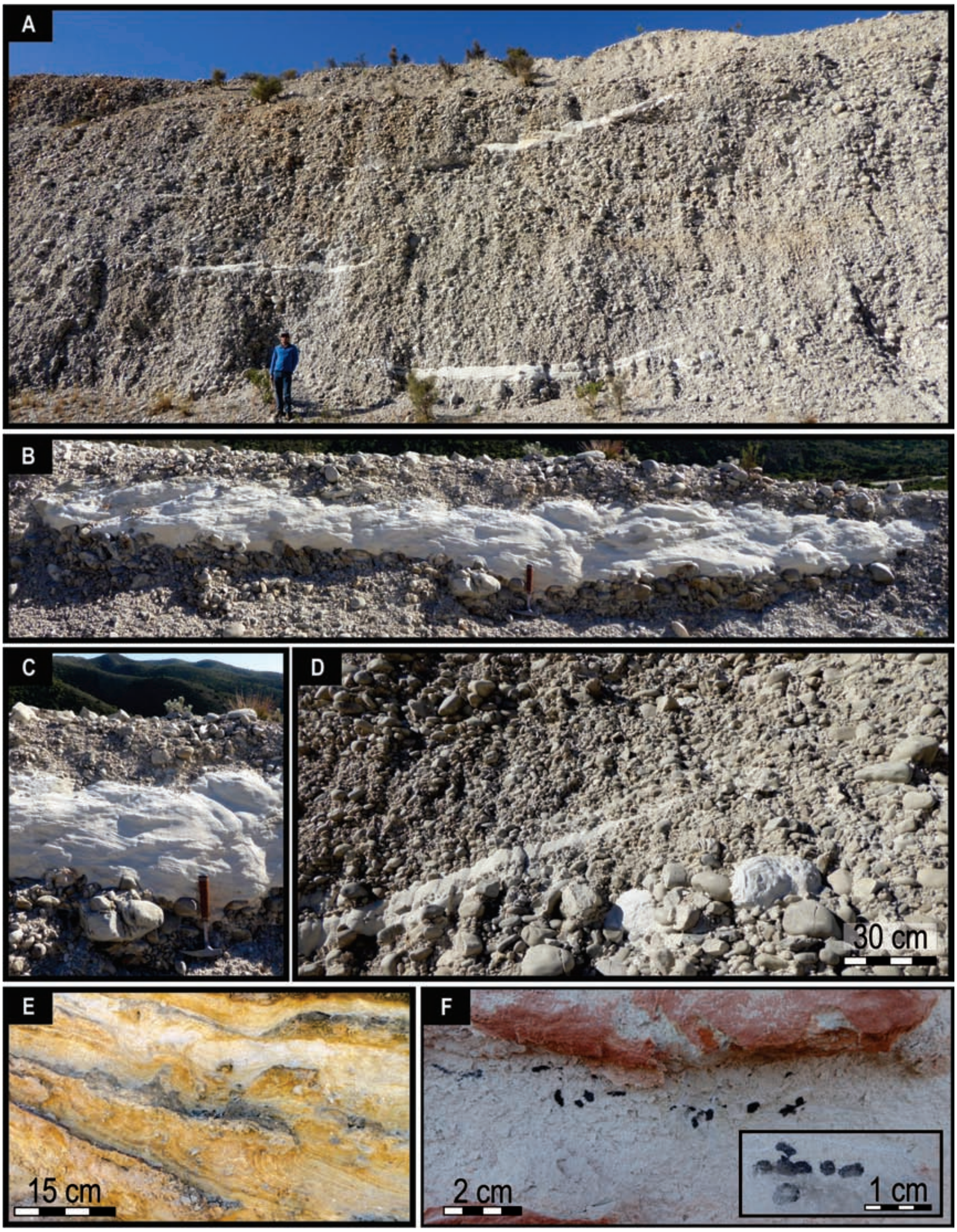

Figure 4. *(**A**) Crudely bedded conglomerates with subordinate white sandstone lenses. (**B**) Sandstone lens with trough cross-bedding. (**C**) Close-up image of the trough cross-bedding shown in B. (**D**) Rare, sub-rounded rip-up sandstone boulders in conglomerate. (**E**) Soft sediment deformation structures (water escape feature) in sandstone lenses in the Enon Formation. (**F**) Angular and rounded charcoal clasts in sandstones of the Enon Formation. All images are from the Gamtoos Basin.*

Genesis

Sedimentary characteristics (coarse clast sizes, massive beds, etc.) suggest that the Enon Formation was deposited by high-energy alluvial and debris flow processes. The steep gradient necessary for these energetic continental sediment transport processes were likely maintained by extensional faulting along rift basin margins. Fluvial deposition, likely by braided rivers on braid plains, alluvial fan depositional environments and scree deposits on an immature, rugged landscape are proposed for the Enon Formation (Shone, 1976; Holzforster, 2007; van der Linde, 2017).

Boundaries

Lower boundary

As the earliest Mesozoic basin-fill, the Enon Formation rests unconformably on, and is easily distinguished from, the basement Cape Supergroup or locally the Cape Granite Suite, Karoo Supergroup and Suurberg Group (Mossel Bay, Worcester/Nuy and northern Algoa Basins, respectively). The nature of the boundary with the underlying Suurberg Group remains uncertain. Hill (1972) considered it to be conformable, while others suspected a hiatus of several millions of years (e.g. Rogers et al., 1929). Unfortunately there are no known outcrops that can unequivocally confirm the stratigraphic relationship between the units. Dating of the Enon itself is hampered by the scarcity of radiometrically datable material and absence of well-preserved, age diagnostic fossils.

Upper boundary

Extreme denudation of the onland rift basin deposits restricts observation of the character of the boundary between the generally resistant Enon and the overlying softer Kirkwood Formation, but where possible, the contact is usually gradational. Where the Kirkwood is absent, e.g. in parts of the Mossel Bay, Heidelberg and Oudtshoorn Basins (Lock et al., 1975; Lock, 1978; Viljoen and Malan, 1993), the Enon is unconformably overlain by the Buffelskloof Formation.

Lateral boundary

The Enon Formation, being diachronous, locally displays a laterally gradational, interfingering, contact with the Kirkwood Formation. Where this is the case, the boundary is regarded as the point where conglomerates, which are dominant in the Enon Formation, give way to sand- and mudstone dominated lithologies typical of the Kirkwood Formation. It is also possible that the Kirkwood Formation onlaps the Enon Formation in places, a configuration that is conformable but difficult to test due to limited laterally extensive outcrops.

Subdivision

Although Hill (1972) introduced a local and informal 'Basal Enon Sandstone' in the Algoa Basin, no official subdivision exists for the Enon Formation. Following Du Preez, (1944), Lock et al. (1975) argued for the subdivision of conglomerates in the Oudtshoorn Basin and refer to the 'Lower'- and 'Upper Enon Beds' following the observation that the conglomerates in the northern parts of the basin seemingly occupy a stratigraphically higher interval than those in the south. This overlying unit of conglomerate was subsequently named the Buffelskloof Formation (Theron et al., 1991; Viljoen and Malan, 1993).

An obvious difference in colour from red/orange in some regions to white in others occurs commonly, leading some authors to use this as a subdivision. However, this variation can be attributed to processes of secondary alteration and is therefore not regarded as significant (Du Preez, 1944).

Regional aspects

Geographic distribution

The Enon Formation has a scattered distribution, but is present in all of the Mesozoic rift basins in the Western Cape and Eastern Cape Provinces (Figure 1), mainly near their margins and locally in the interior parts of the basin fill packages. Borehole data from both onshore and offshore areas confirm a scattered distribution (Shone, 1976; Dingle et al., 1983; Malan and Theron, 1987; Malan and Viljoen, 1990; Shone, 2006; Malan and Viljoen, 2016).

Criteria for lateral extension

Immature conglomerate-dominated Mesozoic lithologies with a variety of clasts, most commonly but not limited to a Cape Supergroup origin, are used to extend the unit from its type locality. In conjunction with its stratigraphic position, this lateral extension places the Enon Formation in a position unconformably overlying the Cape Supergroup and older units. The Enon Formation is conformably overlain by and interfingers with the Kirkwood Formation. Where the latter is absent, it is unconformably overlain by the Buffelskloof Formation.

Correlation

Although the Enon Formation was first formally described from the Algoa Basin, identical lithologies exist in all the Mesozoic rift basins of the Western Cape and Eastern Cape Provinces and are here included in the classification. Coarse conglomerate-dominated units in each basin are considered part of the Enon Formation with the exception of the informal Buffelskloof Formation (Mossel Bay, Heidelberg and Oudtshoorn Basins) and Robberg Formations (Cape Infanta, St. Blaize and Robberg), which have similar but not identical lithological character and distinctly different stratigraphic relations (Reddering, 2003). These latter units are both mappable and easily observed in the field.

Stratotypes

No official stratotype exists for the Enon Formation, possibly due to the homogenous nature of the unit, but the natural cliff faces at the type locality near Enon village in the Algoa Basin (Figure 1) are regarded as a representative section with which similar lithologies in other basins can be compared. The outcrops at the type locality are best viewed from a distance and this is also the case with most Enon Formation cliff faces, which exhibit thickly to very thickly bedded, massive, conglomerate-dominated lithologies without significant vertical or lateral variations. An easily accessible site in a roadside quarry south-west of Hankey in the Gamtoos Basin was selected to represent the general characteristics of the Enon in most areas. The schematic log derived from the quarry exposures is represented here as the Unit Stratotype (Figure 5), the location of which is shown in Figure 6.

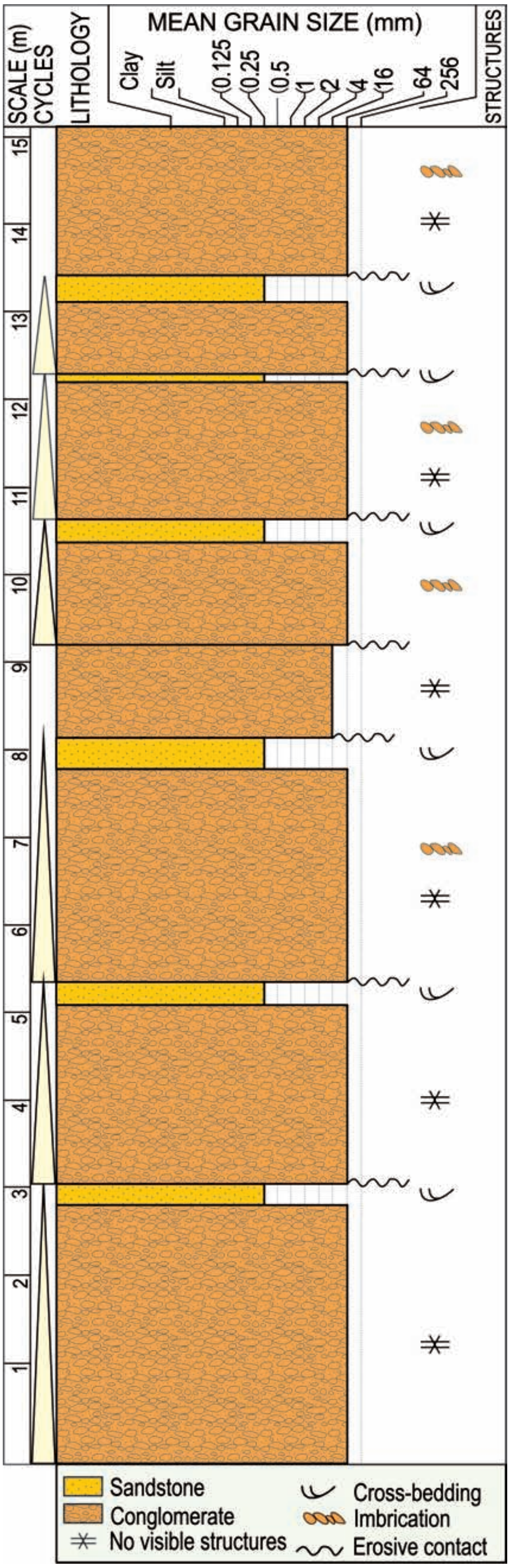

Figure 5. *Schematic stratotype representation of part of the Enon Formation based on adjacent outcrops in a roadside quarry near Hankey in the Gamtoos Basin.*

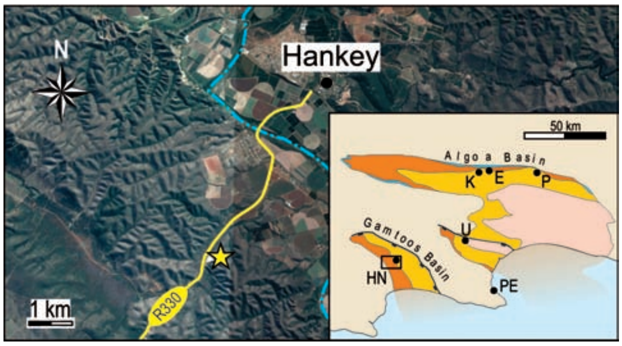

Figure 6. *Location of the quarry (yellow star) selected as the stratotype for the Enon Formation.*

Acknowledgements

Field assistants from the Sedimentology-Palaeontology Research Group at the University of Cape Town are thanked for their help during several field trips to study the Enon Formation. This project was supported by grants from the National Research Foundation African Origins Platform (GUN 91601 to EMB) and the DST-NRF Centre of Excellence in Palaeosciences (GUN CoE2017-050; COE2016-347 to EMB). A doctoral bursary to RM is provided by the DST-NRF Centre of Excellence in Palaeosciences. We gratefully acknowledge their financial contributions. The careful reviews provided by Drs Hayley Cawthra and Nigel Hicks, as well as Coenie de Beer improved the final manuscript. Opinions expressed and conclusions arrived at are those of the authors and are not necessarily to be attributed to the CoE in Palaeosciences or NRF AOP.

References

Atherstone, W.G., 1857. Geology of Uitenhage. Eastern Province Monthly Magazine, 1, 518-532.

Dingle, R.V., Siesser, W.G. and Newton, A.R., 1983. Mesozoic and Tertiary geology of southern Africa. Rotterdam, Balkema, 375p.

Du Preez, J.W., 1944. Lithology, structure and mode of deposition of the Cretaceous deposits in the Oudtshoorn area. Annals, University of Stellenbosch, 22, 209-237.

Engelbrecht, L.N.J., Coertze, F.J. and Snyman, A.A., 1962. Die geologie van die gebied tussen Port Elizabeth en Alexandria, Kaapprovinsie. Explanation of 1:125,000 scale Sheets 3325D Port Elizabeth and 3326C Alexandria, Geological Survey of South Africa, 54p.

Fouché, J., Bate, K.J. and Van der Merwe, R., 1992. Plate tectonic setting of the Mesozoic Basins, southern offshore, South Africa: A review. In: M.J. De Wit, I.G.D. Ransome (Editors). Inversion Tectonics of the Cape Fold Belt, Karoo and Cretaceous Basins of Southern Africa. A.A. Balkema, Rotterdam, 33-48.

Haughton, S.H., 1928. The geology of the country between Grahamstown and Port Elizabeth. Explanation of Cape Sheet 9 (Port Elizabeth), Geological Survey of South Africa, 50p.

Hill, R.S., 1972. The geology of the northern Algoa Basin, Port Elizabeth. Unpublished M.Sc.Thesis, University of Stellenbosch, 62p.

Holzforster, F., 2007. Alluvial fan systems in the Late Mesozoic Oudtshoorn Basin, South Africa, and their implications for basin development. Beringeria, 37, 81-93.

Joubert, P. and Johnson, M.R., 1998. Abridged lexicon of South African stratigraphy. South African Committee for Stratigraphy (SACS), Council for Geoscience, Pretoria, 160p.

Kirstein, L.A., 1997. Magmatism in southern Uruguay and the early rifting of the South Atlantic. Unpublished Ph.D. thesis, The Open University, 376p.

Lock, B.E., Shone, R., Coates, A.T. and Hatton, C.J., 1975. Mesozoic Newark-Type sedimentary basins within the Cape Fold Belt of South Africa. Proceedings of the 9th International Congress of Sedimentology, Nice, 2, 217-225.

Lock, B.E., 1978. The Cape Fold Belt of South Africa; tectonic control of sedimentation. Proceedings, Geological Association, 89, 263-281.

Malan, J.A. and Theron, J.N., 1987. Notes on an Enon basin north-east of Bredasdorp, Southern Cape Province. Annals, Geological Survey of South Africa, 21, 83-87.

Malan, J.A. and Viljoen, J.H.A., 1990. Mesozoic and Cenozoic geology of the Cape South Coast. Guidebook Geocongress '90, Geological Society of South Africa, PO3, 81p.

Malan, J.A. and Viljoen, J.H.A., 2016. Southern Cape Geology: Evolution of a rifted margin. Field Trip Guide, 35th International Geological Congress, Cape Town, Post 11, 64p.

Marsh, J.G., 2016. New Evidence for the Correlation of Basalts of the Suurberg Group with the Upper Part of the Karoo Basalt Sequence of Lesotho. In: B. Linol and M. De Wit (Editors). Origin and Evolution of the Cape Mountains and Karoo Basin. Springer International Publishing, 59-65.

McLachlan, I.R. and McMillan, I.K., 1976. Review and stratigraphic significance of southern Cape Mesozoic paleontology. Transactions of the Geological Society of South Africa, 79, 197-212.

McMillan, I.K., Brink, G.I., Broad, D.S. and Maier, J.J., 1997. Late Mesozoic sedimentary basins off the south coast of South Africa. Sedimentary Basins World, 3, 319-376.

Muir, R.A. and Bordy, E.M., 2016. Stratigraphic framework for the Kirkwood Formation in the southern Cape region: invertebrate biostratigraphy and zircon geochronology. In: 19th Palaeontological Society of South Africa biennial conference, Stellenbosch University, 65p.

Paton, D.A., 2006. Influence of crustal heterogeneity on normal fault dimensions and evolution: southern South Africa extensional system. Journal of Structural Geology, 28, 868-886.

Reddering, J.S.V., 2003. Lithostratigraphy of the Robberg Formation (Uitenhage Group), including the Sebastian Point Member. Lithostratigraphic Series, South African Committee for Stratigraphy (SACS), 40, 18p.

Richardson, J.C., Hodgson, D.M., Paton, D., Craven, B., Rawcliffe, A. and Lang, A., 2017. Where is my sink? Reconstruction of landscape development in southwestern Africa since the Late Jurassic. Gondwana Research, 45, 43-64.

Rigassi, D.A. and Dixon, G.E., 1972. Cretaceous of the Cape Province, Republic of South Africa. In: T.F.J. Dessauvagie and A.J. Whiteman (Editors). African Geology. Geology Department, University of Ibadan, Nigeria, 513-527.

Rogers, A.W., 1905. Geological survey of parts of the Divisions of Uitenhage and Alexandria. Annual report of the Geological Commission of the Cape of Good Hope, 1-18.

Rogers, A.W., Hall, A.L., Wagner, P.A. and Haughton, S.H., 1929. Union of South Africa. Handbuch der Regionalen Geologie, Heft 27. Carl Winters Universitatsbuchhandlung, Heidelberg, Germany. Cretaceous System, 9, 143-148.

SACS, 1980 (See South African Committee for Stratigraphy).

Shone, R.W., 1976. The sedimentology of the Mesozoic Algoa Basin. Unpublished M.Sc. thesis, University of Port Elizabeth, 48p.

Shone, R.W., 2006. Onshore post-Karoo Mesozoic deposits. In: M.R. Johnson, C.R. Anhaeusser and R.J. Thomas (Editors). The Geology of South Africa, Geological Society of South Africa, Johannesburg, and Council for Geoscience, Pretoria, 541-571.

South African Committee for Stratigraphy (SACS), 1980. Stratigraphy of South Africa. Part 1: Lithostratigraphy of the Republic of South Africa, South West Africa/Namibia, and the Republics of Bophuthatswana, Transkei and Venda. Handbook, Geological Survey of South Africa, 8, 690p.

Tankard, A.J. Jackson, M.P.A., Eriksson, K.A., Hobday, D.K., Hunter, D.R., and Minter, W.E.L., 1982. Fragmentation and Mesozoic Paleogeography. In: Crustal Evolution of Southern Africa. Springer-Verlag, New York, 407-423.

Theron, J.N., Wickens, H. de V. and Gresse, P.G., 1991. Die geologie van die gebied Ladismith. Explanation of 1:250,000 scale Sheet 3320 Ladismith, Geological Survey of South Africa, 99p.

Toerien, D.K. (compiler), 1991. Geological Map 3324 Port Elizabeth. 1:250 000 Geological Map Series, Geological Survey of South Africa, Pretoria.

Truswell, J.F., 1967. A critical review of stratigraphic terminology as applied in South Africa. Transactions of the Geological Society of South Africa, 70, 81-116.

Van der Linde, C., 2017. Sediment supply processes and patterns in the Enon Formation, Gamtoos Basin, Eastern Cape, South Africa. Unpublished M.Sc. thesis, University of Cape Town, 82p.

Viljoen, J.H.A. and Malan, J.A., 1993. Die geologie van die gebiede 3422AA Mosselbaai en 3421BB Herbertsdale. Explanation of 1:50,000 scale Sheets 3422 AA and 3421 BB, Geological Survey of South Africa, 79p.

Winter, H. de la R., 1973. Geology of the Algoa Basin, South Africa, In: G. Blant (Editor). Sedimentary basins of the African coasts, Part 2, South and East Coast. Association of African Geological Surveys, Paris, 17-48.

Winter, H. de la R., 1979. Application of basic principles of stratigraphy to the Jurassic-Cretaceous interval in southern Africa. In: A.M. Anderson and W.A. Van Biljon (Editors). Geocongress 77: Some Sedimentary Ore Deposits in South Africa. Special Publication, Geological Society of South Africa 6, 183-196.

Editorial handling: C.H. de Beer

Lithostratigraphy of the Kirkwood Formation (Uitenhage Group), including the Bethelsdorp, Colchester and Swartkops Members, South Africa

R.A. Muir
Department of Geological Sciences, University of Cape Town, Private Bag X3, Rondebosch 7701, South Africa
e-mail: mrxrob009@myuct.ac.za

E.M. Bordy
Department of Geological Sciences, University of Cape Town, Private Bag X3, Rondebosch 7701, South Africa
e-mail: emese.bordy@uct.ac.za

J.S.V. Reddering
Council for Geoscience, P.O. Box 5347 Walmer, Port Elizabeth, 6065, South Africa
(Desceased)

J.H.A. Viljoen
Council for Geoscience, P.O. Box 572, Bellville 7535, Cape Town, South Africa
e-mail: jviljoen@geocience.org.za

Abstract

The Jurassic – Cretaceous Kirkwood Formation forms part of the Uitenhage Group, the earliest deposits to fill Mesozoic rift basins that developed in what is now the southern Cape of South Africa during the breakup of Gondwana. The Kirkwood Formation is not only palaeontologically extremely important, having yielded diverse assemblages of vertebrate, invertebrate and plant fossil taxa, but also contains suitable source rocks for hydrocarbon systems offshore of the southern Cape of South Africa. The Kirkwood Formation comprises chronostratigraphic markers in the form of radiometrically dateable volcaniclastic deposits and age-diagnostic invertebrate fossils, which may provide robust dates for the depositional history of the Uitenhage Group. The Kirkwood, including the Bethelsdorp, Colchester and Swartkops Members, is 2210 m at its thickest and comprises sandstones and mudstones deposited in fluvial and lacustrine depositional settings from the Tithonian to Valanginian. These microfossil-based ages may only apply to the unit in its type area in the Algoa Basin and not to its lithostratigraphic correlatives in the other Mesozoic rift basins, which have highly variable ages ranging from Middle Jurassic to Early Cretaceous.

Introduction

The Kirkwood Formation is part of the Uitenhage Group, which is an assemblage of Mesozoic successions that occupy several rift basins (Lock et al., 1975) formed along the southern margin of South Africa during the breakup of Gondwana. Here we address primarily the onshore sequence, but make reference to offshore boreholes where relevant. Outcrops of the onshore Kirkwood Formation are discontinuous and located in basins along the Worcester-Pletmos and Oudtshoorn-Gamtoos basin lines, in the Algoa Basin and in the Haasvlakte, Jubilee and Soutpansvlakte Basins near Bredasdorp (Figure 1). The Kirkwood is palaeontologically highly productive and its organic-matter rich, lacustrine shale units are considered potential source rocks for hydrocarbons in the southern Cape (McMillan et al., 1997; Roux and Davids, 2016).

There is considerable variation in the stratigraphy of the Kirkwood Formation with early authors referring to sandstone-dominated layers that contain fossil logs as the 'Wood Beds' (Atherstone, 1857), while Rogers and Schwarz (1901) refer to the mudstone units as 'Variegated Marls'. Haughton (1928) realized the connection between sandstone- and mudstone-dominated deposits and referred to the combined package as 'Variegated Marls and Wood Beds' even though he pointed out that 'marl' is a misnomer because the mudstones lack calcium carbonate. Engelbrecht et al. (1962) referred to the formation as the 'Wood Beds and Variegated Marls Stage' and also pointed out the 'marl' misnomer. The 'Wood Beds' were called the Bezuidenhouts Formation by Rigassi and Dixon (1972) who also included the current Swartkops Member and part of the Kirkwood Formation in the other basins. Winter (1973, 1979) was the first to group the sandstone- and mudstone-dominated deposits together and call them the 'Kirkwood Formation'. These classifications initially referred to the succession in the Algoa Basin, which is where the unit is most widely exposed and within which its type locality, 3 km south of the town of Kirkwood, is located (Figure 1). Lithological correlatives in the other Mesozoic rift basins are given the same name, a pragmatic trend we support based on their shared lithological character, and similar stratigraphic relations (SACS, 1980).

A predominantly sandy unit low down in the Kirkwood Formation near Uitenhage was first mapped and named the 'Swartkop Sandstone' by Atherstone (1857). It was renamed the 'Swartkops Member' by Winter (1973, 1979) and approved by SACS (1980). Rigassi and Dixon (1972) suggested the name 'Colchester Formation' for a dark shale unit in the Kirkwood Formation, which Winter (1973, 1979) later termed the Colchester Member and was accepted by SACS (1980). McMillan (2010) limited the use of 'Colchester Formation' to include only the lacustrine shale in the Sundays River Trough of the Algoa Basin, naming the marine shales in the Uitenhage Trough at Bethelsdorp and farther offshore the Bethelsdorp 'Formation'. We propose that due to their limited and mostly subsurface distribution, these units should remain Members of the Kirkwood Formation as accepted by SACS (1980) and used by Joubert and Johnson (1998).

Shone (1976) also proposed two additional locally observed minor sandstone-rich units, the Lindores and Mfuleni Members, and although he referred to surface sections (which he illustrates), he did not provide any description or characteristics of these members (Shone, 1978; p. 7 and 21; sections RS132 and RS 5 and Plates 2 and 3).

Stratigraphic position and age

The Kirkwood Formation is underlain by the Enon Formation and overlain by the Sundays River and (informal) Buffelskloof Formations. It is considered to be the partial lateral time equivalent of the Enon Formation in all southern coast Mesozoic basins (Dingle et al., 1983) and usually occupies the inner parts of

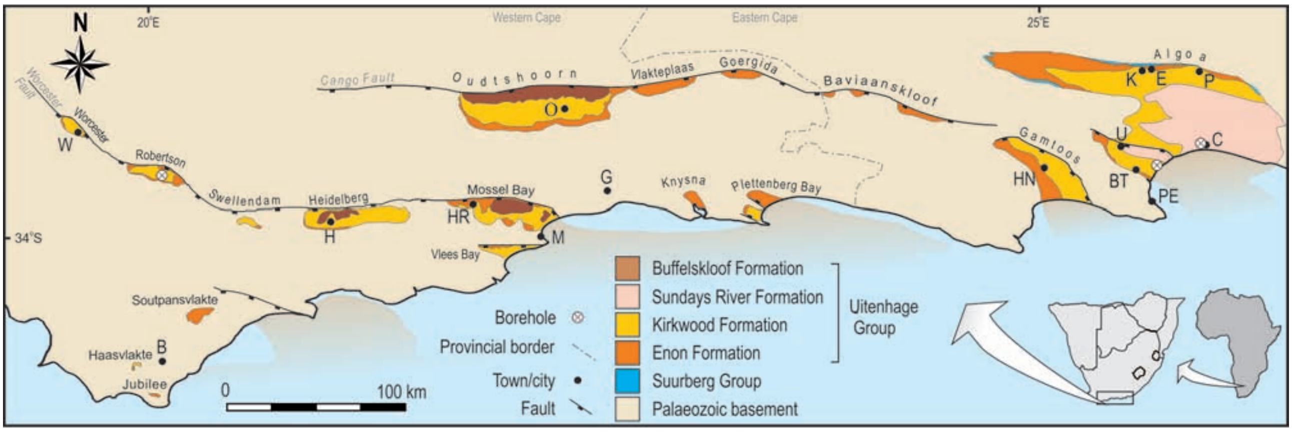

Figure 1. *Mesozoic rift basins of the Eastern and Western Cape provinces of South Africa and the major units of the onshore Uitenhage Group. The offshore extension of the Uitenhage Group is only shown schematically. The Worcester-Pletmos basin line comprises the Worcester, Robertson, Swellendam, Heidelberg, Mossel Bay, Knysna and Plettenberg Bay Basins, whereas the Gamtoos-Oudtshoorn basin line contains the Oudtshoorn, Vlakteplaas, Georgida, Baviaanskloof and Gamtoos Basins. The exceptionally long, parallel fault arrays (Cango and Worcester Faults) exploit pre-existing weaknesses in the Cape Fold Belt (Fouché et al., 1992; Paton, 2006). The Jurassic Suurberg Group is shown in the Algoa Basin, but the contentious Suurberg Fault, supposedly bounding the Algoa Basin to the north, is not included (Toerien, 1991). White crossed circles indicate location of boreholes referenced in text. The Robberg, Hartenbos and Brenton Formations, which are also constituents of the Uitenhage Group, are not shown due to their small aerial extent. Abbreviations: E = Enon; B = Bredasdorp; BT = Bethelsdorp; C = Colchester; G = George; H = Heidelberg; HN = Hankey; HR = Herbertsdale; K = Kirkwood; M = Mossel Bay; O = Oudtshoorn; P = Paterson; PE = Port Elizabeth; U = Uitenhage; W = Worcester*

each basin, while the latter is developed close to their margins. In some parts of the Algoa Basin, the sandy Swartkops Member is the basal unit of the Kirkwood Formation, whereas elsewhere, the shaly Colchester and Bethelsdorp Members occupy this position.

Numerous macrofossils have been recovered from the Kirkwood, but most of them are not age diagnostic, with the result that the age of the beds can only be broadly defined as Jurassic to Early Cretaceous. Microfossil assemblages from the Bethelsdorp and Colchester Members in the lower part of the Kirkwood Formation of the Algoa Basin are dated as Tithonian (McMillan et al., 1997; McMillan, 2010), whereas the uppermost parts are inferred to be Lower Cretaceous in age based on a probable temporal equivalence with the lower part of the Valanginian – Hauterivian Sundays River Formation (McLachlan and McMillan, 1976; Shone, 1978; McMillan, 2003). Although the Kirkwood Formation likely spans the Tithonian – Valanginian in the Algoa Basin, this may not necessarily represent the age of its lithostratigraphic correlatives in the Mesozoic rift basins further to the west, which contain datable volcaniclastic deposits that are currently under investigation. Preliminary U-Pb analyses of zircon from these strata point to a highly variable Middle Jurassic – Early Cretaceous depositional age for the Kirkwood Formation (Muir and Bordy, 2016).

Geological description

Basic unifying features

The Kirkwood Formation is a continental succession of interstratified sandstones and varicoloured mudstones containing diverse terrestrial and lacustrine fossils. In contrast to the conformably underlying and laterally equivalent conglomerate-dominated Enon Formation, it contains only small, isolated conglomerate units that are usually interbedded with sandstone. In turn, the Buffelskloof Formation (Theron et al., 1991), which unconformably overlies the Kirkwood Formation in the Oudtshoorn, Heidelberg and Mossel Bay basins, comprises predominantly conglomerates with only minor sandstone and mudstone. The aerially restricted Hartenbos Formation (Viljoen, 2009) is distinguished from the Kirkwood Formation in the Mossel Bay Basin by an angular relationship and different proportions of sandstone. The Kirkwood Formation differs from the overlying and partially contemporaneous marine Sundays River Formation in the Algoa Basin in that the former contains abundant red-coloured strata with palaeosols (including *in situ* rootlets) and terrestrial fossils, all of which are absent in the Sundays River Formation.

The Swartkops Member is a sandstone-rich unit, while the Colchester and Bethelsdorp Members both consist primarily of dark grey mudstones and minor sandstones, but respectively contain lacustrine and marine fossils.

Thickness

The thickness of the Kirkwood Formation is highly variable, but it reaches its maximum measured thickness in the Algoa Basin, where 2210 m was intersected by borehole AL 1/69 and wedges out towards the southern and western basin margins (Winter, 1973). Although there is limited borehole data outside of the Algoa Basin, a similar thinning towards the basin edges could be expected in the other Mesozoic rift basins. At least 1900 m was intercepted in the Gamtoos Basin (Dingle et al., 1983) and 186.5 m in the Robertson Basin. Boreholes in the offshore Bredasdorp Basin intercepted a similarly wide range of thicknesses varying from 1499 m in the north to just 79 m in the south (Dingle et al., 1983).

The Colchester Member is about 140 m thick in boreholes CO 1/69 and CO 3/71, the Bethelsdorp Member is ~400 m thick in SW1/08 and the Swartkops Member attains a 100 m thickness in the same borehole (McLachlan and McMillan, 1976) (see stratotypes section).

Lithology

Mudstone (50 to 100%)

The mudstones and silty mudstones are variegated, colour-mottled, moderate to dark reddish-brown (10R 4/6, 10R 3/4)*, moderate pink (5R 7/4), light red (5R 6/6), greyish yellow green (5GY 7/2), pale olive (10Y 6/2), greyish green (10GY 5/2) or dark grey (N3) with variable calcrete-rich palaeosols (Frost, 1996) and sandstone interbeds (Winter, 1973; Shone, 1976) (Figures 2A to G). The mudstone packages exhibit either finely laminated units that are in places interbedded with altered tuffs, or they are massive with extensive calcareous palaeosols in the upper part of upward fining cycles.

Sandstone (10 to 50%)

Coarse- to fine-grained, moderate red (5R 4/6), pale red (10R 6/2), pale reddish brown (10R 5/4), light brown (5YR 6/4), pale brown (5YR 5/2), pale yellowish orange (10YR 8/6), greyish orange (10YR 7/4), moderate yellowish brown (10YR 5/4), moderate yellow (5Y 7/6), light grey (N7), very light grey (N8) and white (N9) sandstone interbedded with mudstones as either tabular beds, 'U-shaped' lenses or fully developed point bars (Figures 2A, B, E, F, and G). Sandstone units typically form upward fining successions with pebbly conglomerate lags at the base and mudstones at the top of each cycle. Thicker sandstone beds commonly exhibit cross-bedding or are massive, and contain variable amounts of charcoal, as well-displayed at the Bezuidenhouts River Bridge (Algoa Basin) (Muir et al., 2015) and in cuttings at the old Calitzdorp railway station (Oudtshoorn Basin). Wood fragments and logs are also common in sandstone beds, often in association with charcoal (Figure 2F).

Conglomerate (0 to 10%)

Thin conglomerate lags and lenses are common at the base of sandstone-dominated successions and rarely attain thicknesses of more than 1 m. Clasts comprise either extrabasinal Cape Supergroup lithologies or intrabasinal mudstone rip-ups. Charcoal fragments and fossil logs also occur as clasts in some conglomerate beds.

*All colour codes follow those outlined in the Munsell Rock Colour Chart of 2009.

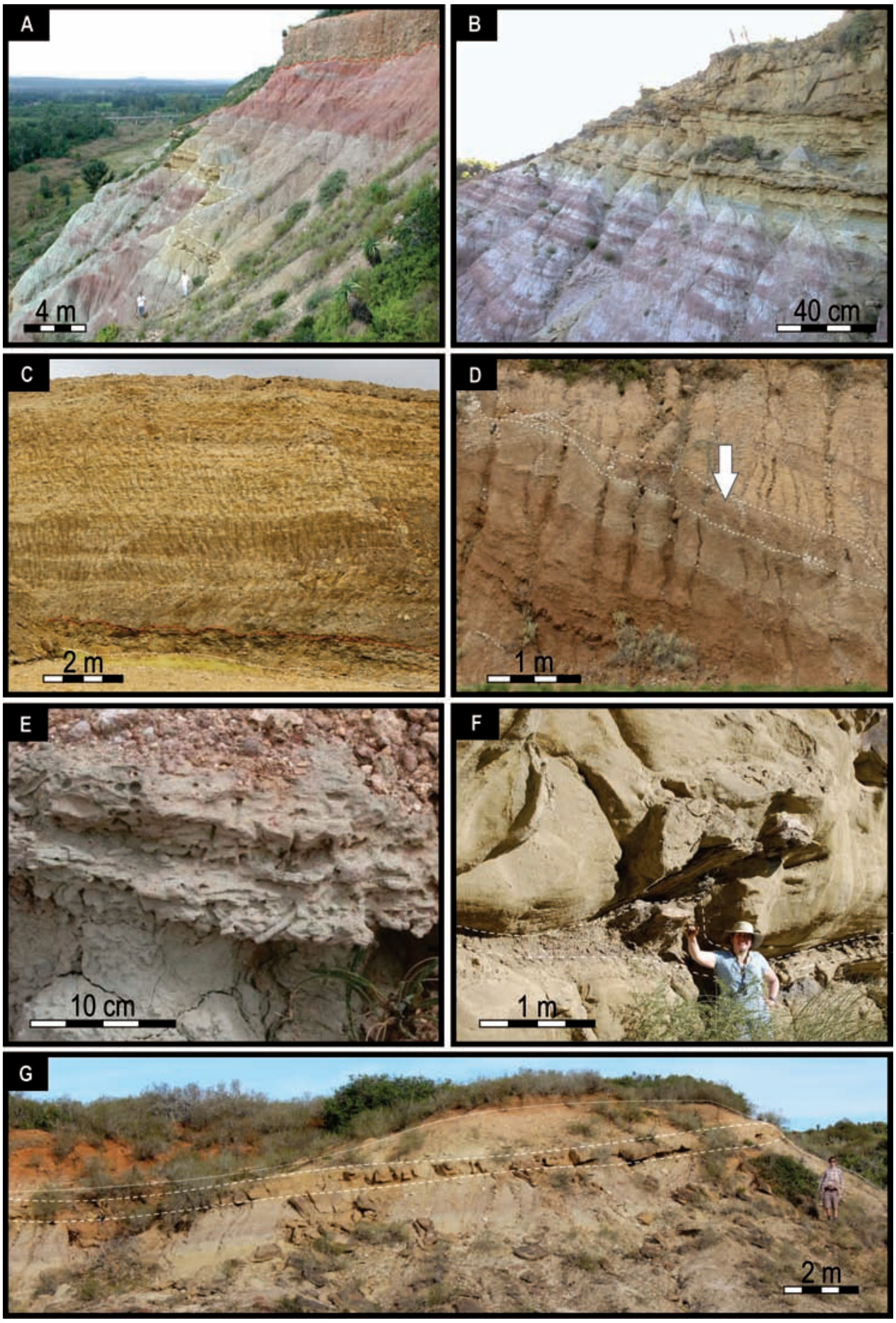

Figure 2.(***A***) *Interbedded variegated mudstones with calcareous palaeosols and yellow-brown sandstones, delineated with white dashed line, at the stratotype exposure on a natural cliff 3 km south of Kirkwood in the Algoa Basin. The red dashed line marks the unconformable contact with the overlying Cenozoic gravels (photo courtesy of Dr. W. de Klerk). (**B**) Sandstone overlying variegated horizontally bedded, mostly massive mudstones that typify the Kirkwood Formation in the Algoa Basin and elsewhere in the southern Cape Mesozoic basins (photo courtesy of Dr. W. de Klerk). (**C**) Volcaniclastic bentonite (1.5 m thick) beneath an erosive contact (red dashed line) overlain by subaqueously deposited conglomerate, sandstones and finely laminated mudstones in an upward-fining lacustrine succession in the Heidelberg Basin. White dotted line marks quarry floor. (**D**) Interbedded red-brown mudstones and sandstones with volcaniclastic bentonite (between white dashed lines) at a road-cutting in the Robertson Basin. Arrow points to 'popcorn' weathering of montmorillonite clay in bentonite. (**E**) Randomly oriented sub-cylindrical invertebrate burrows in greyish-green, laterally extensive, up to 20 to 25 cm thick sandstone interbeds in the red mudstones that contain calcareous palaeosols in the Algoa Basin (image taken from Almond, 2012). (**F**) Fossilized logs embedded in a charcoal-rich sandstone bed in the Kirkwood Formation along the Bezuidenhouts River. (**G**) Outcrop of the marine Bethelsdorp Member near Jachtvlakte, 6 km south of Uitenhage in the Algoa Basin exhibits dark grey laminated mudstones and tabular yellow-brown sandstones (delineated by white dashed lines). White dotted line separates the unit from orange soil horizons above.*

Volcaniclastics (0 to 5%)

Pale greenish yellow (10Y 8/2), moderate brown (5YR 4/4), light brown (5YR 6/4), moderate yellowish brown (10YR 5/4), light grey (N7), very light grey (N8) to white (N9), light red (5R 6/6), pale pink (5RP 8/2), and moderate pink (5R 7/4) volcaniclastic deposits (Figures 2C and D) consisting of tuff, tuffite and bentonite (altered tuff) are documented from most of the Mesozoic rift basins.

Palaeontology

The Kirkwood Formation, being the most fossil-rich Jurassic – Cretaceous unit in southern Africa, contains a highly diverse non-marine fossil biota such as macroplants (e.g., bryophytes, ferns, bennettitaleans, cycads, conifers, fossil logs, amber, charcoal), freshwater algae (charophytes), freshwater crustaceans (conchostracans), bivalves, insects, fish scales, reptile (e.g., sauropod, ornithopod and theropod dinosaurs, frogs, turtles, sphenodontids, crocodiles) and some mammalian bones (McLachlan and McMillan, 1976; Anderson and Anderson,1985; Bamford,1986; de Klerk et al., 2000; Gomez et al., 2002; Shone, 2006; Almond et al., 2009; McMillan, 2010; Almond, 2012; Forster et al., 2009; Muir et al., 2015; McPhee et al., 2016).

Genesis

Most of the Kirkwood Formation was deposited by meandering fluvial systems and in lacustrine environments (Shone, 1976; Muir et al., 2015). The Colchester Member in the Algoa Basin is lacustrine in origin while the Bethelsdorp Member is a marine unit (McMillan, 2010; Almond, 2012). The sandstones that comprise the Swartkops Member are considered fluvial or locally lacustrine (McLachlan and McMillan, 1976; SACS, 1980).

Boundaries

Lower boundary

The Kirkwood Formation conformably overlies and laterally grades into the Enon Formation, but their gradational, interfingering relationship is not easily delineated in the field due to the lack of laterally and vertically extensive outcrops. In some areas the Kirkwood Formation unconformably overlies older Suurberg Group (e.g., in the northern Algoa Basin near Paterson) or older Cape Supergroup rocks.

Upper boundary

Erosion has in most cases removed the overlying units; hence the top boundary of the Kirkwood is usually not apparent in the field. However, in the Algoa Basin either a conformable (Shone, 1978) or unconformable (Winter, 1973; McLachlan and McMillan, 1976) boundary separates it from the overlying Sundays River Formation, with which it also partly shares a gradational interfingering relationship. The Kirkwood Formation is locally unconformably overlain by the Miocene – Pliocene marine Alexandria Formation deposits in the Algoa Basin. An angular, unconformable contact separates the Kirkwood Formation from the overlying Buffelskloof Formation in the Oudtshoorn, Heidelberg and Mossel Bay basins.

Lateral boundaries

A lateral gradational interfingering boundary exists with parts of the Enon Formations in all Mesozoic rift basins that contain the Kirkwood Formation. A similar relationship exists in part with the Sundays River Formation in the Algoa Basin (Figure 3).

Subdivision

Two members of the Kirkwood Formation have been accepted by South African Committee for Stratigraphy (SACS, 1980; Joubert and Johnson, 1998). The most notable is the Colchester Member (Winter, 1973), encountered mainly in boreholes as a potential oil-source rock near the base of the Kirkwood Formation in the Algoa Basin. The Colchester Member lies at a depth of 2171 m in borehole CO 1/67 at Colchester, its type area, and was intersected in several other nearby boreholes in the Algoa Basin (Winter, 1979). Earlier authors consider the member to extend beyond the type area in the Sundays River Trough to

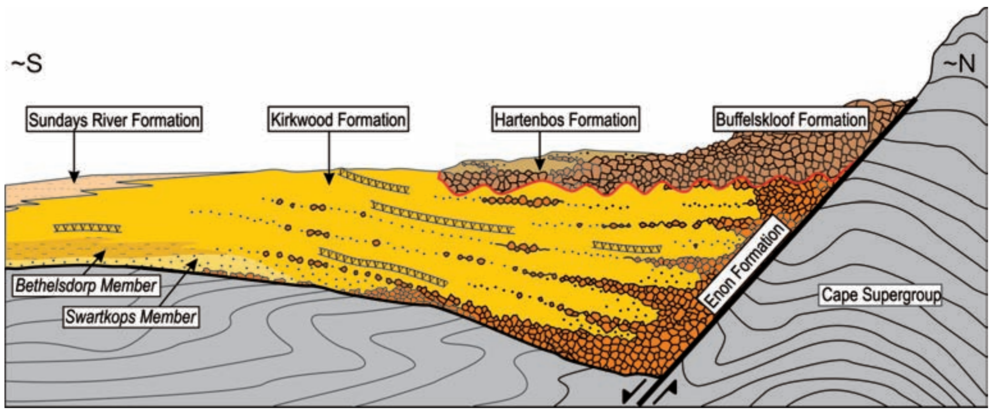

Figure 3. *Schematic representation of the main units of the Uitenhage Group and their stratigraphic position in the Mesozoic rift basins (not to scale). Not all these units or the volcaniclastic deposits (vvvv) are present in all basins.*

other troughs of the Algoa Basin (Winter, 1973; McLachlan and McMillan, 1976; Winter 1979). However, McMillan (2010) highlights subtle lithological and micropalaeontological differences between the units in each trough of the Algoa Basin and prefers a separation of the unit into two, which he names the Colchester Formation (limited to the Sundays River Trough) and Bethelsdorp Formation (of the Uitenhage and Port Elizabeth Troughs). The present authors do not support the elevation of these units to formation level, because they occur mostly in the subsurface and are limited to the Algoa Basin, but do recognise the importance of the divergent micropalaeontological assemblages in each (McMillan, 2010).

The shale in boreholes near Colchester, the type locality for the traditional Colchester Member, contains no clear marine microfossils, whereas the similar dark grey shale in the Uitenhage and Port Elizabeth troughs hosts marine macro- and microfossils (McMillan, 2010; Almond, 2012). We therefore propose a new stratigraphic unit, the Bethelsdorp Member, for the marine grey mudstone-dominated and subordinate sandstone unit in the Uitenhage and Port Elizabeth troughs, and prefer to use Colchester Member to refer only to the lacustrine (as opposed to marine) grey shale encountered in several boreholes around the type area near Colchester in the Algoa Basin. Most notably, these have been identified in borehole CO 1/67. Given the subdivision of the original Colchester Member (Winter, 1979) into a reduced unit with the same name and the newly defined Bethelsdorp Member, several revisions are required. Firstly, the reference material in the CO 1/67 borehole (Figure 4) below 2171 m applies to the newly defined Colchester Member only and does not include the Bethelsdorp Member. Secondly, the new Colchester Member has a reduced thickness of 140 m from the original SACS accepted thickness of <400 m (Joubert and Johnson, 1998). Finally, the depositional environment of the Colchester Member is not mixed marine/estuarine/lacustrine as frequently described (e.g., McLachlan and McMillan, 1976) but instead is limited to probable lacustrine deposition only.

The Bethelsdorp Member is here defined as the 400 m thick grey shale unit that contains marine fossils near the base of the Kirkwood Formation in the Uitenhage (onshore) and Port Elizabeth (offshore) Troughs of the Algoa Basin. The microfossil assemblages point to a Tithonian age for this unit (McLachlan and McMillan, 1976; McMillan et al., 1997; McMillan, 2010) and a likely temporal correlation with the Colchester Member of the Sundays River Trough. In outcrops near Jachtvlakte (Figure 2G), which is the best place to view the Bethelsdorp Member, the bioturbated, grey, mudstone-rich unit exhibits tabular sandstone beds and no palaeosols, in contrast with other parts of the Kirkwood Formation nearby that have well developed red palaeosols, terrestrial fossils and lenticular sandstones (Almond, 2012).

A third member of the Kirkwood Formation accepted by SACS (1980), is the Swartkops Member, first briefly suggested by Atherstone (1857; 'Zwartkops variegated sandstone') and later mentioned by Haughton (1928) as the 'Zwartkops Sandstone'. Both descriptions are unclear, but it was later formalized in its present stratigraphic context by Winter (1973) to denote a thick

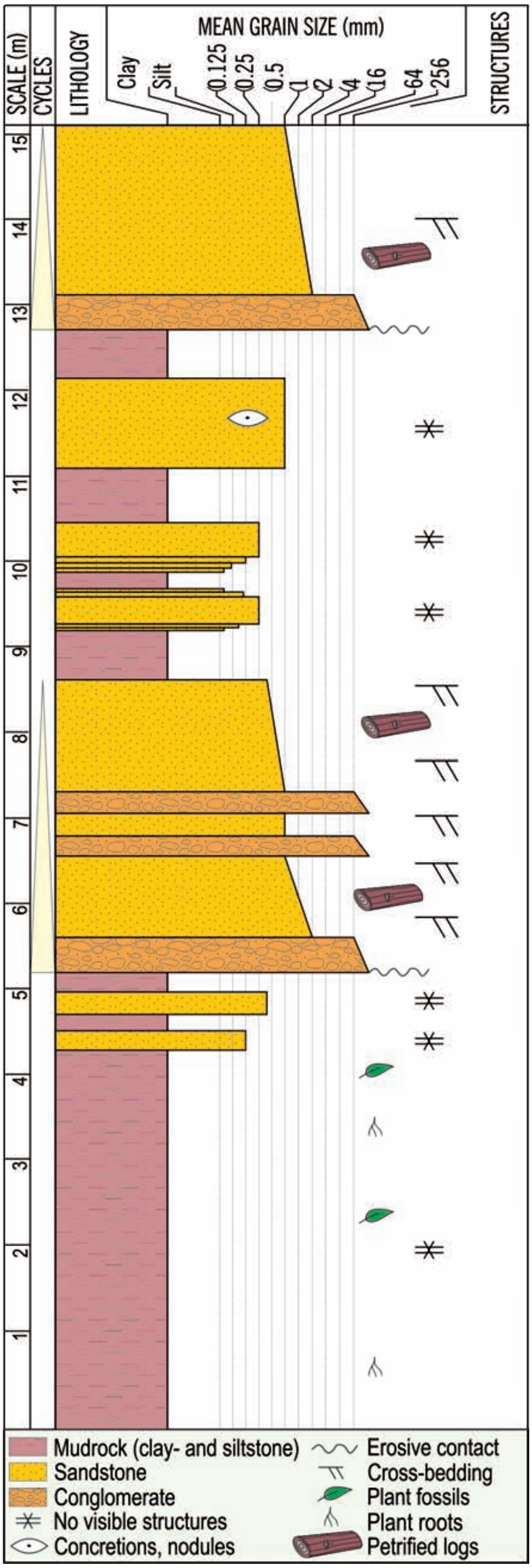

Figure 4. *Stratotype for the Kirkwood Formation in a natural cliff south of Kirkwood, Algoa Basin. See Figure 5 for locality map and Figure 1 for its regional position.*

sandstone package directly above the Enon Formation, but below the Colchester Member. Given the proposed subdivision of the original Colchester Member into two parts, its stratigraphic position is better described as below the Bethelsdorp Member. It outcrops in the Swartkops River valley west of Uitenhage and has otherwise only been encountered in boreholes such as SW 1/08, from which it was described and depicted by McLachlan and McMillan (1976). The Swartkops Member is not given much mention in literature probably because it is rarely exposed and palaeontologically mostly barren (McLachlan and McMillan, 1976).

The 'grey facies' in the Heidelberg Basin (Figure 2C) was predominantly deposited in a lacustrine environment as indicated by horizontally laminated grey mudstones with fresh-water invertebrates and laterally continuous volcaniclastic deposits (Viljoen, 1992) and is not correlated with any of the above members of the Kirkwood, but instead is regarded as a lacustrine or 'grey facies' unit that also exists in some of the other basins (e.g., Haasvlakte and northern Algoa Basins) but with reduced vertical and lateral extent (Malan and Viljoen, 2016).

Regional aspects

Geographic distribution

The Kirkwood Formation was first described from the Algoa Basin; however, deposits with identical lithological characteristics and stratigraphic position also exist in most other Mesozoic rift basins further to the west like the Gamtoos, Plettenberg Bay, Oudtshoorn, Mossel Bay, Vlees Bay, Heidelberg, Swellendam, Robertson and Worcester Basins (Figure 1). The Kirkwood Formation also outcrops in basins near Bredasdorp (Soutpansvlakte, Haasvlakte and Jubilee Basins). The three official Members of the unit, the Bethelsdorp, Colchester and the Swartkops, are all restricted to the Algoa Basin (Shone, 1976; Dingle et al., 1983; Malan and Theron, 1987; Malan and Viljoen, 1990; Shone, 2006; Malan and Viljoen, 2016).

Criteria for lateral extension

Mesozoic variegated mudstones, sandstones and minor conglomerates with terrestrial or lacustrine fossils can be used to extend the Kirkwood Formation from the type area in the northern Algoa Basin to other basins. Three members can be identified in the Algoa Basin: two with abundant dark grey mudstones and minor sandstones with either lacustrine (Colchester Member) or marine (Bethelsdorp Member) fossils, and a sandstone-rich, fossil-poor Swartkops Member.

Correlation

The Kirkwood Formation is found in several Mesozoic rift basins within the Eastern and Western Cape provinces. Correlation between each of these outcrop areas is purely lithostratigraphic, and because of the poorly constrained depositional ages, chronostratigraphic correlation between these units remains speculative. Borehole data confirm that the Kirkwood Formation extends into all offshore basins (McMillan et al., 1997; Roux and Davids, 2016). Parts of the Kirkwood Formation are coeval with the Enon and Sundays River Formations (as explained in earlier sections). The Infanta Formation is the offshore equivalent of the Kirkwood Formation (Joubert and Johnson, 1998), while the Colchester Member is coeval with the marine Bethelsdorp Formation in the Uitenhage Trough of the Algoa Basin (McMillan, 2010).

Some confusion has arisen regarding oyster-bearing sandstones in the Dunbrody area of the Algoa Basin. McMillan and McLachlan (1976) first assigned these beds to the Colchester Member but later McMillan et al. (1997) considers this correlation erroneous and attributes it to a tongue of the Sundays River Formation, which outcrops nearby. A second contention is the correlation of the marine parts of the original Colchester Member, now the Bethelsdorp Member, with the Brenton Formation at Knysna (Dingle and Klinger, 1972), which is

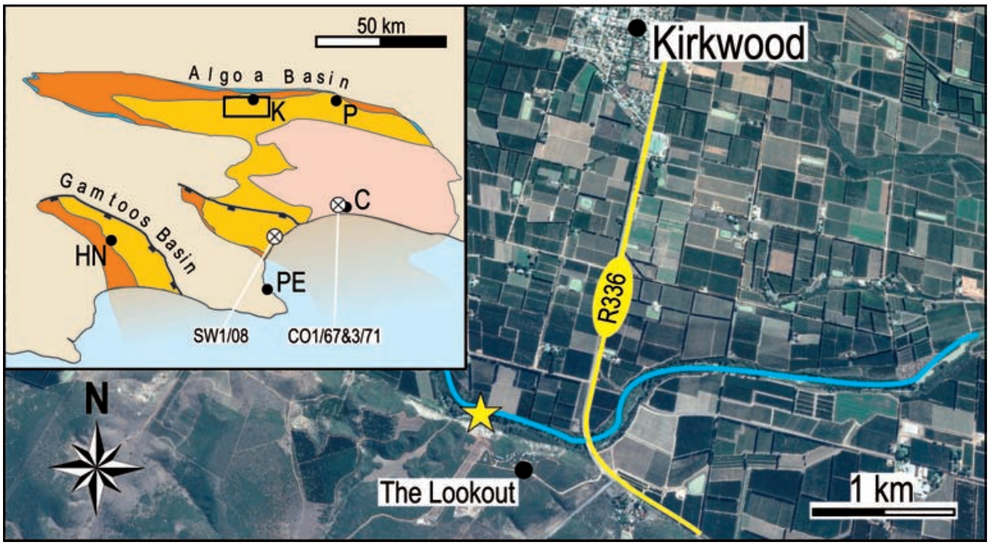

Figure 5. *Type area of the Kirkwood Formation is near the town of Kirkwood in the Eastern Cape. The unit stratotype (locality indicated by yellow star) is on the banks of the Sundays River (blue line) near The Lookout restaurant and lodge. See Figure 4 for the stratotype log.*

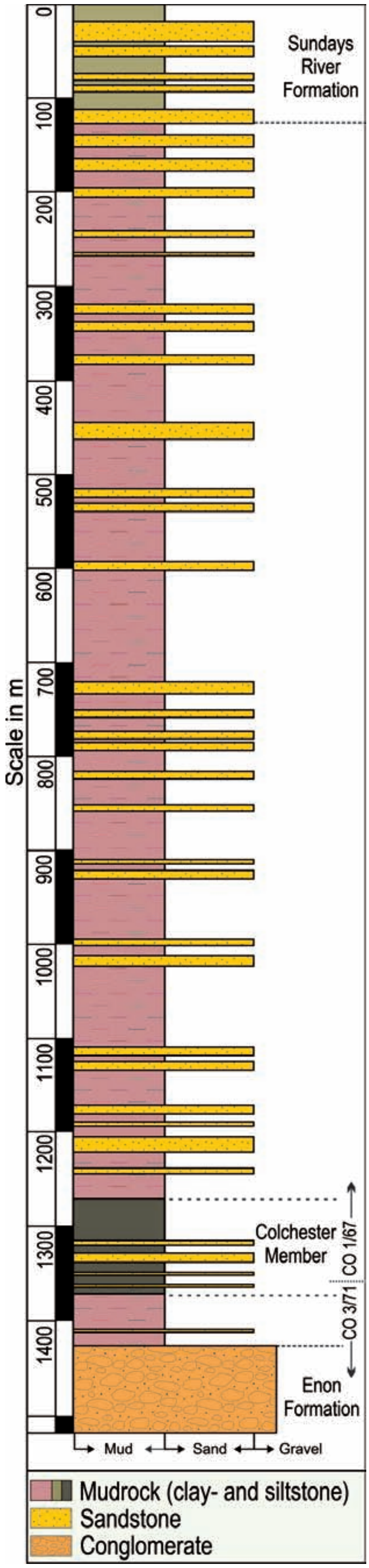

Figure 6. *Composite reference stratotype from boreholes CO1/67 and CO 3/71 (reproduced from Winter, 1979).*

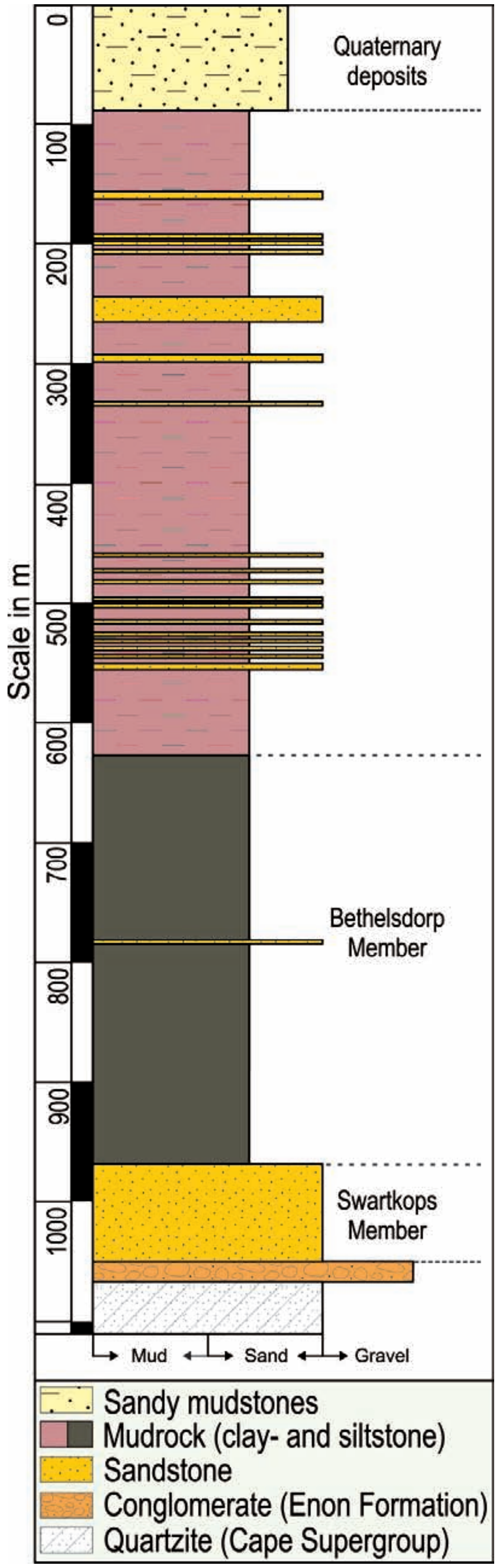

Figure 7. *Reference stratotype from borehole SW1/08 containing both Bethelsdorp and Swartkops Members, as well as the lower contact with the Enon Formation (reproduced from McLachlan and McMillan, 1976). See Figures 1 and inset in Figure 5 for location.*

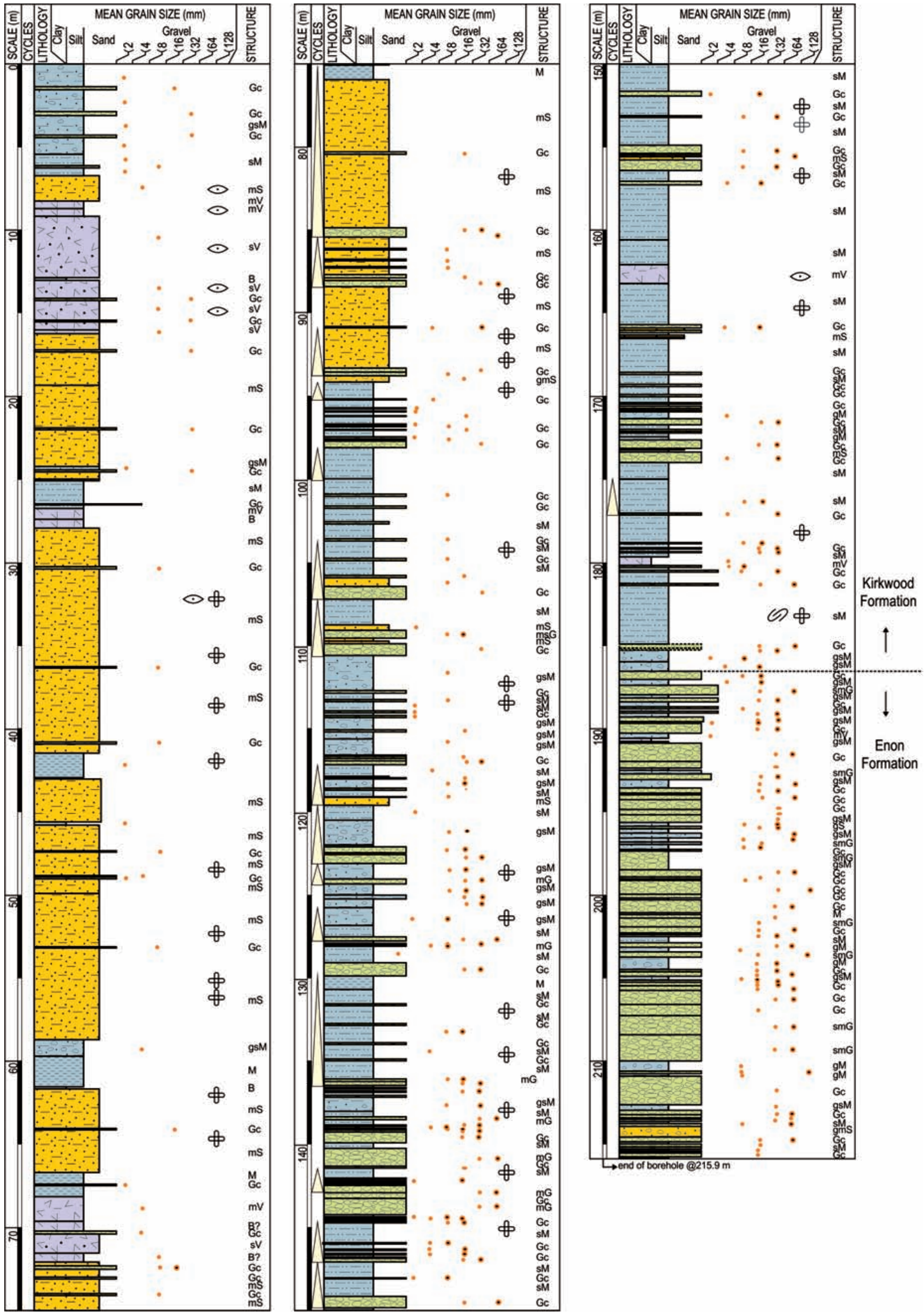

Figure 8. *Reference stratotype of the Kirkwood Formation in borehole W202 drilled near Robertson (Western Cape); for location, see Figure 1. The core of this borehole is stored at the National Core Library of the Council for Geoscience at Donkerhoek, Pretoria. Beds are structureless unless otherwise indicated (See Figure 9 for symbology).*

dismissed by McLachlan et al. (1976) in a subsequent study that instead correlates the Brenton Formation with the Sundays River Formation.

Stratotypes

The unit stratotype for the Kirkwood Formation presented here is a natural cliff 3 km south of Kirkwood and 650 m west of the R336 bridge across the Sundays River in the Algoa Basin (33°25'39"S; 25°26'07"E) (Figures 4 and 5). The cliff face is easily visible from the R336 and farm roads north of the Sundays River, however access from that direction is impossible. Instead, the outcrop is best accessed by foot walking northwards down the very steep slope from the northern end of the shooting range adjacent 'The Lookout' lodge that is situated above the cliff face. The stratotype covers only a limited portion of the Kirkwood, and none of its adjoining units or formally recognised members in the Algoa Basin, but adequately displays most of its general features.

Winter (1979) compiled a composite section for the complete Kirkwood Formation at Colchester in the Algoa Basin (including its Colchester Member) using Soekor boreholes CO1/67 (33°40'58.96"S; 25°47'30.58"E) and CO3/71 (33°40'46.71"S; 25°47'43.38"E) drilled within 500 m of each other (inset in Figure 5). CO1/67 contains the upper boundary with the Sundays River Formation but ends within the Colchester Member while CO3/71 provides a view of the bottom portion of the Formation and its contact with the Enon Formation (Figure 6). Currently, the core/cuttings are stored at the National Core Library of the Council for Geoscience at Donkerhoek, Pretoria.

The SW1/08 borehole (33°52'45.91"S; 25°36'51.78"E) was one of the earliest drilled in the Uitenhage Group of the Algoa Basin (Figure 1 and inset, Figure 5). In the literature, it is commonly referred to as the 'Old Swartkops' or 'Swartkops' borehole (McLachlan and McMillan, 1976). We suggest that it be used as a reference stratotype, because this section contains the Bethelsdorp and the Swartkops Members, as well as the contact with the Enon Formation (Figure 7). According to Winter (1979), the Swartkops Member stratotype is the section of the old Swartkop borehole between 986m (3 234 feet) and 1 049 m (3 443 feet) where there is evidence of interfingering with the overlying Colchester Member above and the Enon Formation below. The cuttings of this borehole are stored at the Port Elizabeth Museum.

To compensate for the dominance of information on the Kirkwood Formation coming from Uitenhage Group lithostratigraphy in the Algoa Basin (Figure 1), an additional reference stratotype from borehole W202 (33°49'05"S; 19°58'00"E) in the Robertson Basin is included here (Figure 7). The borehole intersects 186.5 m of Kirkwood Formation with typical sandstone, varicoloured mudstone, minor conglomeratic interbeds and numerous volcaniclastic deposits before ending in the Enon Formation (Figures 8 and 9). A more detailed record of the reference stratotype can be viewed online (https://doi.org/10.6084/m9.figshare.5155018.v1).

Acknowledgements

Field assistants from the Sedimentology-Palaeontology Research Group at the University of Cape Town are thanked for their help

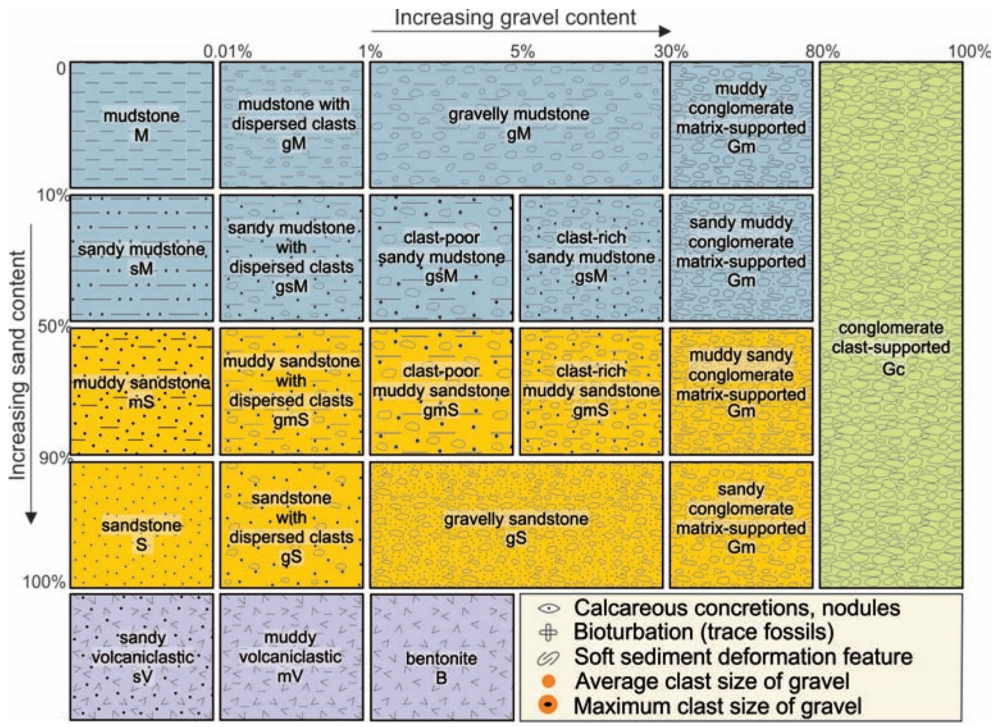

Figure 9. *Lithologies and symbols, arranged by grain size, in the reference stratotype from borehole W202 (see Figure 8).*

during several field trips to study the Kirkwood Formation. This project was supported by grants from the National Research Foundation African Origins Platform (GUN 91601 to EMB) and the DST-NRF Centre of Excellence in Palaeosciences (GUN CoE2017-050; COE2016-347 to EMB). A doctoral bursary to RM is provided by the DST-NRF Centre of Excellence in Palaeosciences. We gratefully acknowledge their financial contributions. The careful reviews provided by Drs Hayley Cawthra and Nigel Hicks, as well as Coenie de Beer improved the final manuscript. Opinions expressed and conclusions arrived at are those of the authors and are not necessarily to be attributed to the CoE in Palaeosciences or NRF AOP.

References

Almond, J.E., de Klerk, W.J. and Gess, R., 2009. Palaeontological heritage of the Eastern Cape. Interim SAHRA technical report, Natura Viva cc, Cape Town, 51p.

Almond, J.E., 2012. Proposed Jachtvlakte Precinct Human Settlement Plan, Nelson Mandela Bay Municipality, Eastern Cape. Natura Viva c, Palaeontological Assessment: Combined Desktop and Scoping Study, 22p.

Anderson, J.M. and Anderson, H.M., 1985. Palaeoflora of Southern Africa. Prodromus of South African Megafloras, Devonian to Lower Cretaceous. A.A. Balkema, Rotterdam, 422p.

Atherstone, W.G., 1857. Geology of Uitenhage: Eastern Province Monthly Magazine, 1, 518-532.

Bamford, M.K., 1986. Aspects of the palaeoflora of the Kirkwood and Sundays River Formations, Algoa Basin, South Africa. Unpublished M.Sc. thesis, University of Witwatersrand, Johannesburg, 160p.

De Klerk, W.J., Forster, C.A., Sampson, S.D., Chinsamy, A. and Ross, C.F., 2000. A new coelurosaurian dinosaur from the Early Cretaceous of South Africa. Journal of Vertebrate Paleontology, 20/2, 324-332.

Dingle, R.V. and Klinger, H.C., 1972. The stratigraphy and ostracod fauna of the Upper Jurassic sediments from Brenton, in the Knysna Outlier, Cape Province. Transactions of the Royal Society of South Africa, 40, 4, 279-298.

Dingle, R.V., Siesser, W.G. and Newton, A.R., 1983. Mesozoic and Tertiary geology of southern Africa. A.A. Balkema, Rotterdam, 375p.

Engelbrecht, L.N.J., Coertze, F.J. and Snyman, A.A., 1962. Die geologie van die gebied tussen Port Elizabeth en Alexandria, Kaapprovinsie. Explanation of 1:125,000 scale Sheets 3325D Port Elizabeth and 3326C Alexandria, Geological Survey South Africa, 54p.

Fouché, J., Bate, K.J. and Van de Merwe, R., 1992. Plate tectonic setting of the Mesozoic Basins, southern offshore, South Africa: A review. In: M.J. De Wit and I.G.D. Ransome (Editors). Inversion Tectonics of the Cape Fold Belt. Karoo and Cretaceous Basins of Southern Africa. A.A. Balkema, Rotterdam, 33-48.

Frost, S., 1996. Early Cretaceous alluvial palaeosols (Kirkwood Formation, Algoa Basin, South Africa) and their palaeoenvironmental and palaeoclimatological significance. Unpublished M.Sc. thesis, University of Rhodes, Grahamstown, 177p.

Forster, C.A., Farke, A.A., McCartney, J.A., De Klerk, W.J. and Ross, C.F., 2009. A 'basal' tetanuran from the Lower Cretaceous Kirkwood Formation of South Africa. Journal of Vertebrate Paleontology, 29, 283-285.

Gomez, B., Martinez-Delclos, X., Bamford, M. and Philippe, M., 2002. Taphonomy and palaeoecology of plant remains from the oldest African Early Cretaceous amber locality. Lethaia 35, 300-308.

Haughton, S.H., 1928. The geology of the country between Grahamstown and Port Elizabeth. Explanation of Cape Sheet 9 (Port Elizabeth), Geological Survey of South Africa, 50p.

Joubert, P. and Johnson, M.R., 1998. Abridged lexicon of South African stratigraphy. South African Committee for Stratigraphy (SACS), Council for Geoscience, Pretoria, 160p.

Lock, B.E., Shone, R., Coates, A.T. and Hatton, C.J., 1975. Mesozoic Newark-Type sedimentary basins within the Cape Fold Belt of South Africa. Proceedings of the 9th International Congress of Sedimentology, Nice, 2, 217-225.

Malan, J.A. and Theron, J.N., 1987. Notes on an Enon basin north-east of Bredasdorp, Southern Cape Province. Annals, Geological Survey of South Africa, 21, 83-87.

Malan, J.A. and Viljoen, J.H.A., 1990. Mesozoic and Cenozoic geology of the Cape South Coast. Guidebook Geocongress '90, Geological Society of South Africa, PO3, 81p.

Malan, J.A. and Viljoen, J.H.A., 2016. Southern Cape Geology: Evolution of a rifted margin. Field Trip Guide, 35th International Geological Congress, Cape Town, Post11, 64p.

McLachlan, I.R., Brenner, P.W. and McMillan, I.K., 1976. The Stratigraphy and Micropalaeontology of the Cretaceous Brenton Formation and the PB-A/1 well, near Knysna, Cape Province. Transaction of the Geological Society of South Africa, 79, 341-370.

McLachlan, I.R. and McMillan, I.K., 1976. Review and stratigraphic significance of southern Cape Mesozoic palaeontology. Transactions of the Geological Society of South Africa, 79, 197-212.

McMillan, I.K., Brink, G.I., Broad, D.S. and Maier, J.J., 1997. Late Mesozoic sedimentary basins off the south coast of South Africa. Sedimentary Basins of the World, 3, 319-376.

McMillan, I.K., 2003. The Foraminifera of the Late Valanginian to Hauterivian (Early Cretaceous) Sundays River Formation of the Algoa Basin, Eastern Cape Province, South Africa. Annals of the South Africa Museum, 106, 1-274.

McMillan, I.K., 2010. The Foraminifera of the Portlandian (Late Jurassic) Bethelsdorp Formation of the onshore Algoa Basin, Eastern Cape Province. Les Rosalines Press, Clovelly, 176p.

McPhee, B.W., Mannion, P.D., de Klerk, W.J. and Choiniere, J.N., 2016. High diversity in the sauropod dinosaur fauna of the Lower Cretaceous Kirkwood Formation of South Africa: implications for the Jurassic - Cretaceous transition. Cretaceous Research, 59, 228-248.

Muir, R.A. and Bordy, E.M., 2016. Stratigraphic framework for the Kirkwood Formation in the southern Cape region: invertebrate biostratigraphy and zircon geochronology. In: 19th Palaeontological Society of South Africa biennial conference, Stellenbosch University, 65p.

Muir, R.A., Bordy, E.M. and Prevec, R., 2015. Lower Cretaceous deposit reveals first evidence of a post-wildfire debris flow in the Kirkwood Formation, Algoa Basin, Eastern Cape, South Africa. Cretaceous Research, 56, 161-179.

Paton, D.A., 2006. Influence of crustal heterogeneity on normal fault dimensions and evolution: southern South Africa extensional system. Journal of Structural Geology, 28, 868-886.

Rigassi, D.A. and Dixon, G.E., 1972. Cretaceous of the Cape Province, Republic of South Africa. In: T.F.J. Dessauvagie and A.J. Whiteman (Editors). African Geology. Geology Department, University of Ibadan, Nigeria, 513-527.

Rogers, A.W. and Schwarz, E.H.L., 1901. Report on parts of the Uitenhage and Port Elizabeth Divisions. Annual Report, Geological Commission of the Cape of Good Hope, 5, 1-18.

Roux, J. and Davids, A., 2016. Structural Evolution of the Gamtoos Basin, based on 2D seismic data, 35th IGC Conference, Cape Town, Poster Abstract.

SACS (South African Committee for Stratigraphy), 1980. Stratigraphy of South Africa. Part 1 (Compiler L. E. Kent). Lithostratigraphy of the Republic of South Africa, South West Africa/Namibia, and the Republics of Bophuthatswana, Transkei and Venda. Handbook, Geological Survey of South Africa, 8, 690p.

Shone, R.W., 1976. The sedimentology of the Mesozoic Algoa Basin. Unpublished M.Sc. thesis, University of Port Elizabeth, 48p.

Shone, R.W., 1978. A case for lateral gradation between the Kirkwood and Sundays River Formations, Algoa Basin. Transactions of the Geological Society of South Africa, 81, 319-326.

Shone, R.W., 2006. Onshore post-Karoo Mesozoic deposits. In: M.R. Johnson, C.R. Anhaeusser and R.J. Thomas (Editors). The Geology of South Africa, Geological Society of South Africa, Johannesburg, and Council for Geoscience, Pretoria, 541-571.

Theron, J.N., Wickens, H. de V. and Gresse, P.G., 1991. Die geologie van die gebied Ladismith. Explanation of sheet 3320 Ladismith, Geological Survey of South Africa, 99p.

Toerien, D.K. (compiler), 1991. Geological Map 3324 Port Elizabeth. 1:250 000 Geological Map Series, Geological Survey of South Africa.

Viljoen, J.H.A., 1992. The stratigraphy of the Heidelberg/Riversdale Mesozoic Basin. In: M.J. De Wit and I.G.D. Ransome (Editors). Inversion Tectonics of the Cape Fold Belt. Karoo and Cretaceous Basins of Southern Africa.

A.A. Balkema, Rotterdam, 77-84.

Viljoen, J.H.A., 2009. Hartenbos Formation (Uitenhage Group) In: M.R. Johnson (Editor). Catalogue of South African Lithostratigraphic Units. South African Committee for Stratigraphy, 10, 9-10.

Winter, H. de la R., 1973. Geology of the Algoa Basin, South Africa, In: G. Blant, (Editor). Sedimentary basins of the African coasts, Part 2, South and East Coast. Association of African Geological Surveys, Paris, 17-48.

Winter, H. de la R., 1979. Application of basic principles of stratigraphy to the Jurassic-Cretaceous interval in southern Africa. In: A.M. Anderson and W.A. Van Biljon (Editors). Geocongress 77: Some Sedimentary Ore Deposits in South Africa. Special Publication, Geological Society of South Africa, 6, 183-196.

Editorial handling: C.H. de Beer.